



HAL
open science

Nouvelles formules de blending et de flambage multi-échelles pour améliorer l'optimisation déterministe des structures multicouches anisotropes

Marco Picchi Scardaoni

► To cite this version:

Marco Picchi Scardaoni. Nouvelles formules de blending et de flambage multi-échelles pour améliorer l'optimisation déterministe des structures multicouches anisotropes. Mécanique [physics.med-ph]. HESAM Université; Università degli studi (Pise, Italie), 2021. Français. NNT : 2021HESAE002 . tel-03482764

HAL Id: tel-03482764

<https://pastel.hal.science/tel-03482764>

Submitted on 16 Dec 2021

HAL is a multi-disciplinary open access archive for the deposit and dissemination of scientific research documents, whether they are published or not. The documents may come from teaching and research institutions in France or abroad, or from public or private research centers.

L'archive ouverte pluridisciplinaire **HAL**, est destinée au dépôt et à la diffusion de documents scientifiques de niveau recherche, publiés ou non, émanant des établissements d'enseignement et de recherche français ou étrangers, des laboratoires publics ou privés.



UNIVERSITÀ DI PISA
DIPARTIMENTO DI INGEGNERIA CIVILE
E INDUSTRIALE
DOTTORATO DI RICERCA IN
INGEGNERIA INDUSTRIALE

ARTS ET MÉTIERS PARISTECH
INSTITUT DE MÉCANIQUE ET
D'INGÉNIERIE – I2M
ÉCOLE DOCTORALE 432: SCIENCE DES
MÉTIERS DE L'INGÉNIEUR

New Blending and Multi-Scale Buckling Formulations to Improve the Deterministic Optimisation of Anisotropic Multilayered Structures

THESIS SUBMITTED IN PARTIAL FULFILMENT OF THE REQUIREMENTS FOR THE
DEGREE OF DOCTOR OF PHILOSOPHY IN

AEROSPACE ENGINEERING

MÉCANIQUE

Candidate

Marco PICCHI SCARDAONI

Supervisors

Prof. Mario Rosario CHIARELLI

Prof. Marco MONTEMURRO

Dott. Vittorio CIPOLLA

Prof. Enrico PANETTIERI

Coordinators of the Ph.D. Programs

Prof. Giovanni MENGALI

Prof. Fodil MERAGHNI

Jury members			
Prof. Sergio DE ROSA	Full Professor	UNINA (Naples)	President
Prof. Paolo VANNUCCI	Full Professor	UVSQ (Paris)	Reviewer
Prof. Paul M. WEAVER	Full Professor	UL (Limerick)	Reviewer
Prof. Angela VINCENTI	Associate Professor	UPMC (Paris)	Examiner
Prof. Marco MONTEMURRO	Full Professor	ENSAM (Bordeaux)	Examiner
Prof. Mario R. CHIARELLI	Associate Professor	UNIFI (Pisa)	Examiner
Prof. Enrico PANETTIERI	Associate Professor	ENSAM (Bordeaux)	Examiner
Dr. Vittorio CIPOLLA	Assistant Professor	UNIFI (Pisa)	Examiner
Prof. Aldo FREDIANI	Full Professor	UNIFI (Pisa)	Invited
Prof. Roberto PARONI	Full Professor	UNIFI (Pisa)	Invited

Pisa, 26 January 2021
XXXIII cycle

Copyright
Marco Picchi Scardaoni, 2021
All rights reserved.

To my family and to Elisabetta

[...] esiste una logica dietro a ogni cosa.
E la magia, che è così facile, non la sa fare nessuno.
Mauro dell'Orso

Ξυνηλών τε λέγω τήν τε πᾶσαν πόλιν τῆς Ἑλλάδος παιδευσιν εἶναι καὶ καθ' ἕκαστον
δοκεῖν ἄν μοι τόν αὐτόν ἄνδρα παρ' ἡμῶν ἐπὶ πλεῖστ' ἄν εἶδῃ καὶ μετὰ χαρίτων μάλιστ'
ἄν εὐτραπέλως τὸ σῶμα αὐταρκες παρέχεσθαι.
Thucydides, History of the Peloponnesian War, II XLI

Le mieux est l'ennemi du bien
Voltaire, La Béguéule

I thought that instead of the great number of precepts of which logic is composed, I would have enough with the four following ones, provided that I made a firm and unalterable resolution not to violate them even in a single instance.

The first rule was never to accept anything as true unless I recognized it to be evidently such: that is, carefully to avoid precipitation and prejudgement, and to include nothing in my conclusions unless it presented itself so clearly and distinctly to my mind that there was no occasion to doubt it.

The second was to divide each of the difficulties which I encountered into as many parts as possible, and as might be required for an easier solution.

The third was to think in an orderly fashion, beginning with the things which were simplest and easiest to understand, and gradually and by degrees reaching toward more complex knowledge, even treating as though ordered materials which were not necessarily so.

The last was always to make enumerations so complete, and reviews so general, that I would be certain that nothing was omitted.

René Descartes, Discours de la Méthode, Eng. Transl. (Sent to me at the beginning of my Ph.D.)

Acknowledgements

Gennaio, andiamo. È tempo di ringraziare.

Ringrazio innanzitutto i miei supervisors, Marco Montemurro, Mario Chiarelli, Enrico Panettieri, Vittorio Cipolla, per avermi dato la possibilità di realizzare al meglio il percorso di dottorato. Li ringrazio per avermi introdotto a tematiche importanti ed interessanti, per il costante e puntuale supporto e per la loro indubbia professionalità che mai è venuta meno nel corso degli anni, anche nei momenti di "stallo tesiistico". Un riconoscimento speciale a Marco, Enrico ed Anita Catapano per l'accoglienza a Bordeaux e per il prezioso aiuto.

Un ringraziamento particolare va ad Aldo Frediani. Ho avuto il piacere di averlo come docente, anni or sono, ed è lui che mi ha trasmesso la passione per continuare con lo studio, l'approfondimento e la ricerca. Senza di lui non starei qui.

Dicevo di Bordeaux. Sicuramente sono stati quindici mesi che ricorderò per sempre con piacere. Ringrazio i miei compagni di avventura - francesi, ritals e affini - per aver alleggerito le giornate lavorative, per i momenti di svago e le belle - talvolta movimentate - serate. Grazie dunque Alberto, Alexandre, Amaia, Carolina, Clement, (il "povero") Dario, Giulia, Giulio, Juanjo, Lorenzo, Marco, Michele, Preshit, Rachel, Ruben, Soukaina (Zucchina), Thibaut (x2), Thomas.

Ormai sono nove anni che Pisa mi ospita. Ho conosciuto molte persone con le quali ho stretto amicizia, tra i banchi all'università ma anche fuori. Siete tanti, ma voglio ringraziarvi singolarmente: Antonio, Dimitri, Gabriele, Gianmario, Giuseppe, Jammy, Luca, Mattia, Noemi, Piergiuseppe, Pierpaolo, i Racca brothers.

Un grazie anche agli amici e "compagni di merende" del DIA (e affini): Alessandro, Alessio, Andrea, Bruno, Davide, Emanuele, Fabio (in fondo sei un ingegnere anche tu), Federico (l'unico vero uomo), Francesco, Karim, Giuseppe, Roberta, Torquato e, in particolare, Vincenzo Binante.

Un grazie anche ai miei fantastici ex coinquilini di Via S. Michele degli Scalzi: Daniele, Federica, Francesco, Giulia, Giuseppe, Marta. L'avevo scritto nei ringraziamenti della tesi magistrale, che speravo potesse nascere una bella amicizia. Oggi ne ho la conferma.

Un grazie anche ai miei nuovi compagni di viaggio e amici di Strutture (e affini): Massimiliano, Matteo, Paolo (x2), Riccardo, Roberto (x2). In particolare grazie a Roberto Paroni, che mi ha introdotto a tematiche affascinanti e che mi ha offerto l'opportunità di poterle continuare ad esplorare.

Non dimentichiamoci delle origini. Ringrazio i miei amici di sempre Anne, Edoardo, Fabiana, Francesco (aka Ciccio), Giulia, Guglielmina (aka Peppa), Rita per la loro "secolare" amicizia nata tra i banchi di una piccola classe di un liceo della piccola gloriosa città di Rieti. Non ve lo dirò più, forse, ma siete la squadra migliore che si possa chiedere. Grazie per esserci sempre stati.

Un grazie enorme alla mia famiglia. Grazie mamma Tilde e nonna Renata. Se oggi sono qui, questo è sicuramente un vostro merito e successo personale. Grazie anche a nonno Cesare, anche se è in qualche mondo misterioso e incomprensibile ai vivi. Se alla fine faccio sempre di testa mia, lo devo a te.

Tra i vari banchi dove si possono conoscere persone, ci sono anche quelli di un aula di un (ex) dipartimento di Ing. Aerospaziale, dove possono svolgersi lezioni di Academic English. Galeotta fu la dispensa della Spataro e chi la scrisse. Un gigantesco grazie ad Elisabetta per il supporto quotidiano, la comprensione quotidiana, il sostegno nei momenti di sconforto e per il costante confronto su qualsiasi argomento. Grazie per aver compreso questi tre anni difficili e per essere ancora qui.

Funding

This Thesis has been funded by the research project PARSIFAL ("PrandtlPlane ARchitecture for the Sustainable Improvement of Future AirpLanes"), financed by the European Union under the Horizon 2020 Research and Innovation Program (Grant Agreement n.723149).

The candidate is profoundly grateful for the support.



Abstract

English The goal of this Thesis is to provide an improved design framework for the optimal design of multilayer composite structures by using deterministic algorithms. The improvement is based on the formalisation of two aspects which deeply affect the reliability and the likelihood of the final solution.

The first one involves multi-scale considerations of the structural responses. In fact, some structural criticalities manifest themselves at different scales: the transition of scale is required to better catch these phenomena. In this work, attention is paid on buckling instability of stiffened panels. However, the scale transition must be considered in the derivation of the response gradient, to be provided to the deterministic algorithm of the solution search.

The second one involves the so-called blending requirement. It is a problem about the correct junction of adjacent laminates of different thickness, requiring that all the plies of the thinner laminate must be contained in the stack of the thickest one, without ply intersections. Moreover, blending makes thickness variations possible. Due to its importance, blending is a manufacturing requirement which must be assessed since the preliminary design phases. Moreover, the development of a general strategy for the retrieval of blended stacking sequence for the structure is faced in this work, to provide a solution which can be manufactured. Two possible approaches are presented: a pure numerical one and a combinatorial one, wherein the solution search is carried out in the class of *quasi-trivial* stacking sequences. After a comparison, the former is preferred for the applications.

Once formalised and included in an optimisation framework, the multi-scale approach for the deterministic optimisation, the blending requisite and the numerical approach for the stack recovery are employed for a complete optimal design of an innovative as well as complex aircraft structure: the wing-box of the PrandtlPlane developed within the PAR-SIFAL project. The obtained results are encouraging.

Besides those aspects of the work, the Thesis also presents insights on two touched topics: the non-convexity of the laminate feasibility domain and the rational modelling choice of stiffened plates. For both topics new unexpected theoretical findings have been found.

Français L'objectif de cette Thèse est de développer une méthodologie de conception multi-échelle innovante utilisant un algorithme déterministe pour la conception de structures composites multicouches. L'innovation par rapport aux travaux existants est représentée par la formalisation de deux aspects qui influent grandement sur la fiabilité et la qualité de la solution finale.

Le premier aspect porte sur la prise en compte de l'intégration dans la formulation du

problème de conception des réponses structurelles critiques intervenants aux différentes échelles du problème. En effet, puisque certaines réponses se manifestent à différentes échelles d'observation, la transition d'échelle se révèle nécessaire afin de bien saisir ces phénomènes. Dans ce travail, une attention particulière sera portée sur l'évaluation de la charge critique de flambage de panneaux raidis constituant l'élément fondamental de la structure des aéronefs. Cependant, la transition d'échelle doit être prise en compte dans la dérivation du gradient des réponses physiques, nécessaire au bon fonctionnement de l'algorithme déterministe pour la recherche de l'optimum.

Le deuxième aspect porte sur la contrainte technologique dite de *blending*, un problème intrinsèquement lié à la variation du nombre de plis (et des orientations associées) entre stratifiés adjacents de différentes épaisseurs. En effet, les plis des stratifiés plus minces doivent être contenus dans l'empilement des stratifiés les plus épais, sans intersection entre plis. De plus, le *blending* permet une modulation de l'épaisseur de la structure. De par son importance, il est nécessaire de prendre en compte la contrainte de *blending* dès les premières phases de conception. De plus, une stratégie générale dont l'objectif est d'identifier la séquence d'empilement des couches du composite en satisfaisant la contrainte de *blending* a été développée : permettant ainsi de proposer une solution faisable. Deux approches possibles sont présentées : la première est une approche numérique et la seconde une approche combinatoire, basée sur la recherche des solutions dans une classe particulière de stratifiés (les séquences quasi-triviales).

Une fois formalisée, cette approche a été appliquée au problème de la conception d'une architecture aéronautique complexe et innovante : le caisson alaire du PrandtlPlane développé au sein du projet PARSIFAL. Les résultats obtenus sont prometteurs.

A côté de ces aspects, les travaux de Thèse abordent aussi deux sujets purement théoriques : la non-convexité du domaine de faisabilité des laminés, ainsi que une justification variationnelle de la modélisation des panneaux raidis. Des résultats inattendus et originaux ont été déterminés pour chacun de ces deux thèmes.

Italiano L'obiettivo di questa Tesi è migliorare la progettazione di strutture composite multistrato attraverso lo sviluppo di un framework incentrato su algoritmi deterministici. Il miglioramento si basa sulla formalizzazione di due aspetti che influenzano profondamente l'affidabilità e la qualità della soluzione finale.

Il primo aspetto riguarda il comportamento multiscala delle risposte strutturali. Infatti, alcune criticità strutturali si manifestano in scale diverse: il passaggio di scala è quindi necessario per meglio descrivere questi fenomeni. In questo lavoro, l'attenzione è rivolta all'instabilità di pannelli irrigiditi. Chiaramente, la transizione di scala deve essere considerata nella formulazione del gradiente della risposta, da fornire all'algoritmo deterministico per la ricerca della soluzione.

Il secondo aspetto riguarda il requisito del *blending*. Si tratta di un problema inerente la corretta giunzione dei laminati di diverso spessore. Si richiede che tutte gli strati del laminato più sottile debbano essere contenuti nella sequenza di laminazione del laminato più spesso, senza intersezione delle stesse. Inoltre, il *blending* rende possibili variazioni di spessore all'interno della struttura. Per la sua importanza, il *blending* è un requisito di manifattura che deve essere considerato sin dalle fasi preliminari di progettazione. In questo lavoro si affronta anche lo sviluppo di una strategia generale per il recupero delle sequenze di laminazione che soddisfino il requisito di *blending*, in modo da fornire, alla fine, una soluzione ottimale che possa essere effettivamente realizzata. Vengono presentati due possibili approcci: uno puramente numerico e uno combinatorio, basato sulla conoscenza di una particolare classe di laminati (le sequenze quasi-triviali).

Una volta formalizzati ed inseriti in un quadro di ottimizzazione, l'approccio multi-scala

Contents

List of Figures	xvii
List of Tables	xix
List of Algorithms	xxi
List of Theorems, Propositions and Lemmata	xxiii
List of Definitions	xxv
Nomenclature	xxv
I Preamble	1
1 Introduction	3
1.1 The PARSIFAL Project and the Thesis Context	3
1.2 Thesis Objectives and Original Contributions	9
1.3 Thesis Structure	11
2 Literature Review	15
2.1 Optimisation Methodologies for Anisotropic Structures	15
2.1.1 Generalities	15
2.1.2 Direct Stiffness Modelling	17
2.1.3 The Multi-scale Multi-level Composite Laminates Optimisation	18
2.1.4 The Choice of Algorithms	20
2.1.5 Global-local Modelling Strategies for Anisotropic Structures	22
2.2 Design of Anisotropic Structures Including Manufacturing Constraints	23
2.2.1 Generalities	23
2.2.2 Blending	24
2.3 Approaches for Wing Design	27
2.3.1 Structural Analyses of PrandtlPlane Lifting System	27
2.3.2 Global-local Approaches for Wing Design	28
2.4 Conclusions	29

II	Theoretical Background	31
3	Fundamentals of Optimisation Methods and Algorithms	33
3.1	Generalities on Optimisation	33
3.1.1	Mathematical Programming	33
3.1.2	Programming Classifications	34
3.2	Deterministic Algorithms for CNLPPs	37
3.2.1	Optimality Conditions	37
3.2.2	The Deterministic Algorithm <i>fmincon</i>	38
3.3	Meta-heuristic Algorithms for CNLPPs and MICNLPPs	39
3.3.1	Introduction to Meta-heuristics	39
3.3.2	The Ant Colony Optimisation Algorithm MIDACO®	40
3.3.2.1	Generalities on Ant Colony Optimisation Algorithms	40
3.3.2.2	MIDACO®	41
3.4	Conclusions	42
4	Fundamentals of Polar Method and of Composite Laminates Mechanics	43
4.1	Polar Representation of Plane Elasticity Tensors	43
4.1.1	Second-order Tensors	44
4.1.2	Fourth-order Tensors	44
4.1.3	Thermodynamic Existence Conditions	46
4.2	Polar Formalism and Composite Laminates	46
4.2.1	First-order Shear Deformation Theory	47
4.2.2	Polar Description of Laminate Stiffness Tensors	49
4.2.3	Polar Description of Laminate Strength Tensors	51
4.2.4	Elastic and Geometrical Bounds	54
4.3	Quasi-trivial Stacking Sequences	55
4.4	Conclusions	57
5	Fundamentals of Elasticity and Variational Methods	59
5.1	Fundamentals of Elasticity	59
5.1.1	Finite Elasticity	60
5.1.1.1	Analysis of Deformation	60
5.1.1.2	Analysis of Stress	61
5.1.1.3	Constitutive Equations	62
5.1.1.4	Equilibrium Problem: Strong and Weak Formulations	63
5.1.2	Linearised Elasticity	65
5.2	The Direct Method of the Calculus of Variations	67
5.3	Γ -convergence	69
5.4	Conclusions	73
III	Improving the Optimal Design of Composite Structures	75
6	On Buckling and Blending	77
6.1	Multi-scale Formulation of Buckling Requirement	77
6.1.1	Constraint	78
6.1.2	Buckling Factor Gradient in Multi-scale Context	79
6.1.2.1	Initialisation of the Gradient Expression	79
6.1.2.2	Stress-Stiffness Matrix Expression	83
6.1.2.3	Finalisation of the Gradient Expression	87

6.2	New Blending Constraints Formulation	88
6.2.1	Constraints	89
6.2.2	Gradient	94
6.3	The Stacking Sequence Recovery Phase	94
6.3.1	Stiffness Recovery for a Single Laminate	95
6.3.2	Recovery Stacking Sequences for the Entire Structure	97
6.3.3	The Concept of Search Propagation Direction	98
6.3.3.1	Mathematical Justification of Search Propagation Direction	99
6.4	An Alternative Approach for the Stacking Sequence Recovery Phase	105
6.4.1	An Algorithm for the Search of Quasi-trivial Quasi-homogeneous Stacking Sequences	106
6.4.2	Quasi-trivial Approach	112
6.5	Conclusions	115
7	The Enhanced Deterministic GL-MS2LOS and Case Studies	117
7.1	Generalities on the MS2LOS	118
7.1.1	Laminate Feasibility Constraints	119
7.1.2	Displacement Requirement	121
7.1.3	Laminate Failure Criterion	122
7.1.4	The First-level Problem Formulation	123
7.1.4.1	Continuous Optimisation	123
7.1.4.2	Discrete Optimisation	124
7.1.5	The Second-level Problem Formulation	125
7.2	Case Study 1: a Benchmark on the FLP	126
7.2.1	Problem Definition	126
7.2.2	The First-level Problem Formulation	126
7.2.3	Numerical Strategy	129
7.2.4	The Global/Local Finite Element Modelling Approach	131
7.2.5	Numerical Results	132
7.3	Case Study 2: a Benchmark on the SLP	138
7.3.1	Problem Definition	138
7.3.2	The First-level Problem	138
7.3.2.1	Numerical Strategy	140
7.3.2.2	Numerical Results	142
7.3.3	The Second-level Problem	143
7.3.3.1	Numerical Strategy	143
7.3.3.2	Numerical Results	147
7.3.4	Some Remarks on the Proposed SLP Strategy	148
7.4	Case Study 3: Comparisons Between Stacking Sequence Recovery Techniques	152
7.4.1	The First-level Problem	153
7.4.1.1	Numerical Strategy	154
7.4.1.2	Numerical Results	154
7.4.2	The Second-level Problem	155
7.4.2.1	Numerical Approach Results	155
7.4.2.2	Alternative Quasi-trivial Approach Results	157
7.4.3	Comments on the Comparison Results	157
7.5	Conclusions	158

8	The Optimal Design of Composite PARSIFAL Wing-box	161
8.1	Problem Definition	161
8.1.1	Geometry and Material	161
8.1.2	Design Criteria	165
8.1.3	Load Cases	166
8.2	The First-level Problem Formulation	167
8.2.1	Numerical Strategy	169
8.2.2	The Global and Local Finite Element Models	171
8.2.2.1	The Global Finite Element Model	171
8.2.2.2	Justification of the FE Modelling of Stiffened Plates	172
8.2.2.3	The Local Finite Element Model	174
8.3	The Second-level Problem Formulation	174
8.3.1	Mathematical Formulation	175
8.3.2	Numerical Strategy	175
8.4	Numerical Results	176
8.5	Conclusions	184
IV	New Theoretical Findings	185
9	On the Non-convexity of the Feasible Domain of Laminates	187
9.1	The Non-convexity of the Feasible Domain of Laminates	188
9.1.1	Generalities	188
9.1.2	Lamination Parameters	189
9.1.3	The Non-convexity Proofs of the Feasible Domain	190
9.1.4	Some Exact Solutions for Geometrical Bounds	197
9.1.4.1	Exact Analytic Expression of the Feasible Domain for the Case $n_1 = n_2 = n_3 = n$	203
9.1.5	New Geometrical Bounds	205
9.2	On the Necessary and Sufficient Conditions for Uncoupling and Homogeneity	205
9.3	Conclusions	208
10	Linear Models of Stiffened Plates via Γ-convergence	211
10.1	Problem Description	213
10.2	The Scaled Problem	215
10.3	Compactness Lemmata	217
10.4	Junction Conditions	218
10.4.1	An Important Inequality	218
10.4.2	The Junction Conditions for Displacements	220
10.4.3	Different Regimes for Joining Conditions	222
10.5	The Limit Energy	224
10.6	Convergence of Minima and Minimisers	228
10.7	Conclusions	234
V	Epilogue	235
11	Conclusions and Perspectives	237
11.1	General Conclusions	237
11.2	Perspectives of the Thesis	239

Bibliography	243
A A Note on the Square of the Sum of n Terms	259
B Study of $B^* = 0$ for Blending Constraints	261
C Analytic Expression of Stiffness Matrix Gradient	265
D Analytic Expression of Laminate Strength Matrices Gradient	267
E Analytic Expression of Laminate Stiffness Matrices Gradient	269
F List of Publications	271

List of Figures

1.1	Possible architectures for the civil transport aircraft of the future: Blended Wing Body (BWB), Truss Braced Wings (TBW) and PrandtlPlane (PrP) concepts	4
1.2	Artistic view of the PrandtlPlane object of study in the PARSIFAL project	5
1.3	Boeing 787 material composition from Hale (2006)	7
1.4	Two blended laminates (different colours mean different orientations). . .	8
1.5	A possible way to read this Thesis	13
2.1	Different scales of a composite laminate	16
2.2	Schematic overview of the multi-scale multi-level optimisation	19
2.3	Conceptual scheme of GL approach	23
2.4	Vertical displacement component for the composite PARSIFAL PrP	28
3.1	Classification of Optimisation programming problems	35
3.2	A graph of four vertices and six edges	41
4.1	Mid-plane of a plate and reference frame	47
4.2	Unit-length internal generalised forces \mathbf{r}_{gen}	48
5.1	Placement \mathbf{k} and deformation χ of a body \mathfrak{B}	60
5.2	Loaded body \mathfrak{B} in the reference configuration	64
5.3	Comparison between a LSC and a non LSC function.	68
5.4	Example 1: family of functionals $\mathcal{F}_n := \sqrt{2}enx e^{-n^2x^2}$ and Γ -limit	72
5.5	Example 2: family of functionals $\mathcal{F}_n := \arctan(nx)$ and Γ -limit	72
5.6	Example 3: family of functionals $\mathcal{F}_n := \sin(nx)$ and Γ -limit	73
6.1	Differences between GFEM and LFEM meshes	81
6.2	Two violations of blending definition (Definition 6.3)	89
6.3	Two possible blended arrangements between two given laminates (different colours mean different orientations).	89
6.4	Comparison of blending feasible region delimited by constraints presented in (Panettieri et al., 2019) and by the herein proposed ones for a reference laminate.	92
6.5	Conceptual junction of composite laminates	93
6.6	Blending of three laminates (different colours mean different orientations).	97

6.7	A four-laminate blended structure	100
6.8	Two propagation schemes.	100
6.9	Propagation 3: a propagation which does not ensure automatic blending of adjacent stacks	101
6.10	Some possible blending schemes (from van Campen et al. (2008), Bordogna et al. (2020))	102
6.11	Sketch of the action of the blending map \mathcal{B} and its left-inverse \mathcal{B}_L^{-1}	103
6.12	Injective maps for Propagation 1	104
6.13	Injective maps for Propagation 2	104
6.14	Injective maps for Propagation 3	105
6.15	Tree graph spanned by two labels for an N -ply laminate.	108
6.16	Branch pruning	108
6.17	Number of QT QH SSs up to thirty-nine plies	111
7.1	Model geometry of the of Case Study 1 benchmark structure (The upper skin ($z = H$) is shaded to make the interior part visible)	126
7.2	Optimisation regions of Case Study 1 structure	127
7.3	Workflow of the numerical strategy of Case Study 1	130
7.4	GFEM and related BCs of Case Study 1	131
7.5	LFEM and the related BCs of Case Study 1	132
7.6	Optimal design variables values for Case 1 (n_0 in blue, ρ_{0K} in red, ρ_1 in green, ϕ_1 in black)	133
7.7	Optimal design variables values for Case 2 (n_0 in blue, ρ_{0K} in red, ρ_1 in green, ϕ_1 in black)	135
7.8	Optimal design variables values for Case 3 (n_0 in blue, ρ_{0K} in red, ρ_1 in green, ϕ_1 in black)	136
7.9	Polar diagram of the first component of matrices \mathbf{A} and \mathbf{H} for panel n° 1	136
7.10	Polar diagram of the first component of matrices \mathbf{A} and \mathbf{H} for panel n° 6	137
7.11	Polar diagram of the first component of matrices \mathbf{A} and \mathbf{H} for panel n° 7	137
7.12	Eighteen panels benchmark structure of Case Study 2	138
7.13	Workflow of the numerical strategy of the FLP of Case Study 2	141
7.14	Blending propagation scheme of Case Study 2	146
7.15	Three different blending schemes.	147
7.16	Contributes to the total residual from each panel of Case Study 2	148
7.17	Polar diagrams of some selected panels of Case Study 2	150
7.18	Benchmark structure for the comparison between two different stacking sequence recovery approaches of Case Study 3	152
7.19	Solution propagation for the numerical approach to the stacking sequence recovery	156
7.20	Contributes to the total residual from each panel of Case Study 3	158
8.1	PrP aircraft rendering and \mathcal{T}_B reference frame	162
8.2	Planform of the PrP lifting system, with wing-box position, in the \mathcal{T} reference frame	162
8.3	Some details of the PrP wing-box architecture	164
8.4	Overview of the PrP wing-box architecture	165
8.5	Optimisation regions IDs for the upper skins (in brackets the IDs of the lower counterparts)	167
8.6	Workflow of the numerical strategy of the FLP of the PrP wing design	170
8.7	GFEM mesh particulars of the PrP wing design	172
8.8	Example of ZOI and checking zone of the PrP wing design	173

8.9	Details of the mesh of the FW upper skin LFEM of the PrP wing design	174
8.10	Blending scheme of the PrP wing design	175
8.11	Solution propagation for the upper skin of the FW	176
8.12	Polar diagrams of meaningful panels of upper skin of FW	178
8.13	Polar diagrams of meaningful panels of lower skin of FW	183
8.14	Polar diagrams of meaningful panels of upper skin of RW	183
8.15	Polar diagrams of meaningful panels of lower skin of RW	183
9.1	Indicator function $\chi [\Delta z_i^*]$	191
9.2	Feasibility domain projections for anisotropic (on the left) and membrane-orthotropic (on the right) laminates ($K = 0$) of $N = 4$ plies, on the top in terms of PPs, on the bottom in terms of LPs (discretisation step = 5°). In red the points \hat{P} and \check{P} used in the proofs of Section 9.1.3.	197
9.3	Feasibility domain projection onto the plane (ρ_1, ρ_0) for anisotropic laminates of N plies (equivalent to consider laminates with m distinct orientations, all of them appearing the same number of times within the SS)	198
9.4	Feasibility domain in the space $(\rho_1, \rho_0, \cos 4(\Phi_0^{A^*} - \Phi_1^{A^*}))$ for anisotropic laminates of $N = 3, 4$ plies. In purple the geometrical bound of Eq. (4.44).	199
9.5	Lamination points for $N = 20, m = 2$ (discretisation step = 3°).	200
9.6	Cases B or C for $n_1 = 1, n_2 = 2, n_3 = 3$, (discretisation step = 3°) by permuting indices 1, 2, 3 modulo 3.	202
9.7	Case D for four different laminates (discretisation step = 3°).	202
9.8	Case E for four different laminates.	204
9.9	Lamination points and envelope for the case $n_1 = n_2 = n_3 = n$ (discretisation step = 3°).	204
9.10	Vannucci's geometrical bound (Vannucci, 2012a) and proposed bounds for a laminate having $N = 4$ (discretisation step = 3°)	206
10.1	Geometry of real problem	213
10.2	(Left) Reference system in this Chapter; (Right) Reference system in (Griso, 2005)	219
10.3	Junction conditions discriminant	223
10.4	Cases presented in Aufranc (1990)	223
B.1	Comparison between blending constraints	264

List of Tables

6.1	Quasi-trivial quasi-homogeneous stacking sequences number	111
7.1	Material properties of the T300/5208 pre-preg	127
7.2	Design space for Problem (7.23)	129
7.3	<i>fmincon</i> parameters	129
7.4	Objective function for the optimised solution	133
7.5	Optimal value of design variables	134
7.6	Material properties of the carbon-epoxy IM7/8552 pre-preg.	139
7.7	Design variables range of Problem (7.27)	140
7.8	MIDACO [®] parameters for the discrete optimisation of Case Study 2	142
7.9	Comparison of optimal mass (in kg) of Case Study 2	143
7.10	Numerical solution for the continuous optimisation of the FLP (7.27)	144
7.11	Numerical solutions for the discrete optimisation of the FLP (7.21)	144
7.12	Buckling factors (λ) after the continuous and discrete optimisations of Case Study 2	145
7.13	MIDACO [®] parameters for RSS search for the SLP of Case Study 2	146
7.14	Residuals for different blending schemes of Case Study 2	147
7.15	Optimal stacks solution of Problem (6.52) of Case Study 2	149
7.16	Design variables range of the continuous optimisation problem of Case Study 3	153
7.17	Numerical solution for the continuous optimisation of the FLP of Case Study 3	155
7.18	Numerical solutions for the discrete optimisation of the FLP of Case Study 3	155
7.19	Numerical optimal SSs of Case Study 3	156
7.20	QT optimal SSs of Case Study 3	157
8.1	Wing geometry in the \mathcal{T} reference frame	163
8.2	Wing-box position (reported in chord percent, refer to the planform of Figure 8.2)	163
8.3	Values of stringer pitch, ribs pitch and stringers geometry	164
8.4	Design variables range of the PrP wing design	169
8.5	Parameters of the <i>fmincon</i> algorithm.	170
8.6	MIDACO [®] parameters for the discrete optimisation of the FLP of the PrP wing design	171

List of Tables

8.7	Number of independent variables for sub-problems of SLP	175
8.8	MIDACO [®] parameters for RSS search for the SLP	176
8.9	Optimal values of the design variables of the FLP	177
8.10	Constraint values for the FLP	178
8.11	Stacks of upper skin of FW	179
8.12	Stacks of lower skin of FW of the PrP wing design	180
8.13	Stacks of upper skin of RW of the PrP wing design	181
8.14	Stacks of lower skin of RW of the PrP wing design	182
8.15	Stacks of spar webs and stringers of the PrP wing design	184
10.1	Different junction conditions	233

List of Algorithms

3.1	Active-set deterministic optimisation algorithm	39
3.2	Ant-colony optimisation algorithm	41
6.1	Generation of matrix \mathbf{P} .	82
6.2	Derivation of matrices $\overline{\mathbf{K}}_i$.	84
6.3	Mesoscale blending check.	97
6.4	DLX-Stack Finder	110
6.5	GOF function	112
6.6	GOC function	113
6.7	GOFC function	113
6.8	Stacking sequence recovery with QT QH SSs	114

List of Theorems, Propositions and Lemmata

3.1	Theorem (Existence (and uniqueness) of global minimum for (strictly) convex functions)	36
3.2	Theorem (Karush-Kuhn-Tucker (KKT) first-order necessary conditions for optimality)	37
3.3	Theorem (Second-order sufficient conditions for optimality)	37
5.1	Theorem (Polar decomposition)	61
5.2	Theorem (Hamel & Noll Theorem (Cauchy’s Postulate))	61
5.3	Theorem (Cauchy’s Lemma)	61
5.4	Theorem (Equilibrium of a body portion)	61
5.5	Theorem (Equilibrium as a stationary point of the total potential energy)	64
5.6	Theorem (Elasticity tensor for hyperelastic linear materials)	65
5.7	Theorem (Coercivity of the elasticity tensor)	65
5.8	Theorem (Representation Theorem for hyperelastic linear isotropic elasticity tensor)	65
5.9	Theorem (Existence and uniqueness of the solution for the linearised elasticity equilibrium problem)	66
5.10	Theorem (Total potential energy minimum)	66
5.11	Theorem (Direct Method of the Calculus of Variations)	69
5.12	Theorem (Coercivity on Sobolev H^1 space)	69
5.13	Theorem (Tonelli-Serrin)	69
5.14	Theorem (Korn’s inequality)	69
5.15	Theorem (Convergence of minima and minimisers)	71
5.16	Theorem (Stability under continuous perturbations)	71
6.1	Lemma (Injectivity of the composition of injective functions)	102
6.2	Lemma (Necessary and sufficient conditions for injectivity)	103
9.1	Proposition (Convexity of the layup functions set)	191
9.1	Lemma (Convexity of projections of a convex set)	192
9.2	Proposition (Non-convexity of the feasible domain of anisotropic laminates in the PPs space)	192
9.3	Proposition (Non-convexity of the feasible domain of orthotropic laminates in the PPs space)	195

9.4	Proposition (Non-convexity of the feasible domain of anisotropic laminates in the LPs space)	195
9.5	Proposition (Non-convexity of the feasible domain of orthotropic laminates in the LPs space)	196
9.1	Theorem (Theorem 1 from (Green, 1916))	206
9.2	Theorem (Theorem 2 from (Green, 1916))	207
9.6	Proposition (Condition for quasi-triviality to be a necessary and sufficient one for quasi-homogeneity)	208
10.1	Lemma (Compactness of rescaled plate displacement)	217
10.2	Lemma (Compactness of rescaled stiffener displacements)	217
10.1	Theorem (Theorem 2.3 from (Griso, 2005))	220
10.3	Lemma (Trace approximation)	220
10.4	Lemma (Convergence of components of the rescaled strain energy)	224
10.2	Theorem (Γ -limit)	225
10.3	Theorem (Convergence of the total energy)	229
10.4	Theorem (Strong convergence of minima and minimisers)	229

List of Definitions

3.1	Definition (Feasible region)	36
3.2	Definition (Convex function)	36
3.3	Definition (Global minimiser)	36
3.4	Definition (Local minimiser)	36
3.5	Definition (Convex set)	36
3.6	Definition (Convex programming problem)	36
4.1	Definition (Membrane/bending uncoupling)	50
4.2	Definition (Homogeneity)	50
4.3	Definition (Quasi-homogeneity)	51
4.4	Definition (Stacking sequence)	55
4.5	Definition (Saturated group)	56
4.6	Definition (Quasi-trivial stacking sequences)	56
5.1	Definition (Displacement)	60
5.2	Definition (Green-Saint Venant strain tensor)	61
5.3	Definition (Elastic material)	62
5.4	Definition (Hyperelastic material)	62
5.5	Definition (Symmetry group)	63
5.6	Definition (Saint Venant–Kirchhoff material)	63
5.7	Definition (Kinematically admissible functions set)	64
5.8	Definition (Total potential energy)	64
5.9	Definition (Total potential energy in linearised elasticity)	66
5.10	Definition (Lebesgue L^2 space)	67
5.11	Definition (Sobolev H^1 space)	67
5.12	Definition (Sobolev $H^{1/2}$ trace space)	67
5.13	Definition (Lower and upper limit)	67
5.14	Definition (Lower-semicontinuity)	68
5.15	Definition (Sequentially lower-semicontinuity)	68
5.16	Definition (Sequentially compact set)	68
5.17	Definition (Sequential coercivity)	69
5.18	Definition (Γ -convergence)	70
6.1	Definition (Annihilating operator \mathfrak{J})	79
6.2	Definition (Reducing operator \mathfrak{R})	79

List of Definitions

6.3	Definition (Blending)	88
6.4	Definition (Recovery stacking sequence)	95
6.5	Definition (Search propagation direction)	99
6.6	Definition (Identity function of a set)	102
6.7	Definition (Left-inverse function)	102
6.8	Definition (Subset-sum problem)	106
6.9	Definition (Exact-cover problem)	106
6.10	Definition (M-unsubsummable set)	107
6.11	Definition (Quasi-trivial quasi-homogeneous stacking sequences search problem)	107

Nomenclature

Abbreviations

ACO Ant colony optimisation

BCs Boundary conditions

BFGS Broyden-Fletcher-Goldbarf-Shanno

CLT Classical Laminate Theory

CNLPP Constrained non-linear programming problem

DC Design criterion

DOFs Degrees of freedom

FE, FEM Finite Element Method, Finite Element Method

FLP First-level problem

FSDT First-Order Shear Deformation Theory

FW, RW, VW Front, Rear, Vertical wing

GA Genetic Algorithm

GFEM Global FEM

GL Global-Local

GL-MS2LOS Global-Local Multi-Scale Two-Level Optimisation Strategy

LC Load condition

LFEM Local FEM

LPs Lamination parameters

LSC, SLSC Lower-semicontinuous, sequentially lower-semicontinuous

MICNLPP Mixed-Integer non-linear programming problem

MS2LOS Multi-Scale Two-Level Optimisation Strategy

Nomenclature

NPC Nondeterministic polynomial time complete problems

PPs Polar parameters

QH Quasi-homogeneous

QT Quasi-trivial

RSS Recovery stacking sequence

SLP Second-level problem

SR Stiffness recovery

SS Stacking sequence

UNLPP Unconstrained non-linear programming problem

ZOI Zone of interest

Symbols

$(\cdot_j), \{\cdot_j\}$ Sequence of \cdot , being j the enumeration index

$\bar{\mathbf{K}}$ Matrix for the decomposition of the geometric stiffness matrix

\cdot_L^{-1} Left-inverse function of \cdot

$:=$ Definition

Γ, Λ, Ω Polar parameters of out-of-plane strength tensor

γ, λ, ω Polar parameters of the linear part of the generalised strength criterion

$\Gamma_0, \Gamma_1, \Lambda_0, \Lambda_1, \Omega_0, \Omega_1$ Polar parameters of plane fourth-order strength tensors

\implies Implication

λ, μ Lamé constants

λ, ψ Eigenvalue, eigenvector

\mathbb{C} Elasticity tensor

$\mathbb{M}^{m \times n}$ Real-valued $m \times n$ matrices space

\mathbb{N}, \mathbb{Z} Natural, integer numbers

$\mathbb{R}, \bar{\mathbb{R}}, \mathbb{R}^+$ Real line, extended Real line ($\mathbb{R} \cup \{-\infty, +\infty\}$), non-negative real numbers

$\mathbb{S}\text{ym}, \mathbb{P}\text{sym}$ Vector space of symmetric fourth-order tensors, of symmetric and positive-definite fourth-order tensors

$\mathbf{0}, \mathbf{O}$ Null vector, tensor

$\mathbf{A}, \mathbf{B}, \mathbf{D}, \mathbf{C}, \mathbf{H}$ Membrane, coupling, bending, homogeneity, transverse shear stiffness tensors

\mathbf{E} Strain tensor

\mathbf{F} Deformation gradient

\mathbf{f}	External forces vector
$\mathbf{G}, \hat{\mathbf{G}}, \mathbf{Q}, \hat{\mathbf{Q}}$	In-plane strength tensor, in-plane stiffness tensor, out-of-plane strength tensor, out-of-plane stiffness tensor of a single ply
$\mathbf{G}_A, \mathbf{G}_B, \mathbf{G}_D, \mathbf{G}_H$	Membrane, coupling, bending, transverse shear strength tensors
\mathbf{I}_n	n -dimensional identity tensor
\mathbf{J}	Jacobian matrix
\mathbf{k}	Reference placement of a body
$\mathbf{K}, \mathbf{K}_\sigma$	Stiffness, Geometrical stiffness matrix
$\mathbf{n}, \mathbf{m}, \mathbf{t}$	Membrane, blending, transverse shear forces and moments vectors
$\mathbf{N}_e, \mathbf{B}_e, \mathbf{L}_e$	Shape functions matrix, Deformation matrix, Connectivity matrix of the e -th element
\mathbf{P}	Interpolant operator between GFEM and LFEM BCs
\mathbf{P}, \mathbf{T}	Piola, Cauchy stress tensors
\mathbf{Q}, \mathbf{R}	Elements of $\text{SO}(3)$
\mathbf{r}	Internal reactions vector
$\mathbf{t}, \mathbf{s}, \mathbf{b}, \hat{\mathbf{u}}$	Prescribed stress vector, surface forces, volume forces, prescribed displacement
\mathbf{u}	Displacements vector
\mathcal{E}	Euclidean space
$\mathcal{NB}(\cdot)$	Set of ply indices not interested by blending
$\mathfrak{B}, \mathfrak{B}$	Body, Subbody
\mathfrak{F}	Response function
$\mathfrak{R}, \mathfrak{J}$	Operators on matrices and vectors
e	Euler's number
i	Immaginary unit
$\text{SO}(n)$	Special orthogonal group. Set of n -dimensional rotation tensors
\mathcal{A}	Admissible functions set
\mathcal{B}	Blending operator
\mathcal{C}^n	Set of n -times continuously-differentiable functions
$\mathcal{F}, \mathcal{L}, \mathcal{W}$	Functionals
\mathcal{G}	Group
$\mathcal{P}(\cdot)$	Projection of the set \cdot
$\nabla \cdot$	Gradient of \cdot

Nomenclature

- \oplus Direct sum
- \otimes Kronecker's tensor product
- $\partial \cdot$ Exterior boundary of \cdot
- Φ Objective function
- χ Deformation mapping
- $\boldsymbol{\mu}, \mathbf{w}$ Adjoint vectors
- $\boldsymbol{\sigma}_1, \boldsymbol{\sigma}_2, \boldsymbol{\sigma}_3$ (Pseudo) Pauli's matrices
- $\boldsymbol{\varepsilon}_0, \boldsymbol{\chi}_0, \boldsymbol{\gamma}_0$ Membrane, blending, transverse shear strain, curvature, shear vectors
- $\boldsymbol{\xi}$ Design variables vector
- $\sharp(\cdot)$ Cardinality of \cdot
- $\rightarrow, \rightharpoonup$ Strong, weak convergence
- C Generic constant which may vary line to line
- h, t Thickness
- $H^1(a; b)$ Space of Sobolev functions on a with value in b
- $H^{1,2}(a; b)$ Trace space of $H^1(a, b)$
- $L^2(a; b)$ Space of square-summable functions on a with value in b
- m, ρ Mass, mass density
- n, N Number of
- $n_0, \rho_{0K}(\rho_0), \rho_1, \phi_1$ Dimensionless Polar parameters for membrane tensor \mathbf{A}^*
- T, R, Φ Polar parameters of out-of-plane stiffness tensor
- $T_0, T_1, R_0, R_1, \Phi_0, \Phi_1$ Polar parameters of plane fourth-order stiffness tensors
- \mathbf{c}, \mathbf{g} Equality, Inequality constraint
- $\det(\cdot)$ Determinant of \cdot
- $\text{diag}(a, b, \dots)$ Diagonal (block) matrix with element (matrices) a, b, \dots on the principal diagonal
- $\text{div}(\cdot)$ Divergence of \cdot
- E, G, ν Young's modulus, shear modulus, Poisson's ratio
- $\text{KS}(\cdot)$ Kreisselmeier-Steinhauser function
- Lin, Lin^+ Vector space of second-order tensors, of second-order tensors with non-negative determinant
- Skw Vector space of skew-symmetric second-order tensors
- $\text{sym}(\cdot), \text{skw}(\cdot)$ Symmetric, skew-symmetric part of \cdot

Sym, Psym Vector space of symmetric second-order tensors, of symmetric and positive-definite second-order tensors

$\text{tr}(\cdot)$ Trace of \cdot

$\text{Var}(\cdot)$ Variance of \cdot

Subscripts and Superscripts

\cdot^\dagger Target value of \cdot

\cdot^T Transpose of \cdot

e Index over elements

$b,^b$ Relative to the LFEM (except in Chapter 10)

BC Relative to the boundary conditions

blend Relative to blending

buck Relative to buckling

DOF Relative to the degrees of freedom

feas Relative to feasibility

gen Generalised

IN Relative to the internal nodes

lam Relative to the laminate

lb, ub Lower bound, upper bound

ply Relative to the ply

ref Reference

TH Relative to Tsai-Hill

vars Relative to variables

Part I

Preamble

Introduction

Strong teeth and good digestion too -
this I wish thee!
And once my book's agreed with you,
then surely you'll agree with me!

Friedrich Nietzsche, *Die fröhliche
Wissenschaft*. (Eng. Transl.)

1.1 The PARSIFAL Project and the Thesis Context

According to researches conducted in the last years by the European Commission (European Commission, 2011) and by industry and academia (EREA, 2012; ACARE, 2017), the Air Transport System will deal with three main challenges in next decades:

1. the increase of air traffic demand improving flight safety;
2. the reduction of noxious emissions and noise (both intended per passenger-kilometres);
3. making travellers within Europe able to complete their journey within 4 hours (door-to-door).

Among the possible ways to reach these goals, novel aircraft configurations, conceived to have a higher aerodynamic efficiency, i.e. lift-to-drag ratio, have been proposed. Some of the candidate configurations for future aviation are those shown in Figure 1.1: the Blended Wing Body (BWB), the Truss Braced Wings (TBW) and the Box-Wing. An exhaustive literature review on the BWB is available in (Okonkwo & Smith, 2016), whilst an akin counterpart for the *joined-wing* concepts (TBW, Box-Wing, etc.) is available in

(Cavallaro & Demasi, 2016), together with challenges and perspectives.

The main advantage of the BWB is the reduction of the wetted surface and of the pressure drag due to the junction between fuselage and wing in "tube-and-wing" configurations. The second and the third concepts attempt at reducing the induced drag, the TBW by increasing the aspect ratio of the wing, the Box-Wing by a theoretical aerodynamic result, discussed in the following, without increasing the wingspan.



Figure 1.1: Possible architectures for the civil transport aircraft of the future: *Blended Wing Body (BWB)*, *Truss Braced Wings (TBW)* and *PrandtlPlane (PrP)* concepts

The Box-Wing concept has been studied since early 1990s at University of Pisa, where the attention has been focused on the possible applications in aviation of the so-called Best Wing System (BWS) concept, due to Ludwig Prandtl. In (Prandtl, 1918, 1924), the German scientist claimed the existence, for fixed wingspan and generated lift, of a lifting system which minimises the induced drag, with a proper lift distribution, among all the others lifting systems. According to Prandtl study, this optimal configuration is a box-wing one. Many years later, in (Frediani et al., 1999; Frediani & Montanari, 2009), a closed-form-solution of the optimal lift distribution has been derived, in the class of elliptic-plus-constant lift circulations. Starting from that point, studies have been focused on the application, into aeronautical engineering, of the BWS. The aircraft architecture based on the BWS has been consequently called *PrandtlPlane* (PrP), in Prandtl's honour. Although the induced drag minimisation is the most direct advantage of the PrP concept, other interesting benefits have been found in subsequent studies, for different aircraft categories. In fact, the PrP architecture has a smooth stall behaviour, and the post-stall is characterised by only a partial reduction of manoeuvrability and controllability (Cipolla et al., 2016). Furthermore, from Flight Mechanics point of view, pitch control can be obtained by using counter-rotating elevators (on both front and rear wing), which can introduce a pitching moment without perturbation to the total lift (Oliviero et al., 2016); moreover, the pitch damping of the PrP is higher than in the case of a wing-tail configuration, with benefits in terms of comfort and safety. In addition, as summarised in (Frediani, Cipolla, & Rizzo, 2012; Cavallaro & Demasi, 2016), the PrP flexibility makes it a suitable concept for aircraft of very different dimensions and purposes, such as Light Sport Aircraft, ultra large airliners, freighter aircraft (Frediani et al., 2015) or cryoplanes (Beccasio et al., 2012). The outperforming performance of the PrP in take-off and landing manoeuvres has been recently investigated in (Bertini & Nuti, 2018; Bianchi, 2018; Abu Salem et al., 2020).

This Thesis is framed within the PARSIFAL ("Prandtlplane ARchitecture for the Sus-

tainable Improvement of Future AirpLanes") Project, funded by the European Union under the Horizon 2020 program (Grant Agreement n. 723149) and coordinated by the University of Pisa. Other partners of PARSIFAL Project are: TU Delft (The Netherlands), ONERA (France), ENSAM (France), DLR (Germany) and SkyBox Engineering (Italy). The main objective of PARSIFAL Project is to demonstrate that the application of the PrP configuration to aircraft with a wingspan limited to 36 m, such as Airbus A320 or Boeing B737, can increase the number of transported passenger from about 200 to more than 300, keeping the aircraft dimensions compatible with current airport infrastructures typical of point-to-point air traffic. In this way, the higher lift-to-drag ratio of the PrP is exploited for increasing the payload capabilities and for reducing the fuel consumption per passenger. Benefits are addressed to airlines, which can have higher profit margins, to airport management companies, which can increase the number of travellers without changing the airside infrastructures, and to travellers, which can reasonably have access to lower fares (Jemitola & Fielding, 2012).

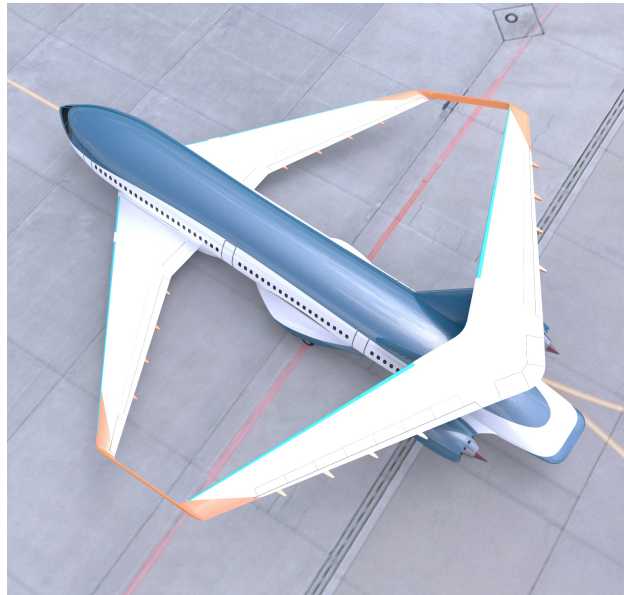


Figure 1.2: *Artistic view of the PrandtlPlane object of study in the PARSIFAL project*

The PARSIFAL Project is a multidisciplinary one. In three years of project, investigations have been performed on Aerodynamics, Flight Mechanics, Structures, Propulsion, Noise and Environmental impact, Economical impact of the PrP into the market, Logistics and ground operations.

This Thesis deals with structural topics, as specified in the following. In the PARSIFAL Project, the Work Package 5, coordinated by ENSAM and held in collaboration with University of Pisa and DLR, was devoted to the structural analyses and optimisation of the configuration. In particular, the University of Pisa determined the first conceptual and preliminary design (Milestone 1), compliant with Top Level Aircraft Requirements, to be used by other partners for further multidisciplinary investigations (Frediani et al., 2017; Abu Salem et al., 2018; Frediani et al., 2019; Picchi Scardaoni et al., 2019a; Cipolla et al., 2020); ENSAM performed the optimisation of the Milestone 1 in the metallic and

composite cases (Izzi, Montemurro, Catapano, Fanteria, et al., 2020; Izzi, Montemurro, Catapano, & Pailhès, 2020; Picchi Scardaoni et al., 2020); DLR performed sensitivity analyses on the joint regions between fuselage and lifting system. Aeroelastic analyses have been performed *externally* by Carlos III University of Madrid.

Indeed, the PrandtlPlane structure, shown in Figure 1.2, represents a challenging one to design, since the conceptual and preliminary design phases. The mutual structural influences between wing and fuselage make Finite Element (FE) modelling anything but a trivial task; the geometry of the aircraft that evolves in the 3D space makes the Finite Element modelling complicated; the large numbers of variables that should be taken into account for a proper design (note that the design of the PARSIFAL wing is approximately the design of three conventional wings at once) makes the design problem formulation not easy, since a trade-off between the number of variables (directly related to quality of the solution) and the computational costs must be found.

Concerning the structural design of the PrP object of study in the PARSIFAL Project, the following main activities have been carried out in the Work Package 5:

- (a) the conceptual design of the fuselage, conceived to fulfil the Top Level Aircraft Requirements, with a detailed study concerning the landing gear and the landing and take-off manoeuvres simulations (Ph. D. Thesis of K. Abu Salem, Ph. D. activities of the candidate, MSc Theses of A. Nuti & F. Bertini, M. Bianchi);
- (b) the preliminary structural sizing using low-fidelity models and Finite Element Methods (FEMs) (MSc Theses of A. Felice, of the candidate, of M. Sansone, of I. L. Navarro, Ph. D. activities of the candidate);
- (c) the optimisation of the PARSIFAL structures adopting traditional metallic and more advanced composite solutions (Ph. D. activities of M. I. Izzi and of the candidate, post-doctoral fellowship activities of E. Panettieri);
- (d) detailed optimisation of fuselage structure adopting traditional metallic and more advanced composite solutions, including variable stiffness composites (Ph. D. Thesis of M. I. Izzi);
- (e) detailed optimisation of wing structure adopting traditional metallic and more advanced composite solutions (Ph.D. Thesis of the candidate);
- (f) experimental validation of the numerical optimisation strategy on simple composite structures and on composite stiffened panels (Ph. D. Thesis of M. I. Izzi, post-doctoral fellowship activities of E. Panettieri);
- (g) aeroelastic analyses of the optimised metallic PrP model (Prof. R. Cavallaro team and Ph. D. activities of R. Bombardieri).

Although the candidate's contributes in points (a) and (b) (Picchi Scardaoni et al., 2017; Picchi Scardaoni et al., 2019a; Picchi Scardaoni & Frediani, 2019a; Picchi Scardaoni & Frediani, 2019b), to define a reference configuration for deeper investigations, and in point

(c) (Picchi Scardaoni et al., 2019b; Picchi Scardaoni et al., 2020), this Thesis focuses on point (e), in particular on the constant stiffness composite solution of the PARSIFAL PrP wing.

Composite materials allow for the tailoring of material properties, with several potential benefits. Indeed, in aerospace structures design, the most relevant is lightness. It is well-known that today's aircraft manufacturers exploit composite solutions for the primary structures of actual aircraft, as shown in Figure 1.3 for the Boeing 787 case, where up to the 50% of the structure is made from composites.

In the recent years, many works have focused on design aspects of composite structures, especially multilayered ones. Hereafter, a (multilayered) *laminated* (or *panel*) is a thin structural component, made of variously-oriented stacked layers (i.e. the *plies*), whereby thickness and elastic properties are constant. Multilayered composite structures are clearly the assembly of different (in thickness and elastic properties) panels. However, an efficient use of composites to build large optimised structures remains one of the main challenges of today aircraft industry (Bordogna et al., 2020). In fact, if compared

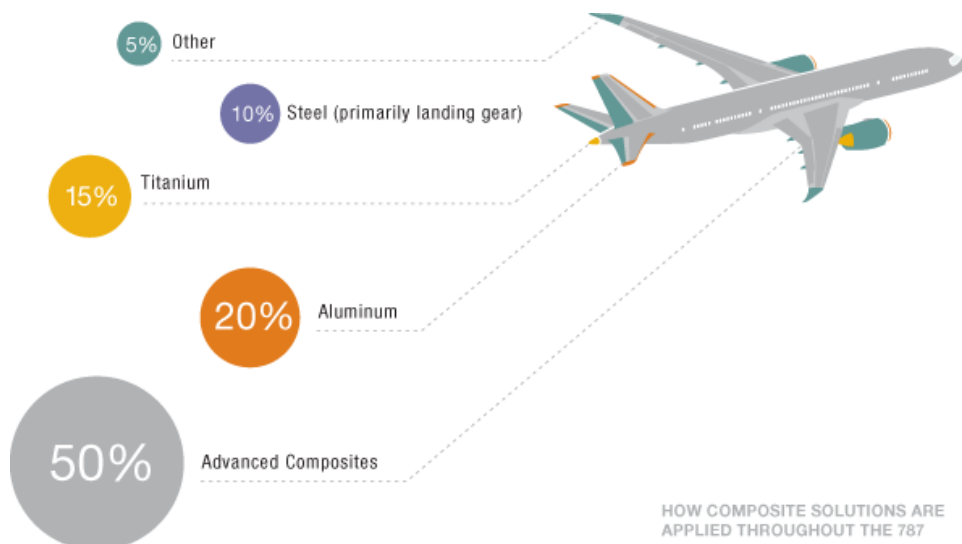


Figure 1.3: Boeing 787 material composition from Hale (2006)

to isotropic light-alloy structures, the design of composite laminates introduces a higher level of complexity due to the increased number of design variables, the mathematical formulation of anisotropy, the heterogeneity of the material, as well as manufacturing and feasibility constraints formulation and modelling. All of these aspects shall be considered since the preliminary design phase.

In general, it is of paramount importance to integrate the most of the requirements since the preliminary design phases. For the case of composite structures, in particular, it is fundamental to include constraints related to the technological and manufacturing process. Among them, of particular importance is the so-called *blending* (or *ply-drop*) constraint. Blending requirement deals with the continuity of ply orientation angles between a pair of adjacent laminates having different thickness. In plain language, given a pair of adjacent laminates, blending is the requirement about the inclusion of the orien-

tation angles of the thinner laminate into the thicker laminate ones. If the requirement is satisfied, the laminates are said *blended*. An example of two blended laminates is shown in Figure 1.4. The desired continuity is essential for the correct junction of panels having

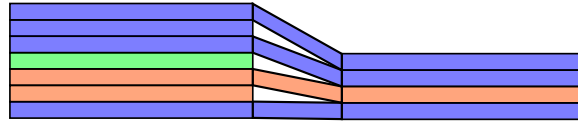


Figure 1.4: Two blended laminates (different colours mean different orientations).

different thickness. From another perspective, blending is necessary to allow thickness variations and modulations on a structure, as for the tapered thickness of a wing. It appears then essential to include blending since the earliest design phases for the manufacturability and for the likelihood of the final solution. Moreover, the blending integration within the design problem should provide, at the end of the design process, the explicit expression of the *blended* (which basically means *manufacturable*) stacking sequences (SSs), i.e. the ordered sequence of oriented layers for each panel of the structure.

When designing thin-walled structures, criteria of different nature shall be included in the problem formulation. For instance: the mass of the structure (to be minimised), requirements about stiffness (expressed, for example, as maximum allowable displacements or rotations in some critical points of the structure), requirements about the mechanical strength of the material, requirements about buckling failure. In addition, the structural responses can be critic at different scales. In fact, a critical phenomenon can appear at the structure global level or only at the macro-component local level. In the case of composite structures, the responses can be critic at the macroscopic scale (panel level) or at the mesoscopic scale (ply-level). For the sake of completeness, further critical phenomena may also appear at the microscopic scale (constitutive phases). However, they are not the topic of this Thesis and will be disregarded in the following. As a consequence, a proper multi-scale approach shall be adopted, in order to implement these considerations within the design process of the structure, without prohibitive computational costs. Thus, a global-local approach to better investigate proper subregions of the main structure is worthy to be considered and integrated (see also the Ph. D. Thesis of M. I. Izzi).

Since, choosing composites, the elastic properties of the material can be tailored, the number of design variables rapidly increases. In this context, meta-heuristic algorithms do not perform efficiently. In fact, for large scale problems, meta-heuristics require a consistent number of evaluations to reach the final solution. This is computational expensive if one considers the typical slow convergence rate of such algorithms (Ghiasi et al., 2009). Conversely, generally speaking, deterministic algorithms have a fast convergence rate (Ghiasi et al., 2009). The resort to deterministic optimisation algorithms, on the one hand mitigates the issues of the number of variables and of the computational cost; on the other hand, the user should provide the analytic expressions of the gradients of objective function and constraints. In particular, the task of considering the scale transition of the global-local approach in the expression of the gradients is anything but trivial.

1.2 Thesis Objectives and Original Contributions

The present Thesis mainly attempts at formalising two important aspects to be taken into account for a more profitable deterministic optimisation of multilayered constant-stiffness thin-walled structures. Those aspects are:

1. a multi-scale global-local approach to properly describe the structural responses of phenomena appearing at different scales. This approach should be suitable for deterministic optimisation. Although in this Thesis it will be developed for the assessment of buckling responses, it can be extended to requirements of different nature;
2. a complete multi-scale blending processing, ensuring blended and manufacturable stacking sequences matching, at the same time, the optimal elastic properties.

Due to the multi-scale focus of the investigation, once formalised, the Thesis findings can be implemented in a multi-scale optimisation framework, as those that will be presented in Chapter 2. In this Thesis, the Multi-Scale Two-Level Optimisation Strategy (MS2LOS), appeared for the first time in (Montemurro et al., 2012b), will be chosen as the preferred framework. Nevertheless, with possibly minor modifications, the proposed findings are substantially valid also for other optimisation frameworks. It is noteworthy that, whichever optimisation framework is chosen to implement the Thesis findings, an enhanced and more complete methodology for the optimal design of composite thin-walled structures results defined. To show the effectiveness of the Thesis' results, several benchmarks, taken from the literature, are proposed. Finally, the composite wing design of the PARSIFAL Project PrP is employed to prove the effectiveness of the enhanced methodology also in dealing with complex *real-world* structures.

Generally speaking, the interest in a more complete methodology can have important practical and industrial interest. In fact, an enhanced reliability of the final solution since the preliminary design phases can be possible, and the explicit expression of blended SSS of laminates composing the structure at hand can be provided. In so doing, the structure could be theoretically manufactured at the end of the design process.

In this context, an answer to the following main research questions (RQs) is provided throughout this Thesis:

RQ1 How to formulate a rigorous global-local approach for the deterministic optimisation framework?

Indeed, when a deterministic algorithm is employed for the solution search of a multi-scale formulation of the optimisation problem, the effect of the scale transition must be taken into account in the formulation of the structural responses gradients. In so doing, the optimisation algorithm "sees" coherency between responses and their gradients, allowing a correct convergence towards a local (or global, depending on the nature of the problem at hand) feasible minimiser. In This thesis, the attention is paid to the global-local buckling requirement.

RQ2 *How to formulate blending requirements to be used within the structural optimisation process? How to recover blended stacking sequences for a complex structure?*

As introduced, the continuity of ply orientations between adjacent panels of different thickness must be considered from the preliminary design phases. Indeed, a blended structure is a manufacturable one. If the explicit expression of blended SSs is not provided, the optimisation results assume only a theoretical meaning, since it remains undefined how to effectively manufacture the structure. It will be clear in the core of the Thesis that the proposed formalisation of the blending strategy, spendable in multi-scale multi-level frameworks, has a double nature. In fact, at first, blending requirement is an optimisation constraint. At a later stage, it is a numerical strategy to determine blended orientations for the panels of the structure at hand, matching the previously-determined optimal elastic properties.

It will also presented an alternative approach, based on the knowledge of a particular class of stacking sequences. This alternative approach for the stack recovery phase will be compared to the numerical approach, the latter being the "official" approach of the Thesis.

RQ3 *Is it possible to formulate the structural optimisation problem, within in the deterministic optimisation framework, by integrating, among others, blending manufacturing requirements and a global-local approach?*

By putting together RQ1 and RQ2, RQ3 regards the joint applicability of such developed elements in a complete optimisation framework. Moreover, a profitable use of the resulting enhanced methodology for complex real applications is sought. It is not *a priori* guaranteed that the high non-linearities, viz. the scale transition and blending constraints, introduced in the design problem can make the deterministic optimisation algorithm to converge towards an optimal feasible solution.

Besides these research questions, other theoretical aspects, linked to research questions RQ1-RQ3, have been worthy deepening. In particular:

RQ4 *Is the feasible domain of laminates convex?*

Is quasi-triviality a necessary and sufficient condition for membrane/bending uncoupling and/or homogeneity?

At the end of the numerical benchmark focusing on blending, some sources of error will be discussed. Among them, the fact that the sharpest expression of the feasible domain of laminate is not known at the present time. This evidence affects the well-posedness of the search of SSs matching some desired properties (and the design problem, in general). A preliminary question about the general problem of the determination of the feasible domain of laminates is then related to its shape, whether it has some nice topological properties. A second question is motivated by the fact that the interest is not on all the laminates, but only on those having some good mechanical properties (namely membrane/bending uncoupling, homogeneity, orthotropy). Are there any necessary and sufficient conditions to achieve

these properties and, hence, to characterise the subset of such laminates?

RQ5 *Which approach to model stiffened plates is closer to the actual linearised 3D elasticity equilibrium problem? Or, which approach to model stiffened plates is justified by the asymptotic limit behaviour of the actual linearised 3D elasticity equilibrium problem?*

The stiffened plate is a structural pattern widely used in thin-walled structures, *a fortiori ratiōne* aeronautic ones, but how to model it? This question arose when creating the FEM for the design of the PARSIFAL PrP wing. Indeed, there are several modelling choices, due to the variety of models available for plates, shells, beams and trusses. In the literature, there is not an unified approach, and the choice of a particular solution seems driven by computational cost considerations only. This investigation tries to clarify, in a rigorous manner, which linear reduced-order models of stiffened plates (e.g. plate and beam, plate and rod, etc.) are asymptotically representative of the "real" 3D elastic equilibrium problem. The results show that only some plate-and-beam model can be justified by a variational energetic approach, whilst others do not have an energetic justification. Results are then used in the FE modelling of the PARSIFAL PrP wing.

1.3 Thesis Structure

This Thesis is outlined as follows.

Chapter 2 presents a state of the art on the main topics touched by the Thesis.

Part II presents a brief collection of the most important theoretical results that will be largely used throughout the Thesis, so to present a self-contained exposition. This Part can be partially or completely skipped by the reader. Chapter 3 resumes the fundamentals of theoretical and numerical Optimisation; Chapter 4 summarises the characterisation of the plane anisotropy of laminates through the polar formalism, with a particular focus on higher-order transversal shear theories; Chapter 5 outlines the most important concepts of non-linear and linearised elasticity, with a particular focus on the variational structure of the elastic equilibrium problem and on a particular variational convergence called Γ -convergence. This latter Chapter is preliminary in view of the exposition of Chapter 10 for answering the research question RQ5.

Part III is dedicated to the answers of research questions RQ1, RQ2, RQ3, together with the numerical applications. Chapter 6 introduces the formalisation of the global-local approach for the assessment of the buckling response, and of the blending processing for the deterministic optimisation framework. An alternative approach to the stacking sequence recovery phase, based on a particular class of laminates, is also presented in the Chapter. Chapter 7 presents the MS2LOS, enhanced with the implementation of the findings exposed in Chapter 6. Successively, some numerical benchmarks, to demonstrate the effectiveness of the Thesis' findings formulations, are presented. The first one is a simplified wing, taken from the literature, to demonstrate the effectiveness of the global-

local approach formulation within the deterministic optimisation framework. The second benchmark is dedicated to prove the effectiveness of the proposed stacking sequence recovery approach, with a focus on blending handling, through the study of a simplified structure, taken from the literature. The third benchmark compares the official numerical approach and the alternative one for the stacking sequence recovery phase. Chapter 8 presents the results of the application of the MS2LOS, including the Thesis' results, to the PARSIFAL PrP wing design.

To avoid any interruption of the main flow of the Thesis, new theoretical findings (research questions RQ4, RQ5) will be exposed in Part IV. In particular, Chapter 9 answers research question RQ4 and addresses the problem of the convexity of the feasible domain of laminates, presenting *unexpected* results. The same Chapter also addresses the problem of necessary and sufficient conditions to obtain uncoupled and/or homogeneous laminates. Chapter 10 answers research question RQ5 and addresses the problem of retrieving homogenised models of stiffened panels starting from the 3D equilibrium problem.

Finally, Part V concludes the Thesis with some meaningful comments and future developments in Chapter 11.

To guide the reader in the reading, a possible way to read the Thesis is depicted in Figure 1.5.

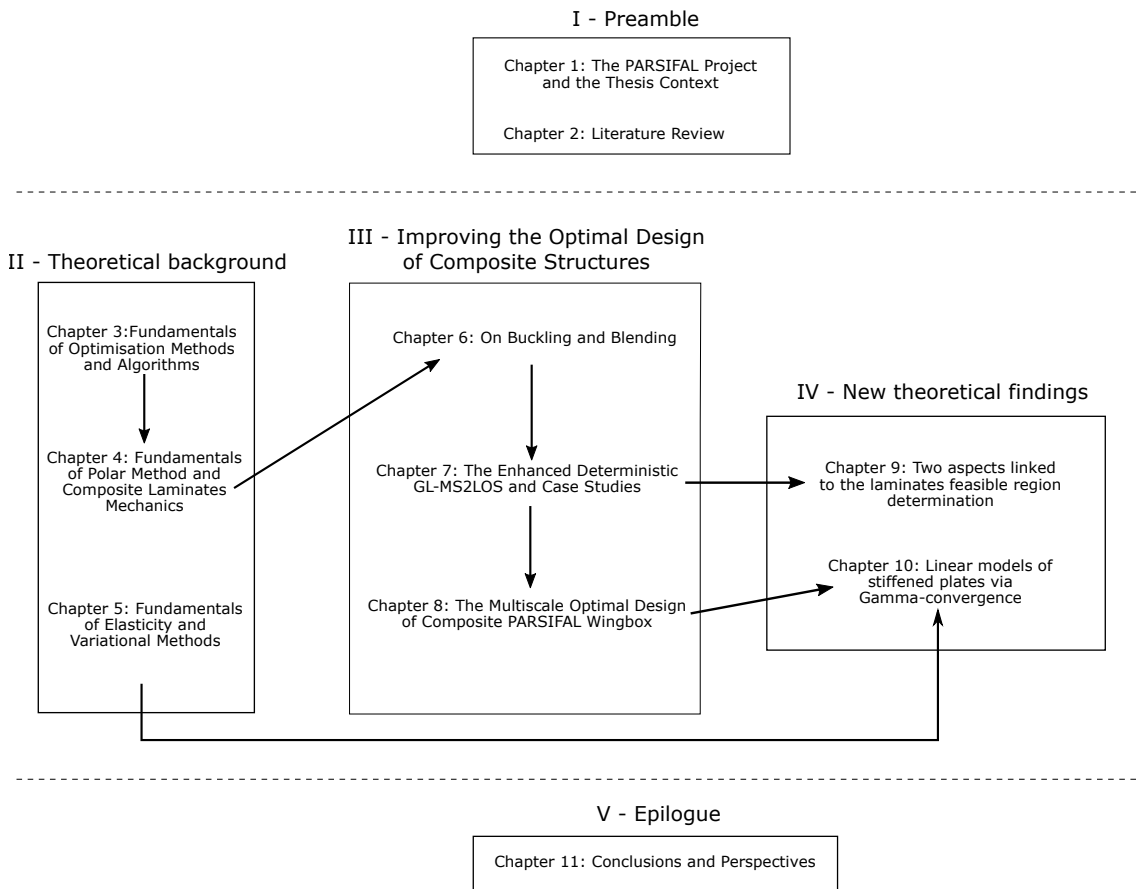


Figure 1.5: A possible way to read this Thesis

Literature Review

This Chapter provides the state of the art on the main topics touched by the Thesis, viz. research questions RQ1, RQ2, RQ3.

Firstly, a summary of multi-scale methods for the design of anisotropic laminates is presented in Section 2.1, with a focus on global-local approaches. Secondly, the state of the art on manufacturing constraints integration within composite laminates optimisation frameworks is discussed in Section 2.2, with a particular attention to blending. Successively, the state of the art on the structural studies of the PrandtlPlane configuration is presented in Section 2.3, together with a survey on the multi-scale methods used in the design of aircraft wings. Finally, some meaningful conclusions are discussed in Section 2.4.

2.1 Optimisation Methodologies for Anisotropic Structures

2.1.1 Generalities

Last decades have seen an increasing interest in the study and in the use of composite materials, especially for aeronautical structures. Composite materials allow for a greater freedom in the design process when compared to traditional metal alloys. In fact, the material itself can be tailored according to the requirements of the problem at hand. Furthermore, high specific stiffness and specific strength make composite materials appealing for the aeronautical industry.

Despite these advantages, many difficulties arise since the initial design phases. Issues are mainly related to the mathematical description of anisotropy, as well as to the scale separation between the most important physical responses to be integrated into the design

process. Three scales are usually identified: the macroscopic scale (at laminate scale), the mesoscopic scale (at ply-level) and the microscopic scale (at constitutive phases scale), which are conceptually depicted in Figure 2.1. Indeed, the three scales are strictly con-

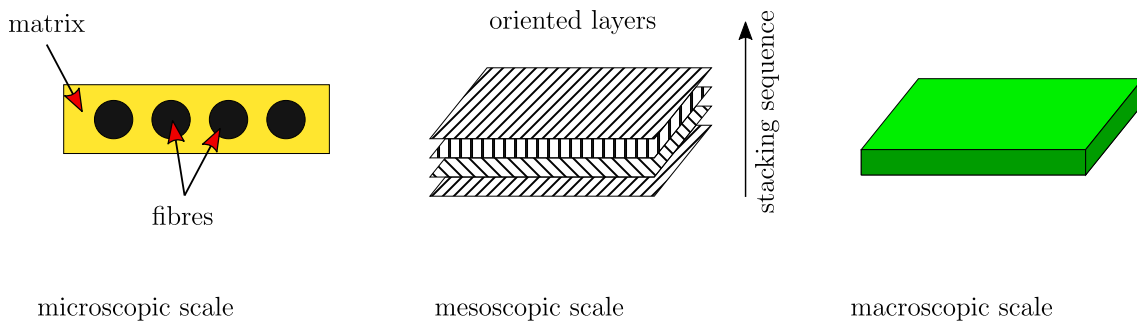


Figure 2.1: Different scales of a composite laminate

nected. In fact, the macroscale behaviour of an anisotropic laminate can be described by the laminate stiffness properties, which are affected by the mesoscopic properties: the laminate's SS (the sequence of orientation of the stacked layers) and the material properties of the layer(s). In turn, the macroscale anisotropy is, *de facto*, a direct consequence of the heterogeneity of the layers at the microscopic scale, i.e., roughly speaking, the embedding of fibres into a resin matrix. It is then clear that the design of a composite laminate is intrinsically a multi-scale task, due to the mutual influence of the three scales. As a consequence, the most general formulation of the design problem of a composite laminate should include all of the three scales. What is conventionally done in the literature is to disregard the microscopic scale in the preliminary design process, thus considering only the mesoscopic and the macroscopic scales. It is done because, basically, phenomena acting at the microscopic scale (debonding, interface phenomena between fibres and matrix, fatigue, etc.) can be at first neglected. Moreover, these phenomena strongly depend on the final geometry of the structure, which is not yet known in the preliminary design stages. Naturally, deeper investigations must follow in the subsequent design phases. As already pointed out, in the reminder of the Thesis, the microscopic scale will not be considered in the design process.

What is, then, the task of the designer? The designer's task is to tailor the stiffness and strength properties of the laminates to achieve the desired final properties of the structure. Traditionally, to each stacked layer within the laminate is assigned a constant fibre orientation angle, thus leading to a constant stiffness laminate. Even though the existence of variable stiffness composites, this Thesis is focused on constant stiffness laminates: elastic properties are constant within a single laminate but generally vary from laminate to laminate.

The industrial interest toward composite laminates is still predominantly restricted to *conventional laminates*, viz. laminates having orientation angles $0, \pm 45, 90$ degrees and symmetric and balanced SSs. The choice of such SSs has been motivated by the limited manufacturing technology at the time. With the recent introduction of new technologies such as the Automated Fibre Placement, fibres can be disposed in any direction.

As a result, interest in non-conventional laminates has been growing up in the last years (Vannucci & Verchery, 2002, 2010; Montemurro et al., 2012a; Vannucci et al., 2012; Montemurro et al., 2018), because laminate design can effectively exploit the benefits of these innovative technologies. Non-conventional laminates provides the largest design space to the designer, thus promising better final results. This could be a blessing and a curse for the designer, where the maximum achievable performance can be attained at the expense of an increased complexity of the design problem (Albazzan et al., 2019). A particular class of unconventional SSs is represented by the so-called quasi-trivial (QT) SSs (Vannucci & Verchery, 2001a; Vannucci, 2017; Garulli et al., 2018), which are exact solution for uncoupled (membrane and bending properties are not coupled) and/or homogeneous laminates (membrane and bending tensors have the same group of symmetry, for further details see Section 4.3). It is noteworthy that, for such SSs, these properties are independent from the particular orientation angle values. QT laminates constitute a by far larger set than the classic symmetric SSs set, as pointed out in (Vannucci & Verchery, 2001a; Garulli et al., 2018). Unfortunately, quasi-triviality is not, in general, a necessary and sufficient condition to achieve uncoupled and/or homogeneous laminates, as will be discussed in Section 9.2. It is noteworthy that, recently, an experimental validation of the effectiveness of the QT SSs has been presented in (Montemurro et al., 2019).

2.1.2 Direct Stiffness Modelling

The search of the optimal stiffness distribution for a multilayered composite structure, fulfilling the constraints of the problem at hand, is usually done acting directly on the stiffness matrix of the laminates. The components of the stiffness tensor are used as design drivers. However, these drivers are not independent and cannot assume arbitrarily any value. As a result, some intermediate variables for the description of the anisotropy are practically used to define univocally the laminate elastic properties. The most common optimisation approaches available in the literature make use of the well-known Lamination parameters (LPs) coupled with the parameters of Tsai and Pagano, see (Tsai & Pagano, 1968; Tsai & Hahn, 1980; Jones, 2018). These parameters unquestionably provide a compact representation of the stiffness tensors of the laminate. Nevertheless, they are not all tensor invariants, as discussed in (Tsai & Hahn, 1980). Both LPs and Tsai and Pagano parameters are easier to understand than PPs, in the sense that the formers are moment-weighted average of trigonometric functions of ply orientations. Moreover, they are closely related to the so-called engineering constants, such as Young modulus, Poisson's ratio, etc. However, LPs are not immediately related to the elastic symmetries of the laminate stiffness tensor, as PPs are. This is quite an important aspect. In fact, if a particular elastic symmetry (e.g. orthotropy) is easier to impose to the design problem, the feasible design region (in this example, the region of orthotropic laminates) assumes "nicer" shape in the PPs space. In so doing, the optimisation problem formulation would enjoy a smoother design search phase, possibly leading to better solutions. A sound alternative for describing the anisotropic behaviour of composite materials and structures is

represented by the polar formalism introduced by Verchery (1979, 1982). Thanks to the polar formalism, it is possible to represent any plane tensor by means of tensor invariants, referred as Polar parameters (PPs), which are related to the symmetries of the tensor. In particular, for a fourth-order elasticity-like plane tensor (i.e. a tensor having both major and minor symmetries), all possible elastic symmetries can be easily expressed in terms of conditions on the tensor PPs. Moreover, the polar formalism offers a frame-invariant description of any plane tensor, see (Verchery, 1982). Recently, the Polar Method has been generalised to the case of higher-order equivalent single layer theories such as First- and Third- Order Shear Deformation Theory (FSDT and TSDT) in (Montemurro, 2015a, 2015b, 2015c). Since the polar formalism is valid for any second order and fourth order plane elasticity-like tensor, the polar formalism has been extended to the analysis of the strength of a laminate (Catapano et al., 2012, 2014), and it has turned out that stiffness and strength PPs are not independent (Catapano & Montemurro, 2018).

A significant advantage of using the direct stiffness modelling approach is the decrease of the number of design variables. Moreover, they are independent from the number of layers of the laminate. For a generic anisotropic laminate, twelve independent parameters are needed to completely characterise its stiffness tensor

Nevertheless, the direct stiffness modelling approach alone is not sufficient for a complete design of a composite structure. In fact, even when the theoretical optimal stiffness distribution is achieved (via a proper numerical optimisation technique), the designer ignores how to built the structure having such optimal properties. In plane language, the knowledge of the optimal stiffness distribution only is not exploitable for any practical purpose. This leads directly to a more refined approach, structured as a multi-scale and multi-level strategy.

In the following, if not specified, it will be tacitly assumed the adoption of the direct stiffness modelling approach.

2.1.3 The Multi-scale Multi-level Composite Laminates Optimisation

In the last years, multi-scale design approaches have attracted the interest of the scientific community (Ghiasi et al., 2009; Ghiasi et al., 2010; Albazzan et al., 2019). Due to the complexity of the laminate design, a multi-level optimisation approach is demanded to efficiently achieve the optimal solution.

The leading idea is splitting the primitive structural problem into many sub-problems, each one focusing on a different phenomenological scale, as schematically shown in Figure 2.2. Composite materials design is a natural environment for this type of approaches. Conventionally, as already pointed out, three scales are generally distinguished:

- the macroscopic scale describing the overall behaviour of the composite;
- the mesoscopic scale describing phenomena at the ply level;

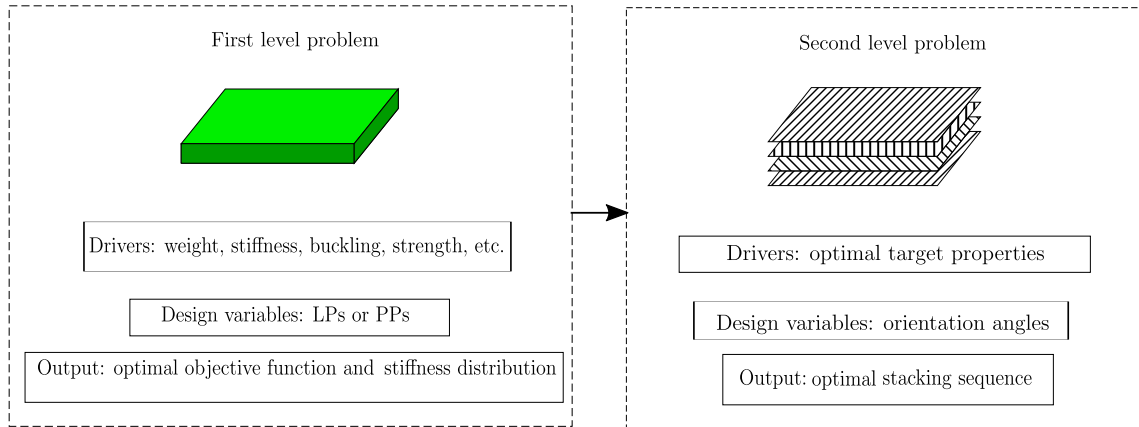


Figure 2.2: Schematic overview of the multi-scale multi-level optimisation

- the microscopic scale describing the interface and interaction between fibres and matrix.

Usually, the microscopic scale is not considered in the preliminary design phase. Structural design drivers such as stiffness, strength, manufacturability, buckling, etc. can be considered in the first-level problem (FLP) (laminate stiffness optimisation), after a proper formulation in terms of design variables. The direct stiffness modelling approach formalism is used in this phase. After the optimal stiffness distribution is obtained, the second-level problem (SLP) (stacking sequence recovery) aims at retrieving at least one SS matching the optimal elastic properties (target properties to be matched) determined at the end of the FLP. This step usually suffers from theoretical performance loss when additional design guidelines and manufacturing constraints are applied to the recovery process. For instance, the design best-practice guidelines resumed in (Irisarri et al., 2014), which act at the mesoscale ply level, can be imposed easily in the SLP, whilst it is difficult, even impossible, to consider them also in the FLP. However, if non-conventional SSs are adopted, those guidelines are questionable or odd.

Many works are present in literature based on multi-scale bi-level approaches. Based on the LPs for describing the macroscopic response of the laminate, some interesting works can be found in (Soremekun et al., 2002; Adams et al., 2004; Seresta et al., 2007; Herencia et al., 2008; Ijsselmuiden et al., 2009; S. Liu et al., 2012; Irisarri et al., 2014; Macquart et al., 2016). The design problem is split into a continuous optimisation problem followed by a discrete optimisation one. In the first step, LPs and thickness of laminates are the design variables, which may vary with continuity. In (B. Liu et al., 2000; D. Liu et al., 2011) a continuous optimisation is used to achieve the minimal mass of the structure. In this approach, only predefined orientation angles values are considered. Design variables are the (continuous) number of plies associated to predefined orientations. Eventually, a second step, based on a permutation GA, allows retrieving the final SS. What is in common with these approaches is the lack of generality of the problem formulation. In fact, predefined SSs or restrictive hypotheses on the SSs are imposed *a priori*, so to deal with conventional SSs. As a consequence, the design space is arbitrarily

reduced, and the final solution is just sub-optimal.

In the framework of the PPs, a multi-scale two-level optimisation strategy (MS2LOS) for composite structures design has been introduced in (Montemurro et al., 2012a; Montemurro et al., 2012b, 2012c) and later extended to the case of variable stiffness composites in (Montemurro & Catapano, 2016, 2017, 2019; Montemurro et al., 2019). The MS2LOS has been successfully used in several works, such as Montemurro et al. (2013), Catapano and Montemurro (2014a, 2014b), Montemurro et al. (2016), Montemurro et al. (2018). The aim of the MS2LOS is to provide optimised solutions for composite structure design problems disregarding simplifying hypotheses on the SS nature, which extremely shrink the solution domain. In the MS2LOS, only macroscopic and mesoscopic scales are involved into the design process, in two different, though correlated, steps. The former step focuses on the macroscopic scale of the laminate and aims at optimising the stiffness distribution to satisfy the requirements of the problem at hand. The latter step focuses on the laminate mesoscopic scale (i.e. the ply-level) and aims at recovering an explicit manufacturable SS (for each laminate composing the structure).

2.1.4 The Choice of Algorithms

Due to the discrete variables involved in the definition of a composite laminate (e.g. the number of plies, the orientation angle of each lamina, etc.), the common choice is to use genetic algorithms (GAs) or other meta-heuristics to perform the solution search during the FLP (Soremekun et al., 2002; Adams et al., 2004; Seresta et al., 2007; Montemurro et al., 2012a; Vannucci, 2012b). Nevertheless, an optimisation based exclusively on meta-heuristics may not be suitable for design problems with a large number of variables. Albeit a deterministic approach is more suited, the price to pay is to transform discrete variables into continuous ones (to be rounded at the end of the procedure) and to possibly accept local optimal solutions instead of the global one. The best choice would be to couple meta-heuristic algorithms with deterministic ones, in order to have the best performance in terms of solution efficacy. In fact, the hybrid algorithms would couple the exploration, typical of meta-heuristics, with local search, typical of deterministic algorithms.

Problems with large number of variables are typical of Topology Optimisation (TO), see for instance the works by Bendsøe and Sigmund (2004), Costa et al. (2017, 2019), Costa, Montemurro, Pailhès, and Perry (2019). The common approach is to use deterministic algorithms together with the analytic expressions of gradients of objective function and constraints, in order to reduce the computational cost. Of course, a similar approach can be used for the multi-scale design of composite structures, by paying a particular attention to the strong non-convexity of the resulting optimisation problem. In the last thirty years, some efforts have been done to employ deterministic optimisation methods for the multi-scale design of composites by considering different physical responses, like compliance, buckling, strength, etc. The first attempts dealing with the integration of a requirement on the first buckling factor of the structure can be found in the works by Rodrigues et al. (1995) and by Neves et al. (1995), where authors use the adjoint method to

derive, with a variational approach, the analytic expression of the buckling factor gradient. Setoodeh et al. (2009) introduced the decomposition of the stress-stiffness matrix of a single element as a linear combination of in-plane forces per unit length and some matrices depending only on the geometry of the element. However, they do not provide the expressions of these matrices, and they do not consider the contributions due to out-of-plane shear stresses. In the article by Ijsselmuiden et al. (2009), authors deal with blending and buckling in a gradient-based optimisation framework. However, buckling is formulated via an empirical (approximated) formula. The same authors, in (Ijsselmuiden et al., 2010), use the approach of Setoodeh et al. (2009) for the buckling load maximisation of variable stiffness laminates. Thomsen et al. (2018) derive the buckling gradient for TO problems in the framework of the Solid Isotropic Material Penalisation (SIMP) approach. Ferrari and Sigmund (2019) revisit the buckling constraint for TO and study the influence of common practices, such as inconsistent gradients, obtained by neglecting some terms as done in the works by Ye et al. (2015), Munk et al. (2016). Finally, Townsend and Kim (2019) propose a level-set topology optimisation for buckling of shell-like structures. Surprisingly, in the aforementioned works, authors do not include out-of-plane shear stresses contribution in the assembly of the stress-stiffness matrix. Such a brief literature survey shows that deterministic optimisation algorithms are suitable for large scale problems, involving constraints of different nature.

As stated before, in the SLP the design variables are orientation angles of the plies, usually taking values in a discrete ranges (i.e. $]-90, 90[$). Note that, at the end of the FLP, the number of plies in the structure is known. Accordingly, the laminates are explicitly modelled with discrete orientation angles, which are the design variables of the problems. It is well known that such an approach for the laminate design is highly non-linear, non-convex, and usually suffers from ill-conditioned objective functions with many local optima (Albazzan et al., 2019). Because of the non-convexity and the presence of several local optima, meta-heuristic algorithms are used for the stack recovery of the SLP. GAs are by far the most popular stochastic methods dealing with discrete angle orientations (Ghiasi et al., 2009). An advantage of using GAs is that gradient information is not required, which is generally computationally expensive for complex structures. However, many function evaluations are needed as the number of variables increases. Basically, all of the aforementioned references make use of GAs for the SLP and, in some cases, also for the FLP. For the SLP others algorithms have been used in the literature. For example, Aymerich and Serra (2008) use an ant-colony optimisation (ACO) algorithm. They find that the ACO algorithm provides comparable or superior results if compared to a GA, suggesting that ACO can provide a rational framework for the development of robust and efficient tools for laminates design. A similar approach is also presented in (Serra & Venini, 2006; Wang et al., 2010; Sebaey et al., 2011; Koide et al., 2013), where ACO algorithms are effectively used also in the FLP for simple benchmark structures.

2.1.5 Global-local Modelling Strategies for Anisotropic Structures

A further issue in the design of composite structures is related to the mathematical model, adopted at each pertinent scale, to assess the physical responses involved in the design problem. In order to reduce the computational cost of the whole optimisation process, in most of the studies mentioned beforehand, analytical (approximate) models are used for the assessment of the response of the structure. Accordingly, the main limitations of these approaches are the lack of accuracy and the limited applicability of such methods that rely on simplifying hypotheses, especially in terms of applied boundary conditions (BCs), which are non-representative of real operative conditions. For instance, laminates of a complex structure are considered as simply supported plates for the buckling factor determination. To go beyond these limitations, some authors proposed the use of enhanced semi-analytical formulations to assess local structural responses. For example, in (Bisagni & Vescovini, 2015), the authors proposed an analytical formulation, based on the Rayleigh-Ritz method, able to better describe the interaction between the skin and the stringers due to buckling, but still neglecting the frames compliance and considering the structure infinitely periodic. In other works, like (Irisarri et al., 2011; Vankan et al., 2014), surrogate models built from results of FE analyses are employed, but the problem of the representativeness of the BCs still persists and the phenomenon of mode switching can lead to a further inaccuracy in the evaluation of the buckling response. Therefore, the use of a proper FE modelling strategy, for both global and local scales phenomena assessment, should be used in these situations. However, as pointed out by Venkataraman and Haftka (2004), its integration in a multi-scale optimisation strategy could be difficult when complex structures characterised by many design variables are considered.

To overcome the aforementioned issues, the dedicated global-local (GL) FE modelling approach, already used in (Izzi, Montemurro, Catapano, Fanteria, et al., 2020; Izzi, Montemurro, Catapano, & Pailhès, 2020; Panettieri et al., 2020; Picchi Scardaoni et al., 2020) for the optimisation of composite structures using GAs, will be in this Thesis improved for the deterministic optimisation. The resulting methodology is referred as GL-MS2LOS. GL modelling strategies are quite commonly used in the structural analysis of the aeronautical structures (Ciampa et al., 2010; Q. Liu et al., 2016; Picchi Scardaoni et al., 2019b; Izzi, Montemurro, Catapano, Fanteria, et al., 2020; Picchi Scardaoni et al., 2020). However, GL modelling strategies are rarely coupled to deterministic optimisation methods due to the following issues:

1. the high computational costs;
2. the lack of pertinent criteria to identify the zones of interest (ZOIs) within the global FE model (GFEM), i.e. the portions of the structures experiencing a certain structural criticality;
3. the lack of suitable modelling strategies to automatically build the local FE models (LFEMs) by extracting pertinent information from the GFEM and by taking into account variable (possibly discontinuous) geometry and mesh;

4. the lack of a proper mathematical formulation to derive the gradient of the physical responses resulting from LFEMs with respect to the design variables describing the model at each pertinent scale (and the related coupling effect between GFEM and LFEMs responses and their derivatives).

Such a GL approach is schematically depicted in Figure 2.3. From the GFEM, a portion (the ZOI) is extracted. A refined LFEM of the same portion is created. BCs are then imposed to the LFEM by interpolating the displacement field from the GFEM solution. The LFEM is then ready for the required FE analysis. This GL modelling strategy is clearly based on the sub-modelling technique by Sun and Mao (1988), Mao and Sun (1991), Whitcomb (1991). If a deterministic optimisation framework is chosen, the sub-modelling effects must be considered in the derivation of constraints (and their gradients) affected by the scale transition. It is anything but trivial, as it will be clearer, and it is never proposed in the literature about composites design.

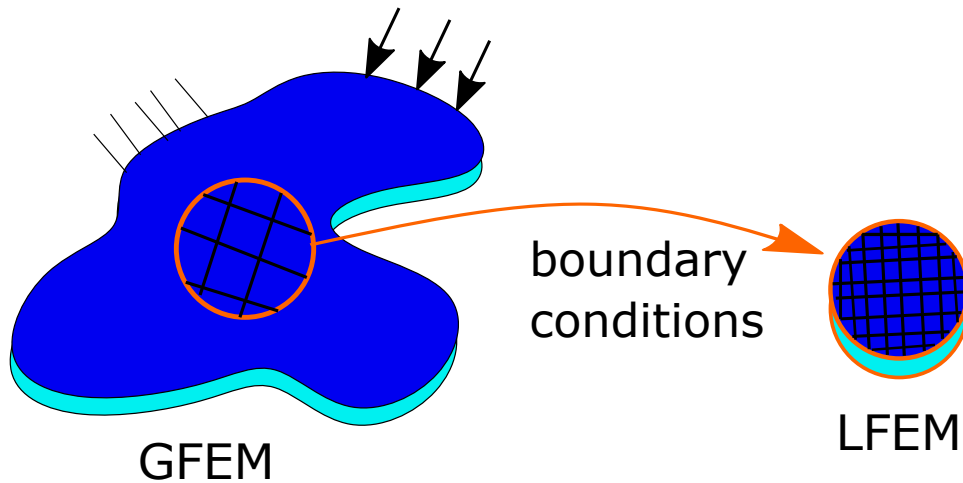


Figure 2.3: *Conceptual scheme of GL approach*

2.2 Design of Anisotropic Structures Including Manufacturing Constraints

2.2.1 Generalities

Manufacturing constraints are linked to limitations, due to different reasons, that must be integrated into the design process to ensure the correct as well as robust manufacturability of the structure. It is clear that manufacturability requirements deeply affect the coherency and the integrity of the whole design process. In fact, a non-manufacturable solution is vane, and without manufacturing constraints the solutions are only theoretical optimal designs.

For a single laminate, design guidelines have been introduced to guarantee its robustness (Baillie et al., 1997). These guidelines for composite materials are the result of a

consistent amount of experience and help the designer to exploit the material strength while alleviating its weaknesses (Albazzan et al., 2019). These guidelines include having symmetric SSs (uncoupled laminates), balanced SSs (no stretching/shearing coupling), a maximum number of consecutive plies of the same orientation, a minimum ply count percentage, a maximum ply angle jump, a minimum ply angle jump, and ± 45 degree external layers (Bailie et al., 1997; Irisarri et al., 2014).

Nevertheless, it is difficult to formalise all these constraints, because the laminate configuration is required but not available in the FLP if the direct stiffness modelling approach is adopted. As a general rule, if a constraint can be formalised, it will reduce the discrepancies between the FLP solution and the SLP stacking sequence design. As a consequence, negligible discrepancies would be observed at the conversion process if the FLP already satisfies these constraints.

Additional continuity constraints must be used for variable thickness structures. In fact, it can happen that specific laminates within a structure can experience ply drops. To tailor the design of specific regions with ply drops, an optimisation approach must be used while accounting for variable thickness and continuity constraints. Ensuring continuity between orientation angles of adjacent laminates is referred to as blending of composite laminates. An example of two blended laminates has been shown in Figure 1.4. Blending constraints can be included in the stiffness optimisation step following the work conducted by Macquart et al. (2016). The authors derived a set of blending constraints in the LPs space to reduce the discrepancies between the FLP results and the stacking sequence recovery phase. Their results demonstrate that including blending constraints in the problem formulation significantly increases the chance of retrieving optimal stacking sequences that closely match the optimal LPs distribution.

2.2.2 Blending

The design of composite structures made by the union of laminates with different number of plies needs the integration of a fundamental requirement of manufacturing/geometrical nature since the preliminary design phase. This requirement is called blending, a term originally introduced in (Kristinsdottir et al., 2001). Blending (or *ply-drop*) requirement deals with the continuity of ply orientation angles between adjacent composite laminates having different thickness. In other words, it is a requirement about the embedding of the orientation angles of the thinner laminate into the thicker laminate ones to avoid manufacturing issues. In fact, this continuity is essential for the correct junction of panels having different thickness. As noted, it appears then essential to include blending considerations since the earliest design phases.

The desiderata would be to include blending requirements in a framework as general as possible, i.e. without assumptions on the SSs, providing at the end of the design process blended stacks for the structure at hand. The design approach should return an optimal structural solution for a set of given design criteria, e.g. mass, buckling, stiffness, strength, etc. However, many are the challenges that blending introduces in the

design process. For example, blending has an intrinsic combinatorial nature, as it will be explained, which makes computational costs rise rapidly and the solution search be difficult, even with the most advanced techniques. Conversely, deterministic optimisation algorithms are more suitable for large-scale continuous problems, like the determination of the optimal stiffness distribution which minimises a specific merit function. The combination of those two aspects, viz. searching for an optimal solution (in some sense) and the explicit expression of the stacks, needs a well-pondered approach and constitutes the main reason of this work.

Blending naturally plays a pivotal role between macroscopic and mesoscopic scales. In the first step, the designer acts directly on the laminate stiffness matrices, regardless of the physiognomy of the stacks. Conversely, in the second step, the designer aims at explicitly retrieving the SSs, matching the optimal elastic properties and thickness resulting from the first step, and meeting also the manufacturing requirements of the structure at hand. Of course, when blending requirement is integrated into the problem formulation, the SSs must ensure the continuity of ply orientations between adjacent panels.

The SLP is not convex because it is posed in terms of orientation angles. As a result, designers have usually used evolutionary algorithms attempting to avoid the local optima in the non-convex design space of orientation angles. Evolutionary algorithms are the most widely used in the conversion step because of their discrete nature (Albazzan et al., 2019).

One of the first investigations on blending appears in (Cairns et al., 1999), focusing on the experimental delamination of differently-blended specimens, not considering the blending as a general design topic. In (Kristinsdottir et al., 2001), blending appears in the design process. The proposed design strategy uses a "ply add and drop" technique and major hypotheses on the SSs. In (Soremekun et al., 2002), a GA is used to determine the best blended SS for a general two-dimensional array of composite panels. A two-step approach is presented: in the first one, panels are independently optimised for the lowest mass. In the second one, blending optimisation is performed considering the fact that the independent-panel optimisation represents the best possible solution. During the blending optimisation, all panels are simultaneously designed using the ply orientations as design variables. This appears to be not totally correct, since not all the plies are truly independent. In fact, due to blending definition, some plies have to be shared between adjacent panels. Moreover, SSs are enforced to be balanced and symmetric. A GA-based approach is also proposed in (Adams et al., 2004; Seresta et al., 2007) together with some simplifying hypotheses on the blending schemes. In fact, authors consider only the so-called inward and outward blending, forcing ply-drop to occur in predefined points within the SSs. Note that all of the aforementioned works consider and solve the structural design problem in one step. GAs are employed because these approaches focus mainly on the discrete combinatorial nature of blending. Since the optimisation problem is not formulated in the most general case, the results have to be considered sub-optimal. Although GAs have been widely used for stacking sequence optimisation, one major shortcoming

is the low convergence rate (Ghiasi et al., 2009). GAs are population-based evolutionary algorithms, and might require several generations before converging to a solution (Ghiasi et al., 2009).

An interesting approach is provided in (Zein et al., 2011). Focusing only on the blended stacks recovery phase, authors solve the problem via a primal-dual backtracking algorithm. Also in this case only a predefined set of orientation angles permutes at each iteration, in order to satisfy the manufacturability and design constraints. However, as pointed out by the authors, this technique does not guarantee to recover the target stiffness of the structure.

In (Irisarri et al., 2014), good practices (commonly known as *blending rules*) for blended panels design together with the concept of SS Tables (SSTs) are introduced. These blending rules synthesise some heuristic best-practices for the conventional design of laminates. It is noteworthy that these rules can be successfully applied only with SST-based approaches, since they operate at the ply-level. Of course, they are applicable if stacks are collected in a SST, which is essentially an arbitrary database of possible stacks wherein the solution is searched. In any case, the design domain is arbitrarily reduced.

In (Macquart et al., 2016) inequality constraints between LPs of adjacent laminates are derived to take into account blending requirement. As pointed out by the authors, multi-step optimisation strategies suffer from performance drops due to the design space discrepancy between the two optimisation steps. Consequently, blending constraints aim at reducing the gap between the two steps, and the overall optimiser performance can be increased. More importantly, they indirectly show that multi-scale design approaches can be conveniently used to include the blending requirement directly at the macroscopic scale of the composite, regardless of the SS nature (Albazzan et al., 2019). In (Bordogna et al., 2016) the blending constraints in the LPs space are applied to a numeric benchmark of an aircraft wing. In the same spirit, in (Panettieri et al., 2019) blending constraints are formulated in the PPs space, focusing on the optimal stiffness distribution search. In (Allaire & Delgado, 2016), authors deal with the blending problem coupled with shape optimisation of layers. Finally, in (Ntourmas et al., 2019), a continuous optimisation is followed by a mixed-integer optimisation, taking into account blending rules. Remarkably, it is possible to infer that in most of the aforementioned works important hypotheses are formulated on the final stacks, thus limiting the design space. As a matter of fact, in all of the aforementioned works, the accuracy of the proposed methodologies in recovering blended SSs matching target elastic properties is not reported.

However, when blending constraints are introduced into the problem formulation, a mismatch between the optimal solutions found at the end of first and second step is observed. This gap can be reduced (but not avoided) by properly formulating the blending requirement. Indeed, this is a crucial aspect to deal with.

Moreover, blending constraints create a strong coupling between all the panels of the structure. This is a sort of chain of dependencies, which makes the second step problem only solvable all at once. In turn, the elastic properties recovery can be affected by the

existence domain of laminates (Vannucci, 2012a), which enters as a bias error in the second step. In fact, if a set of properties cannot be recoverable, one could only approximate the target one, introducing some error. Due to the strong coupling between panels elastic properties, because of the blending constraints, a error chain may rise in the SSs recovery phase, for all the panels within the structure at hand.

2.3 Approaches for Wing Design

2.3.1 Structural Analyses of PrandtlPlane Lifting System

The structural analysis of the PrP aircraft architecture presents many features which make it quite challenging, if compared to a conventional aircraft. Unlike a conventional aircraft architecture, the PrP fuselage and lifting system form an over-constrained structure. Therefore, from a theoretical point of view, the structural problem should be faced as a whole. On the contrary, for conventional aircraft, one may separate the fuselage from the wing, the latter roughly considered as a "cantilever beam". This issue implies some important consequences. Firstly, one cannot separately deal with the structural analysis of the fuselage and the lifting system. Secondly, even if under some simplifying hypotheses it is possible to separate the structural analysis of the lifting system from that of the fuselage, the question about the complexity of the FE analysis still remains open. In this case, the complexity of the FE analysis should be intended in terms of model size, viz. number of degrees of freedom (DOFs), compromise between accuracy and computational cost, choice of the scales of the analysis, choice of the design variables, etc. As an illustrative example, Figure 2.4 shows the vertical displacement component of the PrP (semi-)wing.

This Thesis will consider the wing of the PrandtlPlane as an application of the enhanced methodology for the design of composite structures, including manufacturing constraints and a GL approach. The wing, in fact, is more prone to undergoing evident ply-drop (from the root to the tip and chord-wise) than the fuselage structures. Although the literature about aerodynamics of the PrP configuration is quite rich, there are relatively few works focusing on the structural analysis of the lifting system. The only works on this topic consider a now-obsolete PrP configuration and low-fidelity models Dal Canto et al. (2012), Divoux and Frediani (2012), Frediani, Quattrone, et al. (2012). The *suite* of these three works deals with the design of the metallic wing-box of a PrP, its flutter response and the design of a composite version counterpart. However, no manufacturing constraints are considered, and only the static strength is considered as a design driver. Recently, a FE-based approach for structural analysis of the PrP wing architecture has been proposed in (Diolosà, 2018), but the analysis was still carried out on an obsolete configuration of the wing. Moreover, a structural optimisation of the spars of an ultralight PrP seaplane has been recently presented in (Nardone, 2016; Cipolla et al., 2018) in the framework of IDINTOS project. Paradoxically, in the literature there are more works about PrP aeroelasticity aspects (including non-linear ones) Divoux and Frediani

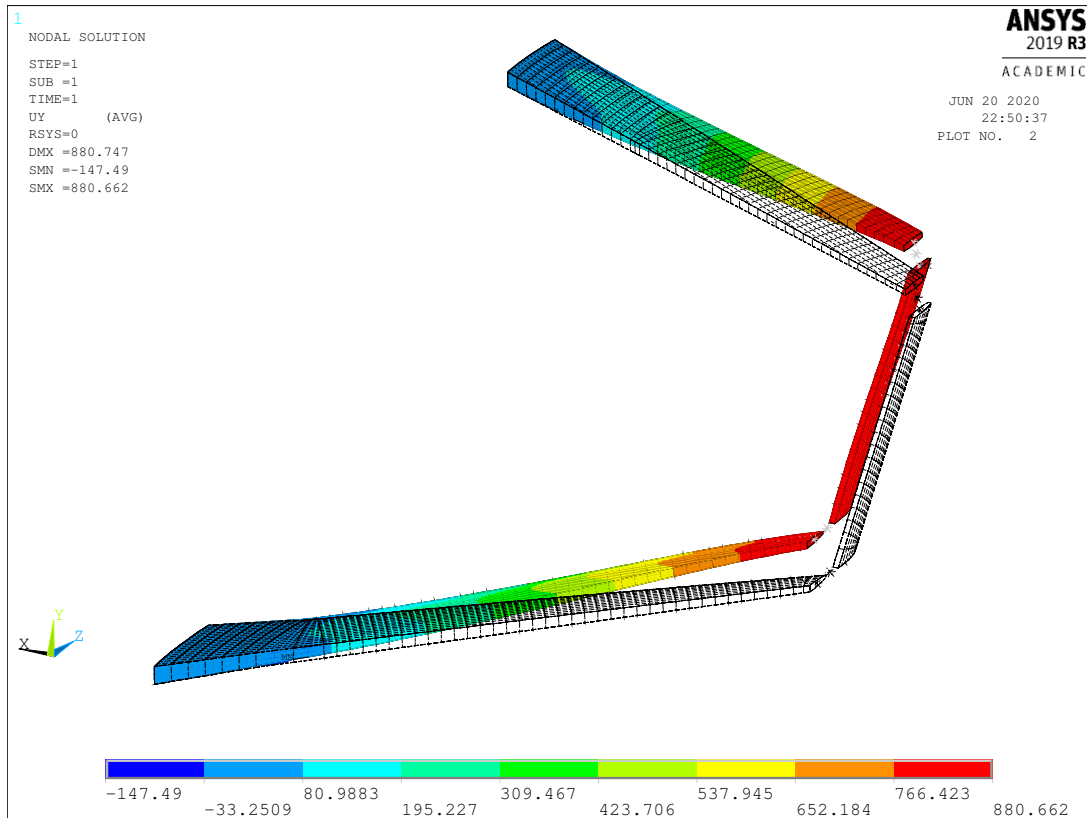


Figure 2.4: Vertical displacement component for the composite PARSIFAL PrP

(2012), Cavallaro (2014), Cavallaro et al. (2015), Cavallaro, Bombardieri, Silvani, et al. (2016), Cavallaro, Demasi, and Bombardieri (2016), Cavallaro et al. (2017), than works focusing on general structural behaviour of the PrP. In particular, some conceptual preliminary studies, collected in (Cavallaro, 2014) investigate the effect of anisotropy and the results of non-linear analyses, post-critical analyses and non-linear buckling analyses. Despite the *per se* interesting findings, these studies consider a too much approximate geometry of the real PrP lifting system. Moreover, these considered topics are far beyond a preliminary design of the PrP lifting system.

2.3.2 Global-local Approaches for Wing Design

Although Dababneha and Kipouros (2018b) represents a recent exhaustive overview on methods for estimating lifting systems mass, authors do not cite GL approaches. Indeed, the vast majority of studies dealing with the structural analysis of (conventional) wing-box architectures for preliminary design purposes do not take into account GL approaches Benaouali and Kachel (2019), Viglietti et al. (2019), Zhao et al. (2019). This is mainly due to the important computational effort required to perform scale transition between global and local models which is often not compatible with the overall time required to perform the optimisation process Dababneha and Kipouros (2018a). However, as far as the de-

velopment of GL strategies for the structural analysis of the lifting system of standard aircraft is concerned, some works can be found in the literature.

In (Arrieta & Stritz, 2005), authors develop a GL strategy dedicated to Damage Tolerance analyses (DTAs), for conventional wings. Of course, DTAs needs a refined models of structural components in order to simulate the growth of cracks. This represents a first example of the need of changing structural scale in optimisation procedures. A more complete approach is presented in (Ciampa et al., 2010). The global model does not take into account stringers and spar-cap, since stiffened panels are modelled as equivalent shells. Furthermore, only continuous variables are considered, which allow authors to use gradient-based techniques for the solution search. In (Chedrik, 2013), a GL strategy for a high-speed wing is presented. The main issue is that local models are re-mapped to rectangular plane stiffened plates, losing geometry effects on instability failures. Furthermore, several constraints are evaluated using analytical formula. In (Chedrik & Tuktarov, 2015), the same authors extend the GL approach for the topology optimisation; nevertheless, the aforementioned issues remain. More recently, Q. Liu et al. (2015) present a GL framework for optimisation of curvilinear spars and ribs (SpaRibs). The problem formulation presents a huge issue on computational cost: the framework needs hundreds of software licences and hundreds of cores to find solutions in acceptable time. Finally, in (Carrera et al., 2018), authors extend the GL approach for a composite material simple wing, in the framework of the Carrera Unified Formulation (CUF). More recently, Panettieri et al. (2020), Picchi Scardaoni et al. (2020) propose a GL approach for the optimal design of a conventional and a PrP lifting system, in light alloy, based on the GL optimisation approach formulated in (Izzi, Montemurro, Catapano, Fanteria, et al., 2020).

2.4 Conclusions

The literature review presented in this Chapter highlights the following features:

- (a) The design of composite structures is generally considered as a multi-scale multi-level approach. Differences arise in the problem formulation. On the one hand, some authors impose restrictive hypotheses on the final design, considering traditional SSs and solutions. On the other hand, other authors attempt at formulating the design problem in a manner as general as possible, thus aiming at achieving true optimal solutions with unconventional SSs.
- (b) The deterministic optimisation framework is suitable for large scale optimisations (in the FLP), involving different nature design drivers: stiffness, strength, buckling, manufacturability, etc. However adopting the direct stiffness modelling approach in the FLP, an expression of these drivers and their gradients must be formalised. As for the SLP, ant colony algorithms are promising but not still widely used.
- (c) The global-local approach is suitable for enhancing the likelihood of structural responses. However, it is not widely used in deterministic optimisation frameworks

because the effect of the scale transition must be considered in the expression of the gradients for the correct matching of a response with its gradient. This is a challenging task to deal with.

- (d) Blending and manufacturability constraints must be imposed in the design process to drive the design towards true manufacturable solutions. A proper formulation of these requirements, to be used in the FLP, must be than properly formalised. In particular, the current blending state-of-the-art can be further improved, by proposing a general treatment, for the FLP and SLP, without imposing simplifying hypotheses on the SSs.
- (e) Modelling strategies are quite commonly used in the structural analysis of the wing-box structure of conventional aircraft. However, such strategies are rarely coupled to deterministic optimisation methods due to three main issues: (a) the high computational costs related to such an approach; (b) the lack of pertinent criteria to identify the ZOIs within the GFEM; (c) the lack of suitable modelling strategies to automatically build the LFEMs by extracting pertinent information from the GFEM and by taking into account the variable geometry and mesh. It is evident the need for a complete GL deterministic optimisation approach, suitable also for complex real structures, which may consider also manufacturing constraints in the problem formulation. Such an approach can be used also with non-conventional aircraft structures, as the PrP lifting system, where complete design still misses.

Part II

Theoretical Background

Fundamentals of Optimisation Methods and Algorithms

Optimisation methods and algorithms have been playing an important role in many research fields since decades. Different Optimisation algorithms have been used in pretty all the significant developments related to this Thesis.

In this Chapter, the main features and concepts of optimisation are introduced. Of course, the Optimisation is intended in the sense of mathematical programming. In particular, Section 3.1 introduces the basic concepts of the mathematical optimisation theory. Section 3.2 gives an overlook on a particular class of optimisation problems, describing also a deterministic algorithm used for the solution search. The presented commercial algorithm will be extensively used in the following of the Thesis, in particular in the applications of Chapters 7 and 8. Section 3.3 provides a general description of the wide panorama of meta-heuristic algorithms. Successively, a particular meta-heuristic one, in view of its extensive usage in the following, is described into detail. Finally, Section 3.4 concludes the Chapter.

For a deeper insight on the topic, the reader is addressed to the classical textbooks Fletcher (1987), Nocedal and Wright (2006), which constitute the source of inspiration for this Chapter.

3.1 Generalities on Optimisation

3.1.1 Mathematical Programming

Roughly speaking, optimisation can be defined as the search and selection of a best element (with regard to some criterion) from a set of available alternatives. For this purpose, a quantitative index of performance of the system at hand must be chosen. This index is called *objective*, or *merit function*, and depends on some system characteristic parameters,

called *design variables*. They can be *bounded* or *unbounded*, depending on their variance within an interval or not. The extrema values of this interval are called *bounds*. Moreover, there may be present some further conditions, called *constraints*, to be satisfied. The aim of Optimisation is to find the set of design variables which minimises the objective, i.e. to find out the *minimiser* of the objective, in compliance with the constraints and the variable bounds. If so, the minimiser is said *feasible*.

The process of formalising an optimisation problem is called *modelling*. It is by far the most delicate phase of the optimisation, since it drastically affects the final result. Once the problem has been formulated, a suitable algorithm is generally used to carry out the solution search, i.e. to find out a feasible minimum and minimiser of the objective.

In the most general way, an optimisation problem can be formally described as follows:

$$\begin{aligned} \min_{\boldsymbol{\xi}} \Phi(\boldsymbol{\xi}), \quad & \text{subject to:} \\ g_i(\boldsymbol{\xi}) \leq 0, \quad & i = 1, \dots, p, \\ c_j(\boldsymbol{\xi}) = 0, \quad & j = 1, \dots, q, \\ \boldsymbol{\xi}_{\text{lb}} \leq \boldsymbol{\xi} \leq \boldsymbol{\xi}_{\text{ub}}, \end{aligned} \tag{3.1}$$

where $n \in \mathbb{N}$ is the number of design variables, $\boldsymbol{\xi} \in \mathbb{R}^n$ is the design variables vector, $\Phi : \mathbb{R}^n \mapsto \mathbb{R}$ is the objective function to be minimised, $g_i : \mathbb{R}^n \mapsto \mathbb{R}$, $i = 1, \dots, p$, $p \in \mathbb{N}$ are the p inequality constraints, $c_j : \mathbb{R}^n \mapsto \mathbb{R}$, $j = 1, \dots, q$, $q \in \mathbb{N}$ are the q equality constraints, $\boldsymbol{\xi}_{\text{lb}} \in \mathbb{R}^n$ and $\boldsymbol{\xi}_{\text{ub}} \in \mathbb{R}^n$ are the lower and upper bound vectors, respectively. The search of $\text{argmin} \Phi(\boldsymbol{\xi})$ can be faced analytically only in special cases. Typically, for real-world engineering problems, the solution search can be performed with a numerical algorithm. The type of strategy can be chosen according to the classification of Problem (3.1).

3.1.2 Programming Classifications

An optimisation programming as Problem (3.1) can be classified in different ways. In the following, a possible classification is briefly outlined, in agreement to that introduced by Nocedal and Wright (2006).

- (a) **Continuous vs Discrete Programming:** Some optimisation problems make sense only if design variables are integer numbers ($\in \mathbb{Z}$), or belong to a prescribed discrete set, e.g. $\xi_i \in \{0, 1\}$. These problems are called *integer programming problems* (IPPs) and are a subset of the *discrete programming problems*, wherein more abstract variables are admitted, e.g. permutations over a set. Conversely, in *continuous programming problems*, design variables may vary with continuity and the objective function and constraints are real-valued functions. If some of the variables are constrained to be integers and other variables are allowed to be continuous, Problem (3.1) is defined as a *mixed-integer programming problem*.

Remarkably, continuous programming problems are generally easier to solve than

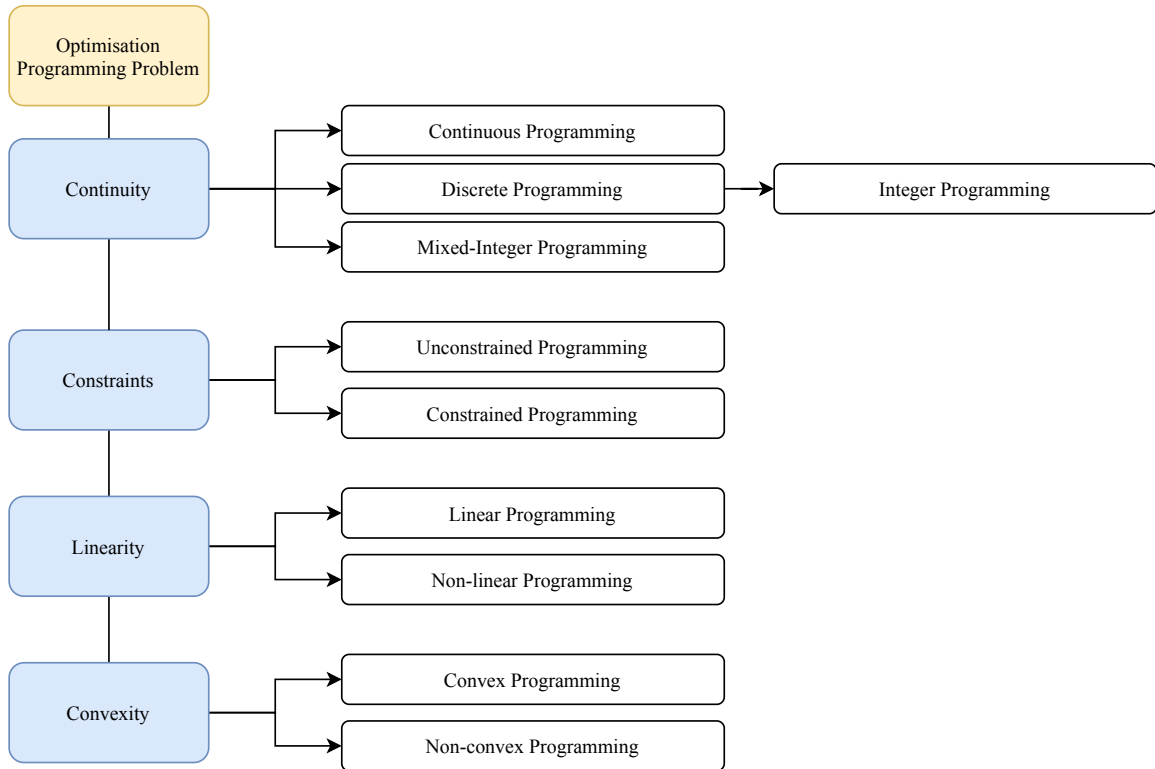


Figure 3.1: Classification of Optimisation programming problems

the discrete counterpart, because of the smoothness and continuity of the involved functions. Moreover, in continuous programming problems, from the objective and constraints values at a given point ξ , it is possible to extract information about the functions behaviour in a neighbourhood of ξ . Conversely, in discrete programming problems the objective function may drastically vary between two "close" points (according to some measure notion). Finally, in some cases, IPPs can be relaxed, ignoring the discrete nature of variables.

- (b) **Constrained vs Unconstrained Programming:** Optimisation problems can be classified according to the presence, or not, of constraints. According to the formulation of Problem (3.1), if $p = q = 0$ and if the design vector is unbounded, the optimisation problem is said an *unconstrained programming problem*. Conversely, if constraints and/or variable bounds are taken into account in the formulation of Problem (3.1), it is denoted as a *constrained programming problem*.
- (c) **Linear vs Non-linear Programming:** For a *linear programming problem* both objective and constraints are linear functions of the design variables. They appear in several applications of Economics and Logistics. On the contrary, if at least one function among objective and constraints is non-linear, the problem is a *non-linear programming problem*. If constraints are taken into account in the problem formulation, *constrained non-linear programming problems* (CNLPPs) are defined. Similarly, a MICNLPP is a constrained non-linear programming problem where some variables are integers and some others continuous numbers. Both categories are common in

Physics and Engineering applications.

(d) **Convex vs Non-convex Programming:**

Point (??) is strictly correlated to the global or local search of minimisers. Preliminary, some definitions must be introduced.

Definition 3.1 (Feasible region). *With reference to Problem (3.1), the feasible region is the set $\Omega := \{\xi : g_i(\xi) \leq 0, c_j(\xi) = 0, \forall i = 1, \dots, p, \forall j = 1, \dots, q\}$.*

Problem (3.1) can be equivalently expressed as

$$\min_{\xi \in \Omega} \Phi(\xi). \quad (3.2)$$

Definition 3.2 (Convex function). *A function $\Phi : \Omega \mapsto \mathbb{R}$ is convex if $\forall \xi_1, \xi_2 \in \Omega$ and $\forall t \in [0, 1]$ $\Phi(t\xi_1 + (1-t)\xi_2) \leq t\Phi(\xi_1) + (1-t)\Phi(\xi_2)$. If $<$ holds instead of \leq , Φ is said strictly-convex.*

Definition 3.3 (Global minimiser). *A point ξ^* is a global minimiser for Φ if $\Phi(\xi^*) \leq \Phi(\xi)$ for every ξ in the feasible domain.*

Definition 3.4 (Local minimiser). *A point ξ^* is a local minimiser for Φ if there exists a neighbourhood of ξ^* such that $\Phi(\xi^*) \leq \Phi(\xi)$ for all ξ in this neighbourhood.*

For convex functions, it can be proved the following well-known result:

Theorem 3.1 (Existence (and uniqueness) of global minimum for (strictly) convex functions). *Let $\Phi : \Omega \mapsto \mathbb{R}$ be a convex function. Then, a local minimum of Φ is also a global minimum. Furthermore, if Φ is strictly-convex, it has exactly one global minimum.*

Consider the following notion of convex set.

Definition 3.5 (Convex set). *Let Ω be a set. If for every elements $x, y \in \Omega$ their convex combination $\alpha x + (1-\alpha)y$ defines an element still belonging to Ω for every $\alpha \in [0, 1]$, then Ω is a convex set.*

The intuition is that every segment connecting two elements of a convex set is still entirely contained in the set. Then, a peculiar class of optimisation problems can be defined:

Definition 3.6 (Convex programming problem). *With reference to Problem (3.1), if the design domain is a convex set and both objective and constraint functions are convex, the optimisation Problem (3.1) is said convex.*

Since linear functions are convex, linear programming problems, possibly constrained ones, are convex programming problems.

As a matter of fact, the vast majority of real-world engineering problems is intrinsically non-convex. Therefore, it is not surprising that searching for a global solution is

prohibitive from a computational point-of-view. Many algorithms search only a local solution, i.e. a point at which the objective is smaller than at all other feasible nearby points. They do not always find the global solution, i.e. the point with lowest function value among all feasible points. Global solutions are difficult to recognise and even more difficult to locate. For convex and linear problems local solutions are also global solutions.

Most of the problems faced in this Thesis are strongly non-convex and non-linear. To deal with these problems, both deterministic and meta-heuristic algorithms have been used. In the following sections, a primer on deterministic and meta-heuristic algorithms is given.

3.2 Deterministic Algorithms for CNLPPs

3.2.1 Optimality Conditions

Consider the following Lagrangian functional associated to the CNLPP (3.1):

$$\mathcal{L}(\xi) := \Phi(\xi) + \sum_{i=1}^p \lambda_i g_i(\xi) + \sum_{j=1}^q \mu_j c_j(\xi). \quad (3.3)$$

The following Theorems can be proved:

Theorem 3.2 (Karush-Kuhn-Tucker (KKT) first-order necessary conditions for optimality). *Let ξ^* be a local solution of Problem (3.1) and let functions Φ , g_i , c_j belong to \mathcal{C}^1 -class. Moreover, suppose the LICQ (Linear Independence Constraint Qualification) condition holds at ξ^* , i.e. the gradients of each constraint function are linearly independent. Then there exist two Lagrangian multiplier vectors, λ^* of components λ_i^* ($i = 1, \dots, p$) and μ^* of components μ_j^* ($j = 1, \dots, q$), such that the following set of condition are simultaneously satisfied (KKT-conditions):*

$$\begin{cases} \nabla_{\xi} \mathcal{L}(\xi^*, \lambda^*, \mu^*) = 0, \\ \lambda_i^* g_i(\xi^*) = 0, \\ \lambda_i \geq 0, \\ c_j(\xi^*) = 0. \end{cases} \quad (3.4)$$

The point $(\xi^*, \lambda^*, \mu^*)$ is called KKT-point.

Theorem 3.3 (Second-order sufficient conditions for optimality). *Assume that functions Φ , g_i , c_j belong to \mathcal{C}^2 -class. Suppose that $(\xi^*, \lambda^*, \mu^*)$ is a KKT-point and assume that the Hessian of the Lagrangian, i.e. $\nabla^2 \mathcal{L}(\xi^*, \lambda^*, \mu^*)$, is positive semi-definite. Then, ξ^* is a local minimiser for Problem (3.1).*

3.2.2 The Deterministic Algorithm *fmincon*

The deterministic optimisation strategies proposed in this Thesis are based on the well-known *fmincon* algorithm implemented into the MATLAB® Optimisation Toolbox (The MathWork Inc., 2011). Among the available algorithms, the *active-set* (Active Set) one has been recognised as the most efficient formulation for the problems discussed in this Thesis. Therefore, in the following, the main features of this algorithm only will be outlined. For a point ξ in the feasible domain, the active-set is the set of constraints for which $c_j(\xi) = 0$ and $g_i(\xi) = 0$ for some $i \leq p$ and some $j \leq q$. In plane language, the active-set is the set of constraints which the current solution lies on or, alternatively, is the set of constraints which hold with equality.

The Active Set algorithm is a particular Sequential Quadratic Programming method with an enhanced constraints handling technique. Sequential Quadratic Programming algorithms are suitable for small or large problems and show their strength with problems having significant non-linearities in the constraints (Nocedal & Wright, 2006).

The main idea consists in approximating the CNLPP (3.1) with a sequence of Quadratic Programming problems. A programming is quadratic if the objective $\Phi(\xi)$ is a quadratic function of the design variables and if constraints depend linearly from the design variables.

The Active Set approach is based on the attempt to identify the constraints which are active at the solution, and to treat these as equality constraints in the Quadratic Programming sub-problems. In so doing, the dimensionality of the minimisation is reduced (Gill et al., 1984). The subset of constraints used as a guess for the solution active-set is called *working set*.

Algorithm 3.1 shows the structure of the code. Once Problem (3.1) has been stated and one initial feasible guess ξ_0 has been provided, the Lagrangian multipliers are initialised and the iteration index k is set to 0. Then, the Lagrangian functional is evaluated (Eq. (3.3)). As for the Hessian, an approximated version is generally considered, according to the well-known Broyden-Fletcher-Goldfarb-Shanno (BFGS) formula. The Quadratic Programming Problem (3.5) is then solved. Note that Problem (3.5) considers a linearisation of the constraints, which can be expressed as $\mathbf{A}_k \mathbf{d} \leq \mathbf{b}_k$, where matrix \mathbf{A}_k collects the gradients of the constraints and \mathbf{b}_k collects the first-order approximation of the constraints. In the Active Set context, only the contributes of the constraints in the working set appear in the \mathbf{A}_k matrix. Problem (3.5) is solved through standard techniques (Gill et al., 1984; Nocedal & Wright, 2006). The minimiser of Eq. (3.5), namely \mathbf{d}_k , is interpreted as the search direction for the k -th iteration of the algorithm. Note that the optimisation constraints of the original Problem (3.1) are linearised, as shown in Eq. (3.5). In the Active Set framework, some internal iterations could be needed to check if the active-set of optimisation constraints has been correctly evaluated and, eventually, Problem (3.5) is updated.

Once the search direction \mathbf{d}_k is obtained, the step length s_k is determined. Lagrange multipliers are then updated together with the design variables array for the next step

Algorithm 3.1 Active-set deterministic optimisation algorithm

```

1: Optimisation Problem (3.1)
2:  $\xi_0, \lambda_0, \mu_0$ 
3:  $k \leftarrow 0$  ▷ Iteration counter
4: while stopping criteria not met do
5:    $\Phi_k \leftarrow \Phi(\xi_k), g_i^k \leftarrow g_i(\xi_k), c_j^k \leftarrow c_j(\xi_k)$ 
6:    $\mathcal{L}_k \leftarrow \Phi_k + \lambda_k^T \mathbf{g}_k + \mu_k^T \mathbf{c}_k$ 
7:    $\nabla \Phi_k \leftarrow \nabla \Phi(\xi_k), \nabla g_i^k \leftarrow \nabla g_i(\xi_k), \nabla c_j^k \leftarrow \nabla c_j(\xi_k)$ 
8:    $\nabla^2 \mathcal{L}(\xi_k) \leftarrow \nabla^2 \mathcal{L}_k \cong \mathbf{H}_k^{BFGS}$ 
9:
       
$$\min_{\mathbf{d} \in \mathbb{R}^n} \left[ (\nabla \Phi_k)^T \mathbf{d} + \frac{1}{2} \mathbf{d}^T \mathbf{H}_k^{BFGS} \mathbf{d} \right], \quad \text{subject to:}$$

       
$$(\nabla g_i^k)^T \mathbf{d} + g_i^k \leq 0, \quad i = 1, \dots, p \quad (3.5)$$

       
$$(\nabla c_j^k)^T \mathbf{d} + c_j^k = 0, \quad j = 1, \dots, q$$

10:   $\mathbf{d}_k \leftarrow \text{argmin [Eq.(3.5)]}$ 
11:  Find step length  $s_k$ 
12:  Evaluate  $\lambda_k, \mu_k$ 
13:   $\xi_{k+1} \leftarrow \xi_k + s_k \mathbf{d}_k$ 
14:   $k \leftarrow k + 1$ 
15:  if stopping criteria are met then
16:    break
17:  end if
18: end while
    
```

ξ_{k+1} . The procedure repeats until a convergence criterion is met (Maximum number of iterations, tolerance on objective function, tolerance on constraints, tolerance on input variables change, tolerance on the gradient norm of the Lagrange's function).

3.3 Meta-heuristic Algorithms for CNLPPs and MICNLPPs

3.3.1 Introduction to Meta-heuristics

Meta-heuristics have been developed in order to overcome the limit of reaching only local optima by deterministic algorithms. In fact, in many practical applications, the global minimum of the objective is desired. Meta-heuristics are generally inspired by natural phenomena or animals behaviour. The purpose of seeking global minimisers is achieved by a suitable balance between exploration of all the design space and exploitation of information from the current best solution and/or from promising design space regions. However, it is noteworthy that no guarantee exists about the ability of a meta-heuristic algorithm to find the global minimiser.

The concept of meta-heuristics is deeply linked to the concept of evolution (Glover, 1977; Fogel et al., 2009). The leading idea is to provide a population of candidate solutions and to make this population evolve towards an improvement of the objective. Partic-

ular interest has been risen by Holland's GA (Goldberg & Holland, 1988; Goldberg, 1989; Holland, 1992). GAs take inspiration from the evolutionary theory by Darwin (Darwin, 1871), from the genetic inheritance laws of Mendel (Mendel, 1865) and from the DNA structure discovered by Watson and Crick (1953).

Another well-known meta-heuristics class is represented by the swarm intelligence: it mimics the behaviour of groups of individuals in nature, as birds, bees, ants, etc. For instance, in the ACO method (Dorigo, 1992; Dorigo et al., 1996; Dorigo et al., 2006), many agents mimic the ants food search strategy. A numerical pheromone is released when numerical "ants" find promising solution. The "scent" of the pheromone leads the ants towards the best solution. Another swarm intelligence is represented by the Particle Swarm Optimisation (Kennedy & Eberhart, 1995), whereby a swarm of candidate solutions (particles) moves in the design space: the progression of the particles is affected both by their own best-known position and by the swarm global best-known position.

Inasmuch the field of meta-heuristics is really wide, in the following the main features of the ACO algorithm MIDACO[®], used in this Thesis, will be described.

3.3.2 The Ant Colony Optimisation Algorithm MIDACO[®]

Most of the following Sections is inspired from Schlüter et al. (2009), Schlueter (2018).

3.3.2.1 Generalities on Ant Colony Optimisation Algorithms

To find food, biological ants start to explore the area around their nest randomly at first. If an ant succeeds in finding a food source, it will return back to the nest, laying down a chemical pheromone trail marking its path. This trail will attract other ants to follow it in the hope of finding food again. Over time the pheromones will start to evaporate and therefore to reduce the attraction of the path. As a consequence, only paths that are updated frequently with new pheromones remain attractive. Short paths from the nest to a food source imply short marching times for the ants, so those paths are updated with pheromones more often than long ones. Consequently more and more ants will be attracted by the shorter paths with ongoing time. As a final result, a very short path will be discovered by the ant colony.

This basic idea of ACO algorithms, for the sake of simplicity presented for the case of integers variables only, is to mimic this biological behaviour with artificial ants *walking* on a graph, which represents a mathematical problem (e.g. the Travelling Salesman Problem). An optimal path in terms of length or some other cost-resource is requested in problems belonging to the field of combinatorial optimisation. By using a parametrised probabilistic model, called pheromone table, the artificial ants choose a path through a completely connected graph $G(V, E)$, where V is the set of vertices and E is the set of connections, as qualitatively illustrated in Figure 3.2. The set V of vertices represents the solution components, which every ant chooses incrementally to create a path. The pheromone values within a pheromone table are used by ants to make these probabilistic

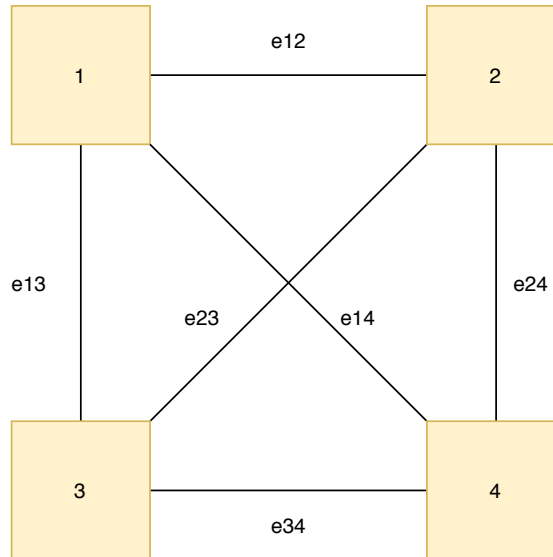


Figure 3.2: A graph of four vertices and six edges

decisions. By updating the pheromone values, according to the most promising information gained on the search domain, and collected in the *Kernel* set, the algorithmic procedure leads to very good and hopefully global optimal solutions, like the biological counterpart. The pseudocode of a generic ACO algorithm is presented in Algorithm 3.2.

Algorithm 3.2 Ant-colony optimisation algorithm

- 1: Optimisation Problem (3.1)
 - 2: n_A, n_K ▷ Number of ants, number of ants in the Kernel, $n_A > n_K$
 - 3: Initialise pheromones (randomly)
 - 4: Initialise algorithm parameters
 - 5: $k \leftarrow 0$ ▷ Iteration counter
 - 6: **while** stopping criteria not met **do**
 - 7: Create generation G_k made of n_A ants, for which the fitness function is evaluated
 - 8: Select the best n_K ants, based on the fitness value, and store them in the Kernel set
 - 9: Update pheromones according to the Kernel
 - 10: Apply ACO evolutionary operators, based on numerical pheromone, to create the next generation G_{k+1} made of n_A ants, expanding the graph exploration
 - 11: Introduce in the Kernel the ants of G_{k+1} having a better fitness than the lowest-ranked ones of the Kernel
 - 12: Discard ants, from the Kernel, having a worse fitness than the n_K -th ant of the Kernel
 - 13: **if** stopping criteria are met **then**
 - 14: **break**
 - 15: **else**
 - 16: $k \leftarrow k+1$
 - 17: **end if**
 - 18: **end while**
-

3.3.2.2 MIDACO®

MIDACO® is a high-performance software for solving single- and multi-objective optimisation problems. Initially developed for MICNLPPs arising from challenging space

applications at the European Space Agency and Astrium (Airbus Group), the software has been extended and constructed as general-purpose solver to fit a wide range of optimisation problems. MIDACO[®] handles problems where the objective functions depend on continuous, integer or both types (mixed integer case) of variables.

MIDACO[®] is based on the ACO algorithm, appeared for the first time in the seminal work of Dorigo (1992). In particular, MIDACO[®] implements and continues ACOs with an extension to mixed integer search domains (Schlüter et al., 2009; Schlüter et al., 2012).

Constraints are handled by the Oracle Penalty Method which is an advanced and self-adaptive method for evolutionary algorithms to reach the global optimal solution (Schlüter & Gerdt, 2009). In (Schlüter et al., 2012) it was also demonstrated that MIDACO[®] can outperform established classical MICNLPP algorithms (like branch & bound) in regard to global optimal capability and runtime performance. The motivation behind MIDACO[®] is to provide a robust algorithm that can deal with complex real world applications, providing optimal solutions in reasonable time. In order to improve the overall performance, many heuristics and algorithms, including a pseudo-gradient based backtracking line-search for fast local convergence, are implemented (Schlüter, 2018). MIDACO[®] is therefore classified as an evolutionary hybrid algorithm (Schlüter et al., 2009).

3.4 Conclusions

In this Chapter, some fundamentals of the mathematical theory of optimisation have been provided. A particular class of optimisation problems, the CNLPPs, has been analysed more in detail from the mathematical point of view. It is the most used optimisation problem class in the following of this Thesis. Besides, details on the two optimisation algorithms to solve CNLPPs, that will be extensively used in the following of the Thesis, have been presented. The first one is the *fmincon* (Active-Set) algorithm, available on the wide-spread computing environment MATLAB[®]; the second one a commercial ACO, called MIDACO[®], suitable also for MICNLPPs. It is noteworthy that the optimisation of constrained non-linear systems (possibly with integers variables) represents the general fundamental framework where the main research of Thesis has been conducted.

Fundamentals of Polar Method and of Composite Laminates Mechanics

This Chapter aims at summarising the most important results of the polar representation of plane tensors via invariants. The polar representation is then applied to the description of anisotropic plates mechanics.

In Section 4.1, the general theory of the Polar Method is introduced. In Section 4.2, the Polar Method is then applied to describe the behaviour of composite laminates in the framework of the FSDT. Both stiffness and strength description is addressed. Section 4.3 introduces the concept of quasi-trivial laminates, that will play a fundamental role in view of the exposition of Section 6.4 and Chapter 9. Finally, Section 4.4 concludes the Chapter with meaningful considerations.

4.1 Polar Representation of Plane Elasticity Tensors

The Polar Method is a mathematical transformation into the complex domain which allows representing any n -th order plane tensor in terms of invariants: this method appeared, for the first time, in (Verchery, 1979, 1982). The following Section aims at presenting the main results of the polar formalism. For a deeper insight in the matter, the reader is addressed to (Vannucci, 2017).

4.1.1 Second-order Tensors

Any second order symmetric plane tensor \mathbf{Z} can be expressed in the local reference frame $\Gamma = \{O, x_1, x_2, x_3\}$ as:

$$\begin{aligned} Z_{11} &= T + R \cos 2\Phi, \\ Z_{12} &= + R \sin 2\Phi, \\ Z_{22} &= T - R \cos 2\Phi, \end{aligned} \quad (4.1)$$

where Z_{ij} , $i, j = 1, 2$ are the Cartesian components of \mathbf{Z} , T is the isotropic modulus, R the deviatoric one and Φ the polar angle. Among them, only the two moduli are tensor invariants, whilst Φ is needed to set the reference frame.

One of the advantages of the Polar representation is that rotations of the reference frame assume a simple form. In fact, the transformation of Eq. (4.1), in a new frame $\Gamma'(O, x, y, z)$ turned counter-clock wise around the x_3 axis of an angle θ , reads

$$\begin{aligned} Z_{xx} &= T + R \cos 2(\Phi - \theta), \\ Z_{xy} &= + R \sin 2(\Phi - \theta), \\ Z_{yy} &= T - R \cos 2(\Phi - \theta). \end{aligned} \quad (4.2)$$

4.1.2 Fourth-order Tensors

Let \mathbf{L} be a fourth-order elasticity-like plane tensor, i.e. with major and minors symmetries. The polar representation of its Cartesian components, in the reference frame $\Gamma = \{O, x_1, x_2, x_3\}$, can be expressed by four polar moduli and two polar angles, namely $T_0, T_1, R_0, R_1, \Phi_0, \Phi_1$. The complete expression reads:

$$\begin{aligned} L_{1111} &= + T_0 + 2T_1 + R_0 \cos 4\Phi_0 + 4R_1 \cos 2\Phi_1, \\ L_{1112} &= + R_0 \sin 4\Phi_0 + 2R_1 \sin 2\Phi_1, \\ L_{1122} &= - T_0 + 2T_1 - R_0 \cos 4\Phi_0, \\ L_{1212} &= + T_0 - R_0 \cos 4\Phi_0, \\ L_{2212} &= - R_0 \sin 4\Phi_0 + 2R_1 \sin 2\Phi_1, \\ L_{2222} &= + T_0 + 2T_1 + R_0 \cos 4\Phi_0 - 4R_1 \cos 2\Phi_1. \end{aligned} \quad (4.3)$$

In Eq. (4.3), T_0 and T_1 are the isotropic moduli, R_0 and R_1 the anisotropic ones, Φ_0 and Φ_1 the polar angles. Among them, only the four moduli and the difference $\Phi_0 - \Phi_1$ are tensor invariants.

The Cartesian components of \mathbf{L} in a new frame $\Gamma'(O, x, y, z)$ turned counter-clock

wise around the x_3 axis of an angle θ , read:

$$\begin{aligned}
 L_{1111} &= +T_0 + 2T_1 + R_0 \cos 4(\Phi_0 - \theta) + 4R_1 \cos 2(\Phi_1 - \theta), \\
 L_{1112} &= + R_0 \sin 4(\Phi_0 - \theta) + 2R_1 \sin 2(\Phi_1 - \theta), \\
 L_{1122} &= -T_0 + 2T_1 - R_0 \cos 4(\Phi_0 - \theta), \\
 L_{1212} &= +T_0 - R_0 \cos 4(\Phi_0 - \theta), \\
 L_{2212} &= - R_0 \sin 4(\Phi_0 - \theta) + 2R_1 \sin 2(\Phi_1 - \theta), \\
 L_{2222} &= +T_0 + 2T_1 + R_0 \cos 4(\Phi_0 - \theta) - 4R_1 \cos 2(\Phi_1 - \theta).
 \end{aligned} \tag{4.4}$$

Another advantage of the Polar Method is that for a fourth order elasticity-like plane tensor the polar invariants are strictly related to the elastic symmetries of the tensor. In particular:

Orthotropy corresponds to the condition $\Phi_0 - \Phi_1 = K \frac{\pi}{4}$, with $K \in \{0, 1\}$;

R₀-Orthotropy can be obtained by imposing $R_0 = 0$; This special case has been studied in (Vannucci, 2002, 2009).

Square symmetry is obtained by imposing $R_1 = 0$ This case represents the 2D counterpart of the well-known 3D cubic syngony;

Isotropy is achieved by imposing $R_0 = R_1 = 0$.

It is remarkable that orthotropy imposes a condition on the cubic invariants of the tensor, namely $\Phi_0 - \Phi_1$, whilst the other symmetries impose conditions on the quadratic invariants, namely R_0 and R_1 .

The norm of \mathbf{L} can be evaluated using the following norm, proposed by Kandil and Verchery (1988):

$$\|\mathbf{L}\| = \sqrt{T_0^2 + 2T_1^2 + R_0^2 + 4R_1^2}. \tag{4.5}$$

Consider the tensor $\mathbf{S} := \mathbf{L}^{-1}$. Still being a fourth-order plane tensor, it admits a polar representation. Let $t_0, t_1, r_0, r_1, \phi_0, \phi_1$ be its PPs. It is possible to show that the PPs of \mathbf{S} are linked to those of \mathbf{L} as follows:

$$\begin{aligned}
 t_0 &= \frac{2}{\det(\mathbf{L})} (T_0 T_1 - R_1^2), \\
 t_1 &= \frac{1}{2 \det(\mathbf{L})} (T_0^2 - R_0^2), \\
 r_0 e^{4i\phi_0} &= \frac{2}{\det(\mathbf{L})} (R_1^2 e^{4i\Phi_1} - T_1 R_0 e^{4i\Phi_0}), \\
 r_1 e^{2i\phi_1} &= \frac{R_1 e^{2i\Phi_1}}{\det(\mathbf{L})} (R_0 e^{4i(\Phi_0 - \Phi_1)} - T_0),
 \end{aligned} \tag{4.6}$$

where

$$\det(\mathbf{L}) = 8T_1(T_0^2 - R_0^2) - 16R_1^2[T_0 - R_0 \cos 4(\Phi_0 - \Phi_1)]. \tag{4.7}$$

4.1.3 Thermodynamic Existence Conditions

Let W be the stored-energy density function for an anisotropic linear hyperelastic material. Then, (under the hypothesis of plane elasticity) this energy density can be expressed as

$$W := \frac{1}{2} \mathbf{T} \cdot \mathbf{E} = Tt + Rr \cos 2(\Phi - \phi), \quad (4.8)$$

being T, R, Φ the PPs of the Cauchy' stress tensor \mathbf{T} and t, r, ϕ the counterparts for the linearised strain tensor \mathbf{E} (see also Section 5.1.2). Since the constitutive equation for the material reads $\mathbf{T} = \mathbb{C}[\mathbf{E}]$ (see also Theorem 5.6), and since \mathbb{C} is a fourth-order elasticity plane tensor of PPs $T_0, T_1, R_0, R_1, \Phi_0, \Phi_1$, Eq. (4.8) reads:

$$W = 4T_1 t^2 + 8R_1 r t \cos 2(\Phi_1 - \phi) + 2r^2 [T_0 + R_0 \cos 4(\Phi_0 - \phi)], \quad (4.9)$$

which can be arranged as a quadratic form of r and t as follows:

$$W = \{r \ t\} \begin{bmatrix} 2 [T_0 + R_0 \cos 4(\Phi_0 - \phi)] & 4R_1 \cos 2(\Phi_1 - \phi) \\ 4R_1 \cos 2(\Phi_1 - \phi) & 4T_1 \end{bmatrix} \begin{Bmatrix} r \\ t \end{Bmatrix}. \quad (4.10)$$

According to the Sylvester's criterion, the following conditions (to be satisfied for all ϕ) are necessary and sufficient for W to be positive-definite:

$$\begin{cases} T_0 + R_0 \cos 4(\Phi_0 - \phi) > 0, \\ T_1 [T_0 + R_0 \cos 4(\Phi_0 - \phi)] > 2R_1^2 \cos^2 2(\Phi_1 - \phi), \end{cases} \quad (4.11)$$

i.e. all of the leading principal minors of the matrix appearing in Eq. (4.10) must have positive determinant. The study of Eq. (4.11), together with the positiveness of R_0 and R_1 , provides the following elastic bounds (Vannucci, 2017):

$$\begin{cases} T_0, T_1, R_0, R_1 > 0, \\ T_0 > R_0, \\ T_1 (T_0^2 - R_0^2) > 2R_1^2 [T_0 - R_0 \cos 4(\Phi_0 - \Phi_1)]. \end{cases} \quad (4.12)$$

4.2 Polar Formalism and Composite Laminates

This section aims at presenting the FSDT for the mechanical description of composite laminates mechanics. Moreover, this theory can be formulated in the framework of polar formalism. Also here, only the main results, available in (Montemurro, 2015a, 2015b), are presented.

4.2.1 First-order Shear Deformation Theory

The FSDT is the generalisation of the CLT (Jones, 2018) and constitutes a general theoretical framework to describe the behaviour of a composite multiplayer plate. The main difference between FSDT and CLT is that fibres orthogonal to the laminate mid-plane (in the un-deformed reference configuration) still remain un-warped but no more perpendicular to the bended mid-plane (Reissner-Mindlin kinematics) in the former theory. With reference to Figure 4.1, the displacement field can be described by Reddy (2003), Barbero (2013)

$$\begin{aligned} u_1(x_1, x_2, x_3) &= u_0(x_1, x_2) + x_3\theta_2(x_1, x_2), \\ u_2(x_1, x_2, x_3) &= v_0(x_1, x_2) - x_3\theta_1(x_1, x_2), \\ u_3(x_1, x_2) &= w_0(x_1, x_2). \end{aligned} \quad (4.13)$$

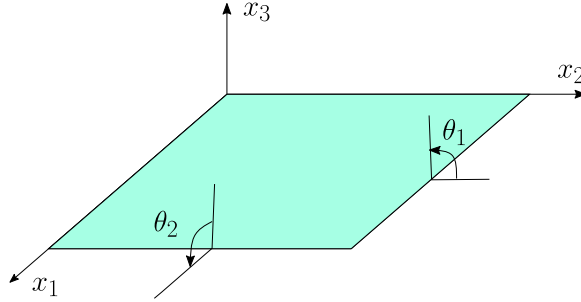


Figure 4.1: *Mid-plane of a plate and reference frame*

The constitutive equation for the laminate reads (the Voigt's notation is tacitly assumed in the following):

$$\mathbf{r}_{\text{gen}} = \mathbf{K}_{\text{lam}}\boldsymbol{\varepsilon}_{\text{gen}}, \quad (4.14)$$

where \mathbf{r}_{gen} and $\boldsymbol{\varepsilon}_{\text{gen}}$ are the vectors of the generalised forces per unit length and generalised strains of the laminate middle plane, respectively, whilst \mathbf{K}_{lam} is the stiffness tensor of the laminate. In the FSDT framework (Reddy, 2003), the analytic expressions of these arrays are

$$\mathbf{r}_{\text{gen}} = \begin{Bmatrix} \mathbf{n} \\ \mathbf{m} \\ \mathbf{t} \end{Bmatrix}, \quad \mathbf{K}_{\text{lam}} = \begin{bmatrix} \mathbf{A} & \mathbf{B} & \mathbf{0} \\ & \mathbf{D} & \mathbf{0} \\ \text{sym} & & \mathbf{H} \end{bmatrix}, \quad \boldsymbol{\varepsilon}_{\text{gen}} = \begin{Bmatrix} \boldsymbol{\varepsilon}_0 \\ \boldsymbol{\chi}_0 \\ \boldsymbol{\gamma}_0 \end{Bmatrix}. \quad (4.15)$$

In Eq. (4.15), \mathbf{A} is the membrane stiffness tensor of the laminate, \mathbf{D} the bending stiffness tensor, \mathbf{H} the out-of-plane shear stiffness tensor, \mathbf{B} the membrane/bending coupling stiffness tensor. Vectors \mathbf{n} , \mathbf{m} , \mathbf{t} are the membrane forces, bending moments and out-of-plane shear forces per unit length, respectively (see Figure 4.2). Vectors $\boldsymbol{\varepsilon}_0$, $\boldsymbol{\chi}_0$, $\boldsymbol{\gamma}_0$ represent the in-plane strains, curvatures and out-of-plane shear strains of the laminate

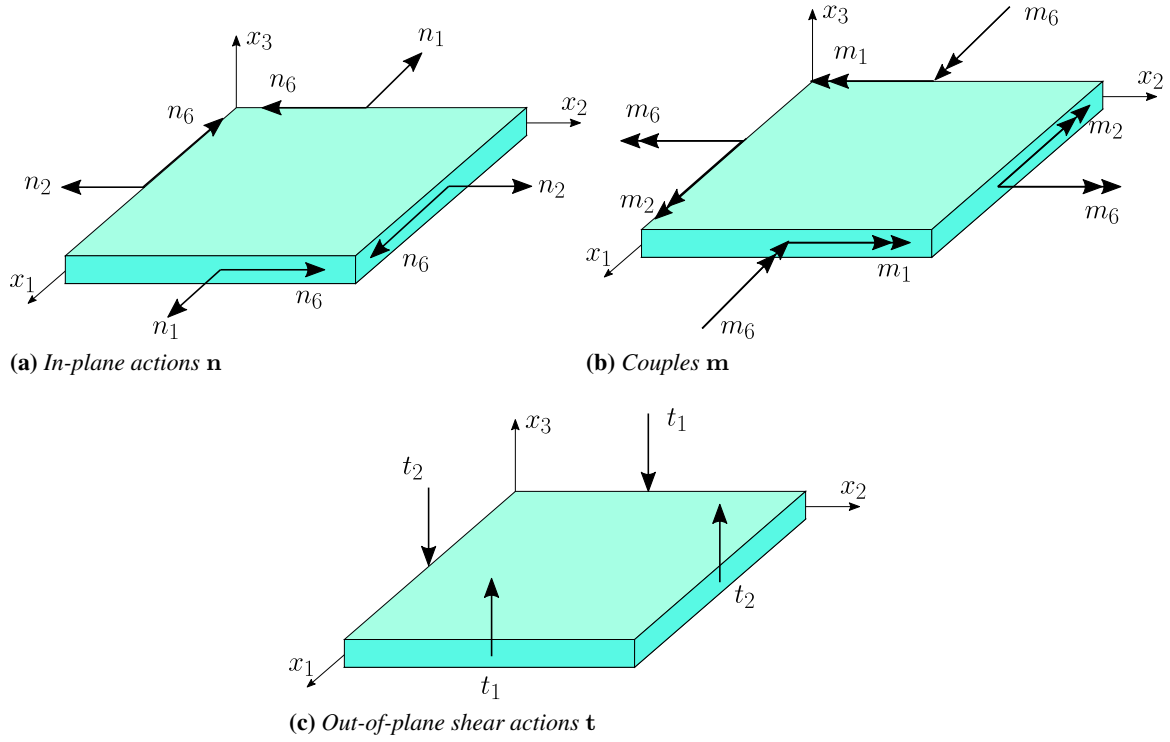


Figure 4.2: Unit-length internal generalised forces \mathbf{r}_{gen}

middle plane, respectively. The strain expressions are:

$$\varepsilon_1^0 = \frac{\partial u_0}{\partial x_1}, \quad \varepsilon_2^0 = \frac{\partial v_0}{\partial x_2}, \quad \varepsilon_6^0 = \frac{\partial u_0}{\partial x_2} + \frac{\partial v_0}{\partial x_1}, \quad (4.16)$$

$$\chi_1^0 = \frac{\partial \theta_2}{\partial x_1}, \quad \chi_2^0 = -\frac{\partial \theta_1}{\partial x_2}, \quad \chi_6^0 = \frac{\partial \theta_2}{\partial x_2} - \frac{\partial \theta_1}{\partial x_1}, \quad (4.17)$$

$$\gamma_2^0 = -\theta_1 + \frac{\partial w_0}{\partial x_2}, \quad \gamma_1^0 = \theta_2 + \frac{\partial w_0}{\partial x_1}. \quad (4.18)$$

Hence (see Figure 4.2)

$$\mathbf{n} = \{n_1, n_2, n_6\}^T, \quad \mathbf{m} = \{m_1, m_2, m_6\}^T, \quad \mathbf{t} = \{t_2, t_1\}^T, \quad (4.19)$$

and

$$\boldsymbol{\varepsilon}_0 = \{\varepsilon_1^0, \varepsilon_2^0, \varepsilon_6^0\}^T, \quad \boldsymbol{\chi}_0 = \{\chi_1^0, \chi_2^0, \chi_6^0\}^T, \quad \boldsymbol{\gamma}_0 = \{\gamma_2^0, \gamma_1^0\}^T. \quad (4.20)$$

It is convenient to introduce also the following normalised tensors:

$$\mathbf{A}^* := \frac{1}{h} \mathbf{A}, \quad \mathbf{B}^* := \frac{2}{h^2} \mathbf{B}, \quad \mathbf{D}^* := \frac{12}{h^3} \mathbf{D}, \quad \mathbf{C}^* := \mathbf{A}^* - \mathbf{D}^*, \quad \mathbf{H}^* := \frac{1}{h} \mathbf{H}, \quad (4.21)$$

where h is the total thickness of the laminate. Note that tensors defined in Eq. (4.21) have dimension of a stress and can be directly compared.

When the laminate is composed of *identical layers* (i.e. plies having same material and thickness), the expressions of the above tensor are:

$$\begin{aligned} \mathbf{A}^* &= \frac{1}{N} \sum_{k=1}^N a_k \mathbf{Q}(\theta_k), & \mathbf{B}^* &= \frac{1}{N^2} \sum_{k=1}^N b_k \mathbf{Q}(\theta_k), & \mathbf{D}^* &= \frac{1}{N^3} \sum_{k=1}^N d_k \mathbf{Q}(\theta_k), \\ \mathbf{H}^* &= \frac{1}{N} \sum_{k=1}^N h_k \hat{\mathbf{Q}}(\theta_k), & \mathbf{C}^* &= \frac{1}{N^3} \sum_{k=1}^N c_k \mathbf{Q}(\theta_k). \end{aligned} \quad (4.22)$$

In Eq. (4.22), N is the number of plies of the laminate, θ_k is the orientation angle of the k -th ply, $\mathbf{Q}(\theta_k)$ is the in-plane reduced stiffness tensor of the k -th ply whose material frame is turned by an angle θ_k with respect to the global reference frame of the laminate. Analogously, $\hat{\mathbf{Q}}(\theta_k)$ is the out-of-plane reduced stiffness tensor of the k -th ply. Furthermore, coefficients a_k, b_k, d_k, h_k and c_k read:

$$\begin{aligned} a_k &= 1, \\ b_k &= 2k - N - 1, \\ d_k &= 12k(k - N - 1) + 4 + 3N(N + 2), \\ h_k &= 1, \\ c_k &= -2N^2 - 12k(k - N - 1) - 4 - 6N. \end{aligned} \quad (4.23)$$

In the following of the Thesis, only laminates composed of identical layers, in the sense specified above, will be considered.

4.2.2 Polar Description of Laminate Stiffness Tensors

In order to properly analyse the mechanical behaviour of a laminate, it is possible to express the stiffness tensors in Eq. (4.22) in terms of their PPs. In particular, \mathbf{A}^* , \mathbf{B}^* , \mathbf{D}^* , and thus \mathbf{C}^* , behave like fourth-order elasticity-like plane tensors, while \mathbf{H}^* like a second-order symmetric plane tensor. The PPs of the laminate stiffness tensors can be expressed as functions of the PPs of the lamina reduced stiffness matrices and of the geometrical properties of the stack (i.e. the layer orientation, position and number). In the following of the Thesis, the special case of laminates made of identical plies, i.e. same material and thickness for the elementary layer, is considered. The polar representations of the homogenised stiffness tensors of the laminate read:

tensor \mathbf{A}^*

$$\begin{aligned} T_0^{A^*} &= T_0, & T_1^{A^*} &= T_1, \\ R_0^{A^*} e^{i4\Phi_0^{A^*}} &= \frac{R_0 e^{i4\Phi_0}}{N} \sum_{k=1}^N a_k e^{i4\theta_k}, & R_1^{A^*} e^{i2\Phi_1^{A^*}} &= \frac{R_1 e^{i2\Phi_1}}{N} \sum_{k=1}^N a_k e^{i2\theta_k}; \end{aligned} \quad (4.24)$$

tensor \mathbf{B}^*

$$\begin{aligned} T_0^{B^*} &= 0, & T_1^{B^*} &= 0, \\ R_0^{B^*} e^{i4\Phi_0^{B^*}} &= \frac{R_0 e^{i4\Phi_0}}{N^2} \sum_{k=1}^N b_k e^{i4\theta_k}, & R_1^{B^*} e^{i2\Phi_1^{B^*}} &= \frac{R_1 e^{i2\Phi_1}}{N^2} \sum_{k=1}^N b_k e^{i2\theta_k}; \end{aligned} \quad (4.25)$$

tensor \mathbf{D}^*

$$\begin{aligned} T_0^{D^*} &= T_0, & T_1^{D^*} &= T_1, \\ R_0^{D^*} e^{i4\Phi_0^{D^*}} &= \frac{R_0 e^{i4\Phi_0}}{N^3} \sum_{k=1}^N d_k e^{i4\theta_k}, & R_1^{D^*} e^{i2\Phi_1^{D^*}} &= \frac{R_1 e^{i2\Phi_1}}{N^3} \sum_{k=1}^N d_k e^{i2\theta_k}; \end{aligned} \quad (4.26)$$

tensor \mathbf{H}^*

$$\begin{aligned} T^{H^*} &= T, \\ R^{H^*} e^{i2\Phi^{H^*}} &= \frac{R e^{i2\Phi}}{N} \sum_{k=1}^N e^{-i2\theta_k}; \end{aligned} \quad (4.27)$$

tensor \mathbf{C}^*

$$\begin{aligned} T_0^{C^*} &= 0, & T_1^{C^*} &= 0, \\ R_0^{C^*} e^{i4\Phi_0^{C^*}} &= \frac{R_0 e^{i4\Phi_0}}{N^3} \sum_{k=1}^N c_k e^{i4\theta_k}, & R_1^{C^*} e^{i2\Phi_1^{C^*}} &= \frac{R_1 e^{i2\Phi_1}}{N^3} \sum_{k=1}^N c_k e^{i2\theta_k}. \end{aligned} \quad (4.28)$$

In the above equations, T_0 , T_1 , R_0 , R_1 , Φ_0 and Φ_1 are the PPs of the in-plane reduced stiffness matrix \mathbf{Q} of the lamina, while T , R , and Φ are those of the out-of-plane shear stiffness matrix $\hat{\mathbf{Q}}$: all of these parameters solely depend upon the ply material properties. Since basic layers are actually orthotropic, without loss of generality it can be assumed that $\Phi_1 = 0$ ($\Phi_0 = K\frac{\pi}{4}$ with $K \in \{0, 1\}$) (Vannucci, 2012a). For further details on the Polar Method in the FSDT framework, the reader is addressed to (Montemurro, 2015a, 2015b).

As a final remark of this Section, it is noteworthy that uncoupling properties between membrane and bending behaviours is often sought in many engineering applications. This property is expressed in the following

Definition 4.1 (Membrane/bending uncoupling). *A laminate is said uncoupled (in membrane and bending responses) if and only if $\mathbf{B}^* = \mathbf{0}$.*

Moreover, in order to have the same properties both in membrane and bending in any direction, i.e. the same group of symmetry, the homogeneity property appears as a natural choice.

Definition 4.2 (Homogeneity). *A laminate is said homogeneous if and only if $\mathbf{C}^* = \mathbf{0}$.*

The two concepts of uncoupling and homogeneity leads to the concept of quasi-homogeneity:

Definition 4.3 (Quasi-homogeneity). *A laminate is said quasi-homogeneous (QH) if and only if uncoupling and homogeneity properties hold.*

As shown in (Montemurro, 2015a, 2015b), the deviatoric part of tensor \mathbf{H}^* , in the framework of FSDT, can be expressed in terms of the membrane PPs of the laminate, as follows:

$$R^{H^*} e^{i2\Phi^{H^*}} = \frac{R}{R_1} R_1^{A^*} e^{i2(\Phi + \Phi_1 - \Phi_1^{A^*})}. \quad (4.29)$$

In many practical applications, the further hypothesis of orthotropy of laminates is required. It is possible to show that, under orthotropy conditions, the membrane PPs assume the following form (Vannucci, 2017):

$$\begin{aligned} T_0^{A^*} &= T_0, & T_1^{A^*} &= T_1, \\ R_{0K}^{A^*} e^{i4\Phi_1^{A^*}} &= \frac{R_0 e^{i4\Phi_0}}{N} \sum_{k=1}^N e^{i4\theta_k}, & R_1^{A^*} e^{i2\Phi_1^{A^*}} &= \frac{R_1 e^{i2\Phi_1}}{N} \sum_{k=1}^N e^{i2\theta_k}, \end{aligned} \quad (4.30)$$

where $R_{0K}^{A^*} = (-1)^K R_0^{A^*}$ and $K = 0, 1$.

If the above hypotheses hold, viz. uncoupling, homogeneity and orthotropy, the design of a laminate is uniquely determined by only four variables: N , $R_{0K}^{A^*}$, $R_1^{A^*}$ and $\Phi_1^{A^*}$. Finally, for design purposes, it is convenient to introduce the following non-dimensional variables:

$$n_0 := \frac{N}{N_{\text{ref}}}, \quad \rho_0 := \frac{R_0^{A^*}}{R_0}, \quad \rho_{0K} := \frac{R_{0K}^{A^*}}{R_0}, \quad \rho_1 := \frac{R_1^{A^*}}{R_1}, \quad \phi_1 := \frac{\Phi_1^{A^*}}{\pi/2}. \quad (4.31)$$

Among them, for the design of QH orthotropic laminates, only four are necessary:

$$n_0 := \frac{N}{N_{\text{ref}}}, \quad \rho_{0K} := \frac{R_{0K}^{A^*}}{R_0}, \quad \rho_1 := \frac{R_1^{A^*}}{R_1}, \quad \phi_1 := \frac{\Phi_1^{A^*}}{\pi/2}. \quad (4.32)$$

4.2.3 Polar Description of Laminate Strength Tensors

Besides the stiffness description of a composite laminate, it is important to consider also its strength description. As discussed in (Catapano et al., 2012), it is possible to formally express all the stress-based failure criteria for composite laminates as

$$F = \boldsymbol{\sigma}^T \mathbf{F} \boldsymbol{\sigma} + \boldsymbol{\sigma}^T \mathbf{f} \leq 1, \quad (4.33)$$

where \mathbf{F} behaves as a fourth-order tensor (it can be interpreted as a *weakness* tensor), $\boldsymbol{\sigma}$ and \mathbf{f} like second order tensors, F is a failure index standing for either Tsai-Wu, Tsai-Hill or Hoffmann failure criterion. As reported in (Catapano et al., 2012; Catapano & Montemurro, 2018), a failure index averaged over the thickness of the laminate can be defined. Under the hypotheses of multilayer plates made of identical plies, in the FSDT

framework, it reads:

$$F_{\text{lam}} = \frac{1}{h} \left(\boldsymbol{\varepsilon}_{\text{gen}}^T \begin{bmatrix} \mathbf{G}_A & \mathbf{G}_B & \mathbf{0} \\ & \mathbf{G}_D & \mathbf{0} \\ \text{sym} & & \mathbf{G}_H \end{bmatrix} \boldsymbol{\varepsilon}_{\text{gen}} + \left\{ \boldsymbol{\varepsilon}_0^T \quad \boldsymbol{\gamma}_0^T \right\} \begin{Bmatrix} \mathbf{g}_A \\ \mathbf{g}_D \end{Bmatrix} \right) \leq 1, \quad (4.34)$$

where \mathbf{G}_A is the laminate membrane strength tensor, \mathbf{G}_B the membrane/bending coupling strength tensor, \mathbf{G}_D the bending strength tensor, \mathbf{G}_H the shear strength tensor, whilst \mathbf{g}_A and \mathbf{g}_D are the membrane and bending strength vectors related to the linear part of the failure criterion. Equation (4.34) represents the polynomial laminate-level failure criterion for a multilayer plate modelled as an equivalent single layer (Catapano & Montemurro, 2018).

It is noteworthy that \mathbf{G}_A , \mathbf{G}_B and \mathbf{G}_D behave like fourth-order elasticity-like tensors, that \mathbf{G}_H behaves like a second-order symmetric tensors, and that \mathbf{g}_A and \mathbf{g}_D behave like second-order symmetric tensors. Then, they can be described through opportune PPs.

In analogy to Section 4.2.2, it is convenient to introduce the dimensionless quantities:

$$\begin{aligned} \mathbf{G}_A^* &:= \frac{1}{h} \mathbf{G}_A, & \mathbf{G}_B^* &:= \frac{2}{h^2} \mathbf{G}_B, & \mathbf{G}_D^* &:= \frac{12}{h^3} \mathbf{G}_D, & \mathbf{G}_H^* &:= \frac{1}{h} \mathbf{G}_H, \\ \mathbf{g}_A^* &:= \frac{1}{h} \mathbf{g}_A, & \mathbf{g}_D^* &:= \frac{2}{h^2} \mathbf{g}_D. \end{aligned} \quad (4.35)$$

With reference to a single lamina, let $\{\Gamma_0, \Gamma_1, \Lambda_0, \Lambda_1, \Omega_0, \Omega_1\}$ be the PPs of the in-plane reduced strength matrix, $\{\Gamma, \Lambda, \Omega\}$ be the PPs of the out-of-plane strength tensor, $\{\gamma, \lambda, \omega\}$ be the PPs of the in-plane strength vector. Then, in analogy to the expressions derived in Section 4.2.2 for the stiffness tensors, the following expressions can be deduced (Catapano & Montemurro, 2018):

tensor \mathbf{G}_A^*

$$\begin{aligned} \Gamma_0^{G_A^*} &= \Gamma_0, & \Gamma_1^{G_A^*} &= \Gamma_1, \\ \Lambda_0^{G_A^*} e^{i4\Omega_0^{G_A^*}} &= \frac{\Lambda_0 e^{i4\Omega_0}}{N} \sum_{k=1}^N e^{i4\theta_k}, & \Lambda_1^{G_A^*} e^{i2\Omega_1^{G_A^*}} &= \frac{\Lambda_1 e^{i2\Omega_1}}{N} \sum_{k=1}^N e^{i2\theta_k}; \end{aligned} \quad (4.36)$$

tensor \mathbf{G}_B^*

$$\begin{aligned} \Gamma_0^{G_B^*} &= 0, & \Gamma_1^{G_B^*} &= 0, \\ \Lambda_0^{G_B^*} e^{i4\Omega_0^{G_B^*}} &= \frac{\Lambda_0 e^{i4\Omega_0}}{N^2} \sum_{k=1}^N b_k e^{i4\theta_k}, & \Lambda_1^{G_B^*} e^{i2\Omega_1^{G_B^*}} &= \frac{\Lambda_1 e^{i2\Omega_1}}{N^2} \sum_{k=1}^N b_k e^{i2\theta_k}; \end{aligned} \quad (4.37)$$

tensor \mathbf{G}_D^*

$$\begin{aligned}\Gamma_0^{G_D^*} &= \Gamma_0, & \Gamma_1^{G_D^*} &= \Gamma_1, \\ \Lambda_0^{G_D^*} e^{i4\Omega_0^{G_D^*}} &= \frac{\Lambda_0 e^{i4\Omega_0}}{N^3} \sum_{k=1}^N d_k e^{i4\theta_k}, & \Lambda_1^{G_D^*} e^{i2\Omega_1^{G_D^*}} &= \frac{\Lambda_1 e^{i2\Omega_1}}{N^3} \sum_{k=1}^N d_k e^{i2\theta_k};\end{aligned}\quad (4.38)$$

tensor \mathbf{G}_H^*

$$\begin{aligned}\Gamma^{G_H^*} &= \Gamma, \\ \Lambda^{G_H^*} e^{i2\Omega^{G_H^*}} &= \frac{\Lambda e^{i2\Omega}}{N} \sum_{k=1}^N e^{-i2\theta_k};\end{aligned}\quad (4.39)$$

vector \mathbf{g}_A^*

$$\begin{aligned}\gamma^{g_A^*} &= \gamma, \\ \lambda^{g_A^*} e^{i2\omega^{g_A^*}} &= \frac{\lambda e^{i2\omega}}{N} \sum_{k=1}^N e^{i2\theta_k};\end{aligned}\quad (4.40)$$

vector \mathbf{g}_D^*

$$\begin{aligned}\gamma^{g_D^*} &= 0, \\ \lambda^{g_D^*} e^{i2\omega^{g_D^*}} &= \frac{\lambda e^{i2\omega}}{N^2} \sum_{k=1}^N b_k e^{i2\theta_k}.\end{aligned}\quad (4.41)$$

However, some simplifications hold. In fact, the deviatoric part of \mathbf{G}_H^* , \mathbf{g}_A^* and \mathbf{g}_D^* can be expressed in terms of the in-plane strength PPs as follows:

$$\begin{aligned}\Lambda^{G_H^*} e^{i2\Omega^{G_H^*}} &= \Lambda_1^{G_A^*} \frac{\Lambda}{\Lambda_1} e^{i2(\Omega + \Omega_1 - \Omega^{G_A^*})}, \\ \lambda^{g_A^*} e^{i2\omega^{g_A^*}} &= \Lambda_1^{G_A^*} \frac{\lambda}{\Lambda_1} e^{i2(\Omega_1^{G_A^*} + \omega - \Omega_1)}, \\ \lambda^{g_D^*} e^{i2\omega^{g_D^*}} &= \Lambda_1^{G_B^*} \frac{\lambda}{\Lambda_1} e^{i2(\Omega_1^{G_B^*} + \omega - \Omega_1)}.\end{aligned}\quad (4.42)$$

Moreover, the following relationships exist between stiffness and strength PPs, as pointed

out in (Catapano & Montemurro, 2018):

$$\begin{aligned}
 \Lambda_0^{G_A^*} e^{i4\Omega_0^{G_A^*}} &= R_0^{A^*} \frac{\Lambda_0}{R_0} e^{i4(\Phi_0^{A^*} + \Omega_0 - \Phi_0)}, \\
 \Lambda_1^{G_A^*} e^{i2\Omega_1^{G_A^*}} &= R_1^{A^*} \frac{\Lambda_1}{R_1} e^{i2(\Phi_1^{A^*} + \Omega_1 - \Phi_1)}, \\
 \Lambda_0^{G_B^*} e^{i4\Omega_0^{G_B^*}} &= R_0^{B^*} \frac{\Lambda_0}{R_0} e^{i4(\Phi_0^{B^*} + \Omega_0 - \Phi_0)}, \\
 \Lambda_1^{G_B^*} e^{i2\Omega_1^{G_B^*}} &= R_1^{B^*} \frac{\Lambda_1}{R_1} e^{i2(\Phi_1^{B^*} + \Omega_1 - \Phi_1)}, \\
 \Lambda_0^{G_D^*} e^{i4\Omega_0^{G_D^*}} &= R_0^{D^*} \frac{\Lambda_0}{R_0} e^{i4(\Phi_0^{D^*} + \Omega_0 - \Phi_0)}, \\
 \Lambda_1^{G_D^*} e^{i2\Omega_1^{G_D^*}} &= R_1^{D^*} \frac{\Lambda_1}{R_1} e^{i2(\Phi_1^{D^*} + \Omega_1 - \Phi_1)}.
 \end{aligned} \tag{4.43}$$

From a physical viewpoint, considering the definition of strength criterion, it means that stiffness and strength of a laminate are correlated, as the deviatoric terms of strength tensors and vectors can be expressed in terms of stiffness PPs. Besides, when passing from CLT to FSDT, the number of PPs that are involved in the design process does not change.

4.2.4 Elastic and Geometrical Bounds

The set of inequalities (4.12) applies also for tensors \mathbf{A}^* and \mathbf{D}^* , taken singularly, since they are positive-definite.

Such conditions on membrane and bending tensors define an elastic domain containing all the admissible values of the PPs. Therefore, \mathbf{A}^* and \mathbf{D}^* can be considered as elastic tensors of two fictitious materials, imagining to build an equivalent single-layer plate with thickness h , having the same extension and bending elastic properties of the laminate in all directions. Conversely, for tensor \mathbf{B}^* is different, because it is not-definite. In particular, the idea of a fictitious material for the coupled response has not a precise mechanical meaning. Vannucci (2012a) has shown that if a laminate is composed by identical layers, there exist more restrictive bounds, given by the combinations of the trigonometric functions appearing in (4.24) and (4.26). Such bounds are said *geometrical bounds* because they arise from the geometry of the stack, i.e. from the combination of the orientation angles and positions within the stack.

Assume $T \in \{A^*, D^*\}$. For a generic uncoupled and anisotropic laminate, they read

$$\left\{ \begin{array}{l} 0 \leq \frac{R_0^T}{R_0} \leq 1, \\ 0 \leq \frac{R_1^T}{R_1} \leq 1, \\ 2 \left(\frac{R_1^T}{R_1} \right)^2 \leq \frac{1 - \left(\frac{R_0^T}{R_0} \right)^2}{1 - (-1)^K \frac{R_0^T}{R_0} \cos 4(\Phi_0^T - \Phi_1^T)}, \end{array} \right. \tag{4.44}$$

and are valid for \mathbf{A}^* or \mathbf{D}^* , taken separately (Vannucci, 2012a). Moreover, Vannucci showed that the geometric domain is always smaller than the elastic domain. More precisely, he proved that the geometric domain is always entirely contained into the elastic domain. Mechanically, this means that laminates constitute a sort of smaller elastic class. Finally, the complete set of constraints that must be considered, in the case of uncoupled, fully-orthotropic laminates is:

$$\begin{cases} 0 \leq \frac{R_0^T}{R_0} \leq 1, \\ 0 \leq \frac{R_1^T}{R_1} \leq 1, \\ 2 \left(\frac{R_1^T}{R_1} \right)^2 - 1 - (-1)^{K_T - K} \frac{R_0^T}{R_0} \leq 0. \end{cases} \quad (4.45)$$

4.3 Quasi-trivial Stacking Sequences

Albeit the concept of SS has been already introduced, its formal definition is now introduced.

Definition 4.4 (Stacking sequence). *A stacking sequence (SS), or stack, of an N -ply laminate is the ordered set*

$$\text{SS} := \{\theta_k : 1 \leq k \leq N\},$$

where θ_k is the orientation angle of the k -th ply. Plies are ordered from the bottom surface to the top one of the laminate.

As already said, a laminate is *uncoupled* if and only if $\mathbf{B}^* = \mathbf{0}$. This means that in-plane forces do not produce curvatures and, similarly, bending moments do not deform the laminate middle plane. A laminate is said *homogeneous* if and only if $\mathbf{C}^* = \mathbf{0}$. The homogeneity property is linked to the design of the pure bending tensor \mathbf{D}^* . The design of \mathbf{D}^* is quite difficult because its properties depend not only on the plies orientation angles, but also on their position within the SS. In order to have the same properties both in membrane and bending in any direction, i.e. the same group of symmetry, the homogeneity property must be imposed.

Since coefficients $\{b_k\}$ assume antisymmetric values with respect to the laminate middle plane, a simple way to obtain $\mathbf{B}^* = \mathbf{0}$ consists of using a symmetric SSs, as commonly done in several works (Adams et al., 2004; Seresta et al., 2007; Bloomfield et al., 2008; Raju et al., 2014; Macquart et al., 2016). Of course, this is only a sufficient condition, since asymmetric uncoupled SSs exist. In (Caprino & Crivelli Visconti, 1982), the existence of uncoupled anti-symmetric stacks was proven, while in (Verchery & Vong, 1986), the existence of completely asymmetric uncoupled SSs was shown. In (Vannucci et al., 1998; Vannucci & Verchery, 2001a), a special class of uncoupled and possibly homogeneous laminates was found; the solutions belonging to this class are called *quasi-trivial*

(QT) and represent a class of arithmetically-exact solutions. Furthermore, authors have shown that the number of independent QT solutions is by far larger than the number of symmetric ones. An efficient enumerating algorithm has been recently proposed in (Garulli et al., 2018).

QT SSs are characterised by an interesting and very useful property: membrane/bending uncoupling and/or homogeneity requirements can be exactly met regardless of the values of the orientation angles. In particular, these requirements can be fulfilled by acting only on the position of the layers into the stack (Vannucci & Verchery, 2001a; Garulli et al., 2018). QT SSs have been efficiently used in many practical problems (Montemurro et al., 2016; Montemurro & Catapano, 2017; Montemurro et al., 2018; Montemurro et al., 2019).

Specifically, a QT stack represents an equivalence class for all possible orientations that each group of ply can assume. As an example, $\{90^\circ, -26^\circ, 90^\circ, 90^\circ, 90^\circ, -26^\circ, 90^\circ\}$ and $\{1^\circ, 42^\circ, 1^\circ, 1^\circ, 1^\circ, 42^\circ, 1^\circ\}$ are elements of the same equivalence class $[\{1, 2, 1, 1, 1, 2, 1\}]$, where 1 and 2 are just labels identifying two possibly distinct orientations. Of course, the choice of the orientations depends upon the desired elastic behaviour of the laminate.

To explain clearly the concept of QT SSs, consider a laminate with N plies and $m \leq N$ different orientations and define

$$G_j := \{k : \theta_k = \theta_j\}, \quad (4.46)$$

the set of indices within the SS sharing the same orientation θ_j . Conditions for uncoupling and homogeneity can be then split as multiple sums over the different sets G_j , $j = 1, \dots, m$ (Garulli et al., 2018). Therefore, the uncoupling condition reads:

$$\sum_{k=1}^N b_k e^{i\beta\theta_k} = \sum_{j=1}^m e^{i\beta\theta_j} \sum_{k \in G_j} b_k = 0, \quad \beta = 2, 4, \quad (4.47)$$

while the homogeneity requirement can be expressed as:

$$\sum_{k=1}^N c_k e^{i\beta\theta_k} = \sum_{j=1}^m e^{i\beta\theta_j} \sum_{k \in G_j} c_k = 0, \quad \beta = 2, 4. \quad (4.48)$$

This leads to the following definitions

Definition 4.5 (Saturated group). *A group of plies oriented at θ_j (for some j), for which*

$$\sum_{k \in G_j} b_k = 0, \quad \sum_{k \in G_j} c_k = 0, \quad (4.49)$$

is said saturated group with respect to coefficients $\{b_k\}$ and $\{c_k\}$, respectively.

Definition 4.6 (Quasi-trivial stacking sequences). *A SS is said quasi-trivial if it is entirely composed of saturated groups. If not specified, the quasi-triviality has to be intended*

with respect to coefficients $\{b_k\}$ and $\{c_k\}$. In this case, the laminate is said quasi-trivial quasi-homogeneous (QT QH).

For more details on the topic, the reader is addressed to (Vannucci, 2017; Garulli et al., 2018).

4.4 Conclusions

In this Chapter, the fundamentals of the Polar Method as a tool to describe plane tensors has been introduced. In particular, it has been shown that the Polar Method is a profitable tool in the description of the anisotropy of multilayered plates. In so doing, it allows for a simple description of both stiffness and strength tensors of uncoupled, homogeneous and orthotropic laminates in the FSDT framework. The aforementioned concepts will be extensively used in the following of the Thesis.

Fundamentals of Elasticity and Variational Methods

This Chapter is focused on the main results of Variational Elasticity and on the main results and properties of the Γ -convergence theory. The principal aim is to provide a theoretical background in view of the exposition of Chapter 10, whose results will be used to justify FE modelling choices in the PARSIFAL box-wing optimisation, discussed in Chapter 8.

In particular, Section 5.1 summarises the classical results of the Theory of Elasticity. From Finite Elasticity, the focus is posed on the Linearised Elasticity. Then, the variational structure of the equilibrium problem is presented. Section 5.2 presents the fundamental notion of lower-semicontinuity and the so-called Direct Method of the Calculus of Variations, by L. Tonelli, to prove the existence and, possibly, the uniqueness, of the elastic equilibrium problem. These concepts are fundamentals also in view of Section 5.3, which introduces the notion of Γ -convergence as a variational tool to derive asymptotic problems, together with its main properties. Finally, Section 5.4 contains some meaningful considerations.

5.1 Fundamentals of Elasticity

The brief collection of results is inspired by the classical textbooks (C. Truesdell & Wang, 1973; C. A. Truesdell, 1977; Gurtin, 1981; Ciarlet, 1994) and by (Morassi, 2008; Paroni, 2008).

5.1.1 Finite Elasticity

5.1.1.1 Analysis of Deformation

Let \mathcal{E} be the three-dimensional Euclidean space. With reference to Figure 5.1, let \mathfrak{B} be a deformable body¹. Assume $\mathbf{k} : \mathfrak{B} \mapsto \mathcal{E}$ to be a placement in \mathcal{E} of this body, which then occupies a certain regular spatial region Ω . The placement \mathbf{k} is assumed as a reference configuration, such that $\Omega := \mathbf{k}(\mathfrak{B})$ and \mathbf{X} are the spatial coordinates of material point X of Ω . Hence, $\mathbf{k}(X) = \mathbf{X}$. With reference to Figure 5.1, consider a different placement of \mathfrak{B} , and let χ be the vector-valued mapping, called *deformation*, from the reference configuration Ω to the new, possibly deformed, one (say $\tilde{\Omega}$). Furthermore, define the deformation gradient as

$$\mathbf{F} := \nabla \chi, \quad (5.1)$$

with $\det(\mathbf{F}) > 0$ so to have \mathbf{F} locally-invertible and orientation-preserving. Moreover, χ is assumed to be a homeomorphism, i.e. a continuous map with a continuous inverse map.

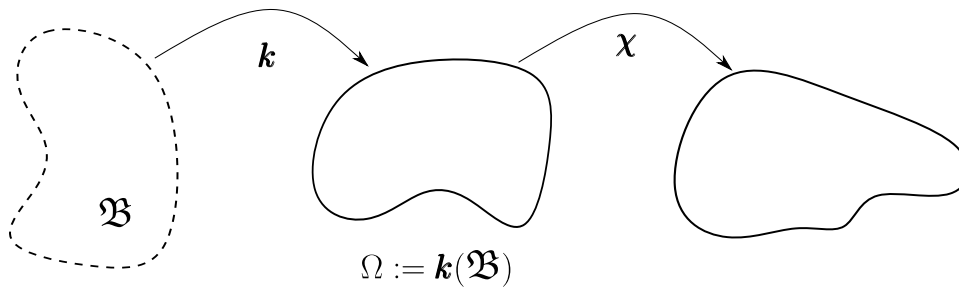


Figure 5.1: Placement \mathbf{k} and deformation χ of a body \mathfrak{B}

It is useful to introduce the notion of displacement.

Definition 5.1 (Displacement). *The displacement of a point $\mathbf{X} \in \Omega$ is defined as*

$$\mathbf{u}(\mathbf{X}) := \chi(\mathbf{X}) - \mathbf{X}. \quad (5.2)$$

The displacement is then the vector joining the position vector \mathbf{X} of point $X \in \Omega$ into its image through χ .

Before continuing, the following important sets shall be introduced. Lin is the set of linear applications from a vectorial space into itself; equivalently, it defines the set of all second-order tensors. Noteworthy subsets are: Lin^+ , the set of second-order tensors with positive determinant; Sym , the set of symmetric second-order tensors; Skw , the set of skew-symmetric second-order tensors; Psym , the set of symmetric and positive-definite second-order tensors. $\text{SO}(n)$ denotes the special orthogonal group, i.e. the set of rotation tensors in the n -dimensional space. For fourth-order tensors, the nomenclature is similar, apart from the *blackboard bold* capital letter: $\mathbb{L}\text{in}$, $\mathbb{S}\text{ym}$, etc.

¹The intuitive notion of body is sufficient for the future developments

Theorem 5.1 (Polar decomposition). *Assume $\mathbf{F} \in \text{Lin}^+$. There exist $\mathbf{U}, \mathbf{V} \in \text{Psym}$ and $\mathbf{R} \in \text{SO}(3)$ such that*

$$\mathbf{F} = \mathbf{R}\mathbf{U} = \mathbf{V}\mathbf{R}. \quad (5.3)$$

The decomposition is unique.

It can be shown that the variations of lengths, areas and volumes are correlated to the so-called Cauchy's right deformation tensor $\mathbf{C} := \mathbf{F}^T\mathbf{F} = \mathbf{U}^2$, so that the deformation measure can be expressed by the following

Definition 5.2 (Green-Saint Venant strain tensor).

$$\mathbf{E} := \frac{1}{2}(\mathbf{C} - \mathbf{I}_3), \quad \mathbf{E} \in \text{Sym}, \quad (5.4)$$

which is a measure of the deviation between a given deformation and a rigid motion. Note that, for rigid deformations, $\mathbf{C} = \mathbf{I}_3 \implies \mathbf{E} = \mathbf{0}$.

5.1.1.2 Analysis of Stress

Assume an arbitrary regular subregion of the configuration $\tilde{\Omega} := \chi(\Omega)$, called *subbody* \mathfrak{B} , such that $\mathfrak{B} \subseteq \tilde{\Omega}$; let $\partial\mathfrak{B}$ denote its external boundary. Suppose that the external forces acting on \mathfrak{B} admit density, and that they can be decomposed as body-forces of density \mathbf{b} (intended per unit-volume) acting on \mathfrak{B} , and as surface tractions of density \mathbf{s} (intended per unit-surface) acting on $\partial\mathfrak{B}$. Then:

Principle 5.1 (Euler's Axiom). *The generic configuration $\tilde{\Omega}$ is equilibrated if the resultants of the forces and moments (with respect to any pole) acting on $\mathfrak{B} \subseteq \tilde{\Omega}$ vanish for every choice of $\mathfrak{B} \subseteq \tilde{\Omega}$.*

Theorem 5.2 (Hamel & Noll Theorem (Cauchy's Postulate)). *In an equilibrated configuration, consider its intersection with any regular surface. Then, there exists a vectorial field $\mathbf{t}(\mathbf{y}, \mathbf{n})$, called tension, depending only on the outer normal vector \mathbf{n} at the point \mathbf{y} belonging to the intersection.*

Theorem 5.3 (Cauchy's Lemma). *In an equilibrated configuration under $\{\mathbf{b}, \mathbf{s}, \mathbf{t}\}$ there exists a tensor field $\mathbf{T}(\mathbf{y})$, called Cauchy's stress tensor, such that $\mathbf{T}(\mathbf{y})\mathbf{n} = \mathbf{t}(\mathbf{y}, \mathbf{n})$ for every point $\mathbf{y} \in \tilde{\Omega}$ and every unitary vector $\mathbf{n}(\mathbf{y})$.*

Theorem 5.4 (Equilibrium of a body portion). *Let \mathfrak{B} be a subbody of $\tilde{\Omega}$ under the action of loads \mathbf{b} , \mathbf{s} and \mathbf{t} . Then, the subbody is in equilibrium if the following relations are satisfied:*

$$\begin{aligned} \text{div}\mathbf{T}(\mathbf{y}) + \mathbf{b}(\mathbf{y}) &= \mathbf{0}, & \mathbf{y} &\in \mathfrak{B} \\ \mathbf{T}(\mathbf{y}) &= \mathbf{T}^T(\mathbf{y}), & \mathbf{y} &\in \mathfrak{B}, \\ \mathbf{T}(\mathbf{y})\mathbf{n}(\mathbf{y}) &= \mathbf{s}(\mathbf{y}), & \mathbf{y} &\in \partial\mathfrak{B}. \end{aligned} \quad (5.5)$$

Of course, these conditions hold *a fortiori ratiōe* also for the particular choice $\mathfrak{P} = \tilde{\Omega}$. In this case, $\tilde{\Omega}$ is an equilibrated configuration.

Note that the equilibrium is defined in the deformed configuration $\tilde{\Omega}$, which in general is unknown, whilst the Kinematics' analysis is defined in the reference configuration Ω . The counterpart of Cauchy' stress tensor, in the reference configuration, is the Piola stress tensor, defined as

$$\mathbf{P} := \det(\mathbf{F})\mathbf{T}\mathbf{F}^{-T}. \quad (5.6)$$

It will be useful in the next Section.

5.1.1.3 Constitutive Equations

The aforementioned results are valid regardless of the particular material properties of the body. In general, different bodies undergo different deformations if experiencing the same stress field. This phenomenological diversity is due to the different behaviour of the materials.

Definition 5.3 (Elastic material). *A material is said elastic if and only if the Cauchy' stress tensor \mathbf{T} depends only upon the point and upon the deformation gradient. In other words, there exists a response function $\mathfrak{F}_{\mathbf{k}}$, with respect to a reference configuration \mathbf{k} , such that*

$$\mathbf{T}(\mathbf{y}) = \mathfrak{F}_{\mathbf{k}}(\mathbf{X}, \mathbf{F}(\mathbf{X})), \quad (5.7)$$

with $\mathbf{F} = \chi(\mathbf{X})$ and $\mathbf{y} = \chi(\mathbf{X})$. If the response function does not depend explicitly upon the point, the response is said homogeneous.

Among the elastic materials, an interesting class is occupied by the hyperelastic materials.

Definition 5.4 (Hyperelastic material). *A material is said hyperelastic if and only if there exists a differential scalar potential $W_{\mathbf{k}} : \Omega \times \text{Lin}^+ \mapsto \mathbb{R}$, called stored-energy density function, such that the Piola stress tensor of Eq. (5.6) can be expressed as*

$$\mathbf{P} = \frac{\partial W_{\mathbf{k}}}{\partial \mathbf{F}}(\mathbf{X}, \mathbf{F}). \quad (5.8)$$

See (Gurtin, 1981) for a physical motivation of such definition.

The stored-energy density function must satisfy some *a priori* restrictions to avoid unphysical mathematical models. Among the physical restrictions on the form of stored-energy density function, one of the most important is expressed by the following

Principle 5.2 (Material frame indifference).

$$W_{\mathbf{k}}(\mathbf{X}, \mathbf{F}) = W_{\mathbf{k}}(\mathbf{X}, \mathbf{Q}\mathbf{F}), \quad \forall \mathbf{Q} \in \text{SO}(3). \quad (5.9)$$

Principle 5.2 expresses the fact that the elastic energy *stored* by a deformed body in the placement \mathbf{k} , under the effect of a deformation χ (whose gradient is \mathbf{F}), must be the

same for two observers placed in different reference frames. Intuitively, Eq. (5.9) states that a rotation applied after the deformation (note that the rotation tensor \mathbf{Q} is applied after the deformation action expressed by \mathbf{F}) does not alter the value of the stored-energy. In particular, the rotation \mathbf{Q} can be interpreted as the passage between two rotated coordinates frames. It can be shown that, if this principle holds, the stored-energy functional cannot be convex.

Materials observable in nature often present some symmetry with respect to their response. This fact motivates the following definition:

Definition 5.5 (Symmetry group).

$$\mathcal{G}_{\mathbf{k}}(\mathbf{X}) = \{\mathbf{Q} \in \text{SO}(3) : W_{\mathbf{k}}(\mathbf{X}, \mathbf{F}) = W_{\mathbf{k}}(\mathbf{X}, \mathbf{F}\mathbf{Q})\} \quad (5.10)$$

The symmetry group of a material is the collection of the orthogonal tensors \mathbf{Q} for which the stored-energy density function is invariant if a rigid rotation is applied before the deformation. If the symmetry group coincides with $\text{SO}(3)$, the material is said isotropic.

The simplest hyperelastic isotropic material admits the following representation

Definition 5.6 (Saint Venant–Kirchhoff material). *There exist two constants, called Lamé constants, $\lambda, \mu > 0$ such that*

$$W_{\mathbf{k}}(\mathbf{E}) = \frac{\lambda}{2} \text{tr}^2 \mathbf{E} + \mu \text{tr} \mathbf{E}^2. \quad (5.11)$$

It can be shown that further restrictions, from thermodynamic considerations, involve the Lamé constants.

5.1.1.4 Equilibrium Problem: Strong and Weak Formulations

The equilibrium problem for an hyperelastic body, in the reference configuration, under the action of assigned loads $\mathbf{b}_{\mathbf{k}}$ and $\mathbf{s}_{\mathbf{k}}$, can be formalised. With reference to Figure 5.2, assuming for the sake of simplicity imposed zero displacements over the surface portion $\partial\Omega_d$, the boundary-value equilibrium problem in the reference placement reads:

$$\left\{ \begin{array}{ll} \text{div} \mathbf{P} + \mathbf{b}_{\mathbf{k}} = \mathbf{0}, & \text{in } \Omega, \\ \mathbf{P} \mathbf{F}^T = \mathbf{F} \mathbf{P}^T, & \text{in } \Omega, \\ \mathbf{P} \mathbf{n}_{\mathbf{k}} = \mathbf{s}_{\mathbf{k}}, & \text{in } \partial\Omega_t, \\ \mathbf{P} = \frac{\partial W_{\mathbf{k}}}{\partial \mathbf{F}}(\mathbf{X}, \mathbf{F}), & \text{in } \Omega, \\ \mathbf{F} = \nabla \chi, & \text{in } \Omega, \\ \mathbf{u}(\mathbf{X}) = \mathbf{0}, & \text{in } \partial\Omega_d, \end{array} \right. \quad (5.12)$$

where $\mathbf{b}_{\mathbf{k}}$ is the body unit-volume body forces, acting on each material point of Ω , $\mathbf{n}_{\mathbf{k}}$ in the outward normal versor at a generic point $X \in \partial\Omega$, $\mathbf{s}_{\mathbf{k}}$ is the surface forces vector

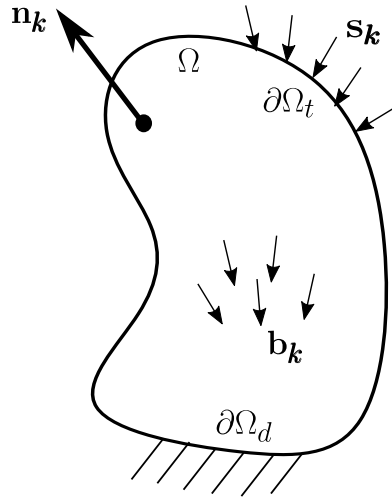


Figure 5.2: Loaded body \mathfrak{B} in the reference configuration

acting over the boundary portion $\partial\Omega_t$. The unknown field is generally the displacement vector field. If a displacement vector field \mathbf{u} satisfies (5.12), it is said a strong solution for the equilibrium problem.

For hyperelastic materials, the equilibrium Problem (5.12) can be formulated in variational terms. To do so, the set of kinematically admissible functions, i.e. the collection of displacements satisfying the boundary displacement condition on $\partial\Omega_d$, must be preliminary introduced.

Definition 5.7 (Kinematically admissible functions set).

$$\mathcal{A} := \{\psi : \bar{\Omega} \mapsto \mathbb{R}^3 : \psi \text{ is smooth and } \psi = \mathbf{0} \text{ on } \partial\Omega_d\}. \quad (5.13)$$

Then, the Total (Potential) energy functional can be defined as:

Definition 5.8 (Total potential energy).

$$\mathcal{F}(\psi) := \int_{\Omega} W_{\mathbf{k}}(\mathbf{X}, \nabla\psi) d\mathbf{X} - \int_{\Omega} \mathbf{b}_{\mathbf{k}} \cdot \psi d\mathbf{X} - \int_{\partial\Omega_t} \mathbf{t}_{\mathbf{k}} \cdot \psi d\mathbf{X}, \quad \psi \in \mathcal{A}. \quad (5.14)$$

The following Theorem finally links the equilibrium Problem (5.12) to the functional (5.14):

Theorem 5.5 (Equilibrium as a stationary point of the total potential energy). *If $\psi \in \mathcal{A}$ satisfies Eq. (5.12), then ψ is, at least formally, a stationary point of \mathcal{F} (Eq. (5.14)).*

The stability of the stationary points of Theorem 5.5 depends on the second variation of the functional (5.14). If $\psi \in \mathcal{A}$ is a stationary point of Eq. (5.14) is said a weak solution of the (weak) equilibrium problem expressed in Theorem 5.5. Of course, a strong solution is so also for the weak equilibrium problem. The converse is not generally true, unless the weak solution is as regular as to make the first equation of Eq. (5.12) meaningful.

5.1.2 Linearised Elasticity

Under further hypotheses of small displacements and small displacement's gradients, assuming an unstressed reference configuration, the stress field linearly depends upon the linearised strain tensor field. Moreover, the strain tensor linearly depends upon the symmetric part of the displacement gradient. In particular, for an hyperelastic linear material:

Theorem 5.6 (Elasticity tensor for hyperelastic linear materials). *There exists a fourth-order tensor,*

$$\mathbb{C} := \frac{\partial W_{\mathbf{k}}}{\partial \mathbf{E}}(\mathbf{X}, \mathbf{E}), \quad \mathbb{C} \in \mathbb{P}_{\text{sym}}, \quad (5.15)$$

called elasticity tensor, such that

(a) (minor symmetries)

$$\mathbb{C}_{ijhk} = \mathbb{C}_{jihk} = \mathbb{C}_{ijkh}, \quad (5.16)$$

(b) (major symmetries)

$$\mathbb{C}_{ijhk} = \mathbb{C}_{hki j}, \quad (5.17)$$

(c) (Cauchy' stress tensor)

$$\mathbf{T} = \mathbb{C}[\mathbf{E}], \quad (5.18)$$

having defined

$$\mathbf{H} := \nabla \mathbf{u}, \quad \mathbf{E} := \text{sym}(\mathbf{H}), \quad \mathbf{W} := \text{skw}(\mathbf{H}). \quad (5.19)$$

In this case of linearised elasticity, tensor \mathbf{E} of Eq. (5.19) constitutes the strain measure. More explicitly, the stored-energy density function is expressed by

$$\frac{1}{2} \mathbf{T} \cdot \mathbf{E} = \frac{1}{2} \mathbb{C}[\mathbf{E}] \cdot \mathbf{E}. \quad (5.20)$$

From the characterisation of the elasticity tensor \mathbb{C} of Theorem 5.6, a further important property descends:

Theorem 5.7 (Coercivity of the elasticity tensor). *There exists a constant $C > 0$ such that*

$$\mathbb{C}[\mathbf{E}] \cdot \mathbf{E} \geq C|\mathbf{E}|^2, \quad \forall \mathbf{E} \in \text{Sym}. \quad (5.21)$$

A representation Theorem holds for hyperelastic isotropic materials:

Theorem 5.8 (Representation Theorem for hyperelastic linear isotropic elasticity tensor). *A fourth-order tensor $\mathbb{C} : \text{Sym} \mapsto \text{Sym}$ is isotropic if and only if there exist two constants*

$\mu > 0$ and λ such that

$$\mathbb{C}[\mathbf{E}] = 2\mu\mathbf{E} + \lambda \operatorname{tr}(\mathbf{E})\mathbf{I}, \quad \forall \mathbf{E} \in \operatorname{Sym}. \quad (5.22)$$

A property of linearised elasticity, i.e. assuming small displacements and gradients, is that the reference configuration is *close* to the deformed one. This means that, neglecting higher-order terms, the two configurations are basically the same up to the first order expansion. As a result, the equilibrium problem can be formulated in the reference configuration, which has the great advantage to be known. Accordingly, the elastic equilibrium problem reads:

$$\left\{ \begin{array}{ll} \operatorname{div} \mathbf{T} + \mathbf{b}_k = \mathbf{0}, & \text{in } \Omega, \\ \mathbf{T} = \mathbf{T}^T, & \text{in } \Omega, \\ \mathbf{T} \mathbf{n}_k = \mathbf{s}_k, & \text{in } \partial\Omega_t, \\ \mathbf{T} = \mathbb{C}[\mathbf{E}], & \text{in } \Omega, \\ \mathbf{E} = \operatorname{sym}(\nabla \mathbf{u}), & \text{in } \Omega, \\ \mathbf{u} = \mathbf{0}, & \text{in } \partial\Omega_d, \end{array} \right. \quad (5.23)$$

where the unknown is the displacement field \mathbf{u} .

In finite elasticity, the existence of the equilibrium solution is still an open topic, at least in the full generality of the problem. The stored-energy functional cannot be convex for physical reasons: for instance, a convex stored-energy density functional would disagree with the principle of Material Frame Indifference (Principle 5.2), as stated before. Moreover, a strictly-convex one would exclude body instabilities and equilibrium point bifurcations. See, for instance, (Ball, 1976; Paroni, 2008). However, in linearised elasticity, an important result of existence and uniqueness holds.

Theorem 5.9 (Existence and uniqueness of the solution for the linearised elasticity equilibrium problem). *Let the external data, viz. external loads and imposed displacements at the boundary, be assigned. The linearised elasticity equilibrium Problem (5.23) admits a unique solution which depends with continuity from the data.*

Of course, also in linearised elasticity the equilibrium problem can be formulated in variational terms. In analogy to finite elasticity, the total energy functional reads:

Definition 5.9 (Total potential energy in linearised elasticity).

$$\mathcal{F}(\boldsymbol{\psi}) := \frac{1}{2} \int_{\Omega} \mathbb{C}[\mathbf{E}] \cdot \operatorname{sym}(\nabla \boldsymbol{\psi}) d\mathbf{X} - \int_{\Omega} \mathbf{b}_k \cdot \boldsymbol{\psi} d\mathbf{X} - \int_{\partial\Omega_t} \mathbf{t}_k \cdot \boldsymbol{\psi} d\mathbf{X}, \quad \boldsymbol{\psi} \in \mathcal{A}. \quad (5.24)$$

Then,

Theorem 5.10 (Total potential energy minimum). *Let the external data, viz. external loads and imposed displacements at the boundary, be assigned. Then, $\mathbf{u} \in \mathcal{A}$ is the unique solution of Problem (5.23) if and only if $\mathcal{F}(\mathbf{u}) = \min_{\boldsymbol{\psi} \in \mathcal{A}} \mathcal{F}(\boldsymbol{\psi})$.*

5.2 The Direct Method of the Calculus of Variations

This section is inspired by the textbooks (Buttazzo, 1989; Dacorogna, 2007; Rindler, 2018). In the previous Section, it has been shown that the elastic equilibrium problem for an hyperelastic body can be formulated in variational terms. Some well-established techniques allow to tackle the equilibrium problem in a variational framework. These techniques are referenced as Direct Method of the Calculus of Variations, deriving from the work of Leonida Tonelli (see, for example (Tonelli, 1915, 1920)).

An abstract problem of the Calculus of Variations, suitable for the topic at hand, is the following minimisation problem of the total energy represented by Eq. (5.24):

$$\begin{aligned} \min_{\psi \in \mathcal{A}} \mathcal{F}(\psi), \\ \mathcal{A} := \{\psi \in W^{1,2}(\Omega; \mathbb{R}^3) \text{ with } \psi|_{\partial\Omega_d} = \mathbf{0}\} \end{aligned} \quad (5.25)$$

where \mathcal{F} is defined in Eq. (5.24), Ω is an open, bounded Lipschitz-regular domain, $W^{1,2}(\Omega; \mathbb{R}^3)$ (or $H^1(\Omega; \mathbb{R}^3)$) is a Sobolev functional space, which happens to be also a Hilbert space, and $\mathbf{0} \in W^{1/2,2}(\partial\Omega_d; \mathbb{R}^3)$ (or $H^{1/2}(\partial\Omega_d; \mathbb{R}^3)$). The involved functional spaces are characterised in the following Definitions.

Definition 5.10 (Lebesgue L^2 space).

$$L^2(\Omega, \mathbb{R}^3) := \left\{ \mathbf{v} : \Omega \mapsto \mathbb{R}^3 : \left(\int_{\Omega} |\mathbf{v}|^2 \right)^{1/2} < \infty \right\}. \quad (5.26)$$

Definition 5.11 (Sobolev H^1 space).

$$H^1(\Omega, \mathbb{R}^3) := \{\mathbf{v} : \Omega \mapsto \mathbb{R}^3 : \mathbf{v} \in L^2(\Omega, \mathbb{R}^3), \nabla \mathbf{v} \in L^2(\Omega, \text{Lin})\}. \quad (5.27)$$

Definition 5.12 (Sobolev $H^{1/2}$ trace space).

$$H^{1/2}(\partial\Omega_d, \mathbb{R}^3) := \{\mathbf{v} \in L^2(\partial\Omega_d; \mathbb{R}^3) \mid \exists \mathbf{u} \in H^1(\Omega; \mathbb{R}^3) : \mathbf{v} = \text{tr}(\mathbf{u}) := \mathbf{u}|_{\partial\Omega_d}\}. \quad (5.28)$$

Some definitions are preliminary needed to introduce in the following some pivotal concepts. Let X be a topological space, and let \mathcal{N} be the family of all open sets containing the generic point $x \in X$. Then, introducing $\bar{\mathbb{R}} := \mathbb{R} \cup \{-\infty, +\infty\}$ as the extended Real Line:

Definition 5.13 (Lower and upper limit). *Assume $\mathcal{F} : X \mapsto \bar{\mathbb{R}}$. The lower limit (\liminf) of \mathcal{F} at $x \in X$ is defined as*

$$\liminf_{y \rightarrow x} \mathcal{F}(y) = \sup_{U \in \mathcal{N}(x)} \inf_{y \in U} \mathcal{F}(y) \quad (5.29)$$

whilst the upper limit (lim sup) of \mathcal{F} at x is defined as

$$\limsup_{y \rightarrow x} \mathcal{F}(y) = \inf_{U \in \mathcal{N}(x)} \sup_{y \in U} \mathcal{F}(y). \quad (5.30)$$

Intuitively, the lower limit of a function at a point x is the largest value, as neighbours of x may vary, among the smallest values assumed by the function in every of such neighbours. Similarly, the upper limit of a function at a point x is the smallest value, as neighbours of x may vary, among the largest values assumed by the function in every of such neighbours.

The following generalised notion of continuity will play a pivotal role in the following.

Definition 5.14 (Lower-semicontinuity). *A function $\mathcal{F} : X \mapsto \bar{\mathbb{R}}$ is lower-semicontinuous (LSC) at a point $x \in X$, if for every $t \in \mathbb{R}$ with $t < \mathcal{F}(x)$, there exists an open set $U \in \mathcal{N}(x)$ such that $t < \mathcal{F}(y)$ for every $y \in U$. \mathcal{F} is LSC on X if it is LSC at each point of X .*

Equivalently, a function is LSC if $\forall t \in \mathbb{R}$ the set $\{x \in X : \mathcal{F}(x) < t\}$ is closed in X .

Just to give an intuition with a mono-dimensional example, Figure 5.3a shows a LSC function. Conversely, Figure 5.3b shows a function which is not LSC. It can be easily verified with the second definition of LSC functions provided in Definition 5.14.

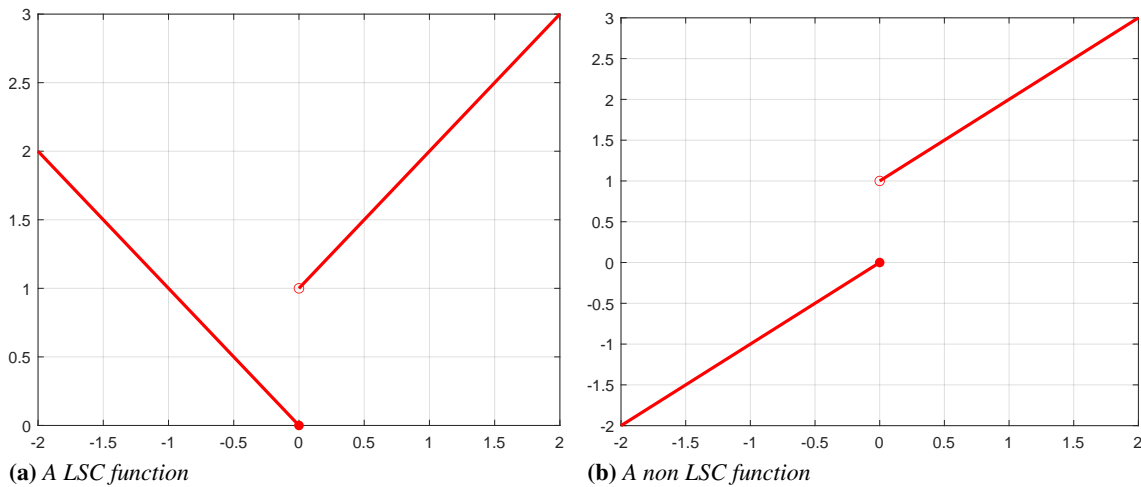


Figure 5.3: Comparison between a LSC and a non LSC function.

To prove the main result of this Section, some further concepts are needed.

Definition 5.15 (Sequentially lower-semicontinuity). *A function $\mathcal{F} : X \mapsto \bar{\mathbb{R}}$ is sequentially lower-semicontinuous (SLSC) at a point $x \in X$, if for every sequence (x_j) converging to x in X*

$$\mathcal{F}(x) \leq \liminf_{j \rightarrow +\infty} \mathcal{F}(x_j). \quad (5.31)$$

Definition 5.16 (Sequentially compact set). *A set $K \subseteq X$ is sequentially compact if every sequence in K has one subsequence converging to an element of K .*

Definition 5.17 (Sequential coercivity). *A function $\mathcal{F} : X \mapsto \bar{\mathbb{R}}$ is sequentially coercive on X if the closure of the set $x \in X : \mathcal{F}(x) < t$ is sequentially compact for every $t \in \mathbb{R}$.*

All these ingredients are enough to state the main Theorem of the Direct Method of the Calculus of Variations:

Theorem 5.11 (Direct Method of the Calculus of Variations). *Let X be a topological space endowed with the weak topology. Let $\mathcal{F} : X \mapsto \bar{\mathbb{R}}$ be a sequentially coercive and SLSC function. Then, Problem (5.25) admits at least one solution.*

In particular, for Problem (5.25) the coercivity and the lower-semicontinuity are ensured by the following Theorems, specialised for the stored-energy density function:

Theorem 5.12 (Coercivity on Sobolev H^1 space). *The hypotheses on the elasticity tensor and Eq. (5.25) \implies sequential coercivity on the space $H^1(\Omega, \mathbb{R}^3)$.*

Theorem 5.13 (Tonelli-Serrin). *An integrand function $f : \Omega \times \text{Lin} \rightarrow [0, \infty)$ that is (Lebesgue-)measurable in the first argument, continuous and convex in the second argument, is SLSC in $H^1(\Omega; \mathbb{R}^3)$.*

It can be shown that the stored-energy functional satisfies Theorem 5.13 and that it is coercive. Therefore, for Theorem 5.11 the elastic linearised problem of equilibrium admits a solution.

This section is concluded by a fundamental inequality (which plays also a pivotal role for the proof of the coerciveness of the stored-energy functional) that will be used in the following:

Theorem 5.14 (Korn's inequality). *Let Ω be a bounded regular domain, having a regular boundary. There exists a constant $C > 0$ such that for each function $\mathbf{v} \in H^1(\Omega)$ vanishing on the boundary,*

$$\|\nabla \mathbf{v}\|_{L^2(\Omega)} \leq C \|\text{sym}(\nabla \mathbf{v})\|_{L^2(\Omega)}. \quad (5.32)$$

The result of this inequality is somewhat *unexpected*, since the nine component of $\nabla \mathbf{v}$ are controlled by six of their linear combinations (components of $\text{sym}(\nabla \mathbf{v})$) in the $L^2(\Omega)$ space.

5.3 Γ -convergence

The brief collection of results is inspired by the classical textbooks on the topic (Dal Maso, 1993; Braides, 2002). In many physical problems, there are some parameters such that, as they may vary, it is possible to obtain an asymptotic property or behaviour of the primitive problem. The asymptotic problems can be used to replace the primitive ones, since, generally, the formers have a simpler and more understandable structure. These peculiar kind of problems may be formalised as the study of the limit (or asymptotic)

behaviour of a family of functionals depending on a scale parameter ε , in some space X_ε , as follows:

$$\min\{\mathcal{F}_\varepsilon(v) : v \in X_\varepsilon\}. \quad (5.33)$$

As stated, the basic idea is to substitute Problem (5.33) with a somehow simpler one, no more depending on ε and which may capture effectively the basic aspects of the actual solution of (5.33). In other words, the asymptotic problem is sought to converge, in a suitable sense to be specified, to the actual one, preserving information on the minimum and minimiser of the actual problem. Formally, the limit problem is of the form

$$\min\{\mathcal{F}_\infty(v) : v \in X\}. \quad (5.34)$$

Keeping this in mind, the Γ -convergence is a suitable tool for this purpose. It is a variational convergence that aims at the convergence of minima and minimisers of the original Problem (5.33) to the minima and minimiser of the limit Problem (5.34). In so doing, it is expected that the main properties of the solution of Problem (5.33) are properly caught by the solution of the asymptotic Problem (5.34). This variational convergence appeared for the first time in the seminal work by Ennio De Giorgi and Tullio Franzoni (De Giorgi & Franzoni, 1975).

Definition 5.18 (Γ -convergence). *Let X be a topological space. A sequence of LSC functions $\mathcal{F}_j : X \mapsto \bar{\mathbb{R}}$ ($j \in \mathbb{N}$) Γ -converges in X to a function $\mathcal{F}_\infty : X \mapsto \bar{\mathbb{R}}$ if the following conditions are satisfied:*

- (lim inf inequality) for every sequence $(x_j) \in X$ converging to $x \in X$

$$\mathcal{F}_\infty(x) \leq \liminf_j \mathcal{F}_j(x_j); \quad (5.35)$$

- (recovery sequence) for all $x \in X$ there exists a sequence $(x_j) \in X$, converging to some $x \in X$ such that

$$\mathcal{F}_\infty(x) = \lim_j \mathcal{F}_j(x_j). \quad (5.36)$$

The function \mathcal{F}_∞ is said the Γ -limit of \mathcal{F}_j , writing $\mathcal{F}_\infty = \Gamma\text{-lim}_j \mathcal{F}_j$.

As a matter of fact, a well-posed Γ -convergence concept must rely on the possibility of obtaining converging sequences from minimisers of Eq. (5.33). A preliminary fundamental question, then, is about the compactness: the candidate space X for the limit problem shall be the one where the compactness argument holds. Moreover, also the lower-semicontinuity plays an important role in the definition. Once a notion of convergence $u_\varepsilon \rightarrow u$ and the environment space have been determined, the functional \mathcal{F}_∞ of (5.34) is obtained as an optimisation between lower and upper bounds of \mathcal{F}_ε . The Γ -convergence of \mathcal{F}_ε is, roughly speaking, the requirement that these two bounds coincide.

Γ -convergence enjoys important properties, such as:

- (a) The Γ -limit, if it exists, is unique;

- (b) The Γ -convergence implies the convergence of minimum problems and the convergence of (sub)sequences of minimisers to the minimisers of the Γ -limit.

Theorem 5.15 (Convergence of minima and minimisers). *Let (\mathcal{F}_j) be a sequence of functions on X such that for all $j \in \mathbb{N}$ there exists a compact $K \subset X$ with the property that $\inf_X \mathcal{F}_j = \inf_K \mathcal{F}_j$. Let $\mathcal{F}_\infty = \Gamma\text{-}\lim_j \mathcal{F}_j$. Then, \mathcal{F}_∞ has a minimiser and*

$$\exists \min_X \mathcal{F}_\infty = \lim_j \inf_X \mathcal{F}_j \quad (5.37)$$

Moreover, if $(x_j) \in X$ is a bounded sequence such that $\lim_j \mathcal{F}_j(x_j) = \lim_j \inf_X \mathcal{F}_j$, then every accumulation point of a convergent subsequence of (x_j) is a minimiser for \mathcal{F}_∞ .

- (c) The Γ -limit is stable under continuous perturbations. This means that the convergence is unaffected if arbitrary continuous terms are added, in the sense specified by the following

Theorem 5.16 (Stability under continuous perturbations). *If (\mathcal{F}_j) Γ -converges to \mathcal{F}_∞ and $g : X \mapsto \bar{\mathbb{R}}$ is a continuous function, then $(\mathcal{F}_j + g)$ Γ -converges to $(\mathcal{F}_\infty + g)$.*

- (d) The Γ -limit \mathcal{F}_∞ is a LSC functional. Then, \mathcal{F}_∞ is suitable to operate in the framework of the Direct Method of Calculus of Variations.

Comparing the Γ -convergence to others variational asymptotic techniques, such as asymptotic expansion, it is possible to see that the former does not require an *ansatz* for the determination of the \mathcal{F}_ε lower bound. Moreover, in the upper-bound search, the ansatz on the minimiser is driven by the lower bound inequality itself.

For a complete treatment of the topic, the reader is addressed to the classical works by Dal Maso (1993), Braides (2002).

In the reminder of the Section, some example on the Real Line will follow, in order to clarify the intuitive notion of Γ -limit. Assume $n \in \mathbb{N}$, $x \in \mathbb{R}$.

Example 1 Consider the family of functionals $\mathcal{F}_n := \sqrt{2\varepsilon} n x e^{-n^2 x^2}$. It is easy to show that the functional converges to the identical null function pointwise. However, the Γ -limit is

$$\mathcal{F}_\infty = \begin{cases} 0, & x \neq 0, \\ -1, & x = 0. \end{cases} \quad (5.38)$$

Generally speaking, the Γ -limit is different from the pointwise limit (in particular the former lies always below the latter) and is LSC. Moreover, the sequence of minima $\{-1\}$ converges to the minima of the Γ -limit, and the sequence of minimiser $\{-1/(\sqrt{2\varepsilon}n)\}$ (which is also the recovery sequence) converges to the Γ -limit infimum.

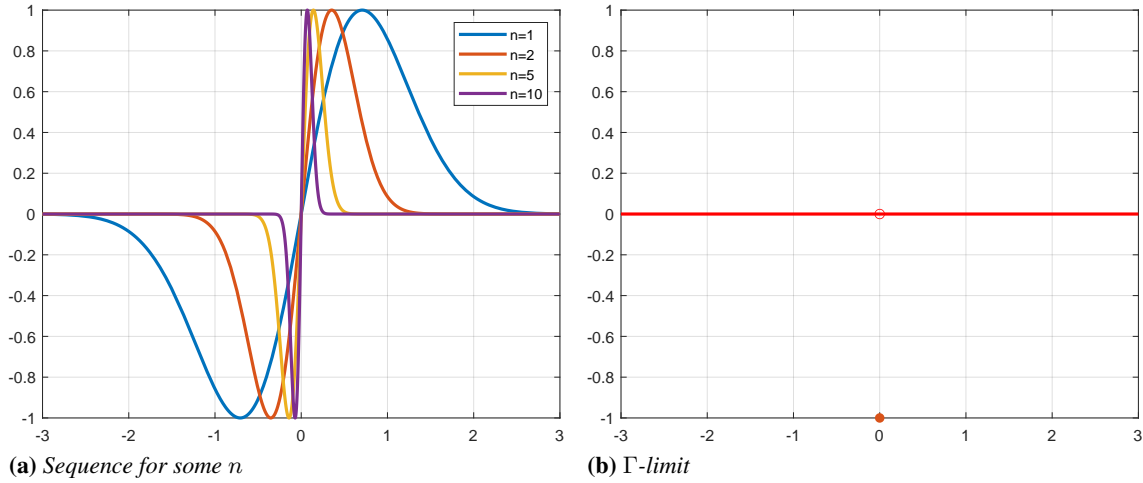


Figure 5.4: Example 1: family of functionals $\mathcal{F}_n := \sqrt{2}e n x e^{-n^2 x^2}$ and Γ -limit

Example 2 Consider the family of functionals $\mathcal{F}_n := \arctan(n x)$. It is easy to show that the functional pointwise converges to the function

$$\mathcal{F} = \begin{cases} \pi/2, & x > 0, \\ 0, & x = 0, \\ -\pi/2, & x < 0. \end{cases} \quad (5.39)$$

However, the Γ -limit is

$$\mathcal{F}_\infty = \begin{cases} \pi/2, & x > 0, \\ -\pi/2, & x \leq 0 \end{cases} \quad (5.40)$$

Also in this case the Γ -limit is different from the pointwise limit and is a LSC function.

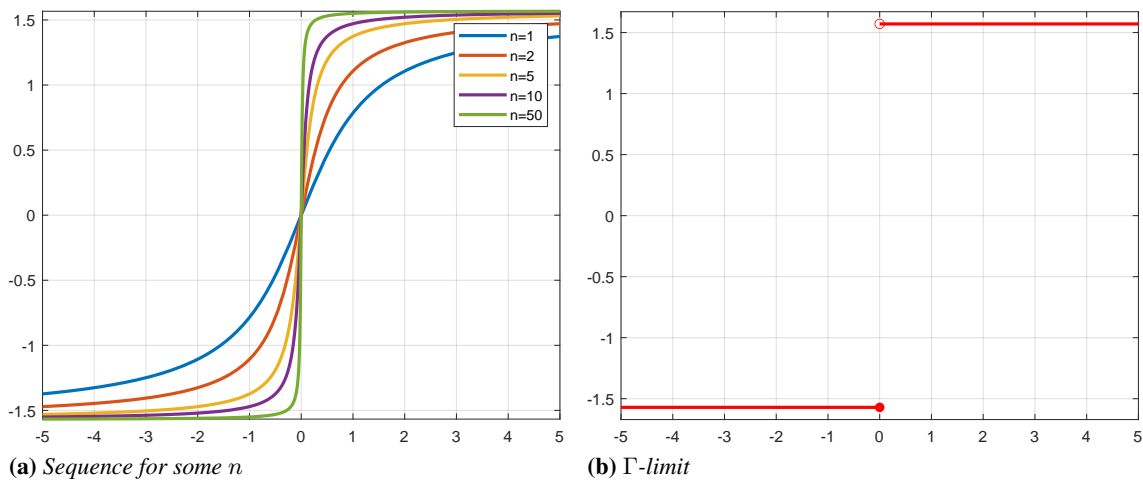


Figure 5.5: Example 2: family of functionals $\mathcal{F}_n := \arctan(n x)$ and Γ -limit

Example 3 Consider the family of functionals $\mathcal{F}_n := \sin(nx)$. It is easy to show that the pointwise limit does not exist, since the functional oscillations around the Real Line. However, the Γ -limit exists, and it is the constant function $\mathcal{F}_\infty = -1$. Also in this case the Γ -limit is a LSC function, and the minima and the minimisers converge.

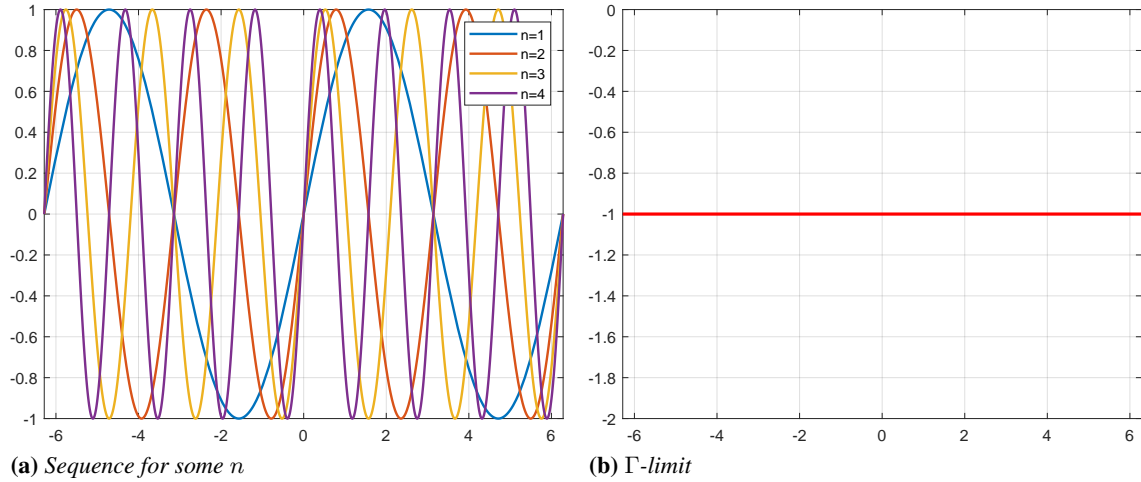


Figure 5.6: Example 3: family of functionals $\mathcal{F}_n := \sin(nx)$ and Γ -limit

5.4 Conclusions

Starting from classic notions of Continuum Mechanics, it has been recalled that the equilibrium problem for hyperelastic materials admits a variational structure. Moreover, some properties of the stored-energy density functional allows for the use of the powerful Direct Method of the Calculus of Variations in establishing the existence and, possibly, the uniqueness of the solution. In this context, the notion of Γ -limit has been introduced, showing its link with the Direct Method and the effectiveness in dealing with the asymptotic model reduction.

Part III

Improving the Optimal Design of Composite Structures

On Buckling and Blending

The goal of this Chapter is to answer research questions RQ1 and RQ2.

Section 6.1 answers research question RQ1. The closed-form expression of the buckling factor and its gradient, calculated on LFEMs, when scale transition is taken into account, is derived. Section 6.2 introduces and formalises the blending problem, where new stricter blending constraints are derived. Section 6.3 faces the problem of the stacking sequence recovery phase. A general numerical approach is presented, together with a mathematical justification. These last two Sections answer research question RQ2. Section 6.4 presents an alternative approach for the stack recovery phase, based on the particular class of QT QH SSs, already presented in Section 4.3. Finally, Section 6.5 concludes the Chapter with some meaningful considerations.

In the following, calculations are performed adopting the polar formalism already introduced in Chapter 4. This choice is due to the fact that PPs are tensor invariant quantities and are related to the material symmetries. Moreover, as explained in Chapter 9, the feasible domain of laminates is non-convex, for either PPs and LPs. However, the latter parameters do not have the aforementioned properties of PPs. Hence, PPs shall be the preferable choice for the description of plane anisotropy. Nevertheless, with the due modifications, the same results can be adapted in the LPs space.

6.1 Multi-scale Formulation of Buckling Requirement

In order to correctly assess local phenomena, such as instabilities, a GL approach must be adopted. As already said, three are the main issues connected with the GL approach:

1. the automatic detection of some ZOIs which are likely to be critical in terms of buckling strength;

2. the automatic generation of a refined LFEMs from the identified ZOIs;
3. the correct transfer of loads from the GFEM into the LFEMs as suitable BCs.

Hereafter, the GL approach will be developed for the buckling response assessment only. In particular, the buckling factors are evaluated in the LFEMs. When using a deterministic optimisation algorithm, two main challenges arise for the analytic derivation of the buckling eigenvalue sensitivity (see Figure 2.3 for a conceptual scheme of the approach. This figure should always be kept in mind.):

1. in the framework of the substructuring technique with imposed displacements on the boundary, under the hypothesis of null unit-volume body forces (see also Eq. (5.12)), the eigenvalue buckling analysis carried out on the LFEM is a pure Dirichlet problem. It means that only non-trivial BCs in terms of generalised displacements are assigned;
2. the BCs imposed on the LFEM are strictly related to the displacement field resulting from the GFEM, thus coupling effects between the GFEM and the LFEM must be integrated into the analytical expression of the gradient of the buckling factor resulting from the LFEM.

6.1.1 Constraint

Preliminary, let n_{DOF} denote the number of DOFs of the unconstrained GFEM. Since BCs are applied at n_{BC} DOFs, the constrained GFEM has $n_{\text{IN}} := n_{\text{DOF}} - n_{\text{BC}}$ DOFs. Let \mathbf{u} be the solution of the equilibrium problem for the GFEM:

$$\mathbf{K}\mathbf{u} - \mathbf{f} = \mathbf{0}, \quad (6.1)$$

where \mathbf{u} is the vector of the unknowns nodal displacements and rotations, \mathbf{f} is the vector of external generalised nodal forces, and $\mathbf{K} \in \mathbb{M}_{s+}^{n_{\text{IN}} \times n_{\text{IN}}}$ is the (constrained) stiffness matrix of the GFEM.

$\mathbb{M}^{m \times n}$ denotes the space of real-valued matrices having m rows and n columns. Noteworthy subsets are defined with the use of subscripts $_s$ and $_{s+}$. The former denotes the set of symmetric matrices, the latter the set of symmetric positive-definite ones (see also Section 5.1.1.1).

The buckling constraint can be formulated as:

$$g_{\text{buck}} = 1 - \lambda \leq 0, \quad (6.2)$$

where λ is the first buckling factor of the associated eigenvalue problem (formulated in the LFEM)

$$(\mathbf{K}^b + \lambda \mathbf{K}_\sigma^b) \boldsymbol{\psi}^b = \mathbf{0}, \quad (6.3)$$

where $\mathbf{K}^b \in \mathbb{M}_{s+}^{n_{\text{IN}}^b \times n_{\text{IN}}^b}$ is the reduced stiffness matrix of the LFEM, $\mathbf{K}_\sigma^b \in \mathbb{M}_s^{n_{\text{IN}}^b \times n_{\text{IN}}^b}$ is the reduced stress-stiffness matrix of the LFEM, $\boldsymbol{\psi}^b$ is the reduced eigenvector associated

to λ . Note that \mathbf{K}_σ^b is not, in general, positive-definite.

Label b , unless specified, will denote quantities defined in the LFEM.

6.1.2 Buckling Factor Gradient in Multi-scale Context

Let n_{vars} be the number of design variables of the optimisation problem. By differentiating Eq. (6.2) with respect to the generic design variable ξ_j (four variables for each panel, see Eq. (4.32)), one obtains:

$$(\nabla_{\xi} g_{\text{buck}})_j := \frac{\partial g_{\text{buck}}}{\partial \xi_j} = -\frac{\partial \lambda}{\partial \xi_j}. \quad (6.4)$$

The next three Subsections of Section 6.1.2 are dedicated to the derivation of the explicit analytical form for Eq. (6.4).

6.1.2.1 Initialisation of the Gradient Expression

Passing to the weak formulation, the generalised eigenvalue problem for the LFEM can be stated as follows:

$$\boldsymbol{\psi}_b^T (\mathbf{K}^b + \lambda \mathbf{K}_\sigma^b) \boldsymbol{\psi}_b = 0, \quad (6.5)$$

As usually done in classical buckling eigenvalue analyses, \mathbf{K}_σ^b is calculated from the stress field solution of the (static) equilibrium boundary problem of the LFEM subject to the same BCs of the original eigenvalue buckling problem. However, in the framework of the considered GL modelling approach, the equilibrium boundary problem of the LFEM is of the Dirichlet's type: non-zero displacements are imposed at some DOFs, which can be collected in the set I_{BC}^b whose cardinality is n_{BC}^b . On the other hand, the unknown DOFs are collected in the set I_{IN}^b whose cardinality is n_{IN}^b . Moreover, BCs depend on the displacement field solution of the GFEM equilibrium Problem (6.1). Therefore, the key-point is to express properly the equilibrium displacement boundary problem (and the related derivatives) for the LFEM. To do so, it is convenient to introduce the following two operators.

Definition 6.1 (Annihilating operator \mathfrak{Z}). *Given a matrix $\mathbf{M} \in \mathbb{M}^{m \times n}$ and the two sets of positive natural numbers $R \subset \{i \mid 1 \leq i \leq m\}$ and $C \subset \{j \mid 1 \leq j \leq n\}$, the operator $\mathfrak{Z}(\mathbf{M}, R, C)$ returns a matrix obtained by annihilating the i -th row and the j -th column of \mathbf{M} , $\forall i \in R$ and $\forall j \in C$. Similarly, $\mathfrak{Z}(\mathbf{v}, R)$ denotes the vector obtained by annihilating the i -th component of vector $\mathbf{v} \in \mathbb{M}^{n \times 1}$, $\forall i \in R$. Operator $\mathfrak{Z}(\cdot)$ preserves the dimensions of its argument.*

Definition 6.2 (Reducing operator \mathfrak{R}). *Given a matrix $\mathbf{M} \in \mathbb{M}^{m \times n}$ and the two sets of positive natural numbers $R \subset \{i \mid 1 \leq i \leq m\}$ and $C \subset \{j \mid 1 \leq j \leq n\}$, the operator $\mathfrak{R}(\mathbf{M}, R, C)$ returns the matrix obtained by suppressing the i -th row and the j -th column of \mathbf{M} , $\forall i \in R$ and $\forall j \in C$. Similarly, $\mathfrak{R}(\mathbf{v}, R)$ denotes the vector obtained by suppressing the i -th row of \mathbf{v} , $\forall i \in R$.*

Since no external nodal forces are applied, the equilibrium equation of the LFEM reads

$$\hat{\mathbf{K}}^b \hat{\mathbf{u}}_0^b = \hat{\mathbf{f}}_0^b, \quad (6.6)$$

where $\hat{\mathbf{K}}^b \in \mathbb{M}_s^{n_{\text{DOF}}^b \times n_{\text{DOF}}^b}$ is the (singular) stiffness matrix of the LFEM, $\hat{\mathbf{u}}_0^b \in \mathbb{M}^{n_{\text{DOF}}^b \times 1}$ is the vector collecting the set of DOFs of the LFEM static analysis (both imposed displacements and unknown ones) and $\hat{\mathbf{f}}_0^b \in \mathbb{M}^{n_{\text{DOF}}^b \times 1}$ is the vector of the unknown nodal forces (occurring at nodes where BCs on generalised displacements are applied). In the above expressions $n_{\text{DOF}}^b = n_{\text{BC}}^b + n_{\text{IN}}^b$.

As discussed in (Reddy, 2005; B. Wu et al., 2007), Problem (6.6) can be solved after a proper rearranging. In particular, if $\hat{u}_s \in \hat{\mathbf{u}}_0^b$ (for some s) is assigned, one must set $\hat{K}_{ss} = 1$, $\hat{K}_{is} = \hat{K}_{si} = 0$ for $i \neq s$ and subtract to the right-hand side the s -th column of the (unmodified) stiffness matrix, multiplied by \hat{u}_s . After this operation, the new system can be reduced, as usually, and the unknown nodal displacements can be determined.

Remark 6.1. Let $A \subset \{i \mid i = 1, \dots, n\}$ and $B \subset \{i \mid i = 1, \dots, n\}$ be two sets such that $A \cap B = \emptyset$ and $\sharp(A \cup B) = n$. Therefore $\mathbf{u} = \mathfrak{Z}(\mathbf{u}, A) \oplus \mathfrak{Z}(\mathbf{u}, B)$, $\forall \mathbf{u} \in \mathbb{M}^{n \times 1}$.

By applying Remark 6.1 to $\hat{\mathbf{u}}_0^b$ and $\hat{\mathbf{f}}_0^b$, one obtains:

$$\begin{aligned} \hat{\mathbf{u}}_0^b &= \mathfrak{Z}(\hat{\mathbf{u}}_0^b, I_{\text{BC}}^b) \oplus \mathfrak{Z}(\hat{\mathbf{u}}_0^b, I_{\text{IN}}^b) := \hat{\mathbf{u}}^b + \hat{\mathbf{u}}_{\text{BC}}^b, \\ \hat{\mathbf{f}}_0^b &= \mathfrak{Z}(\hat{\mathbf{f}}_0^b, I_{\text{BC}}^b) \oplus \mathfrak{Z}(\hat{\mathbf{f}}_0^b, I_{\text{IN}}^b) := \hat{\mathbf{0}} + \hat{\mathbf{f}}_{\text{BC}}^b, \end{aligned} \quad (6.7)$$

where only vector $\hat{\mathbf{u}}_{\text{BC}}^b$ is known, corresponding to the BCs imposed in the LFEM. Therefore, Problem (6.6) becomes

$$\hat{\mathbf{K}}^b \hat{\mathbf{u}}^b + \hat{\mathbf{K}}^b \hat{\mathbf{u}}_{\text{BC}}^b = \hat{\mathbf{0}} + \hat{\mathbf{f}}_{\text{BC}}^b. \quad (6.8)$$

To solve for the unknown part of $\hat{\mathbf{u}}_0^b$, the operator \mathfrak{R} of Definition 6.2 must be applied to Eq. (6.8): the resulting reduced system reads

$$\mathbf{K}^b \mathbf{u}^b + \mathbf{K}_{\text{BC}}^b \mathbf{u}_{\text{BC}}^b = \mathbf{0}, \quad (6.9)$$

where $\mathbf{K} := \mathfrak{R}(\hat{\mathbf{K}}^b, I_{\text{BC}}^b, I_{\text{BC}}^b)$, $\mathbf{u}^b := \mathfrak{R}(\hat{\mathbf{u}}_0^b, I_{\text{BC}}^b)$, $\mathbf{K}_{\text{BC}}^b := \mathfrak{R}(\hat{\mathbf{K}}^b, I_{\text{BC}}^b, I_{\text{IN}}^b)$, $\mathbf{u}_{\text{BC}}^b := \mathfrak{R}(\hat{\mathbf{u}}_0^b, I_{\text{IN}}^b)$ and $\mathfrak{R}(\hat{\mathbf{f}}_{\text{BC}}^b, I_{\text{BC}}^b) = \mathbf{0}$. Inasmuch as \mathbf{u}_{BC}^b depends on the GFEM solution, it is convenient to introduce the linear map

$$\mathbf{P} : \mathbf{u} \mapsto \mathbf{u}_{\text{BC}}^b, \quad \mathbf{P}\mathbf{u} = \mathbf{u}_{\text{BC}}^b, \quad \mathbf{P} \in \mathbb{M}^{n_{\text{BC}}^b \times (n_{\text{DOF}}^b - n_{\text{BC}}^b)}, \quad (6.10)$$

whose aim is to determine the BCs to be imposed to the LFEM (in terms of nodal displacements), starting from the solution of the static analysis carried out on the GFEM. In particular, the number of nodes belonging to the boundary of the LFEM, where BCs are applied, is different (usually larger) than the number of nodes located on the same boundary where the known displacement field is extracted from the GFEM results. Furthermore, meshes may be completely dissimilar, as shown in Figure 6.1 (boundary of LFEM in red,

GFEM mesh in black).

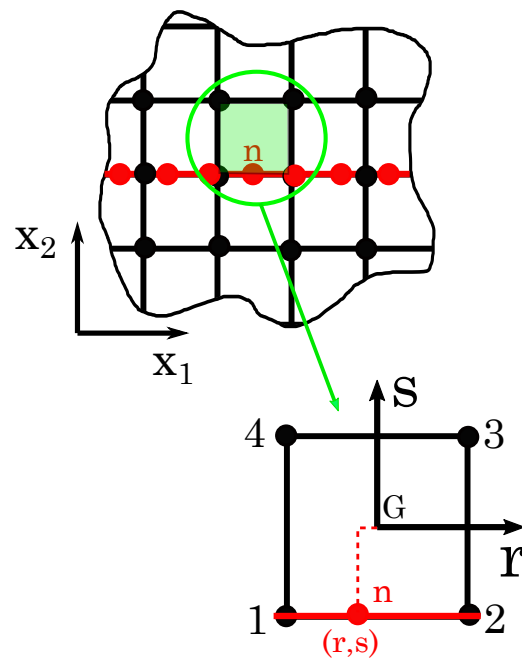


Figure 6.1: Differences between GFEM and LFEM meshes

The construction of \mathbf{P} can be done according to the steps listed in Algorithm 6.1, whose structure refers to the notation provided in Figure 6.1.

Algorithm 6.1 Generation of matrix \mathbf{P} .

- 1: Select a node (whose ID is n in Figure 6.1) located at the boundary of the LFEM where BCs are applied.
- 2: Get the node coordinates (x_{n1}, x_{n2}) in the global frame.
- 3: Select the element of the GFEM containing the projection of node n (green-shadowed in Figure 6.1).
- 4: Evaluate the mapped coordinates r and s of node n with respect to the principal frame of the element, placed at its centroid (frame $\{G, r, s\}$ in Figure 6.1). The mapped coordinates are the results of the following problem:

$$\mathbf{J}(r, s) \begin{pmatrix} r \\ s \end{pmatrix} = \begin{pmatrix} x_{n1} - x_{G1} \\ x_{n2} - x_{G2} \end{pmatrix}, \quad (6.11)$$

where $\mathbf{J} \in \mathbb{M}_{s+}^{2 \times 2}$ is the Jacobian matrix of the element, which depends on the unknowns r and s . \mathbf{J} maps the transformation of the square element into the (possibly) distorted element of the actual GFEM mesh. Problem (6.11) can be solved, for instance, via the `scipy.optimize.minimize` Python's method.

- 5: Evaluate the matrix which maps the element nodal displacements (displacements of nodes 1, 2, 3 and 4) into the displacements at the point of coordinates (r, s) (i.e., $\mathbf{u}_{\text{BC}}^b(r, s)$). If $\mathbf{N}_e \in \mathbb{M}^{6 \times 24}$ is the matrix of the shape functions of the element (Reddy, 2003; Barbero, 2013), the relation can be expressed as

$$\mathbf{u}_{\text{BC}}^b(r, s) = \mathbf{N}_e(r, s)\mathbf{u}_e, \quad (6.12)$$

where \mathbf{u}_e is the vector of DOFs of the element e belonging to the GFEM.

- 6: Properly assemble $\mathbf{N}_e(r, s)$ inside \mathbf{P} .
 - 7: Repeat steps 1-6 for the remaining nodes belonging to the boundary of the LFEM where BCs on nodal displacements are applied.
-

Taking into account the above aspects, Eq. (6.9) reads:

$$\mathbf{K}^b \mathbf{u}^b + \mathbf{K}_{BC}^b \mathbf{P} \mathbf{u} = \mathbf{0}. \quad (6.13)$$

The idea is now to use the so-called adjoint method. Consider, now, the augmented version of Eq. (6.5), by summing to it the null quantities represented by Eq. (6.13) and Eq. (6.1):

$$\boldsymbol{\psi}_b^T (\mathbf{K}^b + \lambda \mathbf{K}_\sigma^b) \boldsymbol{\psi}_b + \boldsymbol{\mu}^T (\mathbf{K}^b \mathbf{u}^b + \mathbf{K}_{BC}^b \mathbf{P} \mathbf{u}) + \mathbf{w}^T (\mathbf{K} \mathbf{u} - \mathbf{f}) = 0, \quad (6.14)$$

where $\boldsymbol{\mu} \neq \mathbf{0}$ and $\mathbf{w} \neq \mathbf{0}$ are the adjoint vectors, to be determined. They can be interpreted as Lagrange's multipliers for Eq. (6.13) and Eq. (6.1). The interpretation of Eq. 6.14 is that the eigenvalue problem (first term) should be solved by considering, at the same time, an equilibrated LFEM (under the action of prescribed boundary displacements) and an equilibrated GFEM (under the action of external loads). The idea is to choose $\boldsymbol{\mu}$ and \mathbf{w} in order to eliminate the explicit dependence from the sensitivities of the displacement fields (with respect to the design variables) of both LFEM and GFEM, respectively (see Section 6.1.2.3)

By differentiating Eq. (6.14) with respect to the generic design variable ξ_j , one obtains:

$$\begin{aligned} \frac{\partial \lambda}{\partial \xi_j} = \frac{\lambda}{\boldsymbol{\psi}_b^T \mathbf{K}^b \boldsymbol{\psi}_b} \left[\boldsymbol{\psi}_b^T \left(\frac{\partial \mathbf{K}^b}{\partial \xi_j} + \lambda \frac{\partial \mathbf{K}_\sigma^b}{\partial \xi_j} \right) \boldsymbol{\psi}_b + \boldsymbol{\mu}^T \left(\frac{\partial \mathbf{K}^b}{\partial \xi_j} \mathbf{u}^b + \mathbf{K}^b \frac{\partial \mathbf{u}^b}{\partial \xi_j} + \dots \right. \right. \\ \left. \left. \dots + \frac{\partial \mathbf{K}_{BC}^b}{\partial \xi_j} \mathbf{P} \mathbf{u} + \mathbf{K}_{BC}^b \mathbf{P} \frac{\partial \mathbf{u}}{\partial \xi_j} \right) + \mathbf{w}^T \left(\frac{\partial \mathbf{K}}{\partial \xi_j} \mathbf{u} + \mathbf{K} \frac{\partial \mathbf{u}}{\partial \xi_j} \right) \right]. \end{aligned} \quad (6.15)$$

6.1.2.2 Stress-Stiffness Matrix Expression

As discussed in (Setoodeh et al., 2009), the stress-stiffness matrix of the generic e -th shell element can be decomposed as a linear combination of internal forces and some matrices depending only on the geometry of the element. In (Setoodeh et al., 2009), the linear combination is composed by three terms. With this choice, only membrane effects are considered for the buckling instability. In the framework of FSDT, there are eight terms: three for membrane effects, three for bending effects and two for the out-of-plane shear effects. Therefore, the decomposition of the stress-stiffness matrix, in the FSDT, reads:

$$\mathbf{K}_{\sigma_e}^b = \sum_{i=1}^8 r_{0ei}^b \bar{\mathbf{K}}_i, \quad (6.16)$$

where r_{0ei}^b are the components of vector \mathbf{r} of Eq. (4.15) (for the e -th element), resulting from the static analysis of Eq. (6.13) carried out on the LFEM, while $\bar{\mathbf{K}}_i \in \mathbb{M}_s^{24 \times 24}$ are matrices depending only on the geometry of the element. The algorithm for retrieving the expression of each matrix $\bar{\mathbf{K}}_i$ for a shell element with four nodes and six DOFs per node (like the SHELL181 ANSYS® shell element), whose kinematics is described in the framework of the FSDT, is presented in Algorithm 6.2. Of course, this algorithm must be

executed off-line, i.e. before the optimisation process, once the element type has been selected. The expressions of $\bar{\mathbf{K}}_i$ for a square SHELL181 element of side L are provided here

Algorithm 6.2 Derivation of matrices $\bar{\mathbf{K}}_i$.

- 1: Build a FE model made of a single element.
 - 2: Set arbitrary material properties for the element. The material properties should be conveniently set in order to obtain a diagonal laminate stiffness matrix \mathbf{K}_{lam} , in order to avoid coupling effects.
 - 3: Impose an elementary strain field ($\varepsilon_{0ei} \neq 0$, $\varepsilon_{0ej} = 0$, $j = 1, \dots, 8$ and $j \neq i$) by using suitable BCs at the four nodes.
 - 4: Run a static analysis and activate the pre-stress option (in this way the commercial FE code builds \mathbf{K}_{σ_e} according to the usual definition, as in (Ansys[®], 2013)).
 - 5: Get r_{0ei} and \mathbf{K}_{σ_e} from the FE software.
 - 6: Calculate $\bar{\mathbf{K}}_i = \frac{\mathbf{K}_{\sigma_e}}{r_{0ei}}$ (since no coupling effects are present).
 - 7: If $i < 8$ set $i = i + 1$ and go to step 3, otherwise stop.
-

below. Each matrix $\bar{\mathbf{K}}_i$ is a symmetric and sparse partitioned block one. Only non-null terms are provided in the following.

To compact the notation, the following matrices may be introduced: three matrices inspired in notation by Pauli's ones (see, for example, (Altmann, 2005)) and the identity matrix in 2D:

$$\begin{aligned} \boldsymbol{\sigma}_1 &= \begin{bmatrix} 0 & 1 \\ 1 & 0 \end{bmatrix}, \quad \boldsymbol{\sigma}_2 = \begin{bmatrix} 0 & 1 \\ -1 & 0 \end{bmatrix}, \quad \boldsymbol{\sigma}_3 = \begin{bmatrix} 1 & 0 \\ 0 & -1 \end{bmatrix}, \\ \mathbf{I}_2 &= \begin{bmatrix} 1 & 0 \\ 0 & 1 \end{bmatrix}. \end{aligned} \tag{6.17}$$

For the sake of completeness, matrices $\boldsymbol{\sigma}_1$ and $\boldsymbol{\sigma}_3$ are Pauli's, whilst the actual Pauli' second matrix is $-i \mathbf{I}_2 \cdot \boldsymbol{\sigma}_2$. The use of the nomenclature *Pauli's matrices* to designate Eq. (6.17) is to be intended, with a slight abuse of nomenclature, only formally.

Introducing the Kronecker product, indicated by \otimes , between two generic matrices $\mathbf{A} \in \mathbb{M}^{m \times n}$ and $\mathbf{B} \in \mathbb{M}^{p \times q}$, which allows to obtain the product matrix $\mathbf{C} \in \mathbb{M}^{pm \times qn}$ as follows

$$\mathbf{C} = \mathbf{A} \otimes \mathbf{B} := \begin{bmatrix} a_{11}\mathbf{B} & \dots & a_{1n}\mathbf{B} \\ \vdots & \ddots & \vdots \\ a_{m1}\mathbf{B} & \dots & a_{mn}\mathbf{B} \end{bmatrix}, \tag{6.18}$$

one obtains:

$$\bar{\mathbf{K}}_1 = \frac{1}{8} (\mathbf{I}_2 - \boldsymbol{\sigma}_1) \otimes \begin{bmatrix} \hat{\mathbf{A}}_1 & \hat{\mathbf{B}}_1 \\ \hat{\mathbf{B}}_1^T & \hat{\mathbf{C}}_1 \end{bmatrix},$$

with, $\hat{\mathbf{A}}_1 = \hat{\mathbf{A}}_1^T$, $\hat{\mathbf{C}}_1 = \hat{\mathbf{C}}_1^T$, and

$$\begin{aligned} \hat{A}_1^{(1,1)} &= -3, \hat{A}_1^{(1,2)} = -1, \hat{A}_1^{(2,2)} = 1, \hat{A}_1^{(3,3)} = 2, \\ \hat{B}_1^{(1,1)} &= 1, \hat{B}_1^{(1,2)} = 1, \hat{B}_1^{(2,1)} = -1, \hat{B}_1^{(2,2)} = -1, \hat{B}_1^{(3,3)} = -2, \\ \hat{C}_1^{(1,1)} &= -3, \hat{C}_1^{(1,2)} = 1, \hat{C}_1^{(2,2)} = 1, \hat{C}_1^{(3,3)} = 2, \end{aligned} \quad (6.19)$$

$$\bar{\mathbf{K}}_2 = \frac{1}{8} (\mathbf{I}_2 - \boldsymbol{\sigma}_1) \otimes \begin{bmatrix} \hat{\mathbf{A}}_2 & \hat{\mathbf{B}}_2 \\ \hat{\mathbf{B}}_2^T & \hat{\mathbf{C}}_2 \end{bmatrix},$$

with, $\hat{\mathbf{A}}_2 = \hat{\mathbf{A}}_2^T$, $\hat{\mathbf{C}}_2 = \hat{\mathbf{C}}_2^T$, and

$$\begin{aligned} \hat{A}_2^{(1,1)} &= 1, \hat{A}_2^{(1,2)} = -1, \hat{A}_2^{(2,2)} = -3, \hat{A}_2^{(3,3)} = 2, \\ \hat{B}_2^{(1,1)} &= 1, \hat{B}_2^{(1,2)} = 1, \hat{B}_2^{(2,1)} = -1, \hat{B}_2^{(2,2)} = -1, \hat{B}_2^{(3,3)} = 2, \\ \hat{C}_2^{(1,1)} &= 1, \hat{C}_2^{(1,2)} = 1, \hat{C}_2^{(2,2)} = -3, \hat{C}_2^{(3,3)} = 2, \end{aligned} \quad (6.20)$$

$$\bar{\mathbf{K}}_3 = \frac{1}{2} (\mathbf{I}_2 - \boldsymbol{\sigma}_1) \otimes \begin{bmatrix} \hat{\mathbf{A}}_3 & \mathbf{0} \\ \mathbf{0} & \hat{\mathbf{C}}_3 \end{bmatrix},$$

with, $\hat{\mathbf{A}}_3 = \hat{\mathbf{A}}_3^T$, $\hat{\mathbf{C}}_3 = \hat{\mathbf{C}}_3^T$, and

$$\hat{A}_3^{(1,2)} = -1, \hat{A}_3^{(3,3)} = 1, \hat{C}_3^{(1,2)} = -1, \hat{C}_3^{(3,3)} = -1, \quad (6.21)$$

$$\bar{\mathbf{K}}_4 = \bar{\mathbf{K}}_5 = \bar{\mathbf{K}}_6 = \mathbf{0}, \quad (6.22)$$

$$\begin{aligned} \bar{\mathbf{K}}_7 &= -\frac{12}{72} (2\mathbf{I}_2 - \boldsymbol{\sigma}_1) \otimes (\mathbf{I}_2 - \boldsymbol{\sigma}_1) \otimes \hat{\mathbf{K}}_7 - \frac{6}{72} (2\boldsymbol{\sigma}_3 \otimes \boldsymbol{\sigma}_3 + \boldsymbol{\sigma}_2 \otimes \boldsymbol{\sigma}_2) \otimes \hat{\mathbf{A}}_7 \\ &\quad + \frac{6}{72} (2\boldsymbol{\sigma}_3 \otimes \boldsymbol{\sigma}_2 + \boldsymbol{\sigma}_2 \otimes \boldsymbol{\sigma}_3) \otimes \hat{\mathbf{B}}_7 + \frac{1}{72} [2\mathbf{I}_2 \otimes (2\mathbf{I}_2 + \boldsymbol{\sigma}_1) + \boldsymbol{\sigma}_1 \otimes (\mathbf{I}_2 + 2\boldsymbol{\sigma}_1)] \otimes \hat{\mathbf{C}}_7, \end{aligned}$$

with, $\hat{\mathbf{K}}_7 = \hat{\mathbf{K}}_7^T$, $\hat{\mathbf{A}}_7 = \hat{\mathbf{A}}_7^T$, $\hat{\mathbf{B}}_7 = -\hat{\mathbf{B}}_7^T$, $\hat{\mathbf{C}}_7 = \hat{\mathbf{C}}_7^T$, and

$$\hat{K}_7^{(1,3)} = 1, \hat{A}_7^{(1,5)} = L, \hat{B}_7^{(1,5)} = -\hat{B}_7^{(5,1)} = -L, \hat{C}_7^{(4,6)} = L^2, \quad (6.23)$$

$$\begin{aligned}
 \overline{\mathbf{K}}_8 &= \frac{12}{72} [\boldsymbol{\sigma}_1 \otimes (\mathbf{I} + 2\boldsymbol{\sigma}_1) - \mathbf{I}_2 \otimes (2\mathbf{I}_2 - \boldsymbol{\sigma}_1)] \otimes \hat{\mathbf{K}}_8 + \frac{6}{72} \boldsymbol{\sigma}_3 \otimes (2\mathbf{I}_2 + \boldsymbol{\sigma}_1) \otimes \hat{\mathbf{A}}_8 \\
 &\quad + \frac{6}{72} \boldsymbol{\sigma}_2 \otimes (\mathbf{I}_2 + 2\boldsymbol{\sigma}_1) \otimes \hat{\mathbf{B}}_8 + \frac{1}{72} [2\mathbf{I}_2 \otimes (2\mathbf{I}_2 + \boldsymbol{\sigma}_1) + \boldsymbol{\sigma}_1 \otimes (\mathbf{I}_2 + 2\boldsymbol{\sigma}_1)] \otimes \hat{\mathbf{C}}_8, \\
 \text{with, } \hat{\mathbf{K}}_8 &= \hat{\mathbf{K}}_8^T, \hat{\mathbf{A}}_8 = \hat{\mathbf{A}}_8^T, \hat{\mathbf{B}}_8 = -\hat{\mathbf{B}}_8^T, \hat{\mathbf{C}}_8 = \hat{\mathbf{C}}_8^T, \text{ and} \\
 \hat{\mathbf{K}}_8^{(2,3)} &= 1, \hat{\mathbf{A}}_8^{(2,4)} = L, \hat{\mathbf{B}}_8^{(2,4)} = -\hat{\mathbf{B}}_8^{(4,2)} = L, \hat{\mathbf{C}}_8^{(5,6)} = L^2,
 \end{aligned} \tag{6.24}$$

The expressions of matrices $\overline{\mathbf{K}}_i$ reported above are supposed independent from the aspect ratio of the element. Of course, this assumption is justified if and only if the mesh of the FE model is structured and regular as much as possible (i.e. composed by pseudo-square elements). It is convenient to introduce the connectivity matrix of element e . For a shell element, with four nodes and six DOFs per node, 24 are the DOFs. This kind of elements will be mainly used in the following. The connectivity matrix is defined as

$$\mathbf{L}_e : \mathbf{u} \mapsto \mathbf{u}_e, \quad \mathbf{L}_e \mathbf{u} = \mathbf{u}_e, \quad \mathbf{L}_e \in \mathbb{M}^{24 \times n_{\text{IN}}}. \tag{6.25}$$

Besides, it is convenient to introduce the matrix \mathbf{B}_e , representing the product of the linear differential operator and the shape function matrices, i.e.

$$\mathbf{B}_e : \mathbf{u}_e \mapsto \boldsymbol{\varepsilon}_{\text{gen } e}, \quad \mathbf{B}_e \mathbf{u}_e = \boldsymbol{\varepsilon}_{\text{gen } e}, \quad \mathbf{B}_e \in \mathbb{M}^{8 \times 24}. \tag{6.26}$$

Accordingly, the singular form of the stress-stiffness matrix reads:

$$\begin{aligned}
 \hat{\mathbf{K}}_\sigma^b &= \sum_{e=1}^{N_e^b} \hat{\mathbf{L}}_e^{bT} \sum_{i=1}^8 r_{0ei}^b \overline{\mathbf{K}}_i \hat{\mathbf{L}}_e^b = \sum_{e=1}^{N_e^b} \hat{\mathbf{L}}_e^{bT} \sum_{i=1}^8 (\mathbf{K}_e^{\text{lam}} \mathbf{B}_e \mathbf{u}_{e0}^b)_i \overline{\mathbf{K}}_i \hat{\mathbf{L}}_e^b \\
 &= \sum_{e=1}^{N_e^b} \hat{\mathbf{L}}_e^{bT} \sum_{i=1}^8 \left(\mathbf{K}_e^{\text{lam}} \mathbf{B}_e \hat{\mathbf{L}}_e^b \hat{\mathbf{u}}_0^b \right)_i \overline{\mathbf{K}}_i \hat{\mathbf{L}}_e^b,
 \end{aligned} \tag{6.27}$$

and the non-singular counterpart can be obtained as

$$\mathbf{K}_\sigma^b := \mathfrak{R} \left(\hat{\mathbf{K}}_\sigma^b, I_{\text{BC}}^b, I_{\text{BC}}^b \right). \tag{6.28}$$

6.1.2.3 Finalisation of the Gradient Expression

With reference to Eq. (6.15), consider the following quantity:

$$\begin{aligned}
 \hat{\boldsymbol{\psi}}_b^T \frac{\partial \hat{\mathbf{K}}_\sigma^b}{\partial \xi_j} \hat{\boldsymbol{\psi}}_b &= \hat{\boldsymbol{\psi}}_b^T \left(\sum_{e=1}^{N_e^b} \hat{\mathbf{L}}_e^T \left(\sum_{i=1}^8 \frac{\partial}{\partial \xi_j} (\mathbf{K}_e^{\text{lam}} \mathbf{B}_e \mathbf{u}_{e0}^b)_i \bar{\mathbf{K}}_i \right) \hat{\mathbf{L}}_e^b \right) \hat{\boldsymbol{\psi}}_b \\
 &= \sum_{e=1}^{N_e^b} \hat{\boldsymbol{\psi}}_b^T \hat{\mathbf{L}}_e^T \left(\sum_{i=1}^8 \frac{\partial}{\partial \xi_j} (\mathbf{K}_e^{\text{lam}} \mathbf{B}_e \mathbf{u}_{e0}^b)_i \bar{\mathbf{K}}_i \right) \hat{\mathbf{L}}_e^b \hat{\boldsymbol{\psi}}_b \\
 &= \sum_{e=1}^{N_e^b} \boldsymbol{\psi}_{eb}^T \left(\sum_{i=1}^8 \frac{\partial}{\partial \xi_j} (\mathbf{K}_e^{\text{lam}} \mathbf{B}_e \mathbf{u}_{e0}^b)_i \bar{\mathbf{K}}_i \right) \boldsymbol{\psi}_{eb} \\
 &= \sum_{e=1}^{N_e^b} \sum_{i=1}^8 \frac{\partial}{\partial \xi_j} (\mathbf{K}_e^{\text{lam}} \mathbf{B}_e \mathbf{u}_{e0}^b)_i \boldsymbol{\psi}_{eb}^T \bar{\mathbf{K}}_i \boldsymbol{\psi}_{eb} \\
 &= \sum_{e=1}^{N_e^b} \mathbf{s}_{eb}^T \frac{\partial}{\partial \xi_j} (\mathbf{K}_e^{\text{lam}} \mathbf{B}_e \mathbf{u}_{e0}^b) \\
 &= \underbrace{\sum_{e=1}^{N_e^b} \mathbf{s}_{eb}^T \frac{\partial \mathbf{K}_e^{\text{lam}}}{\partial \xi_j} \mathbf{B}_e \hat{\mathbf{L}}_e^b \hat{\mathbf{u}}_0^b}_{\hat{\mathbf{a}}^T} + \underbrace{\sum_{e=1}^{N_e^b} \mathbf{s}_{eb}^T \mathbf{K}_e^{\text{lam}} \mathbf{B}_e \hat{\mathbf{L}}_e^b}_{\hat{\mathbf{b}}^T} \frac{\partial \hat{\mathbf{u}}_0^b}{\partial \xi_j} \\
 &:= \hat{\mathbf{a}}^T \hat{\mathbf{u}}_0^b + \hat{\mathbf{b}}^T \frac{\partial \hat{\mathbf{u}}_0^b}{\partial \xi_j},
 \end{aligned} \tag{6.29}$$

with $\mathbf{s}_{eb} := \{\boldsymbol{\psi}_{eb}^T \bar{\mathbf{K}}_i \boldsymbol{\psi}_{eb} \mid i = 1, \dots, 8\}$.

Remark 6.2. Consider the scalar product $\mathbf{v}^T \mathbf{u}$ of two vectors $\mathbf{u}, \mathbf{v} \in \mathbb{M}^{n \times 1}$. If \mathbf{u} , A and B satisfies conditions of Remark 6.1, then: $\mathbf{v}^T \mathbf{u} = \mathbf{v}^T \mathfrak{Z}(\mathbf{u}, A) \oplus \mathbf{v}^T \mathfrak{Z}(\mathbf{u}, B) = \mathfrak{R}(\mathbf{v}, A)^T \mathfrak{R}(\mathbf{u}, A) \oplus \mathfrak{R}(\mathbf{v}, B)^T \mathfrak{R}(\mathbf{u}, B)$.

By applying Remarks 6.1 and 6.2 to both $\hat{\boldsymbol{\psi}}^b$ and $\hat{\mathbf{u}}_0^b$ of Eq. (6.29), considering that $\mathfrak{R}(\hat{\boldsymbol{\psi}}^b, I_{\text{IN}}^b) = \mathbf{0}$, one obtains:

$$\begin{aligned}
 \hat{\boldsymbol{\psi}}_b^T \frac{\partial \hat{\mathbf{K}}_\sigma^b}{\partial \xi_j} \hat{\boldsymbol{\psi}}_b &= \mathfrak{R}(\hat{\mathbf{a}}, I_{\text{IN}}^b)^T \mathfrak{R}(\hat{\mathbf{u}}_0^b, I_{\text{IN}}^b) + \mathfrak{R}(\hat{\mathbf{a}}, I_{\text{BC}}^b)^T \mathfrak{R}(\hat{\mathbf{u}}_0^b, I_{\text{BC}}^b) + \mathfrak{R}(\hat{\mathbf{b}}, I_{\text{IN}}^b)^T \mathfrak{R} \left(\frac{\partial \hat{\mathbf{u}}_0^b}{\partial \xi_j}, I_{\text{IN}}^b \right) + \\
 &\quad + \mathfrak{R}(\hat{\mathbf{b}}, I_{\text{BC}}^b)^T \mathfrak{R} \left(\frac{\partial \hat{\mathbf{u}}_0^b}{\partial \xi_j}, I_{\text{BC}}^b \right) \\
 &= \mathfrak{R}(\hat{\mathbf{a}}, I_{\text{IN}}^b)^T \mathbf{u}_{\text{BC}}^b + \mathfrak{R}(\hat{\mathbf{a}}, I_{\text{BC}}^b)^T \mathbf{u}^b + \mathfrak{R}(\hat{\mathbf{b}}, I_{\text{IN}}^b)^T \frac{\partial \mathbf{u}_{\text{BC}}^b}{\partial \xi_j} + \mathfrak{R}(\hat{\mathbf{b}}, I_{\text{BC}}^b)^T \frac{\partial \mathbf{u}^b}{\partial \xi_j} \\
 &= \mathfrak{R}(\hat{\mathbf{a}}, I_{\text{IN}}^b)^T \mathbf{P} \mathbf{u} + \mathfrak{R}(\hat{\mathbf{a}}, I_{\text{BC}}^b)^T \mathbf{u}^b + \mathfrak{R}(\hat{\mathbf{b}}, I_{\text{IN}}^b)^T \mathbf{P} \frac{\partial \mathbf{u}}{\partial \xi_j} + \mathfrak{R}(\hat{\mathbf{b}}, I_{\text{BC}}^b)^T \frac{\partial \mathbf{u}^b}{\partial \xi_j}.
 \end{aligned} \tag{6.30}$$

By substituting Eq. (6.30) into Eq. (6.14), and by choosing $\boldsymbol{\mu}$ and \mathbf{w} such that the terms

multiplying $\partial \mathbf{u}^b / \partial \xi_j$ and $\partial \mathbf{u} / \partial \xi_j$ vanish, one finally obtains:

$$\left\{ \begin{array}{l} \frac{\partial \lambda}{\partial \xi_j} = \frac{\lambda}{\boldsymbol{\psi}_b^T \mathbf{K}^b \boldsymbol{\psi}_b} \left[\boldsymbol{\psi}_b^T \frac{\partial \mathbf{K}^b}{\partial \xi_j} \boldsymbol{\psi}_b + \lambda \left(\mathfrak{R}(\hat{\mathbf{a}}, I_{\text{IN}}^b)^T \mathbf{P} \mathbf{u} + \mathfrak{R}(\hat{\mathbf{a}}, I_{\text{BC}}^b)^T \mathbf{u}^b \right) + \right. \\ \left. + \boldsymbol{\mu}^T \left(\frac{\partial \mathbf{K}^b}{\partial \xi_j} \mathbf{u}^b + \frac{\partial \mathbf{K}_{\text{BC}}^b}{\partial \xi_j} \mathbf{P} \mathbf{u} \right) + \mathbf{w}^T \frac{\partial \mathbf{K}}{\partial \xi_j} \mathbf{u} \right], \\ j = 1, \dots, n_{\text{vars}}, \\ \mathbf{K}^b \boldsymbol{\mu} = -\lambda \mathfrak{R}(\hat{\mathbf{b}}, I_{\text{BC}}^b), \\ \mathbf{K} \mathbf{w} = -\mathbf{P}^T \left[\lambda \mathfrak{R}(\hat{\mathbf{b}}, I_{\text{IN}}^b) + \mathbf{K}_{\text{BC}}^{bT} \boldsymbol{\mu} \right]. \end{array} \right. \quad (6.31)$$

Equation (6.31) represents the gradient of the buckling factor of the LFEM subject to non-null imposed BCs, which are related to the displacement field solution of static analysis performed on the GFEM.

The last term of the first formula in Eq. (6.31) is the coupling effect between GFEM and LFEM and is, in general, non-zero $\forall j = 1, \dots, n_{\text{vars}}$.

Conversely, the other terms are non-zero if and only if the design variable ξ_j is defined in the LFEM domain.

The final expression of the gradient is then obtained by considering Eqs. (6.31) and (6.4).

6.2 New Blending Constraints Formulation

A preliminary mathematical formalisation of blending requirement is necessary for the fruitful understanding of the investigation. Firstly, consider the general definition of a stacking sequence, given in Definition 4.4.

Consider two generic laminates, labelled p and q , made of the same elementary ply. For the sake of simplicity, laminate p is assumed to be thicker than laminate q . Therefore, if each laminate has a number of plies N_i , where $i = p, q$ and $N_p > N_q$, the blending can be defined as follows.

Definition 6.3 (Blending). *Blending is an injective map*

$$\begin{aligned} \mathcal{B} : \text{SS}_q &\mapsto \text{SS}_p \\ \theta_{k_q} &\mapsto \theta_{\mathcal{B}(k_q)} =: \theta_{k_p}, \quad \theta_{k_i} \in \text{SS}_i, \quad i \in \{p, q\} \end{aligned} \quad (6.32)$$

such that Eq. (6.32) holds

(a) $\forall 1 \leq k_q \leq N_q$,

(b) for some $1 \leq k_p \leq N_p$ such that $\mathcal{B}(k_q + 1) > \mathcal{B}(k_q)$.

Condition (a) of Definition 6.3 implies that blending is a complete embedding $\text{SS}_q \subseteq \text{SS}_p$: all the plies of the thinner laminate have to be embedded in the stack of the thicker one. Moreover, condition (b) means that blending does not allow intersection of plies. In

fact, the generic $(k_q + 1)$ -th ply cannot be mapped in a ply of SS_p below the image of the k_q -th ply via \mathcal{B} . Figure 6.2 shows the violation of points (a), i.e. blending map does not act on all the plies of the thinner laminate, and (b), i.e. ply intersection, of Definition 6.3.

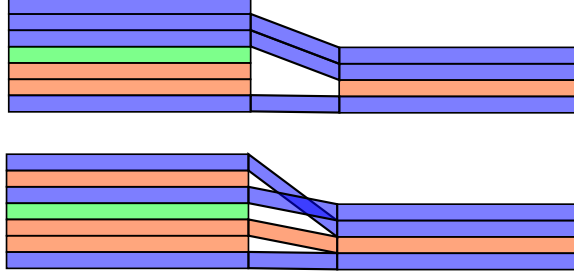


Figure 6.2: Two violations of blending definition (Definition 6.3)

Given two stacks, there may exist many different arrangements satisfying Definition 6.3, as shown qualitatively in Figure 6.3, since no restrictions have been imposed on the schemes of the arrangements, as contrarily done in several works (Adams et al., 2004; Seresta et al., 2007). Finally, it is convenient to introduce the collection of the

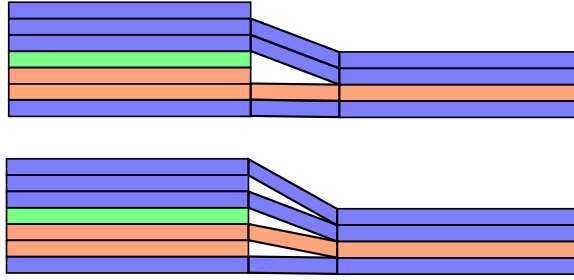


Figure 6.3: Two possible blended arrangements between two given laminates (different colours mean different orientations).

indices of the plies of the thicker laminate which are not interested by blending:

$$\mathcal{NB} := \{k_p : \nexists k_q \in SS_q \text{ such that } \mathcal{B}(k_q) = k_p\}. \quad (6.33)$$

6.2.1 Constraints

The dimensionless anisotropic polar moduli of Eq. (4.30) can be rewritten as:

$$N\rho_{0K}e^{i4\Phi_1^{A*}} = \sum_{k=1}^N e^{i4\theta_k}, \quad N\rho_1e^{i2\Phi_1^{A*}} = \sum_{k=1}^N e^{i2\theta_k}. \quad (6.34)$$

Consider two laminates, still denoted by p and q , the former being thicker than the latter. The member-by-member difference of Eq. (6.34), by considering point (a) of Definition 6.3, together with Eq. (6.33), leads to

$$\Delta_{pq} \left(N\rho_{0K}e^{i4\Phi_1^{A*}} \right) = \sum_{k \in \mathcal{NB}} e^{i4\theta_k}, \quad \Delta_{pq} \left(N\rho_1e^{i2\Phi_1^{A*}} \right) = \sum_{k \in \mathcal{NB}} e^{i2\theta_k}, \quad (6.35)$$

where operator $\Delta_{pq}(\cdot)$ is equivalent to $\cdot_p - \cdot_q$. It is noteworthy that the right-member terms concern only the set of plies not affected by blending. Equation (6.35) holds for both the real and imaginary part, namely

$$\begin{aligned}\Delta_{pq}(N\rho_{0K}c_4) &= \sum_{k \in \mathcal{NB}} \cos 4\theta_k, & \Delta_{pq}(N\rho_{0K}s_4) &= \sum_{k \in \mathcal{NB}} \sin 4\theta_k, \\ \Delta_{pq}(N\rho_1c_2) &= \sum_{k \in \mathcal{NB}} \cos 2\theta_k, & \Delta_{pq}(N\rho_1s_2) &= \sum_{k \in \mathcal{NB}} \sin 2\theta_k,\end{aligned}\tag{6.36}$$

where $c_4 := \cos 4\Phi_1^{A*}$, $s_4 := \sin 4\Phi_1^{A*}$, $c_2 := \cos 2\Phi_1^{A*}$, $s_2 := \sin 2\Phi_1^{A*}$.

In Eq. (6.36), the right-hand members are not independent and cannot be treated separately. Taking the square of both sides and summing member-by-member analogous expressions, one obtains

$$[\Delta_{pq}(N\rho_{0K}c_4)]^2 + [\Delta_{pq}(N\rho_{0K}s_4)]^2 = \left(\sum_{k \in \mathcal{NB}} \cos 4\theta_k \right)^2 + \left(\sum_{k \in \mathcal{NB}} \sin 4\theta_k \right)^2\tag{6.37}$$

and

$$[\Delta_{pq}(N\rho_1c_2)]^2 + [\Delta_{pq}(N\rho_1s_2)]^2 = \left(\sum_{k \in \mathcal{NB}} \cos 2\theta_k \right)^2 + \left(\sum_{k \in \mathcal{NB}} \sin 2\theta_k \right)^2.\tag{6.38}$$

Equations (6.37) and (6.38) simplify to (by taking into account the fundamental properties recalled in Appendix A)

$$[\Delta_{pq}(N\rho_{0K}c_4)]^2 + [\Delta_{pq}(N\rho_{0K}s_4)]^2 = N_p - N_q + 2 \sum_{\substack{k, j \in \mathcal{NB} \\ j > k}} \cos 4(\theta_k - \theta_j),\tag{6.39}$$

and

$$[\Delta_{pq}(N\rho_1c_2)]^2 + [\Delta_{pq}(N\rho_1s_2)]^2 = N_p - N_q + 2 \sum_{\substack{k, j \in \mathcal{NB} \\ j > k}} \cos 2(\theta_k - \theta_j).\tag{6.40}$$

It is noteworthy that Eqs. (6.39) and (6.40) cannot be used in their current form within the FLP, since orientation angles of plies do not enter within the problem formulation. Therefore, Eqs. (6.39) and (6.40), must be opportunely bounded by means of quantities which do not depend upon layers orientation angles. Applying the triangle inequality, and

considering the properties given in Appendix A, the following estimate is found:

$$\begin{aligned}
 [\Delta_{pq}(N\rho_{0K}c_4)]^2 + [\Delta_{pq}(N\rho_{0K}s_4)]^2 &\leq N_p - N_q + 2 \left| \sum_{\substack{k,j \in \mathcal{NB} \\ j > k}} \cos 4(\theta_k - \theta_j) \right| \\
 &\leq N_p - N_q + 2 \sum_{\substack{k,j \in \mathcal{NB} \\ j > k}} |\cos 4(\theta_k - \theta_j)| \\
 &\leq N_p - N_q + 2 \sum_{\substack{k,j \in \mathcal{NB} \\ j > k}} 1 \\
 &\leq N_p - N_q + 2 \frac{(N_p - N_q)(N_p - N_q - 1)}{2} \\
 &\leq (N_p - N_q)^2,
 \end{aligned} \tag{6.41}$$

and, in a similar fashion,

$$[\Delta_{pq}(N\rho_1c_2)]^2 + [\Delta_{pq}(N\rho_1s_2)]^2 \leq (N_p - N_q)^2. \tag{6.42}$$

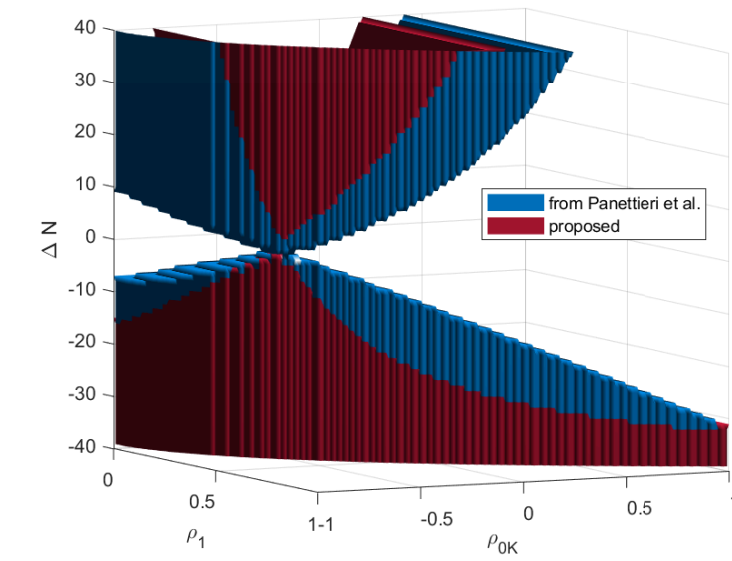
Finally, for a generic couple of adjacent panels, the blending constraint reads:

$$\begin{aligned}
 g_{\text{blend}-0} &:= [\Delta_{pq}(N\rho_{0K}c_4)]^2 + [\Delta_{pq}(N\rho_{0K}s_4)]^2 - (N_p - N_q)^2, \\
 g_{\text{blend}-1} &:= [\Delta_{pq}(N\rho_1c_2)]^2 + [\Delta_{pq}(N\rho_1s_2)]^2 - (N_p - N_q)^2, \\
 g_{\text{blend}-i} &\leq 0, \quad i = 0, 1.
 \end{aligned} \tag{6.43}$$

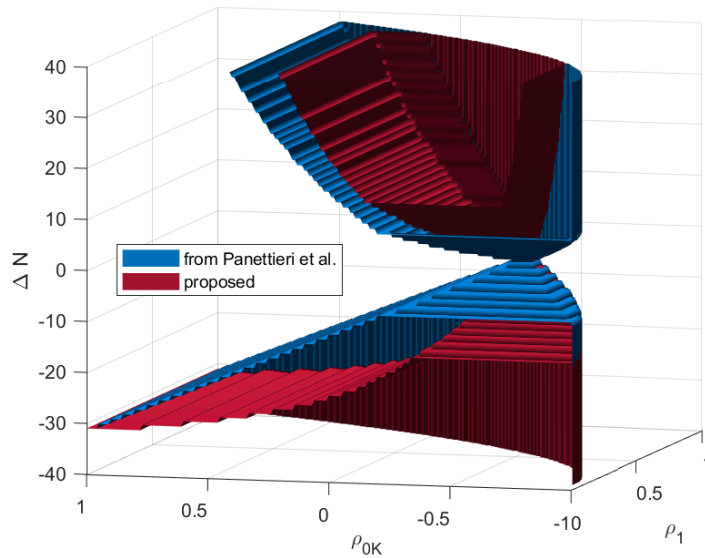
Equation (6.43) represents the expression of the blending requirement in the PPs space when the laminate is orthotropic. These constraints must be imposed, for each couple of adjacent panels, during the FLP.

The geometrical interpretation of each inequality of Eq. (6.43) is the following. Assume p , for example, to be the reference panel of the couple; then, in the space having coordinates $\{N\rho_{0K}c_4, N\rho_{0K}s_4\}$ (or $\{N\rho_1c_2, N\rho_1s_2\}$), the properties of q lie in a ball centred in that of p , namely the point $(N\rho_{0K}c_4; N\rho_{0K}s_4)|_p$ (or $(N\rho_1c_2; N\rho_1s_2)|_p$), having radius equal to the difference between the number of plies of the two laminates, i.e. $|N_p - N_q|$.

Figure 6.4 shows that the proposed formulation induces a feasibility domain stricter than the one presented in (Panettieri et al., 2019). The reason is that considering Eq. (6.34) as the starting point makes terms related to blended plies to drop-off, whilst in (Macquart et al., 2016; Panettieri et al., 2019) they generate further terms in the right-hand side of equations, making the final estimate not as sharp as Eq. (6.43). Of course, the "jump" of PPs between two blended laminates is attributable to the plies not interested by blending. To highlight the main differences between the new expression of blending constraints and the previous one (Panettieri et al., 2019), in Figure 6.4, a reference laminate characterised by $N_{\text{ref}} = 40$, $\rho_{0K} = -0.6$, $\rho_1 = 0.4$, $\phi_1 = 0$ is considered; a second laminate (with $\phi_1 = 0$ and having a variable number N of plies) is blended with the reference one if it lies



(a) View 1



(b) View 2

Figure 6.4: Comparison of blending feasible region delimited by constraints presented in (Panettieri et al., 2019) and by the herein proposed ones for a reference laminate.

inside the domain delimited by the purple surface. In the Figures, $\Delta N := N - N_{\text{ref}}$. The plot is restricted to laminates up to $2N$ plies for graphical reasons. Of course, if $\Delta N < 0$ the second laminate is thinner than the reference one. Conversely, if $\Delta N > 0$, the second laminate is thicker than the reference one. It is noteworthy that, when $N = N_{\text{ref}}$, the feasible domain degenerates into a point. Of course, two laminates both made of N plies can be blended if and only if the two SSs are the same (as a trivial consequence, the elastic properties are the same).

It is noteworthy that only condition (a) of Definition 6.3 has been used to derive Eq. (6.43). This is expected, since Eq. (6.43) derives from the expression of membrane

PPs, which is not influenced by the position of the plies within the stack. Appendix B is dedicated to the possible contribution of the uncoupling condition on blending constraints.

In this following, the extension of the transition zones between adjacent laminates is neglected. It is a major hypothesis. The transition zone cannot be too tapered (Irisarri et al., 2014), so that the relative extension in the nominal panel dimensions could not be negligible at all. The situation is conceptually depicted in Figure 6.5, where a real-world-like solution is presented, despite the modelling approach adopted so far for the transition zone. Two laminates of thickness $t_1 > t_2$, of nominal dimension $H \times L$, are joined along a side. The transition zone is tapered, and the voids are filled by resin pockets. The transition zone extension in the longitudinal direction, if α denotes the taper of this zone, is $\frac{t_1 - t_2}{\tan \alpha}$. The question is whether $\frac{t_1 - t_2}{2 \tan \alpha} \ll L$ or not. In this Thesis, the answer is assumed always positive.

Note that the transition region is likely to undergo failure: the ply-drop creates geometry and material discontinuities which act as sources for delamination initiation and propagation (see (He et al., 2000) for a review). Common values for α are $\alpha < 15$ deg or $\alpha = 5.71$ deg, corresponding to a 10 : 1 taper ratio of the transition zone (He et al., 2000). However, at least for the preliminary investigation goal of the Thesis, the transition regions can be neglected and not modelled in the conceptual and preliminary design phase, as often done in the literature.

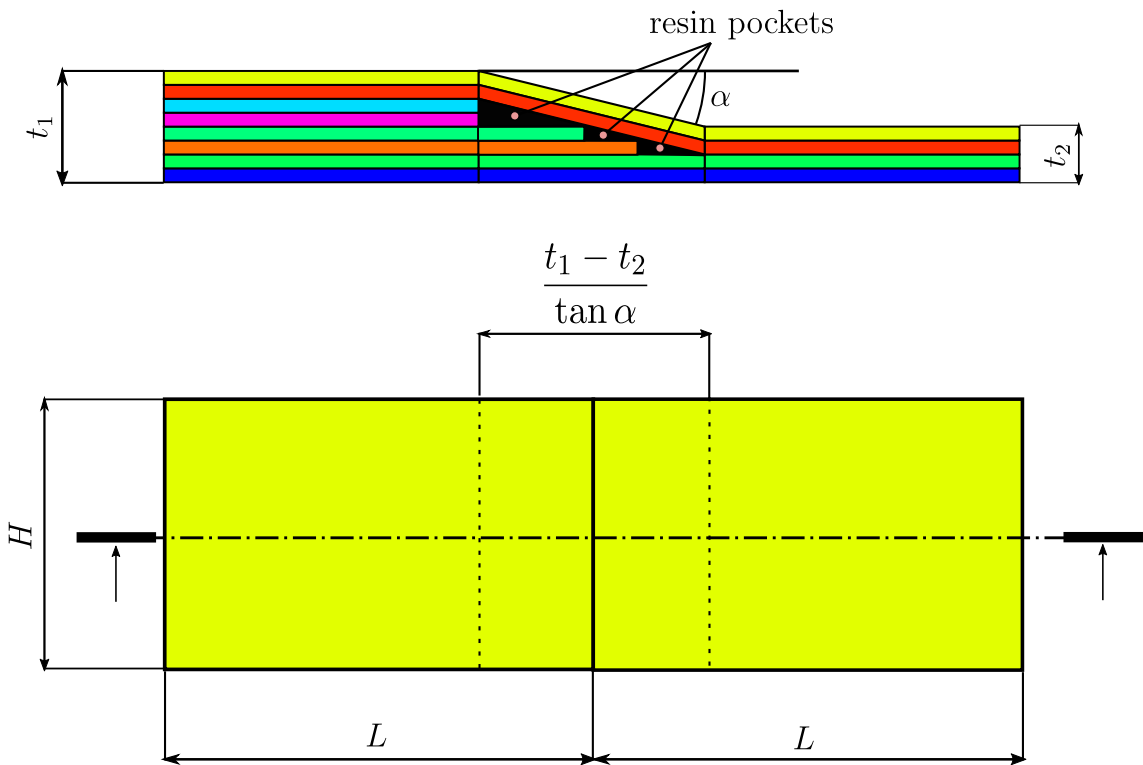


Figure 6.5: Conceptual junction of composite laminates

6.2.2 Gradient

Defining, for brevity of notation

$$\begin{aligned}
 c_1 &= [\Delta_{pq} (N\rho_{0K}c_4)], & c_2 &= [\Delta_{pq} (N\rho_{0K}s_4)], \\
 c_3 &= [\Delta_{pq} (N\rho_1c_2)], & c_4 &= [\Delta_{pq} (N\rho_1s_2)] \\
 c_5 &= N_p - N_q,
 \end{aligned} \tag{6.44}$$

the gradient of Eq. (6.43), for $j = 1, \dots, n_{\text{vars}}$, reads:

$$\frac{\partial g_{\text{blend-0}}}{\partial \xi_j} = \begin{cases} 2c_1 \rho_{0K}^{(p)} \cos(2\pi\phi_1^{(p)}) + 2c_2 \rho_{0K}^{(p)} \sin(2\pi\phi_1^{(p)}) - 2c_5, & \text{if } \xi_j = n_p, \\ 2c_1 n_p \cos(2\pi\phi_1^{(p)}) + 2c_2 n_p \sin(2\pi\phi_1^{(p)}), & \text{if } \xi_j = \rho_{0K}^{(p)}, \\ -4\pi c_1 n_p \rho_{0K}^{(p)} \sin(2\pi\phi_1^{(p)}) + 4\pi c_2 n_p \rho_{0K}^{(p)} \cos(2\pi\phi_1^{(p)}), & \text{if } \xi_j = \phi_1^{(p)}, \\ -2c_1 \rho_{0K}^{(q)} \cos(2\pi\phi_1^{(q)}) - 2c_2 \rho_{0K}^{(q)} \sin(2\pi\phi_1^{(q)}) + 2c_5, & \text{if } \xi_j = n_q, \\ -2c_1 n_q \cos(2\pi\phi_1^{(q)}) - 2c_2 n_q \sin(2\pi\phi_1^{(q)}), & \text{if } \xi_j = \rho_{0K}^{(q)}, \\ 4\pi c_1 n_q \rho_{0K}^{(q)} \sin(2\pi\phi_1^{(q)}) - 4\pi c_2 n_q \rho_{0K}^{(q)} \cos(2\pi\phi_1^{(q)}), & \text{if } \xi_j = \phi_1^{(q)}, \\ 0, & \text{otherwise,} \end{cases} \tag{6.45}$$

and

$$\frac{\partial g_{\text{blend-1}}}{\partial \xi_j} = \begin{cases} 2c_1 \rho_1^{(p)} \cos(\pi\phi_1^{(p)}) + 2c_2 \rho_1^{(p)} \sin(\pi\phi_1^{(p)}) - 2c_5, & \text{if } \xi_j = n_p, \\ 2c_1 n_p \cos(\pi\phi_1^{(p)}) + 2c_2 n_p \sin(\pi\phi_1^{(p)}), & \text{if } \xi_j = \rho_1^{(p)}, \\ -2\pi c_1 n_p \rho_1^{(p)} \sin(\pi\phi_1^{(p)}) + 2\pi c_2 n_p \rho_1^{(p)} \cos(\pi\phi_1^{(p)}), & \text{if } \xi_j = \phi_1^{(p)}, \\ -2c_1 \rho_1^{(q)} \cos(\pi\phi_1^{(q)}) - 2c_2 \rho_1^{(q)} \sin(\pi\phi_1^{(q)}) + 2c_5, & \text{if } \xi_j = n_q, \\ -2c_1 n_q \cos(\pi\phi_1^{(q)}) - 2c_2 n_q \sin(\pi\phi_1^{(q)}), & \text{if } \xi_j = \rho_1^{(q)}, \\ 2\pi c_1 n_q \rho_1^{(q)} \sin(\pi\phi_1^{(q)}) - 2\pi c_2 n_q \rho_1^{(q)} \cos(\pi\phi_1^{(q)}), & \text{if } \xi_j = \phi_1^{(q)}, \\ 0, & \text{otherwise.} \end{cases} \tag{6.46}$$

6.3 The Stacking Sequence Recovery Phase

As said in Section 2.1.3, in the multi-scale multi-level approaches the goal of the SLP is to search for at least one blended SS, for the whole structure, recovering at the same time the optimal value of thickness and of elastic properties resulting from the resolution of the FLP. Therefore, a numerical strategy must be developed. It must be able to find at least one SS, blended in the sense of Definition 6.3, which meets the target elastic properties determined in the FLP. The process of recovering the stiffness properties will be referenced as *stiffness recovery* (SR).

From a manufacturing point of view, the stand-alone solution in terms of optimal stiffness distribution is not enough in the sense that, at the end of the FLP, it is unknown how to manufacture the blended laminates, because only optimised stiffness properties and thickness are available. What is necessary is an explicit expression of stacking sequences. This is intrinsically due to the multi-level design formulations. In fact, in the FLP, one "gives up" to know information related to the mesoscale of laminates, in order to facilitate the design considering homogenised laminates. However, in the SLP, the designer strives on recovering the lost information. It is clear that the design problem integrating the blending requirement, which is essentially about manufacturability, can be (and must be) considered solved only when at least one manufacturable SS, having some characteristics in the sense specified above, is provided for the whole structure.

6.3.1 Stiffness Recovery for a Single Laminate

The basic step for the mathematical formulation of the SS recovery phase for blended structures is the formalisation of the SR for a single laminate. Of course, in this particular case, the design variables vector coincides with the SS of the laminate, as in Definition 4.4. Therefore, there are as many independent design variables as the number of plies of the laminate. Hereafter, target PPs will be labelled with the symbol \dagger : $\rho_{0K}^\dagger, \rho_1^\dagger, \phi_1^\dagger$. Nevertheless, it is more convenient to consider the following equivalent set of parameters in place of ρ_{0K}^\dagger :

$$K^{A*\dagger} = \begin{cases} 0, & \text{if } \rho_{0K}^\dagger \geq 0, \\ 1, & \text{if } \rho_{0K}^\dagger < 0, \end{cases} \quad \rho_0^\dagger = \frac{\rho_{0K}^\dagger}{(-1)^{K^{A*\dagger}}}. \quad (6.47)$$

As discussed in (Montemurro et al., 2012a; Montemurro, 2015a), it is useful to consider the following dimensionless quantities:

$$\begin{aligned} \mathcal{R}_1(\theta_k) &:= \frac{\|\mathbf{B}^*(\theta_k) - \mathbf{0}^\dagger\|_{L^2}}{\mathcal{M}}, & \mathcal{R}_2(\theta_k) &:= \frac{\|\mathbf{C}^*(\theta_k) - \mathbf{0}^\dagger\|_{L^2}}{\mathcal{M}}, \\ \mathcal{R}_3(\theta_k) &:= |2(\phi_0(\theta_k) - \phi_1(\theta_k)) - K^{A*\dagger}|, & \mathcal{R}_4(\theta_k) &:= |\rho_0(\theta_k) - \rho_0^\dagger|, \\ \mathcal{R}_5(\theta_k) &:= |\rho_1(\theta_k) - \rho_1^\dagger|, & \mathcal{R}_6(\theta_k) &:= |\phi_1(\theta_k) - \phi_1^\dagger|, \end{aligned} \quad (6.48)$$

and

$$\mathcal{R}(\theta_k) := \sum_{i=1}^6 \mathcal{R}_i^2(\theta_k). \quad (6.49)$$

In Eq. (6.48), \mathcal{M} is a suitable modulus which can be defined in different ways. In the following, it is assumed equal to Eq. (4.5). The quantities appearing in Eq. (6.48) can be interpreted as the distances (residuals) from target properties (labelled with \dagger) for a uncoupled, homogeneous, orthotropic laminate, whilst Eq. (6.49) is the residual function for a single laminate, i.e. the sum of the square of all the aforementioned six terms.

Definition 6.4 (Recovery stacking sequence). A *recovery stacking sequence (RSS)* is a stack for which $\mathcal{R} = 0$.

Equation (6.49) represents a suitable distance from a laminate having desired mechanical properties. Of course, its extremal value is zero, reached when all the terms \mathcal{R}_i , $i = 1, \dots, 6$ are null, i.e. when all the target properties are matched. The physical meaning of \mathcal{R}_i , $i = 1, \dots, 6$, is straightforward: \mathcal{R}_1 represents the uncoupling condition, \mathcal{R}_2 the homogeneity condition, \mathcal{R}_3 the orthotropy condition, \mathcal{R}_4 , \mathcal{R}_5 and \mathcal{R}_6 the conditions over target PPs.

The RSS can be found by means of a dedicated numerical tool. In fact, the RSS is solution of the following SR problem:

$$\min_{\theta_k} \mathcal{R}(\theta_k), \theta_k \in \text{SS}, k = 1, \dots, N, \quad (6.50)$$

which is an *unconstrained non-linear programming problem* (UNLPP). Problem (6.50) may admit more than one solution because of the non-bijective relationship between the SS and the laminate PPs (Montemurro, 2015a, 2015b).

The design variables of Problem (6.50) are the layers orientation angles. As a consequence, the problem is strongly non-convex because of the trigonometric functions linking the PPs and such design variables. Moreover, as detailed in (Montemurro et al., 2012a; Montemurro et al., 2012b, 2012c; Catapano & Montemurro, 2014a, 2014b; Montemurro, 2015a, 2015b, 2015c; Montemurro et al., 2016; Montemurro et al., 2019), the merit function of Problem (6.50) has some interesting properties:

- it is a non-negative function in the PPs space (in particular, it can be expressed as a quadratic form);
- design requirements on elastic symmetries and laminate stiffness tensors properties can be easily formulated in terms of tensor invariants and do not depend upon the considered frame;
- the values of the global minima are known *a priori*, corresponding to the zeros of the function.

A further advantage of such a formulation is that Problem (6.50) is an UNLPP, which is easier to solve than a CNLPP. In the formulation proposed in Eq. (6.50), the residual contributions are dimensionless, see Eq. (6.48), and are aggregated by means of a simple sum. In so doing, it is assumed that the requirements of Eq. (6.48) have the same weight because they have the same importance. Of course, one could consider as objective function a weighted sum of the residuals provided in Eq. (6.48), to privilege, for instance, the uncoupling and homogeneity conditions rather than the recovery of the PPs of the membrane stiffness tensor. In the following, the former approach proposed by Montemurro (2015a, 2015b, 2015c) has been preferred.

6.3.2 Recovery Stacking Sequences for the Entire Structure

The design variables of Problem (6.50) for a single laminate are the orientation angles.

However, if multi-laminate blended structures are considered, the problem is more complicated. At the laminate mesoscale, the blending constraint is merely a decision problem whether points (a) and (b) of Definition 6.3 are satisfied or not. Considering the generic couple of adjacent panels, labelled with subscripts p and q , the decision problem can be handled through Algorithm 6.3 (for the sake of simplicity, assume $N_p > N_q$):

Algorithm 6.3 Mesoscale blending check.

```

1:  $j \leftarrow 1$ .
2: for  $k = 1, \dots, N_p$  do
3:   if  $SS_p[k] = SS_q[j]$  then
4:      $j \leftarrow j + 1$ 
5:   end if
6:   if  $j = N_q + 1$  then
7:     return 0 ▷ Blending requirement satisfied
8:   end if
9: end for
10: return 1 ▷ Blending requirement not satisfied
    
```

Problem (6.50), formulated for one panel, can be extended to the search of blended RSSs for the whole structure as follows:

$$\min_{SS_j} \sum_{j=1}^{n_{\text{pan}}} \mathcal{R}^{(j)}, \text{ subject to:} \quad (6.51)$$

Algorithm 6.3 returns 0 \forall couples of adjacent panels,

where n_{pan} is the number of laminates composing the structure. Unlike Problem (6.50), Problem (6.51) is a CNLPP and presents two main issues. Firstly, in Problem (6.51) it is not clear the dependence of the merit function from the $SS_j, j = 1, \dots, n_{\text{pan}}$. Secondly, the dimension of the design space is not *a priori* known. Blending constraints, in fact, create a strong non-univocal coupling between SSs of panels.

To clarify this aspect, consider, for the sake of simplicity, three laminates $p, q,$ and r as in Figure 6.6. Unlike the case wherein the three panels are independent, i.e. when

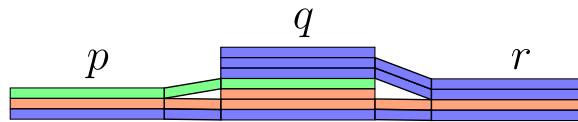


Figure 6.6: Blending of three laminates (different colours mean different orientations).

blending is not taken into account, the design space has not dimension $N_p + N_q + N_r$, and $\mathcal{R}^{(j)}$ does not depend only on $SS_j, j \in \{p, q, r\}$. For the case of Figure 6.6, the design space has dimension N_q , whilst the dependence is not unique, because it is affected by the *search propagation direction*, which plays a pivotal role.

Before introducing a formal definition, consider, as an illustrative example, the following two possible propagations. To solve Problem (6.51) for the structure of Figure 6.6, one could either:

- (a) find a RSS for panel p , by solving Problem (6.50). For panel q , $N_q - N_p$ orientations need to be determined and inserted within SS_p , to achieve SS_q . Note that blending constraints between p and q are satisfied *by construction*. Successively, SS_r can be obtained by choosing N_r orientations from SS_q . Note that, also in this case, the blending requirements between q and r are satisfied *by construction*. Therefore, at the end, there are N_q independent design variables, and the following chain of dependences between stacks is determined: $SS_q = SS_q(SS_p, (N_q - N_p) \text{ angles})$ and $SS_r = SS_r(SS_q(SS_p, (N_q - N_p) \text{ angles}))$.
- (b) find a RRS for panel q , by solving Problem (6.50). Panels p and r SSs can be determined by choosing N_p and N_r orientations from SS_q , respectively. Note that, also in this case, the blending requirements are satisfied *by construction*. Again, the number of independent design variables is N_q . The chain of dependences is $SS_p = SS_p(SS_q)$ and $SS_r = SS_r(SS_q)$.

Separately minimising $\mathcal{R}^{(j)}$, $j \in \{p, q, r\}$, as done in the two aforementioned propagations, does not guarantee the minimisation of the global \mathcal{R} . This is an issue especially when the propagation moves from a thicker to a thinner panel, as in the first propagation scheme. In fact, when passing from q to r , the RSS search degenerates in extracting a N_r -sised subset from SS_q , respecting blending. The optimal choice is, of course the minimiser of $\mathcal{R}^{(r)}$. Nevertheless, for this combinatorial problem, one should try all the possible N_r -sised subsets from an N_q -sised one. From a computational point of view, this is impractical, since the number of the possible arrangements is of the order of $\binom{N_q}{N_r}$. Moreover, the minimised residual $\mathcal{R}^{(r)}$ could not be close to zero, because the only degree of freedom for the designer is the blending arrangement.

6.3.3 The Concept of Search Propagation Direction

A strategy to avoid these problems could be transforming the CNLPP of Eq. (6.51) into an UNLPP. This can be done imposing blending *by construction*. For instance, when passing from a thicker laminate to a thinner one, blending decision problem of Algorithm 6.3 is automatically satisfied if the thinner SS is obtained by extracting a subset from the thicker SS. The extraction can be *a priori* imposed, according to some predefined blending scheme, or even random. The determination of the orientation values must be carried out to minimise the global \mathcal{R} for the structure. A similar approach can be arranged when passing from thinner to thicker laminates. The orientation angles are by far the most impacting parameters to minimise \mathcal{R} .

Therefore, the following operative definition can be given for the *search propagation*:

Definition 6.5 (Search propagation direction). *The search propagation direction is the order, among the laminates constituting the structure, according to which the blended SSs are built. For each pair of adjacent laminates, the construction is performed as follows:*

- *if the propagation moves from a thinner to a thicker laminate, plies are added within the SS of the former;*
- *if the propagation moves from a thicker to a thinner laminate, plies are dropped from the SS of the former.*

In so doing, a proper propagation must ensure that blending requirements are automatically satisfied among all of the adjacent laminates of the structure.

As it will be discussed in the next Section, the position whereby inserting or dropping plies does not affect propagation directions satisfying Definition 6.5. Once a proper propagation direction has been determined, it remains only to determine the orientation values matching the desired optimal elastic properties of the structure. In so doing, the recovery for blended laminates has been reduced in similarity to the recovery of a single laminate. Note that the procedure described in Definition 6.5 satisfies points (a) and (b) of Definition 6.3: injectivity and no-self-intersection are preserved.

6.3.3.1 Mathematical Justification of Search Propagation Direction

In this Section, conditions to transform Problem (6.51) into an UNLPP are established. The idea is to find a search propagation direction which guarantees the blending requirements satisfaction between each pair of adjacent laminates, regardless of the particular plies interested by blending.

It has been stated that, when imposing blending by construction, the constrained Problem (6.51) can be transformed into an unconstrained one. As a consequence, the recovery becomes a more handy unconstrained SR problem. The key point is to find a proper solution propagation path, which may allow for such a simplification.

To illustrate this point, consider, for example, the structure of Figure 6.7, composed by $n_{\text{pan}} = 4$ laminates having 31, 8, 19 and 11 plies, respectively. For the sake of simplicity, laminates are named after their number of plies: e.g. “31” is the laminate having 31 plies, etc. Of course, as will be clear, the particular search propagation determines the number of independent variables (orientations) within the stack recovery phase problem.

Consider two propagations for the same problem of Figure 6.7, as shown in Figure 6.8. Propagation 1 (Figure 6.8a) starts from “8” (s is a reminder of *starting laminate*). Hence, there are 8 independent orientations that must be determined. Then, it moves to “11”, and $11 - 8 = 3$ further independent variables are introduced in the problem. Successively, the propagation moves to “19”, introducing 8 additional variables. Finally, it moves to “31” (a is a reminder of *arrival laminate*), adding 12 more variables. At the end, according to Propagation 1, the stack recovery phase has $n_{\text{vars}} = 31$ independent variables to determine. It is easy to see that, since the progressive addition of plies during the

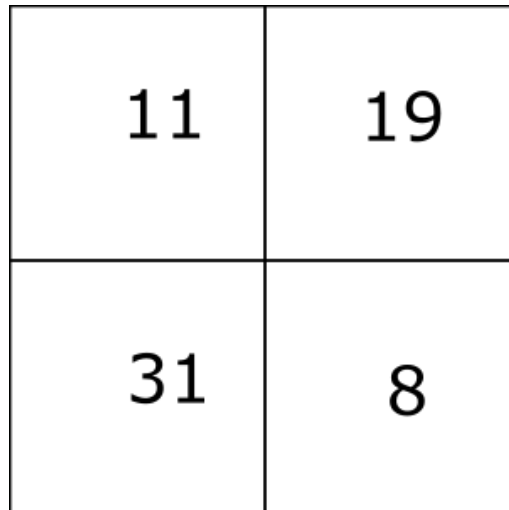


Figure 6.7: A four-laminate blended structure

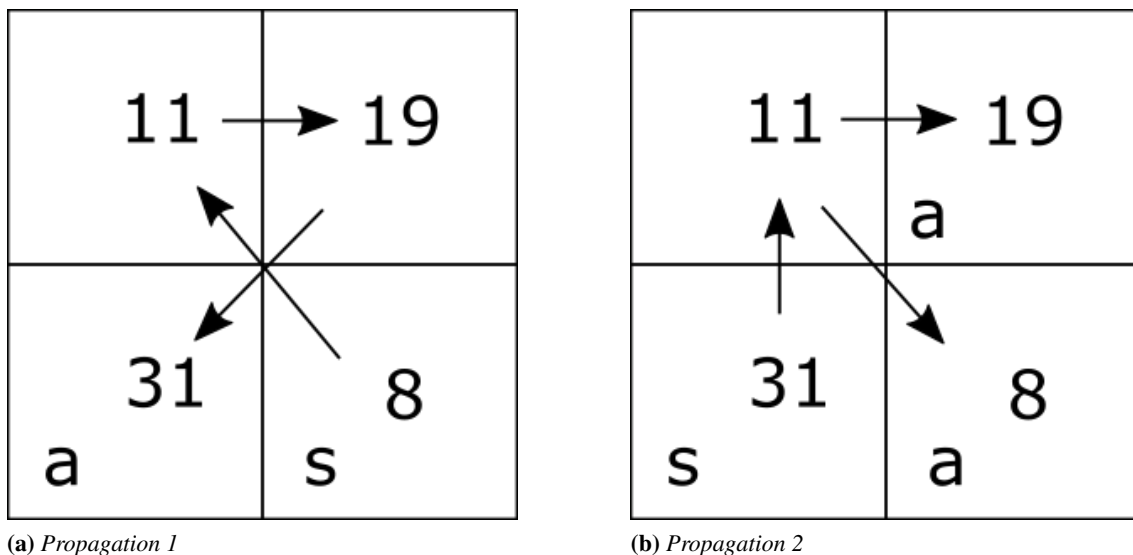


Figure 6.8: Two propagation schemes.

search propagation, for every possible pair or adjacent laminates the thinner SS is always contained in the thicker one. Therefore, the conclusion is that the structure is blended, regardless of the particular orientation values and regardless of the particular indices in the SSs interested by the ply-drop.

Propagation 2 (Figure 6.8b) starts from “31” with 31 independent variables. Then, it moves to “11”, but no more variables are added, since the stack of “11” is a subset of the stack of “31”. Again, the passage to “8” does not introduce further variables. On the contrary, the passage from “11” to “19” introduces 8 independent variables. At the end, according to Propagation 2, the stack recovery phase has $n_{\text{vars}} = 39$ independent variables. It is easy to see that the SS of “8” is necessarily contained in the SS of “19” and “31” regardless of the particular orientation values and regardless of the particular indices in the SSs interested by the ply-drop. Therefore, the structure is blended.

Some remarks are needed:

- (a) The search propagation for the same structure is not unique, as trivially shown in Figure 6.8 for the structure of Figure 6.7;
- (b) The number of independent variables within the stack recovery phase depends on the particular propagation adopted;
- (c) The blending requirement satisfaction is independent from the particular insertion position within a stack of additional plies when passing from a thinner to a thicker laminate. For example, when passing from “8” to “11”, the 3 additional plies can be added in any position within the stack of “8”.
- (d) The blending requirement satisfaction is independent from the particular suppression position within a stack of “extra” plies when passing from a thicker to a thinner laminate. For example, when passing from “11” to “8”, 3 extra plies can be suppressed in any position within the stack of “11”, without jeopardising blending.

Points (a) and (b) allow the user to choose any propagation which ensures the satisfaction of blending constraints of adjacent laminates by construction (see Definition 6.5). This is the only non-automated part of the strategy, since it heavily depends on the particular problem at hand. Moreover, it is a crucial step, since it allows transforming the constrained Problem (6.50) into an unconstrained one. If more propagations are available, it is preferable to choose the one which maximises the number of independent variables. In so doing, the larger design space allows for smaller residual \mathcal{R} .

As a counter example, Figure 6.9 shows a *bad* propagation, since “11” and “19” are not necessarily blended. In fact, “11” and “19” are the result of two distinct paths (“8”-“19” and “8”-“31”-“11”), which are independent. In fact, there may be some orientations in “19” which cannot be present in “11”, thus jeopardising the blending of the structure.

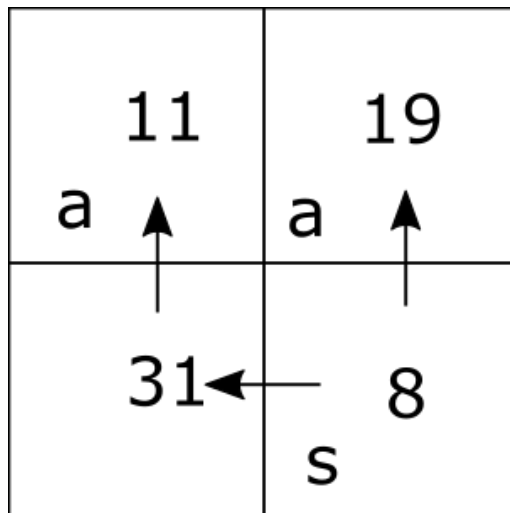


Figure 6.9: Propagation 3: a propagation which does not ensure automatic blending of adjacent stacks

Points (c) and (d) allow for different blending schemes to be imposed, regardless of the particular propagation: inner and outer blending, ply drop with continuity of the out-

ermost plies, random, customised, etc.. Some of them are represented in Figure 6.10. It allows the user to choose a blending scheme that may be suitable for the particular

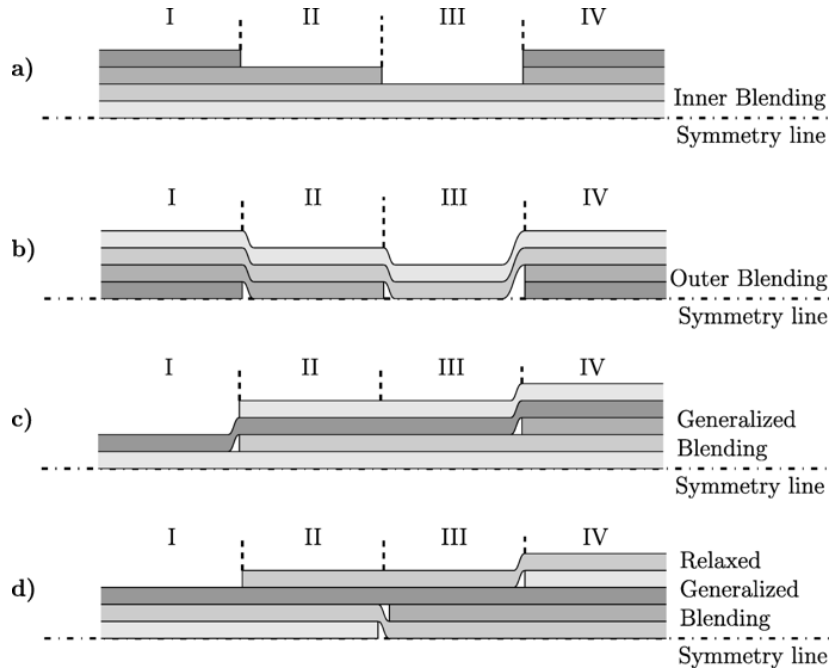


Figure 6.10: Some possible blending schemes (from van Campen et al. (2008), Bordogna et al. (2020))

problem at hand.

Once a proper solution propagation has been determined, and a blending scheme is chosen, the SLP just solves the SR problem for all of the n_{pan} laminates:

$$\min_{SS_j} \sum_{j=1}^{n_{\text{pan}}} \mathcal{R}^{(j)}, \quad (6.52)$$

where the stacks are function of the n_{vars} ¹ orientation angles and are built by the numerical algorithm used for the solution search. In fact, once blending constraints are automatically satisfied, the only parameters to address are the n_{vars} orientation angles, in order to recover the desired stiffness properties. Therefore, the SR problem has been transformed in an unconstrained problem, analogously to the stiffness recovery of a single laminate.

To state the formal condition which makes the propagation proper, some results and definitions must be introduced (see, for example, (Munkres, 2000)).

Lemma 6.1 (Injectivity of the composition of injective functions). *Let $f : A \mapsto B$ and $g : B \mapsto C$ be two injective functions. Then, the composition $g \circ f : A \mapsto C$ is injective.*

Definition 6.6 (Identity function of a set). *Let C be a set. The identity function for the set C is the map $I_C : C \mapsto C$ given by the rule $I_C(x) = x \forall x \in C$.*

¹Also for the SLP n_{vars} designates the number of variables. However, for the SLP, they are different in number and typology from those of the FLP.

Definition 6.7 (Left-inverse function). *Let $f : A \mapsto B$ be a function. The function $g : B \mapsto A$ is a left-inverse for f if $g \circ f = I_A$. The left-inverse of f is denoted as f_L^{-1}*

Lemma 6.2 (Necessary and sufficient conditions for injectivity). *Let $f : A \mapsto B$ be a function. Then, f is injective if and only if there exists a left-inverse function $g : B \mapsto A$.*

Blending operator definition has been given in Definition 6.3. Accordingly, given two laminates p and q , with $N_p > N_q$, the blending is the injective map $\mathcal{B} : SS_q \mapsto SS_p$ such that all orientations within SS_q , at a certain position within SS_q , are mapped into some possibly different positions within SS_p , without ply intersections. According to Lemma 6.2, there exists also a left-inverse mapping $\mathcal{B}_L^{-1} : SS_p \mapsto SS_q$. The action of the blending mapping and of its left-inverse is conceptually sketched in Figure 6.11. A possible choice for the left-inverse blending map is as follows:

$$\mathcal{B}_L^{-1}(\theta_j) := \begin{cases} \mathcal{B}^{-1}(\theta_j), & \text{if } \theta_j \in \mathcal{B}(SS_q), \\ c, & \text{if } \theta_j \in SS_p \setminus \mathcal{B}(SS_q), \end{cases} \quad (6.53)$$

where c is an arbitrary element of SS_q .

By construction, when passing from a thinner (say, SS_q) to a thicker laminate (say, SS_p), the introduction in any position within SS_q of $N_p - N_q$ plies preserves the condition of no-intersection of plies, as already noted. The same consideration holds if the thinner laminate is created by dropping $N_p - N_q$ plies from the thicker laminate. In so doing, only injectivity of blending mappings between adjacent laminates must be controlled.

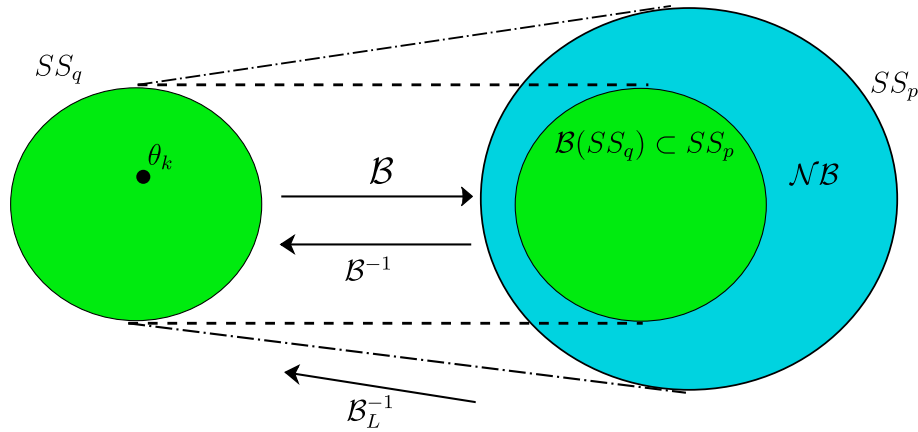


Figure 6.11: Sketch of the action of the blending map \mathcal{B} and its left-inverse \mathcal{B}_L^{-1} .

To illustrate the condition, consider the three graphs, relative to Propagation 1, 2 and 3 illustrated in Figures 6.12, 6.13 and 6.14, respectively. Each square represents a laminate of the structure of Figure 6.7, with inside the number of plies. Black arrows represent the solution propagation, as already considered in Figures 6.8a, 6.8b and 6.9. Red arrows represent the injective blending maps between adjacent laminates (from the thinnest to the thickest of each pair).

In Figure 6.12, Propagation 1 maps SS_8 to SS_{11} through the injective map f . Then, the propagation maps SS_{11} to SS_{19} through the injective map g and, finally, maps SS_{19}

to SS_{31} through the injective map h . As a result, there are defined, between each pair of adjacent laminates, injective maps, i.e. $g, g \circ f, h \circ g$ and $h \circ g \circ f$ (see also Lemma 6.1).

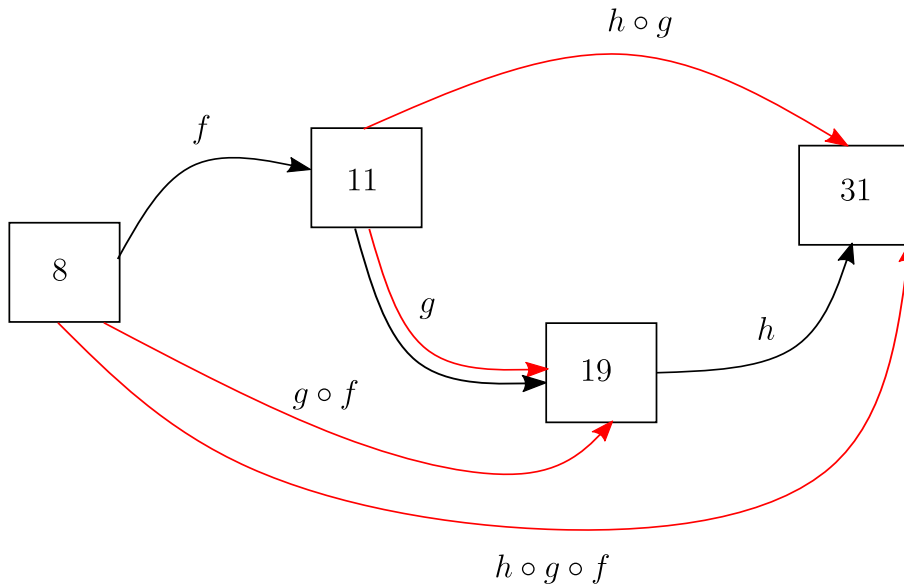


Figure 6.12: *Injective maps for Propagation 1*

In Figure 6.13, Propagation 2 maps SS_{31} to SS_{11} through the left-inverse map f_L^{-1} . Note that, for blending, its "inverse" map (f) must be injective. Therefore, f_L^{-1} exists and is well-defined. Then, the propagation maps SS_{11} to SS_{19} through the injective map h and, finally, maps SS_{11} to SS_8 through the left-inverse map g_L^{-1} . As a result, there are defined, between each pair of adjacent laminates, injective maps, i.e. $f, h, h \circ g$ and $f \circ g$ (see also Lemma 6.1).

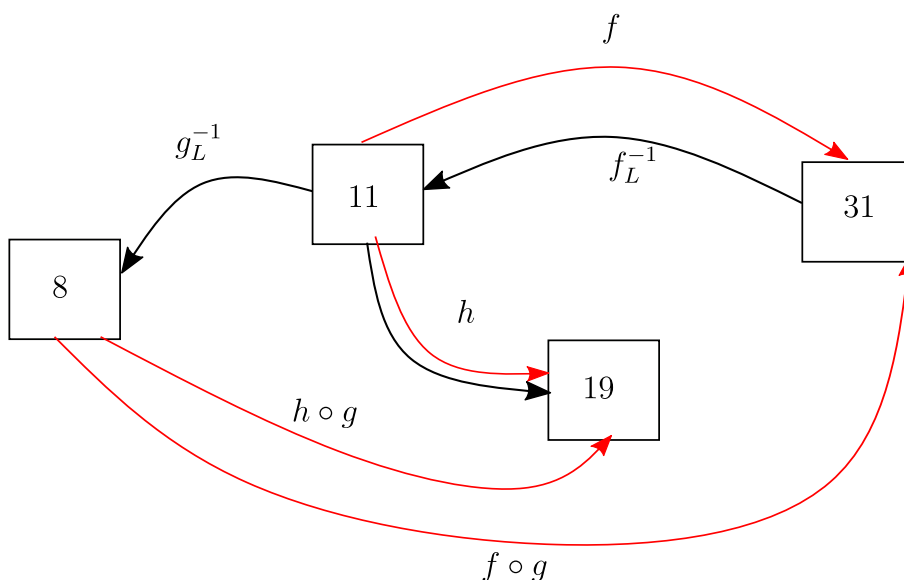


Figure 6.13: *Injective maps for Propagation 2*

In Figure 6.14, Propagation 3 maps SS_8 to SS_{19} through the injective map h . Then, the propagation maps SS_8 to SS_{31} through the injective map f and, finally, maps SS_{31} to SS_{11} through the left-inverse map g_L^{-1} . As a result, there are defined, between each pair

of adjacent laminates, injective maps, i.e. f, h, g and a non injective map $h \circ h_L^{-1} \circ g$ (the left-inverse is generally not injective). As a result, laminates "11" and "19" may be not

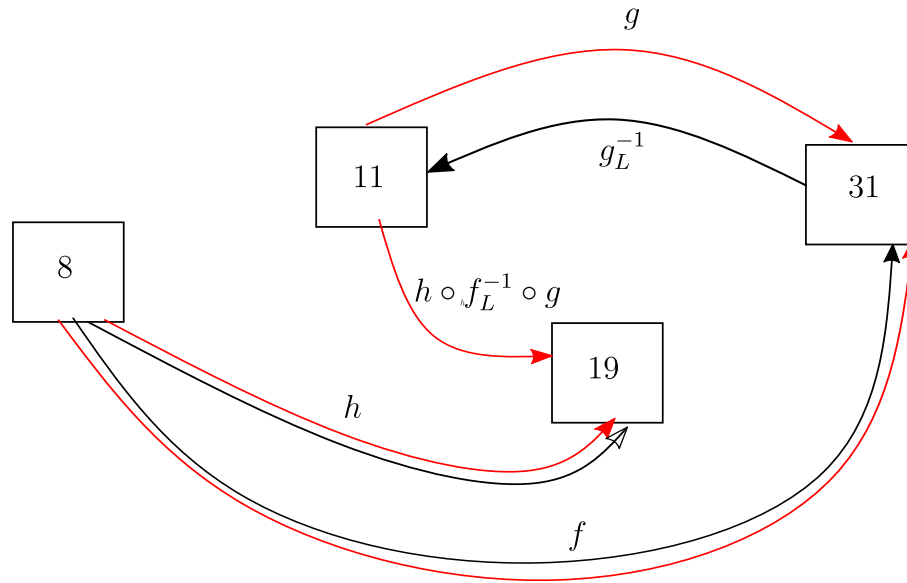


Figure 6.14: Injective maps for Propagation 3

satisfy blending requirement.

To conclude, proper propagations are those for which injective maps arise between each pair of adjacent laminates. An automated strategy to find out solution propagations goes beyond the aim of this Thesis, and such problem will not be addressed. Nor, the problem of find the propagation which maximises the number of variables has not been taken into account. In the following, proper propagation schemes have been find out manually. Of course, this is possible for relatively small structure, whilst for more complex ones an automated strategy should be established.

6.4 An Alternative Approach for the Stacking Sequence Recovery Phase

In Sections 6.2 and 6.3, a strategy for the SS recovery has been introduced and discussed. It is based on a numeric approach, trying to match the target properties, determined in the FLP, taking blending into account in the already discussed strategy. In particular, the SR is done by minimising a residual function composed by six contributes (see Eq. (6.48)) for each laminate of the structure.

In Section 4.3 QT QH SSs have been introduced. It is noteworthy that QT QH SSs are exact solutions for uncoupled and homogeneous laminates: one may wonder whether the use of such QT QH SSs in the stack recovery phase can be profitable. In fact, the part of residual associated to the recovery of uncoupling and homogeneity (residuals \mathcal{R}_1 and \mathcal{R}_2 of Eq. (6.48)) is exactly zero by definition of QT QH SSs.

The stack recovery phase using QT QH SSs can be performed if they are known in

advance, for laminates of any number of plies. A database up to $N = 35$ plies has been already proposed by Garulli et al. (2018) using a dedicated algorithm for the search. The database contains only *independent* QT QH SSs, i.e. SSs whose saturated groups do not contain any other saturated subgroups. In this Chapter, an alternative version of the algorithm by Garulli et al. (2018), Garulli (2020) is presented. Based on the observation that the QT QH SSs search can be view as the contribute of two well-known combinatorial problems, the proposed version of the algorithm has brought to the extension of the QT QH SSs database up to $N = 39$ plies.

The knowledge of all the QT QH SSs, although limited to a relatively small number of plies, would allow to recover blended SSs for the structure at hand. A possible strategy for employing QT QH SSs in blending structures is also presented in this Chapter. In particular, Section 6.4.1 introduces DLX-Stack Finder, the new algorithm for the search of QT QH SSs. Then, Section 6.4.2 shows the stack recovery approach based on the knowledge of QT QH SSs.

6.4.1 An Algorithm for the Search of Quasi-trivial Quasi-homogeneous Stacking Sequences

Although QT QH SSs, in general, are not the *full* set of uncoupled and homogeneous laminates, they constitute a *large* family. In (Garulli et al., 2018), a database of all QT QH SSs has been presented, for SSs up to $N = 35$. However, this approach has, as a drawback, the very rapid increasing of the necessary computational sources to make computations. A different approach has been then developed, in order to expand the database towards thicker laminates. In particular, the focus has been to retrieve the uncoupled and homogeneous laminates for $N > 35$.

The problem of finding QT QH SSs can be decomposed into two well-known combinatorial decision problems: the *Subset-sum problem* and the *Exact-cover problem*, which are known to be nondeterministic polynomial time complete problems (NPC). A decision problem is a yes-or-no question. NPC is a complexity class used to label decision problems for which the instances having answer *yes* can be verified in polynomial time. Polynomial time means that, if the instance to be verified has size n , the verification takes n^k time, for some positive k . However, the solution search for NPC problems cannot be computed in polynomial time, at least for the current state of the art in Algorithmics². For deeper insights, which go beyond this Thesis, see the classical textbook (Cormen et al., 2001).

Definition 6.8 (Subset-sum problem). *Given a set S of integers, find (if it exists) one proper non-empty subset S' (i.e. $S' \subset S$, $S' \neq \emptyset$) whose elements sum up to a predefined integer M .*

²The *P vs NP* problem wonders whether it is actually possible or not. It is one of the most celebrated unresolved problems in Computer Science. In plane language, it asks whether there is a fast procedure to answer all questions that have short answers that are easy to verify mechanically (Aaronson, 2016)

Definition 6.9 (Exact-cover problem). *Given a collection C of subsets of a set S , an exact cover of S is a subcollection C^* of C such that subsets in C^* are pairwise disjoint and the union of the subsets of C^* is S . Then, find (if it exists) one of such subcollections C^* .*

Before stating the definition of the problem of the QT QH SSs search, the following definition is needed:

Definition 6.10 (M-unsubsummable set). *A set S of integers whose elements sum up to $M \in \mathbb{Z}$ and which does not contain a proper non-empty subset whose elements sum up again to M is said M-unsubsummable.*

Then, the enumeration problem of QT QH SSs can be formulated as follows:

Definition 6.11 (Quasi-trivial quasi-homogeneous stacking sequences search problem). *Given a number of plies $N \in \mathbb{N}$, consider the sets of integer coefficients $\mathcal{B}_N := \{b_k : k = 1, \dots, N\}$ and $\mathcal{C}_N := \{c_k : k = 1, \dots, N\}$, whose elements belong to \mathbb{Z} . Then, find all the zero-unsubsummable subsets of \mathcal{B}_N and \mathcal{C}_N (Subset-sum problem) which are at the same time exact cover of \mathcal{B}_N and \mathcal{C}_N , respectively (Exact-cover problem).*

The requirement of zero-unsubsummability (see Definition 6.10 with $M = 0$) of the subsets of \mathcal{B}_N and \mathcal{C}_N is stronger than the saturated group requisite of Definition 4.5. Moreover, it imposes that only independent solutions (in the sense of Garulli et al. (2018)) are sought. This means that cases in which a QT QH SS contains at least one non zero-unsubsummable group are disregarded. In fact, a non zero-unsubsummable SS having m_1 groups can be interpreted as the degeneration of another SS, having $m_2 > m_1$ groups, in the sense that $m_2 - m_1$ orientations coincide. For example, the QT QH SS $[1/2_2/1_2/2/1/2/1_2/2_2/1]$ (two saturated groups) is generated from $[1/2/3/1_2/3/1/2/1_2/2/3/1]$ (three saturated groups) by collapsing orientation 3 into orientation 2.

A C++ code, called DLX-Stack Finder, has been developed in order to solve the problem of Definition 6.11 for QT QH laminates. By selecting the desired number of plies N to be investigated, DLX-Stack Finder tries to build progressively and iteratively all the possible N-ply-SSs spanned by the use of orientations labels 1 and 2. The possible constructions can be visualised through a tree graph, as qualitatively shown in Figure 6.15. Since the first orientation can be labelled 1 without loss of generality, there are 2^{N-1} possible SSs (paths) and $2^N - 1$ nodes for laminates of N plies. Of course, the verification of the satisfaction of Definition 6.11 for all the 2^{N-1} stacks, even though it takes polynomial time, is not computationally efficient even for relatively large numbers of plies. To this purpose, the construction of the candidate QT QH SSs is done in such a way that is possible to check *in itinere* if the stack under construction (i.e. less than N orientations are determined) has chances to be a QT QH SS of N plies. If not, the associated branch of the binary tree of Figure 6.15 is *pruned*.

For example, with reference to Figure 6.16, DLX-Stack Finder has built the SS $[1_2]$ by choosing the light-blue coloured nodes in the tree. At the next iteration, it builds the SS

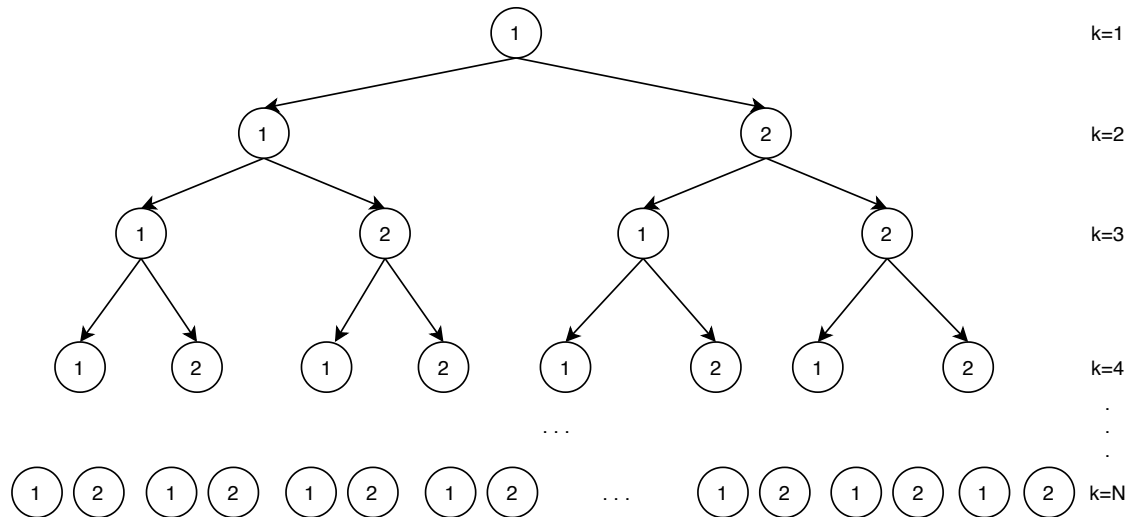


Figure 6.15: Tree graph spanned by two labels for an N -ply laminate.

[1_3]. However, recognising that it has no chances to become a QT QH N -ply SS³, DLX-Stack Finder prunes the associated branch (red-coloured nodes and arrows), moving to the SS [$1_2/2$]. The pruned branch will not be further investigated. As a results, for a cut at

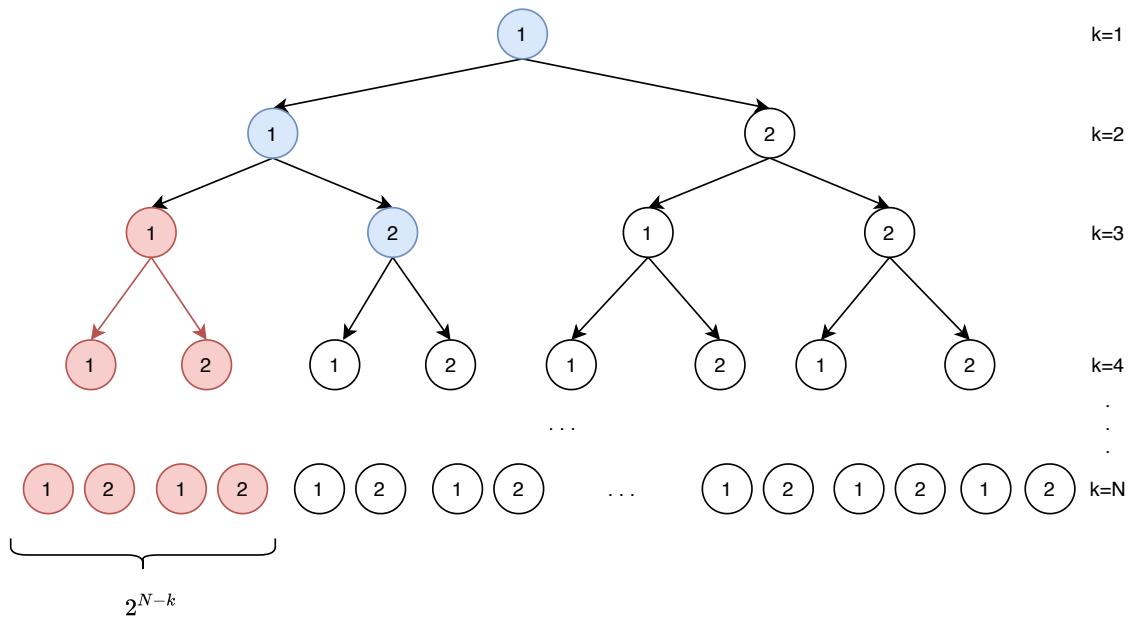


Figure 6.16: Branch pruning

a certain k ($= 3$ in Figure 6.16), there are automatically disregarded 2^{N-k} SSs: they will not be built and checked, resulting in a computational time saving. Just to give an idea, for $N = 20$, there are 524288 possible SSs and 1048575 nodes. However DLX-Stack Finder just reaches 7535 of them because of the 3705 branch prunings.

When an N -ply SS is found, DLX-Stack Finder checks whether the candidate SS is zero-unsubsummable (*Sieving* phase). If yes, a solution is found and stored. If not, the orientations of the subset (possibly, subsets) summing up to zero are incrementally re-

³It is a dummy example. The reader shall not understand that a QH QT SS cannot be of the form [$1_3/\dots$].

labelled (3, 4, 5, ...), and the check whether the "new" N -ply SS is zero-unsubsummable is performed iteratively. At the end, a solution with more than two saturated groups is found and stored. This part corresponds to the *Upping* phase by Garulli et al. (2018), Garulli (2020).

For example, for the SS $[1/2_2/1_2/2/1/2/1_2/2_2/1]$ the set of orientations labelled by 2 is not zero-unsubsummable. Then, the algorithm makes a third group to appear: $[1/2/3/1_2/3/1/2/1_2/2/3/1]$ ⁴. New checks confirm that the latter SS is a solution for the Problem of Definition 6.11 for $N = 13$.

However, DLX-Stack Finder disregards also the SSs for which the set of orientations labelled by 1 is not zero-unsubsummable. In fact, such SSs, after the Upping phase, are equal to SSs which, in any case, are eventually built by DLX-Stack Finder.

At the end of DLX-Stack Finder run, the freeware utility CMSort (Maas, 2000), specialised in handling huge files, processes the outputs files to remove eventual duplicated entries and to sort the SSs in lexicographic order.

The Exact-cover problem component of DLX-Stack Finder is addressed by an *ad-hoc* modified implementation of the well-known *Dancing Links* algorithm, or *Algorithm-X*⁵, originally appeared in (Knuth, 2000). Dancing Links algorithm is based on two basic properties of circular doubly-linked lists of nodes (see Gaddis, 2015, Chapter 17), and formalises any Exact-cover problem with a "toroidal" binary matrix representation. The algorithm is particularly efficient in dealing with backtracking, and it has been successfully used to efficiently solve large NPC problems such as Sudoku (Harrysson & Laestander, 2014) and the 18-Queen problem (Knuth, 2000).

The Subset-sum problem component of the problem of Definition 6.11 is addressed through dedicated checks whether the candidate solution of k plies, $k < N$, has chances to be an N -ply QT QH SS or not, regardless of the $N - k$ plies to be eventually determined. In the former case, DLX-Stack Finder accepts the SS under construction and goes on determining the next orientation (*Covering* phase⁶). In the latter case, the algorithm backtracks (*Uncovering* phase⁶) and prunes the associated branch. Roughly speaking, the Subset-sum problem component is composed by many conditions which are used to forecast and prune dead branches of the tree spanned by all the possible combinations of forming an N -ply SS. Among them (in the following, "coefficients" means $\{b_k\}$ and $\{c_k\}$):

- The negative coefficients cannot be all assigned to a single orientation;
- The number of groups to be still saturated must be less than the number of orientations to be still determined;
- When negative coefficients have been all assigned to an orientation, the partial sums

⁴Of course, the choice $[1/3/2/1_2/2/1/3/1_2/3/2/1]$ is equivalent. It is important to point out that the two SSs cannot be appear in the final solution database, since they are essentially the same SS. DLX-Stack Finder avoids this possibility.

⁵From which the name DLX-Stack Finder.

⁶ Standard language of Dancing Links algorithm

of coefficients related to every determined orientation cannot be positive, or the relative group cannot be saturated (only positive coefficients remain);

- Among the coefficients relative to the not-assigned orientations, there must be subsets summing up to minus each of the partial sums of coefficients associated to every determined orientation;
- At the last ply determination, the sums of coefficients associated to every group must vanish.

The conceptual structure of DLX-Stack Finder is reported in Algorithm 6.4.

Algorithm 6.4 DLX-Stack Finder

```

1: Enter the number of plies  $N$  to be investigated.
2: Initialise Dancing Link algorithm
3:  $k \leftarrow 0$  ▷ Number of determined orientations
4: function DLX-STACK FINDER
5:   if a candidate QT QH SS of  $N$  plies is found then ▷  $k = N$ 
6:     Check if the QT QH SS is zero-unsubsummable (Sieving)
7:     if it is then
8:       Store the QT QH SS in a solution file
9:     else
10:      Recursive Upping and Sieving (lines 6-9).
11:    end if
12:    return
13:  else ▷  $k < N$ 
14:     $k \leftarrow k+1$ 
15:    Continue constructing a candidate QT QH SS (Cover) ▷ Determine  $k$ -th orientation
16:    Check if the  $k$ -ply SS has chances to be a candidate QT QH SS
17:    if it has chances then
18:      DLX-STACK FINDER ▷ Recursive call
19:    end if
20:    Uncover
21:     $k \leftarrow k-1$ 
22:  end if
23:  Uncover
24:  return
25: end function

```

DLX-Stack Finder has been validated by recovering the same number of solutions reported in (Garulli et al., 2018) for QH laminates up to 35 plies. The extension of the database of Garulli et al. (2018), employing DLX-Stack Finder, is listed in Table 6.1. Figure 6.17 shows the number of QT QH SSs up to $N = 39$ (Garulli, 2020) with a best-fit approximation.

Albeit the small range of the new number of plies, it should be noted that the search of the QT QH SSs becomes more and more time consuming as the number of plies increases. Therefore, huge efforts are needed to further expanding the range.

The major drawbacks of DLX-Stack Finder are essentially two. On the one hand, the computational price has been moved to CPU capabilities of the calculator (less than 10

Table 6.1: *Quasi-trivial quasi-homogeneous stacking sequences number*

N of plies	Number of groups						Total solutions
	2	3	4	5	6	7	
36	9735	1492595	132505	1721	8	-	1636564
37	-	21796951	63557555	5270490	86095	-	90711091
38	26	26630644	36296309	2174102	21747	51	65122879
39	-	26191328	32897211	1726500	3390	-	60818429

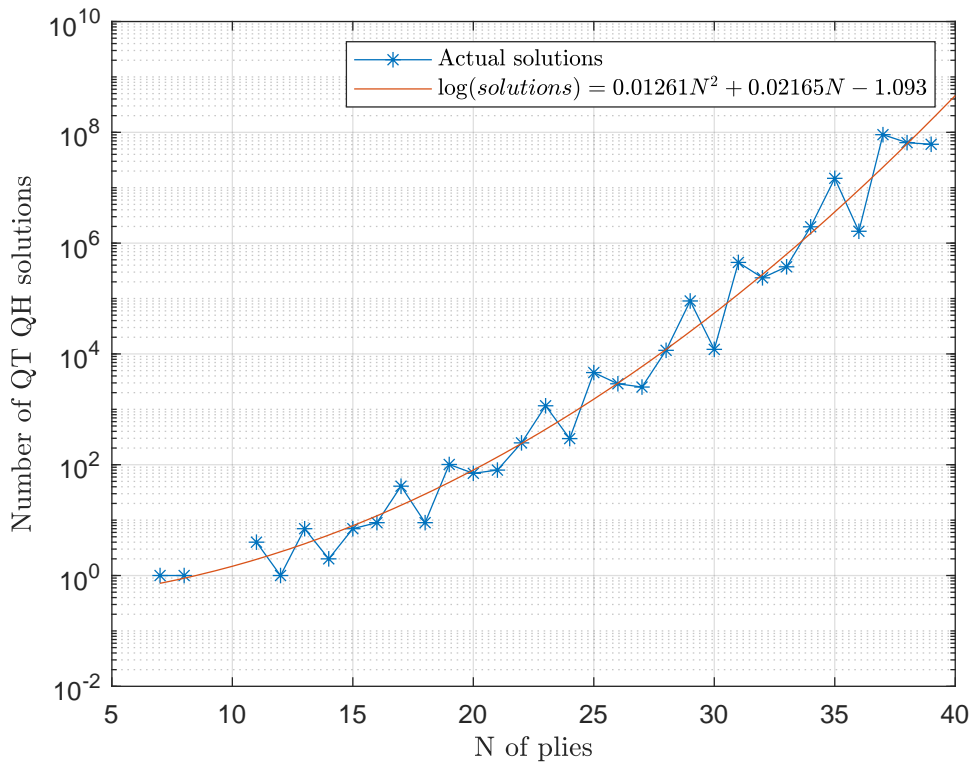


Figure 6.17: *Number of QT QH SSs up to thirty-nine plies*

MB of RAM are required to DLX-Stack Finder to perform its computations). However, the number of solutions dramatically grows up as the number of plies increases, as shown in Table 6.1 and, even if the pruning of the tree spanned by all the possible combinations, the computational time becomes of the order of months. Indeed, powerful calculators can reduce the computational time. On the other hand, the large number of solutions makes it difficult to find an efficient manner to store all of them. Currently, text files are used. Indeed, DLX-Stack Finder can be improved by reducing the CPU time of the algorithm and by developing a more efficient way of stocking the solutions. Moreover, a version of DLX-Stack Finder for solving problem of Definition 6.11 only for uncoupled or only for homogeneous laminates shall be implemented.

6.4.2 Quasi-trivial Approach

The "quasi-trivial" approach relies on the knowledge of the QT QH SSs for all the thicknesses, i.e. the numbers of plies, involved in the structure. Then, the stacking recovery approach can be defined into two steps:

- (a) find blended QT QH SSs for the structure at hand by exploiting a QT QH SSs database;
- (b) determine the values of the independent orientations, in order to match the target elastic properties.

The first point is, basically, equivalent to finding a blending scheme and solution propagation. Once found out, an optimisation must be performed to determine the values of orientations, matching the optimal elastic properties from the FLP. This step is needed since QT QH SSs define equivalence classes, as pointed out in Section 4.3, and are independent from the particular orientations.

The first point is, by far, the most challenging. The proposed strategy is based on a recursive algorithm, developed in Python language, which makes extensively use of the concept of *generators*. Roughly speaking, a Python generator is a function that saves the states of the local variables every time the *yield* statement is performed. Later on, the function continues from there on successive calls.

The use of generators is due to the fact that QT QH SSs database files are huge to handle, and cannot all be stored in the temporary memory of the calculator. A more efficient way to "read" these files is to use an iterator, created by a generator function, which returns at each call the *next* element of the file. This algorithm, called *Generator over file* (GOF), is shown in Algorithm 6.5. Note that the *yield* keyword just pauses the loop and returns the "next" SS at each call of GOF.

Algorithm 6.5 GOF function

```
1: function GOF(filename)
2:   Open filename.txt (from the database) as f
3:   while f is open do
4:     for any SS in f do
5:       yield SS
6:     end for
7:   Close f
8:   end while
9: end function
```

Another reason for the use of generators/iterators is the following. The QT QH SSs database contains only the zero-unsubsummable SSs. However, from each zero-unsubsummable SS many other SSs can be derived. For example, by collapsing the orientation 3 into the orientation 1, the QT QH SS $[1/2/3/1_2/3/1/2/1_2/2/3/1]$ gives birth to $[1/2/1_5/2/1_2/2/1_2]$. The former SS is defined *parent* SS, the latter *child* SS. Considering also child SSs is very important when Algorithm 6.3 is used to check whether two

6.4. An Alternative Approach for the Stacking Sequence Recovery Phase

SSs are blended. For example, the SS [1/2/1] is not blended with [1/2/3/2]. However, the child SS [3/1/2/1], obtained by a permutation of the orientation labels of the latter one, satisfies the blending requirement. Note that QT QH SSs admit permutations of the orientations labels, since their properties are independent from the particular angle values. The algorithm that generates the children SSs from a parent SS is called *Generator over children* (GOC) and is reported in Algorithm 6.6. Given a parent SS made of n_g saturated groups, the algorithm basically generates all the permutations of n_g elements of the set $\{1, \dots, n_g\}$. A check is done to discard solutions which would have too few or too many distinct orientations. The former requirement is imposed to consider only SSs having at least two saturated groups, thus avoiding mono-oriented SSs. The latter requirement is imposed to avoid too much fragmented SSs, which make blending a more difficult task. Then, the *next* child SS is returned at every call of GOC.

Algorithm 6.6 GOC function

```

1: Define  $n_{gmin}, n_{gmax}$  ▷ For instance,  $n_{gmin} = 2$ 
2: function GOC( $n_g, n_{gmin}, n_{gmax}, ss$ )
3:   for any  $n_g$ -permutation of  $\{1, \dots, n_g\}$  do
4:      $ngp \leftarrow$  number of distinct elements within the  $ng$ -permutation
5:     if  $n_{gmin} \leq ngp \leq n_{gmax}$  then ▷ Discard solutions which have too many or too few distinct orientations
6:       yield permuted ss ▷ Children stack of ss
7:     end if
8:   end for
9: end function

```

The ensemble of GOF and GOC is used to define a third generator, Generator over file and children (GOFC), reported in Algorithm 6.7. It returns, at every call, the next child SS of a parent of the database. When the children SSs (for that particular parent SS) have been exhausted, GOFS returns the next parent SS in the database file, and so on.

Algorithm 6.7 GOFC function

```

1: Define  $n_{gmin}, n_{gmax}$  ▷ For instance,  $n_{gmin} = 2$ 
2: function GOFC( $gof, n_{gmin}, n_{gmax}$ )
3:   while True do
4:      $ss \leftarrow$  next( $gof$ ) ▷ Next parent stack
5:      $n_g \leftarrow$  number of groups within ss
6:      $goc \leftarrow$  GOC( $n_g, n_{gmin}, n_{gmax}, ss$ )
7:     while True do
8:        $child\_ss \leftarrow$  next( $goc$ ) ▷ Next child stack from the parent (ss)
9:       yield  $child\_ss$ 
10:    end while
11:  end while
12: end function

```

The main algorithm for the search of blended QT QH SSs is described in Algorithm 6.8. Once the FLP is solved, a sequence of laminates processed by Algorithm 6.8 must be defined. It is not necessary that this sequence corresponds to the a Search Propagation

Direction. The sequence is then passed to Algorithm 6.8 as an array, said Solution Propagation array (SPA), which also contains information on the adjacent laminates for each of them. For the first element within the SPA, the associated GOFC is created. Then, a loop over the laminates (elements in the SPA) is performed. For each of them, a GOFC iterator is created (apart for the first laminate) and invoked for the next child SS. If this stack satisfies blending with the adjacent laminates (see Algorithm 6.3), it is stored in the solution array, and the procedure repeats for the next panel in the SPA, until a complete solution is achieved. Conversely, if the child SS does not satisfy blending, the next child SS is generated, blending satisfaction is checked, and so forth.

Algorithm 6.8 Stacking sequence recovery with QT QH SSs

```

1:  $k = 0$ 
2: Create SPA
3:  $\text{gofc}_0 \leftarrow$  GOFC for the first panel in SPA
4: Create empty solution array
5: while True do
6:    $\text{SS}_0 \leftarrow \text{next}(\text{gofc}_0)$ 
7:   Store  $\text{SS}_0$  in the solution array  $\triangleright$  For the first panel, the SS can be stored directly into the
   solution array
8:   function RECURSIVE_BLOCK
9:      $k \leftarrow k + 1$ 
10:     $\text{gofc}_k \leftarrow$  GOFC for the  $k$ -th panel in SPA
11:    while True do
12:       $\text{SS}_k \leftarrow \text{next}(\text{gofc}_k)$ 
13:      if  $\text{SS}_k$  satisfies blending with adjacent laminates then
14:        Store  $\text{SS}_k$  in the solution array
15:        if panels are not finished then
16:          RECURSIVE_BLOCK  $\triangleright$  Recursive call
17:        else
18:          Store the complete solution
19:        end if
20:      end if
21:    end while
22:     $k \leftarrow k - 1$ 
23:    return
24:  end function
25: end while

```

It is evident the combinatorial nature of the problem of finding QT QH SSs and of the problem of finding blended QT QH SSs. It is noteworthy that, in this alternative approach, the SR phase is uncoupled from the search of blended SSs. In other words, blended QT QH SSs from Algorithm 6.8 are encoded sequences of arbitrary orientations. A further step is required for the determination of the independent orientation angles, by solving Problem (6.52).

6.5 Conclusions

This Chapter provided answers to research questions RQ1 and RQ2.

The expression of the buckling factor, considering the transition of scale from the GFEM to the LFEM, has been derived. It contains the effect of the LFEM BCs which depend on the design variables of the FLP. The dependency is expressed by the second adjoint vector which takes into account the sensitivity of the displacement field of the GFEM.

A secondary, but crucial, problem has been also addressed. The closed-form expression of the stress stiffness matrix has been derived, through a dedicated strategy, for a shell element having four nodes and six DOFs per node. The expression is a linear combination of the internal forces per unit-length and eight matrices depending only from the geometry of the element. The explicit expressions of those matrices have been retrieved and provided, thus allowing for the final expression of the buckling factor gradient.

As for blending, a general mathematical definition has been provided. Because of its wide generality, this definition allows for a blending treatment without *a priori* assumptions. New blending constraints have been derived, stricter than those available in the literature.

A dedicated numerical strategy has been proposed for the stacking sequence recovery phase of the SLP. It is based on the concept of *search propagation direction* which allows for the definition of blended orientation regardless of the particular plies affected by ply-dropping. A mathematical justification of the functioning of such an approach has been provided, as well.

Finally, an alternative approach for the stack recovery phase has been presented. It is based on the exploitation of a particular class of laminates which are exact solutions for quasi-homogeneous laminates. In so doing, the uncoupling and quasi-homogeneity residuals are exactly zero in the residual function of the stiffness recovery phase. For this approach, a new algorithm, called DLX-Stack Finder, has been developed starting from an existing one (Garulli et al., 2018). DLX-Stack Finder has expanded the database of all QT QH SSs up to 39 plies, and there is margin to further extend it if some drawbacks, discussed in the text, will be mitigated.

The Enhanced Deterministic GL-MS2LOS and Case Studies

This Chapter aims at answering research question RQ3. Since the initial choice to settle the problem in the PPs space, due to the advantages of this parametrisation discussed in Chapters 4 and 6, the elements formalised in Chapter 6 have been implemented in the MS2LOS. The enhanced methodology, indicated as GL-MS2LOS, aims at the deterministic optimisation of composite structures, involving phenomena appearing at different scales and blending of laminates.

Section 7.1 introduces an overview on the methodology, that will be mathematically developed in the following Sections. In particular, the fundamental concepts at the basis of the MS2LOS are presented. Apart from those derived in Chapter 6, other requirements of different types are formulated in terms of design variables and presented.

Successively, two case studies, taken from the literature, are presented to prove the effectiveness of the methodology, with a particular focus on the two elements formalised in Chapter 6. In particular, the first case study, described in Section 7.2, focuses on the GL approach and the buckling requirement. A simplified wing-box structure is optimised, in the least-weight sense, through a deterministic algorithm. Attention is paid to the effectiveness of the gradient of the buckling factor formulation when scale transition is performed. The second study case, described in Section 7.3, focuses on the optimisation of a 18-panel structure. The focus is on the new blending constraints formulation and on the stacking sequence recovery phase, presented in Section 6.3. At the end of the Section, some critical comments are provided: some of them are the basis for deeper investigations that will be presented in Chapter 9.

Section 7.4 compares the numerical approach for the stacking sequence recovery of Section 6.3 with the alternative approach, based on QT QH SSs, presented in Section 6.4.

Finally, Section 7.5 concludes the Chapter with meaningful considerations.

7.1 Generalities on the MS2LOS

The MS2LOS is formulated in terms of two distinct (but related) problems.

First-level Problem (FLP) The aim of this phase, which focuses on the laminate macroscopic scale, is the determination of the optimum distribution of the mechanical and geometric design variables, describing the behaviour of each laminate, which minimises a given objective function by fulfilling a set of design requirements (formulated as optimisation constraints). At this level, the generic laminate is modelled as an equivalent homogeneous anisotropic plate, whose behaviour is described in terms of laminate PPs. Framed in the FSDT, the FLP contemplates four design variables for each laminate: the (continuous) number of plies n and three PPs: ρ_{0K} , ρ_1 , ϕ_1 . Thanks to this formulation, at this stage, the designer can add further requirements (e.g. manufacturing constraints, strength and damage criteria, etc.) by introducing suitable constraints on the laminate PPs and thickness. Of course, the derivation of suitable equivalent constraints to be imposed on the laminate PPs corresponding to manufacturing requirements involved at the ply-level (like the the maximum angular difference among two consecutive plies) is anything but trivial. However, some manufacturing constraints can still be introduced at this level, like feasibility and blending requirements. In this Thesis, the following requirements are considered:

1. laminate feasibility (Section 7.1.1);
2. displacement requirements (Section 7.1.2);
3. laminate static failure (Section 7.1.3);
4. buckling (with GL approach) (Section 6.1);
5. blending of laminates with different thickness (Section 6.2).

A first novelty in this formulation of the FLP is the rigorous multi-scale global-local approach for the assessment of the buckling factor in the deterministic optimisation framework (Section 6.1). Note that a GL approach has been already presented in the MS2LOS context for the genetic optimisation framework in (Izzi, Montemurro, Catapano, Fanteria, et al., 2020; Izzi, Montemurro, Catapano, & Pailhès, 2020; Panettieri et al., 2020), based on the sub-modelling technique (Sun & Mao, 1988; Mao & Sun, 1991; Whitcomb, 1991). Selected portions of the structure, called ZOIs, which are likely to undergo buckling failure, are extracted from the GFEMs and analysed. Refined LFEMs are then generated from the GFEMs geometry, and buckling factors are evaluated.

A second novelty is the implementation of new blending requirements as a set of equivalent optimisation constraints on the laminate PPs and number of plies (Section 6.2). These constraints define a stricter regions if compared to the existing ones

(Macquart et al., 2016; Panettieri et al., 2019).

Finally, an intermediate step, called *discrete optimisation*, is needed to get laminates with a discrete number of plies.

Second-level Problem (SLP) The SLP of the strategy focuses on the laminate mesoscopic scale and aims at determining optimal SSs, satisfying the blending requirement between adjacent laminates, in such a way to recover the optimised PPs and thickness resulting from the FLP. The design variables of the SLP are the plies orientation angles.

The novelty of this SLP formulation is the implementation of the numerical strategy presented in Section 6.3 to recover blended SSs matching the optimal elastic properties determined in the FLP (Section 6.3). The stack recovery phase approach, addressed through a meta-heuristic algorithm, is suitable for laminates with any number of plies.

7.1.1 Laminate Feasibility Constraints

In the FLP, geometric and feasibility constraints on the PPs must be considered (Vannucci, 2012a), in order to ensure that the optimal values of PPs correspond to a feasible SS (to be determined in the SLP of the procedure). Since orthotropy and quasi-homogeneity properties are imposed (i.e. membrane/bending uncoupling with the same group of symmetry in membrane and bending), such constraints read (Vannucci, 2012a) (see Eq. (4.45)):

$$\begin{cases} -1 \leq \rho_{0K} \leq +1, \\ 0 \leq \rho_1 \leq 1, \\ 2\rho_1^2 - 1 - \rho_{0K} \leq 0. \end{cases} \quad (7.1)$$

The first two equations of (7.1) can be considered as bounds for the design variables PPs; therefore, the feasibility constraint is represented only by the third equation of (7.1), which must be evaluated for each of the n_{pan} panels in the structure at hand. It is noteworthy that the homogeneity property allows for the design of the bending stiffness tensor without introducing further variables than those used to characterise the membrane tensor. Moreover, homogeneity makes the membrane and bending behaviours to agree in terms of orthotropy axes orientation. Physically, it avoids the equivalent single-layer membrane behaviour to be different from the bending counterpart.

However, in order to avoid a large number of constraints (and gradients), which may lead to a over-constrained optimisation problem, one may use suitable aggregation strategies, i.e. by introducing the well-know maximum operator. Inasmuch as max operator is not everywhere differentiable with continuity (\mathcal{C}^0 class), a continuous and differentiable approximation (at least of class \mathcal{C}^1) must be introduced.

Let \mathbf{x} be a generic vector of n components, and let the following operator, called Kreisselmeier-Steinhauser (KS) function or α -LogSumExp, often used in machine learn-

ing and artificial neural networks (Haykin, 1998; Calafiore & El Ghaoui, 2014; Nielsen & Sun, 2016), be introduced:

$$\text{KS}_\alpha(\mathbf{x}) := \frac{1}{\alpha} \ln \left(\sum_{i=1}^n e^{\alpha x_i} \right), \quad (7.2)$$

where α is a parameter which can be chosen according to the variance $\text{Var}(\mathbf{x})$ and to the values of vector \mathbf{x} . The higher α , the more accurate is the KS_α approximation.

It can be easily shown that the family KS_α approaches the max operator by excess; in particular, the following estimate holds:

$$\max \mathbf{x} \leq \text{KS}_\alpha \leq \max \mathbf{x} + \frac{1}{\alpha} \ln(n). \quad (7.3)$$

Equation (7.3) is much more accurate as $\text{Var}(\mathbf{x})$ and/or α assume large values. Furthermore, KS_α is a convex and strictly-monotonically-increasing function in its domain (Calafiore & El Ghaoui, 2014). Equation (7.3) is a fundamental inequality, since it ensures that the approximated constraints are conservative. The value of α is chosen as a trade-off between two conflicting requirements. On the one hand, it should be reasonably small in order to avoid too sharp approximations and numerical overflows. On the other hand, it should be sufficiently high to maintain the discrete effect of the max operator and to reasonably approximate the maximum value. The aggregation strategy can be explained also from the Active Set algorithm (see Section 3.2.2) used in the next Chapter for the numerical applications. Since the number of possible working sets grows exponentially with the number of inequalities, a phenomenon which is referred to as the *combinatorial difficulty* of non-linear programming, the algorithm cannot consider all the possible choices for the working set (Nocedal & Wright, 2006). Hence, the "reduction" of the constraints, by means of the proposed aggregation, is beneficial, because it reduces the number of possibilities of estimating the solution active-set.

For each of the n_{pan} laminate composing the structure, inequality (7.1) must be imposed. Those values can be collected in the vector \mathbf{g} and can be replaced by the condition

$$g_{\text{feas}} := \text{KS}_\alpha(\mathbf{g}), \quad \alpha \gg 1. \quad (7.4)$$

Let n_{vars} be the number of variables. The gradient of of Eq. (7.4), with respect to the generic design variable ξ_j (four variables for each panel, see Eq. (4.32)), reads:

$$(\nabla_{\boldsymbol{\xi}} g_{\text{feas}})_j := \frac{\partial g_{\text{feas}}}{\partial \xi_j} = \frac{\sum_{i=1}^{n_{\text{pan}}} e^{\alpha g_i} \frac{\partial g_i}{\partial \xi_j}}{\sum_{i=1}^{n_{\text{pan}}} e^{\alpha g_i}}, \quad \alpha \gg 1, \quad j = 1, \dots, n_{\text{vars}}, \quad (7.5)$$

where

$$\frac{\partial g_i}{\partial \xi_j} = \begin{cases} -1, & \text{if } \xi_j = \rho_{0K}^i, \\ 4\rho_1^i, & \text{if } \xi_j = \rho_1^i, \\ 0, & \text{otherwise.} \end{cases} \quad (7.6)$$

It is assumed, for calculation practicality, that the derivatives of α with respect to the generic design variable are zero. This means that, even though α is chosen depending on $\text{Var}(\mathbf{x})$, its derivatives are negligible with respect to the problem variables.

7.1.2 Displacement Requirement

The displacement requirement is measured on the GFEM and is considered as a bound on a displacement component of a meaningful node, chosen *a priori*, of the GFEM mesh.

Let index k denote the position, in \mathbf{u} , of the displacement component (at the chosen node) to be bounded. Then, if u_0 denotes the maximum allowable displacement, one obtains the displacement requirement as

$$g_{\text{disp}} := \frac{u_k}{u_0} - 1 \leq 0. \quad (7.7)$$

It is convenient to introduce the vector \mathbf{a} , whose its unique non-zero component has unit value in position k , such that

$$\frac{\partial u_k}{\partial \xi_j} = \mathbf{a}^T \frac{\partial \mathbf{u}}{\partial \xi_j}. \quad (7.8)$$

Under the hypothesis that external generalised nodal forces do not depend on design variables:

$$\frac{\partial \mathbf{f}}{\partial \xi_j} = \mathbf{0}, \quad \forall j = 1, \dots, n_{\text{vars}}, \quad (7.9)$$

Equation (7.8) can be augmented (adjoint method) with the null quantity obtained by differentiation of Eq. (6.1):

$$\frac{\partial u_k}{\partial \xi_j} = \mathbf{a}^T \frac{\partial \mathbf{u}}{\partial \xi_j} + \boldsymbol{\mu}^T \left(\frac{\partial \mathbf{K}}{\partial \xi_j} \mathbf{u} + \mathbf{K} \frac{\partial \mathbf{u}}{\partial \xi_j} \right). \quad (7.10)$$

The expression of $\partial \mathbf{K} / \partial \xi_j$ is given in Appendix C.

The adjoint vector $\boldsymbol{\mu}$ is chosen in such a way that the term multiplying $\frac{\partial \mathbf{u}}{\partial \xi_j}$ vanishes from Eq. (7.10). Finally, the gradient reads:

$$\begin{cases} (\nabla_{\boldsymbol{\xi}} g_{\text{disp}})_j := \frac{1}{u_0} \frac{\partial u_k}{\partial \xi_j} = \boldsymbol{\mu}^T \frac{\partial \mathbf{K}}{\partial \xi_j} \frac{\mathbf{u}}{u_0}, & \forall j = 1, \dots, n_{\text{vars}}, \\ \mathbf{K} \boldsymbol{\mu} = -\mathbf{a}. \end{cases} \quad (7.11)$$

7.1.3 Laminate Failure Criterion

The requirement on the laminate strength is based on the results of the works by Catapano et al. (2012, 2014), Catapano and Montemurro (2018), whose main results have been reported in Section 4.2.3. The authors introduce a laminate failure index, in the framework of the FSdT, averaged on the laminate thickness h , having the form reported in Eq. (4.34). Under the hypothesis of quasi-homogeneity and by considering the Tsai-Hill criterion, Eq. (4.34) reduces to

$$F_{\text{TH}} := \frac{1}{h} \left(\boldsymbol{\varepsilon}_{\text{gen}}^{\text{T}} \mathbf{G} \boldsymbol{\varepsilon}_{\text{gen}} \right) - 1 \leq 0, \quad \text{with } \mathbf{G} := \text{diag}(\mathbf{G}_A, \mathbf{G}_D, \mathbf{G}_H). \quad (7.12)$$

Equation (7.12) is evaluated for all the elements of the GFEM belonging to the *check zone*, the set of elements where the strain field assumes meaningful values. The check zone is composed by n_e elements. To avoid a large number of constraints (and gradients), the aggregation based on the approximated maximum operator is adopted also in this case:

$$g_{\text{TH}} = \text{KS}_\alpha \left(\frac{1}{h_e} \boldsymbol{\varepsilon}_{\text{gen } e}^{\text{T}} \mathbf{G}_e \boldsymbol{\varepsilon}_{\text{gen } e} \right) - 1 \leq 0, \quad e = 1, \dots, n_e, \quad \alpha \gg 1. \quad (7.13)$$

Adopting the approximation of Eq. (7.2), and adding the null quantity of Eq. (6.1), Eq. (7.13) becomes:

$$g_{\text{TH}} = \text{KS}_\alpha(\boldsymbol{\delta}) + \boldsymbol{\mu}^{\text{T}} (\mathbf{K}\mathbf{u} - \mathbf{f}) - 1 \leq 0, \quad e = 1, \dots, n_e, \quad \alpha \gg 1, \quad (7.14)$$

where vector $\boldsymbol{\delta}$ collects the quantity

$$\delta_e := \frac{1}{h_e} \boldsymbol{\varepsilon}_{\text{gen } e}^{\text{T}} \mathbf{G}_e \boldsymbol{\varepsilon}_{\text{gen } e}, \quad e = 1, \dots, n_e. \quad (7.15)$$

By differentiating Eq. (7.14), remembering assumption (7.9), one obtains:

$$\begin{aligned} (\nabla_{\boldsymbol{\xi}} g_{\text{TH}})_j &:= \frac{\partial g_{\text{TH}}}{\partial \xi_j} = \frac{\sum_{e=1}^{n_e} e^{\alpha \delta_e} \frac{\partial \delta_e}{\partial \xi_j}}{\sum_{e=1}^{n_e} e^{\alpha \delta_e}} + \boldsymbol{\mu}^{\text{T}} \left(\frac{\partial \mathbf{K}}{\partial \xi_j} \mathbf{u} + \mathbf{K} \frac{\partial \mathbf{u}}{\partial \xi_j} \right), \\ \alpha \gg 1, \quad j &= 1, \dots, n_{\text{vars}}. \end{aligned} \quad (7.16)$$

By substituting Eqs. (6.25) and (6.26) in Eq. (7.15) and by differentiating, one obtains:

$$\begin{aligned} \frac{\partial \delta_e}{\partial \xi_j} &:= \boldsymbol{\beta}_e \frac{\partial \mathbf{u}}{\partial \xi_j} + \eta_{ej}, \quad \text{with :} \\ \boldsymbol{\beta}_e &:= \frac{2}{h_e} \boldsymbol{\varepsilon}_{\text{gen } e}^{\text{T}} \mathbf{G}_e \mathbf{B}_e \mathbf{L}_e, \quad \eta_{ej} := \frac{1}{h_e} \left(\boldsymbol{\varepsilon}_{\text{gen } e}^{\text{T}} \frac{\partial \mathbf{G}_e}{\partial \xi_j} \boldsymbol{\varepsilon}_{\text{gen } e} - \delta_e \frac{\partial h_e}{\partial \xi_j} \right). \end{aligned} \quad (7.17)$$

The expression of $\partial \mathbf{G}_e / \partial \xi_e$, appearing in the above formula, is provided in Appendix D. By substituting Eq. (7.17) into Eq. (7.16), one obtains:

$$\begin{aligned} \frac{\partial g_{\text{TH}}}{\partial \xi_j} &= \eta_j + \boldsymbol{\mu}^T \frac{\partial \mathbf{K}}{\partial \xi_j} \mathbf{u} + (\boldsymbol{\beta}^T + \boldsymbol{\mu}^T \mathbf{K}) \frac{\partial \mathbf{u}}{\partial \xi_j}, \quad \text{with :} \\ \boldsymbol{\beta}^T &:= \frac{\sum_{e=1}^{n_e} e^{\alpha \delta_e} \boldsymbol{\beta}_e^T}{\sum_{e=1}^{n_e} e^{\alpha \delta_e}}, \quad \eta_j := \frac{\sum_{e=1}^{n_e} e^{\alpha \delta_e} \eta_{ej}}{\sum_{e=1}^{n_e} e^{\alpha \delta_e}}. \end{aligned} \quad (7.18)$$

In Eq. (7.18), the vector $\boldsymbol{\mu}$ can be chosen in such a way that the term multiplying $\frac{\partial \mathbf{u}}{\partial \xi_j}$ vanishes; accordingly, one finally obtains the following expression:

$$\begin{cases} (\nabla_{\boldsymbol{\xi}} g_{\text{TH}})_j := \eta_j + \boldsymbol{\mu}^T \frac{\partial \mathbf{K}}{\partial \xi_j} \mathbf{u}, & j = 1, \dots, n_{\text{vars}}, \\ \mathbf{K} \boldsymbol{\mu} = -\boldsymbol{\beta}, \\ \alpha \gg 1. \end{cases} \quad (7.19)$$

7.1.4 The First-level Problem Formulation

The FLP can be, now, correctly formulated. Of course, the proposed formulation is a general one, since some constraints can be removed, depending on cases. The FLP itself is divided into two sub-steps. The *continuous optimisation* aims at the optimal distribution of stiffness; in this sub-step, the thickness can vary with continuity in the admissible range. The *discrete optimisation* aims at finding the solution with a discrete number of plies *closest* to the continuous one.

7.1.4.1 Continuous Optimisation

Firstly, the main results detailed in the previous Sections are summarised. As stated, in the FLP formulation, geometric and feasibility constraints, in terms of PPs, must be considered (Vannucci, 2012a). These constraints ensure that the optimal values of PPs, determined in the FLP, correspond to a feasible laminate. Their expression, g_{feas} , has been addressed in Section 7.1.1.

If some displacement component values, at some node, must be bounded, e.g. the maximum tip displacement, the correspondent constraint g_{disp} has been retrieved in Section 7.1.2.

The static failure of laminates has been addressed through a failure index averaged over the laminate thickness. The expression of the corresponding constraints, g_{TH} , has been addressed in Section 7.1.3.

Buckling constraints involve the evaluation, for each ZOI, of the buckling factor. Formally, for each LFEM, the buckling constraint g_{buck} must be evaluated, as discussed in Section 6.1.

Only blended solutions must be considered. For the FLP, the blending requirement g_{blend} is derived in Section 6.2.

In the light of the previous considerations, collecting the results, the CNLPP of the con-

tinuous optimisation can be formulated as follows:

$$\begin{aligned}
 & \min_{\boldsymbol{\xi}} \Phi(\boldsymbol{\xi}), \quad \text{subject to:} \\
 & \left. \begin{aligned} & \mathbf{K}\mathbf{u} - \mathbf{f} = \mathbf{0}, \\ & \mathbf{K}^b \mathbf{u}^b + \mathbf{K}_{BC}^b \mathbf{P}\mathbf{u} = \mathbf{0}, \end{aligned} \right\} \text{ in the GFEM,} \\
 & \left. \begin{aligned} & g_{TH}(\boldsymbol{\xi}) \leq 0, \text{ (one constraint for all the elements in the check zone),} \\ & g_{disp}(\boldsymbol{\xi}) \leq 0, \end{aligned} \right\} \forall \text{ bounded displacement components,} \\
 & g_{feas}(\boldsymbol{\xi}) \leq 0, \text{ (one constraint for all the design regions),} \\
 & \left. \begin{aligned} & g_{buck}(\boldsymbol{\xi}) \leq 0, \end{aligned} \right\} \forall \text{ LFEMs,} \\
 & \left. \begin{aligned} & g_{blend-j}(\boldsymbol{\xi}) \leq 0, \end{aligned} \right\} \forall \text{ couples of adjacent panels, } j = 0, 1 \\
 & \boldsymbol{\xi}_{lb} \leq \boldsymbol{\xi} \leq \boldsymbol{\xi}_{ub},
 \end{aligned} \tag{7.20}$$

where Φ is the objective function, $\boldsymbol{\xi}$ is the design variable vector and $\boldsymbol{\xi}_{lb}$, $\boldsymbol{\xi}_{ub}$ are the lower and upper bound vectors of the design variables, respectively. Variables n_0^j , $j = 1, \dots, n_{pan}$, are assumed continuous in this sub-step.

7.1.4.2 Discrete Optimisation

A second sub-step, hereafter referenced as *discrete optimisation*, is needed to round up the continuous solution of Problem (7.20) to discrete numbers of plies, while complying to the full set of constraints of Eq. (7.20).

Let $\boldsymbol{\xi}_c$ be the solution of the continuous optimisation Problem (7.20). The discrete optimisation problem aims at finding a solution, $\boldsymbol{\xi}_d$, at a minimal distance from $\boldsymbol{\xi}_c$, having integer number of plies. The formulation of the resulting MICNLPP reads:

$$\begin{aligned}
 & \min_{\boldsymbol{\xi}} \|\boldsymbol{\xi}_c - \boldsymbol{\xi}\|_{L^2}^2, \quad \text{subject to :} \\
 & \left. \begin{aligned} & g_{feas}(\boldsymbol{\xi}) \leq 0, \\ & \frac{[n_0 N_{ref}]}{N_{ref}} =: n_{0d}, \end{aligned} \right\} \forall \text{ laminates} \\
 & \left. \begin{aligned} & g_{blend-j}(\boldsymbol{\xi}, n_{0d}) \leq 0, \quad j = 0, 1, \\ & |\Delta_{pq} n_{0d}| \left(\frac{\Delta N_{min}}{N_{ref}} - |\Delta_{pq} n_{0d}| \right) \leq 0, \end{aligned} \right\} \forall \text{ couples of adjacent laminates } p, q \\
 & \boldsymbol{\xi}_{lb} \leq \boldsymbol{\xi} \leq \boldsymbol{\xi}_{ub}.
 \end{aligned} \tag{7.21}$$

Problem (7.21) takes into account only blending and manufacturability constraints, while allowing for changes in the optimal PPs values of $\boldsymbol{\xi}_c$ in order to satisfy the new set of constraints. It is noteworthy that this formulation does not require further FE evaluations. However, Problem (7.21) imposes that, for each panel, the discrete dimensionless number of ply, i.e. n_{0d} , defined in Eq. (7.21), must be greater than or equal to the continuous

counterpart n_0 . Even though this results in an increase of the final mass of the structure, it represents a security margin against buckling failure. In fact, the thickness of the laminate is the most influencing parameter on buckling factor. This claim can be justified by comparing the order of magnitude of buckling factor sensitivity terms related to the thickness with those related to the laminate PPs. The formers are by far more important than the latter. This margin of safety is required since the formulation of Problem (7.21) can affect the satisfaction of buckling constraints, which do not enter directly in the formulation (7.21). Of course, an interactive convergence procedure between the discrete optimisation and new FE analyses to ensure the compliance of all the mechanical constraints should be carried out in this phase. However, it is tacitly assumed that the new solution ξ_d , which, roughly speaking, is a “perturbation” of ξ_c , does not violates the fulfilling of mechanical constraints in a too severe way.

Blending constraints are evaluated with the discrete number of plies $N_i = n_{0d}N_{\text{ref}}$ ($i = p, q$) for each generic couple of adjacent laminates p and q . The last constraint of Problem (7.21) imposes that the difference of number of plies between two adjacent panels must be zero or greater than a predefined ΔN_{min} . From a mathematical point of view, this requirements help the SLP, as it will be explained in the following of the Chapter. Physically, it avoids impractical and meaningless drops of very few plies, imposing that slightly-different panels (in terms of thickness and PPs values) converge into mechanically and geometrically identical panels. In fact, panels having the same number of plies are blended if and only if they have the same SS (geometrical identity) and, as a trivial consequence, the same elastic behaviour (mechanical identity). Generally speaking, ΔN_{min} should be chosen according to the trend of the results of the continuous optimisation. For instance, consider a continuous solution of three laminates resulting in 100, 102 and 98 plies. If one chooses $\Delta N_{\text{min}} = 10$, clearly the discrete solution will be very far from the continuous one. Conversely, if the continuous solution, for the same panels, is characterised by 100, 108 and 99 plies, the application of the same ΔN_{min} would result in a discrete solution closer to the continuous one.

7.1.5 The Second-level Problem Formulation

Once the FLP is solved, target properties must be recovered by blended SSs. The generalities and the basic hypotheses of the Stacking sequence recovery phase have been already discussed in Section 6.3. The SLP formulation within this MS2LOS can be summarised by the following steps:

- (a) Find a proper Search Propagation Direction (Definition 6.5);
- (b) Select a Blending Scheme;
- (c) Solve Problem (6.52).

7.2 Case Study 1: a Benchmark on the FLP

7.2.1 Problem Definition

A numerical benchmark, taken from (B. Liu et al., 2000; D. Liu et al., 2011; Panettieri et al., 2019), has been considered. The benchmark consists in a simplified wing-box model, made of composite laminates, subject to bending and twist moment at the tip section, with a clamped root section ($x = 0$). The geometry of the structure is presented in Figure 7.1. The wing-box has length $L = 3543$ mm, width $W = 2240$ mm and height $H = 381$ mm. Loads and BCs are deeply discussed in Section 7.2.4. In the model, ribs, spars and stringers are replaced by continuous equally spaced composite plates with a pre-defined stacking sequence: $[(\pm 45^\circ)_{11}]_S$. The constitutive ply, used for all laminates

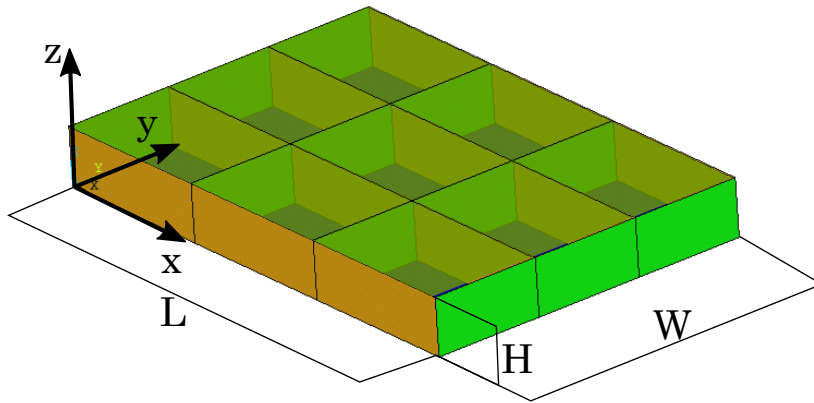


Figure 7.1: Model geometry of the of Case Study 1 benchmark structure (The upper skin ($z = H$) is shaded to make the interior part visible)

composing the structure, is made of a carbon-epoxy T300/5208 pre-preg (Catapano, 2013; Zhang et al., 2019), whose properties are listed in Table 7.1, in terms of both technical constants and PPs. Optimisation regions are the upper ($z = H$) and lower ($z = 0$) skins of the wing-box. Each skin is subdivided into nine regions (or panels), numbered as in Figure 7.2, for a total number of panels n_{pan} equal to 18.

7.2.2 The First-level Problem Formulation

The FLP aims at determining the optimal distribution of PPs and numbers of plies in the structure, minimising the structure mass by satisfying, simultaneously, the design requirements that will be specified.

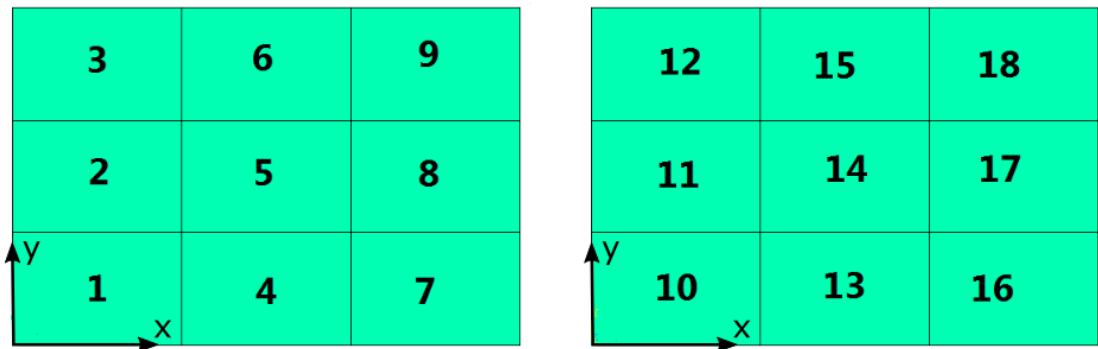
The objective function can be formulated as follows:

$$\Phi(\xi) := \frac{m_0 + \sum_{i=1}^{n_{\text{pan}}} A_i n_{0i} n_{\text{ref}} t_{\text{ply}} \rho_{\text{ply}}}{m_{\text{ref}}}, \quad (7.22)$$

where m_0 is the mass of the part of the structure which remains unchanged during the optimisation, $m_{\text{ref}} = 314.12$ kg (D. Liu et al., 2011) is a reference mass, A_i , n_{0i} are the area

Table 7.1: Material properties of the T300/5208 pre-preg

Technical constants		Polars parameters of \mathbf{Q}^a		Polars parameters of $\hat{\mathbf{Q}}^b$	
E_1 [GPa]	181	T_0 [MPa]	26898.96	T [MPa]	5398.38
E_2 [GPa]	10.3	T_1 [MPa]	24710.25	R [MPa]	1771.61
G_{12} [GPa]	7.17	R_0 [MPa]	19728.96	Φ [deg]	90
G_{23} [GPa]	3.78	R_1 [MPa]	21426.38		
G_{13} [GPa]	7.17	Φ_0 [deg]	0		
ν_{12}	0.27	Φ_1 [deg]	0		
ν_{23}	0.42				
ν_{13}	0.27				
Density and thickness		Polars parameters of \mathbf{G}^c		Polars parameters of $\hat{\mathbf{G}}^d$	
ρ_{ply} [kg mm ⁻³]	1.76×10^{-6}	Γ_0	7531.02	Γ	10633.53
t_{ply} [mm]	0.125	Γ_1	2113.80	Λ	484.30
n_{ref}	150	Λ_0	3586.81	Ω [deg]	90
		Λ_1	1603.36		
		Ω_0 [deg]	45		
		Ω_1 [deg]	0		
Limit stresses					
X [MPa]	1500				
Y [MPa]	246				
S_{12} [MPa]	68				
S_{23} [MPa]	36				
S_{13} [MPa]	68				

^aIn-plane ply stiffness matrix^bOut-of-plane ply shear stiffness matrix^cIn-plane ply strength matrix^dOut-of-plane ply shear strength matrix(a) Upper ($z = H$) laminates numbering(b) Lower ($z = 0$) laminates numbering**Figure 7.2:** Optimisation regions of Case Study 1 structure

and the dimensionless number of plies of the i -th region, respectively, ρ_{ply} is the density

of the single ply. Formally, the optimisation problem can be stated as a CNLPP:

$$\begin{aligned}
 & \min_{\boldsymbol{\xi}} \Phi(\boldsymbol{\xi}), \quad \text{subject to:} \\
 & \mathbf{K}\mathbf{u} - \mathbf{f} = \mathbf{0}, \\
 & \mathbf{K}^b \mathbf{u}^b + \mathbf{K}_{BC}^b \mathbf{P}\mathbf{u} = \mathbf{0}, \\
 & g_{\text{feas}}(\boldsymbol{\xi}) \leq 0, \\
 & g_{\text{disp}}(\boldsymbol{\xi}) \leq 0, \\
 & g_{\text{TH}}(\boldsymbol{\xi}) \leq 0, \\
 & g_{\text{blend}}(\boldsymbol{\xi}) \leq 0, \\
 & g_{\text{buck}}(\boldsymbol{\xi}) \leq 0, \\
 & \boldsymbol{\xi}_{\text{lb}} \leq \boldsymbol{\xi} \leq \boldsymbol{\xi}_{\text{ub}}.
 \end{aligned} \tag{7.23}$$

Actually, for the FLP of this benchmark, the implemented blending constraints are those presented by Panettieri et al. (2019), because those of Section 6.2 have not yet been derived.

The parameter α of KS function appearing in Eqs. (7.4) and (7.5), after some empirical tuning, has been set as follows:

$$\alpha(\text{Var}(\mathbf{g})) = \begin{cases} 70, & \text{if } \text{Var}(\mathbf{g}) \leq 0.001, \\ 50, & \text{if } 0.001 < \text{Var}(\mathbf{g}) \leq 0.1, \\ 10, & \text{if } \text{Var}(\mathbf{g}) \geq 0.1. \end{cases} \tag{7.24}$$

The requirement on the bounded displacement regards the maximum vertical displacement measured at the tip of the wing-box, as will be detailed in Section 7.2.4. For the static strength requirements, the check zone consists in the elements of the lower skin of the wing-box GFEM. This choice is due to the fact that the lower skin undergo tension. The parameter α appearing in Eqs. (7.13) and (7.19), after some empirical tuning, has been set as follows:

$$\alpha(\text{Var}(\boldsymbol{\delta})) = \begin{cases} 50, & \text{if } \text{Var}(\boldsymbol{\delta}) \leq 0.001, \\ 30, & \text{if } 0.001 < \text{Var}(\boldsymbol{\delta}) \leq 0.1, \\ 10, & \text{if } 0.1 < \text{Var}(\boldsymbol{\delta}) \leq 0.3, \\ 2, & \text{if } \text{Var}(\boldsymbol{\delta}) \geq 0.3. \end{cases} \tag{7.25}$$

For the buckling requirement, the ZOI is the upper skin ($z = H$), from which a LFEM is generated. This choice is due to the fact that the upper skin ($z = H$) undergo compression. Details will be provided in Section 7.2.4. Table 7.2 reports lower and upper bounds for the considered design variables of Eq. (4.32). The number of plies, which is a discrete variable, is assumed as a continuous one.

Table 7.2: Design space for Problem (7.23)

Variable*	lower bound	upper bound
n_0^j	0.14	1
ρ_{0K}^j	-1	1
ρ_1^j	0	1
ϕ_1^j	-1	1

* $j = 1, \dots, n_{\text{pan}}$

Since the SLP will not be performed in this case study, the discrete optimisation step is disregarded.

7.2.3 Numerical Strategy

Problem (7.23) is a non-convex CNLPP in terms of both geometrical and mechanical design variables. The non-convexity is mainly due to the buckling eigenvalue as well as to strength and blending design requirements.

The solution search is performed via the *active-set* algorithm of the *fmincon* family, available in the Optimization Toolbox of MATLAB® (The MathWorks Inc., 2011). The parameters tuning the behaviour of the algorithm have been kept to their default values, as summarised in Table 7.3. Of course, the strategy is not affected by the particular choice of other deterministic algorithm, such as a different *active-set* implementation or an *interior-point* algorithm. Such kinds of algorithms are available also in many open-source libraries, e.g. *Scipy* (e.g. SLSQP algorithm) or *PyOpt* (e.g. IPOPT algorithm). In any case, algorithm parameters are left unmodified with respect to the standard tuning, as in Table 7.3 for the *fmincon active-set* choice.

Table 7.3: *fmincon* parameters

Parameter	Value
Solver	Active-set
Maximum number of iterations	1000
Tolerance on objective function	1×10^{-6}
Tolerance on constraints	1×10^{-6}
Tolerance on input variables change	1×10^{-6}
Tolerance on gradient norm of the Lagrange's function	1×10^{-6}

Figure 7.3 shows the work-flow of the numerical strategy for the resolution of the FLP. The MATLAB® script invokes, at each iteration, the Python routines controlling the generation of the FE models (both global and local ones) used to assess the objective function and the optimisation constraints. Both the GFEM and the LFEMs are built in the ANSYS® environment through suitable ANSYS® Parametric Design Language (APDL) scripts. For each iteration, a new set of design variables ξ is passed from MATLAB® to a Python Class which represents the GFEM Object which invokes the APDL script

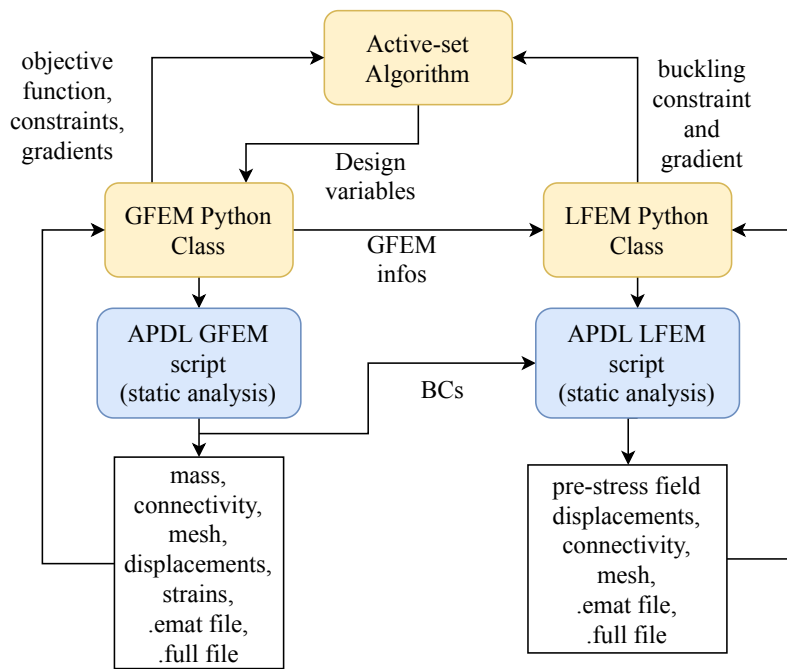


Figure 7.3: Workflow of the numerical strategy of Case Study 1

generating the GFEM. Then, a static analysis is performed on the GFEM, and some fundamental information such as connectivity, nodes coordinates, displacement and strain fields, are passed to the GFEM Object (by means of `.emat` and `.full` files generated from ANSYS® at the end of the analysis). Subsequently, the GFEM Object evaluates feasibility, blending, maximum displacement and maximum strain constraints, together with their gradients. After this phase, the GFEM Object creates a new Object: the LFEM. The LFEM Object inherits some useful GFEM information (connectivity, etc.) and calls an APDL script generating the LFEM for the most critical ZOI. Once BCs extracted from the GFEM are applied to the LFEM, a static analysis with pre-stress effects is solved on the LFEM. Some information such as pre-stress displacements, connectivity, etc. are passed back to the LFEM Object. Matrix \mathbf{K}_σ^b is assembled by the LFEM Class, according to the expression presented in Section 6.1.2. The LFEM Class also solves the eigenvalue buckling problem on the LFEM via `scipy.sparse.linalg.eigsh` routine, based on the ARPACK software and the Implicitly Restarted Lanczos Method (Lehoucq et al., 1998). Finally, the buckling constraint of Eq. (6.4) and its gradient are evaluated (according to the procedure detailed in Section 6.1.2).

The objective function and the optimisation constraints, with the related gradients, are then passed to the optimisation algorithm. The loop is repeated until one of the convergence criteria, listed in Table 7.3, is satisfied.

The choice of assembling the LFEM stress-stiffness matrix in Python environment, instead of just exploiting the `.emat` file provided by ANSYS®, is due to the fact that ANSYS® software makes use of some correction factors, not provided in the ANSYS® manual (Ansys®, 2013), which depend on the element geometric and material properties. Moreover, as detailed in Section 6.1.2, in this work, an alternative (general) definition of

the element stress-stiffness matrix (different from that used in classic FE codes) has been used in order to derive an efficient closed-form expression of the buckling factor gradient. All these details are of paramount importance for a correct assessment of the buckling factor gradient and represent the reason at the basis of using Python instead of ANSYS® for the resolution of the eigenvalue problem.

7.2.4 The Global/Local Finite Element Modelling Approach

As stated above, the FE models integrated in the optimisation process are based on a GL modelling approach, more precisely on the sub-modelling technique, see the works by Sun and Mao (1988), Mao and Sun (1991), Whitcomb (1991) for more details on this topic. According to the strategy discussed in (Izzi, Montemurro, Catapano, & Pailhès, 2020), two different FE models are created: the GFEM for the assessment of the global behaviour of the wing-box, and a refined LFEM in order to properly evaluate the local responses (in this case the first buckling factor). The LFEM is created only at the most critical ZOI (from a buckling strength perspective), which is represented by the upper panels ($z = H$) composing the wing-box, as illustrated in Figure 7.5. Therefore, inasmuch as for the simple benchmark considered in this study the most critical ZOI is known *a-priori*, there is no need to introduce suitable criteria for automatically identifying the most critical ZOIs, as done in (Izzi, Montemurro, Catapano, & Pailhès, 2020). Nevertheless, as deeply discussed in Section 6.1.2, the coupling effects between GFEM and LFEM are still important when evaluating the gradient of the buckling factor for optimisation purposes.

Both GFEM and LFEMs are fully parametric and are built using the commercial FE code ANSYS®. The GFEM is illustrated in Figure 7.4. The root section is clamped, whilst external forces $F_1 = 90009$ N, $F_2 = F_3 = 187888$ N, $F_4 = 380176$ N are applied at the tip section nodes (from B to E) as illustrated in the same figure. The model is made of SHELL181 elements, which are based on Reissner-Mindlin kinematics (Reddy, 2003) and have four nodes with six DOFs per node. The GFEM is composed of about 560 elements and 3000 DOFs. The mesh size has been chosen after a sensitivity study (not reported here for the sake of brevity) in order to find a compromise between accuracy and computational cost.

The LFEM model is created to evaluate the first buckling load of the upper skin ($z = H$) of the wing-box, as shown in Figure 7.5, and it is generated via a dedicated APDL script. BCs on generalised displacements, extracted from the results of the global analysis and illustrated in Figure 7.5, are imposed to all the boundary nodes belonging to the skin of each upper panel (representing the connections between ribs, spars and stringers). The LFEM is made of SHELL181 elements, and the mesh is finer than the upper skin ($z = H$) of the GFEM. Therefore, BCs extracted from the boundary nodes of each panel composing the GFEM are properly interpolated during the transfer from the GFEM to the LFEM (by using the element shape functions). To set a suitable value of the element size of the LFEM, a sensitivity analysis of the first buckling factor to this

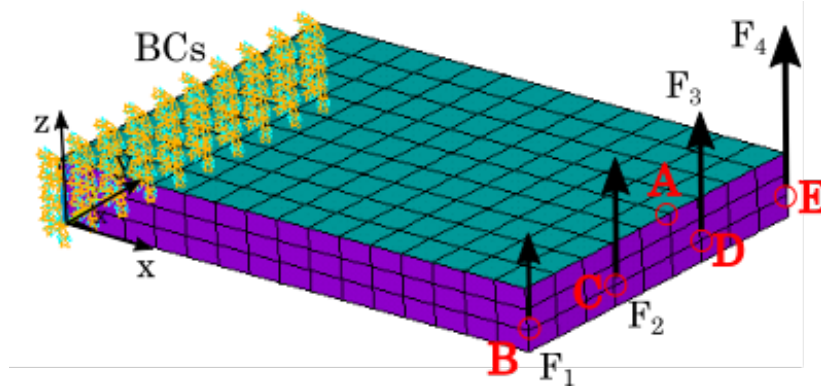


Figure 7.4: GFEM and related BCs of Case Study 1

parameter has been performed also in this case (and it is not reported here for the sake of brevity). As a result, the LFEM is characterised by approximately 490 elements and 3200 DOFs.

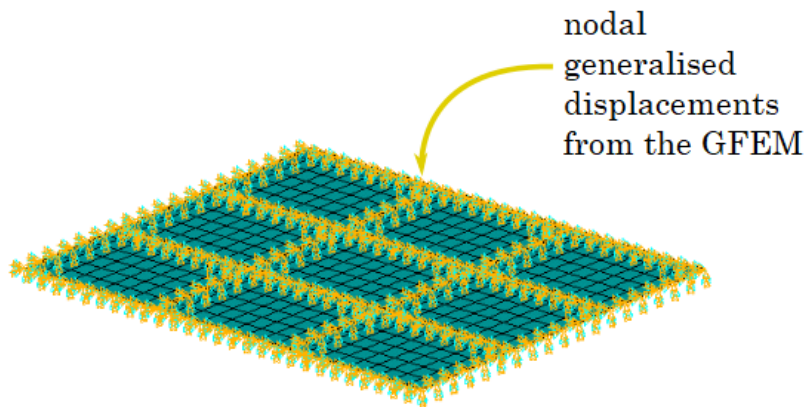


Figure 7.5: LFEM and the related BCs of Case Study 1

7.2.5 Numerical Results

Since the objective function of Eq. (7.22) is an hyper-plane in the $\mathbb{R}^{n_{\text{vars}}}$ space, due to its linearity with respect to geometrical variables, it is expected that the optimal solution exists, and that it is located at the boundary of the feasible region. Because of the high complexity of Problem (7.23), the choice of a feasible starting guess is of paramount importance.

In the following, three test cases are discussed, showing the importance of the buckling constraint and the differences in the optimised solution when neglecting the out-of-plane shear contribution in the expression of \mathbf{K}_{σ}^b .

The best known value for the optimised mass is 276.47 kg, corresponding to a normalised value of 0.88, obtained via a meta-heuristic algorithm in (Panettieri et al., 2019), even though a slightly different formulation of Problem (7.23).

Table 7.4 reports the numerical values of objective function and constraints, whilst

Table 7.5 lists the optimal values of the design variables.

Table 7.4: Objective function for the optimised solution

Case	Objective function	g_{feas}	g_{blend}	g_{TH}	g_{disp}	g_{buck}
Panettieri et al., 2019	0.88	—	—	—	—	—
Case 1	0.5603	-0.9215	-0.0125	-6×10^{-7}	-0.3202	—
Case 2	0.8440	-0.0897	-3×10^{-5}	-2×10^{-5}	-0.4316	-7×10^{-5}
Case 3	0.8461	-0.0540	-1×10^{-5}	-6×10^{-6}	-0.4322	-1×10^{-5}

Case 1: Optimisation Without Buckling Strength Requirement

Firstly, Problem (7.23) has been solved without considering the design requirement on the first buckling factor evaluated on the LFEM. The starting point has been set to $n_0^j = 0.4$, $\rho_{0K}^j = \rho_1^j = \phi_1^j = 0.0$, $j = 1, \dots, n_{\text{pan}}$ (see Figure 7.2). Such a starting point, in the feasible domain, represents a wing-box structure composed of isotropic laminates because the anisotropic moduli are null.

The algorithm converges towards a feasible solution after 400 iterations. The optimal value of the design variables is shown in Figure 7.6, whilst Table 7.5 reports the numerical values. Due to the absence of an optimisation constraint on the first buckling load,

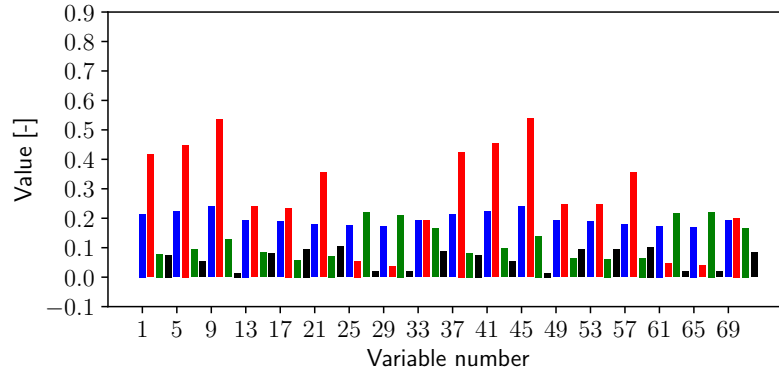


Figure 7.6: Optimal design variables values for Case 1 (n_0 in blue, ρ_{0K} in red, ρ_1 in green, ϕ_1 in black)

the resulting structural mass takes low value: the objective function is $\Phi = 0.5603$, corresponding to an overall mass of 176 kg, as indicated in Table 7.4. It is noteworthy that the solution is almost symmetric between upper ($z = H$) and lower ($z = 0$) panels. The active constraint is the maximum strain, as reported in Table 7.4. This confirms the expectations stated at the preamble of this section: the solution lies on the boundary of the feasible domain.

Case 2: Only Membrane Contribution in K_v^b

The introduction of the design requirement on the first buckling factor introduces a strong

Table 7.5: Optimal value of design variables

Panel	Case 1					Case 2					Case 3				
	n_0	ρ_{0K}	ρ_1	ϕ_1	ϕ_1	n_0	ρ_{0K}	ρ_1	ϕ_1	ϕ_1	n_0	ρ_{0K}	ρ_1	ϕ_1	ϕ_1
1	0.2147	0.4171	0.0788	0.0757	0.7001	0.9423	0.5172	0.0144	0.6972	0.9999	0.4980	0.0020			
2	0.2237	0.4491	0.0943	0.0532	0.7208	0.9655	0.4782	0.0241	0.7159	0.9855	0.4846	0.0111			
3	0.2404	0.5361	0.1281	0.0142	0.7700	0.8791	0.5016	0.0498	0.7655	1.0000	0.5247	0.0316			
4	0.1941	0.2394	0.0833	0.0805	0.6065	0.6783	0.3666	-0.0086	0.6120	0.7837	0.4157	0.0239			
5	0.1893	0.2349	0.0583	0.0958	0.6287	0.7077	0.4110	-0.0075	0.6240	0.7463	0.4112	0.0291			
6	0.1782	0.3547	0.0714	0.1039	0.6760	0.6056	0.3973	0.0266	0.6729	0.8434	0.4293	0.0531			
7	0.1758	0.0543	0.2202	0.0182	0.4164	1.0000	0.4044	0.0001	0.4493	1.0000	0.5426	-0.0104			
8	0.1712	0.0366	0.2109	0.0197	0.4300	1.0000	0.4490	0.0099	0.4293	1.0000	0.4601	0.0032			
9	0.1924	0.1921	0.1661	0.0860	0.4742	1.0000	0.4789	0.0393	0.4828	1.0000	0.5285	0.0379			
10	0.2136	0.4243	0.0817	0.0750	0.1400	0.5765	0.7271	0.0518	0.1400	0.6775	0.8847	0.0460			
11	0.2224	0.4540	0.0962	0.0537	0.1569	0.6728	0.8896	0.0540	0.1400	0.6751	0.8941	0.0463			
12	0.2388	0.5391	0.1400	0.0146	0.1882	0.7071	0.7977	0.0565	0.1988	0.6505	0.7723	0.0459			
13	0.1919	0.2456	0.0626	0.0937	0.1444	0.4969	0.7190	0.0394	0.1399	0.6668	0.8815	0.0447			
14	0.1892	0.2457	0.0620	0.0936	0.1400	0.4570	0.6813	0.0637	0.1400	0.6645	0.8843	0.0467			
15	0.1787	0.3562	0.0651	0.1018	0.1548	0.5285	0.7068	0.1063	0.1553	0.5504	0.7293	0.0986			
16	0.1736	0.0463	0.2156	0.0202	0.1400	0.4527	0.6744	0.0631	0.1400	0.6582	0.8853	0.0434			
17	0.1703	0.0399	0.2211	0.0199	0.1400	0.4447	0.6748	0.0641	0.1548	0.4525	0.6936	0.0248			
18	0.1925	0.2011	0.1667	0.0839	0.1468	0.3883	0.6004	0.1000	0.1400	0.3575	0.5462	0.1215			

non-linear behaviour into the optimisation problem formulation. This non-linear behaviour is due, on the one hand, to the assessment of the buckling factor on a refined LFEM, and, on the other hand, to the definition of the structure stress-stiffness matrix \mathbf{K}_σ^b as a function of the design variables of the problem at hand. In a first time, the effect of only the membrane contribution in the definition of \mathbf{K}_σ^b (viz. matrices $\bar{\mathbf{K}}_1, \bar{\mathbf{K}}_2, \bar{\mathbf{K}}_3$ in Section 6.1.2) on the optimised solution is considered. In order to help the convergence,

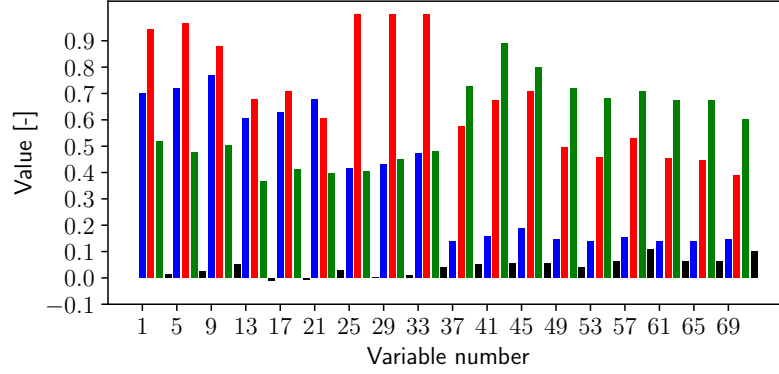


Figure 7.7: Optimal design variables values for Case 2 (n_0 in blue, ρ_{0K} in red, ρ_1 in green, ϕ_1 in black)

the starting point has been set to $n_0^j = 0.8$, $\rho_{0K}^j = \rho_1^j = \phi_1^j = 0.0$, $j = 1, \dots, 9$ for upper panels ($z = H$) and to $n_0^j = 0.4$, $\rho_{0K}^j = \rho_1^j = \phi_1^j = 0.0$, $j = 10, \dots, n_{\text{pan}}$ for the lower ones (see Figure 7.2). This starting point, which lies in the feasible domain, is more likely to be closer to the optimal point. Moreover, also in this case, the starting point is an isotropic solution.

The algorithm converges after 500 iterations. Although the starting point is inside the feasible domain, the algorithm experiences many difficulties in find the good path, due to the strong non-linear nature of the problem. The objective function value is $\Phi = 0.8440$, corresponding to a mass equal to 265.12 kg. As expected, the mass is slight lower then the value reported in (Panettieri et al., 2019), because of the neglected out-of-plane shear contribution in the expression of the stress-stiffness matrix. As in (Panettieri et al., 2019), the solution lies on the boundary of the buckling constraint.

The optimal value of the design variables is illustrated in Figure 7.7 (n_0 in blue, ρ_{0K} in red, ρ_1 in green, ϕ_1 in black), whilst the numerical values are reported in Table 7.5. The objective function and the optimisation constraints are listed in Table 7.4. A quick glance to this result highlights an enhanced exploitation of the anisotropy, especially for upper panels ($z = H$) (variables 1 up to 36), if compared to the optimal solution of case 1.

Case 3: Membrane and Out-of-plane Shear Contributions in \mathbf{K}_σ^b

This case considers both the membrane and the out-of-plane shear contributions in the expression of \mathbf{K}_σ^b (see Section 6.1.2). This formulation is really close to that implemented in ANSYS® software.

The starting point has been set to $n_0^j = 0.8$, $\rho_{0K}^j = \rho_1^j = \phi_1^j = 0.0$, $j = 1, \dots, 9$ for upper

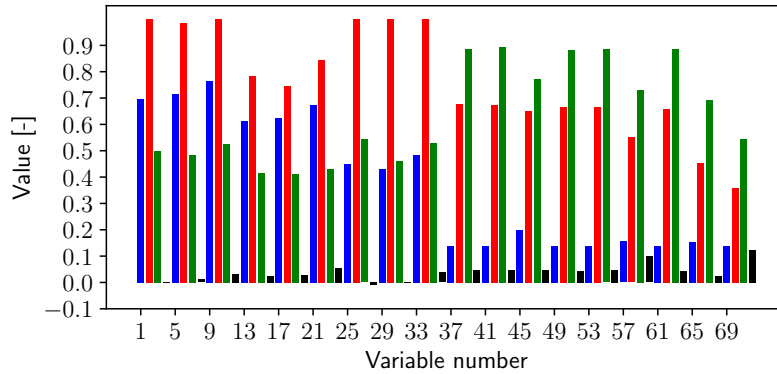


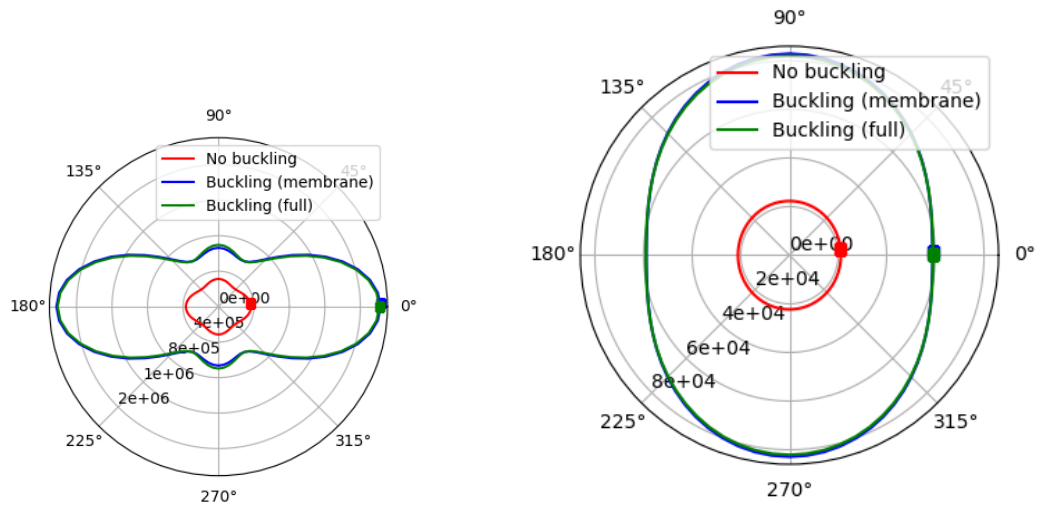
Figure 7.8: Optimal design variables values for Case 3 (n_0 in blue, ρ_{0K} in red, ρ_1 in green, ϕ_1 in black)

panels ($z = H$) and to $n_0^j = 0.4$, $\rho_{0K}^j = \rho_1^j = \phi_1^j = 0.0$, $j = 10, \dots, n_{\text{pan}}$ for the lower ones (see Figure 7.2). Also in this case the starting point is an isotropic solution.

The algorithm converges after 400 iterations. The objective function value is 0.8461, corresponding to an overall mass of 265.72 kg. The optimal value of the design variables is shown in Figure 7.8 and listed in Table 7.5. The values of the objective function and of the optimisation constraints are reported in Table 7.4. When compared to the solution of case 2, this configuration is characterised by a more pronounced effect of the anisotropy on the buckling strength (especially in terms of ρ_{0K} and ρ_1 contributions) and by a different orientation of the main orthotropy axis (related to the value of the polar angle). However, since the problem is strongly non-convex in terms of the buckling factor requirement, both solutions are characterised by similar values of the mass and of the buckling factor constraint.

As an example, Figures 7.9a, 7.10a, 7.11a show the first component of the membrane tensor \mathbf{A} , whilst Figures 7.9b, 7.10b, 7.11b illustrate the first component of the out-of-plane shear tensor \mathbf{H} , for panels 1, 6, 7, respectively. The square mark shows the relative angle Φ_1^{A*} .

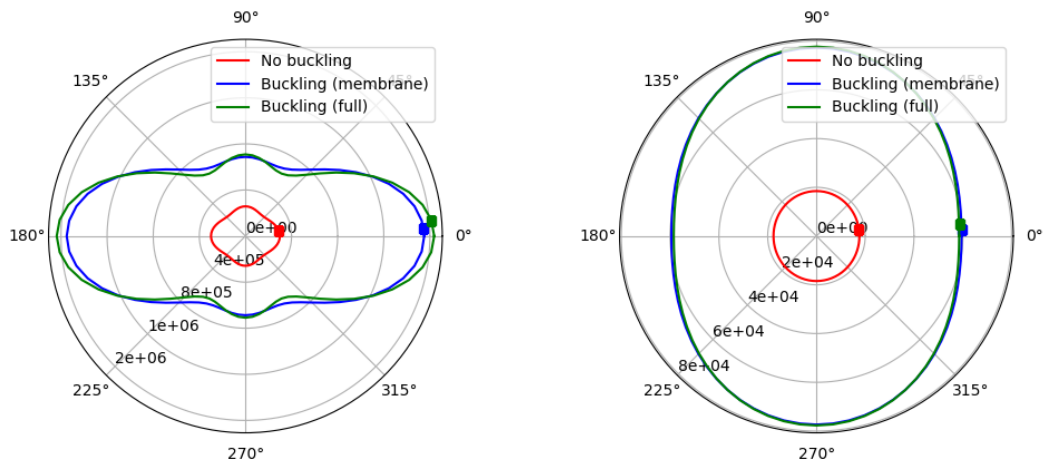
It is evident the impact of considering the buckling strength requirement on the optimised value of the laminate PPs: the polar diagram of the laminate stiffness matrices changes considerably for the considered cases. Conversely, the effect of the membrane and shear contributions involved in the definition of the stress-stiffness matrix it is more pronounced only for panels 6 and 7, as it can be inferred from Table 7.5 and Figures 7.10 and 7.11.



(a) A_{11} coefficient

(b) H_{11} coefficient

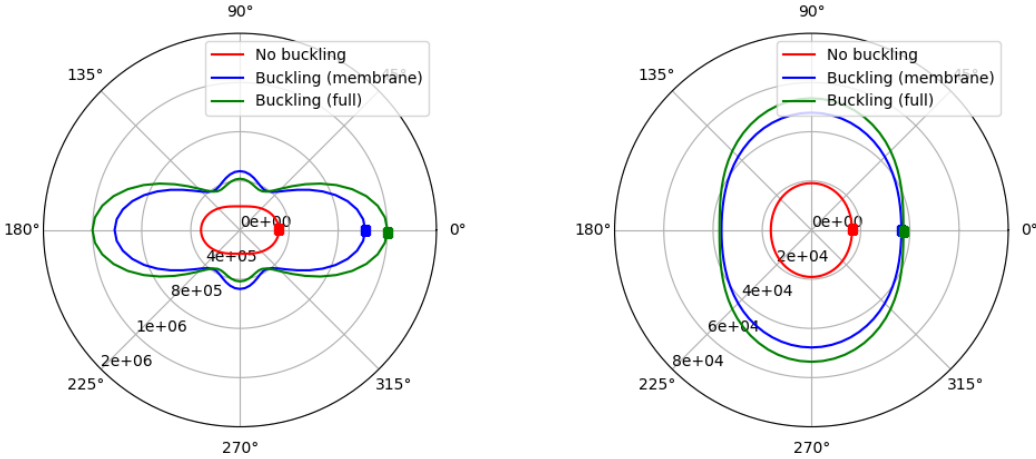
Figure 7.9: Polar diagram of the first component of matrices \mathbf{A} and \mathbf{H} for panel $n^o 1$



(a) A_{11} coefficient

(b) H_{11} coefficient

Figure 7.10: Polar diagram of the first component of matrices \mathbf{A} and \mathbf{H} for panel $n^o 6$



(a) A_{11} coefficient

(b) H_{11} coefficient

Figure 7.11: Polar diagram of the first component of matrices \mathbf{A} and \mathbf{H} for panel $n^\circ 7$

7.3 Case Study 2: a Benchmark on the SLP

7.3.1 Problem Definition

To analyse the impact of the blending constraints in FLP and SLP, a numerical benchmark taken from the literature (Soremekun et al., 2002; Adams et al., 2004; Ijsselmuiden et al., 2009) is considered. The system is an eighteen-panel structure. Each panel is subject to biaxial compressive loads, as shown in Figure 7.12. Besides, each panel is simply-supported along its boundary edges, and no load redistribution is considered, since loads at panels level are assumed known and fixed (Macquart et al., 2016). This is equivalent to consider the plates mechanically-independent between them; the coupling effect is hence limited to the blending constraints between adjacent panels.

The material of the elementary lamina is a carbon-epoxy IM7/8552 pre-preg (Ijssel-

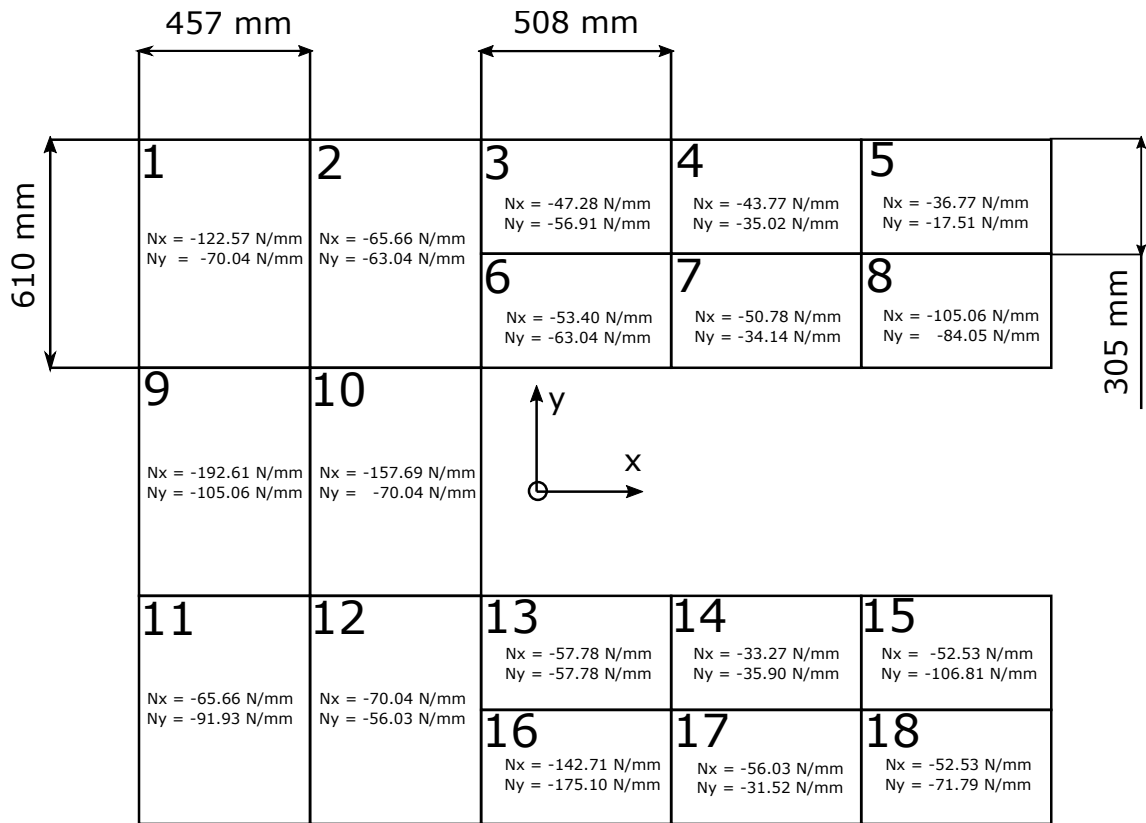


Figure 7.12: Eighteen panels benchmark structure of Case Study 2

muiden et al., 2009), whose properties are summarised in Table 7.6, in terms of both engineering constants and PPs.

7.3.2 The First-level Problem

Each panel is characterised by four design variables, introduced in Eq. (4.32). The structure of Figure 7.12 is then described through 72 variables collected in the design variables vector $\xi := \{n_0^j, \rho_{0K}^j, \rho_1^j, \phi_1^j \mid j = 1, \dots, 18\}$. The objective function is expressed as

Table 7.6: Material properties of the carbon-epoxy IM7/8552 pre-preg.

Technical constants		Polar parameters of \mathbf{Q}	
E_1 [GPa]	141	T_0 [MPa]	20285.37
E_2 [GPa]	9.03	T_1 [MPa]	19604.71
G_{12} [GPa]	4.27	R_0 [MPa]	16015.37
ν_{12}	0.32	R_1 [MPa]	16605.14
ν_{23}	0.42	Φ_0 [deg]	0
		Φ_1 [deg]	0
Density and thickness		Polar parameters of $\hat{\mathbf{Q}}$	
ρ_{ply} [kg mm ⁻³]	1.572×10^{-6}	T [MPa]	3724.78
t_{ply} [mm]	0.191	R [MPa]	545.21
N_{ref}	40	Φ [deg]	90
ΔN_{min}	4		

follows:

$$\Phi(\boldsymbol{\xi}) := \frac{N_{\text{ref}} t_{\text{ply}} \rho_{\text{ply}}}{m_{\text{ref}}} \sum_{j=1}^{18} A_j n_0^j, \quad (7.26)$$

where $m_{\text{ref}} = 29.46$ kg is the reference mass (Ijsselmuiden et al. (2009)), N_{ref} is a reference number of plies to rescale the actual one (see Table 7.6), A_i , n_0^j are the area and the dimensionless number of plies of the j -th panel, respectively, ρ_{ply} , t_{ply} are the density and the thickness of the single ply, respectively (see Table 7.6). In this case study, the FLP formulation deals with the minimisation of the mass of the structure, subject to feasibility, blending and buckling constraints. A safety factor of 1.1 has been added in the buckling constraint (Izzi, Montemurro, Catapano, & Pailhès, 2020). Finally, the continuous optimisation problem can be formulated as:

$$\begin{aligned} & \min_{\boldsymbol{\xi}} \Phi(\boldsymbol{\xi}), \quad \text{subject to:} \\ & \left. \begin{aligned} & \mathbf{K}(\boldsymbol{\xi}) \mathbf{u}(\boldsymbol{\xi}) - \mathbf{f} = \mathbf{0} \\ & (\mathbf{K} - \lambda \mathbf{K}_{\sigma}) \boldsymbol{\psi} = \mathbf{0}, \\ & g_{\text{feas}}(\boldsymbol{\xi}) \leq 0 \\ & g_{\text{buck}}(\boldsymbol{\xi}) \leq 0 \end{aligned} \right\} \forall \text{ panels,} \\ & \left. \begin{aligned} & g_{\text{blend-}j}(\boldsymbol{\xi}) \leq 0, \quad j = 0, 1 \end{aligned} \right\} \forall \text{ couples of adjacent panels,} \\ & \boldsymbol{\xi}_{\text{lb}} \leq \boldsymbol{\xi} \leq \boldsymbol{\xi}_{\text{ub}}. \end{aligned} \quad (7.27)$$

The employed blending constraints are those presented in Section 6.2. Moreover, for the sake of completeness, since the GL approach is not used, the expression of the buckling factor gradient (Eq. (6.31)) is more simple, because terms coupling the global and the local scales identically vanish.

Table 7.7 reports the lower and upper bounds of design variables. Variables n_0^j , $j = 1, \dots, 18$ are assumed continuous for the first optimisation phase, i.e. the *continuous op-*

timisation, for the resolution of the FLP (7.27). The parameter α appearing in Eq. (7.4) and (7.5) has been set as in Eq. (7.24).

Table 7.7: Design variables range of Problem (7.27)

Variable	lower bound	upper bound
n_0^j	0.25	1
ρ_{0K}^j	-1	1
ρ_1^j	0	1
ϕ_1^j	-1	1

$j = 1, \dots, 18$

The mathematical formulation of the discrete optimisation is identical to the one reported in Eq. (7.21) with $\Delta N_{\min} = 4$.

7.3.2.1 Numerical Strategy

Problem (7.27) is a non-convex CNLPP in terms of both geometrical and mechanical design variables. The non-convexity is due to the set of constraints. The solution search of the continuous problem is performed via *fmincon* algorithm, available in the Optimization Toolbox of MATLAB® (The MathWork Inc., 2011). The default values, summarised in Table 7.3, have been used.

At each iteration, the MATLAB® script invokes the Python routines which control the creation of the FE models and the evaluation of the objective function, of the constraints and of the corresponding gradients, as detailed in Chapter 6. The optimisation procedure is coupled with ANSYS® FE commercial software. Figure 7.13 shows the conceptual work-flow of the numerical strategy for the FLP. At each iteration of the deterministic algorithm:

- a new set of design variables ξ is passed to a Python Class which controls the FEMs generation;
- ANSYS® is invoked: an ANSYS® Parametric Design Language (APDL) script generates the panels FEMs;
- once Problem (6.1) is solved, for each panel, fundamental information such as connectivity, nodes coordinates, displacement fields, etc. are passed back to the Python Class;
- the Python Class evaluates the objective function and optimisation constraints, together with their gradients.

Matrix \mathbf{K}_σ is assembled within the Python Class, which also solves the eigenvalue problem via the *scipy.sparse.linalg.eigh* routine, based on the ARPACK software and the Implicitly Restarted Lanczos Method (Lehoucq et al., 1998). The use of this approach,

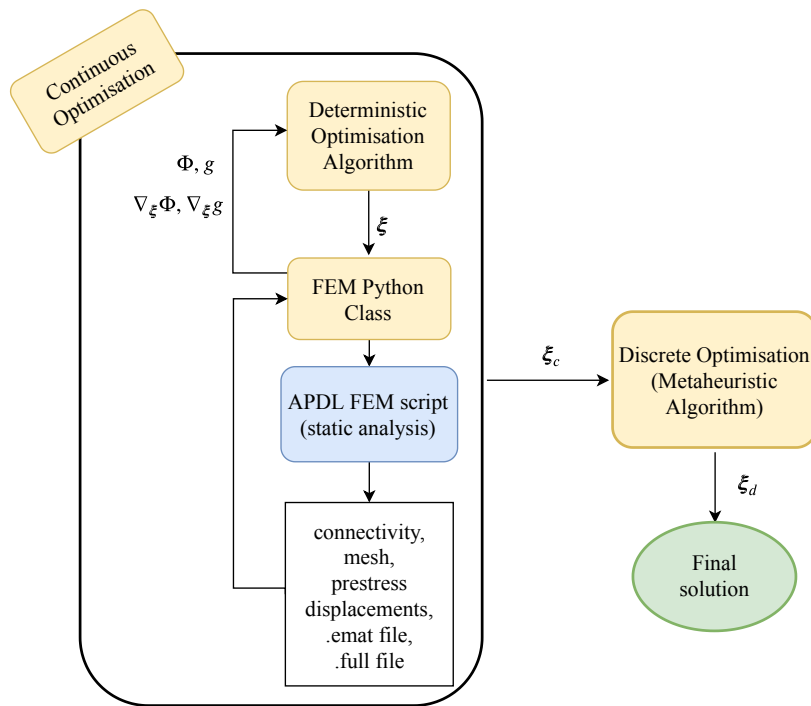


Figure 7.13: Workflow of the numerical strategy of the FLP of Case Study 2

already explained in Section 6.1 and 7.2.3, is mainly due to the perfect coherence between buckling factor and its gradient. In this case, K_σ is evaluated for every panel. For each panel the buckling factor is evaluated separately, since no mechanical coupling is considered between adjacent laminates. As a consequence, each panel depends only on its variables, and the buckling factor gradient expression simplifies (coupling terms are identically null).

The objective function value and all of the constraints (and gradients) are then passed to the optimisation algorithm. The loop is repeated until one of the convergence criteria of the *fmincon* algorithm is satisfied, as in Table 7.3.

The ACO meta-heuristic algorithm MIDACO[®], specialised in mixed-integer programmings, is used (Dorigo et al., 2006; Schlüter et al., 2009; Schlüter & Gerdts, 2009; Schlüter et al., 2012) to perform the solution search for Problem (7.21). This choice is due to the fact that MIDACO[®] is specialised in MICNLPPs and provide good results for a wide class of problems, as discussed in the above works. Moreover, the solver is claimed to be the state-of-the-art for evolutionary computing on MICNLPPs¹. MIDACO[®] parameters have been tuned as reported in Table 7.8. After a preliminary tuning, 200 Ants and a 20-ant based Kernel resulted as a good trade-off between the exploration of the design space and the convergence of results. A high Focus value facilitates the exploration of the neighbourhood of the starting guess, which is set to ξ_c . In so doing, the final solution would not be so different from the initial guess, as desired. The Oracle parameter, which is suggested to be assumed equal to the expected (or desired) objective function optimal value (Schlueter (2018)), is set equal to 0. The convergence criterion for the algorithm is

¹From <http://www.midaco-solver.com/index.php/about>

the number of evaluations of the objective function (*Evalstop* parameter), and it has been set to three millions.

Table 7.8: MIDACO[®] parameters for the discrete optimisation of Case Study 2

Parameter	Value
Ants	200
Kernel	20
Focus	1×10^6
Oracle	0
Evalstop	3×10^6

Each panel of the structure is made of SHELL181 elements, which are based on Reissner-Mindlin kinematics (Reddy, 2003) and have four nodes with six DOFs per node. Each panel is composed of about 60 elements and has 460 DOFs. The mesh size has been chosen after a sensitivity study (not reported here for the sake of brevity) in order to find a compromise between accuracy and computational cost. As stated in Section 7.3.1, each panel is simply-supported along the edges, whilst the load condition is a biaxial compressive load, as reported in Figure 7.12.

7.3.2.2 Numerical Results

Two cases have been simulated:

- (a) the optimisation of individual panels without blending constraints;
- (b) the optimisation of the eighteen-panel structure enforcing blending constraints.

The initial guess for both cases has been chosen as an isotropic ($\rho_0^j = \rho_1^j = \phi_1^j = 0$, $j = 1, \dots, 18$) feasible solution, having $n_0^1 = 0.9$, $n_0^{2,11,12,16} = 0.8$, $n_0^{3,8,15} = 0.7$, $n_0^{4,7,14,17} = 0.5$, $n_0^{5,6,13,18} = 0.6$, $n_0^{9,10} = 1$. In so doing, the anisotropy can "freely" emerge as the optimisation algorithm evolves.

Since no hypotheses have been formulated on the final stacks, e.g. symmetric, balanced, or restricted to the use of few orientations, the final solutions for both cases are lighter than the reference ones available in the literature. Table 7.9 compares the optimal masses from (Soremekun et al., 2002; Adams et al., 2004; Ijsselmuiden et al., 2009; Irisarri et al., 2014; Macquart et al., 2016) with the results of this work, while Table 7.10 reports the optimal value of the design variables at the end of the continuous optimisation. Of course, the optimal solutions found in the above works make use of some restrictive assumptions on the stacks. It is noteworthy that the use of the FE method for the evaluation of buckling factor instead of an approximated formula, coupled with the wide generality of the proposed blending constraints, lead to a lower mass of the structure. Moreover, the blended solution is 6% heavier than the not-blended counterpart, but still 7% lighter than the reference one. It is noteworthy that, despite the introduction of a safety factor

Table 7.9: Comparison of optimal mass (in kg) of Case Study 2

Reference Optimisation method	No blending		With blending	
	continuous	discrete	continuous	discrete
Soremekun et al., 2002		27.28		29.27
Adams et al., 2004				28.63
Ijsselmuiden et al., 2009		27.28		29.46
Irisarri et al., 2014				28.85
Macquart et al., 2016				27.63
Proposed method	25.50	25.98	25.86	27.28

in Eq. (6.2), the proposed solution is lighter than the other ones presented in the literature, obtained without safety factor. Table 7.11 reports the optimal solutions for Problem (7.21). The little increase of weight (see Table 7.9) due to blending is contained by a major exploitation of anisotropy, as clearly shown in the results. Furthermore, the conservative rounding of the continuous solutions makes the discrete solution compliant with buckling requirements since, for every panel, the buckling eigenvalue has been checked to still be greater than one. It is noteworthy that this is not true for some approaches as in (Adams et al., 2004; Macquart et al., 2016).

As reported in Tables 7.10 and 7.11, the compliance with blending constraints may require substantial modifications in terms of PPs and number of plies (see, for instance, panel 17). Moreover, when blending requirement is not taken into account, the discrete optimisation step achieves a solution very close to the continuous one. Conversely, when blending is taken into account, the strong coupling between laminates may introduce more important discrepancies, which are always conservative (in terms of buckling factor values).

The buckling factors for both cases (with and without blending) and after both continuous and discrete optimisation steps are reported in Table 7.12. It is noteworthy that the continuous optimisation, with and without blending constraints, is able to find a local minimiser located on the boundary of the feasible domain, i.e. all buckling factors are equal to 1.1. Moreover, the rounding of laminates thickness carried out during the discrete optimisation step is conservative and creates a security margin against buckling failure varying between +14% (panel 16) and +56% (panel 2).

7.3.3 The Second-level Problem

The SLP formulation is the same provided in Section 7.4.2. However, the search propagation direction must be introduced and discussed.

7.3.3.1 Numerical Strategy

The determination of the number of design variables for the SLP strictly depends on the FLP solution. The actual structure of Figure 7.12, with reference to the FLP solution reported in Table 7.11, can be represented with a graph, as in Figure 7.14. Each panel

Table 7.10: Numerical solution for the continuous optimisation of the FLP (7.27)

Panel	No blending					With blending				
ID	n_0	$n_0 N_{\text{ref}}$	ρ_{0K}	ρ_1	ϕ_1	n_0	$n_0 N_{\text{ref}}$	ρ_{0K}	ρ_1	ϕ_1
1	0.7451	29.8040	-0.1462	0.6533	0	0.7567	30.2662	-0.5877	0.4318	0
2	0.5865	23.4600	-0.3940	0.5504	0	0.6038	24.1529	-0.7409	0.2875	0
3	0.5184	20.7360	-0.6444	0	0	0.5411	21.6448	-0.7094	0.2035	0
4	0.4314	17.2560	-0.9320	0	0	0.4315	17.2588	-0.9184	0	0
5	0.3250	13	-1	0	0	0.3262	13.0488	-0.9686	0	0
6	0.5361	21.4440	-0.6553	0	0	0.5638	22.5513	-0.7203	0.2347	0
7	0.4201	16.8040	-1	0	0	0.4207	16.8299	-0.9565	0	0
8	0.5780	23.1200	-0.9315	0	0	0.5781	23.1226	-0.9259	0	0
9	0.8687	34.7480	-0.1264	0.6609	0	0.8767	35.0665	-0.4765	0.4974	0
10	0.8193	32.7720	-0.0361	0.6942	0	0.8310	33.2416	-0.4903	0.4685	0
11	0.5767	23.0680	-0.7003	0.3870	0	0.5778	23.1126	-0.7452	0.3506	0
12	0.6062	24.2480	-0.3000	0.5916	0	0.6242	24.9690	-0.7659	0.2920	0
13	0.5174	20.6960	-0.7581	0	0	0.5386	21.5441	-0.7276	0.1784	0
14	0.4428	17.7120	-0.7089	0	0	0.4431	17.7223	-0.7809	0	0
15	0.6451	25.8040	-0.4180	0	0	0.6452	25.8075	-0.4121	0	0
16	0.7553	30.2120	-0.6326	0	0	0.7637	30.5482	-0.6105	0.0556	0
17	0.4012	16.0480	-1	0	0	0.4024	16.0972	-0.9637	0	0
18	0.5594	22.3760	-0.0159	0	0	0.5620	22.4816	-0.5647	0	0

Table 7.11: Numerical solutions for the discrete optimisation of the FLP (7.21)

Panel	No blending				With blending			
ID	N	ρ_{0K}	ρ_1	ϕ_1	N	ρ_{0K}	ρ_1	ϕ_1
1	30	-0.1462	0.6533	0	31	-0.5878	0.4095	0
2	24	-0.3940	0.5504	0	27	-0.7409	0.3148	0
3	21	-0.6444	0	0	23	-0.7095	0.2035	0
4	18	-0.9320	0	0	18	-0.9184	0	0
5	13	-1	0	0	14	-0.9686	0	0
6	22	-0.6553	0	0	23	-0.7095	0.2035	0
7	17	-1	0	0	18	-0.9184	0	0
8	24	-0.9315	0	0	24	-0.9259	0	0
9	35	-0.1264	0.6609	0	36	-0.4903	0.4685	0
10	33	-0.0361	0.6942	0	36	-0.4903	0.4685	0
11	24	-0.7003	0.3870	0	26	-0.7658	0.2677	0
12	25	-0.3000	0.5916	0	26	-0.7658	0.2677	0
13	21	-0.7581	0	0	22	-0.7276	0.1784	0
14	18	-0.7089	0	0	18	-0.8514	0	0
15	26	-0.4180	0	0	27	-0.4122	0	0
16	31	-0.6326	0	0	31	-0.6105	0.0582	0
17	17	-1	0	0	18	-0.8514	0	0
18	23	-0.0159	0	0	23	-0.5647	0	0

Table 7.12: Buckling factors (λ) after the continuous and discrete optimisations of Case Study 2

Panel	Buckling factor			
	Continuous optimisation		Discrete optimisation	
ID	No blending	With blending	No blending	With blending
1	1.1000	1.1000	1.1215	1.1709
2	1.1000	1.1000	1.1769	1.5650
3	1.1000	1.1000	1.1423	1.3192
4	1.1000	1.1000	1.2477	1.2476
5	1.1000	1.1000	1.0990	1.3580
6	1.1000	1.1000	1.1874	1.1747
7	1.1000	1.1000	1.1384	1.3452
8	1.1000	1.1000	1.2296	1.2295
9	1.1000	1.1000	1.1239	1.1890
10	1.1000	1.1000	1.1229	1.3958
11	1.1000	1.1000	1.2378	1.5235
12	1.1000	1.1000	1.2048	1.2255
13	1.1000	1.1000	1.1486	1.1711
14	1.1000	1.1000	1.1542	1.1524
15	1.1000	1.1000	1.1247	1.2590
16	1.1000	1.1000	1.1874	1.1475
17	1.1000	1.1000	1.3063	1.4934
18	1.1000	1.1000	1.1147	1.1776

is represented by a circle characterised by the number of plies obtained at the end of the discrete optimisation step of the FLP (panels having the same thickness and PPs are depicted once, the panel ID being in the yellow diamond). The solution propagation starts from the thinnest panel, having 14 plies. Following the solution path in Figure 7.14, additional variables (reported in light-blue labels) are introduced when moving from a thinner to a thicker laminate. Conversely, when passing from a thicker to a thinner laminate, no further variables are introduced (red arrows). It is noteworthy that, with such a propagation, blending requirements at the mesoscale are automatically satisfied, regardless of the particular adopted blending scheme. The propagation scheme of Figure 7.14 is specific for the case at hand, since propagation heavily depends on the FLP solution. During the SLP, the construction of blended SSs is enforced following the propagation of Figure 7.14. Once the blended SSs are formally generated, at each iteration, the residual for the whole structure must be minimised by acting on the design variables, i.e. the determining the orientation angles. The information related to the specific propagation scheme is set by the user and passed as an input of the SLP, i.e. as the order of generation of each SS (basically, the path formed by the arrows in Figure 7.14). As said before, different propagation schemes can be set by the user. Problem (6.52) has 56 independent design variables, while the overall number of plies in the structure is 441. Consider the passage from the generic laminate p to laminate q . If $N_p > N_q$, SS_q is obtained by a random suppression of a number of plies equal to $N_p - N_q$. Otherwise, if $N_p < N_q$, SS_q is obtained by the insertion, at random position in SS_p , of a number of new design variables equal to

7.3.3.2 Numerical Results

Since the propagation is independent from the particular adopted blending scheme, several stack recoveries have been performed. In particular, four different blending schemes have been considered, qualitatively depicted in Figure 7.15, but many others are possible. The results of Problem (6.52) are listed in Table 7.14. It is observed that the Random

Table 7.14: Residuals for different blending schemes of Case Study 2

Blending scheme	Residual
Random	1.4378
Outward $[0, \pm 45, 90]$ deg	0.8462
Outward	0.5743
Inward with continuity of two external plies	0.4381

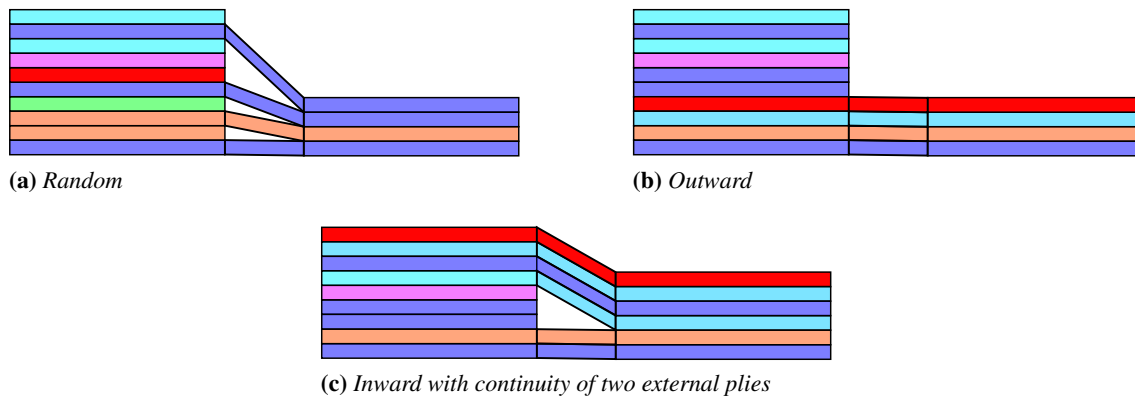


Figure 7.15: Three different blending schemes.

scheme has the highest residual. It is probably due to the fact that the dropped plies change at every iteration in an unpredictable way, thus causing difficulties to the algorithm. However, it remarks the fact that the solution propagations are independent from the particular blending scheme: even a random one may work in the strategy. Remarkably, the Outward blending considering only classical orientations, i.e. $[0, \pm 45, 90]$ deg, is farther from the target than the counterpart allowing non-conventional orientations. The closest solution to the target, among the considered four, is the Inward blending with the imposed continuity of the two outermost plies. This case can be employed, for example, for aeronautic surfaces, because it guarantees a smooth side, that can be wet by the air flow without aerodynamic penalisation, whilst the other side is "protected" by two (in this case) external covering plies. Hereafter, only this latter solution will be considered for the illustration and discussion of the results.

Results are reported in Table 7.15, together with the residuals $\mathcal{R}^{(i)}$, $i = 1, \dots, 18$ of the SR for each panel and the buckling factor evaluated with the properties associated to the recovered SS. For the structure, the value of the objective function is $\mathcal{R} = 0.4381$. As it can be seen, no panels violate the buckling requirement, i.e. all panels have a buckling

factor greater than 1. Moreover, some reservoir against buckling failure is maintained, from +6% (panel 14) to +45% (panel 2). It is a noteworthy result, since other approaches, such as (Macquart et al., 2016), at the end do not provide feasible SSs from the buckling failure viewpoint.

The decomposition of the total residual into the single contributions appearing in Eq. (6.48), for each panel, is shown in Figure 7.16. It is clear that the major contributors are from the ρ_1 recovery (\mathcal{R}_5) especially for panels 1, 9, 10; from the ρ_0 recovery (\mathcal{R}_4) for panel 5; from the uncoupling recovery (\mathcal{R}_1) for panel 9, 10, 1, 15. Except from these panels, the recovery of uncoupling (\mathcal{R}_1) and/or homogeneity (\mathcal{R}_2) requirements is generally good. Finally, the ϕ_1 recovery (\mathcal{R}_6) and the orthotropy recovery (\mathcal{R}_3) is generally satisfying.

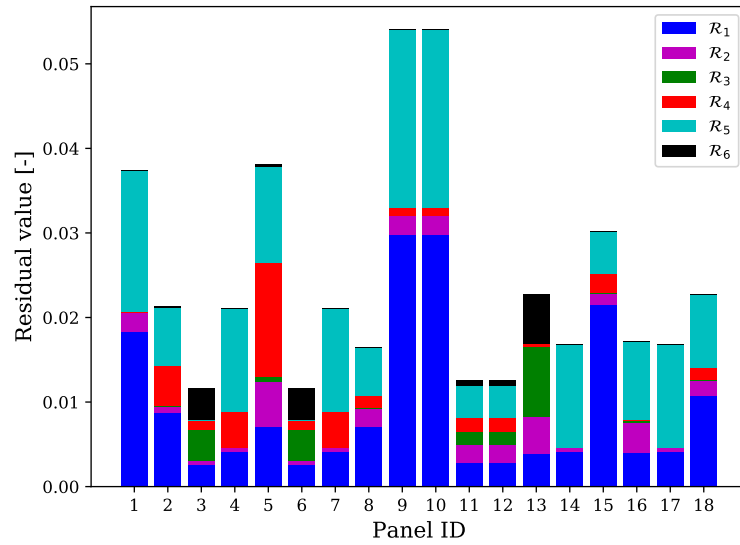


Figure 7.16: *Contributes to the total residual from each panel of Case Study 2*

Figure 7.17 shows the polar diagrams of $(\mathbf{A}^*)_{11}^\dagger$, $(\mathbf{A}^*)_{11}$, $(\mathbf{B}^*)_{11}$, $(\mathbf{C}^*)_{11}$ ($(\mathbf{B}^*)_{11}^\dagger$ and $(\mathbf{C}^*)_{11}^\dagger$ are null) for the thinnest laminate, the thickest laminates, and for the laminates having the smallest and largest residual, see Table 7.15.

If compared to previous works, where the stack recovery is performed for single laminates (Montemurro et al. (2012a), Montemurro et al. (2012c), Montemurro (2015b), Montemurro et al. (2019)), it is clear that the SLP for single laminates is simpler to solve, since residuals are definitely smaller.

It would be interesting comparing the results of the SLP provided in this study with other methodologies proposed in the literature. Unfortunately, these works do not provide any measure of the fitness (viz. the residuals of Table 7.15) of the SLP solution.

7.3.4 Some Remarks on the Proposed SLP Strategy

When dealing with multi-scale optimisation of composite structures including blending constraints, numerous factors introduce uncertainty and error. The following remarks can be inferred from a critical analysis of the results of both the FLP and the SLP.

Table 7.15: Optimal stacks solution of Problem (6.52) of Case Study 2

Panel	Stack	Residual	Buckling factor (λ)
1	42/ - 45/36/ - 37/14/ - 10/ - 11/ - 41/45/20/ - 33/41/24/ - 37/ - 8/47/ - 49/ - 37/32/ - 43/44/51/ - 44/ - 44/28/42/ - 46/50/ - 22/36/ - 47/	0.0374	1.1201
2	42/ - 45/ - 11/ - 41/45/20/ - 33/41/24/ - 37/ - 8/47/ - 49/ - 37/32/ - 43/44/51/ - 44/ - 44/28/42/ - 46/50/ - 22/36/ - 47/	0.0213	1.4563
3	42/ - 45/ - 33/41/24/ - 37/ - 8/47/ - 49/ - 37/32/ - 43/44/51/ - 44/ - 44/28/42/ - 46/50/ - 22/36/ - 47/	0.0116	1.3219
4	42/ - 45/47/ - 49/ - 37/32/ - 43/44/51/ - 44/ - 44/28/42/ - 46/50/ - 22/36/ - 47/	0.0211	1.1408
5	42/ - 45/ - 43/44/51/ - 44/ - 44/28/42/ - 46/50/ - 22/36/ - 47/	0.0381	1.1962
6	42/ - 45/ - 33/41/24/ - 37/ - 8/47/ - 49/ - 37/32/ - 43/44/51/ - 44/ - 44/28/42/ - 46/50/ - 22/36/ - 47/	0.0116	1.1952
7	42/ - 45/47/ - 49/ - 37/32/ - 43/44/51/ - 44/ - 44/28/42/ - 46/50/ - 22/36/ - 47/	0.0211	1.2112
8	42/ - 45/47/ - 46/45/ - 44/46/ - 47/47/ - 49/ - 37/32/ - 43/44/51/ - 44/ - 44/28/42/ - 46/50/ - 22/36/ - 47/	0.0164	1.1556
9	42/ - 45/ - 7/21/ - 13/ - 40/40/36/ - 37/14/ - 10/ - 11/ - 41/45/20/ - 33/41/24/ - 37/ - 8/47/ - 49/ - 37/32/ - 43/44/51/ - 44/ - 44/28/42/ - 46/50/ - 22/36/ - 47/	0.0540	1.1198
10	42/ - 45/ - 7/21/ - 13/ - 40/40/36/ - 37/14/ - 10/ - 11/ - 41/45/20/ - 33/41/24/ - 37/ - 8/47/ - 49/ - 37/32/ - 43/44/51/ - 44/ - 44/28/42/ - 46/50/ - 22/36/ - 47/	0.0540	1.3461
11	42/ - 45/ - 41/45/20/ - 33/41/24/ - 37/ - 8/47/ - 49/ - 37/32/ - 43/44/51/ - 44/ - 44/28/42/ - 46/50/ - 22/36/ - 47/	0.0126	1.3711
12	42/ - 45/ - 41/45/20/ - 33/41/24/ - 37/ - 8/47/ - 49/ - 37/32/ - 43/44/51/ - 44/ - 44/28/42/ - 46/50/ - 22/36/ - 47/	0.0126	1.1832
13	42/ - 45/41/24/ - 37/ - 8/47/ - 49/ - 37/32/ - 43/44/51/ - 44/ - 44/28/42/ - 46/50/ - 22/36/ - 47/	0.0227	1.1635
14	42/ - 45/47/ - 49/ - 37/32/ - 43/44/51/ - 44/ - 44/28/42/ - 46/50/ - 22/36/ - 47/	0.0168	1.0577
15	42/ - 45/77/ - 19/21/ - 75/66/13/ - 47/ - 89/ - 4/47/ - 49/ - 37/32/ - 43/44/51/ - 44/ - 44/28/42/ - 46/50/ - 22/36/ - 47/	0.0301	1.2160
16	42/ - 45/ - 21/26/62/ - 57/ - 81/ - 41/45/20/ - 33/41/24/ - 37/ - 8/47/ - 49/ - 37/32/ - 43/44/51/ - 44/ - 44/28/42/ - 46/50/ - 22/36/ - 47/	0.0172	1.0845
17	42/ - 45/47/ - 49/ - 37/32/ - 43/44/51/ - 44/ - 44/28/42/ - 46/50/ - 22/36/ - 47/	0.0168	1.3621
18	42/ - 45/66/13/ - 47/ - 89/ - 4/47/ - 49/ - 37/32/ - 43/44/51/ - 44/ - 44/28/42/ - 46/50/ - 22/36/ - 47/	0.0227	1.1173
		0.4381	

(a) **Guarantee to satisfy constraints.** In analogy with all multi-level optimisation methods available in the literature, there is no guarantee that the final design, i.e. the recovered SSs, is compliant with mechanical constraints (in this work only a requirement on the buckling factor has been considered). As shown in Table 7.15, all panels satisfy the constraint on the buckling factor (assessed *a posteriori* through an eigen-

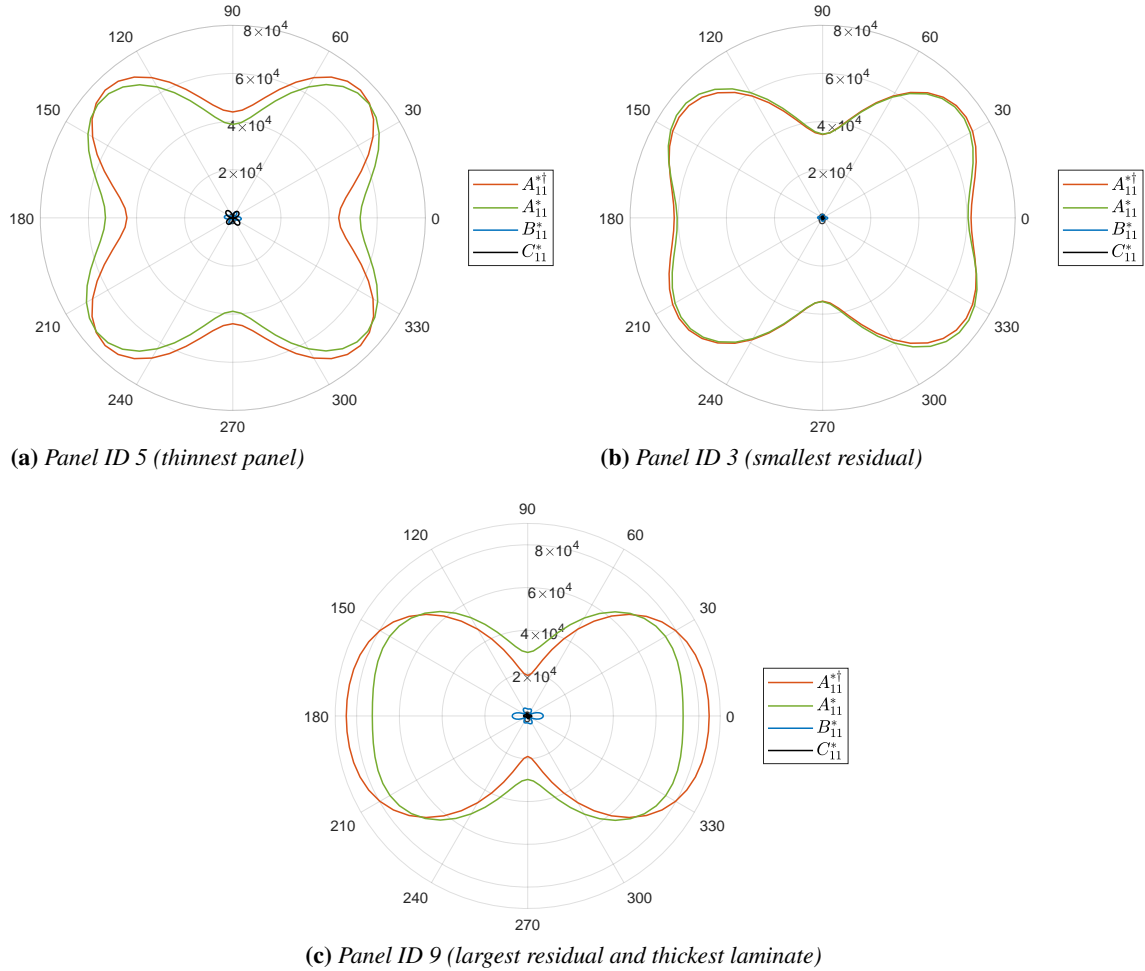


Figure 7.17: Polar diagrams of some selected panels of Case Study 2

value buckling analysis). It is due to the introduction in the FLP of a suitable safety factor ($= 1.1$) that prevents the violation of the mechanical requirements, as done in (Montemurro et al., 2018; Montemurro et al., 2019).

- (b) **Orientations discretisation.** In the FLP, PPs can assume any value inside the feasible domain of Eq. (4.45). In the SLP, orientation angles are sampled with a step of 1 deg. Assuming arbitrarily a coarser discretisation (conventional composites consider few orientation angles, viz. $\pm 45, 0, 90$ deg) worsens the situation, since SLPs based on few angles values can generate only an enumerable set of PPs, which does not cover the whole feasible domain with continuity.
- (c) **Blending constraints only on membrane PPs.** As stated in Section 6.2, blending constraints of Eq. (6.43) are deducible by studying membrane properties. As reported in Appendix B, the study of blended uncoupled laminates does not add further restrictive constraints. As a result, the non-intersection condition of plies (point (b) of Definition 6.3) does not enter in the FLP. Conversely, in step two, the blending constraint of Algorithm 6.3 takes this aspect into account. Therefore, an inconsistency between the two steps is inevitably introduced, making Problem (6.52) over-constrained.

- (d) **Dual attitude towards SSs in the MS2LOS.** The use of PPs in the FLP formulation introduces a necessary loss of information about SSs geometry. It is evident in Eq. (6.41) when orientation angles disappear from blending constraints, determining the passage from an equation to an inequality. On the contrary, in the SLP, the designer strives for recovery the lost information. Since the two sub-problems are not bijective (and the exact recovery may be impossible, see next point), the optimal target solution resulting from the FLP can be approximately achieved only through numerical methods, e.g. optimisation by means of meta-heuristic algorithms. Remarkably, the estimate (6.41) is the sharpest possible, thus minimising the discrepancy between FLP and SLP results.
- (e) **Feasibility domain in the PPs space.** A serious error source is connected to the feasibility of laminates, characterised by an arbitrary PPs[†] set inside the feasible domain of Eq. (4.45). In fact, the FLP formulation rely on the existence, in every point of the feasibility domain, of uncoupled, homogeneous, orthotropic laminates. Actually, this hypothesis is not necessarily true. Naively, given a SS, a PPs set necessarily derives, whilst given a set of PPs, there may exist no SS matching the reference set. As a consequence, the expression of a proper feasibility domain of laminates is a major still-open problem of composite design, and will be object of preliminary investigations in Chapter 9. Uncertainty on laminates feasibility domain introduces an unavoidable bias error in the SLP: if a set of optimal PPs is unrecoverable, the RSS introduce by default an error on the final solution. This fact is linked to the next point.
- (f) **Error chain.** Bias error may propagate throughout the structure, due to the strong coupling between all the connected panels. In fact, laminates PPs lie in the neighbourhood, determined by Eq. (6.43), of PPs of adjacent panels. Consider, for instance, the case depicted in Figure 6.6. Suppose that for laminate p target PPs _{p} [†] are not recoverable at all. Therefore, PPs _{q} [†] may lie outside the ball determined by Eq. (6.43) centred in the recovered PPs _{p} (different from PPs _{p} [†]). A similar case may happen when passing from q to r . The final error is affected by the initial bias error, because of the strong coupling of laminates PPs.

Apart from the benchmark problem discussed in this Chapter, there are some shrewdness to reduce the error.

- (a) **Increasing the ΔN_{\min}** makes thickness changes to appear only when necessary. As a consequence, there will be more panels sharing the same PPs and thickness. Of course, adjacent similar panels do not introduce further error. However, as noticed, the choice of this parameter depends on the trend of the FLP solution.
- (b) **Increasing the thickness of the laminates** reduces the bias error linked to the feasibility domain of laminates, since the feasibility region should coincide with the region delimited by Eq. (4.45) as the number of plies increases, as detailed in Chapter 9. Moreover, thin laminates PPs are more difficult to recover, as shown in (Montemurro et al., 2012a).

- (c) **Reducing the thickness of the constitutive ply** by adopting thin plies will be surely beneficial for both FLP and SLP formulations. In fact, the use of thin plies introduces a greater freedom in the design process allowing for an increased number of plies in the same thickness, with possibly different orientation angles. On the one hand, this allows finding better solutions in terms of mass and mechanical performances (buckling, stiffness, strength, etc.) at the end of the FLP. On the other hand, this allows reducing the gap between the solutions of FLP and SLP because of the increased number of design variables for the SLP.
- (d) **Determine stricter bounds for the laminate feasible domain:** finding the sharpest feasibility domain for an N -ply laminate would eliminate the bias error, as deeply discussed in Chapter 9.

7.4 Case Study 3: Comparisons Between Stacking Sequence Recovery Techniques

To test the stack recovery phase based on QT QH SSs, a very simple benchmark structure has been used. It is a rectangular simply-supported laminate, subdivided into twelve design regions and undergoing biaxial compression, as depicted in Figure 7.18. This is the panel 1 of the benchmark structure of Figure 7.12. The twelve design regions are

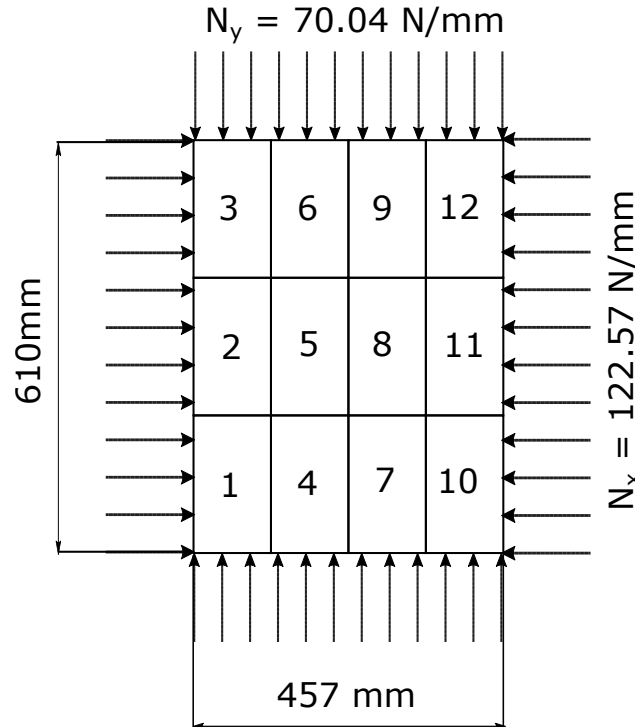


Figure 7.18: Benchmark structure for the comparison between two different stacking sequence recovery approaches of Case Study 3

coupled by means of blending constraints and load redistribution. Conceptually, the same methodology already described in Section 7.3 has been used.

7.4.1 The First-level Problem

The FLP is completely similar to the one already described in Section 7.3, including the material properties of the basic layer, the mathematical formulation of the problem (only buckling (no additional safety factor), blending and feasibility constraints have been considered as design drivers for the lightest solution), the adopted numerical strategy. In particular, the continuous optimisation problem can be formulated as:

$$\begin{aligned}
 & \min_{\xi} \Phi(\xi), \quad \text{subject to:} \\
 & \left. \begin{aligned} & \mathbf{K}\mathbf{u} - \mathbf{f} = \mathbf{0}, \\ & (\mathbf{K} - \lambda\mathbf{K}_\sigma)\boldsymbol{\psi} = \mathbf{0}, \end{aligned} \right\} \text{ in the global structure,} \\
 & \left. \begin{aligned} & g_{\text{feas}} \leq 0, \\ & g_{\text{buck}} \leq 0, \end{aligned} \right\} \text{ one constraint for the twelve regions,} \\
 & \left. \begin{aligned} & g_{\text{blend-}j} \leq 0, \quad j = 0, 1, \end{aligned} \right\} \forall \text{ couples of adjacent panels,} \\
 & \xi_{\text{lb}} \leq \xi \leq \xi_{\text{ub}},
 \end{aligned} \tag{7.28}$$

where the objective function Φ is the panel mass, defined as $\frac{12 A \rho_{\text{ply}} t_{\text{ply}} N_{\text{ref}}}{m_{\text{ref}}} \sum_{j=1}^{12} n_0^j$, being A the area of a single design region. The reference mass m_{ref} has been taken equal to 1 kg. The basic ply is the carbon-epoxy IM7/8552 pre-preg, whose properties are listed in Table 7.6. Also in this case, the expression of the buckling factor gradient is simpler than the one provided in Eq. (6.31), since the terms involving the coupling between global and local scales identically vanish. The design variables range is listed in Table 7.16.

Table 7.16: Design variables range of the continuous optimisation problem of Case Study 3

Variable*	lower bound	upper bound
n_0^j	0.1	0.8
ρ_{0K}^j	-1	1
ρ_1^j	0	1
ϕ_1^j	-1	1

* $j = 1, \dots, 12$

Variables n_0^j , $j = 1, \dots, 12$ are assumed continuous for the first optimisation phase, i.e. the *continuous optimisation*, for the resolution of the FLP (7.28). The parameter α appearing in Eq. (7.4) and (7.5) has been set as in Eq. (7.24).

The mathematical formulation of the discrete optimisation is identical to the one reported in Eq. (7.21) with $\Delta N_{\text{min}} = 4$. It is noteworthy that Eq. (7.21), as said in Section 7.1.4.2, does not take load redistribution into account. Indeed, load redistribution is a major concern of actual structures. However, since this investigation is focused on the stack recovery phase and not on the effective strength of the structure, Eq. (7.21) is

considered valid, as a first approximation.

7.4.1.1 Numerical Strategy

Problem (7.28) is a non-convex CNLPP in terms of both geometrical and mechanical design variables. The non-convexity is due to the set of constraints. The solution search of the continuous problem is performed via *fmincon* algorithm. The default values, summarised in Table 7.3, have been used.

At each iteration, the MATLAB[®] script invokes the Python routines which control the creation of the FE model of the panel and the evaluation of the objective function, of the constraints and of the corresponding gradients. The optimisation procedure is coupled with ANSYS[®] FE software. The conceptual work-flow of the numerical strategy for the FLP is basically identical to the one depicted in Figure 7.13. At each iteration of the deterministic algorithm, a new set of design variables ξ is passed to a Python Class which controls the FEM generation. ANSYS[®] is then invoked: an ANSYS[®] APDL script generates the panel FEM. Once Problem (6.1) has been solved, fundamental information such as connectivity, nodes coordinates, displacement fields, etc. are passed back to the Python Class, which evaluates the objective function and optimisation constraints, together with their gradients.

Matrix K_σ is assembled within the Python Class, which also solves the eigenvalue problem via the *scipy.sparse.linalg.eigsh* routine. The use of this approach have been already motivated in Section 6.1 and 7.2.3. The objective function value and all of the constraints (and gradients) are then passed to the optimisation algorithm. The loop is repeated until one of the convergence criteria of the *fmincon* algorithm is satisfied, as in Table 7.3.

The ACO meta-heuristic algorithm MIDACO[®] is used to perform the solution search for Problem (7.21). MIDACO[®] parameters have been tuned as reported in Table 7.8.

The panel is made of SHELL181 elements, which are based on Reissner-Mindlin kinematics (Reddy, 2003) and have four nodes with six DOFs per node. The panel is composed of about 400 elements and has about 10000 DOFs. The mesh size has been chosen after a sensitivity study (not reported here for the sake of brevity) in order to find a compromise between accuracy and computational cost. As stated, the panel is simply-supported along the four external edges, whilst the load condition is a biaxial compressive load, as reported in Figure 7.18.

7.4.1.2 Numerical Results

The results of the continuous optimisation of the FLP are reported in Table 7.17. The optimal mass is 1.8134 kg, whilst the buckling factor is equal to one. The starting point is characterised by all the twelve design regions having $n_0^j = 0.75$, $\rho_{0K}^j = \rho_1^j = \phi_1^j = 0$, $j = 1, \dots, 12$.

Results of the discrete optimisation problem are collected in Table 7.18. The resulting mass is 1.8694 kg.

Table 7.17: Numerical solution for the continuous optimisation of the FLP of Case Study 3

ID	n_0	$n_0 N_{\text{ref}}$	ρ_{0K}	ρ_1	ϕ_1
1	0.7730	30.92	-0.8405	0.1892	-0.0232
2	0.2667	10.66	-0.7815	0.2757	0.0059
3	0.7941	31.76	-0.8620	0.1674	0.0341
4	0.1965	7.86	-0.5332	0.4264	-0.0346
5	0.4278	17.11	-0.5557	0.0000	-0.0007
6	0.3542	14.16	-0.7938	0.1307	-0.0001
7	0.7745	30.98	-0.5715	0.0161	0.0125
8	0.7911	31.64	-0.5499	0.0000	0.0127
9	0.4291	17.16	-0.7501	0.1172	-0.0174
10	0.6466	25.86	-0.7658	0.1733	-0.0087
11	0.2545	10.18	-0.6276	0.3941	-0.0176
12	0.7927	31.70	-0.8277	0.1969	-0.0337

Table 7.18: Numerical solutions for the discrete optimisation of the FLP of Case Study 3

ID	N	ρ_{0K}	ρ_1	ϕ_1
1	31	-0.8405	0.1887	-0.0232
2	11	-0.7814	0.2762	0.0059
3	32	-0.8617	0.1669	0.0341
4	8	-0.5330	0.4265	-0.0338
5	19	-0.5542	0.0000	-0.0007
6	15	-0.7936	0.1314	-0.0001
7	32	-0.5676	0.0012	0.0125
8	32	-0.5676	0.0012	0.0125
9	19	-0.7489	0.1161	-0.0172
10	26	-0.7670	0.1726	-0.0087
11	11	-0.6275	0.3929	-0.0176
12	32	-0.8217	0.1969	-0.0337

7.4.2 The Second-level Problem

The SLP has been firstly solved by using the numerical approach already described in Chapter 6 and Section 7.3, and then by using the alternative approach based on the knowledge of QT QH SSs.

7.4.2.1 Numerical Approach Results

The numerical approach makes use of the solution propagation depicted in Figure 7.19, which defines 74 design variables, i.e. the number of independent orientations to be determined. The numerical method solves Problem (6.52) with the same strategy presented in Section 7.3. The MIDACO[®] algorithm has been used tuned as reported in Table 7.13. Since it is expected that the blending scheme using QT QH SSs will be akin to the *Random* scheme, for a more fair comparison it has been chosen. The resulting optimal SSs, together with the residuals, are listed in Table 7.19. Of course, as shown in Section 7.3,

7.4. Case Study 3: Comparisons Between Stacking Sequence Recovery Techniques

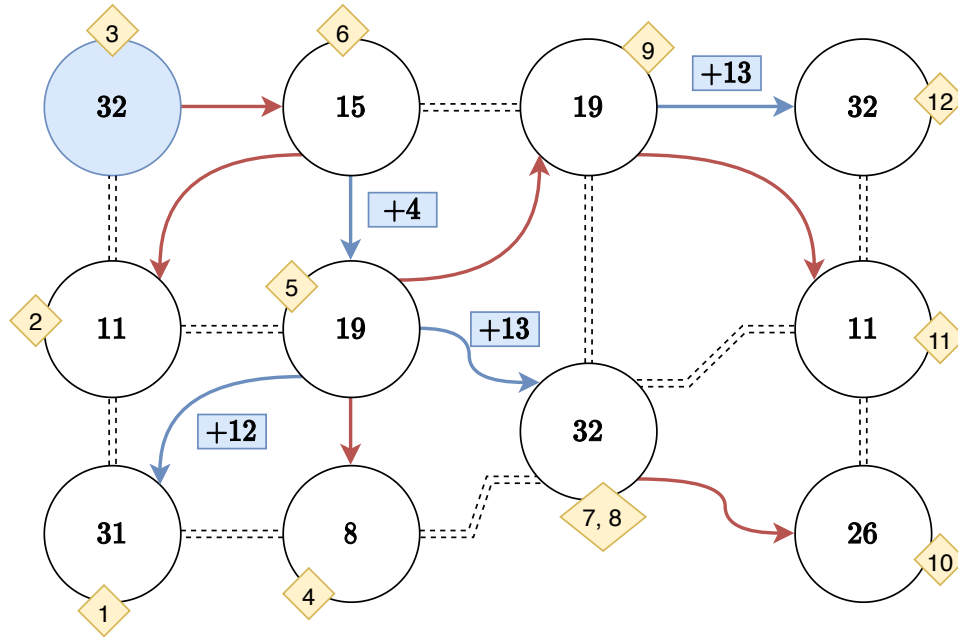


Figure 7.19: Solution propagation for the numerical approach to the stacking sequence recovery

there are different blending schemes which may reduce the residual values.

Table 7.19: Numerical optimal SSs of Case Study 3

Panel	Stack	Residual
1	28/ -47/ 24/ 30/ 13/ -53/ -45/ 31/ 41/ -56/ -48/ -37/ -45/ -41/ 22/ 21/ -45/ 11/ 1/ 17/ 30/ -72/ 56/ -67/ -48/ 26/ 22/ 35/ 66/ -49/ -42/	0.0933
2	28/ -47/ 30/ -45/ 11/ -48/ 26/ 22/ 35/ -49/ -42/	0.0546
3	28/ -47/ 30/ 26/ -45/ 41/ -55/ -37/ -86/ -45/ 11/ 50/ -51/ 26/ 30/ -48/ -22/ -29/ -67/ 45/ 26/ 22/ 35/ 48/ 24/ -21/ -37/ 27/ -49/ 29/ -42/ -78/	0.1336
4	24/ -37/ -45/ -41/ 21/ 11/ 35/ -49/	0.0242
5	28/ -47/ 24/ 30/ -45/ 41/ -37/ -45/ -41/ 21/ -45/ 11/ 30/ -48/ 26/ 22/ 35/ -49/ -42/	0.1416
6	28/ -47/ 30/ -45/ 41/ -37/ -45/ 11/ 30/ -48/ 26/ 22/ 35/ -49/ -42/	0.0489
7	28/ 62/ -47/ 30/ 24/ 30/ -45/ 41/ -37/ -45/ 56/ -54/ -41/ 41/ 21/ -45/ 11/ 52/ 30/ -48/ 66/ 26/ 22/ -34/ 35/ -10/ -56/ 13/ -58/ -52/ -49/ -42/	0.0613
8	28/ 62/ -47/ 30/ 24/ 30/ -45/ 41/ -37/ -45/ 56/ -54/ -41/ 41/ 21/ -45/ 11/ 52/ 30/ -48/ 66/ 26/ 22/ -34/ 35/ -10/ -56/ 13/ -58/ -52/ -49/ -42/	0.0613
9	28/ -47/ 24/ 30/ -45/ 41/ -37/ -45/ -41/ 21/ -45/ 11/ 30/ -48/ 26/ 22/ 35/ -49/ -42/	0.0513
10	28/ 62/ -47/ 30/ 24/ -45/ 41/ -37/ -45/ -54/ -41/ 41/ 21/ -45/ 11/ 30/ -48/ 66/ 26/ 22/ 35/ -10/ -58/ -52/ -49/ -42/	0.0538
11	28/ -47/ 30/ -37/ -41/ 21/ -45/ 30/ 26/ 22/ -42/	0.0399
12	28/ -47/ 24/ 30/ -45/ 41/ -37/ 2/ -68/ -45/ -77/ -41/ 21/ -79/ 56/ -45/ 49/ 35/ 11/ 30/ 51/ -27/ 36/ -7/ -48/ 26/ 22/ 35/ -49/ -66/ -31/ -42/	0.1388
		0.9037

7.4.2.2 Alternative Quasi-trivial Approach Results

The alternative approach, based on the knowledge of QT QH SSs, has been already introduced in Section 6.4. Once a blended QT QH SS for the structure has been retrieved by Algorithm 6.8, Problem (6.52) has been solved via MIDACO[®] algorithm in a similar fashion as for the numerical approach. The number of independent design variables is 8. Table 7.20 lists the optimal SSs and the residuals.

Table 7.20: *QT optimal SSs of Case Study 3*

Panel	Stack	Residual
1	20 ₂ / - 46/ - 48/ - 46/32/ - 76 ₂ /32 ₂ / - 76/ - 48/32/ - 76/32/20/ - 46/20 ₂ / - 48/ - 46/20 ₂ / - 46/ - 76/ - 46/20/ - 48/32 ₂ / - 76	0.0463
2	20/ - 46 ₂ /20 ₂ / - 46/20 ₂ / - 46 ₂ /20	0.0643
3	20 ₄ / - 46 ₂ / - 52/20/ - 52/ - 46/20/ - 46/20 ₄ / - 46/20 ₂ / - 52/20 ₃ / - 46/20 ₂ / - 46/20 ₂ / - 52/ - 46/20	0.2788
4	20/ - 46 ₂ /20/ - 46/20 ₂ / - 46	0.0311
5	20 ₃ / - 46 ₂ /20 ₂ / - 46/20 ₇ / - 46 ₂ /20 ₂	0.8610
6	20 ₃ / - 46/20/ - 46/20 ₇ / - 46/20	0.9365
7, 8	-46/20/ - 48/20 ₄ / - 46/20/ - 46/20 ₂ / - 46/20 ₂ / - 48/20/ - 48/20 ₃ / - 46 ₂ /20 ₃ / - 46 ₂ / - 48/20 ₃	0.4029
9	20 ₃ / - 46 ₂ /20 ₂ / - 46/20 ₇ / - 46 ₂ /20 ₂	0.6999
10	-46/ - 48/20 ₅ / - 46/20 ₂ / - 46/20 ₂ / - 48 ₂ /20 ₃ / - 46 ₂ /20/ - 46/ - 48/20 ₃	0.2319
11	20/ - 46/20/ - 46/20 ₃ / - 46/20/ - 46/20	0.2112
12	20 ₂ / - 30/20/ - 46 ₂ / - 52/20/ - 52/ - 46/20/ - 46/20 ₃ / - 30/ - 46/ - 30/20/ - 52/20 ₃ / - 46/20 ₂ / - 46/20/ - 30/ - 52/ - 46/20	0.1320
		4.2988

7.4.3 Comments on the Comparison Results

As seen, the alternative QT approach results present definitely larger residuals than the numerical approach. Although QT QH SSs do not contribute to the residual function of the SLP for the terms involving uncoupling and homogeneity, they heavily contribute for the terms related to the recovery of the elastic target properties. Is it basically due to the uncoupling between the SR and the building of blended SSs. In fact, Algorithm 6.8 cannot control the associated elastic properties for each SS, since there are infinite possibilities (see also the concept of equivalence class of Section 4.3). Moreover, the blending of QT QH SSs is a very hard problem, in the sense that blended QT QH SSs may not even exist given two arbitrary number of plies. An empirical existence rule is that the two laminates must have a certain difference in the number of plies, say 4 plies.

The decomposition of the total residual into the single contributions appearing in Eq. (6.48), for each panel, is shown in Figure 7.20 for the two approaches. The scale is the same, so that plots are directly comparable. For the alternative QT approach, it is clear that the major contributors are from the orthotropy recovery (\mathcal{R}_3) and from the ρ_1 recovery (\mathcal{R}_5). For the numerical approach, it is evident that the major sources of residual

come from ρ_0 and ρ_1 recovery (\mathcal{R}_4 and \mathcal{R}_5 , respectively).

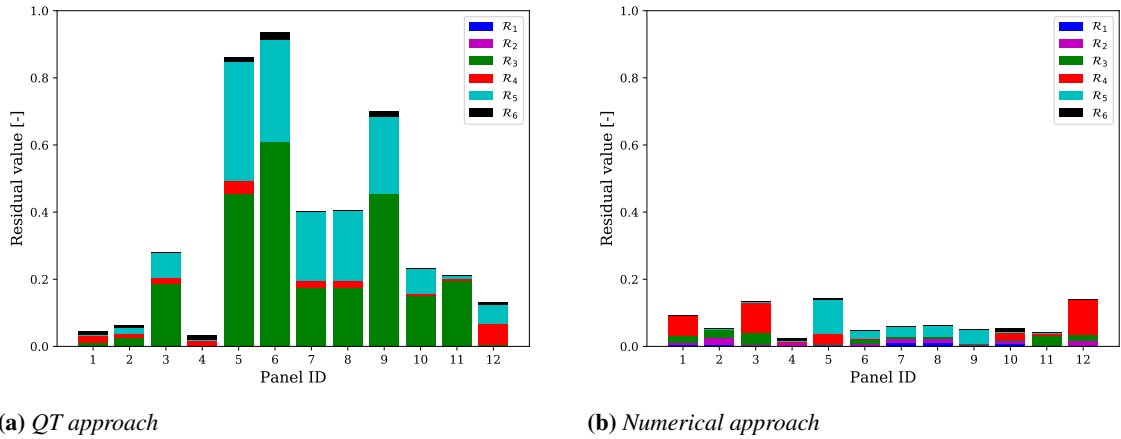


Figure 7.20: *Contributes to the total residual from each panel of Case Study 3*

Acting on the number of saturated groups has two consequences. If the number of groups increases, chances to find blended SSs decrease, since SSs are more and more fragmented. On the other side, if eventually blended SSs are found, it introduces more design variables in the SR phase, thus allowing for lower residuals. For the problem at hand, there are only 8 design variables in the SLP to be determined to annihilate the residual function. For the numerical approach, there are 74 variables.

A further drawback of the alternative approach is that its combinatorial nature makes the computational time extremely large, and there is not even guarantee to find out at least one solution. Furthermore, when thick laminates are involved in the structure, the number of child SSs processed by Algorithm 6.8 dramatically increases. Besides, it is not clear how to deal with laminates having a number of plies not contemplated by the QT QH SSs database. Conversely, the numerical approach is suitable regardless of the thickness of the laminates, and find always a solution in a reasonable amount of time.

For all those reasons, the numerical approach of Section 6.3 has been preferred to the QT one and implemented in the MS2LOS for the stack recovery phase.

7.5 Conclusions

The Chapter provided answer to research question RQ3.

The elements formalised in the previous Chapter have been implemented in the MS2LOS framework for the deterministic optimisation of composite structures. The approach is based on the polar formalism for the description of the anisotropy and on the first-order shear deformation theory to represent the laminate kinematics at the macroscopic scale. It is based on a general formulation of the design problem, assuming only uncoupling, homogeneity and orthotropy of laminates. The design variables are the full set of geometric and mechanical parameters defining the behaviour of the composite structure at each pertinent scale.

The effectiveness of the FLP formulation of the enhanced MS2LOS has been tested firstly through a numerical benchmark, taken from the literature, dealing with the least-weight design of a simplified wing-box structure: the numerical results, in terms of optimised solutions, are very encouraging. Successively, the effectiveness of the SLP formulation has been tested on a numerical benchmark, taken from the literature, dealing with the least-weight design of a eighteen-panel structure. As a final result, the best blended stacking sequence for the structure is provided, without making any simplifying assumption neither on the stacking sequence nature nor on the blending kinematics.

The proposed methodology highlights several still-open problems of composite design laminates, which consistently affect the fitness of the final result. Regarding the FLP three aspects deserve to be deeply investigated.

Firstly, the major uncertainty source has been recognised in the expression of the feasible domain bounds, for a given number of plies and for desired laminates characteristics, viz. uncoupling, orthotropy, homogeneity.

Secondly, inasmuch as the FLP deals with laminate homogenised properties, deriving an equivalent expression of manufacturing constraints related to the geometrical features of the stack (e.g. the maximum difference between consecutive plies orientation angles, etc.) is anything but trivial. Nevertheless, these requirements should be introduced since the FLP formulation in order to reduce the discrepancy when optimal stacks are retrieved at the end of the SLP.

Finally, the issues related to the load redistribution, a problem of capital importance in real-world engineering applications, should be opportunely integrated in the formulation of the discrete optimisation of the FLP.

The Chapter provided also a comparison between two approaches for the stack recovery phase: the numerical one, implemented in the MS2LOS, and the alternative one, based on the knowledge of QT QH SSs, collected in a database. The numerical approach has achieved better results in a simple benchmark structure. The reasons are basically due to the fact that the stiffness recovery phase for the alternative approach is ruled by few orientation angles, which fail in providing a good match of the target elastic properties. Moreover, the proposed alternative strategy does not guarantee to find at least a blended solution, and it fails when thick laminates (especially if the number of plies lies outside the database) are present. Although the interest in exploiting exact uncoupled and homogenous SSs, their employment seems to be harsh in practical purposes, when more laminates, possibly thick, are present in the structure.

The Optimal Design of Composite PARSIFAL Wing-box

In this Chapter, the MS2LOS described in Chapter 7, endowed with the elements formalised in Chapter 6, is applied to a complex structure: the lifting system of the PARSIFAL PrP. Results are provided for both the FLP and SLP.

Section 8.1 describes the geometry of the PrP lifting system, together with the load cases and the design criteria. Section 8.2 introduces the FLP formulation and the numerical strategy. Section 8.3 is dedicated to the SLP formalisation. The results of both FLP and SLP are presented in Section 8.4. Finally, Section 8.5 concludes the Chapter with meaningful considerations.

8.1 Problem Definition

The PrP lifting system considered in this case study is the result of a preliminary aerodynamic study presented in (Abu Salem et al., 2018). The PrP lifting system can be ideally split into three (semi-)wings: the front wing (FW), the rear wing (RW) and the vertical wing (VW), as shown in Figure 8.1. In the same picture the global Body reference frame $\mathcal{T}_B(\text{CG}; X_B, Y_B, Z_B)$, centred at the aircraft centre of mass CG is illustrated. Due to the symmetry of the structure with respect to the aircraft longitudinal plane $X_B - Z_B$, the structural analysis is limited to the left-side part.

8.1.1 Geometry and Material

For each wing of the PrP configuration, the external geometry is assigned in terms of the leading edge coordinates, chords and profiles of a small number of reference sections (viz. root, kink and tip sections). As a result, the geometrical features affecting the out-plane shape of the wing, viz. dihedral and twist angles, are automatically taken into account.

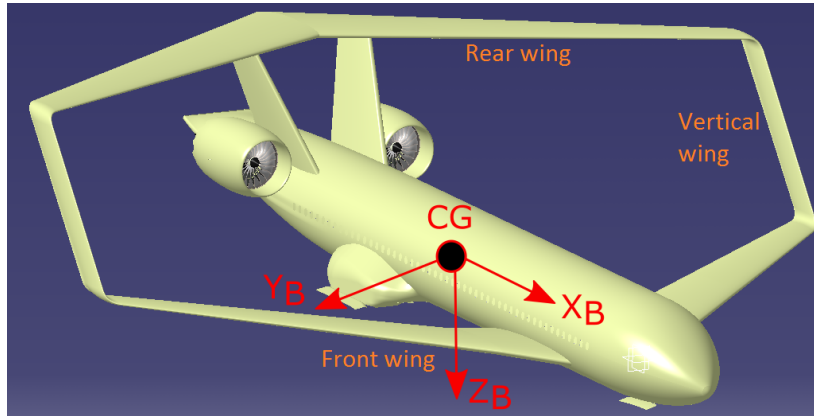


Figure 8.1: *PrP aircraft rendering and \mathcal{T}_B reference frame*

All of the aforementioned quantities, which are summarised in Table 8.1, are known at the three sections (only two for the VW), and linearly vary between them. The same Table adopts the reference frame $\mathcal{T}(O; x, y, z)$ where the origin O coincides with the orthogonal projection of the leading edge of the FW onto the aircraft symmetry plane $X_B - Z_B$, the x axis is parallel to the X_B axis (but opposite direction) and the z axis is parallel to the Y_B axis (but opposite direction). The airfoil F15 – 11, taken from (CERAS, 2014; Risse et al., 2015), is considered. This profile is used to describe the shape of the wing sections parallel to the free-stream direction.

The width of the wing box is obtained from the assumptions about front and rear spar positions, defined as chord percents according to Table 8.2. According to (CERAS, 2014; Risse et al., 2015), a span-wise linear behaviour of both front and rear spars, for each wing, is adopted. The position of spars, with respect to the considered wing planform, is shown in Figure 8.2 (in the \mathcal{T} reference frame) and reported in Table 8.2.

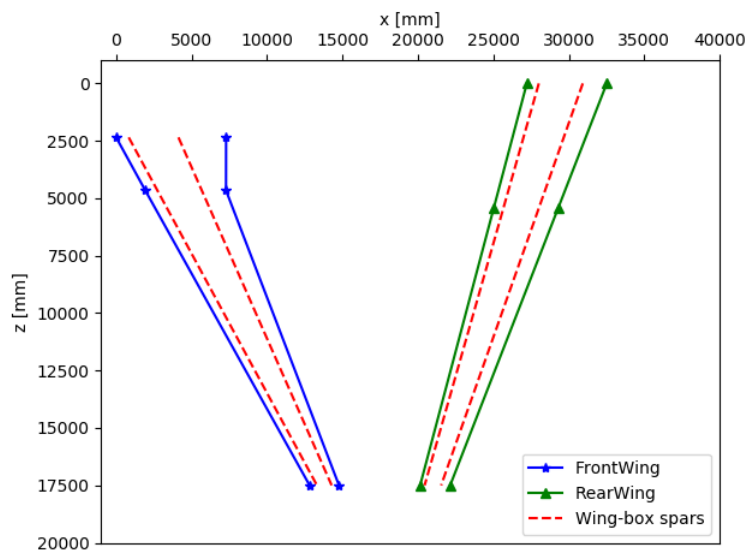


Figure 8.2: *Planform of the PrP lifting system, with wing-box position, in the \mathcal{T} reference frame*

Regarding the modelling of the structural components, the following simplifications

Table 8.1: *Wing geometry in the \mathcal{T} reference frame*

	Leading edge coordinates [mm]	Chord [mm]	Twist angle [deg]
Front Wing			
Root	(0, 0, 2350)	7287	3.05
Kink	(1932, 200, 4661)	5350	3.9
Tip	(12820, 810, 17500)	1949	1.5
Rear Wing			
Root	(26138, 7926, 0)	5295	3.7
Kink	(23955, 7926, 5400)	4276	2.99
Tip	(19064, 7926, 17500)	1991	1.4
Vertical Wing			
Root	(13623, 1310, 18000)	1852	1.5
Tip	(18261, 7426, 18000)	1922	1.4

Table 8.2: *Wing-box position (reported in chord percent, refer to the planform of Figure 8.2)*

	Root	Kink	Tip
Front Wing	11%	15%	25%
	57%	70%	75%
Rear Wing	15%	15%	15%
	70%	70%	70%
Vertical Wing	20%	-	20%
	80%	-	77%

are introduced:

- only major structural components are modelled (viz. skin, stringers, ribs and spars);
- at the interfaces between the structural components, perfect bonding conditions apply;
- connection zones and opening/cut-out are neglected and not considered in the preliminary design phase.

For both FW and RW, ribs are parallel to the free stream direction between root and kink sections, whilst they are perpendicular, respectively, to the rear and front spar between kink and tip sections (see Figures 8.3a and 8.4). For the VW, ribs are perpendicular to both front and rear spars. However, in order to ensure a gradual change in the orientation between root-kink and kink-tip sectors, some transition ribs at intermediate angles are introduced, as illustrated in Figures 8.3a and 8.4. Inasmuch as the goal is the preliminary optimisation of the PrP wing-box architecture, a simplified rib geometry is considered,

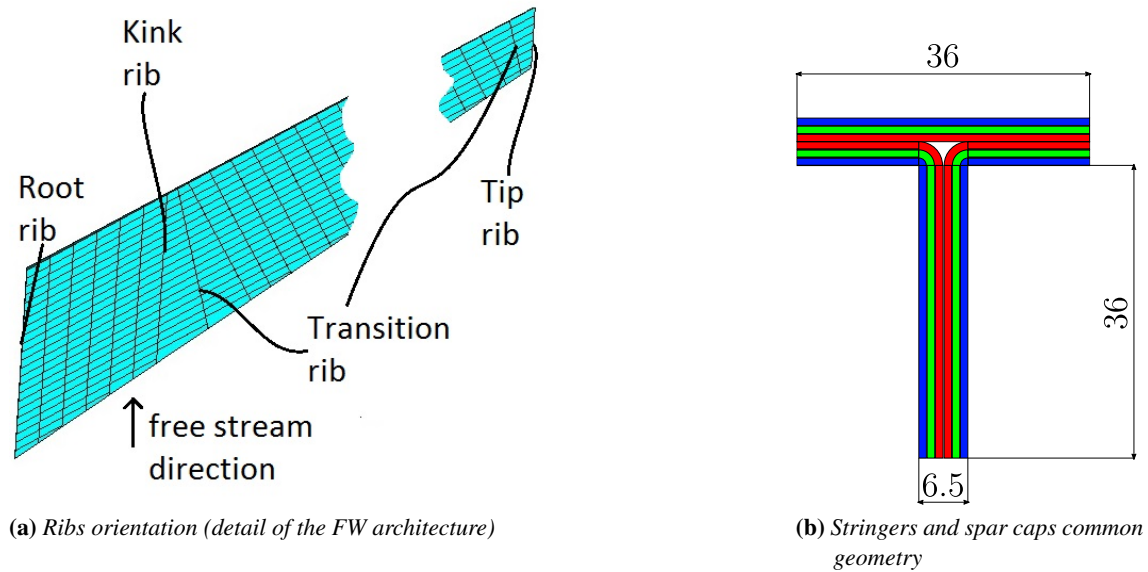


Figure 8.3: Some details of the PrP wing-box architecture

i.e. a continuous plate without cuts. As far as ribs are concerned, a predefined SS is considered: $[(\pm 45^\circ)_{11}]_S$ (D. Liu et al., 2011).

Due to the lack in the literature of reference values for such an aircraft architecture, a preliminary genetic optimisation run has been performed to assess the values of some variables not handled by the current formulation, viz. stringers and ribs number; and stringers (and spar caps) geometry and stiffness. The problem formulation is conceptually similar to the one of the FLP discussed in Section 8.2, but with less optimisation regions. For the solution search, the genetic optimisation algorithm ERASMUS (Evolutionary Algorithm for optimisation of Modular Systems) algorithm has been used (for more details on the algorithm, see Montemurro (2018)). Stringers and spar caps are characterised only by the cross-sectional area (because they are modelled as bar elements, see Section 8.2.2.1). The values for these geometrical parameters are listed in Table 8.3 and are kept constant during the FLP optimisation. Figure 8.3b shows the cross section of the stiffeners (stringers and spar caps). Qualitatively, in the same figure, the manufacturing technique is shown: a basic SS (represented by a blue, a green and a red ply) is doubled in order to achieve, both in flanges and webs, the same elastic properties. The preliminary genetic optimisation run furnished $\rho_0 = 0.6165$, $\rho_1 = 0.1936$, $\phi_1 = 0$. These values of PPs, together with stringers and ribs pitches, are kept constant during the FLP optimisation.

Table 8.3: Values of stringer pitch, ribs pitch and stringers geometry

	FW	RW
Upper stringers pitch [mm]	133	166
Lower stringers pitch [mm]	153	168
Ribs pitch [mm]	395	430
Stringers and spar caps cross-sectional area [mm ²]	468	468

Both GFEM and LFEM, presented in Section 8.2.2, do not take into account for explicit modelling of shear tie, stringer-tie and tear-strap.

The selected material is a carbon-epoxy T300/5208 pre-preg lamina. The elastic and strength properties of the lamina, expressed both in engineering constant and in PPs, are listed in Table 7.1. Figure 8.4 gives an overview of the resulting PrP wing-box geometry.

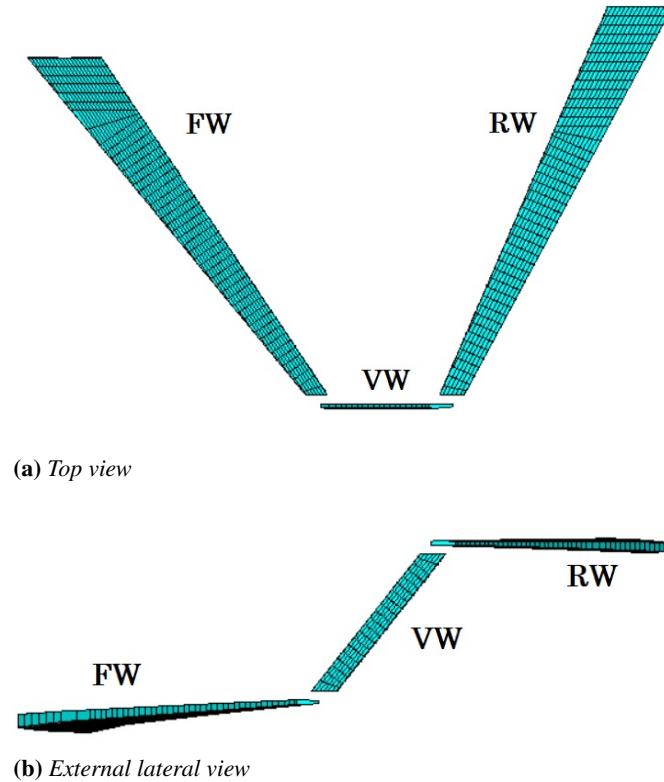


Figure 8.4: Overview of the PrP wing-box architecture

8.1.2 Design Criteria

Only symmetric static loads are considered in this work. Certification specifications (EASA, 2018) identify two types of loading conditions: limit loads (LLs) and ultimate loads (ULs). LLs are the maximum loads expected in service that the structure must withstand without detrimental permanent deformations. ULs are equal to limit loads multiplied by a prescribed safety factor (usually 1.5). The structure must withstand ULs without failure for at least 3 seconds. For instance, for civil aircraft, LLs in symmetrical manoeuvres occur at load factors $n_z = 2.5$ and $n_z = -1$. This study focuses on this class of loads.

The following set of design criteria (DCs) is integrated in the formulation of the optimisation problem.

- DC1: The global stiffness of the structure must be greater than a predefined reference value.

- DC2: The laminate-level failure index, obtained by using the phenomenological failure criterion of Tsai-Hill expressed in the PPs space (Catapano et al., 2012, 2014; Catapano & Montemurro, 2018), for skin and spar webs, multiplied by a safety factor $F_S = 1.5 \times 2$, must be lower than or equal to the unit value. The contribute in the F_S equal to 1.5 comes from airworthiness regulations (see CS 25.303 (EASA, 2018)), whilst the contribute equal to 2 consider the fact that the failure index is applied at the laminate level, i.e. it is averaged over the thickness of the laminate, thus it can be too conservative with respect to the first-ply failure criterion.
- DC3: No buckling must occur in the stiffened panels when LLs are applied, considering a safety factor $F_S = 1.5$.
- DC4: Only feasible laminates are considered.
- DC5: Only manufacturable solutions are considered. To this end, the blending requirement between adjacent laminates is considered.
- DC6: Only homogeneous, uncoupled fully orthotropic laminates are considered.

DC1 is expressed in terms of maximum tip displacement of the lifting system. DC2 is expressed in terms of the laminate-level failure index by using the Tsai-Hill failure criterion, evaluated in a proper mesh subset in order to neglect the effects of local strain concentrations due to the GFEM modelling. DC3 is expressed in terms of no-buckling condition for the FW and RW upper and lower skin (as discussed in Section 8.2.2.3). Of course, the evaluation of the first buckling load for such regions is done through dedicated LFEMs. DC4 is expressed by a set of inequalities defining the laminate feasible region in the PPs space (see Eq. (7.1)). DC5 is expressed in terms of two inequalities, to be imposed to each couple of adjacent laminates (see Section 6.2). DC6 is expressed by imposing conditions $\mathbf{B}^* = \mathbf{0}$, $\mathbf{C}^* = \mathbf{0}$ and $\Phi_0^{A^*} - \Phi_1^{A^*} = K^{A^*} \frac{\pi}{4}$, with $K^{A^*} = 0, 1$ (see Chapter 4).

8.1.3 Load Cases

Aerodynamic loads are calculated through the Vortex Lattice Method solver AVL (Drela & Youngren, 2013), implemented in the preliminary aircraft design tool AEROSTATE (AERodynamic optimisation with STatic stability and Trim Evaluator), developed at University of Pisa (Rizzo, 2007; Rizzo & Frediani, 2009). AEROSTATE has been used for the preliminary study of the reference configuration definition, together with medium and high fidelity corrections. For more details, the reader is addressed to (Abu Salem et al., 2018; Cipolla et al., 2018; Frediani et al., 2019). The resulting lift distribution is interpolated and decomposed into a set of point forces and moments (applied to the centre of gravity of the ribs of each wing) to obtain a statically-equivalent system of forces. The aerodynamic loads are evaluated for a Mach number of 0.79, altitude of 11000 m, adopting the Standard Atmosphere model, in cruise condition. These loads define the fundamental basic load case (BLC) used in this study, which is denoted as BLC_{1g} .

For the sake of simplicity, two load cases have been considered. The first one corresponds to a load factor $n_z = 2.5$ (pull-up manoeuvre), whilst the second one is characterised by $n_z = -1$ (push-down manoeuvre), according to the flight envelope for civil transport aircraft. The lift distribution for all the previous cases is obtained by a simple scaling of the BLC_{1g} which has been calculated for $n_z = 1$. DCs 1, 2 and 3 are evaluated for the two load cases. Of course, DCs 4, 5 and 6 are independent from the load cases. It is noteworthy that the two considered load cases are commonly used in the preliminary design of civil aircraft wing-box structures at the boundary of the flight envelope (Niu, 1988; Stanford & Dunning, 2015; Panettieri et al., 2020; Picchi Scardaoni et al., 2020).

8.2 The First-level Problem Formulation

In this study, the FLP formulation deals with the minimisation of the mass of the PrP wing-box structure, subject to feasibility, blending, static failure, stiffness and buckling requirements. The goal is to find the optimal feasible distribution of thickness and stiffness of the laminates composing the PrP wing-box.

The optimisation region includes the upper and lower skins of the FW and RW, and the spar webs. For each skin, twelve regions are defined, labelled as shown in Figure 8.5. Regarding the spar webs, they correspond to IDs 25 and 26 for the FW (leading and trailing edges side, respectively), and to IDs 51 and 52 for the RW (leading and trailing edges side, respectively).

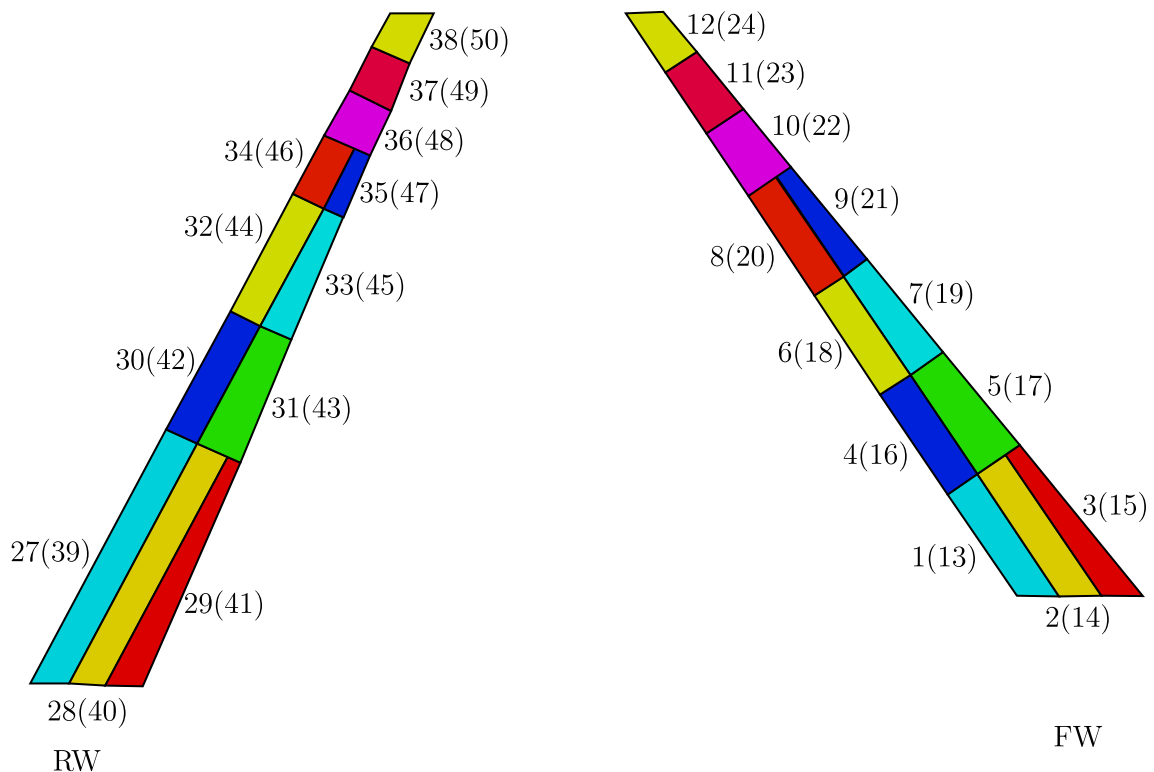


Figure 8.5: Optimisation regions IDs for the upper skins (in brackets the IDs of the lower counterparts)

Each panel is characterised by three design variables, introduced in Eq. (4.32). In fact, for the sake of simplicity, ϕ_1 has been set to zero and is oriented parallel to the wingspan direction of each wing. The structure is then described by 156 variables, since there are 52 panels, collected in the design variables vector $\boldsymbol{\xi} := \{n_0^j, \rho_{0K}^j, \rho_1^j \mid j = 1, \dots, 52\}$. The objective function is expressed as follows:

$$\Phi(\boldsymbol{\xi}) := \frac{m_0}{m_{\text{ref}}} + \frac{N_{\text{ref}} t_{\text{ply}} \rho_{\text{ply}}}{m_{\text{ref}}} \sum_{j=1}^{52} A_j n_0^j, \quad (8.1)$$

where m_0 is the mass of the components not involved in the design process, $m_{\text{ref}} = 10000$ kg is the reference mass, A_i, n_0^j are the area and the dimensionless number of plies of the j -th panel, respectively, $\rho_{\text{ply}}, t_{\text{ply}}$ are the density and the thickness of the single ply, respectively (see Table 7.1).

The CNLPP of Eq. (3.1) can be formulated, for this specific case study, as:

$$\begin{aligned} & \min_{\boldsymbol{\xi}} \Phi(\boldsymbol{\xi}), \quad \text{subject to:} \\ & \mathbf{K}(\boldsymbol{\xi})\mathbf{u}(\boldsymbol{\xi}) - \mathbf{f} = \mathbf{0}, \quad \forall \text{ load cases} \\ & \mathbf{K}^b \mathbf{u}^b + \mathbf{K}_{\text{BC}}^b \mathbf{P}\mathbf{u} = \mathbf{0}, \quad \forall \text{ LFEMs} \\ & g_{\text{feas}}(\boldsymbol{\xi}) \leq 0, \\ & g_{\text{disp}}(\boldsymbol{\xi}) \leq 0, \\ & g_{\text{TH}}(\boldsymbol{\xi}) \leq 0, \quad \left. \vphantom{g_{\text{TH}}(\boldsymbol{\xi})} \right\} (\forall \text{ elements in the check zone } \Omega_c, \text{ see Section 8.2.2.1}) \\ & g_{\text{buck}}(\boldsymbol{\xi}) \leq 0, \quad \left. \vphantom{g_{\text{buck}}(\boldsymbol{\xi})} \right\} \forall \text{ LFEMs} \\ & g_{\text{blend-}j}(\boldsymbol{\xi}) \leq 0, \quad j = 0, 1 \quad \left. \vphantom{g_{\text{blend-}j}(\boldsymbol{\xi})} \right\} \forall \text{ couples of adjacent panels (grouped in one constraint),} \\ & \boldsymbol{\xi}_{\text{lb}} \leq \boldsymbol{\xi} \leq \boldsymbol{\xi}_{\text{ub}}. \end{aligned} \quad (8.2)$$

In Eq. (8.2), the feasibility constraints corresponds to DC4. Since several load cases are considered, the static response must be evaluated for every load case. The stiffness constraint of DC1 is expressed by imposing that the vertical displacement on a tip node of the FW tip section must be less than $0.15b$, where b is the wing semi-span ($= 18$ m). The buckling constraints (DC3) involve the evaluation, for each LFEM, of the buckling factor. A safety factor of 1.5 as prescribed for LLs by regulations, is considered. Regarding blending requirements (DC5), for a generic couple of adjacent panels, the constraints formalised in Section 6.2 are enforced. Requirement against static failure (DC2) is imposed via the Tsai-Hill criterion, according to Eq. (7.14).

The parameter α appearing in Eqs. (7.4) and (7.5) has been set as in Eq. (7.24). Parameter

α appearing in Eqs. (7.13) and (7.19) has been set as follows:

$$\alpha(\text{Var}(\boldsymbol{\delta})) = \begin{cases} 200, & \text{if } \text{Var}(\boldsymbol{\delta}) \leq 0.001, \\ 35, & \text{if } 0.001 < \text{Var}(\boldsymbol{\delta}) \leq 0.01, \\ 25, & \text{if } 0.01 < \text{Var}(\boldsymbol{\delta}) \leq 0.1, \\ 10, & \text{if } 0.1 < \text{Var}(\boldsymbol{\delta}) \leq 0.3, \\ 5, & \text{if } \text{Var}(\boldsymbol{\delta}) \geq 0.3. \end{cases} \quad (8.3)$$

For this case study, the blending constraints have been grouped in a completely similar manner as for feasibility and static strength (Eqs. (7.4) and (7.13)). The tuning parameter α has been tuned as follows ($\boldsymbol{\delta}$ is the vector containing all the blending constraints evaluations for each pair of adjacent laminates):

$$\alpha(\text{Var}(\boldsymbol{\delta})) = \begin{cases} 600, & \text{if } \text{Var}(\boldsymbol{\delta}) \leq 0.001, \\ 300, & \text{if } 0.001 < \text{Var}(\boldsymbol{\delta}) \leq 0.5, \\ 200, & \text{if } \text{Var}(\boldsymbol{\delta}) \geq 0.5. \end{cases} \quad (8.4)$$

Table 8.4 reports the lower and upper bounds of design variables. Variables n_0^j , $j = 1, \dots, 52$ are assumed continuous for the first optimisation phase, i.e. the *continuous optimisation*, for the resolution of the FLP (8.2).

Table 8.4: Design variables range of the PrP wing design

Variable	lower bound	upper bound
n_0^j	0.2	1
ρ_{0K}^j	-1	1
ρ_1^j	0	1
$j = 1, \dots, 52$		

The *discrete optimisation* is needed to round up the continuous solution of Problem (8.2) to discrete numbers of plies, while complying to the full set of constraints of Eq. (8.2). The mathematical formulation is identical to the one reported in Eq. (7.21) with $\Delta N_{\min} = 4$. It is noteworthy that Eq. (7.21), as said in Section 7.1.4.2, does not take load redistribution into account. However, Eq. (7.21) is still considered valid, as a first approximation.

8.2.1 Numerical Strategy

Problem (8.2) is a non-convex CNLPP in terms of both geometrical and mechanical design variables. The non-convexity is due to the set of constraints.

The solution search of the continuous problem is performed via *fmincon* algorithm, available in the Optimisation Toolbox of MATLAB[®] (The MathWork Inc., 2011), tuned as

summarised in Table 8.5. At each iteration, the MATLAB® script invokes the Python

Table 8.5: Parameters of the *fmincon* algorithm.

Parameter	Value
Solver algorithm	Active-set
Tolerance on objective function	1×10^{-3}
Tolerance on constraints	1×10^{-3}
Tolerance on input variables change	1×10^{-3}
Tolerance on gradient norm of the Lagrange's function	1×10^{-3}
Maximum number of iterations	1000

routines which control the creation of the FE models and the evaluation of the objective function, of the constraints and of the corresponding gradients. The optimisation procedure is coupled with ANSYS® FE commercial software. Figure 8.6 shows the conceptual

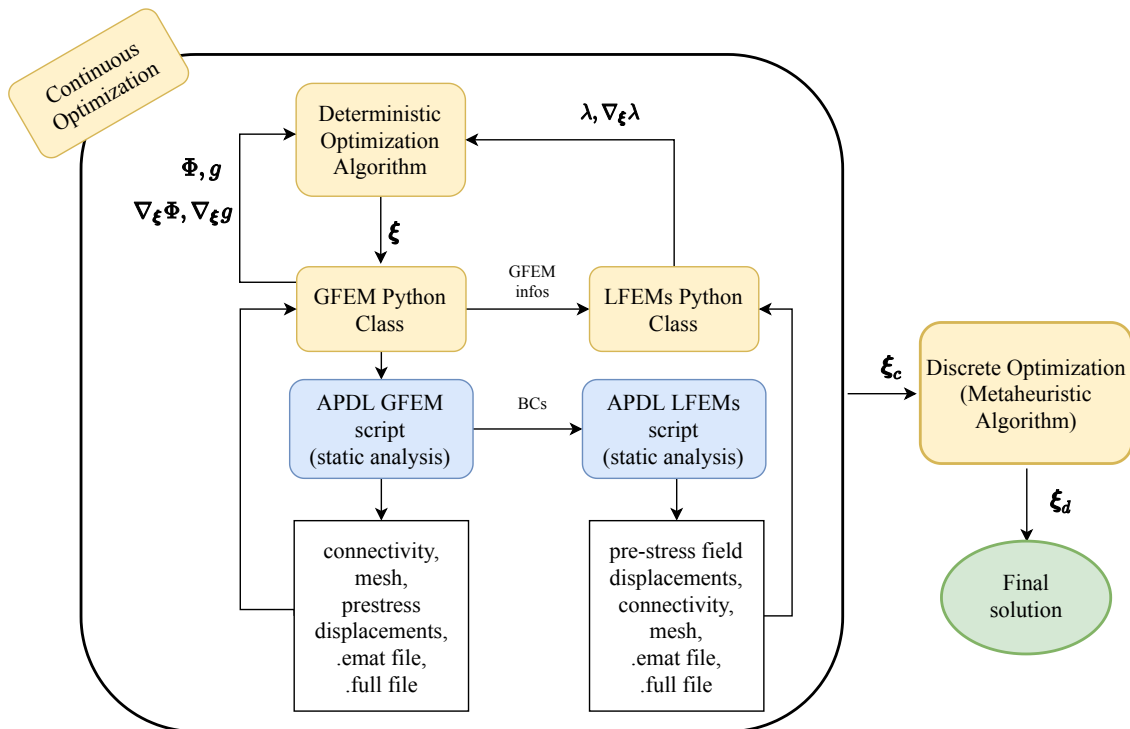


Figure 8.6: Workflow of the numerical strategy of the FLP of the PrP wing design

work-flow of the numerical strategy for the FLP. At each iteration of the deterministic algorithm, a new set of design variables ξ is passed to a Python Class which controls the GFEM generation. ANSYS® is then invoked: an ANSYS® Parametric Design Language (APDL) script generates the GFEM. Once Problem (6.1) has been solved, for each load case, fundamental information such as connectivity, nodes coordinates, displacement fields, etc. are passed back to the Python Class. Then, the Python Class evaluates the objective function and all the optimisation constraints (except the buckling ones), together with their gradients.

Hence, LFEMs are generated in a similar manner. BCs on the boundary of the LFEMs

are imposed by properly interpolating the displacement field resulting from the GFEM (see Section 8.2.2.3). Matrix \mathbf{K}_σ is assembled within the Python Class, which also solves the eigenvalue problem via the *scipy.sparse.linalg.eigsh* routine. The use of this approach is mainly due to the perfect coherence between buckling factor and its gradient. The objective function value and all of the constraints (and gradients) are then passed to the optimisation algorithm. The loop is repeated until one of the convergence criteria of the *fmincon* algorithm is satisfied.

Once the continuous solution is obtained, Problem (7.21) solution search is performed. The MIDACO[®] algorithm, specialised in mixed-integer programmings (Dorigo et al., 2006; Schlüter et al., 2009; Schlüter & Gerdts, 2009; Schlüter et al., 2012), is used to this purpose. MIDACO[®] parameters have been tuned as reported in Table 8.6. A high Focus value facilitates the exploration of the neighbourhood of the starting guess, which is set to ξ_c . The Oracle parameter, which is suggested to be the expected (or desired) objective function optimal value (Schlueter, 2018), is set to 0.

Table 8.6: MIDACO[®] parameters for the discrete optimisation of the FLP of the PrP wing design

MIDACO [®] Parameter	Value
Ants	500
Kernel	10
Focus	1×10^6
Oracle	0
Evalstop	3×10^6

8.2.2 The Global and Local Finite Element Models

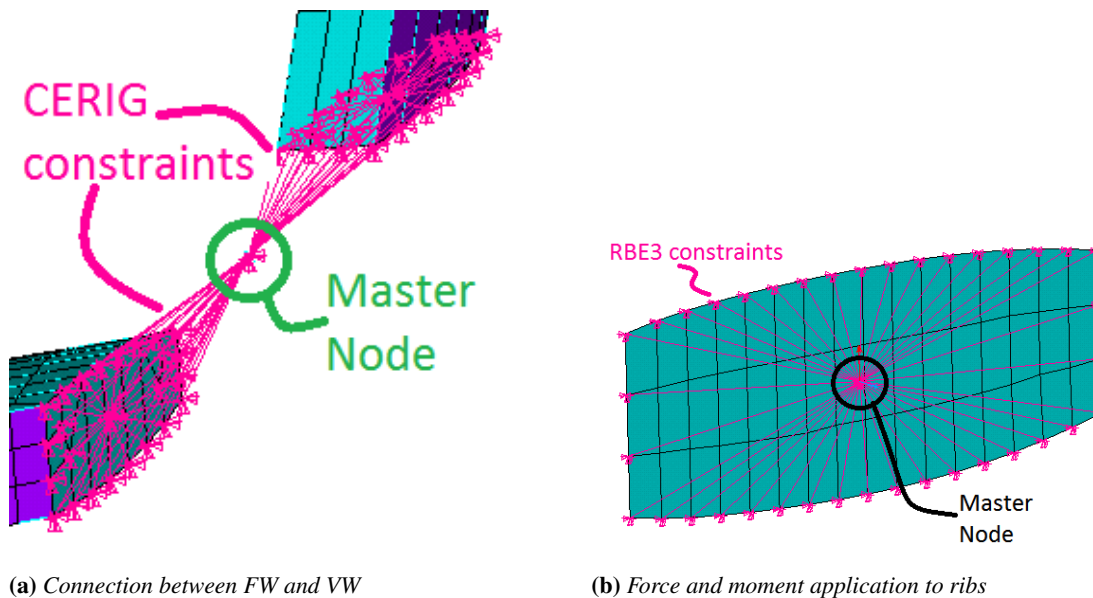
As stated above, the FE models integrated in the optimisation process are based on a GL modelling approach. In particular, two different models are created. The GFEM is used to assess the macroscopic behaviour of each wing, whilst refined LFEMs are generated to properly assess the buckling factor.

8.2.2.1 The Global Finite Element Model

Skin, ribs and spar webs are modelled with 4-node SHELL181 elements (Reissner-Mindlin kinematics), while stringers and spar caps are modelled with 2-node LINK180 elements (Truss model), according to the results presented in Section 8.2.2.2. The GFEM size is of the order of 14000 elements and 50000 DOFs. Link and shell elements are connected together by node merging. Shear-tie components are not modelled, but their mechanical effect (the transfer of shear load from ribs to skin) is ensured by the direct connection between ribs and skin elements.

As shown in Figure 8.4, fillets connecting FW and RW to VW are not explicitly modelled; MPC184 (multi-point constraint) elements with “rigid beam” behaviour (master-slave approach) are used to link extremal ribs nodes with the central master node, as

illustrated in Figure 8.7a.



(a) Connection between FW and VW

(b) Force and moment application to ribs

Figure 8.7: GFEM mesh particulars of the PrP wing design

Aerodynamic forces and moments are applied to a reference node, which, for the sake of simplicity, is created at the centroid of each rib; the master node is then linked to the boundary nodes of each rib via RBE3 elements, as shown in Figure 8.7b.

Since AEROSTATE-AVL gives as an output the position of the pressure centre, for each of the strips in which the lifting surface is subdivided, transport moments can be easily evaluated. As far as BCs of the GFEM are concerned, the 6 DOFs of the nodes lying at the root rib of both FW and RW are null.

After solving the GFEM for each load case, the ZOIs are created. Bays close to the root section, to the connection to the VW and to the kink transition rib are disregarded. Furthermore, the three closest areas to the front and rear spars are not included. As an example, Figure 8.8a shows the ZOI for the upper skin of the FW. From the ZOIs, checking zones element subsets are created, wherein DC2 is evaluated. As an example, Figure 8.8b shows the checking zone for the upper skin of the FW.

Results provided by the GFEM are used for the evaluation of the objective function and all the constraint functions except those related to buckling failure.

8.2.2.2 Justification of the FE Modelling of Stiffened Plates

In the previous Section, it has been claimed that the stiffened panels of the skins have been modelled through SHELL (plate) and LINK (truss, or rod) elements. In the literature there is not an unified approach. For instance, in (Frediani, Quattrone, et al., 2012; Benaouali & Kachel, 2019; Panettieri et al., 2020; Picchi Scardaoni et al., 2020) stringers are modelled via beam elements, whilst in (Roehl et al., 1995; Tang et al., 2013; Dababneha & Kipouros, 2018a; Zhu et al., 2019) via rod elements.

Even though different formulations exist, beam elements surely represent a more com-

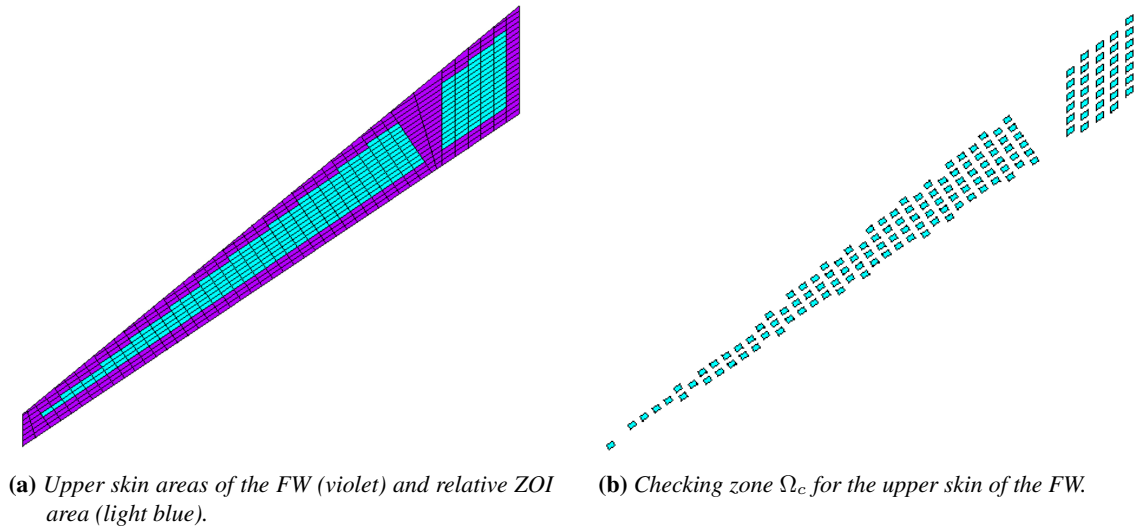


Figure 8.8: Example of ZOI and checking zone of the PrP wing design

plete structural component than rods, in the sense that they can react to axial, transversal and torsional solicitations. However, despite the simplicity of the rod structural response, which is clearly only axial, rod elements make the FE model simpler. This allows for less burdensome computations.

However, the preference of the former or the latter mono-dimensional element shall not be based only on computational cost considerations. Moreover, the coupling (the junction) with shell elements may affect the beam or rod behaviour which, in turn, may affect the plate response. Then, the following answer rises: what kind of structural 2D- and 1D-elements, coupled together, is the most representative to reproduce the actual 3D stiffened panel? In order to provide a rigorous answer to this question, a variational justification via Γ -convergence is provided in Chapter 10. It is retrieved the limit problem of the equilibrium of a 3D stiffened panel (see Figure 10.1), as the plate thickness and the section of the stiffener may scale with different orders. The conclusions are twofold. On the one hand, as the scaling parameters may vary, very different models are retrieved (see Section 10.4.3). As Paroni and Podio-Guidugli (2014) warn:

Which of the several sequences we may associate with a given real problem is the best one? As every other "natural" question, this is ill-posed, unless an optimality criterion is stipulated. Such a stipulation presumes that those features of the real problem that one especially wishes to approximate are chosen, be they the displacement field, the stress field, or other; and that an error measure is selected, in terms of an appropriate norm. Then, the best sequence is the one that delivers a limit problem whose solution is the closest in norm to the real solution.

On the other hand, among all the retrieved models, no one provides a complete and *tout court* "beam+plate" approximation. In fact, in all the cases, the plate and the stiffener interact, and some displacement component, for the plate and/or the beam, are rigid, so

that they do not appear in the limit energy expression.

In this Chapter, the regime C of Table 10.1 has been selected. The stiffener is rigid for transversal and lateral displacements, whilst the axial component is coupled with the plate displacement in the same direction. In such a model, thus, the stiffener actually behaves like a truss.

8.2.2.3 The Local Finite Element Model

LFEMs are generated in order to evaluate structural phenomena which typically appear at a smaller scale with respect to the GFEM one. In this work, the LFEMs are used to assess the first buckling load of the upper and lower skins of the FW and RW. The LFEM are finer-meshed ZOIs, introduced in Section 8.2.2.1. The structural components are entirely modelled by using SHELL181 (Reissner-Mindlin kinematics) elements. Each LFEM has approximately 7000 elements and 43000 DOFs.

Dirichlet-type BCs are interpolated from the GFEM, for the predefined load case, and applied to the nodes of the LFEM lying in correspondence of stringers and ribs intersections with the skin, as illustrated in Figure 8.9. An eigenvalue buckling analysis

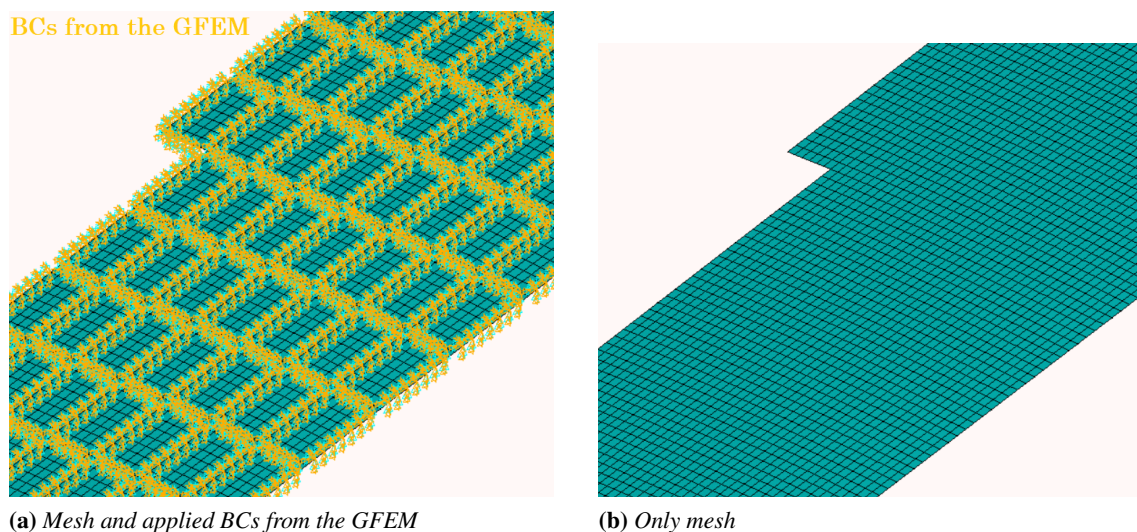


Figure 8.9: Details of the mesh of the FW upper skin LFEM of the PrP wing design

is performed on the LFEM, and the resulting first positive eigenvalue λ is used for the evaluation of the constraint g_{buck} .

8.3 The Second-level Problem Formulation

The goal of the SLP is to search for at least one blended SS, for the whole structure, recovering at the same time the optimal value of thickness and of PPs resulting from the resolution of the FLP, listed in Table 8.9.

8.3.1 Mathematical Formulation

In this work, in order to have a planar and continuous top surface of each skin region, the blending scheme illustrated in Figure 8.10 is assumed. The reason is to have no discontinuities, due to ply drop, in the outer side, which may penalise aerodynamics. Therefore,

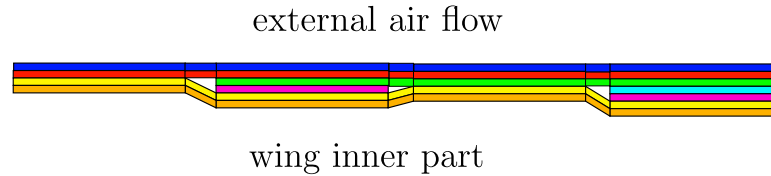


Figure 8.10: *Blending scheme of the PrP wing design*

the top surface of each laminate is the one wet by the external air flow, whilst the bottom side overlooks the wing-box inner part. Moreover, the two innermost plies (yellow and orange in Figure 8.10) are shared by all the laminates as a covering (Irisarri et al., 2014). The determination of the orientation values must be carried out to minimise the global residual function (see Eqs. (6.49) and (6.52)) for the structure.

8.3.2 Numerical Strategy

Problem (6.52) has been split into 9 sub-problems: one for each of upper and lower skins of FW and RW, and one for each of spar webs and stringers which are not affected by blending. For each of these nine sub-problems, Tab. 8.7 lists the number of independent variables.

Table 8.7: *Number of independent variables for sub-problems of SLP*

Sub-problem ID	Region ID	N° independent variables
1	upper skin FW	246
2	lower skin FW	211
3	upper skin RW	230
4	lower skin RW	242
5	25	30
6	26	50
7	51	31
8	52	30
9	Stiffeners	26

The solution search for Problem (6.52), properly adapted to each of the sub-problems, is performed via MIDACO[®] optimisation software, with the parameters listed in Table 8.8. The design variables correspond to the orientation angles which can vary in the range $] - 90, 90]$ deg with a discrete step of 1 deg. As an example, Figure 8.11 shows the solution propagation used for the stack recovery of the upper skin of the FW only. With the same notation of Chapter 7, each panel is represented by a circle characterised by the number of plies obtained at the end of the discrete optimisation step of the FLP (panels

Table 8.8: MIDACO[®] parameters for RSS search for the SLP

Parameter	Value
Ants	100
Kernel	20
Oracle	0
Evalstop	1×10^6

having the same thickness and PPs are depicted once, the panel ID being in the yellow diamond). The solution propagation starts from panel 1, having 51 plies. Following the

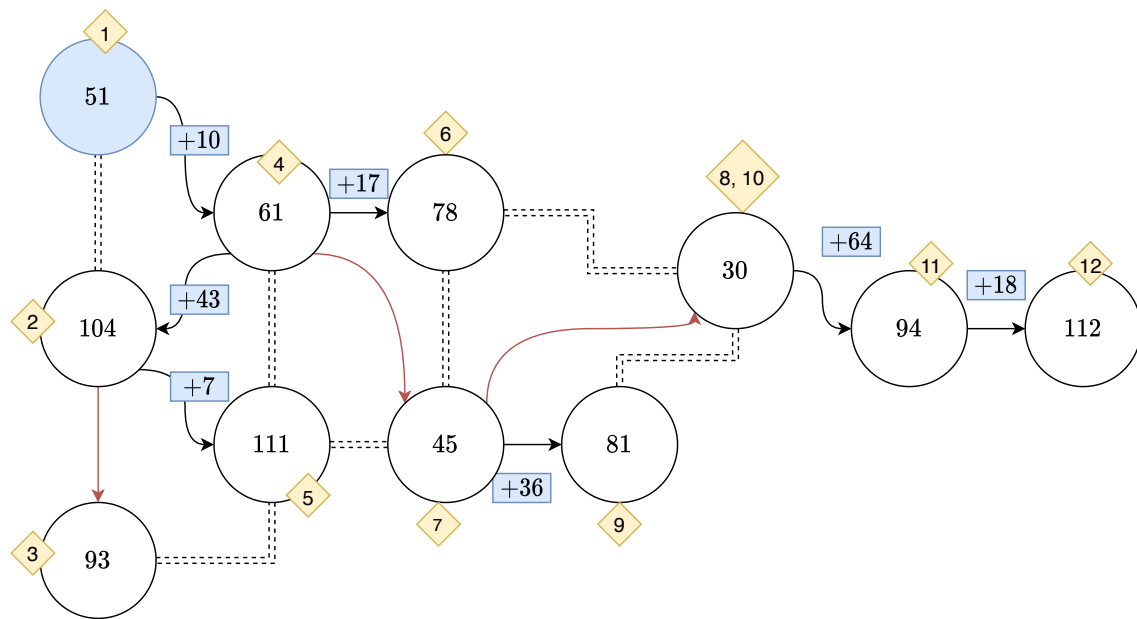


Figure 8.11: Solution propagation for the upper skin of the FW

solution propagation in Figure 8.11, additional variables (reported in light-blue labels) are introduced when moving from a thinner to a thicker laminate. Conversely, when passing from a thicker to a thinner laminate, no further variables are introduced (red arrows). It is recalled that propagation scheme of Figure 8.11 is specific for the case at hand, since propagation heavily depends on the FLP solution. Moreover, also in this case, it has been found manually.

8.4 Numerical Results

The solution of the FLP is summarised in Table 8.9. Specifically, the Table shows the optimal number of plies and the optimal PPs values for each of the 52 optimisation regions. The starting point for the continuous optimisation is $\xi_0 = \{0.8, 0.0, 0.0 \mid j = 1, \dots, 52\}$, whereby the dimensionless mass is 1.14. At the end of the FLP, the resulting dimensionless optimal mass is 0.7912. Therefore, the mass saving is about 30%, in agreement with Dal Canto et al. (2012), Frediani, Quattrone, et al. (2012).

Table 8.10 lists the values of the constraints for the optimal solution for both the con-

Table 8.9: *Optimal values of the design variables of the FLP*

ID	N	ρ_0	ρ_1	ID	N	ρ_0	ρ_1
1	51	0.2971	0.0770	27	70	0.0128	0.0210
2	104	0.0950	0.1743	28	139	0.3917	0.0059
3	93	-0.0225	0.1044	29	107	0.6844	0.0001
4	61	0.0669	0.0946	30	78	-0.1077	0.0295
5	111	0.1488	0.2010	31	139	0.3917	0.0059
6	78	0.1844	0.0380	32	101	0.0151	0.0341
7	45	0.7413	0.0454	33	61	0.2181	0.0092
8	30	-0.0960	0.0254	34	43	-0.2055	0.0094
9	81	-0.0364	0.0167	35	129	-0.4252	0.0000
10	30	-0.1992	0.1108	36	30	0.1610	0.0199
11	94	-0.0645	0.1517	37	30	0.1610	0.0199
12	112	0.1119	0.0170	38	30	0.1610	0.0199
13	86	0.0394	0.0952	39	115	0.0922	0.1929
14	53	0.3827	0.4737	40	58	-0.5996	0.0350
15	119	0.1186	0.0271	41	78	-0.1823	0.0592
16	92	0.1199	0.1439	42	86	-0.2182	0.0002
17	119	0.1186	0.0271	43	86	-0.2182	0.0002
18	37	0.7503	0.4305	44	30	0.2820	0.1829
19	31	0.5630	0.6061	45	30	0.2820	0.1829
20	72	0.2134	0.0452	46	97	0.0559	0.0814
21	31	0.5630	0.6061	47	51	-0.0282	0.0712
22	31	0.5630	0.6061	48	30	0.2820	0.1829
23	84	-0.0059	0.0501	49	90	-0.5986	0.1808
24	88	-0.0761	0.0827	50	45	-0.5318	0.0377
25	30	-0.0613	0.0794	51	31	-0.6774	0.1289
26	50	0.4676	0.6653	52	30	0.1828	0.0352

tinuous and the discrete optimisation. The active constraints in the continuous optimisation are the blending one and the buckling one for the lower skin of the FW. In particular, the latter is slightly violated, but still in tolerance (see Table 8.5). The stiffness constraint, i.e. the requirement on the maximum vertical tip displacement, is verified with a wide margin. This means that the structure is very rigid and that this requirement is, practically, obsolete. Besides, some constraints values suggest that the solution may be further improved. Indeed, the complexity of the structural model and of the problem formulation may have created some difficulties in the convergence of the algorithm. The discrete optimisation step generally makes the constraint values to assume more negative values, with the exception of the constraint related to the buckling of the upper skin of the FW, which is violated (however, the buckling factor is 1.3993). It is clearly due to the stress redistribution, which is not taken into account in the formulation of the discrete optimisation problem, as already pointed out.

As far as the SLP is concerned, the optimal SSs, together with the residuals, are listed in Tables 8.11, 8.12, 8.13, 8.14, 8.15. It is possible to see that for single laminates, MIDACO[®] is able to find solutions which have a very low residual, as it can be seen looking Table 8.15. On the other hand, when blended solutions are sought, the residuals are larger, but still close to zero (Tables 8.11, 8.12, 8.13, 8.14).

Figures 8.12, 8.13, 8.14, 8.15 show the polar diagrams of $(\mathbf{A}^{*\dagger})_{11}$, $(\mathbf{A}^*)_{11}$, $(\mathbf{B}^*)_{11}$ and

Table 8.10: Constraint values for the FLP

Constraint	Value	
	Continuous optimisation	Discrete optimisation
Feasibility	-0.0408	-0.2893
Blending	-0.0001	-0.0127
Strength	-0.0301	-0.1689
Stiffness	-0.6704	-0.6851
Buckling (Upper FW)	-0.0266	+0.0671
Buckling (Lower FW)	+0.0008	-0.3178
Buckling (Upper RW)	-0.1463	-0.1222
Buckling (Lower RW)	-0.0225	-0.1004

$(\mathbf{C}^*)_{11}$ of the panels having lowest (on the left) and largest (on the right) residual for each upper and lower skin of the FW and RW. It is possible to see that uncoupling and homogeneity properties are very well achieved by the solution of the SLP. However, component $(\mathbf{A}^*)_{11}$ seems to have some differences with the target counterpart. However, given the challenges due to blending and the large scale of problems at hand, the final result can be considered satisfactory.

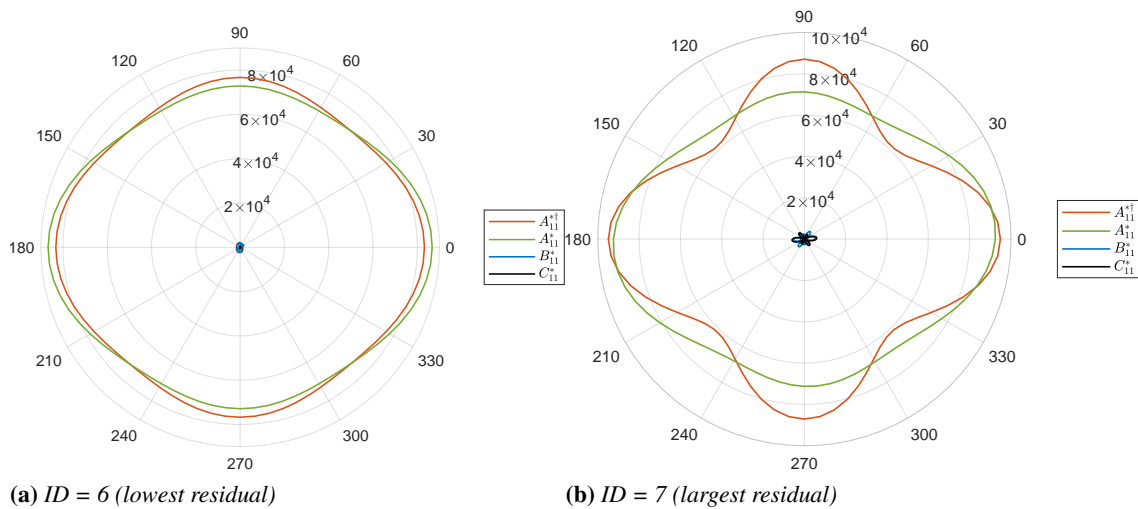


Figure 8.12: Polar diagrams of meaningful panels of upper skin of FW

Table 8.12: Stacks of lower skin of FW of the PrP wing design

ID	Stack	Residual
13	5/-3/-62/-63/77/56/55/50/47/41/-51/-49/-44/-43/-24/6/6/1/-3/-10/-2/-13/7/-46/32/-50/45/51/54/57/58/-61/90/-64/-65/90/78/4/6/10/-16/13/-38/-40/-44/-45/41/44/48/50/-53/90/-3/2/0/0/90/-89/-4/40/-6/0/90/-58/-7/-3/-6/2/-10/14/-82/-5/15/48/3/46/-9/-72/-19/-4/-89/78/-8/8/-39/22	0.048
14	5/-3/90/78/4/6/10/-16/13/-38/-40/-44/-45/41/44/48/50/-53/90/-3/2/0/0/90/-89/-4/40/-6/0/90/-58/-7/-3/-6/2/-10/14/-82/-5/15/48/3/46/-9/-72/-19/-4/-89/78/-8/8/-39/22	0.022
15	5/-3/52/51/52/-54/90/-50/-51/-49/-49/49/-44/-32/90/90/39/16/90/5/4/73/2/0/1/1/83/86/1/-63/-24/90/28/3/71/-62/-63/77/56/55/50/47/41/-51/-49/-44/-43/-24/6/6/1/-3/-10/-2/-13/7/-46/32/-50/45/51/54/57/58/-61/90/-64/-65/90/78/4/6/10/-16/13/-38/-40/-44/-45/41/44/48/50/-53/90/-3/2/0/0/90/-89/-4/40/-6/0/90/-58/-7/-3/-6/2/-10/14/-82/-5/15/48/3/46/-9/-72/-19/-4/-89/78/-8/8/-39/22	0.044
16	5/-3/-63/-24/90/28/3/71/-62/-63/77/56/55/50/47/41/-51/-49/-44/-43/-24/6/6/1/-3/-10/-2/-13/7/-46/32/-50/45/51/54/57/58/-61/90/-64/-65/90/78/4/6/10/-16/13/-38/-40/-44/-45/41/44/48/50/-53/90/-3/2/0/0/90/-89/-4/40/-6/0/90/-58/-7/-3/-6/2/-10/14/-82/-5/15/48/3/46/-9/-72/-19/-4/-89/78/-8/8/-39/22	0.030
17	5/-3/52/51/52/-54/90/-50/-51/-49/-49/49/-44/-32/90/90/39/16/90/5/4/73/2/0/1/1/83/86/1/-63/-24/90/28/3/71/-62/-63/77/56/55/50/47/41/-51/-49/-44/-43/-24/6/6/1/-3/-10/-2/-13/7/-46/32/-50/45/51/54/57/58/-61/90/-64/-65/90/78/4/6/10/-16/13/-38/-40/-44/-45/41/44/48/50/-53/90/-3/2/0/0/90/-89/-4/40/-6/0/90/-58/-7/-3/-6/2/-10/14/-82/-5/15/48/3/46/-9/-72/-19/-4/-89/78/-8/8/-39/22	0.044
18	5/-3/90/-3/2/0/0/90/-89/-4/40/-6/0/90/-58/-7/-3/-6/2/-10/14/-82/-5/15/48/3/46/-9/-72/-19/-4/-89/78/-8/8/-39/22	0.031
19	5/-3/-89/-4/40/-6/0/90/-58/-7/-3/-6/2/-10/14/-82/-5/15/48/3/46/-9/-72/-19/-4/-89/78/-8/8/-39/22	0.044
20	5/-3/71/-89/-71/66/-84/-57/-48/54/-37/46/38/-24/-3/2/2/1/14/8/20/29/-30/-40/-43/-48/-52/-54/49/52/57/-64/-65/64/73/87/73/90/-3/2/0/0/90/-89/-4/40/-6/0/90/-58/-7/-3/-6/2/-10/14/-82/-5/15/48/3/46/-9/-72/-19/-4/-89/78/-8/8/-39/22	0.045
21	5/-3/-89/-4/40/-6/0/90/-58/-7/-3/-6/2/-10/14/-82/-5/15/48/3/46/-9/-72/-19/-4/-89/78/-8/8/-39/22	0.044
22	5/-3/-89/-4/40/-6/0/90/-58/-7/-3/-6/2/-10/14/-82/-5/15/48/3/46/-9/-72/-19/-4/-89/78/-8/8/-39/22	0.044
23	69/-60/55/59/-31/51/60/61/60/-44/-57/-61/63/-65/-56/-63/-69/-89/-4/40/-6/0/90/-58/-7/-3/-6/2/-10/14/-82/-5/15/48/3/46/-9/-72/-19/-4/-89/78/-8/8/-39/22	0.039
24	5/-3/58/-57/45/-46/-55/61/-60/44/68/56/54/54/-47/-58/-58/-54/-14/16/58/-17/-57/-14/49/-27/-50/12/27/21/9/47/5/-1/-37/12/-31/-27/27/20/25/-18/27/20/25/-18/69/-60/55/59/-31/51/60/61/60/-44/-57/-61/63/-65/-56/-63/-69/-89/-4/40/-6/0/90/-58/-7/-3/-6/2/-10/14/-82/-5/15/48/3/46/-9/-72/-19/-4/-89/78/-8/8/-39/22	0.033
		0.468

Table 8.13: Stacks of upper skin of the PrP wing design

ID	Stack	Residual
27	-29/59/-43/40/790/-40/41/-33/46/90/89/2/-46/47/-38/14/11/-9/-87/10/12/-10/-73/-6/80/74/-86/83/40/-47/-88/-28/32/-44/47/38/-36/-37/34/40/-37/-5/-74/29/-67/-87/-15/21/80/-87/5/37/-17/55/-48/-3/67/-56/85/45/-21/-51/17/-1/-64/-16/66/-84/25	0.005
28	-29/59/-21/13/90/5/-59/89/5/87/4/3/-87/89/1/86/2/-19/1/24-24/31/-87/27/73/-15/89/-71/90/87/-74/-75/83/77/2/-89/1/90/1/89/89/0/89/0/1/0/1/89/1/90/90/90/1/10/014-89/1/1/90/0/89/-1/0/-89/-1/-81/49/-48/42/-46/-17/-43/40/790/-40/41/-33/46/90/89/2/-46/47/-38/14/11/-9/-87/10/12/-10/-73/-6/80/74/-86/83/40/-47/-88/-28/32/-44/47/38/-36/-37/34/40/-37/-5/-74/29/-67/-87/-15/21/80/-87/5/37/-17/55/-48/-3/67/-56/85/45/-21/-51/17/-1/-64/-16/66/-84/25	0.200
29	-29/59/2/-89/1/90/1/89/89/0/89/0/1/0/1/89/1/90/90/90/1/1/-89/1/1/1/90/0/89/-1/0/-89/-1/-81/49/-48/42/-46/-17/-43/40/790/-40/41/-33/46/90/89/2/-46/47/-38/14/11/-9/-87/10/12/-10/-73/-6/80/74/-86/83/40/-47/-88/-28/32/-44/47/38/-36/-37/34/40/-37/-5/-74/29/-67/-87/-15/21/80/-87/5/37/-17/55/-48/-3/67/-56/85/45/-21/-51/17/-1/-64/-16/66/-84/25	0.016
30	-29/59/-89/-1/-81/49/-48/42/-46/-17/-43/40/790/-40/41/-33/46/90/89/2/-46/47/-38/14/11/-9/-87/10/12/-10/-73/-6/80/74/-86/83/40/-47/-88/-28/32/-44/47/38/-36/-37/34/40/-37/-5/-74/29/-67/-87/-15/21/80/-87/5/37/-17/55/-48/-3/67/-56/85/45/-21/-51/17/-1/-64/-16/66/-84/25	0.014
31	-29/59/-21/13/90/5/-59/89/5/87/4/3/-87/89/1/86/2/-19/1/24-24/31/-87/27/73/-15/89/-71/90/87/-74/-75/83/77/2/-89/1/90/1/89/89/0/89/0/1/0/1/89/1/90/90/90/1/10/014-89/1/1/90/0/89/-1/0/-89/-1/-81/49/-48/42/-46/-17/-43/40/790/-40/41/-33/46/90/89/2/-46/47/-38/14/11/-9/-87/10/12/-10/-73/-6/80/74/-86/83/40/-47/-88/-28/32/-44/47/38/-36/-37/34/40/-37/-5/-74/29/-67/-87/-15/21/80/-87/5/37/-17/55/-48/-3/67/-56/85/45/-21/-51/17/-1/-64/-16/66/-84/25	0.001
32	-29/59/90/-56/22/18/-48/-35/13/77/55/-57/-2/-72/9/-40/-26/67/7/-6/87/51/79/49/2/-89/-1/-81/49/-48/42/-46/-17/-43/40/790/-40/41/-33/46/90/89/2/-46/47/-38/14/11/-9/-87/10/12/-10/-73/-6/80/74/-86/83/40/-47/-88/-28/32/-44/47/38/-36/-37/34/40/-37/-5/-74/29/-67/-87/-15/21/80/-87/5/37/-17/55/-48/-3/67/-56/85/45/-21/-51/17/-1/-64/-16/66/-84/25	0.038
33	-29/59/89/2/-46/47/-38/14/11/-9/-87/10/12/-10/-73/-6/80/74/-86/83/40/-47/-88/-28/32/-44/47/38/-36/-37/34/40/-37/-5/-74/29/-67/-87/-15/21/80/-87/5/37/-17/55/-48/-3/67/-56/85/45/-21/-51/17/-1/-64/-16/66/-84/25	0.025
34	-29/59/40/-47/-88/-28/32/-44/47/38/-36/-37/34/40/-37/-5/-74/29/-67/-87/-15/21/80/-87/5/37/-17/55/-48/-3/67/-56/85/45/-21/-51/17/-1/-64/-16/66/-84/25	0.022
35	-29/59/46/-75/-53/15/-49/-8/-46/45/45/46/-47/-43/-59/45/-41/45/-41/-41/-29/44/-37/44/44/-61/81/44/-58/43/-32/-55/89/-30/43/42/43/43/43/-62/43/-41/43/43/-34/-44/-44/44/44/-45/-45/-45/-10/46/46/46/47/54/46/46/47/47/-46/-46/-89/-46/-47/-47/89/2/-46/47/-38/14/11/-9/-87/10/12/-10/-73/-6/80/74/-86/83/40/-47/-88/-28/32/-44/47/38/-36/-37/34/40/-37/-5/-74/29/-67/-87/-15/21/80/-87/5/37/-17/55/-48/-3/67/-56/85/45/-21/-51/17/-1/-64/-16/66/-84/25	0.003
36	-29/59/-5/-74/29/-67/-87/-15/21/80/-87/5/37/-17/55/-48/-3/67/-56/85/45/-21/-51/17/-1/-64/-16/66/-84/25	0.003
37	-29/59/-5/-74/29/-67/-87/-15/21/80/-87/5/37/-17/55/-48/-3/67/-56/85/45/-21/-51/17/-1/-64/-16/66/-84/25	0.003
38	-29/59/-5/-74/29/-67/-87/-15/21/80/-87/5/37/-17/55/-48/-3/67/-56/85/45/-21/-51/17/-1/-64/-16/66/-84/25	0.344

Table 8.14: Stacks of lower skin of RW of the PrP wing design

ID	Stack	Residual
39	-81/12/35/85/-83/26/-35/83/34/-12/-17/84/-7/16/-22/6/6/-74/-2/-2/-3/-2/87/85/86/87/-85/-3/-78/0/86/54/-56/-40/44/57/-27/-59/23/48/-44/43/-53/50/-21/90/-40/-6/-1/77/8/5/2/-4/-2/88/88/-89/-89/-47/37/-3/1/-38/-41/48/-55/42/47/47/35/36/-52/30/-34/-49/-41/40/32/-48/62/-47/40/-48/-52/-47/54/53/5/69/-20/86/2/37/-32/46/20/87/-11/16/-63/-67/-18/50/1/-6/-76/50/59/86/-6/25/56/-47/8/-43	0.046
40	-81/12/-47/37/-31/-38/-41/48/-55/42/47/47/35/36/-52/30/-34/-49/-41/40/32/-48/62/-47/40/-48/-52/-47/54/53/5/69/-20/86/2/37/-32/46/20/87/-11/16/-63/-67/-18/50/1/-6/-76/50/59/86/-6/25/56/-47/8/-43	0.088
41	-81/12/48/-44/43/-53/50/-21/90/-40/-6/-1/77/8/5/2/-4/-2/88/88/-89/-89/-47/37/-3/1/-38/-41/48/-55/42/47/47/35/36/-52/30/-34/-49/-41/40/32/-48/62/-47/40/-48/-52/-47/54/53/5/69/-20/86/2/37/-32/46/20/87/-11/16/-63/-67/-18/50/1/-6/-76/50/59/86/-6/25/56/-47/8/-43	0.020
42	-81/12/54/-56/-40/44/57/-27/-59/23/48/-44/43/-53/50/-21/90/-40/-6/-1/77/8/5/2/-4/-2/88/88/-89/-89/-47/37/-3/1/-38/-41/48/-55/42/47/47/35/36/-52/30/-34/-49/-41/40/32/-48/62/-47/40/-48/-52/-47/54/53/5/69/-20/86/2/37/-32/46/20/87/-11/16/-63/-67/-18/50/1/-6/-76/50/59/86/-6/25/56/-47/8/-43	0.011
43	-81/12/54/-56/-40/44/57/-27/-59/23/48/-44/43/-53/50/-21/90/-40/-6/-1/77/8/5/2/-4/-2/88/88/-89/-89/-47/37/-3/1/-38/-41/48/-55/42/47/47/35/36/-52/30/-34/-49/-41/40/32/-48/62/-47/40/-48/-52/-47/54/53/5/69/-20/86/2/37/-32/46/20/87/-11/16/-63/-67/-18/50/1/-6/-76/50/59/86/-6/25/56/-47/8/-43	0.011
44	-81/12/569/-20/86/2/37/-32/46/20/87/-11/16/-63/-67/-18/50/1/-6/-76/50/59/86/-6/25/56/-47/8/-43	0.027
45	-81/12/569/-20/86/2/37/-32/46/20/87/-11/16/-63/-67/-18/50/1/-6/-76/50/59/86/-6/25/56/-47/8/-43	0.027
46	-81/12/-71/-5/43/58/-57/69/-35/-9/-13/-47/15/51/-19/18/3/-86/87/75/15/-33/-58/76/22/-44/54/-59/-30/47/14/13/85/42/-5/-7/-32/-83/44/-33/-86/84/2/-73/-87/-2/9/13/61/49/-53/-30/-16/-87/-7/17/-43/-22/33/-70/43/36/43/-51/-30/43/83/87/-51/5/69/-20/86/2/37/-32/46/20/87/-11/16/-63/-67/-18/50/1/-6/-76/50/59/86/-6/25/56/-47/8/-43	0.0005
47	-81/12/61/49/-53/-30/-16/-87/-7/17/-43/-22/33/-70/43/36/43/-51/-30/43/83/87/-51/5/69/-20/86/2/37/-32/46/20/87/-11/16/-63/-67/-18/50/1/-6/-76/50/59/86/-6/25/56/-47/8/-43	0.001
48	-81/12/569/-20/86/2/37/-32/46/20/87/-11/16/-63/-67/-18/50/1/-6/-76/50/59/86/-6/25/56/-47/8/-43	0.027
49	-81/12/41/41/-41/-41/41/41/-41/-40/41/-40/41/-40/41/-40/41/41/41/-39/41/41/40/40/39/39/39/37/-29/-28/-18/22/-31/-38/-41/-42/-42/-42/90/39/40/40/-42/39/40/-42/-45/-46/-47/41/41/-49/41/42/-50/-51/-51/42/5/69/-20/86/2/37/-32/46/20/87/-11/16/-63/-67/-18/50/1/-6/-76/50/59/86/-6/25/56/-47/8/-43	0.031
50	-81/12/39/40/-42/-45/-46/-47/41/41/-49/41/42/-50/-51/-51/42/5/69/-20/86/2/37/-32/46/20/87/-11/16/-63/-67/-18/50/1/-6/-76/50/59/86/-6/25/56/-47/8/-43	0.108
		0.398

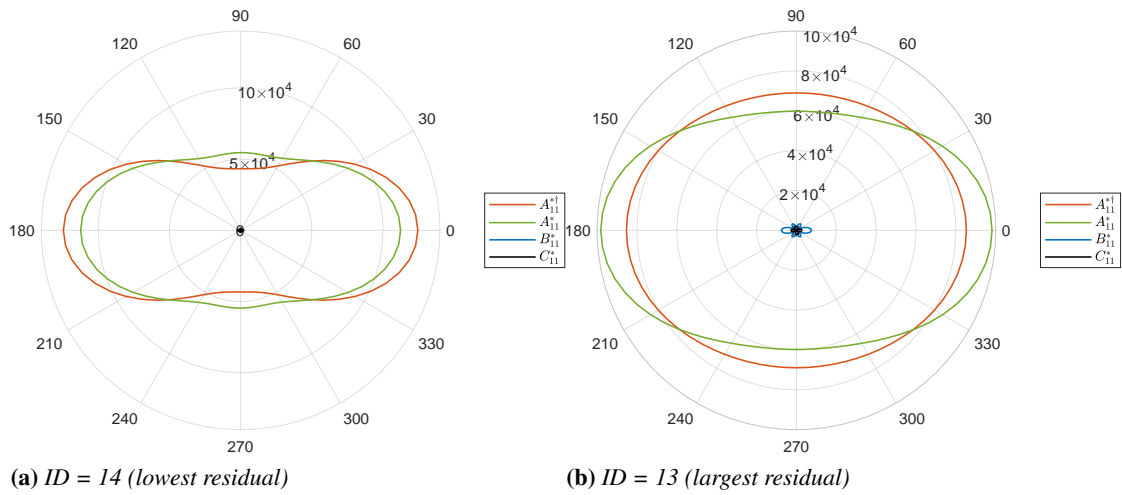


Figure 8.13: Polar diagrams of meaningful panels of lower skin of FW

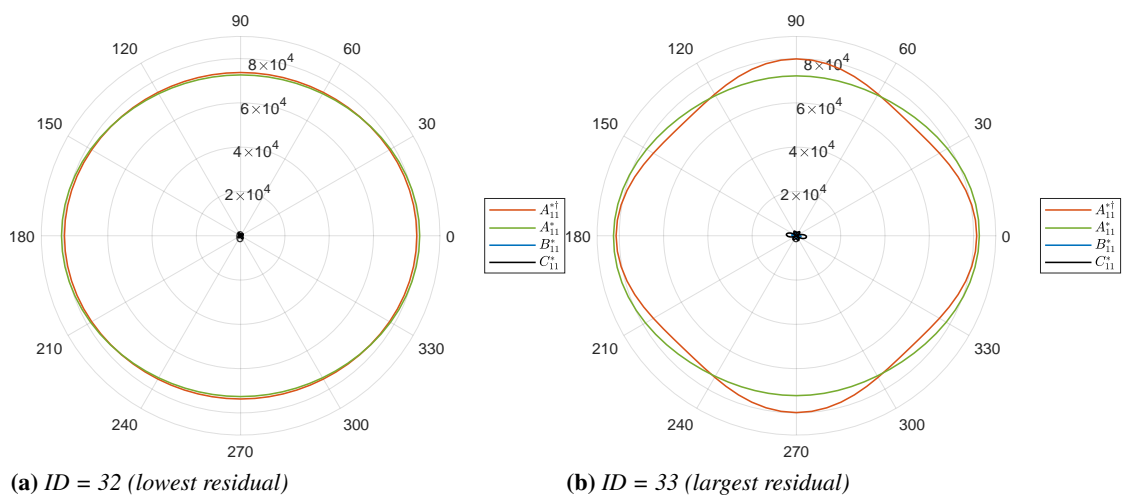


Figure 8.14: Polar diagrams of meaningful panels of upper skin of RW

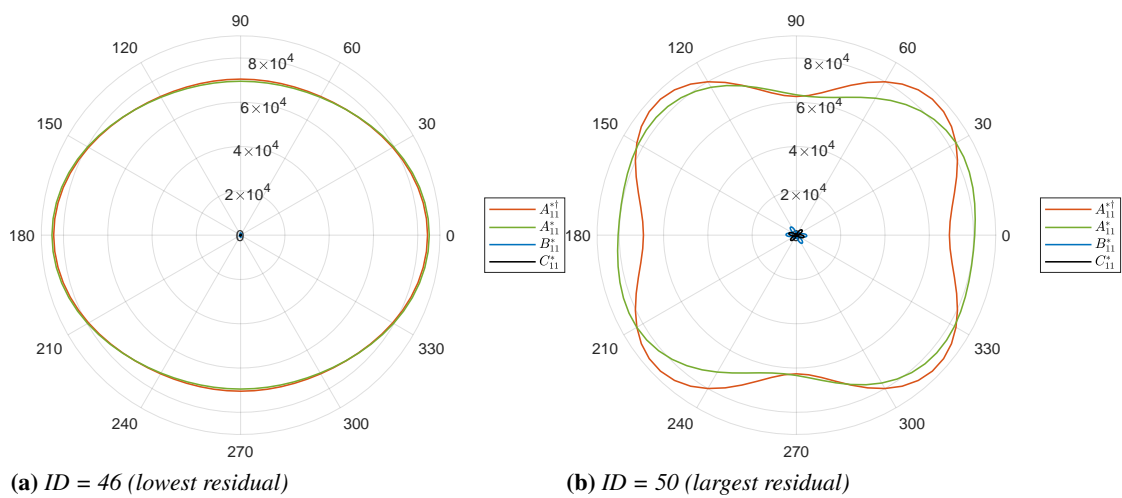


Figure 8.15: Polar diagrams of meaningful panels of lower skin of RW

Table 8.15: *Stacks of spar webs and stringers of the PrP wing design*

ID	Stack	Residual
25	-37/-4/-71/33/56/43/75/-25/-67/-2/11/-85/12/-42/87/42/-52/47/-28/- 26/46/7/-79/29/-28/-40/72/-7/-79/35	3×10^{-5}
26	0/10/16/-11/-39/-10/4/-25/90/7/51/35/-3/-7/-57/-8/3/14/-2/- 9/12/61/8/5/-8/-7/24/-15/3/15/4/1/0/2/-33/-23/-57/5/5/-13/-43/87/50/- 9/33/7/2/10/-11/0	7×10^{-7}
51	44/-47/-54/37/-11/-43/38/-31/46/28/68/56/-33/-30/35/-51/-42/- 51/46/25/-46/38/-45/41/39/-61/-28/-11/53/42/-45	6×10^{-6}
52	-81/46/-3/28/-35/83/-33/-10/77/-11/-70/-77/22/17/8/80/-76/60/-45/- 22/24/-76/50/-24/68/-9/26/84/-3/-63	1×10^{-5}
Stringers	86/-5/-3/-86/29/85/18/-45/-9/-4/83/-7/6/-58/7/1/0/-18/75/3/-75/15/89/- 3/67/-86/	2×10^{-6}

8.5 Conclusions

The enhanced MS2LOS, endowed with the elements formalised in this Thesis, has been employed for the deterministic optimisation of a complex composite structure. In particular, the effectiveness of the approach detailed in the two previous Chapters, is here tested on the optimal design of the PARSIFAL Project PrP lifting system. Despite the complexity of the problem, the results are encouraging. A light structure design has been found, and blended stacking sequences, also for laminates with large number of plies, have been satisfactorily recovered, thus providing an explicit manufacturable solution.

Part IV

New Theoretical Findings

On the Non-convexity of the Feasible Domain of Laminates

This Chapter aims at answering to research question RQ4.

As stated in Section 7.3.4, the stack recovery is affected by the fact that the FLP formulation relies on the existence, in every point of the feasibility domain, of uncoupled, homogeneous, orthotropic laminates. Actually, this hypothesis is not necessarily true. As a consequence, the expression of a proper feasibility domain of laminates is a major still-open problem of composite design, jeopardising the well-formulation of the design problem. The feasible domain shape of laminates is indeed a subset of the domain induced by Eq. (4.44), but it is not clear how it depends on PPs. It can be inferred that the "missing constraints", defining the sharpest feasibility domain, are geometrical bounds, in the sense that they must depend on all the possible stacks for a given number of plies. In particular, the number of ply should appear in their expressions.

This Chapter investigates two preliminary aspects of the more wide problem of the feasibility domain determination. Section 9.1 focuses on the non-convex nature of the feasible domain of anisotropic laminates. Proofs are given on the non-convexity of the feasible domain for full anisotropic and for membrane-orthotropic laminates, either in the LPs space or in the PPs one. Then, adopting the polar formalism, some particular cases are studied, providing analytical expressions of new narrower bounds, in terms of PPs of the membrane stiffness tensor. For a particular case, the exact expression of the membrane feasibility domain is determined. Moreover, new geometrical bounds are derived, defining a stricter region than those presented in Section 4.2.4.

Section 9.2 focuses on the necessary and sufficient conditions to achieve uncoupling and homogeneity properties, clarifying that quasi-triviality is, in general, only a sufficient condition. Finally, Section 9.3 concludes the Chapter with meaningful comments.

9.1 The Non-convexity of the Feasible Domain of Laminates

9.1.1 Generalities

Two still-open problems in anisotropic plane elasticity for composite laminates are:

- the definition of the general expression of the feasibility domain;
- the definition of sufficient and necessary conditions to obtain membrane/bending uncoupled laminates and/or the homogeneity property, defined in Chapter 4.

It is well-known that there is no bijective relationship between arbitrary macroscopic elastic properties of the laminate (in terms of \mathbf{A}^* , \mathbf{B}^* , \mathbf{D}^* and \mathbf{H}^* components) and SSs. This means that, given an arbitrary SS, a set of elastic properties is always uniquely determined, whilst the converse is generally false. This aspect is particularly important in practical applications, such as laminates design and SSs recovery.

As summarised in Section 4.1.3, a first kind of bounds derives directly from thermodynamic considerations, since the elasticity tensor is positive-definite. Therefore, the elastic constants live in a feasibility domain whose boundary constitutes the so-called *elastic-bound* (Vannucci, 2012a). However, a second kind of bounds can be introduced, which are often referred as *geometrical bounds* (Vannucci, 2012a). To this purpose, it is important to adopt some mathematical descriptors of the anisotropy, for instance, LPs or PPs.

In (Hammer et al., 1997), geometrical bounds were derived as a consequence of the nature of the trigonometric functions involved in the definition of the laminate stiffness tensors. Vannucci (2012a) derived the expressions of the geometrical bounds in the framework of the Polar Method (see Section 4.2.4), showing that these bounds are always stricter than the elastic ones: hence only the formers must be considered in practical design problems, as done so far.

Grenestedt and Gudmundson (1993) claimed to provide a proof of the convexity of the feasible domain of general anisotropic laminates in the LPs space. However, as it will be discussed later in this Chapter, the proof provided in (Grenestedt & Gudmundson, 1993) proves only that the projection of the LPs on each axis (in the LPs space, which is of dimension 12) is convex. Moreover, this proof does not respect a more general result of convex analysis (Rockafellar, 1997; Boyd & Vandenberghe, 2019), which states that if a set is convex then any projection is still a convex set, while the converse is not generally true. Many works, dealing with the optimisation of laminates and making use of the formalism based on LPs, use the results of Grenestedt and Gudmundson, 1993, claiming that the convexity of the domain endows the composite design problems with nice properties (Hammer et al., 1997; Diaconu et al., 2002; Setoodeh et al., 2006; Bloomfield et al., 2008; Raju et al., 2014; Macquart et al., 2018).

This work would like to reflect on two different concepts: the geometrical-admissible region (i.e. the region delimited through the geometrical bounds) and the *actual* feasibility region, i.e. the set of all the mapped SSs, through LPs (or PPs), in the corresponding space. In fact, although the geometrical bounds define a region, possibly convex, it may happen that the actual feasible domain, which is a subset of the geometrical-admissible region, is a non-convex set. In the light of this, there could be a conceptual overlapping between the geometrical-admissible region (which can be convex or not) and the actual feasible region, which shall be the object of the investigation of this Chapter.

The derivation of the laminate actual feasibility domain in a closed form is of paramount importance when formulating the laminate design problem as a constrained non-linear programming problem. Keeping this in mind, a simple investigation led to the discovery of the analytic expression of a further bound, valid for any kind of symmetry of the laminate, which makes the feasibility region a stricter non-convex region. These new bounds introduce the dependence from the number of plies.

9.1.2 Lamination Parameters

In this Section, the LPs are introduced, as they are a common mathematical descriptor of the plane anisotropy. They are introduced because the main results of this Section are valid when the anisotropy is described through LPs or PPs. Besides, the results of this Section disprove the fact that the feasible domain of laminates is convex if LPs are adopted. LPs are often used together with the parameters of Tsai and Pagano to describe the anisotropic behaviour of the laminate in the framework of the CLT (Grenstedt & Gudmundson, 1993; Hammer et al., 1997; Reddy, 2003; Jones, 2018). LPs express the properties of a laminate in terms of moments, relative to the plate mid-plane, of the trigonometric functions entering in the frame rotation formulæ (Hammer et al., 1997). For the sake of brevity, the complete expressions of the LPs in the CLT framework are not here reported. The interested reader is addressed to (Jones, 2018).

LPs are closely related to PPs: from a mathematical viewpoint, it is sufficient to report the following identities. The same nomenclature of Vannucci (2017) is adopted.

$$\begin{aligned}
 \xi_1 + i\xi_2 &= \frac{1}{N} \sum_{k=1}^N a_k e^{i4\theta_k}, & \xi_3 + i\xi_4 &= \frac{1}{N} \sum_{k=1}^N a_k e^{i2\theta_k}, \\
 \xi_5 + i\xi_6 &= \frac{1}{N^2} \sum_{k=1}^N b_k e^{i4\theta_k}, & \xi_7 + i\xi_8 &= \frac{1}{N^2} \sum_{k=1}^N b_k e^{i2\theta_k}, \\
 \xi_9 + i\xi_{10} &= \frac{1}{N^3} \sum_{k=1}^N d_k e^{i4\theta_k}, & \xi_{11} + i\xi_{12} &= \frac{1}{N^3} \sum_{k=1}^N d_k e^{i2\theta_k}.
 \end{aligned} \tag{9.1}$$

It is evident that twelve parameters are necessary to completely define the behaviour of the laminate in the CLT framework.

9.1.3 The Non-convexity Proofs of the Feasible Domain

Under the same assumptions reported in Section 4.2.4, when only the membrane tensor is taken into account, the geometrical bounds in the PPs space read (Vannucci, 2012a) (see Eq. (4.44)):

$$\begin{cases} 0 \leq \rho_0 \leq 1, \\ 0 \leq \rho_1 \leq 1, \\ 2\rho_1^2 \leq \frac{1 - \rho_0^2}{1 - (-1)^K \rho_0 \cos 4(\Phi_0^{A*} - \Phi_1^{A*})}, \end{cases} \quad (9.2)$$

where

$$\rho_0 := \frac{R_0^{A*}}{R_0} = \frac{1}{N} \sqrt{\left(\sum_{j=1}^N \cos 4\theta_j\right)^2 + \left(\sum_{j=1}^N \sin 4\theta_j\right)^2}, \quad (9.3)$$

$$\rho_1 := \frac{R_1^{A*}}{R_1} = \frac{1}{N} \sqrt{\left(\sum_{j=1}^N \cos 2\theta_j\right)^2 + \left(\sum_{j=1}^N \sin 2\theta_j\right)^2}. \quad (9.4)$$

In the LPs space, they read (Hammer et al., 1997)

$$\begin{cases} 2\xi_3^2(1 - \xi_1) + 2\xi_4^2(1 + \xi_1) + \xi_1^2 + \xi_2^2 - 4\xi_3\xi_2\xi_4 \leq 1, \\ \xi_3^2 + \xi_4^2 \leq 1, \\ -1 \leq \xi_1 \leq 1. \end{cases} \quad (9.5)$$

In a similar fashion, for a membrane-orthotropic laminate, the geometrical bounds in the PPs space simplify to Eq. (4.45). In the LPs space, they read (Miki, 1982)

$$\begin{cases} -1 \leq \xi_3 \leq 1 \\ 2\xi_3^2 - 1 \leq \xi_1 \leq 1. \end{cases} \quad (9.6)$$

As discussed in (Montemurro, 2015a, 2015b; Vannucci, 2017), the design of a laminate lives in \mathbb{R}^{12} , since four PPs are needed to define the anisotropic part of tensors \mathbf{A}^* , \mathbf{B}^* and \mathbf{D}^* (the deviatoric part of tensor \mathbf{H}^* being directly related, in general, to the anisotropic one of tensors \mathbf{A}^* and \mathbf{D}^*). Regarding LPs, the same remark holds since 12 LPs are needed to fully describe the laminate behaviour in the CLT framework, as stated above. For both representations, the feasibility domain is then a subset of \mathbb{R}^{12} . The determination of the feasible domain, in the most general case, is still an open problem. For example, in (Grenestedt & Gudmundson, 1993), the feasibility domain in the LPs space is claimed to be convex. Conversely, in (Vannucci, 2017), the feasibility domain in the PPs space is claimed to be non-convex for anisotropic laminates and convex for orthotropic ones.

To show the main results of this Chapter, some nomenclature must be introduced, as done by Grenestedt and Gudmundson (1993).

Let $z^* \in [0, 1]$ be the dimensionless coordinate defined through the laminate thickness, from the bottom to the top. The layup function is a combination of piecewise functions defined as

$$\theta(z^*) := \sum_{i=1}^N c_i \chi[\Delta z_i^*], \quad (9.7)$$

where $N \geq 1$, $N \in \mathbb{N}$, $c_i \in [-\frac{\pi}{2}, \frac{\pi}{2}]$ and $\chi[\Delta z_i^*]$ is the indicator function assuming unit value in the interval Δz_i^* . The function $\chi[\Delta z_i^*]$ is defined as:

$$\chi[\Delta z_i^*] := \begin{cases} 1 & \text{if } z^* \in \Delta z_i^*, \\ 0 & \text{otherwise.} \end{cases} \quad (9.8)$$

Intervals Δz_i^* are such that $\bigcup_{i=1}^N \Delta z_i^* = [0, 1]$, $\bigcap_{i=1}^N \Delta z_i^* = \emptyset$ and $\text{meas}(\Delta z_i^*) = 1/N$. It is clear that the range of $\theta(z^*)$ is $[-\frac{\pi}{2}, \frac{\pi}{2}]$. The layup function can be seen as the SS counterpart when the integral description is used instead of summations. The indicator function of Eq. (9.8) is plotted in Figure 9.1.

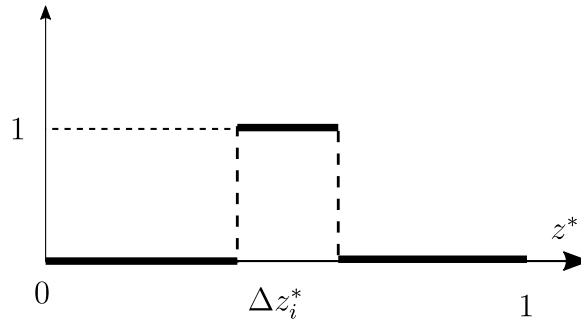


Figure 9.1: Indicator function $\chi[\Delta z_i^*]$

Proposition 9.1 (Convexity of the layup functions set). *The set of layup functions $\Theta_N := \left\{ \theta(z^*) : \theta(z^*) = \sum_{i=1}^N c_i \chi[\Delta z_i^*], c_i \in [-\frac{\pi}{2}, \frac{\pi}{2}] \right\}$ is convex.*

Proof. Assume $\alpha \in [0, 1]$ and suppose that $\hat{\theta}(z^*)$ and $\check{\theta}(z^*)$ belong to Θ_N . Therefore, there exist some \hat{c}_i and \check{c}_i belonging to the interval $[-\frac{\pi}{2}, \frac{\pi}{2}]$ such that $\hat{\theta}(z^*) = \sum_{i=1}^N \hat{c}_i \chi[\Delta z_i^*]$ and $\check{\theta}(z^*) = \sum_{i=1}^N \check{c}_i \chi[\Delta z_i^*]$.

A convex combination of these two elements satisfies the following identity:

$$\begin{aligned} \alpha \hat{\theta} + (1 - \alpha) \check{\theta} &= \alpha \sum_{i=1}^N \hat{c}_i \chi[\Delta z_i^*] + (1 - \alpha) \sum_{i=1}^N \check{c}_i \chi[\Delta z_i^*] \\ &= \sum_{i=1}^N (\alpha \hat{c}_i + (1 - \alpha) \check{c}_i) \chi[\Delta z_i^*] \\ &=: \sum_{i=1}^N \tilde{c}_i \chi[\Delta z_i^*], \end{aligned} \quad (9.9)$$

where \tilde{c}_i are defined through the last equality. Note that $\tilde{c}_i \in [-\frac{\pi}{2}, \frac{\pi}{2}]$. Therefore, the right-hand side member belongs to Θ_N for every α and for every $\hat{\theta}(z^*)$, $\check{\theta}(z^*)$ (see Definition 3.5). This claim is sufficient to conclude the proof. ■

The following Lemma (see Boyd and Vandenberghe, 2019, Section 2.3.2; Rockafellar, 1997, Theorem 3.4 and Corollary 3.4.1) is needed before introducing the main result of this Section.

Lemma 9.1 (Convexity of projections of a convex set). *Let $C \subset \mathbb{R}^{m+n}$ be a convex set. Then, the projection over some of its coordinates $\mathcal{P}(C) = \{x_1 \in \mathbb{R}^m \mid (x_1, x_2) \in C \text{ for some } x_2 \in \mathbb{R}^n\}$ is convex.*

It is then immediate the following

Corollary 9.1. *If a projection $\mathcal{P}(S)$ (in the sense of Lemma 9.1) of a set S is non-convex, then S is a non-convex set.*

Of course, Lemma 9.1 and Corollary 9.1 have an important consequence: if a projection of a set S is convex, the set is not necessarily convex. Indeed, the proof provided in (Grenestedt & Gudmundson, 1993) about the convexity of the LPs space does not take this aspect into account.

Let $\mathbf{p}[\theta]$ denote the vector consisting of twelve PPs (or LPs) obtained with the layup function $\theta(z^*)$. The following four Propositions express the non-convexity of the feasible domain regardless of the anisotropy representation. A more detailed proof is given only for full-anisotropic laminates in the PPs space, the remaining four being conceptually identical.

Proposition 9.2 (Non-convexity of the feasible domain of anisotropic laminates in the PPs space). *The feasible region in the PPs space of all anisotropic laminates composed of N plies $\Pi_N := \{\mathbf{p}[\theta(z^*)] \mid \forall \theta(z^*) \in \Theta_N\}$ is a non-convex bounded subset of \mathbb{R}^{12} for every $N > 1$ ($N \in \mathbb{N}$).*

Proof. For the boundedness, it is sufficient to see that the twelve components of \mathbf{p} are bounded. In fact, the six dimensionless anisotropy moduli (ρ_0, ρ_1 for tensor $\mathbf{A}^*, \mathbf{B}^*, \mathbf{D}^*$) take values in the set $[0, 1]$, whilst the six dimensionless polar angles ($\phi_0 := \frac{\Phi_0}{\pi/4}$ and $\phi_1 := \frac{\Phi_1}{\pi/2}$ for tensors $\mathbf{A}^*, \mathbf{B}^*, \mathbf{D}^*$) take values in the set $[-1, 1]$. Therefore, Π_N is a bounded subset of the 12D-parallelepiped $[0, 1]^6 \times [-1, 1]^6 \subset \mathbb{R}^{12}$.

Let $\hat{\mathbf{p}} := \mathbf{p}[\hat{\theta}(z^*)]$ and $\check{\mathbf{p}} := \mathbf{p}[\check{\theta}(z^*)]$ be two points of the feasible domain for the layup functions $\hat{\theta}(z^*)$ and $\check{\theta}(z^*)$ belonging to Θ_N . Moreover, consider the interval $[0, 1]$ subdivided into N disjoint intervals Δz_i^* of equal length, and let $\alpha \in [0, 1]$.

A convex set, by Definition 3.5, contains the whole line segment that joins any two points belonging to the set. For the characterisation of Π_N , its convexity would imply the existence of a layup function $\tilde{\theta} \in \Theta_N$ such that $\mathbf{p}[\tilde{\theta}] = \alpha \hat{\mathbf{p}} + (1 - \alpha) \check{\mathbf{p}}$ belongs to Π_N for every α and for every $\hat{\mathbf{p}}, \check{\mathbf{p}}$. Therefore, to prove the thesis of the Proposition, it is sufficient to prove the violation of such definition at least for one case. Moreover, thanks

to Proposition 9.1 and Corollary 9.1, it is sufficient to seek the violation in the projection of Π_N into some of its hyper-planes. To this purpose, consider the projection of Π_N onto the plane (ρ_1, ρ_0) .

If layup functions are considered instead of SSs:

$$\begin{aligned} \rho_0[\theta(z^*)] &:= \sqrt{\left(\int_0^1 \cos 4\theta(z^*) dz^*\right)^2 + \left(\int_0^1 \sin 4\theta(z^*) dz^*\right)^2} \\ &= \sqrt{2 \int_0^1 \int_0^1 \cos^2 2(\theta(z^*) - \theta(t^*)) dz^* dt^*} - 1, \end{aligned} \quad (9.10)$$

and

$$\begin{aligned} \rho_1[\theta(z^*)] &:= \sqrt{\left(\int_0^1 \cos 2\theta(z^*) dz^*\right)^2 + \left(\int_0^1 \sin 2\theta(z^*) dz^*\right)^2} \\ &= \sqrt{\int_0^1 \int_0^1 \cos 2(\theta(z^*) - \theta(t^*)) dz^* dt^*}, \end{aligned} \quad (9.11)$$

where the identities $\int f(x) dx \int g(x) dx = \iint f(x)g(t) dx dt$, $\cos(\alpha - \beta) = \cos \alpha \cos \beta + \sin \alpha \sin \beta$ and $\cos(4\alpha) = 2\cos^2 2\alpha - 1$ have been used. Consider two points of the (ρ_1, ρ_0) plane having coordinates $\check{P} = (1, 1)$ and $\hat{P} = (1 - \frac{2}{N}, 1)$. These two points belong to Π_N . In fact, \check{P} corresponds to layup functions of the form $\sum_{i=1}^N c\chi[\Delta z_i^*]$ ($c \in [-\frac{\pi}{2}, \frac{\pi}{2}]$), whilst \hat{P} corresponds to layup functions of the form $\sum_{i=1}^{N-1} c\chi[\Delta z_i^*] + (-\frac{\pi}{2} + c)\chi[\Delta z_N^*]$ ($c \in [-\frac{\pi}{2}, \frac{\pi}{2}]$), as it can be easily verified. Then, assuming that the convex combination of these two points belongs to Π_N , one has:

$$\alpha \begin{pmatrix} 1 - \frac{2}{N} \\ 1 \end{pmatrix} + (1 - \alpha) \begin{pmatrix} 1 \\ 1 \end{pmatrix} = \begin{pmatrix} \rho_1[\tilde{\theta}(z^*)] \\ \rho_0[\tilde{\theta}(z^*)] \end{pmatrix}, \quad (9.12)$$

for some $\tilde{\theta}(z^*) \in \Theta_N$. The second component of Eq. (9.12) is satisfied only if $\rho_0[\tilde{\theta}(z^*)] = 1$. Considering Eq. (9.10), it means that $\int_0^1 \int_0^1 \cos^2 2(\theta(z^*) - \theta(t^*)) dz^* dt^* = 1$. This condition is achieved if $\tilde{\theta}(z^*)$ is the constant function (the line segment represented by Eq. (9.12) would collapse in a point, so this case is disregarded) or if it is of the form

$$\tilde{\theta}(z^*) = \sum_{i=1}^M c\chi[\Delta z_i^*] + \sum_{i=M+1}^N \left(-\frac{\pi}{2} + c\right)\chi[\Delta z_i^*], \quad (9.13)$$

for some $M < N$, $M \in \mathbb{N}$. Assuming $\tilde{\theta}(z^*)$ as in Eq. (9.13), the value of $\rho_1[\tilde{\theta}(z^*)]$ can

be calculated from Eq. (9.11) as:

$$\begin{aligned}
 \rho_1^2[\tilde{\theta}(z^*)] &= \int_0^1 \int_0^1 \cos 2(\tilde{\theta}(z^*) - \tilde{\theta}(t^*)) dt^* dz^* \\
 &= \int_0^1 \int_0^1 \cos 2 \left(\sum_{i=1}^M c \chi[\Delta z_i^*] + \sum_{i=M+1}^N \left(-\frac{\pi}{2} + c\right) \chi[\Delta z_i^*] - \sum_{i=1}^M c \chi[\Delta t_i^*] \right. \\
 &\quad \left. - \sum_{i=M+1}^N \left(-\frac{\pi}{2} + c\right) \chi[\Delta t_i^*] \right) dt^* dz^* \\
 &= \int_0^{M/N} \int_0^{M/N} \cos 2 \left(c \sum_{i=1}^M \chi[\Delta z_i^*] - \chi[\Delta t_i^*] \right) dt^* dz^* \\
 &\quad + \int_0^{M/N} \int_{M/N}^1 \cos 2 \left(c \sum_{i=1}^M \chi[\Delta z_i^*] - \left(-\frac{\pi}{2} + c\right) \sum_{i=M+1}^N \chi[\Delta t_i^*] \right) dt^* dz^* \\
 &\quad + \int_{M/N}^1 \int_0^{M/N} \cos 2 \left(-c \sum_{i=1}^M \chi[\Delta t_i^*] + \left(-\frac{\pi}{2} + c\right) \sum_{i=M+1}^N \chi[\Delta z_i^*] \right) dt^* dz^* \\
 &\quad + \int_{M/N}^1 \int_{M/N}^1 \cos 2 \left(\left(-\frac{\pi}{2} + c\right) \sum_{i=M+1}^N \chi[\Delta z_i^*] - \chi[\Delta t_i^*] \right) dt^* dz^* \\
 &= \left(\frac{M}{N}\right)^2 - \frac{M}{N} \left(1 - \frac{M}{N}\right) - \frac{M}{N} \left(1 - \frac{M}{N}\right) + \left(1 - \frac{M}{N}\right)^2 \\
 &= \left(1 - 2\frac{M}{N}\right)^2,
 \end{aligned} \tag{9.14}$$

and, hence,

$$\rho_1[\tilde{\theta}(z^*)] = \sqrt{\left(1 - 2\frac{M}{N}\right)^2}. \tag{9.15}$$

Finally, from Eqs. (9.12) and (9.15), one obtains

$$1 - \frac{2\alpha}{N} = \sqrt{\left(1 - 2\frac{M}{N}\right)^2} = \begin{cases} 1 - 2\frac{M}{N}, & \text{if } 1 > 2\frac{M}{N}, \\ 2\frac{M}{N} - 1, & \text{otherwise.} \end{cases} \tag{9.16}$$

From Eq. (9.16), either $M = \alpha$ or $M = N - \alpha$. Both results are absurd, since M must be, by definition, an integer number (for all α). Therefore, no $\tilde{\theta}(z^*)$ exists satisfying Eq. (9.12), and the entire line segment between \hat{P} and \check{P} does not belong to the projection of Π_N onto the (ρ_1, ρ_0) plane. This counter-example proves the statement of the Proposition, remembering also Corollary 9.1. \blacksquare

It is noteworthy that Proposition 9.2 considers only geometrical aspects of laminate layups. With the same argument used to prove Proposition 9.2, one can prove that the

feasible domain of laminates with an orthotropic membrane behaviour is a non-convex bounded set.

Proposition 9.3 (Non-convexity of the feasible domain of orthotropic laminates in the PPs space). *The feasible region in the PPs space of all membrane-orthotropic laminates composed of N plies $\Pi_N^{Ort} := \{\mathbf{p}[\theta(z^*)] \mid \Phi_0^{A^*} - \Phi_1^{A^*} = K^{A^*} \frac{\pi}{4}, K^{A^*} \in \{0, 1\}, \forall \theta(z^*) \in \Theta_N\}$ is a non-convex bounded subset of \mathbb{R}^{12} for every $N > 1$ ($N \in \mathbb{N}$).*

Proof. To show the boundedness, the argument is the same of the proof of Proposition 9.2. Adopting the integral description,

$$\begin{aligned} \Phi_0[\theta(z^*)] &:= \frac{1}{4} \arctan \left(\frac{\int_0^1 \sin 4\theta(z^*) dz^*}{\int_0^1 \cos 4\theta(z^*) dz^*} \right), \\ \Phi_1[\theta(z^*)] &:= \frac{1}{2} \arctan \left(\frac{\int_0^1 \sin 2\theta(z^*) dz^*}{\int_0^1 \cos 2\theta(z^*) dz^*} \right). \end{aligned} \quad (9.17)$$

For the non-convexity, it is sufficient to notice that points \hat{P} and \check{P} , used for the proof of Proposition 9.2, actually belong to Π_N^{Ort} (with $K^{A^*} = 0$). ■

Proposition 9.4 (Non-convexity of the feasible domain of anisotropic laminates in the LPs space). *The feasible region in the LPs space of all anisotropic laminates composed of N plies $\Pi_N := \{\mathbf{p}[\theta(z^*)] \mid \forall \theta(z^*) \in \Theta_N\}$ is a non-convex bounded subset of \mathbb{R}^{12} for every $N > 1$ ($N \in \mathbb{N}$).*

Proof. To show the boundedness, the argument is the same as the proof of Proposition 9.2. For the non-convexity, the same argument of Proposition 9.2 is used, but settled in the (ξ_3, ξ_1) plane. Adopting the integral description,

$$\xi_1 = \int_0^1 \cos 4\theta(z^*) dz^*, \quad \xi_3 = \int_0^1 \cos 2\theta(z^*) dz^*. \quad (9.18)$$

Let $\check{P} = (1, 1)$ and $\hat{P} = (1 - \frac{2}{N}, 1)$ be the same points used for Proposition 9.2. These two points belong to Π_N . In fact, \check{P} corresponds to layup functions of the form $\sum_{i=1}^N 0\chi[\Delta z_i^*]$, whilst \hat{P} corresponds to layup functions of the form $\sum_{i=1}^{N-1} 0\chi[\Delta z_i^*] + (-\frac{\pi}{2} + 0)\chi[\Delta z_N^*]$, as it can be easily verified. The convexity condition, to be confuted, reads:

$$\begin{pmatrix} \xi_3[\tilde{\theta}(z^*)] \\ \xi_1[\tilde{\theta}(z^*)] \end{pmatrix} = \alpha \hat{P} + (1 - \alpha) \check{P} = \alpha \begin{pmatrix} 1 - \frac{2}{N} \\ 1 \end{pmatrix} + (1 - \alpha) \begin{pmatrix} 1 \\ 1 \end{pmatrix} \quad (9.19)$$

for some $\tilde{\theta}(z^*) \in \Theta_N$ and for all $\alpha \in [0, 1]$. Considering the second component of Eq. (9.19), $\tilde{\theta}(z^*)$ is necessarily of the form

$$\tilde{\theta}(z^*) = \sum_{i=1}^M c_1 \chi[\Delta z_i^*] + \sum_{i=M+1}^N c_2 \chi[\Delta z_i^*] \quad (9.20)$$

with $c_1, c_2 \in \{0, -\frac{\pi}{2}, \frac{\pi}{2}\}$ and $M < N$, $M \in \mathbb{N}$. As a consequence, it is easy to see that, for all combinations of c_1 and c_2 , $\xi_3[\tilde{\theta}(z^*)] \in \{-1, 1, -1 + 2\frac{M}{N}, 1 - 2\frac{M}{N}\}$. The first component of Eq. (9.19) reads $\{-1, 1, -1 + 2\frac{M}{N}, 1 - 2\frac{M}{N}\} = 1 - \frac{2\alpha}{N}$, which either cannot be satisfied regardless of α or violates the condition $M \in \mathbb{N}$. Considerations similar to those of the proof of Proposition 9.2 can also be repeated for this case, allowing to conclude the proof. ■

Proposition 9.5 (Non-convexity of the feasible domain of orthotropic laminates in the LPs space). *The feasible region in the LPs space of all membrane-orthotropic laminates composed of N plies $\Pi_N^{Ort} := \{\mathbf{p}[\theta(z^*)] \mid \Phi_0^{A^*} - \Phi_1^{A^*} = K^{A^*} \frac{\pi}{4}, K^{A^*} \in \{0, 1\}, \forall \theta(z^*) \in \Theta_N\}$ is a non-convex bounded subset of \mathbb{R}^{12} for every $N > 1$ ($N \in \mathbb{N}$).*

Proof. The proof follows straightforwardly from the previous ones. Indeed, points \hat{P} and \check{P} used in the proof of Proposition 9.4 correspond to membrane-orthotropic laminates (they are a particular case of those chosen in the proof of Proposition 9.2 and 9.3). Therefore, the proof can be considered concluded. ■

Propositions 9.2 and 9.4 claim that, for an anisotropic laminate, the feasible region Π_N , in terms of LPs or PPs, is a non-convex set. Propositions 9.3 and 9.5 state that the non-convexity of the feasible domain holds also in the case of laminates having an orthotropic membrane stiffness tensor. Specifically, the non-convexity is maintained in the projection of the 12-D feasible domain onto either the (ρ_1, ρ_{0K}) or the (ξ_3, ξ_1) plane¹.

A way to visualise the non-convexity of the feasible domain is, trivially, to plot all the possible points of Π_N and Π_N^{Ort} , projected in the corresponding plane according to the anisotropy representation, for an arbitrary number of plies N . Inasmuch as the number of all the possible SSs grows exponentially with the number of layers N , a sampling step is assumed. It is convenient to introduce the notion of *number of groups*, denoted by m , which is the number of distinct orientations within a SS. The number of plies associated to the i -th orientation is denoted by n_i (obviously $\sum_{i=1}^m n_i = N$). Figure 9.2 shows the feasible domain projections for a laminate having $N = 4$ plies ($K = 0$). Indeed, the projected feasible domains are non-convex sets.

In (Grenestedt & Gudmundson, 1993), it was claimed that the feasibility domain in the LPs space is convex. The thesis and the proof of this claim are erroneous. The authors considered one of the twelve components of \mathbf{p} at time. Each component of \mathbf{p} is a

¹In the proof of Proposition 9.3, the non-convexity appears in the (ρ_1, ρ_0) plane. However, since the points \hat{P} and \check{P} correspond to orthotropic laminates with $K^{A^*} = 0$, the line segment delimited by the two points is still not included in the projection of the feasible domain onto the (ρ_1, ρ_{0K}) plane.

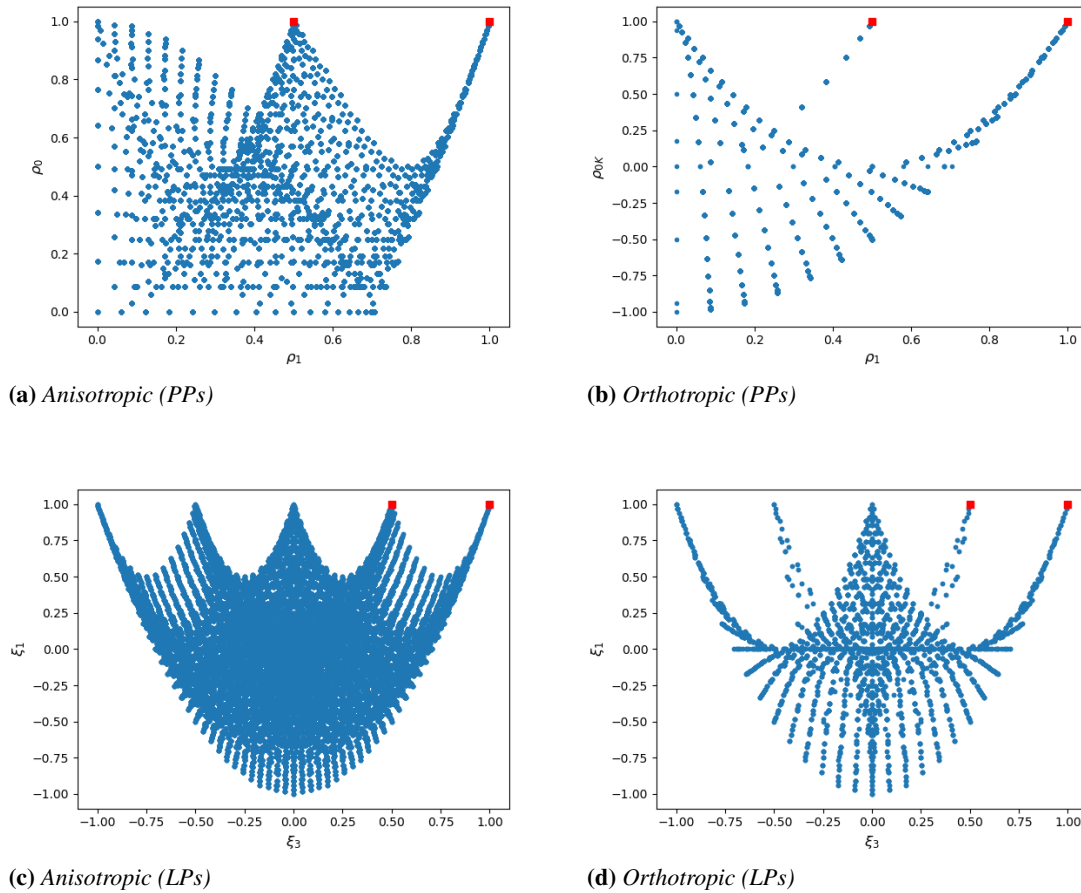


Figure 9.2: Feasibility domain projections for anisotropic (on the left) and membrane-orthotropic (on the right) laminates ($K = 0$) of $N = 4$ plies, on the top in terms of PPs, on the bottom in terms of LPs (discretisation step = 5°). In red the points \hat{P} and \check{P} used in the proofs of Section 9.1.3.

continuous function whose range is a continuous bounded set: in \mathbb{R} such a set (a segment) is necessary convex. Moreover, considering Lemma 9.1, one cannot conclude that a set is convex by knowing that some (not all) of its projections are convex sets. The crucial point is that the components of \mathbf{p} are not independent, since they rely on the same SS. This mutual influence is the actual reason of the shrinkage of the feasible domain from the 12D parallelepiped, as Figure 9.2 clearly shows.

However, a laminate has always a finite number of plies, which makes the determination of Π_N challenging. This is one of the main aspect this Chapter would try to address.

9.1.4 Some Exact Solutions for Geometrical Bounds

In this Section, only anisotropic laminates, in the PPs space, will be considered. The non-convexity of the feasible region Π_N is preserved in the projection onto the (ρ_1, ρ_0) plane.

Figure 9.3 shows some results for the cases $N = 2, \dots, 7$, equivalent to the cases

$m = 2, \dots, 7$ with n_i mutually equal. Figure 9.4 shows the feasibility domain in 3D

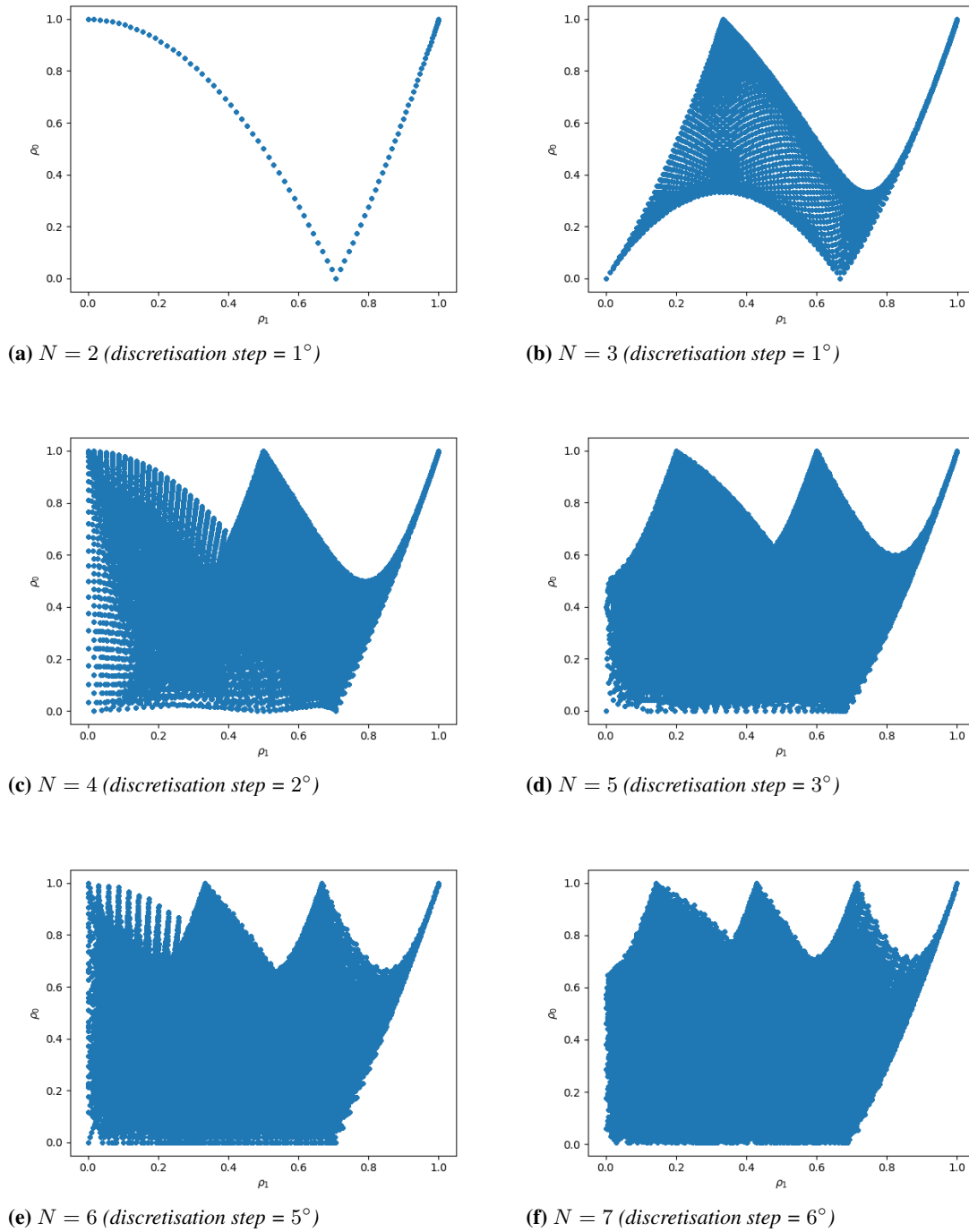


Figure 9.3: Feasibility domain projection onto the plane (ρ_1, ρ_0) for anisotropic laminates of N plies (equivalent to consider laminates with m distinct orientations, all of them appearing the same number of times within the SS)

for the cases $N = 3, 4$. In purple the geometrical bound of Eq. (4.44). It is evident the non-convexity of the feasible domain, which may degenerate to a curve or to a point. In fact, it is easy to see that, if $N = 1$ or $m = 1$, i.e. for laminates wherein all plies share a

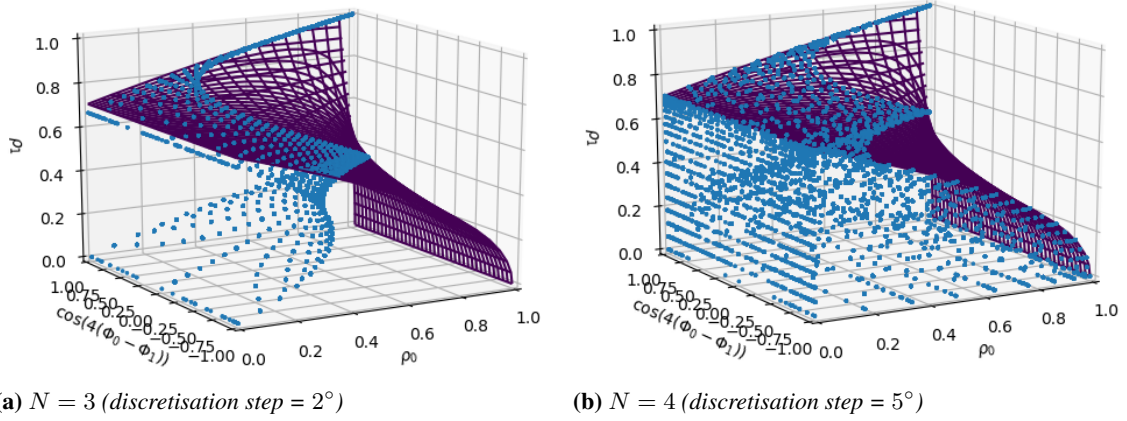


Figure 9.4: Feasibility domain in the space $(\rho_1, \rho_0, \cos 4(\Phi_0^{A*} - \Phi_1^{A*}))$ for anisotropic laminates of $N = 3, 4$ plies. In purple the geometrical bound of Eq. (4.44).

single orientation, $\rho_0 = \rho_1 = 1$.

More interesting is the case $m = 2$. After few calculations, considering that $n_2 = N - n_1$, one achieves the following relation:

$$\rho_0 = \sqrt{\lambda^2 + (1 - \lambda)^2 + 2\lambda(1 - \lambda) \left\{ \left[\frac{\rho_1^2 - \lambda^2 - (1 - \lambda)^2}{2\lambda(1 - \lambda)} \right]^2 - 1 \right\}}, \quad (9.21)$$

or, in the implicit form:

$$F_2(\rho_0, \rho_1, \lambda) := \rho_0 - \sqrt{\lambda^2 + (1 - \lambda)^2 + 2\lambda(1 - \lambda) \left\{ \left[\frac{\rho_1^2 - \lambda^2 - (1 - \lambda)^2}{2\lambda(1 - \lambda)} \right]^2 - 1 \right\}}, \quad (9.22)$$

where $\lambda := n_1/N$. Equation (9.21) means that, for $m = 2$, the locus of lamination points, i.e. the pairs (ρ_1, ρ_0) , is represented by a family of curves, parametrised with the relative number of plies of each orientation within the SS. Equation (9.21) intersects the axis $\rho_0 = 1$ for the following values of ρ_1 :

$$\begin{cases} 1 - 2\lambda, & \text{if } \lambda \leq 1/2, \\ 2\lambda - 1, & \text{if } \lambda \geq 1/2, \\ 1, & \text{if } \lambda = N, \end{cases} \quad (9.23)$$

in perfect agreement with the proof of Proposition 9.2. The family of implicit curves, expressed by Eq. (9.22) in the form of $F_2(\rho_0, \rho_1, \lambda) = 0$, admits envelope, represented by the well-known geometrical-bound $\rho_0 = 2\rho_1^2 - 1$ (Vannucci, 2012a). As an example, Figure 9.5 shows the lamination points locus for a laminate having $N = 20$, $m = 2$, when n_1 varies in the range $[0, N]$ as a subset of \mathbb{N} . The analytic solution of Eq. (9.21) is represented by the red curves. It is noteworthy the discrete nature of the locus, due to the

discrete nature of the stack.

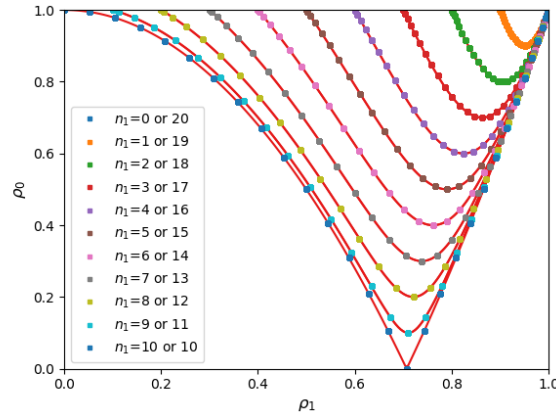


Figure 9.5: Lamination points for $N = 20$, $m = 2$ (discretisation step = 3°).

The process may be conceptually extended to higher number of groups. However, computations become intricate. For the sake of simplicity, consider the case $m = 3$. Equations (9.3) and (9.4) can be rearranged as (see Appendix A)

$$\rho_0 = \frac{1}{N} \sqrt{\sum_{i=1}^3 n_i^2 - 2 \sum_{i=1}^2 \sum_{j=i+1}^3 n_i n_j + 4 \sum_{i=1}^2 \sum_{j=i+1}^3 n_i n_j \cos^2(2\Delta\theta_{ij})}, \quad (9.24)$$

$$\rho_1 = \frac{1}{N} \sqrt{\sum_{i=1}^3 n_i^2 + 2 \sum_{i=1}^2 \sum_{j=i+1}^3 n_i n_j \cos(2\Delta\theta_{ij})}. \quad (9.25)$$

Substituting, for example, the expression of $\cos(2\Delta\theta_{13})$ from Eq. (9.25) into Eq. (9.24), one obtains

$$\begin{aligned} F_3(\rho_0, \rho_1; \Delta\theta_{12}, \Delta\theta_{23}) := & \rho_0 - \frac{1}{N} \left[\sum_{i=1}^3 n_i^2 - 2 \sum_{i=1}^2 \sum_{j=i+1}^3 n_i n_j \right. \\ & \left. + 4 \sum_{i=1}^2 n_i n_{(i+1)} \cos^2(2\Delta\theta_{i(i+1)}) \right. \\ & \left. + \frac{1}{n_1 n_3} \left(N^2 \rho_1^2 - \sum_{i=1}^3 n_i^2 - 2 \sum_{i=1}^2 n_i n_{(i+1)} \cos(2\Delta\theta_{i(i+1)}) \right)^2 \right]^{1/2}. \end{aligned} \quad (9.26)$$

For the envelope, the following system must be solved:

$$\begin{cases} F_3(\rho_0, \rho_1; \Delta\theta_{12}, \Delta\theta_{23}) = 0, \\ \frac{\partial F_3}{\partial \Delta\theta_{12}}(\rho_0, \rho_1; \Delta\theta_{12}, \Delta\theta_{23}) = 0, \\ \frac{\partial F_3}{\partial \Delta\theta_{23}}(\rho_0, \rho_1; \Delta\theta_{12}, \Delta\theta_{23}) = 0, \end{cases} \quad (9.27)$$

which simplifies to

$$\begin{cases} F_3(\rho_0, \rho_1; \Delta\theta_{12}, \Delta\theta_{23}) = 0, \\ \sin(2\Delta\theta_{12}) \left[N^2\rho_1^2 - \sum_{j=1}^3 n_j^2 - 2n_1(n_2 + n_3) \cos(2\Delta\theta_{12}) - 2n_2n_3 \cos(2\Delta\theta_{23}) \right] = 0, \\ \sin(2\Delta\theta_{23}) \left[N^2\rho_1^2 - \sum_{j=1}^3 n_j^2 - 2n_3(n_1 + n_2) \cos(2\Delta\theta_{23}) - 2n_1n_2 \cos(2\Delta\theta_{12}) \right] = 0. \end{cases} \quad (9.28)$$

Four are the possibilities to annihilate the last two expressions of Eq. (9.28).

Case A: $2\Delta\theta_{12} = K_{12}\pi$, $2\Delta\theta_{23} = K_{23}\pi$, $K_{12}, K_{23} \in \mathbb{Z}$. Therefore, $\cos(2\Delta\theta_{i(i+1)}) = (-1)^{K_{i(i+1)}}$, $i = 1, 2$. This case corresponds to a SS composed by parallel laminae. This condition corresponds to the point $\rho_0 = \rho_1 = 1$.

Case B: $2\Delta\theta_{12} = K_{12}\pi$, $2\Delta\theta_{23} \neq K_{23}\pi$, $K_{12}, K_{23} \in \mathbb{Z}$. From Eq. (9.28)₃, one obtains the expression of $\cos(2\Delta\theta_{23})$, and thus

$$\begin{cases} \cos(2\Delta\theta_{23}) = \frac{N^2\rho_1^2 - \sum_{i=1}^3 n_i^2 - 2n_1n_2(-1)^{K_{12}}}{2n_3(n_1 + n_2)}, \\ \rho_0 = \frac{1}{N} \left[\sum_{j=1}^3 n_j^2 - 2 \sum_{i=1}^2 \sum_{j=i+1}^3 n_i n_j + 4n_1n_2 + 4n_3(n_1 + n_2) \cos^2(2\Delta\theta_{23}) \right]^{1/2}. \end{cases} \quad (9.29)$$

Only the case $K_{12} = 0$ is effective, corresponding to the case $m = 2$, because orientations 1 and 2 coincide.

Case C: $2\Delta\theta_{12} \neq K_{12}\pi$, $2\Delta\theta_{23} = K_{23}\pi$, $K_{12}, K_{23} \in \mathbb{Z}$. This case is analogous to case B, exchanging indices 1, 2 with 2, 3, respectively. Figure 9.6 depicts the curves of cases B or C for a laminate having $N = 6$, $m = 3$ and $n_1 = 1$, $n_2 = 2$, $n_3 = 3$, obtained by permuting indices 1, 2, 3 modulo 3. This is due to the arbitrary substitution of $\cos(2\Delta\theta_{13})$ in the derivation of Eq. (9.26). Because of the cyclic permutation, cases B and C coincide.

Case D: $2\Delta\theta_{12} \neq K_{12}\pi$, $2\Delta\theta_{23} \neq K_{23}\pi$, $K_{12}, K_{23} \in \mathbb{Z}$. Subtracting term by term the last two formulæ of Eq. (9.28), one gets the condition $\cos(2\Delta\theta_{12}) = \cos(2\Delta\theta_{23})$.

$$\begin{cases} \cos(2\Delta\theta_{12}) = \cos(2\Delta\theta_{23}) = \frac{N^2\rho_1^2 - \sum_{j=1}^3 n_j^2}{2 \sum_{i=1}^2 \sum_{j=i+1}^3 n_i n_j}, \\ F_3(\rho_0, \rho_1; \Delta\theta_{12}, \Delta\theta_{23}) = 0. \end{cases} \quad (9.30)$$

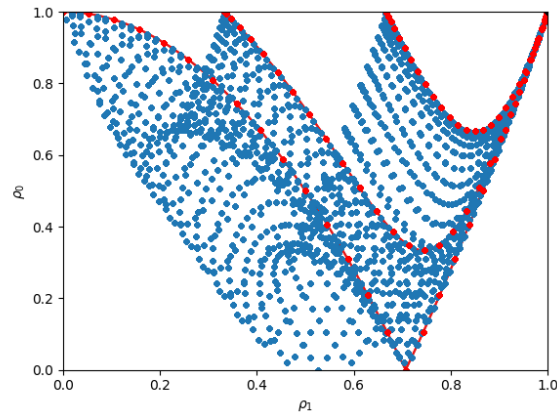


Figure 9.6: Cases B or C for $n_1 = 1$, $n_2 = 2$, $n_3 = 3$, (discretisation step = 3°) by permuting indices 1, 2, 3 modulo 3.

Figure 9.7 depicts the bound. It can be shown that it defines a lower bound for the feasible

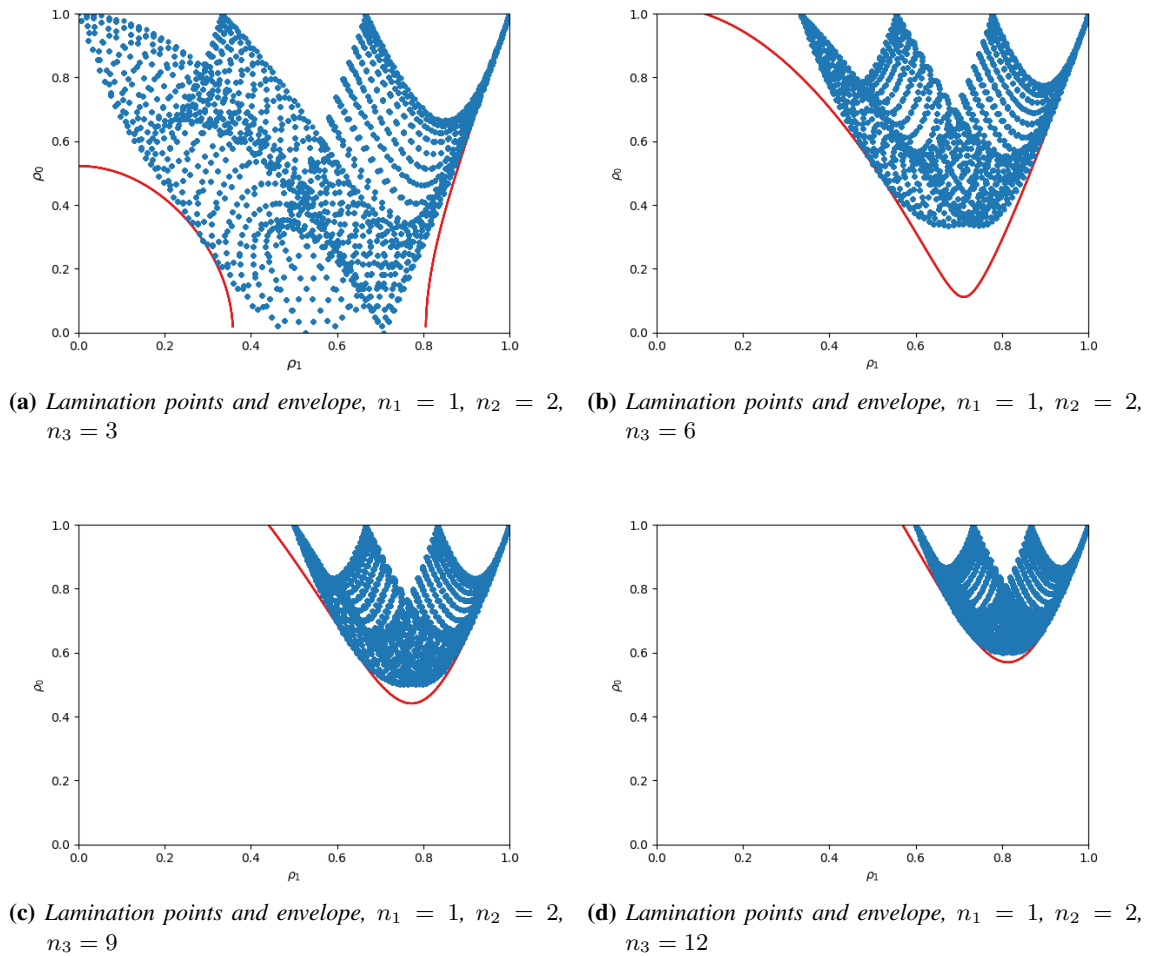


Figure 9.7: Case D for four different laminates (discretisation step = 3°).

region.

A further case, arising from a different change of variables, is noteworthy to be considered.

Case E: $2\Delta\theta_{12} \neq K_{12}\pi, 2\Delta\theta_{23} \neq K_{23}\pi, K_{12}, K_{23} \in \mathbb{Z}$. Subtracting term by term the last two formulæ of Eq. (9.28), one gets the condition $\cos(2\Delta\theta_{12}) = \cos(2\Delta\theta_{23})$. Note that $\cos(2\Delta\theta_{13}) = \cos(2\Delta\theta_{12} + 2\Delta\theta_{23})$. From Eq. (9.25) one obtains the value of parameter $\cos(2\Delta\theta_{12})$.

$$\begin{cases} \cos(2\Delta\theta_{12}) = \cos(2\Delta\theta_{23}) = \frac{N^2\rho_1^2 - \sum_{i=1}^3 n_i^2 - 2n_1n_3}{2n_2(n_1 + n_3)}, & \text{if } 2\Delta\theta_{12} = -2\Delta\theta_{23}, \\ \cos(2\Delta\theta_{12}) = \cos(2\Delta\theta_{23}) = \frac{-b \pm \sqrt{b^2 - 4c}}{2}, & \text{if } 2\Delta\theta_{12} = 2\Delta\theta_{23}, \\ F_3(\rho_0, \rho_1; \Delta\theta_{12}, \Delta\theta_{23}) = 0, \end{cases} \quad (9.31)$$

where

$$b = \frac{n_2(n_1 + n_3)}{2n_1n_3}, \quad c = -\frac{N^2\rho_1^2 - \sum_{i=1}^3 n_i^2 + 2n_1n_3}{4n_1n_3}. \quad (9.32)$$

Figure 9.8 depicts the bound. The area it encloses is always inside the actual feasible region.

9.1.4.1 Exact Analytic Expression of the Feasible Domain for the

Case $n_1 = n_2 = n_3 = n$

In the case $n_1 = n_2 = n_3 = n$, for every $N = 3n$, the aforementioned relationships can be further simplified. It is noteworthy that for this case, Eqs. (6.26) and (9.31) provide the analytic expression of the actual projection of the feasible domain, i.e.

$$\begin{cases} 0 \leq \rho_0 \leq 1, \\ 0 \leq \rho_1 \leq 1, \\ \rho_0 \leq \rho_1 |3\rho_1 + 2|, \\ \rho_0 \geq \rho_1 |3\rho_1 - 2|, \\ \rho_0 \leq \frac{1}{3} \sqrt{1 + \frac{(9\rho_1^2 - 5)^2}{2}}, \end{cases} \quad (9.33)$$

which, of course, does not depend on N . Figure 9.9 shows the result for this case. At the best of our knowledge, it is the first time that an exact closed-form expression for the projection of feasibility domain of a laminate is given.

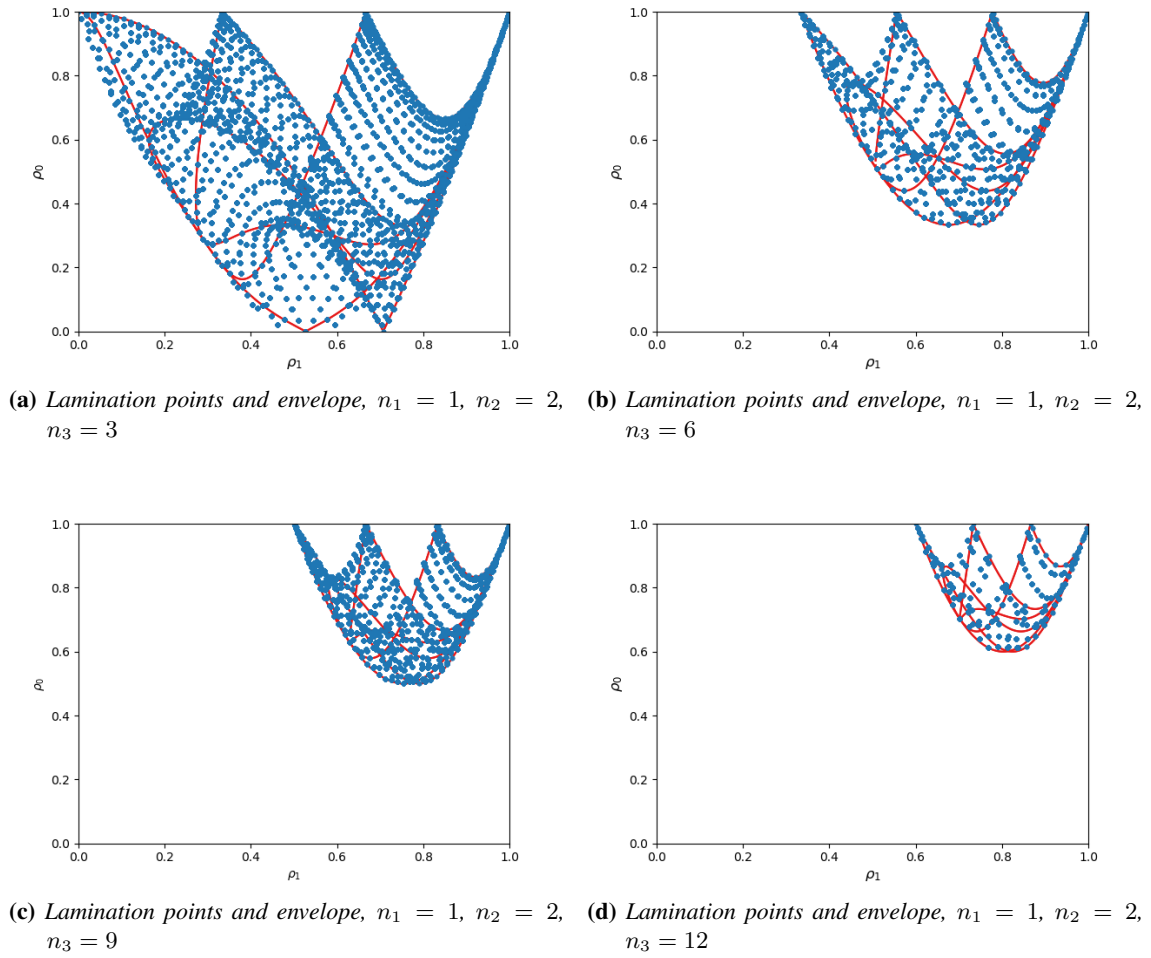


Figure 9.8: Case E for four different laminates.

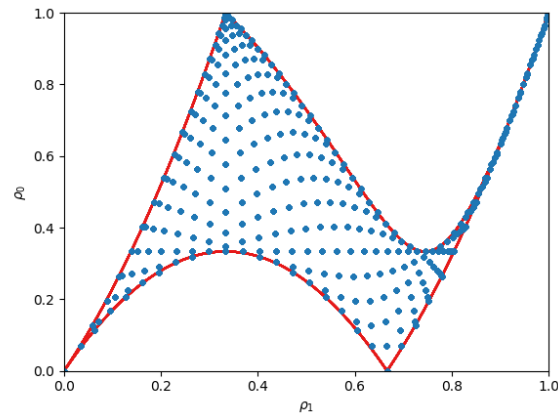


Figure 9.9: Lamination points and envelope for the case $n_1 = n_2 = n_3 = n$ (discretisation step = 3°).

9.1.5 New Geometrical Bounds

It is possible to infer that Eq. (9.22) evaluated for $\lambda = 1/N$, i.e. $F_2(\rho_0, \rho_1, 1/N) = 0$, is, in any case, a geometrical bound for anisotropic laminates. Similarly, $F_2((-1)^K \rho_{0K}, \rho_1, 1/N) = 0$ is a geometrical bound for membrane-orthotropic laminates.

From the proofs of Propositions 9.2 and 9.3, there exists a region in the (ρ_1, ρ_0) plane that is excluded from the feasible domain projection. This results has a physical interpretation. For a SS made of N plies, the case $m = 2$, $n_1 = 1$, $n_2 = N - 1$ is the minimal condition to make the feasible domain not to degenerate into a point (case $n_1 = 0$). Therefore, no lamination points can lie in the epigraph of $F_2(\rho_0, \rho_1, 1/N) = 0$. If so, plies would be a non-integer number, leading, thus, to a contradiction. The excluded area is more important for relative small N , whilst it can be negligible as N increases.

Therefore, new geometrical bounds can be proposed for a general anisotropic laminate:

$$\begin{cases} 0 \leq \rho_0 \leq 1, \\ 0 \leq \rho_1 \leq 1, \\ 2\rho_1^2 \leq \frac{1 - \rho_0^2}{1 - (-1)^K \rho_0 \cos 4(\Phi_0^{A*} - \Phi_1^{A*})}, \\ F_2(\rho_0, \rho_1, 1/N) \leq 0. \end{cases} \quad (9.34)$$

Moreover, for a laminate having an orthotropic membrane stiffness tensor, the above bounds simplifies to

$$\begin{cases} -1 \leq \rho_{0K} \leq 1, \\ 0 \leq \rho_1 \leq 1, \\ 2\rho_1^2 - 1 - (-1)^K \rho_{0K} \leq 0 \\ F_2((-1)^K \rho_{0K}, \rho_1, 1/N) \leq 0. \end{cases} \quad (9.35)$$

It is noteworthy that, for a quasi-homogeneous laminate, Eqs. (9.34) and (9.35) offer a description of the laminate feasible domain richer than those available in the literature (Miki, 1982; Vannucci, 2012a).

Figure 9.10 shows the Vannucci's geometrical bounds (Vannucci, 2012a) and the proposed bound for anisotropic (Eq. (9.34)) and membrane-orthotropic (Eq. (9.35)) laminates with $N = 4$.

It is remarkable that the proposed bounds formulation depends also on the number of plies of the laminate.

9.2 On the Necessary and Sufficient Conditions for Uncoupling and Homogeneity

In this Section, a discussion on the necessary and sufficient conditions to get membrane/bending uncoupled and/or homogeneous laminates is presented. It is proved

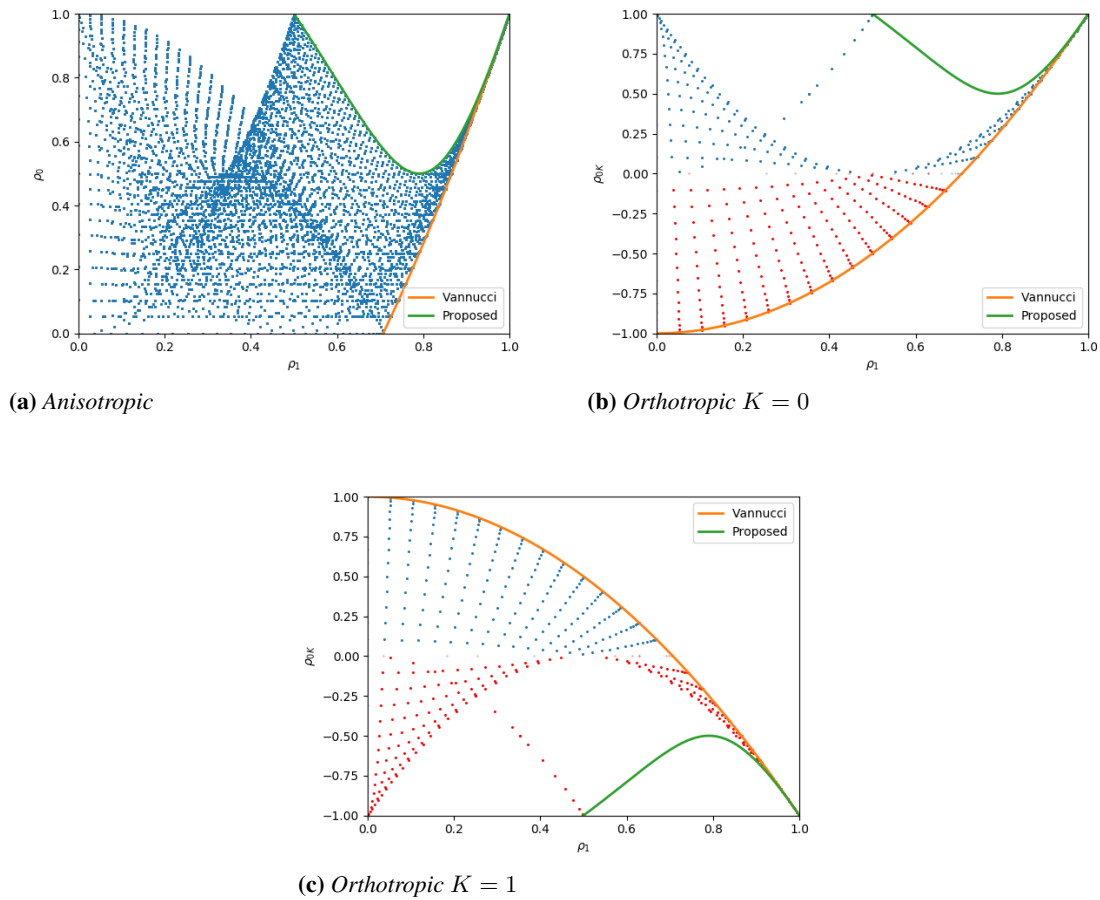


Figure 9.10: Vannucci's geometrical bound (Vannucci, 2012a) and proposed bounds for a laminate having $N = 4$ (discretisation step = 3°)

that, when the distinct orientations within the stack are two, quasi-triviality (see Section 4.3) represents a necessary and sufficient condition to achieve uncoupling and/or quasi-homogeneity. More in general, quasi-triviality is only a sufficient condition.

Up to now, it is not clear if quasi-triviality is a sufficient or even necessary condition to have uncoupled and/or homogeneous laminates. This Chapter aims at clarifying this aspect, by showing that quasi-triviality is, in general, only a sufficient condition. However, for a particular case, quasi-triviality becomes also a necessary condition. In other words, for that particular case, QT solutions constitute the full set of all possible uncoupled and/or homogeneous SSs.

Two Theorems of Linear Algebra are used to prove that quasi-triviality is only a sufficient condition for uncoupling and/or homogeneity for $m \geq 3$, and to prove that, for $m = 2$, quasi-triviality is also a necessary one. The results are based on the following two Theorems by Green (1916), which are reported here for the sake of completeness.

Theorem 9.1 (Theorem 1 from (Green, 1916)). *Consider the p -dimensional cube $A := (-\pi/2, \pi/2)^p$. Let y_1 and y_2 be functions of the p independent variables u_1, u_2, \dots, u_p for which all partial derivatives of the first order, $\partial y_1 / \partial u_k, \partial y_2 / \partial u_k, (k = 1, 2, \dots, p)$ exist*

throughout the region A . Furthermore, suppose that one of the functions, i.e. y_i , does not vanish in A . Then, if all the two-rowed determinants in the matrix

$$\begin{bmatrix} y_1 & y_2 \\ \frac{\partial y_1}{\partial u_1} & \frac{\partial y_2}{\partial u_1} \\ \frac{\partial y_1}{\partial u_2} & \frac{\partial y_2}{\partial u_2} \\ \vdots & \vdots \\ \frac{\partial y_1}{\partial u_p} & \frac{\partial y_2}{\partial u_p} \end{bmatrix} \quad (9.36)$$

vanish identically in A , y_1 and y_2 are linearly dependent in A .

Theorem 9.2 (Theorem 2 from (Green, 1916)). Consider the p -dimensional cube $A := (-\pi/2, \pi/2)^p$. Moreover, consider the matrix $\mathbf{M}_s(y_1, y_2, \dots, y_r)$ in which the first row consists of the functions y_1, y_2 up to y_r (for some r) and the other s rows of derivatives of these functions:

$$\mathbf{M}_s = \begin{bmatrix} y_1 & y_2 & \dots & y_r \\ y_1^{(1)} & y_2^{(1)} & \dots & y_r^{(1)} \\ \vdots & \vdots & \vdots & \vdots \\ y_1^{(s)} & y_2^{(s)} & \dots & y_r^{(s)} \end{bmatrix}. \quad (9.37)$$

Let the set of n functions y_1, y_2, \dots, y_n of the p independent variables u_1, u_2, \dots, u_p possess enough partial derivatives, of any order whatever, to form a matrix $\mathbf{M} = \mathbf{M}_{(n-2)}(y_1, y_2, \dots, y_n)$, of n columns and $n-1$ rows, in which at least one of the $(n-1)$ -rowed determinants, i.e.

$$\mathbf{W}_n = \begin{bmatrix} y_1 & y_2 & \dots & y_{n-1} \\ y_1^{(1)} & y_2^{(1)} & \dots & y_{n-1}^{(1)} \\ \vdots & \vdots & \vdots & \vdots \\ y_1^{(n-2)} & y_2^{(n-2)} & \dots & y_{n-1}^{(n-2)} \end{bmatrix}, \quad (9.38)$$

vanishes nowhere in A . Moreover, suppose that all of the first derivatives of each of the elements of the above matrix \mathbf{M} exist, and adjoin to the matrix \mathbf{M} such of these derivatives as do not already appear in \mathbf{M} , to form the new matrix $\mathbf{M}' = \mathbf{M}_q(y_1, y_2, \dots, y_n)$, which has n columns and at least n rows, so that $q \geq n-1$. Then if all the n -rowed determinants of the matrix \mathbf{M}' in which the determinant \mathbf{W}_n is a first minor vanish identically in A , the functions y_1, y_2, \dots, y_n are linearly dependent in A .

Thanks to the above Theorems, the following Proposition can be introduced.

Proposition 9.6 (Condition for quasi-triviality to be a necessary and sufficient one for quasi-homogeneity). *QT SSs represent a necessary and sufficient condition to satisfy membrane/bending uncoupling and/or homogeneity requirements when the number of saturated groups m is equal to two.*

Proof. Consider a laminate with a SS composed of m different orientations and apply Theorem 9.1 to the set of functions $e^{i\beta\theta_j}$, $j = 1, \dots, m$, $\beta = 2, 4$. When $m = 2$, Eq. (9.36) reads

$$\begin{bmatrix} e^{i\beta\theta_1} & e^{i\beta\theta_2} \\ i\beta e^{i\beta\theta_1} & 0 \\ 0 & i\beta e^{i\beta\theta_2} \end{bmatrix}. \quad (9.39)$$

One can easily check that none of the two-rowed determinants of Eq. (9.39) is singular in $A = (-\pi/2, \pi/2)^2$. In fact, the determinants would vanish if $e^{i\beta\theta_1} e^{i\beta\theta_2} = 0$. However, this condition reads $\cos \beta(\theta_1 + \theta_2) + i \sin \beta(\theta_1 + \theta_2)$, which clearly is never zero. Therefore, it follows that, for $m = 2$, the combination of functions $e^{i\beta\theta_j}$, $j = 1, 2$, $\beta = 2, 4$ is linearly independent on A . Accordingly, the proof can be considered concluded. ■

Remark 9.1. *Proposition 9.6 means that uncoupled and/or homogeneous laminates imply the annealing of the sum of coefficients $\{b_k\}$ and/or $\{c_k\}$ associated to each orientation. In other words, when $m = 2$, uncoupled and/or homogeneous laminates are QT and vice versa.*

Remark 9.2. *In the light of Theorem 9.1 and Proposition 9.6, it is not possible to obtain extensionally-isotropic laminates with only two different orientations, since the sum of coefficients a_k cannot be zero. This result is in agreement with the evidence that no isotropic SS is known having only two distinct orientation angles (Warren & Norris, 1953; K. M. Wu & Avery, 1992; Vannucci, 2017).*

Remark 9.3. *For $m \geq 3$, there exist uncoupled and/or homogeneous laminates which are not QT. It is a result discussed in (Vannucci & Verchery, 2001b), where the authors have shown that the QT solutions are not the only possible ones. As a consequence, since the combination of exponential functions may sum up to zero for some particular choice of orientations, there exist uncoupled and/or homogeneous laminates which are not necessarily QT. Theorem 9.2 formalises this fact.*

9.3 Conclusions

This Chapter provided an answer to research question RQ4.

Accordingly, the choice of using Polar parameters to describe plane anisotropy seems more valuable, in view of the nice physical properties (invariance and relationships with material symmetries) enjoyed by the Polar parameters.

The Chapter clarifies some preliminary aspects of the feasibility domain determination problem. Although tackling the problem in full generality is probably impractical, a closed form of stricter feasibility bounds has been derived in terms of the membrane stiffness tensor Polar parameters. This is an aspect of paramount importance in the optimisation of composite laminates, where the anisotropy is tailored to satisfy some merit functions and constraints.

Moreover, the problem of retrieving sufficient and necessary conditions for membrane/bending uncoupling and homogeneity has been addressed. It has been shown that, in general, quasi-triviality is only a sufficient condition. It becomes also a necessary one if the stacking sequence has only two distinct orientations.

Linear Models of Stiffened Plates via Γ -convergence

L'operaio conosce cento parole, il padrone mille. Per questo è lui il padrone.

Lorenzo Milani

This Chapter aims at answering research question RQ5.

Thin-walled structures are widely used in many engineering fields, such as aeronautic, aerospace and naval structures, pressurised vessels design, civil and mechanical constructions, etc. Since the widespread use of such structures, many models, based on *a priori* kinematics assumptions on the displacement field, has been developed in the history of Mechanics, in order to design and size structures, and to predict the behaviour of actual loaded structures. Even though these models have been used successfully by generations of engineers, scientists and - why not - students, they all defect the fact of relying on heuristic, yet reasonable, assumptions. From a theoretical and ontological point of view, as reasonable as these assumptions may sound, they are hypotheses that jeopardise the validity of the models.

In the last years, attention has been paid to the rigorous justification of the classical theories and models of Mechanics: beams, shells, plates, etc. The common approach is to study the asymptotic behaviour of 3-dimensional problem formulations and letting some "small" parameter going to zero (plate thickness, beam cross section etc.). After a suitable passage to the limit, the asymptotic behaviour is obtained and, possibly, the limit solution is recognised as one of the classic models.

In model dimension reduction, a special position is reserved to junctions of bodies, possibly having different asymptotic dimensions: for instance, the junction of a 3D-body with a "2D-body". Several contributes, especially from the "French school", can be counted (Ciarlet et al., 1989; Le Dret, 1989; Ciarlet, 1990; Le Dret, 1992; Gruais,

1993a, 1993b). More recently, (Nardinocchi, 2002; Gaudiello et al., 2007; Gaudiello & Zappale, 2010; Leugering et al., 2018) have studied the junction between multi-domain bodies using classical variational techniques.

Conversely, in the last few years, especially in the "Italian school", the dimension reduction problem has been faced via Γ -convergence, a well-known variational tool, appeared for the first time in the seminal work of Ennio De Giorgi and Tullio Franzoni (De Giorgi & Franzoni, 1975) (see Chapter 5). Among the others, many interesting results have been obtained via Γ -convergence. For example, in (Freddi et al., 2007) authors justify the Vlasov theory of torsion and the well-known Bredt's formulæ. Γ -convergence has been successfully used to justify models for beams and plates in linear and non-linear elasticity, in isotropic and anisotropic elasticity, also under residual stress condition or not (Freddi et al., 2004; Freddi et al., 2009; Freddi et al., 2010; Paroni & Tomassetti, 2011; Freddi et al., 2013; Davini et al., 2014a, 2014b).

Curiously, among the work about the limit models of plates and beams, there is a lack of models of stiffened plates. At the best of the candidate's knowledge, only the work by Aufranc (1990) has been found in the literature dealing with this problem of practical interest. However, this work considers an indeed-generalisable case, since the stiffener cross-section scales uniformly. Hereby, it is addressed the problem of the asymptotic model of a stiffened plate in the framework of linear isotropic elasticity, as the plate thickness and the stiffener cross-section go to zero, possibly with different velocities. The variational convergence is obtained via Γ -convergence, a versatile tool which establishes the validation of results on rigorous bases. Moreover, results are not derived with *a priori* assumptions on the deformation kinematics, but in full generality.

A family of rectangular stiffened plates of thickness of order ε presenting a blade-stiffener whose rectangular cross-section scales by ε^w and ε^h is thus considered in this Chapter. As ε goes to zero, the limit problem is identified and, in the case of linear homogeneous isotropic materials, under suitable mild assumptions on the external loads, the three-dimensional equilibrium solution Γ -converges to displacements of the Kirchhoff-Love and Bernoulli-Navier classes. However, depending on the values of the scaling factors, the limit junction conditions affect the limit energy in its form. As a noteworthy result, in no case the limit energy considers all the contributes from all the limit displacement fields of the plate and of the beam.

Section 10.1 introduces the setting of the variational problem, whilst Section 10.2 introduces the mapping from the 3-dimensional equilibrium problem to a scaled family of thin domains. Section 10.3 introduces two compactness results. They are needed for the application of the Direct Method of the Calculus of Variations, as exposed in Section 5.2. Section 10.4 is dedicated to the limit joining conditions on displacements between the plate and the stiffener. In Section 10.5 the expression of the limit energy is obtained, together with the main Γ -convergence Theorem. Section 10.6 shows the strong convergence of minima and minimisers. Finally, Section 10.7 concludes the Chapter with meaningful considerations.

The following notation is used throughout the Chapter. The Euclidean (Frobenius) product is indicated with \cdot and the corresponding induced norm by $|\cdot|$. A generic constant is indicated by letter C : its value may vary line to line. Indices $\alpha, \beta, \gamma, \delta$ take values in the set $\{1, 2\}$, indices a, b, c, d in the set $\{2, 3\}$, and indices i, j in the set $\{1, 2, 3\}$. $\bar{f}_\Omega f(x) dX$ denotes the average value of a function over its domain, i.e. $\frac{1}{|\Omega|} \int_\Omega f(x) dX$.

10.1 Problem Description

Let the real parameter ε , which takes values in a sequence of positive numbers converging to zero, be introduced. The actual 3D structure is a plate-like body of thickness ε and with in-plane dimension $2L \times 2L$ lying in the negative semi-space spanned by x_3 . This body has a blade-like stiffener lying in the positive semi-space spanned by x_3 , as depicted in Figure 10.1. The junction region lies in the plane $x_3 = 0$.

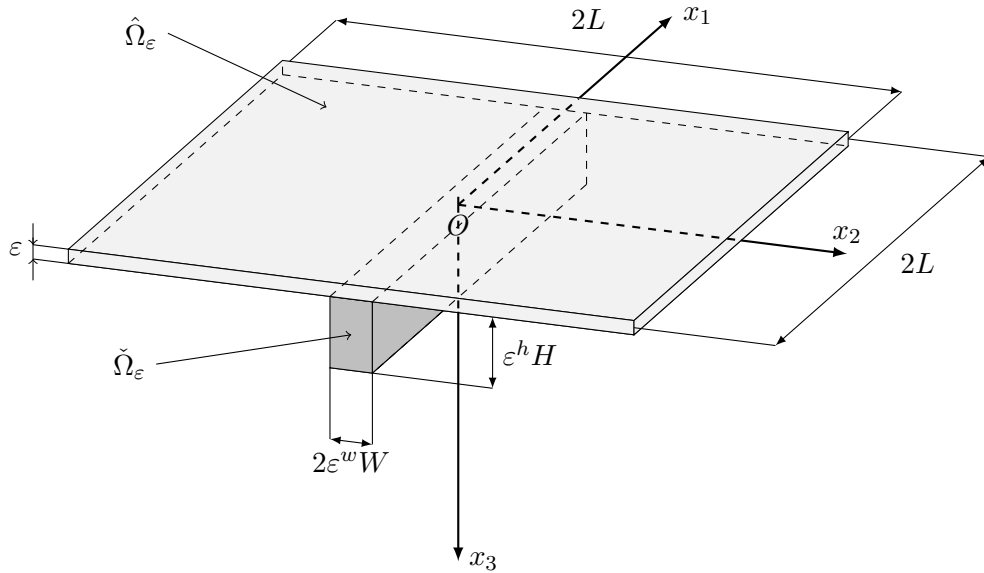


Figure 10.1: Geometry of real problem

Let the plate-like body cross-section domain be denoted by

$$\hat{\omega} := (-L, +L) \times (-L, +L), \quad (10.1)$$

and the cross-section of the stiffener by

$$\check{\omega}_\varepsilon := \varepsilon^w (-W, +W) \times \varepsilon^h (0, H) \quad w, h \in \mathbb{R}^+. \quad (10.2)$$

Hence, the plate-like body domain reads

$$\hat{\Omega}_\varepsilon := \hat{\omega} \times (-\varepsilon, 0), \quad (10.3)$$

the stiffener domain reads

$$\check{\Omega}_\varepsilon := (-L, +L) \times \check{\omega}_\varepsilon, \quad (10.4)$$

the body domain reads

$$\Omega_\varepsilon := \hat{\Omega}_\varepsilon \cup \check{\Omega}_\varepsilon \cup (-L, +L) \times \varepsilon^w(-W, +W) \times \{0\}, \quad (10.5)$$

and the junction domain reads

$$\omega_J^\varepsilon := (-L, +L) \times \varepsilon^w(-W, +W) \times \{0\}. \quad (10.6)$$

For simplicity' sake, consider the body clamped at section $x_1 = +L$, and denote the clamped area by

$$\partial_D \Omega_\varepsilon := \partial_D \hat{\Omega}_\varepsilon \cup \partial_D \check{\Omega}_\varepsilon, \quad (10.7)$$

where $\partial_D \hat{\Omega}_\varepsilon := \{+L\} \times (-L, +L) \times (-\varepsilon, 0)$ and $\partial_D \check{\Omega}_\varepsilon := \{+L\} \times \check{\omega}_\varepsilon$.

Considering Definitions 5.10 and 5.11, the Sobolev's space defined on the set Ω is denoted by

$$H^1(\Omega, \mathbb{R}^3) := \{\mathbf{v} : \Omega \mapsto \mathbb{R}^3 : \mathbf{v} \in L^2(\Omega, \mathbb{R}^3), \nabla \mathbf{v} \in L^2(\Omega, \mathbb{R}^{3 \times 3})\}, \quad (10.8)$$

where

$$L^2(\Omega, \mathbb{R}^3) := \left\{ \mathbf{v} : \Omega \mapsto \mathbb{R}^3 : \left(\int_{\Omega} |\mathbf{v}|^2 \right)^{1/2} < \infty \right\} \quad (10.9)$$

is the L^2 space defined on the same set. Besides, let

$$H_{\text{bc}}^1 := \{\mathbf{v} \in H^1(\Omega_\varepsilon, \mathbb{R}^3) : \mathbf{v} = \mathbf{0} \text{ in } \partial_D \Omega_\varepsilon\} \quad (10.10)$$

denote the set of displacements which satisfy boundary conditions. According to Eq. (5.19), the elastic strain is measured by means of the symmetric second-order tensor ¹

$$\mathbf{E}\mathbf{v} := \frac{\nabla \mathbf{v} + \nabla \mathbf{v}^T}{2}, \quad \mathbf{E}\mathbf{v} \in \text{Sym}. \quad (10.11)$$

symmetric part of the displacements gradient tensor

$$\mathbf{H}\mathbf{v} := \nabla \mathbf{v}, \quad \mathbf{H}\mathbf{v} \in \text{Lin}. \quad (10.12)$$

According to Eq. (5.20), let the stored-energy functional be expressed by $\widetilde{\mathcal{W}}_\varepsilon : \Omega_\varepsilon \mapsto \mathbb{R}^+$, defined as

$$\widetilde{\mathcal{W}}_\varepsilon(\mathbf{v}) := \frac{1}{2} \int_{\Omega_\varepsilon} \mathbb{C}[\mathbf{E}\mathbf{v}] \cdot \mathbf{E}\mathbf{v} \, dX, \quad (10.13)$$

where $\mathbb{C} \in \mathbb{P}\text{sym}$ is the fourth-order elasticity tensor, positive definite, having the usual symmetries (see Theorem 5.6), and coercive. This means that there exists a positive constant C such that the coercivity property expressed by Theorem 5.7 holds.

¹In this Chapter, following a notation typical of Solid Mechanics, the writing $\mathbf{E}\mathbf{v}$ (and similar expressions) must not be intended as a tensor-vector product, but in the sense of the operator \mathbf{E} (it returns the symmetric part of the gradient of the argument) applied to the vector (the argument) \mathbf{v} , i.e. the writing is equivalent to $\mathbf{E} \circ \mathbf{v}$.

The set of displacements of Kirchhoff-Love's type is denoted by

$$\text{KL}(\hat{\Omega}_\varepsilon) := \left\{ \mathbf{u} \in H^1(\hat{\Omega}_\varepsilon) : \exists \hat{\xi}_\alpha \in H^1(\hat{\omega}), \exists \hat{\xi}_3 \in H^2(\hat{\omega}), u_3 = \hat{\xi}_3, u_\alpha = \hat{\xi}_\alpha - x_3 \hat{\xi}_{3,\alpha} \right\}, \quad (10.14)$$

and the set of displacements of Bernoulli-Navier's type by

$$\text{BN}(\check{\Omega}_\varepsilon) := \left\{ \mathbf{u} \in H^1(\check{\Omega}_\varepsilon) : \exists \check{\xi}_1 \in H^1((-L, +L)), \exists \check{\xi}_A \in H^2((-L, +L)), \right. \\ \left. u_1 = \check{\xi}_1 - x_3 \check{\xi}_{3,1} - x_2 \check{\xi}_{2,1}, u_a = \check{\xi}_a(x_1) \right\}. \quad (10.15)$$

Note that the Kirchhoff-Love's displacement components are referred to the plate face lying on the plane $x_3 = 0$ and not, as usual, to the mid-plane. A similar consideration holds for the stiffener, where the displacement field is not referred to the centreline.

Of course, for the particular choice of $\varepsilon = 1$, one has

$$\hat{\Omega} := \hat{\Omega}_1, \quad \check{\Omega} := \check{\Omega}_1, \quad \Omega := \Omega_1. \quad (10.16)$$

10.2 The Scaled Problem

Suppose that the elasticity tensor of the structure may be decomposed as follows:

$$\mathbb{C} := \begin{cases} \hat{\mathbb{C}}, & \text{in } \hat{\Omega}_\varepsilon, \\ \varepsilon^{2q+1} \check{\mathbb{C}}, & \text{in } \check{\Omega}_\varepsilon, \end{cases} \quad (10.17)$$

where $q \in \mathbb{R}$. Consequently, the elastic stored-energy functional of the system is defined as

$$\widetilde{\mathcal{W}}_\varepsilon(\mathbf{u}) = \frac{1}{2} \int_{\hat{\Omega}_\varepsilon} \hat{\mathbb{C}}[\mathbf{E}\mathbf{u}] \cdot \mathbf{E}\mathbf{u} \, dX + \frac{1}{2} \int_{\check{\Omega}_\varepsilon} \varepsilon^{2q+1} \check{\mathbb{C}}[\mathbf{E}\mathbf{u}] \cdot \mathbf{E}\mathbf{u} \, dX. \quad (10.18)$$

As commonly done, after a proper change of variables, the functional is rescaled over a fixed domain (see (Anzellotti et al., 1994)). For the plate, the following mapping is introduced:

$$\hat{\mathbf{q}}_\varepsilon : \hat{\Omega} \mapsto \hat{\Omega}_\varepsilon, \\ \hat{\mathbf{q}}_\varepsilon(x_1, x_2, x_3) := (x_1, x_2, \varepsilon x_3), \\ \hat{\mathbf{Q}}_\varepsilon := \nabla \hat{\mathbf{q}}_\varepsilon = \text{diag}(1, 1, \varepsilon), \\ \hat{\mathbf{u}}_\varepsilon := \hat{\mathbf{Q}}_\varepsilon \mathbf{u} \circ \hat{\mathbf{q}}_\varepsilon. \quad (10.19)$$

Differentiating, one obtains

$$\hat{\mathbf{H}}_\varepsilon \hat{\mathbf{u}}_\varepsilon := (\mathbf{H}\mathbf{u}) \circ \hat{\mathbf{q}}_\varepsilon = \hat{\mathbf{Q}}_\varepsilon^{-1} \mathbf{H} \hat{\mathbf{u}}_\varepsilon \hat{\mathbf{Q}}_\varepsilon^{-1} = \begin{pmatrix} (\mathbf{H}\hat{\mathbf{u}}_\varepsilon)_{11} & (\mathbf{H}\hat{\mathbf{u}}_\varepsilon)_{12} & (\mathbf{H}\hat{\mathbf{u}}_\varepsilon)_{13} \\ (\mathbf{H}\hat{\mathbf{u}}_\varepsilon)_{21} & (\mathbf{H}\hat{\mathbf{u}}_\varepsilon)_{22} & (\mathbf{H}\hat{\mathbf{u}}_\varepsilon)_{23} \\ \frac{(\mathbf{H}\hat{\mathbf{u}}_\varepsilon)_{31}}{\varepsilon} & \frac{(\mathbf{H}\hat{\mathbf{u}}_\varepsilon)_{32}}{\varepsilon} & \frac{(\mathbf{H}\hat{\mathbf{u}}_\varepsilon)_{33}}{\varepsilon^2} \end{pmatrix}, \quad (10.20)$$

and

$$\hat{\mathbf{E}}_\varepsilon \hat{\mathbf{u}}_\varepsilon := (\mathbf{E}\mathbf{u}) \circ \hat{\mathbf{q}}_\varepsilon = \hat{\mathbf{Q}}_\varepsilon^{-1} \mathbf{E} \hat{\mathbf{u}}_\varepsilon \hat{\mathbf{Q}}_\varepsilon^{-1} = \begin{pmatrix} (\mathbf{E}\hat{\mathbf{u}}_\varepsilon)_{11} & (\mathbf{E}\hat{\mathbf{u}}_\varepsilon)_{12} & \frac{(\mathbf{E}\hat{\mathbf{u}}_\varepsilon)_{13}}{\varepsilon} \\ & (\mathbf{E}\hat{\mathbf{u}}_\varepsilon)_{22} & \frac{(\mathbf{E}\hat{\mathbf{u}}_\varepsilon)_{23}}{\varepsilon} \\ \text{sym} & & \frac{(\mathbf{E}\hat{\mathbf{u}}_\varepsilon)_{33}}{\varepsilon^2} \end{pmatrix}. \quad (10.21)$$

In a similar fashion, the following mapping is introduced for the stiffener

$$\begin{aligned} \check{\mathbf{q}}_\varepsilon &: \check{\Omega} \mapsto \check{\Omega}_\varepsilon, \\ \check{\mathbf{q}}_\varepsilon(x_1, x_2, x_3) &:= (x_1, \varepsilon^w x_2, \varepsilon^h x_3), \\ \check{\mathbf{Q}}_\varepsilon &:= \nabla \check{\mathbf{q}}_\varepsilon = \text{diag}(1, \varepsilon^w, \varepsilon^h), \\ \check{\mathbf{u}}_\varepsilon &:= \check{\mathbf{Q}}_\varepsilon \mathbf{u} \circ \check{\mathbf{q}}_\varepsilon. \end{aligned} \quad (10.22)$$

Differentiating, one obtains

$$\check{\mathbf{H}}_\varepsilon \check{\mathbf{u}}_\varepsilon := (\mathbf{H}\mathbf{u}) \circ \check{\mathbf{q}}_\varepsilon = \check{\mathbf{Q}}_\varepsilon^{-1} \mathbf{H} \check{\mathbf{u}}_\varepsilon \check{\mathbf{Q}}_\varepsilon^{-1} = \begin{pmatrix} (\mathbf{H}\check{\mathbf{u}}_\varepsilon)_{11} & \frac{(\mathbf{H}\check{\mathbf{u}}_\varepsilon)_{12}}{\varepsilon^w} & \frac{(\mathbf{H}\check{\mathbf{u}}_\varepsilon)_{13}}{\varepsilon^h} \\ \frac{(\mathbf{H}\check{\mathbf{u}}_\varepsilon)_{21}}{\varepsilon^w} & (\mathbf{H}\check{\mathbf{u}}_\varepsilon)_{22} & \frac{(\mathbf{H}\check{\mathbf{u}}_\varepsilon)_{23}}{\varepsilon^h} \\ \frac{(\mathbf{H}\check{\mathbf{u}}_\varepsilon)_{31}}{\varepsilon^h} & \frac{(\mathbf{H}\check{\mathbf{u}}_\varepsilon)_{32}}{\varepsilon^{w+h}} & \frac{(\mathbf{H}\check{\mathbf{u}}_\varepsilon)_{33}}{\varepsilon^{2h}} \end{pmatrix}, \quad (10.23)$$

and

$$\check{\mathbf{E}}_\varepsilon \check{\mathbf{u}}_\varepsilon := (\mathbf{E}\mathbf{u}) \circ \check{\mathbf{q}}_\varepsilon = \check{\mathbf{Q}}_\varepsilon^{-1} \mathbf{E} \check{\mathbf{u}}_\varepsilon \check{\mathbf{Q}}_\varepsilon^{-1} = \begin{pmatrix} (\mathbf{E}\check{\mathbf{u}}_\varepsilon)_{11} & \frac{(\mathbf{E}\check{\mathbf{u}}_\varepsilon)_{12}}{\varepsilon^w} & \frac{(\mathbf{E}\check{\mathbf{u}}_\varepsilon)_{13}}{\varepsilon^h} \\ & \frac{(\mathbf{E}\check{\mathbf{u}}_\varepsilon)_{22}}{\varepsilon^{2w}} & \frac{(\mathbf{E}\check{\mathbf{u}}_\varepsilon)_{23}}{\varepsilon^{w+h}} \\ \text{sym} & & \frac{(\mathbf{E}\check{\mathbf{u}}_\varepsilon)_{33}}{\varepsilon^{2h}} \end{pmatrix}. \quad (10.24)$$

For simplicity of notation, the following parameter is introduced:

$$2k := 2q + w + h, \quad (10.25)$$

which will play a fundamental role in the following of this Chapter. Rescaling the problem over the fixed domain, one obtains

$$\begin{aligned} \frac{\widetilde{\mathcal{W}}_\varepsilon}{\varepsilon} &:= \mathcal{W}_\varepsilon(\hat{\mathbf{u}}_\varepsilon, \check{\mathbf{u}}_\varepsilon) = \frac{1}{2} \int_{\hat{\Omega}} \hat{\mathbf{C}} [\hat{\mathbf{E}}_\varepsilon \hat{\mathbf{u}}_\varepsilon] \cdot \hat{\mathbf{E}}_\varepsilon \hat{\mathbf{u}}_\varepsilon \, dX + \frac{1}{2} \int_{\check{\Omega}} \check{\mathbf{C}} [\varepsilon^k \check{\mathbf{E}}_\varepsilon \check{\mathbf{u}}_\varepsilon] \cdot \varepsilon^k \check{\mathbf{E}}_\varepsilon \check{\mathbf{u}}_\varepsilon \, dX, \\ &=: \widetilde{\mathcal{W}}_\varepsilon(\hat{\mathbf{u}}_\varepsilon) + \widetilde{\mathcal{W}}_\varepsilon(\varepsilon^k \check{\mathbf{u}}_\varepsilon). \end{aligned} \quad (10.26)$$

10.3 Compactness Lemmata

According to Section 5.3, the (sequentially) compactness of the candidate space is a fundamental preliminary property to assess a Γ -convergence result. In this Section, the compactness of some properly rescaled sequences of displacements, both for the plate and the stiffener, is proved, and the candidate space is defined.

Lemma 10.1 (Compactness of rescaled plate displacement). *Let $\{\hat{\mathbf{u}}_\varepsilon\} \subset H_b^1(\hat{\Omega})$ be a sequence such that $\sup_\varepsilon \mathcal{W}_\varepsilon(\hat{\mathbf{u}}_\varepsilon) \leq \infty$. Then, there exist a sub-sequence (not relabelled) $\{\hat{\mathbf{u}}_\varepsilon\}$ and one element $\hat{\mathbf{u}} \in \text{KL}(\hat{\Omega})$ such that $\hat{\mathbf{u}}_\varepsilon \rightharpoonup \hat{\mathbf{u}}$ in $H^1(\hat{\Omega})$.*

Proof. Since $\hat{\mathbb{C}}$ is positive-definite, from Korn's inequality (see Theorem 5.14) it follows that

$$C \sup_\varepsilon \|\hat{\mathbf{u}}_\varepsilon\|_{H^1(\hat{\Omega})}^2 \leq \sup_\varepsilon \left\| \hat{\mathbf{E}}_\varepsilon \hat{\mathbf{u}}_\varepsilon \right\|_{L^2(\hat{\Omega})}^2 < \infty. \quad (10.27)$$

Hence, up to a subsequence, $\hat{\mathbf{u}}_\varepsilon \rightharpoonup \hat{\mathbf{u}}$ for a certain $\hat{\mathbf{u}} \in H^1(\hat{\Omega}, \mathbb{R}^3)$. Therefore, the sequences

$$\left\{ (\mathbf{E}\hat{\mathbf{u}}_\varepsilon)_{\alpha\beta} \right\}, \left\{ \frac{(\mathbf{E}\hat{\mathbf{u}}_\varepsilon)_{\alpha 3}}{\varepsilon} \right\}, \left\{ \frac{(\mathbf{E}\hat{\mathbf{u}}_\varepsilon)_{33}}{\varepsilon^2} \right\},$$

are bounded in $L^2(\hat{\Omega})$. This fact implies that, in $L^2(\hat{\Omega})$,

$$\begin{aligned} \hat{u}_{\varepsilon\alpha,3} + \hat{u}_{\varepsilon 3,\alpha} &\rightharpoonup \hat{u}_{\alpha,3} + \hat{u}_{3,\alpha} = 0, \\ \hat{u}_{\varepsilon 3,3} &\rightharpoonup \hat{u}_{3,3} = 0. \end{aligned} \quad (10.28)$$

Hence, it is easy to deduce that $\hat{\mathbf{u}} \in \text{KL}(\hat{\Omega})$. ■

Lemma 10.2 (Compactness of rescaled stiffener displacements). *Let $\{\varepsilon^k \check{\mathbf{u}}_\varepsilon\} \subset H_b^1(\check{\Omega})$ be a sequence such that $\sup_\varepsilon \check{\mathcal{W}}_\varepsilon(\varepsilon^k \check{\mathbf{u}}_\varepsilon) \leq \infty$; then, there exist a sub-sequence (not relabelled) $\{\varepsilon^k \check{\mathbf{u}}_\varepsilon\}$ and one element $\check{\mathbf{u}} \in \text{BN}(\check{\Omega})$ such that $\varepsilon^k \check{\mathbf{u}}_\varepsilon \rightharpoonup \check{\mathbf{u}}$ in $H^1(\check{\Omega})$.*

Proof. Since $\check{\mathbb{C}}$ is positive-definite, from Korn's inequality (see Theorem 5.14) it follows that

$$C \sup_\varepsilon \|\varepsilon^k \check{\mathbf{u}}_\varepsilon\|_{H^1(\check{\Omega})}^2 \leq \sup_\varepsilon \left\| \varepsilon^k \check{\mathbf{E}}_\varepsilon \check{\mathbf{u}}_\varepsilon \right\|_{L^2(\check{\Omega})}^2 < \infty. \quad (10.29)$$

Hence, up to a subsequence, $\varepsilon^k \check{\mathbf{u}}_\varepsilon \rightharpoonup \check{\mathbf{u}}$ for a certain $\check{\mathbf{u}} \in H^1(\check{\Omega}, \mathbb{R}^3)$. As a consequence, sequences

$$\left\{ (\varepsilon^k \check{\mathbf{E}}_\varepsilon \check{\mathbf{u}}_\varepsilon)_{ij} \right\}$$

are bounded in $L^2(\check{\Omega})$. This fact implies that, in $L^2(\check{\Omega})$,

$$\begin{aligned} \varepsilon^k \check{u}_{\varepsilon 1,2} + \varepsilon^k \check{u}_{\varepsilon 2,1} &\rightharpoonup \check{u}_{1,2} + \check{u}_{2,1} = 0, \\ \varepsilon^k \check{u}_{\varepsilon 1,3} + \varepsilon^k \check{u}_{\varepsilon 3,1} &\rightharpoonup \check{u}_{1,3} + \check{u}_{3,1} = 0, \\ \varepsilon^k \check{u}_{\varepsilon 3,2} + \varepsilon^k \check{u}_{\varepsilon 2,3} &\rightharpoonup \check{u}_{3,2} + \check{u}_{2,3} = 0, \\ \varepsilon^k \check{u}_{\varepsilon a,a} &\rightharpoonup \check{u}_{a,a} = 0. \end{aligned} \quad (10.30)$$

Hence, it is easy to deduce that $\check{\mathbf{u}} \in \text{BN}(\check{\Omega})$. ■

The candidate spaces are then the $\text{KL}(\hat{\Omega})$ one for the displacements of the plate, and the $\text{BN}(\check{\Omega})$ one for the displacements of the stiffener.

10.4 Junction Conditions

Whereas the problem has been split into two sub-domains $\hat{\Omega}$ and $\check{\Omega}$, considering two displacements fields $\hat{\mathbf{u}}_\varepsilon$ and $\check{\mathbf{u}}_\varepsilon$ defined over these sets (respectively), some joining conditions between these two fields must be introduced. In particular, it must be imposed the equality of the displacement components in the fixed-domain. Since the aforementioned expressions of \mathbf{u} in terms of $\hat{\mathbf{u}}_\varepsilon$ and $\check{\mathbf{u}}_\varepsilon$, one must impose

$$\hat{\mathbf{Q}}_\varepsilon^{-1} \hat{\mathbf{u}}_\varepsilon \circ \hat{\mathbf{q}}_\varepsilon^{-1} = \check{\mathbf{Q}}_\varepsilon^{-1} \check{\mathbf{u}}_\varepsilon \circ \check{\mathbf{q}}_\varepsilon^{-1} \quad \text{in } (-L, +L) \times (-\varepsilon^w W, +\varepsilon^w W) \times \{0\}, \quad (10.31)$$

which may be rewritten as

$$\varepsilon^k \check{\mathbf{Q}}_\varepsilon \hat{\mathbf{Q}}_\varepsilon^{-1} \hat{\mathbf{u}}_\varepsilon \circ \hat{\mathbf{q}}_\varepsilon^{-1} \circ \check{\mathbf{q}}_\varepsilon = \varepsilon^k \check{\mathbf{u}}_\varepsilon \quad \text{in } (-L, +L) \times (-\varepsilon^w W, +\varepsilon^w W) \times \{0\}. \quad (10.32)$$

More explicitly,

$$\begin{aligned} \varepsilon^k \hat{u}_1^\varepsilon(x_1, \varepsilon^w x_2, 0) &= \varepsilon^k \check{u}_1^\varepsilon(x_1, x_2, 0), \\ \varepsilon^{k+w} \hat{u}_2^\varepsilon(x_1, \varepsilon^w x_2, 0) &= \varepsilon^k \check{u}_2^\varepsilon(x_1, x_2, 0), \\ \varepsilon^{k+h-1} \hat{u}_3^\varepsilon(x_1, \varepsilon^w x_2, 0) &= \varepsilon^k \check{u}_3^\varepsilon(x_1, x_2, 0), \end{aligned} \quad (10.33)$$

for all $(x_1, x_2) \in (-L, +L) \times (-\varepsilon^w W, +\varepsilon^w W) \times \{0\}$. Note that right members of Eq. (10.33) have a straightforward passage to limit, because of the continuity of the trace operator property and Lemma 10.2. Conversely, left-side terms require more involved calculations. In fact, if the generic function $f(x_1, x_2, x_3)$ belongs to $H^1(\Omega)$, its trace $f(x_1, x_2, 0)$ belongs to $H^{1/2}(\partial\Omega) \hookrightarrow L^2(\partial\Omega)$ and the trace is a bounded continuous operator. However, $f(x_1, 0, 0)$ is not well-defined as the trace of $f(x_1, x_2, 0)$, because it can be shown that the trace of a L^2 function is not bounded, in general. Besides, the continuity of the trace operator does not hold.

10.4.1 An Important Inequality

An important estimate, which will be used in the derivation of the limit junction conditions, is derived in this Section. Some arguments presented in (Griso, 2005) are adapted, where a scaled reference system, as depicted in Figure 10.2, is considered. With reference

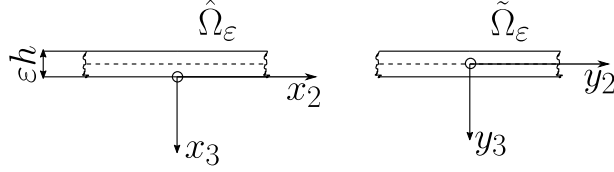


Figure 10.2: (Left) Reference system in this Chapter; (Right) Reference system in (Griso, 2005)

to Figure 10.2, consider the quantity $\tilde{\Omega}_\varepsilon := \hat{\omega} \times (-\varepsilon/2, +\varepsilon/2)$ and the mapping

$$\begin{aligned} \tilde{\mathbf{q}} : \hat{\Omega} &\mapsto \tilde{\Omega}_\varepsilon, \\ \tilde{\mathbf{q}}(x_1, x_2, x_3) &:= (x_1, x_2, \varepsilon(x_3 + \frac{1}{2})) := (y_1, y_2, y_3), \\ \tilde{\mathbf{Q}}_\varepsilon &:= \nabla \tilde{\mathbf{q}} = \text{diag}(1, 1, \varepsilon). \end{aligned} \quad (10.34)$$

Consider the displacement field

$$\tilde{\mathbf{u}}_\varepsilon : \tilde{\Omega}_\varepsilon \mapsto \mathbb{R}^3, \quad \tilde{\mathbf{u}}_\varepsilon := \tilde{\mathbf{Q}}_\varepsilon^{-1} \hat{\mathbf{u}}_\varepsilon \circ \tilde{\mathbf{q}}_\varepsilon^{-1}, \quad (10.35)$$

and the following quantities:

$$\begin{aligned} \tilde{\mathbf{m}}_\varepsilon(\mathbf{y}') &:= \int_{-\varepsilon/2}^{\varepsilon/2} \tilde{\mathbf{u}}_\varepsilon dy_3, & \tilde{\mathbf{r}}_\varepsilon(\mathbf{y}') &:= \frac{3}{2(\varepsilon/2)^3} \int_{-\varepsilon/2}^{\varepsilon/2} y_3 \mathbf{e}_3 \wedge \tilde{\mathbf{u}}_\varepsilon dy_3, \\ \tilde{\mathbf{u}}_\varepsilon^t &:= \tilde{\mathbf{m}}_\varepsilon + y_3 \tilde{\mathbf{r}}_\varepsilon \wedge \mathbf{e}_3, & \tilde{\mathbf{u}}_\varepsilon^r &:= \tilde{\mathbf{u}}_\varepsilon - \tilde{\mathbf{u}}_\varepsilon^t. \end{aligned} \quad (10.36)$$

Moreover, define

$$\begin{aligned} \hat{\mathbf{m}}_\varepsilon(\mathbf{x}') &:= \int_{-1}^0 \hat{\mathbf{u}}_\varepsilon dx_3, & \hat{\mathbf{r}}_\varepsilon(\mathbf{x}') &:= \frac{3}{2(1/2)^3} \int_{-1}^0 (x_3 + \frac{1}{2}) \mathbf{e}_3 \wedge \hat{\mathbf{u}}_\varepsilon dx_3, \\ \hat{\mathbf{u}}_\varepsilon^t &:= \hat{\mathbf{m}}_\varepsilon + (x_3 + \frac{1}{2}) \hat{\mathbf{r}}_\varepsilon \wedge \mathbf{e}_3, & \hat{\mathbf{u}}_\varepsilon^r &:= \hat{\mathbf{u}}_\varepsilon - \hat{\mathbf{u}}_\varepsilon^t. \end{aligned} \quad (10.37)$$

Given $\hat{\mathbf{u}}_\varepsilon$, define

$$\mathbf{H}_\varepsilon \hat{\mathbf{u}}_\varepsilon := \tilde{\mathbf{Q}}_\varepsilon^{-1} \nabla \hat{\mathbf{u}}_\varepsilon \tilde{\mathbf{Q}}_\varepsilon^{-1}, \quad \mathbf{E}_\varepsilon \hat{\mathbf{u}}_\varepsilon := \text{sym}(\mathbf{H}_\varepsilon \hat{\mathbf{u}}_\varepsilon). \quad (10.38)$$

Then:

$$\hat{\mathbf{m}}_\varepsilon(\mathbf{x}') = \int_{-1}^0 \hat{\mathbf{u}}_\varepsilon dx_3 = \int_{-1}^0 \tilde{\mathbf{Q}}_\varepsilon \tilde{\mathbf{u}}_\varepsilon \circ \tilde{\mathbf{q}}_\varepsilon dx_3 = \int_{-\varepsilon/2}^{+\varepsilon/2} \tilde{\mathbf{Q}}_\varepsilon \tilde{\mathbf{u}}_\varepsilon dy_3 =: \tilde{\mathbf{Q}}_\varepsilon \tilde{\mathbf{m}}_\varepsilon \quad (10.39)$$

and

$$\begin{aligned}
 \hat{\mathbf{r}}_\varepsilon(\mathbf{x}') &= \frac{3}{2(1/2)^3} \int_{-1}^0 \left(x_3 + \frac{1}{2}\right) \mathbf{e}_3 \wedge \hat{\mathbf{u}}_\varepsilon \, dx_3 = \frac{3}{2(1/2)^3} \int_{-1}^0 \left(x_3 + \frac{1}{2}\right) \mathbf{e}_3 \wedge \tilde{\mathbf{Q}}_\varepsilon \tilde{\mathbf{u}}_\varepsilon \circ \tilde{\mathbf{q}}_\varepsilon \, dx_3 \\
 &= \frac{3}{2(1/2)^3} \int_{-\varepsilon/2}^{+\varepsilon/2} \frac{y_3}{\varepsilon} \mathbf{e}_3 \wedge \tilde{\mathbf{Q}}_\varepsilon \tilde{\mathbf{u}}_\varepsilon \frac{dy_3}{\varepsilon} = \tilde{\mathbf{Q}}_\varepsilon \frac{3\varepsilon}{2(\varepsilon/2)^3} \int_{-\varepsilon/2}^{+\varepsilon/2} y_3 \mathbf{e}_3 \wedge \tilde{\mathbf{u}}_\varepsilon \, dy_3 \\
 &=: \varepsilon \tilde{\mathbf{Q}}_\varepsilon \tilde{\mathbf{r}}_\varepsilon.
 \end{aligned} \tag{10.40}$$

Then:

$$\begin{aligned}
 \tilde{\mathbf{Q}}_\varepsilon^{-1} \hat{\mathbf{u}}_\varepsilon^t \circ \tilde{\mathbf{q}}_\varepsilon^{-1} &= \tilde{\mathbf{Q}}_\varepsilon^{-1} \left[\hat{\mathbf{m}}_\varepsilon + \frac{y_3}{\varepsilon} \hat{\mathbf{r}}_\varepsilon \wedge \mathbf{e}_3 \right] = \tilde{\mathbf{m}}_\varepsilon + y_3 \tilde{\mathbf{r}}_\varepsilon \wedge \mathbf{e}_3 =: \tilde{\mathbf{u}}_\varepsilon^t, \\
 \tilde{\mathbf{u}}_\varepsilon^r &:= \tilde{\mathbf{u}}_\varepsilon - \tilde{\mathbf{u}}_\varepsilon^t = \tilde{\mathbf{Q}}_\varepsilon^{-1} \hat{\mathbf{u}}_\varepsilon^r \circ \tilde{\mathbf{q}}_\varepsilon^{-1}.
 \end{aligned} \tag{10.41}$$

Theorem 10.1 (Theorem 2.3 from (Griso, 2005)).

$$\left\| \mathbf{E} \tilde{\mathbf{u}}_\varepsilon^t \right\|_{L^2(\tilde{\Omega}_\varepsilon)}^2 + \left\| \mathbf{H} \tilde{\mathbf{u}}_\varepsilon^r \right\|_{L^2(\tilde{\Omega}_\varepsilon)}^2 + \frac{1}{\varepsilon^2 (1/2)^2} \left\| \tilde{\mathbf{u}}_\varepsilon^r \right\|_{L^2(\tilde{\Omega}_\varepsilon)}^2 \leq C \left\| \mathbf{E} \hat{\mathbf{u}}_\varepsilon \right\|_{L^2(\tilde{\Omega}_\varepsilon)}^2. \tag{10.42}$$

Proof. see (Griso, 2005). ■

Rearranging Eq. (10.42), one obtains

$$\begin{aligned}
 &\left\| \mathbf{E} \left[\tilde{\mathbf{Q}}_\varepsilon^{-1} \hat{\mathbf{u}}_\varepsilon^t \circ \tilde{\mathbf{q}}_\varepsilon^{-1} \right] \right\|_{L^2(\tilde{\Omega}_\varepsilon)}^2 + \left\| \mathbf{H} \left[\tilde{\mathbf{Q}}_\varepsilon^{-1} \hat{\mathbf{u}}_\varepsilon^r \circ \tilde{\mathbf{q}}_\varepsilon^{-1} \right] \right\|_{L^2(\tilde{\Omega}_\varepsilon)}^2 + \frac{1}{\varepsilon^2 (1/2)^2} \left\| \tilde{\mathbf{Q}}_\varepsilon^{-1} \hat{\mathbf{u}}_\varepsilon^r \circ \tilde{\mathbf{q}}_\varepsilon^{-1} \right\|_{L^2(\tilde{\Omega}_\varepsilon)}^2 \\
 &\leq C \left\| \mathbf{E} \left[\tilde{\mathbf{Q}}_\varepsilon^{-1} \hat{\mathbf{u}}_\varepsilon \circ \tilde{\mathbf{q}}_\varepsilon^{-1} \right] \right\|_{L^2(\tilde{\Omega}_\varepsilon)}^2 \\
 &\left\| \tilde{\mathbf{Q}}_\varepsilon^{-1} \mathbf{E} \hat{\mathbf{u}}_\varepsilon^t \tilde{\mathbf{Q}}_\varepsilon^{-1} \right\|_{L^2(\tilde{\Omega})}^2 + \left\| \tilde{\mathbf{Q}}_\varepsilon^{-1} \mathbf{H} \hat{\mathbf{u}}_\varepsilon^r \tilde{\mathbf{Q}}_\varepsilon^{-1} \right\|_{L^2(\tilde{\Omega})}^2 + \frac{1}{\varepsilon^2 (1/2)^2} \left\| \tilde{\mathbf{Q}}_\varepsilon^{-1} \hat{\mathbf{u}}_\varepsilon^r \right\|_{L^2(\tilde{\Omega})}^2 \\
 &\leq C \left\| \tilde{\mathbf{Q}}_\varepsilon^{-1} \mathbf{E} \hat{\mathbf{u}}_\varepsilon \tilde{\mathbf{Q}}_\varepsilon^{-1} \right\|_{L^2(\tilde{\Omega})}^2 \\
 &\left\| \hat{\mathbf{E}}_\varepsilon \hat{\mathbf{u}}_\varepsilon^t \right\|_{L^2(\hat{\Omega})}^2 + \left\| \hat{\mathbf{H}}_\varepsilon \hat{\mathbf{u}}_\varepsilon^r \right\|_{L^2(\hat{\Omega})}^2 + \frac{1}{\varepsilon^2 (1/2)^2} \left\| \tilde{\mathbf{Q}}_\varepsilon^{-1} \hat{\mathbf{u}}_\varepsilon^r \right\|_{L^2(\hat{\Omega})}^2 \leq C \left\| \hat{\mathbf{E}}_\varepsilon \hat{\mathbf{u}}_\varepsilon \right\|_{L^2(\hat{\Omega})}^2.
 \end{aligned} \tag{10.43}$$

Therefore, remembering the compactness result of Lemma 10.1, the main result of this section reads:

$$\frac{1}{\varepsilon^2} \left\| \tilde{\mathbf{Q}}_\varepsilon^{-1} \hat{\mathbf{u}}_\varepsilon^r \right\|_{L^2(\hat{\Omega})}^2 < +\infty. \tag{10.44}$$

10.4.2 The Junction Conditions for Displacements

The following Lemma can be now proved.

Lemma 10.3 (Trace approximation). *Let $\hat{\mathbf{u}}_\varepsilon \in H^1(\hat{\Omega})$ be a sequence of functions such that $\hat{\mathbf{u}}_\varepsilon \rightharpoonup \hat{\mathbf{u}}$ in the $H^1(\hat{\Omega})$ norm, $\hat{\mathbf{u}} \in \text{KL}$. Then $\hat{\mathbf{u}}_\varepsilon(x_1, \varepsilon^w x_2, 0)$ converges in the $L^2(\hat{\omega})$ norm to the trace of $\hat{\mathbf{u}}$ in $(-L, +L) \times \{0\} \times \{0\}$ if and only if $0 < w < 2$.*

Proof. First of all, consider the following change of variables between the displacement components defined on the midplane and those defined on the external face of the plate

$$\tilde{\xi}_3 = \hat{\xi}_3, \quad \tilde{\xi}_\alpha = \hat{\xi}_\alpha + \frac{1}{2}\hat{\xi}_{3,\alpha}, \quad (10.45)$$

and the following identity:

$$\hat{\xi}(x_1, 0) = \left(\tilde{\xi} + \frac{1}{2}(-\mathbf{e}_3 \wedge \nabla \tilde{\xi}_3) \wedge \mathbf{e}_3 \right) (x_1, 0). \quad (10.46)$$

The thesis of the Lemma is proved by showing that

$$\begin{aligned} & \left\| \hat{\mathbf{u}}_\varepsilon(x_1, \varepsilon^w x_2, 0) - \hat{\xi}(x_1, 0) \right\|_{L^2(\hat{\Omega})} \leq \\ & \left\| \hat{\mathbf{u}}_\varepsilon(x_1, \varepsilon^w x_2, 0) - \hat{\mathbf{u}}_\varepsilon^t(x_1, \varepsilon^w x_2, 0) \right\|_{L^2(\hat{\Omega})} \\ & + \left\| \hat{\mathbf{u}}_\varepsilon^t(x_1, \varepsilon^w x_2, 0) - \left(\hat{\mathbf{m}}_\varepsilon + \frac{1}{2}\hat{\mathbf{r}}_\varepsilon \wedge \mathbf{e}_3 \right) (x_1, \varepsilon^w x_2) \right\|_{L^2(\hat{\Omega})} \\ & + \left\| \left(\hat{\mathbf{m}}_\varepsilon + \frac{1}{2}\hat{\mathbf{r}}_\varepsilon \wedge \mathbf{e}_3 \right) (x_1, \varepsilon^w x_2) - \left(\hat{\mathbf{m}}_\varepsilon + \frac{1}{2}\hat{\mathbf{r}}_\varepsilon \wedge \mathbf{e}_3 \right) (x_1, 0) \right\|_{L^2(\hat{\Omega})} \\ & + \left\| \left(\hat{\mathbf{m}}_\varepsilon + \frac{1}{2}\hat{\mathbf{r}}_\varepsilon \wedge \mathbf{e}_3 \right) (x_1, 0) - \left(\tilde{\xi} + \frac{1}{2}(-\mathbf{e}_3 \wedge \nabla \tilde{\xi}_3) \wedge \mathbf{e}_3 \right) (x_1, 0) \right\|_{L^2(\hat{\Omega})} \rightarrow 0. \end{aligned} \quad (10.47)$$

The four norms at the right-side member are referenced as row1, row2, row3, and row4, respectively.

It is easy to show that $\hat{\mathbf{m}}_\varepsilon \rightharpoonup \tilde{\xi}$ in $H^1(\hat{\omega})$ and that $\hat{\mathbf{r}}_\varepsilon \rightharpoonup -\mathbf{e}_3 \wedge \nabla \tilde{\xi}_3$ in $H^1(\hat{\omega})$. Then, it has been proved that row4 tends to zero.

(row3)² can be rewritten as

$$\begin{aligned} & \int_{-1}^0 \int_{\hat{\omega}} \left| \int_0^{\varepsilon^w x_2} \partial_2 \left(\hat{\mathbf{m}}_\varepsilon + \frac{1}{2}\hat{\mathbf{r}}_\varepsilon \wedge \mathbf{e}_3 \right) (x_1, t_2) dt_2 \right|^2 dx_1 dx_2 dx_3 \\ & \leq \int_{-1}^0 \int_{\hat{\omega}} |\varepsilon^w x_2| \int_0^{\varepsilon^w x_2} \left| \partial_2 \left(\hat{\mathbf{m}}_\varepsilon + \frac{1}{2}\hat{\mathbf{r}}_\varepsilon \wedge \mathbf{e}_3 \right) (x_1, t_2) \right|^2 dt_2 dx_1 dx_2 dx_3 \\ & \leq C\varepsilon^w \int_{-1}^0 \int_{\hat{\omega}} \left| \partial_2 \left(\hat{\mathbf{m}}_\varepsilon + \frac{1}{2}\hat{\mathbf{r}}_\varepsilon \wedge \mathbf{e}_3 \right) (x_1, t_2) \right|^2 dt_2 dx_1 dx_3 \\ & \leq C\varepsilon^w \end{aligned} \quad (10.48)$$

which tends to zero, since the integrand function is bounded in $H^1(\hat{\omega})$ and $w > 0$.

As for row2, it is trivially true that is equal to zero.

Consider $(\text{row1})^2$ together with Eq. (10.44).

$$\begin{aligned}
 \left\| \hat{\mathbf{u}}_\varepsilon(x_1, \varepsilon^w x_2, 0) - \hat{\mathbf{u}}_\varepsilon^t(x_1, \varepsilon^w x_2, 0) \right\|_{L^2(\hat{\Omega})}^2 &= \left\| \hat{\mathbf{u}}_\varepsilon^r(x_1, \varepsilon^w x_2, 0) \right\|_{L^2(\hat{\Omega})}^2 \\
 &\leq \frac{1}{\varepsilon^w} \left\| \hat{\mathbf{u}}_\varepsilon^r(x_1, x_2, 0) \right\|_{L^2(\hat{\Omega})}^2 \\
 &= \frac{1}{\varepsilon^w} \left\| \hat{\mathbf{Q}}_\varepsilon \hat{\mathbf{Q}}_\varepsilon^{-1} \hat{\mathbf{u}}_\varepsilon^r(x_1, x_2, 0) \right\|_{L^2(\hat{\Omega})}^2 \\
 &\leq \frac{1}{\varepsilon^w} \left\| \hat{\mathbf{Q}}_\varepsilon \right\|_{L^2(\hat{\Omega})}^2 \left\| \hat{\mathbf{Q}}_\varepsilon^{-1} \hat{\mathbf{u}}_\varepsilon^r(x_1, x_2, 0) \right\|_{L^2(\hat{\Omega})}^2 \\
 &\leq \frac{\varepsilon^2}{\varepsilon^w} C \left\| \hat{\mathbf{Q}}_\varepsilon \right\|_{L^2(\hat{\Omega})}^2
 \end{aligned} \tag{10.49}$$

which tends to zero if $2 > w$. ■

The limit of Eq. (10.33) can be now taken in the $L^2(\hat{\Omega})$ norm. However, the limit depends on the relative values of the exponents k , w and h . This dependency is taken into account by introducing the following functions: $\hat{\chi} : \mathbb{R} \times (0, 2) \times \bar{\mathbb{R}}^+ \mapsto \{0, 1\}^3$, $\hat{\chi}(k, w, h) \mapsto \{0, 1\}^3$ and $\check{\chi} : \mathbb{R} \times (0, 2) \times \bar{\mathbb{R}}^+ \mapsto \{0, 1\}^3$, $\check{\chi}(k, w, h) \mapsto \{0, 1\}^3$, defined as follows:

$$\hat{\chi} := \begin{cases} \hat{\chi}_1 = \begin{cases} 0 & \text{if } k > 0 \\ 1 & \text{if } k \leq 0 \end{cases} \\ \hat{\chi}_2 = \begin{cases} 0 & \text{if } k + w > 0 \\ 1 & \text{if } k + w \leq 0 \end{cases} \\ \hat{\chi}_3 = \begin{cases} 0 & \text{if } k + h - 1 > 0 \\ 1 & \text{if } k + h - 1 \leq 0, \end{cases} \end{cases}, \quad \check{\chi} := \begin{cases} \check{\chi}_1 = \begin{cases} 0 & \text{if } k < 0 \\ 1 & \text{if } k \geq 0 \end{cases} \\ \check{\chi}_2 = \begin{cases} 0 & \text{if } k + w < 0 \\ 1 & \text{if } k + w \geq 0 \end{cases} \\ \check{\chi}_3 = \begin{cases} 0 & \text{if } k + h - 1 < 0 \\ 1 & \text{if } k + h - 1 \geq 0, \end{cases} \end{cases} \tag{10.50}$$

so that the limit junction conditions reads:

$$\hat{\mathbf{X}}(k, w, h) \hat{\xi}(x_1, 0) = \check{\mathbf{X}}(k, w, h) \check{\xi}(x_1), \tag{10.51}$$

where $\hat{\mathbf{X}} := \text{diag}(\hat{\chi}_1, \hat{\chi}_2, \hat{\chi}_3)$ and $\check{\mathbf{X}} := \text{diag}(\check{\chi}_1, \check{\chi}_2, \check{\chi}_3)$.

10.4.3 Different Regimes for Joining Conditions

Considering Eq. (10.51), the following regimes are possible, depending on values of k (q), w and h . The general scenario can be graphically depicted in Figure 10.3, where the red, green and blue planes represents the conditions $\hat{\chi}_i = \check{\chi}_i = 1$, respectively.

The cases reported in (Aufranc, 1990) correspond to the particular choice $w = h = 1$ and $q = -a/4$ (a is an exponent used in (Aufranc, 1990) for the stiffener material properties scaling. Aufranc (1990) considers the cases $a = 4, 6$).

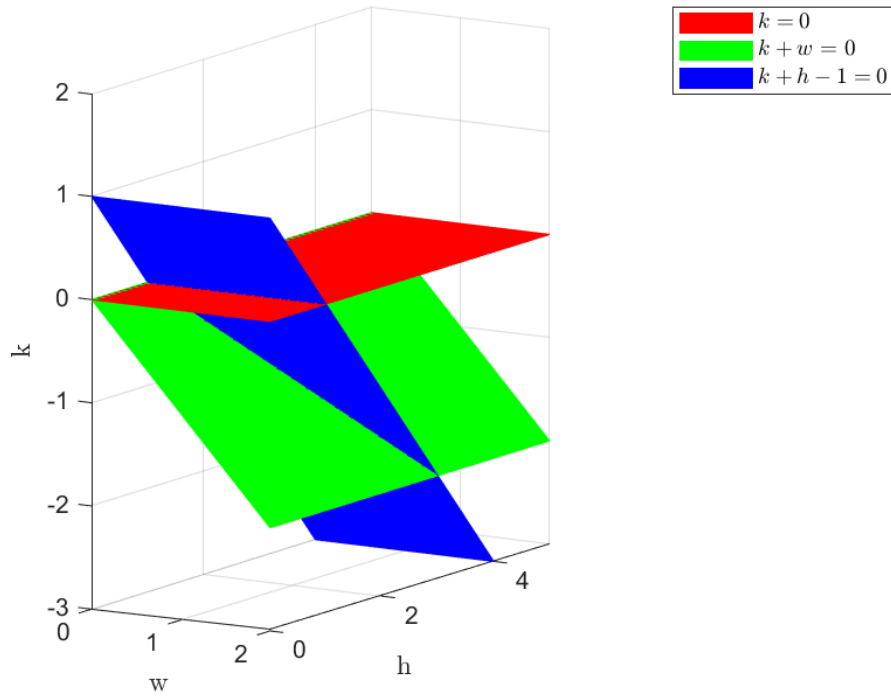
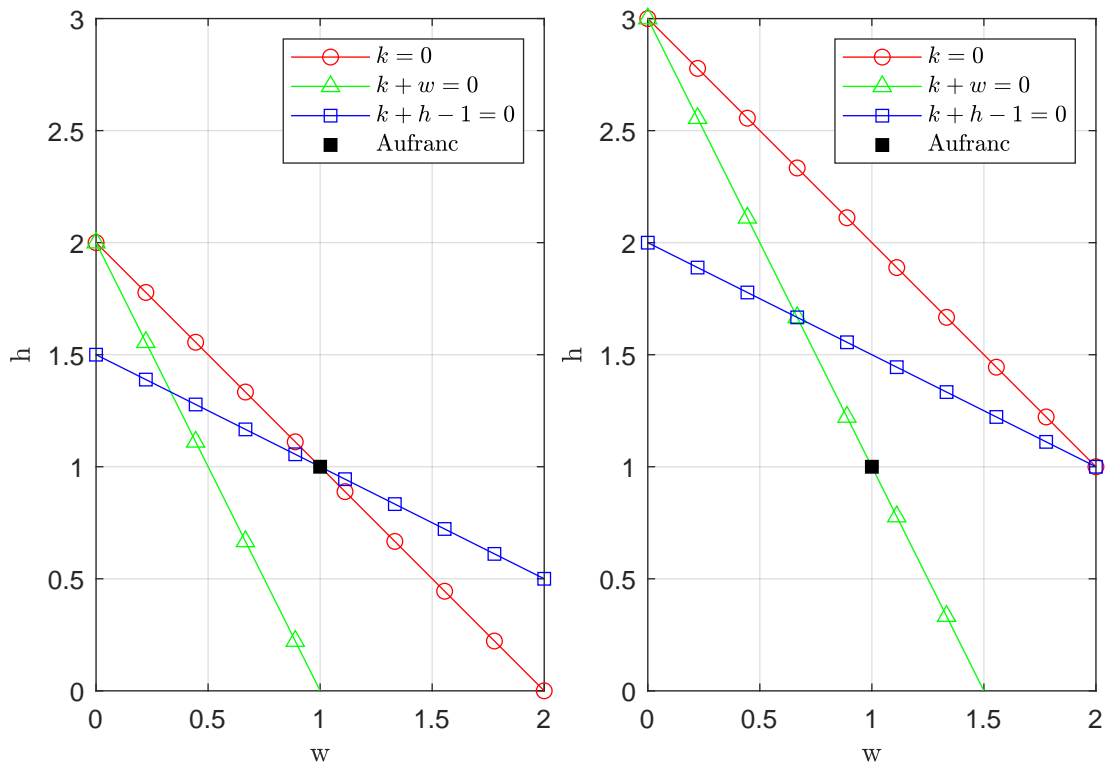


Figure 10.3: Junction conditions discriminant



(a) Case $q = -1$ (corresponding to the case $a = 4$) (b) Case $q = -3/2$ (corresponding to the case $a = 6$)

Figure 10.4: Cases presented in Aufranc (1990)

Analysing Figure 10.3, it is noteworthy to see that for no combination of k, w, h (re-

member that w and h are strictly positive) the three joining conditions in Eq. (10.51) are non-trivial at the same time. For the same reasons, the first and second conditions cannot be simultaneously non-trivial. However, for $h = 1$ the first and third joining conditions are necessarily non-trivial, whilst for $h = w + 1$ the second and the third conditions are so. Table 10.1 reports all the possible regimes as defined from the relative values of the scaling parameters (see Figure 10.3).

10.5 The Limit Energy

In this Section, the limit energy is deduced. Firstly, the convergence of some components of the rescaled strain energy is established.

Lemma 10.4 (Convergence of components of the rescaled strain energy). *Under the same assumptions, up to sub-sequences, in the weak $L^2(\check{\Omega})$ topology,*

$$\varepsilon^k (\check{\mathbf{E}}_\varepsilon \check{\mathbf{u}}_\varepsilon)_{11} \rightharpoonup D_1 \check{u}_1 \text{ weakly in } L^2(\check{\Omega}) \quad (10.52)$$

Proof. To prove (10.52) it is sufficient to notice that $\varepsilon^k (\check{\mathbf{E}}_\varepsilon \check{\mathbf{u}}_\varepsilon)_{11} = \varepsilon^k D_1 \check{u}_{\varepsilon 1}$ and to apply Lemma 10.2. \blacksquare

Define

$$\begin{aligned} \hat{f}_0(\hat{E}_{\alpha\beta}) &:= \min_{A_{i3}} \{ \hat{f}(\mathbf{A}) : \mathbf{A} \in \text{Sym}, A_{\alpha\beta} = \hat{E}_{\alpha\beta} \}, \\ \check{f}_0(\check{E}_{11}) &:= \min_{A_{12}, A_{13}, A_{ab}} \{ \check{f}(\mathbf{A}) : \mathbf{A} \in \text{Sym}, A_{11} = D_1 \check{u}_1 \}; \end{aligned} \quad (10.53)$$

as linear homogeneous isotropic materials are considered, the stored-energy density function is of the form (see Theorem 5.8)

$$\begin{aligned} \hat{f}(\mathbf{A}) &= \frac{1}{2} \hat{\mathbf{C}}[\mathbf{A}] \cdot \mathbf{A} = \hat{\mu} |\mathbf{A}|^2 + \frac{\hat{\lambda}}{2} |\text{tr} \mathbf{A}|^2 \\ \check{f}(\mathbf{A}) &= \frac{1}{2} \check{\mathbf{C}}[\mathbf{A}] \cdot \mathbf{A} = \check{\mu} |\mathbf{A}|^2 + \frac{\check{\lambda}}{2} |\text{tr} \mathbf{A}|^2. \end{aligned} \quad (10.54)$$

A direct computation shows that

$$\begin{aligned} \hat{\mathbf{Z}}(\hat{E}_{\alpha\beta}) &:= \text{argmin} \hat{f}_0 = \hat{E}_{\alpha\beta} \mathbf{e}_\alpha \otimes \mathbf{e}_\beta - \frac{\hat{\nu}}{1 - \hat{\nu}} (\hat{E}_{11} + \hat{E}_{22}) \mathbf{e}_3 \otimes \mathbf{e}_3, \\ \check{\mathbf{Z}}(D_1 \check{u}_1) &:= \text{argmin} \check{f}_0 = \check{E}_{11} [\mathbf{e}_1 \otimes \mathbf{e}_1 - \check{\nu} (\mathbf{e}_2 \otimes \mathbf{e}_2 + \mathbf{e}_3 \otimes \mathbf{e}_3)], \end{aligned} \quad (10.55)$$

and

$$\begin{aligned} \hat{f}_0 &= \hat{\mu} \left(\frac{\hat{E}_{11}^2 + \hat{E}_{22}^2 + 2\hat{\nu} \hat{E}_{11} \hat{E}_{22}}{1 - \hat{\nu}} + 2\hat{E}_{12}^2 \right), \\ \check{f}_0 &= \frac{1}{2} \check{E} \check{E}_{11}^2, \end{aligned} \quad (10.56)$$

where $E := \frac{\mu(2\mu + 3\lambda)}{\mu + \lambda}$ is the Young modulus and $\nu = \frac{\lambda}{2(\lambda + \mu)}$ is the Poisson's coefficient. Of course, labels $\hat{\cdot}$ and $\check{\cdot}$ specify if these quantities are referred to the plate-like or stiffener-like body.

Let the set of the pairs of admissible displacements be introduced:

$$\mathcal{A} := \{(\hat{\mathbf{u}}, \check{\mathbf{u}}) : \hat{\mathbf{u}} \in \text{KL}_b(\hat{\Omega}), \check{\mathbf{u}} \in \text{BN}_b(\check{\Omega}), \text{ satisfying (10.51) and the boundary conditions}\}. \quad (10.57)$$

The stored-energy can be extended as the functional $\mathcal{W}(\hat{\mathbf{u}}, \check{\mathbf{u}}) : H^1(\hat{\Omega}) \times H^1(\check{\Omega}) \mapsto [0, +\infty]$ defined by

$$\mathcal{W}(\hat{\mathbf{u}}, \check{\mathbf{u}}) := \begin{cases} \hat{\mathcal{W}}(\hat{\mathbf{u}}) + \check{\mathcal{W}}(\check{\mathbf{u}}), & \text{if } (\hat{\mathbf{u}}, \check{\mathbf{u}}) \in \mathcal{A} \\ +\infty, & \text{otherwise,} \end{cases} \quad (10.58)$$

where

$$\hat{\mathcal{W}}(\hat{\mathbf{u}}) := \int_{\hat{\Omega}} \hat{f}_0 \, dX, \quad \check{\mathcal{W}}(\check{\mathbf{u}}) := \int_{\check{\Omega}} \check{f}_0 \, dX. \quad (10.59)$$

The main result of the Chapter is the following (see Definition 5.18)

Theorem 10.2 (Γ -limit). *As $\varepsilon \rightarrow 0^+$, the sequence of functionals \mathcal{W}_ε Γ -converges to the functional \mathcal{W} in the following sense:*

(a) (*lim inf inequality*) for every sequence $\varepsilon_n \rightarrow 0^+$ ($\varepsilon_n > 0 \forall n$) and for every sequence $(\hat{\mathbf{u}}_{\varepsilon_n}, \check{\mathbf{u}}_{\varepsilon_n}) \in \mathcal{A}_{\varepsilon_n}$ such that

$$\begin{aligned} \hat{\mathbf{u}}_{\varepsilon_n} &\rightharpoonup \hat{\mathbf{u}} \text{ in } H^1(\hat{\Omega}), \\ \varepsilon_n^k \check{\mathbf{u}}_{\varepsilon_n} &\rightharpoonup \check{\mathbf{u}} \text{ in } H^1(\check{\Omega}), \end{aligned} \quad (10.60)$$

one obtains

$$\liminf_{n \rightarrow +\infty} \mathcal{W}_{\varepsilon_n}(\hat{\mathbf{u}}_{\varepsilon_n}, \varepsilon_n^k \check{\mathbf{u}}_{\varepsilon_n}) \geq \mathcal{W}(\hat{\mathbf{u}}, \check{\mathbf{u}}) \quad (10.61)$$

(b) (*Recovery sequence*) for every sequence $\varepsilon_n \rightarrow 0^+$ ($\varepsilon_n > 0 \forall n$) and for every $(\hat{\mathbf{u}}, \check{\mathbf{u}}) \in \mathcal{A}$ there exists a sequence $(\hat{\mathbf{u}}_{\varepsilon_n}, \check{\mathbf{u}}_{\varepsilon_n}) \in \mathcal{A}_{\varepsilon_n}$, called recovery sequence, such that

$$\begin{aligned} \hat{\mathbf{u}}_{\varepsilon_n} &\rightharpoonup \hat{\mathbf{u}} \text{ in } H^1(\hat{\Omega}), \\ \varepsilon_n^k \check{\mathbf{u}}_{\varepsilon_n} &\rightharpoonup \check{\mathbf{u}} \text{ in } H^1(\check{\Omega}), \end{aligned} \quad (10.62)$$

and

$$\limsup_{n \rightarrow +\infty} \mathcal{W}_{\varepsilon_n}(\hat{\mathbf{u}}_{\varepsilon_n}, \varepsilon_n^k \check{\mathbf{u}}_{\varepsilon_n}) \leq \mathcal{W}(\hat{\mathbf{u}}, \check{\mathbf{u}}). \quad (10.63)$$

Proof. Firstly, the liminf inequality is proved. Without loss of generality, suppose that

$$\liminf_{n \rightarrow +\infty} \mathcal{W}_{\varepsilon_n}(\hat{\mathbf{u}}_{\varepsilon_n}, \varepsilon_n^k \check{\mathbf{u}}_{\varepsilon_n}) < +\infty$$

otherwise there is nothing to prove; hence,

$$\sup_n \mathcal{W}_{\varepsilon_n}(\hat{\mathbf{u}}_{\varepsilon_n}, \varepsilon_n^k \check{\mathbf{u}}_{\varepsilon_n}) < +\infty.$$

Thus, Lemmata 10.1, 10.2 and 10.4 hold. Taking into account the decomposition given in Eq. (10.26), it is sufficient to show that

$$\liminf_{n \rightarrow +\infty} \mathcal{W}_{\varepsilon_n}(\hat{\mathbf{u}}_{\varepsilon_n}) \geq \int_{\hat{\Omega}} \hat{f}_0 \, dX, \quad \liminf_{n \rightarrow +\infty} \mathcal{W}_{\varepsilon_n}(\varepsilon_n^k \check{\mathbf{u}}_{\varepsilon_n}) \geq \int_{\check{\Omega}} \check{f}_0 \, dX. \quad (10.64)$$

By minimality condition represented by Eq. (10.53), one has that $\hat{f} \geq \hat{f}_0$ and $\check{f} \geq \check{f}_0$. Denoting with $\hat{\mathbf{E}}$ the limit $\hat{\mathbf{E}}_{\varepsilon_n} \hat{\mathbf{u}}_{\varepsilon_n} \rightharpoonup \hat{\mathbf{E}}$ in $L^2(\hat{\Omega})$, one obtains

$$\begin{aligned} \liminf_{n \rightarrow +\infty} \mathcal{W}_{\varepsilon_n}(\hat{\mathbf{u}}_{\varepsilon_n}) &= \liminf_{n \rightarrow +\infty} \int_{\hat{\Omega}} \hat{f}(\hat{\mathbf{E}}_{\varepsilon_n} \hat{\mathbf{u}}_{\varepsilon_n}) \, dX \\ &= \liminf_{n \rightarrow +\infty} \int_{\hat{\Omega}} \hat{f}(\hat{\mathbf{E}}_{\varepsilon_n} \hat{\mathbf{u}}_{\varepsilon_n} - \hat{\mathbf{E}}) \, dX - \int_{\hat{\Omega}} \hat{f}(\hat{\mathbf{E}}) \, dX + \int_{\hat{\Omega}} \hat{\mathbf{C}}[\hat{\mathbf{E}}_{\varepsilon_n} \hat{\mathbf{u}}_{\varepsilon_n}] \cdot \hat{\mathbf{E}} \, dX \\ &\geq \liminf_{n \rightarrow +\infty} \int_{\hat{\Omega}} \hat{\mathbf{C}}[\hat{\mathbf{E}}_{\varepsilon_n} \hat{\mathbf{u}}_{\varepsilon_n}] \cdot \hat{\mathbf{E}} \, dX - \int_{\hat{\Omega}} \hat{f}(\hat{\mathbf{E}}) \, dX \\ &= \int_{\hat{\Omega}} \hat{\mathbf{C}}[\hat{\mathbf{E}}] \cdot \hat{\mathbf{E}} \, dX - \int_{\hat{\Omega}} \hat{f}(\hat{\mathbf{E}}) \, dX \\ &= \int_{\hat{\Omega}} \hat{f}(\hat{\mathbf{E}}) \, dX \\ &\geq \int_{\hat{\Omega}} \hat{f}_0(\hat{\mathbf{Z}}) \, dX = \int_{\hat{\Omega}} \hat{f}_0(\hat{E}_{11}, \hat{E}_{22}, \hat{E}_{12}) \, dX. \end{aligned} \quad (10.65)$$

Similarly, denoting with $\check{\mathbf{E}}$ the limit of $\varepsilon_n^k \check{\mathbf{E}}_{\varepsilon_n} \check{\mathbf{u}}_{\varepsilon_n} \rightharpoonup \check{\mathbf{E}}$ in $L^2(\check{\Omega})$, one obtains

$$\begin{aligned}
 \liminf_{n \rightarrow +\infty} \mathcal{W}_{\varepsilon_n}(\varepsilon_n^k \check{\mathbf{u}}_{\varepsilon_n}) &= \liminf_{n \rightarrow +\infty} \int_{\check{\Omega}} \check{f}(\varepsilon_n^k \check{\mathbf{E}}_{\varepsilon_n} \check{\mathbf{u}}_{\varepsilon_n}) \, dX \\
 &= \liminf_{n \rightarrow +\infty} \int_{\check{\Omega}} \check{f}(\varepsilon_n^k \check{\mathbf{E}}_{\varepsilon_n} \check{\mathbf{u}}_{\varepsilon_n} - \check{\mathbf{E}}) \, dX - \int_{\check{\Omega}} \check{f}(\check{\mathbf{E}}) \, dX + \int_{\check{\Omega}} \check{\mathbb{C}}[\varepsilon_n^k \check{\mathbf{E}}_{\varepsilon_n} \check{\mathbf{u}}_{\varepsilon_n}] \cdot \check{\mathbf{E}} \, dX \\
 &\geq \liminf_{n \rightarrow +\infty} \int_{\check{\Omega}} \check{\mathbb{C}}[\varepsilon_n^k \check{\mathbf{E}}_{\varepsilon_n} \check{\mathbf{u}}_{\varepsilon_n}] \cdot \check{\mathbf{E}} \, dX - \int_{\check{\Omega}} \check{f}(\check{\mathbf{E}}) \, dX \\
 &= \int_{\check{\Omega}} \check{\mathbb{C}}[\check{\mathbf{E}}] \cdot \check{\mathbf{E}} \, dX - \int_{\check{\Omega}} \check{f}(\check{\mathbf{E}}) \, dX \\
 &= \int_{\check{\Omega}} \check{f}(\check{\mathbf{E}}) \, dX \\
 &\geq \int_{\check{\Omega}} \check{f}_0(\check{\mathbf{Z}}) \, dX = \int_{\check{\Omega}} \check{f}_0(\check{E}_{11}) \, dX.
 \end{aligned} \tag{10.66}$$

A recovery sequence is now found. For the sake of simplicity, the rest of the proof is limited for the particular case B of Table 10.1, for which $k = 0$ and $h = 1$. Suppose that $\mathcal{W} < +\infty$, otherwise there is nothing to prove. Assume $(\hat{\mathbf{u}}, \check{\mathbf{u}})$ to be smooth and equal to zero near $x_1 = B$. The convergence of these elements and the characterisation the limit functions have been already accomplished. Introduce the function $\mathbf{u}^{0,\varepsilon}$ whose components are defined as follows:

$$\begin{aligned}
 u_1^{0,\varepsilon} &:= \begin{cases} \hat{\xi}_1 - x_3 \hat{\xi}_{3,1} & \text{in } \hat{\Omega} \\ \hat{\xi}_1(x_1, 0) - x_3 \hat{\xi}_{3,1}(x_1, 0) + \check{\nu} \varepsilon^{2w} \frac{x_2^2}{2} x_3 \hat{\xi}_{3,111}(x_1, 0) & \text{in } \check{\Omega} \end{cases} \\
 u_2^{0,\varepsilon} &:= \begin{cases} \hat{\xi}_2 - x_3 \hat{\xi}_{3,2} & \text{in } \hat{\Omega} \\ -\check{\nu} \varepsilon^{2w} \left[x_2 \hat{\xi}_{1,1}(x_1, 0) - x_2 x_3 \hat{\xi}_{3,11}(x_1, 0) \right] & \text{in } \check{\Omega} \end{cases} \\
 u_3^{0,\varepsilon} &:= \begin{cases} \hat{\xi}_3 - \varepsilon^2 \frac{\hat{\nu}}{1 - \hat{\nu}} x_3 \left[\hat{\xi}_{1,1} + \hat{\xi}_{2,2} - \frac{x_3}{2} \left(\hat{\xi}_{3,11} + \hat{\xi}_{3,22} \right) \right] & \text{in } \hat{\Omega} \\ \hat{\xi}_3(x_1, 0) - \check{\nu} \varepsilon^{2h} \left[x_3 \hat{\xi}_{1,1}(x_1, 0) - \frac{x_3^2}{2} \hat{\xi}_{3,11}(x_1, 0) \right] - \check{\nu} \varepsilon^{2w} \frac{x_2^2}{2} \hat{\xi}_{3,11}(x_1, 0) & \text{in } \check{\Omega} \end{cases}
 \end{aligned} \tag{10.67}$$

It can be seen that the function satisfies boundary conditions at $x_1 = B$, the junction conditions of Eq. (10.51) and the conditions:

$$\begin{aligned}
 \|\hat{\mathbf{E}}_\varepsilon \mathbf{u}^{0,\varepsilon} - \hat{\mathbf{Z}}\|_{L^2(\hat{\Omega})} &\rightarrow 0, \quad \|\check{\mathbf{E}}_\varepsilon \mathbf{u}^{0,\varepsilon} - \check{\mathbf{Z}}\|_{L^2(\check{\Omega})} \rightarrow 0, \\
 \|\mathbf{u}^{0,\varepsilon} - \hat{\mathbf{u}}\|_{H^1(\hat{\Omega})} &\rightarrow 0, \quad \|\mathbf{u}^{0,\varepsilon} - \check{\mathbf{u}}\|_{H^1(\check{\Omega})} \rightarrow 0.
 \end{aligned} \tag{10.68}$$

Hence, in this case, $\mathbf{u}^{0,\varepsilon_n}$ is a recovery sequence. The case for non-smooth $\mathbf{u}^{0,\varepsilon_n}$ is achieved by approximating $\mathbf{u}^{0,\varepsilon_n}$ in H^1 by a smooth function satisfying boundary and junction conditions, concluding with a standard diagonal argument. \blacksquare

The limit energies have the following formal expressions

$$\mathcal{W}^{\check{}} = \frac{1}{2} \int_{-B}^{+B} \begin{bmatrix} \check{E} A & -\check{E} S_2 \\ -\check{E} S_2 & \check{E} J_2 \end{bmatrix} \begin{pmatrix} \hat{\xi}_{1,1}(x_1, 0) \\ \hat{\xi}_{3,11}(x_1, 0) \end{pmatrix} \cdot \begin{pmatrix} \hat{\xi}_{1,1}(x_1, 0) \\ \hat{\xi}_{3,11}(x_1, 0) \end{pmatrix} dx_1, \quad (10.69)$$

where

$$A := \int_{\check{\omega}} dx_2 dx_3 = WH, \quad S_2 := \int_{\check{\omega}} x_3 dx_2 dx_3 = W \frac{H^2}{2}, \quad J_2 := \int_{\check{\omega}} x_3^2 dx_2 dx_3 = W \frac{H^3}{3}, \quad (10.70)$$

and

$$\mathcal{W}^{\hat{}} = \frac{1}{2} \int_{\check{\omega}} \begin{bmatrix} \mathbf{A} & \mathbf{B} \\ \mathbf{B} & \mathbf{D} \end{bmatrix} \begin{pmatrix} \hat{\xi}_{1,1} \\ \hat{\xi}_{2,2} \\ \hat{\xi}_{1,2} + \hat{\xi}_{2,1} \\ \hat{\xi}_{3,11} \\ \hat{\xi}_{3,22} \\ \hat{\xi}_{3,12} \end{pmatrix} \cdot \begin{pmatrix} \hat{\xi}_{1,1} \\ \hat{\xi}_{2,2} \\ \hat{\xi}_{1,2} + \hat{\xi}_{2,1} \\ \hat{\xi}_{3,11} \\ \hat{\xi}_{3,22} \\ \hat{\xi}_{3,12} \end{pmatrix} dx_1 dx_3, \quad (10.71)$$

where

$$\mathbf{A} := \frac{\hat{E} 1}{1 - \hat{\nu}^2} \begin{bmatrix} 1 & \hat{\nu} & 0 \\ & 1 & 0 \\ \text{sym} & & \frac{1-\hat{\nu}}{2} \end{bmatrix}, \quad \mathbf{B} := -\frac{\hat{E} 1^2}{2(1 - \hat{\nu}^2)} \begin{bmatrix} 1 & \hat{\nu} & 0 \\ & 1 & 0 \\ \text{sym} & & \frac{1-\hat{\nu}}{2} \end{bmatrix}, \quad (10.72)$$

$$\mathbf{D} := \frac{\hat{E} 1^3}{3(1 - \hat{\nu}^2)} \begin{bmatrix} 1 & \hat{\nu} & 0 \\ & 1 & 0 \\ \text{sym} & & 2(1 - \hat{\nu}) \end{bmatrix}.$$

Remark 10.1. Considering $\check{\xi}_3 = 0$ in Eq. (10.67), one obtains easily the recovery sequence also for the case C of Table 10.1. The consequent limit energy simplifies to

$$\mathcal{W}^{\check{}} = \frac{1}{2} \int_{-B}^{+B} \check{E} A \hat{\xi}_{1,1}^2(x_1, 0) dx_1 \quad (10.73)$$

for the stiffener, whilst for the plate the limit energy is the same of Eq. (10.71). Since the stiffener participates to the energy functional only through extensional displacements, the stiffener behaves actually like a truss.

10.6 Convergence of Minima and Minimisers

Theorem 5.15 presents conditions to achieve the convergence of minima and minimiser of the "real" problem, ruled by \mathcal{F}_ε , with those of the limit problem ruled by \mathcal{F} .

The total energy $\widetilde{\mathcal{F}}_\varepsilon$ of the system (see Definition 5.9) can be written as the sum of the strain energy $\widetilde{\mathcal{W}}_\varepsilon$ minus the work done by external loads $\widetilde{\mathcal{L}}_\varepsilon$

$$\widetilde{\mathcal{F}}_\varepsilon(\mathbf{u}) := \widetilde{\mathcal{W}}_\varepsilon(\mathbf{u}) - \widetilde{\mathcal{L}}_\varepsilon(\mathbf{u}), \quad (10.74)$$

where the external loads work is of the form

$$\widetilde{\mathcal{L}}_\varepsilon(\mathbf{u}) := \int_{\Omega_\varepsilon} \mathbf{b}_\varepsilon \cdot \mathbf{u} \, dX, \quad (10.75)$$

and where the body forces \mathbf{b}_ε belong to $L_2(\Omega)$.

After a scaling akin to Section 10.2, let $\mathcal{L}_\varepsilon(\hat{\mathbf{u}}_\varepsilon, \check{\mathbf{u}}_\varepsilon) := \frac{1}{\varepsilon} \widetilde{\mathcal{L}}_\varepsilon(\mathbf{u}_\varepsilon) = \hat{\mathcal{L}}_\varepsilon(\hat{\mathbf{u}}_\varepsilon) + \check{\mathcal{L}}_\varepsilon(\varepsilon^k \check{\mathbf{u}}_\varepsilon)$ denote the rescaled work. Assume that the contributes of the plate and of the stiffener in the rescaled work continuously converge to some limit functionals $\hat{\mathcal{L}}(\hat{\mathbf{u}})$ and $\check{\mathcal{L}}(\check{\mathbf{u}})$, respectively, in the sense of the convergence used in Theorem 10.2.

Therefore, the following result holds:

Theorem 10.3 (Convergence of the total energy). *As $\varepsilon \rightarrow 0^+$, the sequence of functionals $\mathcal{F}_\varepsilon(\mathbf{u}_\varepsilon) := \mathcal{W}_\varepsilon(\mathbf{u}_\varepsilon) - \mathcal{L}_\varepsilon(\mathbf{u}_\varepsilon)$ Γ -converges to the limit functional $\mathcal{F}(\mathbf{u}) := \mathcal{W}(\mathbf{u}) - \mathcal{L}(\mathbf{u})$ in the sense specified by Theorem 10.2.*

Proof. The proof directly follows from the well-known stability of Γ -convergence with respect to continuous, real-valued perturbations (Theorem 5.16) see also, Dal Maso (1993, Proposition 6.20). ■

Theorem 10.4 (Strong convergence of minima and minimisers). *The minimisation problem for the Γ -limit functional $\mathcal{F} = \mathcal{W} - \mathcal{L}$*

$$\min \{ \mathcal{F}(\hat{\mathbf{u}}, \check{\mathbf{u}}) : \hat{\mathbf{u}} \in KL(\hat{\Omega}), \check{\mathbf{u}} \in BN(\check{\Omega}), \hat{\mathbf{u}} = \check{\mathbf{u}} = \mathbf{0} \text{ on } \partial_D \Omega, \text{ equation (10.51) is satisfied} \} \quad (10.76)$$

admits a unique solution $(\hat{\mathbf{u}}_\#, \check{\mathbf{u}}_\#)$. Moreover, as $\varepsilon \rightarrow 0^+$,

1. $\hat{\mathbf{u}}_{\#\varepsilon} \rightarrow \hat{\mathbf{u}}_\#$ strongly in $H^1(\hat{\Omega})$;
2. $\check{\mathbf{u}}_{\#\varepsilon} \rightarrow \check{\mathbf{u}}_\#$ strongly in $H^1(\check{\Omega})$;
3. $\mathcal{F}_\varepsilon(\hat{\mathbf{u}}_{\#\varepsilon}, \check{\mathbf{u}}_{\#\varepsilon})$ converges to $\mathcal{F}(\hat{\mathbf{u}}_\#, \check{\mathbf{u}}_\#)$.

Proof. The existence of a solution for Problem (10.76) can be proved through the Direct Method of the Calculus of Variations (see Section 5.2, in particular Theorem 5.11); its uniqueness follows from the strictly convexity of the functional \mathcal{F} .

From Theorem 10.3, from well-known properties of Γ -limits and, in particular, from Dal Maso (1993, Proposition 6.8 and 8.16 (lower-semicontinuity of sequential Γ -limits), Theorem 7.8 (coercivity of Γ -limits) and Corollary 7.24 (convergence of minima and minimiser)), it follows that points (1) and (2) are satisfied in the weak convergence and that

point (3) is proved. To show that the converge of points (1) and (2) is actually strong, some arguments proposed by Freddi et al. (2004), Freddi et al. (2007) are adapted.

Denote by \mathbf{a}_ε the approximate minimiser of Problem (10.76), defined as the recovery sequence of the Γ -limit Theorem, but with $(\hat{\xi}, \check{\xi})$ replaced by $(\hat{\xi}_\#, \check{\xi}_\#)$. Even if the new sequence is no more a recovery sequence, since it does not satisfy the boundary conditions, estimates (10.68) still hold if $(\hat{\xi}, \check{\xi})$ are replaced by $(\hat{\xi}_\#, \check{\xi}_\#)$. Therefore, one obtains:

$$\lim_{\varepsilon \rightarrow 0^+} \mathcal{F}_\varepsilon(\hat{\mathbf{a}}_\varepsilon, \check{\mathbf{a}}_\varepsilon) = \mathcal{F}(\hat{\xi}_\#, \check{\xi}_\#), \quad \lim_{\varepsilon \rightarrow 0^+} \mathcal{L}_\varepsilon(\hat{\mathbf{a}}_\varepsilon, \check{\mathbf{a}}_\varepsilon) = \mathcal{L}(\hat{\xi}_\#, \check{\xi}_\#). \quad (10.77)$$

In particular,

$$\begin{aligned} \lim_{\varepsilon \rightarrow 0^+} \left(\hat{\mathcal{F}}_\varepsilon(\hat{\mathbf{u}}_{\#\varepsilon}) - \hat{\mathcal{F}}_\varepsilon(\hat{\mathbf{a}}_\varepsilon) \right) &= 0, & \lim_{\varepsilon \rightarrow 0^+} \left(\check{\mathcal{F}}_\varepsilon(\check{\mathbf{u}}_{\#\varepsilon}) - \check{\mathcal{F}}_\varepsilon(\check{\mathbf{a}}_\varepsilon) \right) &= 0, \\ \lim_{\varepsilon \rightarrow 0^+} \hat{\mathcal{L}}_\varepsilon(\hat{\mathbf{u}}_{\#\varepsilon} - \hat{\mathbf{a}}_\varepsilon) &= 0, & \lim_{\varepsilon \rightarrow 0^+} \check{\mathcal{L}}_\varepsilon(\check{\mathbf{u}}_{\#\varepsilon} - \check{\mathbf{a}}_\varepsilon) &= 0. \end{aligned} \quad (10.78)$$

As a preliminary observation, quadratic forms of the type of Eq. (10.54) satisfy the identity

$$f(\mathbf{U}) = f(\mathbf{A}) + \mathbb{C}[\mathbf{A}] \cdot (\mathbf{U} - \mathbf{A}) + f(\mathbf{U} - \mathbf{A}) \quad (10.79)$$

for every 3×3 matrices \mathbf{A} , \mathbf{U} . By the coercivity condition (Theorem 5.7), one obtains the following inequality:

$$f(\mathbf{U}) \geq f(\mathbf{A}) + \mathbb{C}[\mathbf{A}] \cdot (\mathbf{U} - \mathbf{A}) + \mu |\mathbf{U} - \mathbf{A}|^2. \quad (10.80)$$

Then,

$$\begin{aligned} \hat{\mathcal{F}}_\varepsilon(\hat{\mathbf{u}}_{\#\varepsilon}) - \hat{\mathcal{F}}_\varepsilon(\hat{\mathbf{a}}_\varepsilon) &\geq \int_{\hat{\Omega}} \hat{\mathbb{C}}[\hat{\mathbf{E}}_\varepsilon \hat{\mathbf{a}}_\varepsilon] \cdot \hat{\mathbf{E}}_\varepsilon(\hat{\mathbf{u}}_{\#\varepsilon} - \hat{\mathbf{a}}_\varepsilon) dX + \hat{\mu} \left\| \hat{\mathbf{E}}_\varepsilon \hat{\mathbf{u}}_{\#\varepsilon} - \hat{\mathbf{E}}_\varepsilon \hat{\mathbf{a}}_\varepsilon \right\|_{L^2(\hat{\Omega})}^2 \\ &\quad - \hat{\mathcal{L}}_\varepsilon(\hat{\mathbf{u}}_{\#\varepsilon} - \hat{\mathbf{a}}_\varepsilon), \\ \check{\mathcal{F}}_\varepsilon(\check{\mathbf{u}}_{\#\varepsilon}) - \check{\mathcal{F}}_\varepsilon(\check{\mathbf{a}}_\varepsilon) &\geq \int_{\check{\Omega}} \check{\mathbb{C}}[\check{\mathbf{E}}_\varepsilon \check{\mathbf{a}}_\varepsilon] \cdot \check{\mathbf{E}}_\varepsilon(\check{\mathbf{u}}_{\#\varepsilon} - \check{\mathbf{a}}_\varepsilon) dX + \check{\mu} \left\| \check{\mathbf{E}}_\varepsilon \check{\mathbf{u}}_{\#\varepsilon} - \check{\mathbf{E}}_\varepsilon \check{\mathbf{a}}_\varepsilon \right\|_{L^2(\check{\Omega})}^2 \\ &\quad - \check{\mathcal{L}}_\varepsilon(\check{\mathbf{u}}_{\#\varepsilon} - \check{\mathbf{a}}_\varepsilon). \end{aligned} \quad (10.81)$$

It is now proved that

$$\begin{aligned} \lim_{\varepsilon \rightarrow 0^+} \int_{\hat{\Omega}} \hat{\mathbb{C}}[\hat{\mathbf{E}}_\varepsilon \hat{\mathbf{a}}_\varepsilon] \cdot \hat{\mathbf{E}}_\varepsilon(\hat{\mathbf{u}}_{\#\varepsilon} - \hat{\mathbf{a}}_\varepsilon) dX &= 0, \\ \lim_{\varepsilon \rightarrow 0^+} \int_{\check{\Omega}} \check{\mathbb{C}}[\check{\mathbf{E}}_\varepsilon \check{\mathbf{a}}_\varepsilon] \cdot \check{\mathbf{E}}_\varepsilon(\check{\mathbf{u}}_{\#\varepsilon} - \check{\mathbf{a}}_\varepsilon) dX &= 0. \end{aligned} \quad (10.82)$$

For brevity's sake, the following notation (to be specialised for the plate and the stiffener

with the usual symbols) is introduced:

$$\mathbf{A}_\varepsilon := \mathbf{E}_\varepsilon \mathbf{a}_\varepsilon, \quad \mathbf{U}_\varepsilon := \mathbf{E}_\varepsilon \mathbf{u}_{\#\varepsilon}, \quad \mathbf{\Delta}_\varepsilon := \mathbf{U}_\varepsilon - \mathbf{A}_\varepsilon, \quad (10.83)$$

so that Eq. (10.81) rewrites

$$\begin{aligned} \hat{\mathcal{F}}_\varepsilon(\hat{\mathbf{u}}_{\#\varepsilon}) - \hat{\mathcal{F}}_\varepsilon(\hat{\mathbf{a}}_\varepsilon) &\geq \int_{\hat{\Omega}} \hat{\mathbf{C}}[\hat{\mathbf{A}}_\varepsilon] \cdot \hat{\mathbf{\Delta}}_\varepsilon dX + \hat{\mu} \|\hat{\mathbf{\Delta}}_\varepsilon\|_{L^2(\hat{\Omega})}^2 - \hat{\mathcal{L}}_\varepsilon(\hat{\mathbf{u}}_{\#\varepsilon} - \hat{\mathbf{a}}_\varepsilon), \\ \check{\mathcal{F}}_\varepsilon(\check{\mathbf{u}}_{\#\varepsilon}) - \check{\mathcal{F}}_\varepsilon(\check{\mathbf{a}}_\varepsilon) &\geq \int_{\check{\Omega}} \check{\mathbf{C}}[\check{\mathbf{A}}_\varepsilon] \cdot \check{\mathbf{\Delta}}_\varepsilon dX + \check{\mu} \|\check{\mathbf{\Delta}}_\varepsilon\|_{L^2(\check{\Omega})}^2 - \check{\mathcal{L}}_\varepsilon(\check{\mathbf{u}}_{\#\varepsilon} - \check{\mathbf{a}}_\varepsilon), \end{aligned} \quad (10.84)$$

and the integrands in Eq. (10.82) rewrite

$$2\hat{\mu} \left(\hat{A}_{ij}^\varepsilon \hat{\Delta}_{ij}^\varepsilon \right) + \hat{\lambda} \left(\hat{A}_{ii}^\varepsilon \hat{\Delta}_{jj}^\varepsilon \right), \quad 2\check{\mu} \left(\check{A}_{ij}^\varepsilon \check{\Delta}_{ij}^\varepsilon \right) + \check{\lambda} \left(\check{A}_{ii}^\varepsilon \check{\Delta}_{jj}^\varepsilon \right). \quad (10.85)$$

By Eq. (10.68), one obtains

$$\begin{aligned} \hat{\mathbf{A}}_\varepsilon &\rightarrow \hat{\mathbf{Z}}(D_1 \hat{u}_{\#1}, D_2 \hat{u}_{\#2}, D_2 \hat{u}_{\#1}, D_1 \hat{u}_{\#2}) \text{ in } L^2(\hat{\Omega}), \\ \check{\mathbf{A}}_\varepsilon &\rightarrow \check{\mathbf{Z}}(D_1 \check{u}_{\#1}) \text{ in } L^2(\check{\Omega}), \end{aligned} \quad (10.86)$$

and from Lemma 10.1, Lemma 10.2 and Eq. (10.86) one has that $\hat{\mathbf{\Delta}}_\varepsilon$ and $\check{\mathbf{\Delta}}_\varepsilon$ are bounded in $L^2(\hat{\Omega})$ and $L^2(\check{\Omega})$, respectively. Thus, from (10.86), it is immediately deduced that

$$\begin{aligned} \lim_{\varepsilon \rightarrow 0^+} \int_{\hat{\Omega}} \hat{A}_{\alpha 3}^\varepsilon \hat{\Delta}_{\alpha 3}^\varepsilon dX &= 0, \\ \lim_{\varepsilon \rightarrow 0^+} \int_{\check{\Omega}} \check{A}_{ij}^\varepsilon \check{\Delta}_{ij}^\varepsilon dX &= 0, \quad ij \neq 11, 22, 33. \end{aligned} \quad (10.87)$$

From (10.86) and points (1) and (2) (weak convergence version) it follows that $\hat{\Delta}_{\alpha\beta} \rightharpoonup 0$ in $L^2(\hat{\Omega})$ and that $\check{\Delta}_{11} \rightharpoonup 0$ in $L^2(\check{\Omega})$, and therefore

$$\lim_{\varepsilon \rightarrow 0^+} \int_{\hat{\Omega}} \hat{A}_{ij}^\varepsilon \hat{\Delta}_{\alpha\beta}^\varepsilon dX = 0, \quad \lim_{\varepsilon \rightarrow 0^+} \int_{\check{\Omega}} \check{A}_{ij}^\varepsilon \check{\Delta}_{11}^\varepsilon dX = 0. \quad (10.88)$$

Let $\hat{\Delta}_{33}$ be the weak limit in $L^2(\hat{\Omega})$ of $\hat{\Delta}_{33}^\varepsilon$ and $\check{\Delta}_{aa}$ be the weak limit in $L^2(\check{\Omega})$ of $\check{\Delta}_{aa}^\varepsilon$.

Putting all together, one has

$$\begin{aligned}
 \lim_{\varepsilon \rightarrow 0^+} \int_{\hat{\Omega}} \hat{\mathbf{C}} \hat{\mathbf{A}}_\varepsilon \hat{\Delta}_\varepsilon \, dX &= \lim_{\varepsilon \rightarrow 0^+} \int_{\hat{\Omega}} 2\hat{\mu} \hat{A}_{33}^\varepsilon \hat{\Delta}_{33}^\varepsilon + \hat{\lambda} \hat{A}_{ii}^\varepsilon \hat{\Delta}_{33}^\varepsilon \, dX \\
 &= \int_{\hat{\Omega}} \hat{\Delta}_{33} D_\alpha \hat{u}_{\#\alpha} \frac{\hat{\lambda}(1-2\hat{\nu}) - 2\hat{\mu}\hat{\nu}}{1-\hat{\nu}} \, dX = 0, \\
 \lim_{\varepsilon \rightarrow 0^+} \int_{\check{\Omega}} \check{\mathbf{C}} \check{\mathbf{A}}_\varepsilon \check{\Delta}_\varepsilon \, dX &= \lim_{\varepsilon \rightarrow 0^+} \int_{\check{\Omega}} 2\check{\mu} \check{A}_{aa}^\varepsilon \check{\Delta}_{aa}^\varepsilon + \check{\lambda} \check{A}_{ii}^\varepsilon \check{\Delta}_{bb}^\varepsilon \, dX \\
 &= \int_{\check{\Omega}} \check{\Delta}_{aa} D_1 \check{u}_{\#1} (\check{\lambda} - 2\check{\nu}(\check{\mu} + \check{\lambda})) \, dX = 0,
 \end{aligned} \tag{10.89}$$

since the relationships between elastic moduli (E , ν) and Lamé constants (λ , μ) nullify the integrand functions. Those relationships read:

$$E := \frac{\mu(3\lambda + 2\mu)}{\lambda + \mu}, \quad \nu := \frac{\lambda}{2(\lambda + \mu)}. \tag{10.90}$$

Hence, considering (10.81) and (10.78), it has been shown that

$$\left\| \hat{\mathbf{E}}_\varepsilon \hat{\mathbf{u}}_{\#\varepsilon} - \hat{\mathbf{E}}_\varepsilon \hat{\mathbf{a}}_\varepsilon \right\|_{L^2(\hat{\Omega})}^2 \rightarrow 0, \quad \left\| \check{\mathbf{E}}_\varepsilon \check{\mathbf{u}}_{\#\varepsilon} - \check{\mathbf{E}}_\varepsilon \check{\mathbf{a}}_\varepsilon \right\|_{L^2(\check{\Omega})}^2 \rightarrow 0. \tag{10.91}$$

Applying the standard Korn's inequality (see Theorem 5.14), it follows that

$$\left\| \hat{\mathbf{u}}_{\#}^\varepsilon - \hat{\mathbf{a}}^\varepsilon \right\|_{H^1(\hat{\Omega})} \rightarrow 0, \quad \left\| \check{\mathbf{u}}_{\#}^\varepsilon - \check{\mathbf{a}}^\varepsilon \right\|_{H^1(\check{\Omega})} \rightarrow 0. \tag{10.92}$$

From this fact and from the last two of (10.68) applied to \mathbf{a}_ε the thesis of the strong convergence, claimed in points (1) and (2), is obtained. \blacksquare

Table 10.1: Different junction conditions

Case:	A	B	C	D	E
	$k = 0$	$k = 0$	$k = 0$	$-w$	$-w$
	w	w	w	$k + w = 0$	$k + w = 0$
	$h < 1$	$h = 1$	$h > 1$	$h < w + 1$	$h = w + 1$

Comp. 1	$\hat{\xi}_1(x_1, 0) = \check{\xi}_1(x_1)$	$\hat{\xi}_1(x_1, 0) = \check{\xi}_1(x_1)$	$\hat{\xi}_1(x_1, 0) = \check{\xi}_1(x_1)$	$\hat{\xi}_1(x_1, 0) = 0$	$\hat{\xi}_1(x_1, 0) = 0$
Comp. 2	$0 = \check{\xi}_2(x_1)$	$0 = \check{\xi}_2(x_1)$	$0 = \check{\xi}_2(x_1)$	$\hat{\xi}_2(x_1, 0) = \check{\xi}_2(x_1)$	$\hat{\xi}_2(x_1, 0) = \check{\xi}_2(x_1)$
Comp. 3	$\hat{\xi}_3(x_1, 0) = 0$	$\hat{\xi}_3(x_1, 0) = \check{\xi}_3(x_1)$	$0 = \check{\xi}_3(x_1)$	$\hat{\xi}_3(x_1, 0) = 0$	$\hat{\xi}_3(x_1, 0) = \check{\xi}_3(x_1)$

Case:	F	G	H	I	J
	$-w$	$-h + 1 > 0$	$-h + 1 < 0$	$-h + 1 < 0$	$k > 0$
	$k + w = 0$	$w - h + 1 > 0$	$w - h + 1 > 0$	$w - h + 1 < 0$	$k + w > 0$
	$h > w + 1$	$k + h - 1 = 0$	$k + h - 1 = 0$	$k + h - 1 = 0$	$k + h - 1 > 0$

Comp. 1	$\hat{\xi}_1(x_1, 0) = 0$	$0 = \check{\xi}_1(x_1)$	$\hat{\xi}_1(x_1, 0) = 0$	$\hat{\xi}_1(x_1, 0) = 0$	$0 = \check{\xi}_1(x_1)$
Comp. 2	$\hat{\xi}_2(x_1, 0) = \check{\xi}_2(x_1)$	$0 = \check{\xi}_2(x_1)$	$0 = \check{\xi}_2(x_1)$	$\hat{\xi}_2(x_1, 0) = 0$	$0 = \check{\xi}_2(x_1)$
Comp. 3	$0 = \check{\xi}_3(x_1)$	$\hat{\xi}_3(x_1, 0) = \check{\xi}_3(x_1)$	$\hat{\xi}_3(x_1, 0) = \check{\xi}_3(x_1)$	$\hat{\xi}_3(x_1, 0) = \check{\xi}_3(x_1)$	$0 = \check{\xi}_3(x_1)$

Case:	K	L	M	N	O
	$k > 0$	$k < 0$	$k < 0$	$k < 0$	$k < 0$
	$k + w > 0$	$k + w > 0$	$k + w > 0$	$k + w < 0$	$k + w < 0$
	$k + h - 1 < 0$	$k + h - 1 > 0$	$k + h - 1 < 0$	$k + h - 1 < 0$	$k + h - 1 > 0$

Comp. 1	$0 = \check{\xi}_1(x_1)$	$\hat{\xi}_1(x_1, 0) = 0$			
Comp. 2	$0 = \check{\xi}_2(x_1)$	$0 = \check{\xi}_2(x_1)$	$0 = \check{\xi}_2(x_1)$	$\hat{\xi}_2(x_1, 0) = 0$	$\hat{\xi}_2(x_1, 0) = 0$
Comp. 3	$\hat{\xi}_3(x_1, 0) = 0$	$0 = \check{\xi}_3(x_1)$	$\hat{\xi}_3(x_1, 0) = 0$	$\hat{\xi}_3(x_1, 0) = 0$	$0 = \check{\xi}_3(x_1)$

10.7 Conclusions

The problem of the limit energy derivation of the equilibrium of a 3D plate-and-stiffener elastic solid has been addressed through the Γ -convergence variational approach. Only the normal and the out-of-plane displacement fields are considered in this Chapter. As the scaling parameters go to zero, fifteen different limit models are found out. As a noteworthy remark, no limit model includes all the contributes (related to the displacements field components) in the expression of the limit energy. It is basically due to the mutual interaction between the plate and the stiffener. Roughly speaking, it means that the stiffener and the plate have a spurious behaviour when coupled together.

This investigation, performed on a simple structural pattern, raises awareness to the problem of obtaining and justifying, in a rigorous manner the classic structural models. Even though many results have been achieved, as presented in the Introduction of this Chapter, many others still remain to be found. In particular, the recovering of the limit problem for structures presenting junctions, scaling parameters with different scaling velocities is anything but trivial.

Part V

Epilogue

Conclusions and Perspectives

In this final Chapter, there are summarised the main conclusions of this Ph.D. Thesis (Section 11.1) and the main general ideas, challenges and trends for future researches (Section 11.2).

11.1 General Conclusions

The work presented in this Thesis has been carried out in the framework of the PARSI-FAL Project.

Several are major contributions of this Thesis.

First of all, there have been developed and formalised two elements for an enhanced and more reliable design of composite multilayered structures. These elements, presented in Chapter 6, are: (i) the derivation of the explicit form of the gradient of the buckling factor when transition of scale (sub-modelling technique) occurs, from the global model of the structure to a more refined local model of critical areas, whereby the buckling factor is evaluated; (ii) a dedicated blending strategy, without the use of simplifying hypotheses on the stacking sequences, with a general numerical strategy for the recovery of blended stacks matching some target elastic properties.

These elements have been formulated using the Polar Method for the description of the plane anisotropy and in the context of the First-order Shear Deformation Theory, so taking transversal shear effects into account. Eventually, these two elements have been implemented in the Multi-Scale Two-Level Optimisation Strategy framework, extended to the deterministic optimisation in Chapter 7. As a result, an enhanced global-local modelling approach for the optimisation of composite structures has been defined, without introducing simplifying hypotheses on the laminate stack and by considering, as design variables, the full set of geometric and mechanical parameters defining the behaviour of the com-

posite structure at each pertinent scale. In this background, a variety of constraints has been integrated in the deterministic optimisation problem formulation, expressed in the Polar parameters space; moreover, the analytic form of their gradients has been derived. The global-local modelling approach has been integrated in the formulation of the related optimisation strategy, in order to assess the physical responses involved at different levels. Of course, the coupling effect between global and local models on the gradient of the physical responses, evaluated on the refined local models, has been taken into account thanks to the Thesis results.

New blending constraints have been derived in the Polar parameters space to be integrated in the first-level of the optimisation problem formulation (focusing on the laminate macroscopic scale). Moreover, a general resolution scheme has been developed for the stacking sequence recovery phase (dealing with the laminate mesoscopic scale) taking into account general stacking sequences and blending schemes.

In parallel, an alternative approach for blending has been presented. It is based on the knowledge of a special class of laminates, said quasi-trivial, which are exact solutions for membrane/bending uncoupled and homogeneous laminates. The actual knowledge of all such a laminates has been extended up to laminates made of 39 plies. It has been possible by means of the development of a new algorithm, DLX-Stack Finder, based on a combinatorial formulation of the quasi-trivial stack finding problem.

The effectiveness of the Thesis achievements has been tested on several numerical benchmarks, taken from the literature, dealing with the least-weight design of simple structures. The results have shown an encouraging trend. Finally, the complete Optimisation Strategy has been applied to the least-weight design of the lifting system of the PrandtlPlane aircraft developed within the PARSIFAL Project (Chapter 8). The results are encouraging for this complex *real-word* structure, as well.

Secondly, the Thesis has been an occasion to study in deep two theoretical aspects related to the multi-scale design of composite structures. Firstly, in Chapter 9, two aspects linked to the nature of the feasible domain of composite laminates have been studied. Proofs of the non-convexity of the feasible domain in Polar parameters and Lamination parameters spaces have been provided for both anisotropic and orthotropic laminates. This investigation clarifies some preliminary aspects of the feasible domain determination problem. Although tackling the problem in full generality is probably impractical, a closed form of stricter feasibility bounds has been derived in terms of the membrane stiffness tensor Polar parameters. This is an aspect of paramount importance in the optimisation of composite laminates, where the anisotropy is tailored to satisfy some merit functions and constraints. Successively, the problem of retrieving sufficient and necessary conditions for membrane/bending uncoupling and homogeneity has been addressed in this study. It has been shown that, in general, quasi-triviality is only a sufficient condition. It becomes also a necessary one if the stacking sequence has only two distinct orientations.

The second theoretical aspect, discussed in Chapter 10, has been the derivation of the

limit energy of a stiffened plate-like body, as the thickness of the plate-like body and the stiffener-like body cross-sectional dimensions become really small. By means of a variational notion of convergence, i.e. the Γ -convergence, it has been shown that the scaled dimensions, as may go to zero in different velocities, determine many different models of "plate and beam". Remarkably, the plate and the beam interact in such a way that the junction of a plate and a beam is not asymptotically equivalent to consider those elements as independent. In other words, the junction provides, asymptotically, spurious plate and beam models. This study has been used to support a rational finite element modelling of the PrandtlPlane wing.

11.2 Perspectives of the Thesis

The results and the findings presented in this Thesis are by far to be exhaustive for the dealt topics. Indeed, many questions naturally rise from this work: they constitute opportunities for future researches.

Regarding the deterministic global-local approach, following the path of the buckling gradient formalisation provided in Section 6.1, many other kind of requirements can be formulated considering the scale transition between the global model and refined local models of critical areas. Of course, the approach hereby provided shall be used as a guide for the explicit formalisation of other structural requirements, to be used as optimisation constraints, upon the specific formulation of the problem at hand.

Moreover, more element types can be included in the implementation, to generalise the field of validity of the numerical implementation. For example, more evolute shell elements, beam elements, truss elements, solid elements can be used in the problem formulation. The major effort is, basically, to derive the expressions of the matrices for the decomposition of the stress-stiffness matrix of the single element at hand. A roadmap has been provided in Algorithm 6.2. Besides, more complex problem formulations, including many load cases and local models, can be formulated.

The study of blending of laminates highlighted several still-open problems of composite design laminates, which consistently affect the fitness of the final result. In particular, four aspects deserve to be deeply investigated.

Firstly, the major uncertainty source has been recognised in the expression of the feasible domain bounds in the Polar parameters space (and, equivalently, in the Lamination parameters space), for a given number of plies and for desired laminates characteristics, viz. uncoupling, orthotropy, homogeneity. In the future, the problem of determining stricter bounds for the laminate feasible domain in the polar parameters space (or in the Lamination parameters one) could be faced, in order to reduce the discrepancy between results provided by both first-level and second-level problems.

Secondly, inasmuch as the first-level problem deals with laminate homogenised properties, deriving an equivalent expression of manufacturing constraints related to the geometrical features of the stack (e.g. the percentage rule, the maximum difference between

consecutive plies orientation angles) in either the Lamination parameters space or in the Polar parameters one is anything but trivial. Nevertheless, if considered as a design driver, these requirements should be introduced since the first-level problem formulation in order to reduce the discrepancy when optimal stacks are retrieved at the end of the second-level problem.

Thirdly, the issues related to the load redistribution, a problem of capital importance in real-world engineering applications, should be opportunely addressed and integrated in the formulation of the discrete optimisation of the first-level problem.

Finally, inasmuch the search propagation direction is concerned, an existence criterion for the search propagation direction shall be derived. Besides, a pertinent approach should be developed in order to determine automatically (i.e. without the user's intervention) the best search propagation direction when looking for optimised blended stacking sequences.

The alternative approach for blending, i.e. using quasi-trivial quasi-homogeneous stacking sequences, deserves deeper studies. First of all, a more efficient storing strategy for the DLX-Stack Finder algorithm must be found out and implemented. Moreover, some version of the algorithm can be developed to attain only uncoupled or only homogeneous quasi-trivial laminates.

The presented approach for the stack recovery phase using quasi-trivial stacking sequences is still embryonic. A more evolved strategy can be developed, starting from the one hereby presented, to alleviate the non-control of the recovery of the target elastic properties and to guarantee the finding of at least one solution. Moreover, a strategy to deal with thick laminates shall be found out.

The proposed blending strategy needs to be validated and, eventually, corrected. The transition zones between adjacent panels are likely to be critical from stability and delamination point of view. Their effect shall be included in the future in the proposed strategy for blending. It is of the uttermost importance that experimental tests shall study these effects, in the case of non-conventional laminates, so to properly tune the numerical strategy.

As far the problem of the feasible domain of laminates is concerned, the derivation of the analytic expressions of the feasible domain of laminates (either in Lamination parameters or Polar parameters spaces), at least for the membrane stiffness tensor, shall be derived in more general cases, maintaining the dependence from the number of plies. These expressions must be included in the formulation of the optimisation problem of the composites in order to get true feasible optimal solutions. Moreover, to support the composite design, necessary and sufficient conditions to achieve uncoupled and/or homogeneous and/or isotropic laminates shall be derived. This could represent a step-forward to the definition of the feasible domain considering membrane and bending stiffness tensors at once.

Of course, the main (and most difficult) problem to address still remains the derivation of the actual feasible domain of a laminate when the full stiffness matrix is considered either in the fully anisotropic case or when introducing some hypotheses on the laminate

stiffness tensors elastic symmetries. This aspect is of paramount importance for the well-posedness of the problem of composite laminates design.

The proof of the non-convexity of the feasible domain of laminates, shall suggest the adoption of the Polar parameters as a unified formalisation of the plane anisotropy. Polar parameters are *true* tensor invariant quantities, are strictly related to the elastic symmetries, provide a description for high-order shear theories and a compact mathematical description for engineering-interest laminates. Conversely, Lamination parameters do not have all these properties. Since the feasibility domain is non-convex either using the former or the latter description of the plane anisotropy, the choice of Lamination parameters seems an obsolete one.

The asymptotic study of the behaviour of a stiffened-plate-like body fosters many perspectives, as well. This investigation suggests the study of different structural patterns to support more rational modelling choices of the designers, either in linearised or finite elasticity, either considering isotropic or anisotropic materials. This kind of studies is interesting *per se*, because it provides a rational ansatz-free justification of the structural models commonly used in structural design problems. Besides, the asymptotic study of "joint" structures may be at the basis for the formulation of new finite elements, to be used for a more profitable modelling of junction regions between different structural models. This kind of studies is very important, since it contributes to set the current mechanical models and theories on firmer grounds. Even though many results have been achieved, many others still remain to be found in an open-wide scenario. For instance, the recovering of the limit problem for structures with junctions, hierarchical structures, multi-scale structures, lattice structures, nanomaterials (e.g. graphene), non-Euclidean elastic bodies (i.e. frustrated states with residual stresses), multi-phase and phase-transforming solids gels and films, and many others applications.

Bibliography

- Aaronson, S. (2016). $P = NP$? In J. F. Nash & M. T. Rassias (Eds.), *Open problems in mathematics* (pp. 1–122). Springer International Publishing. https://doi.org/10.1007/978-3-319-32162-2_1
- Abu Salem, K., Binante, V., Cipolla, V., & Maganzi, M. (2018). Parsifal project: A breakthrough innovation in air transport. *Aerotec. Missili Spaz.*, 97(1), 40–46. <https://doi.org/https://doi.org/10.1007/BF03404764>
- Abu Salem, K., Palaia, G., Bianchi, M., Zanetti, D., Cipolla, V., & Binante, V. (2020). Preliminary Take-Off Analysis and Simulation of PrandtlPlane Commercial Aircraft. *Aerotecnica Missili & Spazio*. <https://doi.org/10.1007/s42496-020-00056-0>
- ACARE. (2017). *Strategic Research and Innovation Agenda (SRIA)* (tech. rep.). Advisory Council for Aviation Research and Innovation in Europe.
- Adams, D. B., Watson, L. T., Gürdal, Z., & Anderson-Cook, C. M. (2004). Genetic algorithm optimization and blending of composite laminates by locally reducing laminate thickness. *Advances in Engineering Software*, 35(1), 35–43. <https://doi.org/10.1016/j.advengsoft.2003.09.001>
- Albazzan, M. A., Harik, R., Tatting, B. F., & Gürdal, Z. (2019). Efficient design optimization of nonconventional laminated composites using lamination parameters: A state of the art. *Composite Structures*, 209, 362–374. <https://doi.org/10.1016/j.compstruct.2018.10.095>
- Allaire, G., & Delgado, G. (2016). Stacking sequence and shape optimization of laminated composite plates via a level-set method. *Journal of the Mechanics and Physics of Solids*, 97, 168–196. <https://doi.org/10.1016/j.jmps.2016.06.014>
- Altmann, S. (2005). *Rotations, quaternions, and double groups*. Dover Publications.
- Ansys®. (2013). *Ansys® Mechanical APDL Basic Analysis Guide. Release 15.0*. ANSYS Inc. Southpointe, 257 Technology Drive: Canonsburg, PA 15317.
- Anzellotti, G., Baldo, S., & Percivale, D. (1994). Dimension reduction in variational problems, asymptotic development in Γ -convergence and thin structures in elasticity. *Asymptot. Anal.*, 9(1), 61–100.
- Arrieta, A., & Stritz, A. G. (2005). Optimal design of aircraft structures with damage tolerance requirements. *Struct Multidisc Optim.*, 30. <https://doi.org/10.1007/s00158-004-0510-0>

- Aufranc, M. (1990). Plaques radiés par des poutres. *Comptes rendus de l'Académie des Sciences - Série I - Mathématique*.
- Aymerich, F., & Serra, M. (2008). Optimization of laminate stacking sequence for maximum buckling load using the ant colony optimization (ACO) metaheuristic. *Composites Part A: Applied Science and Manufacturing*, 39(2), 262–272. <https://doi.org/10.1016/j.compositesa.2007.10.011>
- Bailie, J. A., Ley, R. P., & Pasricha, A. (1997). *A Summary and Review of Composite Laminate Design Guidelines* (tech. rep. NAS1-19347). Northrop Grumman Military Aircraft Systems Division.
- Ball, J. M. (1976). Convexity conditions and existence theorems in nonlinear elasticity. *Archive for Rational Mechanics and Analysis*, 63(4), 337–403. <https://doi.org/10.1007/bf00279992>
- Barbero, E. J. (2013, December 11). *Finite Element Analysis of Composite Materials Using ANSYS®*. Taylor & Francis Inc.
- Beccasio, N., Tesconi, M., & Frediani, A. (2012). PrandtlPlane propelled with liquid hydrogen: A preliminary study. In *Springer optimization and its applications* (pp. 1–25). Springer US. https://doi.org/10.1007/978-1-4614-2435-2_1
- Benaouali, A., & Kachel, S. (2019). Multidisciplinary design optimization of aircraft wing using commercial software integration. *Aerospace Science and Technology*, 92, 766–776. <https://doi.org/10.1016/j.ast.2019.06.040>
- Bendsøe, M. P., & Sigmund, O. (2004). *Topology Optimization*. Springer Berlin Heidelberg. <https://doi.org/10.1007/978-3-662-05086-6>
- Bertini, F., & Nuti, A. (2018). *Design and Dynamic Modelling of a Fuselage-Mounted Main Landing Gear for a PrandtlPlane Civil Transport Aircraft* (Master's thesis). University of Pisa. <https://etd.adm.unipi.it/theses/available/etd-01312018-182845/>
- Bianchi, M. (2018). *Analysis of take-off performance of a Prandtlplane 300 seat civil transport aircraft* (Master's thesis). University of Pisa. <https://etd.adm.unipi.it/t/etd-09112018-020609/>
- Bisagni, C., & Vescovini, R. (2015). A fast procedure for the design of composite stiffened panels. *The Aeronautical Journal*, 119(1212), 185–201. <https://doi.org/10.1017/S0001924000010332>
- Bloomfield, M. W., Diaconu, C. G., & Weaver, P. M. (2008). On feasible regions of lamination parameters for lay-up optimization of laminated composites. *Proceedings of the Royal Society A: Mathematical, Physical and Engineering Sciences*, 465(2104), 1123–1143. <https://doi.org/10.1098/rspa.2008.0380>
- Bordogna, M. T., Lancelot, P., Bettebghor, D., & Breuker, R. D. (2020). Static and dynamic aeroelastic tailoring with composite blending and manoeuvre load alleviation. *Structural and Multidisciplinary Optimization*. <https://doi.org/10.1007/s00158-019-02446-w>
- Bordogna, M. T., Macquart, T., Bettebghor, D., & Breuker, R. D. (2016). Aeroelastic optimization of variable stiffness composite wing with blending constraints. In *17th AIAA/ISSMO multidisciplinary analysis and optimization conference*. <https://doi.org/10/ggr55h>
- Boyd, S., & Vandenberghe, L. (2019). *Convex optimization*. Cambridge University Press.
- Braides, A. (2002). *Γ -convergence for Beginners*. Oxford University Press.

- Buttazzo, G. (1989). *Semicontinuity, Relaxation and Integral Representation in the Calculus of Variations*. Longman Higher Education.
- Cairns, D., Mandell, J., Scott, M., & Maccagnano, J. (1999). Design and manufacturing considerations for ply drops in composite structures. *Composites Part B: Engineering*, 30(5), 523–534. [https://doi.org/10.1016/s1359-8368\(98\)00043-2](https://doi.org/10.1016/s1359-8368(98)00043-2)
- Calafiore, G., & El Ghaoui, L. (2014, October 31). *Optimization models*. Cambridge University Press.
- Caprino, G., & Crivelli Visconti, I. (1982). A note on specially orthotropic laminates. *Journal of Composite Materials*, 16(5), 395–399. <https://doi.org/10.1177/002199838201600504>
- Carrera, E., Pagani, A., & Silva, G. (2018). Global-local structural analysis of composite wings. In *31th congress of the international council of the aeronautical sciences*. https://www.icas.org/ICAS_ARCHIVE/ICAS2018/data/papers/ICAS2018_0245_paper.pdf
- Catapano, A. (2013). *Stiffness and strength optimisation of the anisotropy distribution for laminated structures* (Doctoral dissertation) [English]. Université Pierre et Marie Curie - Paris VI. <https://tel.archives-ouvertes.fr/tel-00952372/document>
- Catapano, A., Desmorat, B., & Vannucci, P. (2012). Invariant formulation of phenomenological failure criteria for orthotropic sheets and optimisation of their strength. *Mathematical Methods in the Applied Sciences*, 35(15), 1842–1858. <https://doi.org/10.1002/mma.2530>
- Catapano, A., Desmorat, B., & Vannucci, P. (2014). Stiffness and strength optimization of the anisotropy distribution for laminated structures. *Journal of Optimization Theory and Applications*, 167(1), 118–146. <https://doi.org/10.1007/s10957-014-0693-5>
- Catapano, A., & Montemurro, M. (2014a). A multi-scale approach for the optimum design of sandwich plates with honeycomb core. part i: Homogenisation of core properties. *Composite Structures*, 118, 664–676. <https://doi.org/10.1016/j.compstruct.2014.07.057>
- Catapano, A., & Montemurro, M. (2014b). A multi-scale approach for the optimum design of sandwich plates with honeycomb core. part II: The optimisation strategy. *Composite Structures*, 118, 677–690. <https://doi.org/10.1016/j.compstruct.2014.07.058>
- Catapano, A., & Montemurro, M. (2018). On the correlation between stiffness and strength properties of anisotropic laminates. *Mechanics of Advanced Materials and Structures*, 26(8), 651–660. <https://doi.org/10.1080/15376494.2017.1410906>
- Cavallaro, R. (2014). *Nonlinear aeroelastic analysis of joined-wing configurations* (Doctoral dissertation). San Diego State University. <https://escholarship.org/content/qt1p85h6q2/qt1p85h6q2.pdf>
- Cavallaro, R., Bombardieri, R., Demasi, L., & Iannelli, A. (2015). Prandtlplane joined wing: Body freedom flutter, limit cycle oscillation and freeplay studies. *Journal of Fluids and Structures*, 59, 57–84. <https://doi.org/10.1016/j.jfluidstructs.2015.08.016>
- Cavallaro, R., Bombardieri, R., & Santos, J. (2017). Discrete gust response of a box-wing configuration. In *6th CEAS Conference, Bucarest*.
- Cavallaro, R., Bombardieri, R., Silvani, S., Demasi, L., & Bernardini, G. (2016). Aeroelasticity of the prandtlplane: Body freedom flutter, freeplay, and limit cycle oscillation. In G. Buttazzo & A. Frediani (Eds.), *Variational analysis and aerospace engineering: Mathematical challenges for the aerospace of the future*. Springer. https://doi.org/10.1007/978-3-319-45680-5_3

- Cavallaro, R., & Demasi, L. (2016). Challenges, ideas, and innovations of joined-wing configurations: A concept from the past, an opportunity for the future. *Progress in Aerospace Sciences*, 87, 1–93. <https://doi.org/10.1016/j.paerosci.2016.07.002>
- Cavallaro, R., Demasi, L., & Bombardieri, R. (2016). Aeroelasticity of joined wings: Unique aspects and challenges. In *57th AIAA/ASCE/AHS/ASC structures, structural dynamics, and materials conference*. <https://doi.org/10.2514/6.2016-0238>
- CERAS. (2014). Ceras-csr01: Short range reference aircraft. <http://ceras.ilr.rwthachen.de/trac/wiki/CeRAS/AircraftDesigns/CSR01>
- Chedrik, V. (2013). Two-level design optimization of aircraft structures under stress, buckling and aeroelasticity constraints. In *10th world congress on structural and multidisciplinary optimisation*.
- Chedrik, V., & Tuktarov, S. (2015). Structural design of aircraft wing based on topology and global-local optimization. In *11th world congress on structural and multidisciplinary optimisation*. http://web.aeromech.usyd.edu.au/WCSMO2015/papers/1160_paper.pdf
- Ciampa, P. D., Nagel, B., & Tooren, M. (2010, April). Global Local Structural Optimization of Transportation Aircraft Wings. In *51st AIAA/ASME/ASCE/AHS/ASC structures, structural dynamics, and materials conference*. <https://doi.org/10.2514/6.2010-3098>
- Ciarlet, P. G. (1990). *Plates and Junctions in Elastic Multi-Structures: An Asymptotic Analysis*. Masson.
- Ciarlet, P. G. (1994). *Mathematical Elasticity. Volume 1: Three Dimensional Elasticity*. North Holland.
- Ciarlet, P. G., Le Dret, H., & Nzenywa, R. (1989). Junctions between three-dimensional and two-dimensional linear elastic structures. *J. Math. Pures Appl. (9)*, 68(3), 261–295.
- Cipolla, V., Binante, V., & Nardone, A. (2018). Design, optimization and manufacturing of metallic wings of light aircraft. *Aerotecnica Missili e spazio*, 97(4), 219–227. <https://doi.org/10.19249/ams.v97i4.350>
- Cipolla, V., Frediani, A., & Lonigro, E. (2016). Aerodynamic design of a light amphibious prandtlplane: Wind tunnel tests and cfd validation. *Aerotecnica Missili & Spazio*, 94(2). <https://doi.org/10.19249/ams.v94i2.128>
- Cipolla, V., Salem, K. A., Picchi Scardaoni, M., & Binante, V. (2020). Preliminary design and performance analysis of a box-wing transport aircraft. In *AIAA scitech 2020 forum*. <https://doi.org/10.2514/6.2020-0267>
- Cormen, T. H., Leiserson, C. E., Rivest, R. L., & Stein, C. (2001). *Introduction to algorithms*. The MIT Press.
- Costa, G., Montemurro, M., & Pailhès, J. (2017). A 2d topology optimisation algorithm in NURBS framework with geometric constraints. *International Journal of Mechanics and Materials in Design*, 14(4), 669–696. <https://doi.org/10.1007/s10999-017-9396-z>
- Costa, G., Montemurro, M., & Pailhès, J. (2019). NURBS hyper-surfaces for 3d topology optimization problems. *Mechanics of Advanced Materials and Structures*, 1–20. <https://doi.org/10.1080/15376494.2019.1582826>
- Costa, G., Montemurro, M., Pailhès, J., & Perry, N. (2019). Maximum length scale requirement in a topology optimisation method based on NURBS hyper-surfaces. *CIRP Annals*, 68(1), 153–156. <https://doi.org/10.1016/j.cirp.2019.04.048>

- Dababneha, O., & Kipouros, T. (2018a). Influence of High Fidelity Structural Models on the Predicted Mass of Aircraft Wing Using Design Optimization. *Aerosp. Sci. Technol.* <https://doi.org/https://doi.org/10.1016/j.ast.2018.05.043>
- Dababneha, O., & Kipouros, T. (2018b). A review of aircraft wing mass estimation methods. *Aerosp. Sci. Technol.*, 72. <https://doi.org/https://doi.org/10.1016/j.ast.2017.11.006>
- Dacorogna, B. (2007). *Direct Methods in the Calculus of Variations*. Springer New York. <https://doi.org/10.1007/978-0-387-55249-1>
- Dal Canto, D., Frediani, A., Ghiringhelli, G. L., & Terraneo, M. (2012). The lifting system of a prandtlplane, part 1: Design and analysis of a light alloy structural solution. In G. Buttazzo & A. Frediani (Eds.), *Variational analysis and aerospace engineering: Mathematical challenges for aerospace design*. Springer. https://doi.org/https://doi.org/10.1007/978-1-4614-2435-2_9
- Dal Maso, G. (1993, January 1). *An Introduction to Γ -Convergence*. Birkhäuser Boston.
- Darwin, C. (1871). *On the origin of species*. D. Appleton; Co. <https://doi.org/10.5962/bhl.title.28875>
- Davini, C., Freddi, L., & Paroni, R. (2014a). Linear Models for Composite Thin-Walled Beams by Γ -Convergence. Part I: Open Cross Sections. *SIAM Journal on Mathematical Analysis*, 46(5), 3296–3331. <https://doi.org/10.1137/140951473>
- Davini, C., Freddi, L., & Paroni, R. (2014b). Linear Models for Composite Thin-Walled Beams by Γ -Convergence. Part II: Closed Cross-Sections. *SIAM Journal on Mathematical Analysis*, 46(5), 3332–3360. <https://doi.org/10.1137/140964321>
- De Giorgi, E., & Franzoni, T. (1975). Su un tipo di convergenza variazionale. *Atti Accademia Nazionale dei Lincei. Classe di Scienze Fisiche, Matematiche e Naturali. Rendiconti*, 58(8), 842–850.
- Diaconu, C. G., Sato, M., & Sekine, H. (2002). Feasible region in general design space of lamination parameters for laminated composites. *AIAA Journal*, 40(3), 559–565. <https://doi.org/10.2514/2.1683>
- Diolosa, L. M. F. (2018). *Preliminary studies for the structural optimization of a prandtlplane wing* (Master's thesis). University of Pisa, Department of Civil and Industrial Engineering, Aerospace division. <https://etd.adm.unipi.it/theses/available/etd-09032018-165921/>
- Divoux, N., & Frediani, A. (2012). The lifting system of a prandtlplane, part 2: Preliminary study on flutter characteristics. In G. Buttazzo & A. Frediani (Eds.), *Variational analysis and aerospace engineering: Mathematical challenges for aerospace design*. Springer. https://doi.org/https://doi.org/10.1007/978-1-4614-2435-2_10
- Dorigo, M., Maniezzo, V., & Colorni, A. (1996). Ant system: Optimization by a colony of cooperating agents. *IEEE Transactions on Systems, Man, and Cybernetics, Part B (Cybernetics)*, 26(1), 29–41. <https://doi.org/10.1109/3477.484436>
- Dorigo, M. (1992). *Optimization, Learning and Natural Algorithms* (Doctoral dissertation). Politecnico di Milano.
- Dorigo, M., Birattari, M., & Stutzle, T. (2006). Ant colony optimization. *IEEE Computational Intelligence Magazine*, 1(4), 28–39. <https://doi.org/10.1109/mci.2006.329691>
- Drela, M., & Youngren, H. (2013). Avl overview. <http://web.mit.edu/drela/Public/web/avl/>

- EASA. (2018). Certification specifications and acceptable means of compliance for large aeroplanes, cs 25 amendment 22. <https://www.easa.europa.eu/document-library/certification-specifications/cs-25-amendment-22>
- EREA. (2012). *Study on the Air Transport System in 2050 from vision towards a planning for research and innovation* (tech. rep.). European Research Establishments in Aeronautics.
- European Commission. (2011). *Flightpath 2050: Europe's Vision for Aviation* (tech. rep.). European Commission, Directorate General for Research, Innovation, Directorate General for Mobility, and Transport.
- Ferrari, F., & Sigmund, O. (2019). Revisiting topology optimization with buckling constraints. *Structural and Multidisciplinary Optimization*, 59(5), 1401–1415. <https://doi.org/10.1007/s00158-019-02253-3>
- Fletcher, R. (1987). *Practical Methods of Optimization* (Second). John Wiley & Sons.
- Fogel, L. J., Owens, A. J., & Walsh, M. J. (2009). Artificial intelligence through simulated evolution. In *Evolutionary computation*. IEEE. <https://doi.org/10.1109/9780470544600.ch7>
- Freddi, L., Morassi, A., & Paroni, R. (2007). Thin-walled beams: a derivation of Vlassov theory via Γ -convergence. *Journal of Elasticity*, 86, 263–296. <https://doi.org/https://doi.org/10.1007/s10659-006-9094-9>
- Freddi, L., Mora, M., & Paroni, R. (2013). Nonlinear Thin-Walled Beams with a Rectangular Cross-Section. *Mathematical Models and Methods in Applied Sciences*, 23(04), 743–775. <https://doi.org/10.1142/s0218202512500595>
- Freddi, L., Morassi, A., & Paroni, R. (2004). Thin-Walled Beams: the Case of the Rectangular Cross-Section. *Journal of Elasticity*, 76(1), 45–66. <https://doi.org/10.1007/s10659-004-7193-z>
- Freddi, L., Murat, F., & Paroni, R. (2009). Anisotropic inhomogeneous rectangular thin-walled beams. *SIAM Journal on Mathematical Analysis*, 40(5), 1923–1951.
- Freddi, L., Murat, F., & Paroni, R. (2010). Saint-Venant's theory for beams with multi-connected cross-section: Justification and error estimate. *Asymptotic Analysis*, 70(3-4), 177–197. <https://doi.org/10.3233/ASY-2010-1013>
- Frediani, A., Cipolla, V., Abu Salem, K., Binante, V., & Picchi Scardaoni, M. (2019). Conceptual design of prandtlplane civil transport aircraft. *Proceedings of the Institution of Mechanical Engineers, Part G: Journal of Aerospace Engineering*. <https://doi.org/https://doi.org/10.1177/0954410019826435>
- Frediani, A., & Montanari, G. (2009). Best wing system: An exact solution of the prandtl's problem. In G. Buttazzo & A. Frediani (Eds.), *Variational analysis and aerospace engineering*. Springer. https://doi.org/https://doi.org/10.1007/978-0-387-95857-6_11
- Frediani, A., Quattrone, F., & Contini, F. (2012). The lifting system of a prandtlplane, part 3: Structures made in composites. In G. Buttazzo & A. Frediani (Eds.), *Variational analysis and aerospace engineering: Mathematical challenges for aerospace design*. Springer. https://doi.org/https://doi.org/10.1007/978-1-4614-2435-2_11
- Frediani, A., Cipolla, V., Abu Salem, K., Binante, V., & Picchi Scardaoni, M. (2017). On the preliminary design of PrandtlPlane civil transport aircraft. In *Proceedings of the 7th European Conference for Aeronautics and Space Sciences (EUCASS)*. <https://doi.org/10.13009/EUCASS2017-546>

- Frediani, A., Cipolla, V., & Rizzo, E. (2012). The PrandtlPlane configuration: Overview on possible applications to civil aviation. In *Springer optimization and its applications* (pp. 179–210). Springer US. https://doi.org/10.1007/978-1-4614-2435-2_8
- Frediani, A., Montanari, G., & Pappalardo, M. (1999). Sul problema di prandtl della minima resistenza indotta di un sistema portante. In *Xv congresso aidaa (associazione italiana di aeronautica e astronautica), torino*.
- Frediani, A., Oliviero, F., & Rizzo, E. (2015). Design of an airfreight system based on an innovative PrandtlPlane aircraft. In *56th AIAA/ASCE/AHS/ASC structures, structural dynamics, and materials conference*. <https://doi.org/10.2514/6.2015-1186>
- Gaddis, T. (2015). *Starting out with C++*. From Control Structures through Objects (8th). Pearson.
- Garulli, T. (2020). *Design and validation of Fully-Uncoupled Multi-Directional lay-ups to evaluate interlaminar fracture toughness* (Doctoral dissertation) [English]. Université de Bordeaux, Università di Pisa. <https://tel.archives-ouvertes.fr/tel-02968779/document>
- Garulli, T., Catapano, A., Montemurro, M., Jumel, J., & Fanteria, D. (2018). Quasi-trivial stacking sequences for the design of thick laminates. *Composite Structures*, 200, 614–623. <https://doi.org/10.1016/j.compstruct.2018.05.120>
- Gaudiello, A., Monneau, R., Mossino, J., Murat, F., & Sili, A. (2007). Junction of elastic plates and beams. *ESAIM: Control, Optimisation and Calculus of Variations*, 13(3), 419–457. <https://doi.org/10.1051/cocv:2007036>
- Gaudiello, A., & Zappale, E. (2010). A Model of Joined Beams as Limit of a 2D Plate. *Journal of Elasticity*, 103(2), 205–233. <https://doi.org/10.1007/s10659-010-9281-6>
- Ghiasi, H., Fayazbakhsh, K., Pasini, D., & Lessard, L. (2010). Optimum stacking sequence design of composite materials Part II: Variable stiffness design. *Composite Structures*, 93(1), 1–13. <https://doi.org/10.1016/j.compstruct.2010.06.001>
- Ghiasi, H., Pasini, D., & Lessard, L. (2009). Optimum stacking sequence design of composite materials Part I: Constant stiffness design. *Composite Structures*, 90(1), 1–11. <https://doi.org/10.1016/j.compstruct.2009.01.006>
- Gill, P. E., Murray, W., Saunders, M. A., & Wright, M. H. (1984). Procedures for optimization problems with a mixture of bounds and general linear constraints. *ACM Transactions on Mathematical Software*, 10(3), 282–298. <https://doi.org/10.1145/1271.1276>
- Glover, F. (1977). Heuristics for Integer Programming Using Surrogate Constraints. *Decision Sciences*, 8(1), 156–166. <https://doi.org/10.1111/j.1540-5915.1977.tb01074.x>
- Goldberg, D. E. (1989). *Genetic Algorithms in Search, Optimization, and Machine Learning*. Addison-Wesley Professional.
- Goldberg, D. E., & Holland, J. H. (1988). Genetic algorithms and machine learning. *Machine Learning*, 3(2/3), 95–99. <https://doi.org/10.1023/a:1022602019183>
- Graham, R. L., Knuth, D. E., & Patashnik, O. (1994, February 1). *Concrete mathematics: A foundation for computer science*. Addison Wesley Pub. Co. Inc.
- Green, G. M. (1916). The linear dependence of functions of several variables, and completely integrable systems of homogeneous linear partial differential equations. *Transactions of the American Mathematical Society*, 17(4), 483–483. <https://doi.org/10.1090/s0002-9947-1916-1501055-6>

- Grenestedt, J. L., & Gudmundson, P. (1993). Layup optimization of composite material structures. In *Optimal design with advanced materials* (pp. 311–336). Elsevier. <https://doi.org/10.1016/b978-0-444-89869-2.50027-5>
- Griso, G. (2005). Asymptotic behavior of Structures made of Plates. *Analysis and applications*, 3(4), 325–356. <https://doi.org/10.1142/S0219530505000613>
- Gruais, I. (1993a). Modeling of the junction between a plate and a rod in nonlinear elasticity. *Asymptotic Analysis*, 7(3), 179–194. <https://doi.org/10.3233/ASY-1993-7302>
- Gruais, I. (1993b). Modélisation de la jonction entre une plaque et une poutre en élasticité linéarisée. *ESAIM: Mathematical Modelling and Numerical Analysis - Modélisation Mathématique et Analyse Numérique*, 27(1), 77–105. http://www.numdam.org/item/M2AN_1993__27_1_77_0
- Gurtin, M. (1981). *An Introduction to Continuum Mechanics*. Academic Press Inc.
- Hale, J. (2006). Boeing 787 from the Ground Up. *Aeromagazine*, 24(6), 17–24. https://www.boeing.com/commercial/aeromagazine/articles/qtr_4_06/AERO_Q406.pdf
- Hammer, V., Bendsøe, M., Lipton, R., & Pedersen, P. (1997). Parametrization in laminate design for optimal compliance. *International Journal of Solids and Structures*, 34(4), 415–434. [https://doi.org/10.1016/s0020-7683\(96\)00023-6](https://doi.org/10.1016/s0020-7683(96)00023-6)
- Harrysson, M., & Laestander, H. (2014). *Solving Sudoku efficiently with Dancing Links* (Master's thesis). KTH Royal Institute of Technology. https://www.kth.se/social/files/58861771f276547fe1dbf8d1/HLaestanderMHarrysson_dkand14.pdf
- Haykin, S. (1998). *Neural networks: A comprehensive foundation*. Prentice Hall.
- He, K., Hoa, S., & Ganesan, R. (2000). The study of tapered laminated composite structures: A review. *Composites Science and Technology*, 60(14), 2643–2657. [https://doi.org/10.1016/s0266-3538\(00\)00138-x](https://doi.org/10.1016/s0266-3538(00)00138-x)
- Herencia, J. E., Weaver, P. M., & Friswell, M. I. (2008). Initial sizing optimisation of anisotropic composite panels with t-shaped stiffeners. *Thin-Walled Structures*, 46(4), 399–412. <https://doi.org/10.1016/j.tws.2007.09.003>
- Holland, J. H. (1992). *Adaptation in natural and artificial systems: An introductory analysis with applications to biology, control, and artificial intelligence (complex adaptive systems)*. A Bradford Book.
- Ijsselmuiden, S. T., Abdalla, M. M., & Gürdal, Z. (2010). Optimization of variable-stiffness panels for maximum buckling load using lamination parameters. *AIAA Journal*, 48(1), 134–143. <https://doi.org/10.2514/1.42490>
- Ijsselmuiden, S. T., Abdalla, M. M., Seresta, O., & Gürdal, Z. (2009). Multi-step blended stacking sequence design of panel assemblies with buckling constraints. *Composites Part B: Engineering*, 40(4), 329–336. <https://doi.org/10.1016/j.compositesb.2008.12.002>
- Irisarri, F.-X., Lasseigne, A., Leroy, F.-H., & Riche, R. L. (2014). Optimal design of laminated composite structures with ply drops using stacking sequence tables. *Composite Structures*, 107, 559–569. <https://doi.org/10.1016/j.compstruct.2013.08.030>
- Irisarri, F.-X., Laurin, F., Leroy, F.-H., & Maire, J.-F. (2011). Computational strategy for multi-objective optimization of composite stiffened panels. *Composite Structures*, 93(3), 1158–1167. <https://doi.org/10.1016/j.compstruct.2010.10.005>

- Izzi, M., Montemurro, M., Catapano, A., Fanteria, D., & Pailhès, J. (2020). Multi-scale optimisation of thin-walled structures by considering a global/local modelling approach. *Proceedings of the Institution of Mechanical Engineers, Part G*. <https://doi.org/10.1177/0954410020939338>
- Izzi, M., Montemurro, M., Catapano, A., & Pailhès, J. (2020). A multi-scale two-level optimisation strategy integrating a global/local modelling approach for composite structures. *Composite Structures*. <https://doi.org/10.1016/j.compstruct.2020.111908>
- Jemitola, P. O., & Fielding, J. P. (2012). Box wing aircraft conceptual design. In *28th congress of the international council of the aeronautical sciences (icas 2012)*.
- Jones, R. M. (2018). *Mechanics of composite materials*. CRC Press. <https://doi.org/10.1201/9781498711067>
- Kandil, N., & Verchery, G. (1988). New methods of design for stacking sequences of laminates. *Computer aided design in composite material technology*, 243–257.
- Kennedy, J., & Eberhart, R. (1995). Particle swarm optimization. In *Proceedings of icnn'95 - international conference on neural networks*. <https://doi.org/10.1109/ICNN.1995.488968>
- Knuth, D. E. (2000). Dancing links. *Millennial Perspectives in Computer Science, 2000*, 187–214arXiv cs/0011047v1.
- Koide, R. M., von Zeska de França, G., & Luersen, M. A. (2013). An ant colony algorithm applied to lay-up optimization of laminated composite plates. *Latin American Journal of Solids and Structures*, 10(3), 491–504. <https://doi.org/10.1590/s1679-78252013000300003>
- Kristinsdottir, B. P., Zabinsky, Z. B., Tuttle, M. E., & Neogi, S. (2001). Optimal design of large composite panels with varying loads. *Composite Structures*, 51(1), 93–102. [https://doi.org/10.1016/s0263-8223\(00\)00128-8](https://doi.org/10.1016/s0263-8223(00)00128-8)
- Le Dret, H. (1992). *Problemes variationnels dans les multi-domaines: modelisation des jonctions et applications*. Masson.
- Le Dret, H. (1989). Modeling of the junction between two rods. *J. Math. Pures Appl. (9)*, 68(3), 365–397.
- Lehoucq, R. B., Sorensen, D. C., & Yang, C. (1998). *ARPACK users guide*. Society for Industrial; Applied Mathematics. <https://doi.org/10.1137/1.9780898719628>
- Leugering, G., Nazarov, S. A., & Slutskiy, A. S. (2018). The asymptotic analysis of a junction of two elastic beams. *ZAMM - Journal of Applied Mathematics and Mechanics / Zeitschrift für Angewandte Mathematik und Mechanik*, 99(1), e201700192. <https://doi.org/10.1002/zamm.201700192>
- Liu, B., Haftka, R., & Akgün, M. (2000). Two-level composite wing structural optimization using response surfaces. *Structural and Multidisciplinary Optimization*, 20(2), 87–96. <https://doi.org/10.1007/s001580050140>
- Liu, D., Toropov, V. V., Querin, O. M., & Barton, D. C. (2011). Bilevel optimization of blended composite wing panels. *Journal of Aircraft*, 48(1), 107–118. <https://doi.org/10.2514/1.c000261>
- Liu, Q., Jrad, M., Mulani, S. B., & Kapania, R. K. (2015). Integrated global wing and local panel optimization of aircraft wing. In *56th AIAA/ASCE/AHS/ASC structures, structural dynamics, and materials conference*. <https://doi.org/10.2514/6.2015-0137>

- Liu, Q., Jrad, M., Mulani, S. B., & Kapania, R. K. (2016). Global/local optimization of aircraft wing using parallel processing. *AIAA Journal*, *54*(11), 3338–3348. <https://doi.org/10.2514/1.j054499>
- Liu, S., Hou, Y., Sun, X., & Zhang, Y. (2012). A two-step optimization scheme for maximum stiffness design of laminated plates based on lamination parameters. *Composite Structures*, *94*(12), 3529–3537. <https://doi.org/10.1016/j.compstruct.2012.06.014>
- Maas, C. (2000). Cmsort. <http://www.chmaas.handshake.de/delphi/freeware/cmsort/cmsort.htm>
- Macquart, T., Maes, V., Bordogna, M. T., Pirrera, A., & Weaver, P. (2018). Optimisation of composite structures – enforcing the feasibility of lamination parameter constraints with computationally-efficient maps. *Composite Structures*, *192*, 605–615. <https://doi.org/10.1016/j.compstruct.2018.03.049>
- Macquart, T., Bordogna, M. T., Lancelot, P., & Breuker, R. D. (2016). Derivation and application of blending constraints in lamination parameter space for composite optimisation. *Composite Structures*, *135*, 224–235. <https://doi.org/10.1016/j.compstruct.2015.09.016>
- Mao, K. M., & Sun, C. T. (1991). A refined global-local finite element analysis method. *International Journal for Numerical Methods in Engineering*, *32*(1), 29–43. <https://doi.org/10.1002/nme.1620320103>
- Mendel, G. (1865). Versuche über pflanzen-hybriden. *Verhandlungen des naturforschenden Vereines in Brünn*, *4*, 3–47.
- Miki, M. (1982). Material design of composite laminates with required in-plane elastic properties [ICCM-IV, Tokyo]. In T. Hayashi, K. Kawata, & S. Umekawa (Eds.).
- Montemurro, M. (2018). *A contribution to the development of design strategies for the optimisation of lightweight structures* (HDR thesis). Université de Bordeaux. <http://hdl.handle.net/10985/15155>
- Montemurro, M., Vincenti, A., & Vannucci, P. (2012a). Design of the elastic properties of laminates with a minimum number of plies. *Mechanics of Composite Materials*, *48*(4), 369–390. <https://doi.org/10.1007/s11029-012-9284-4>
- Montemurro, M. (2015a). An extension of the polar method to the First-order Shear Deformation Theory of laminates. *Composite Structures*, *127*, 328–339. <https://doi.org/10.1016/j.compstruct.2015.03.025>
- Montemurro, M. (2015b). Corrigendum to “An extension of the polar method to the First-order Shear Deformation Theory of laminates”. *Composite Structures*, *131*, 1143–1144. <https://doi.org/10.1016/j.compstruct.2015.06.002>
- Montemurro, M. (2015c). The polar analysis of the third-order shear deformation theory of laminates. *Composite Structures*, *131*, 775–789. <https://doi.org/10.1016/j.compstruct.2015.06.016>
- Montemurro, M., & Catapano, A. (2016). A new paradigm for the optimum design of variable angle tow laminates. In *Variational analysis and aerospace engineering* (pp. 375–400). Springer International Publishing. https://doi.org/10.1007/978-3-319-45680-5_14
- Montemurro, M., & Catapano, A. (2017). On the effective integration of manufacturability constraints within the multi-scale methodology for designing variable angle-tow laminates. *Composite Structures*, *161*, 145–159. <https://doi.org/10.1016/j.compstruct.2016.11.018>

- Montemurro, M., & Catapano, A. (2019). A general B-Spline surfaces theoretical framework for optimisation of variable angle-tow laminates. *Composite Structures*, 209, 561–578. <https://doi.org/10.1016/j.compstruct.2018.10.094>
- Montemurro, M., Catapano, A., & Doroszewski, D. (2016). A multi-scale approach for the simultaneous shape and material optimisation of sandwich panels with cellular core. *Composites Part B: Engineering*, 91, 458–472. <https://doi.org/10.1016/j.compositesb.2016.01.030>
- Montemurro, M., Izzi, M. I., El-Yagoubi, J., & Fanteria, D. (2019). Least-weight composite plates with unconventional stacking sequences: Design, analysis and experiments. *Journal of Composite Materials*, 53(16), 2209–2227. <https://doi.org/10.1177/0021998318824783>
- Montemurro, M., Pagani, A., Fiordilino, G. A., Pailhès, J., & Carrera, E. (2018). A general multi-scale two-level optimisation strategy for designing composite stiffened panels. *Composite Structures*, 201, 968–979. <https://doi.org/10.1016/j.compstruct.2018.06.119>
- Montemurro, M., Vincenti, A., Koutsawa, Y., & Vannucci, P. (2013). A two-level procedure for the global optimization of the damping behavior of composite laminated plates with elastomer patches. *Journal of Vibration and Control*, 21(9), 1778–1800. <https://doi.org/10.1177/1077546313503358>
- Montemurro, M., Vincenti, A., & Vannucci, P. (2012b). A two-level procedure for the global optimum design of composite modular structures—application to the design of an aircraft wing. *Journal of Optimization Theory and Applications*, 155(1), 1–23. <https://doi.org/10.1007/s10957-012-0067-9>
- Montemurro, M., Vincenti, A., & Vannucci, P. (2012c). A two-level procedure for the global optimum design of composite modular structures—application to the design of an aircraft wing. *Journal of Optimization Theory and Applications*, 155(1), 24–53. <https://doi.org/10.1007/s10957-012-0070-1>
- Morassi, A. (2008). Strain, Stress and Linearized Elasticity. In A. Morassi & R. Paroni (Eds.), *Classical and advanced theories of thin structures* (pp. 1–34). Springer.
- Munk, D. J., Vio, G. A., & Steven, G. P. (2016). A simple alternative formulation for structural optimisation with dynamic and buckling objectives. *Structural and Multidisciplinary Optimization*, 55(3), 969–986. <https://doi.org/10.1007/s00158-016-1544-9>
- Munkres, J. R. (2000). *Topology*. Prentice Hall, Inc.
- Nardinocchi, P. (2002). Modelling junctions of thin plates. *European Journal of Mechanics - A/Solids*, 21(3), 523–534. [https://doi.org/10.1016/s0997-7538\(02\)01222-6](https://doi.org/10.1016/s0997-7538(02)01222-6)
- Nardone, A. (2016). *Progetto di ali di velivoli leggeri costruite per saldatura di lamiere sottili di alluminio* (Master's thesis) [in italian]. University of Pisa, Department of Civil and Industrial Engineering, Aerospace division. <https://etd.adm.unipi.it/theses/available/etd-05222016-162117/>
- Neves, M. M., Rodrigues, H., & Guedes, J. M. (1995). Generalized topology design of structures with a buckling load criterion. *Structural Optimization*, 10(2), 71–78. <https://doi.org/10.1007/bf01743533>
- Nielsen, F., & Sun, K. (2016). Guaranteed bounds on information-theoretic measures of univariate mixtures using piecewise log-sum-exp inequalities. *Entropy*, 18(12), 442. <https://doi.org/10.3390/e18120442>
- Niu, M. C. Y. (1988). *Airframe structural design*. Conmilit Press Ltd.

- Nocedal, J., & Wright, S. (2006). *Numerical Optimization*. Springer-Verlag New York. <https://doi.org/10.1007/978-0-387-40065-5>
- Ntourmas, G., Ozcan, E., Chronopoulos, D., Glock, F., & Daoud, F. (2019). Towards a streamlined stacking sequence optimisation methodology for blended composite aircraft structures. In *Proceedings of the 8th European Conference for Aeronautics and Space Sciences (EUCASS)*. <https://doi.org/10.13009/EUCASS2019-632>
- Okonkwo, P., & Smith, H. (2016). Review of evolving trends in blended wing body aircraft design. *Progress in Aerospace Sciences*, 82, 1–23. <https://doi.org/10.1016/j.paerosci.2015.12.002>
- Oliviero, F., Zanetti, D., & Cipolla, V. (2016). Flight dynamics model for preliminary design of prandtlplane wing configuration with sizing of the control surfaces. *Aerotecnica Missili & Spazio*, 95(4). <https://doi.org/10.19249/ams.v95i4.289>
- Panettieri, E., Montemurro, M., & Catapano, A. (2019). Blending constraints for composite laminates in polar parameters space. *Composites Part B: Engineering*, 168, 448–457. <https://doi.org/10.1016/j.compositesb.2019.03.040>
- Panettieri, E., Montemurro, M., Fanteria, D., & Coccia, F. (2020). Multi-scale least-weight design of a wing-box through a global/local modelling approach. *Journal of Optimization Theory and Applications*. <https://doi.org/10.1007/s10957-020-01693-y>
- Paroni, R. (2008). Constitutive Equations and Variational Elasticity. In A. Morassi & R. Paroni (Eds.), *Classical and advanced theories of thin structures* (pp. 35–59). Springer.
- Paroni, R., & Podio-Guidugli, P. (2014). On variational dimension reduction in structure mechanics. *Journal of Elasticity*, 118(1), 1–13. <https://doi.org/10.1007/s10659-014-9473-6>
- Paroni, R., & Tomassetti, G. (2011). From non-linear elasticity to linear elasticity with initial stress via Γ -convergence. *Continuum Mechanics and Thermodynamics*, 23(4), 347–361. <https://doi.org/10.1007/s00161-011-0184-y>
- Picchi Scardaoni, M., Binante, V., & Cipolla, V. (2017). WAGNER: A new code for parametrical structural study of fuselages of civil transport aircraft. *Aerotecnica Missili & Spazio*, 96(3), 136–147. <https://doi.org/10.1007/bf03404748>
- Picchi Scardaoni, M., Cipolla, V., & Binante, V. (2019a). Overall Preliminary Sizing and Optimization of the Metallic Structures of a PrandtlPlane Civil Transport Aircraft. In *Proceedings of the 8th European Conference for Aeronautics and Space Sciences (EUCASS)*. <https://doi.org/10.13009/EUCASS2019-802>
- Picchi Scardaoni, M., & Frediani, A. (2019a). General closed-form solution of piecewise circular frames of aircraft. *AIAA Journal*, 57(3), 1338–1342. <https://doi.org/10.2514/1.j057712>
- Picchi Scardaoni, M., Izzi, M. I., Panettieri, E., & Montemurro, M. (2019b). Prandtlplane Aircraft Least-Weight Design: A Multi-Scale Optimisation Strategy. In *Italian association of aeronautics and astronautics (aidaa) xxv international congress*. AIDAA.
- Picchi Scardaoni, M., Panettieri, E., & Montemurro, M. (2020). Prandtlplane wing-box least-weight design: A multi-scale optimisation approach. *Aerospace Science and Technology*. <https://doi.org/10.1016/j.ast.2020.106156>
- Picchi Scardaoni, M., & Frediani, A. (2019b). Analytical and finite element approach for the in-plane study of frames of non-conventional civil aircraft. *Aerotecnica Missili & Spazio*, 98(1), 45–61. <https://doi.org/10.1007/s42496-018-00004-z>
- Prandtl, L. (1918). Der Induzierte Widerstand von Mehrdeckern. *Technische Berichte*, 3, 309–315.

- Prandtl, L. (1924). *Induced drag of multiplanes* (technical note No. 182). NACA.
- Raju, G., Wu, Z., & Weaver, P. (2014). On further developments of feasible region of lamination parameters for symmetric composite laminates. In *55th AIAA/ASME/ASCE/AHS/ASC structures, structural dynamics, and materials conference*. <https://doi.org/10.2514/6.2014-1374>
- Reddy, J. N. (2003). *Mechanics of laminated composite plates and shells: Theory and analysis* (Second). CRC Press.
- Reddy, J. N. (2005). *An introduction to the finite element method*. McGraw-Hill Education.
- Rindler, F. (2018). *Calculus of variations*. Springer International Publishing. <https://doi.org/10.1007/978-3-319-77637-8>
- Risse, K., Schäfer, K., Schültke, F., & Stumpf, E. (2015). Central reference aircraft data system (CeRAS) for research community. *CEAS Aeronautical Journal*, 7(1), 121–133. <https://doi.org/10.1007/s13272-015-0177-9>
- Rizzo, E. (2007). *Optimization methods applied to the preliminary design of innovative, non conventional aircraft configurations* (Doctoral dissertation). University of Pisa, Department of Civil and Industrial Engineering, Aerospace division.
- Rizzo, E., & Frediani, A. (2009). Application of optimisation algorithms to aircraft aerodynamics. In G. Buttazzo & A. Frediani (Eds.), *Variational analysis and aerospace engineering*. Springer. https://doi.org/https://doi.org/10.1007/978-0-387-95857-6_23
- Rockafellar, R. (1997). *Convex analysis*. Princeton University Press.
- Rodrigues, H. C., Guedes, J. M., & Bendsøe, M. P. (1995). Necessary conditions for optimal design of structures with a nonsmooth eigenvalue based criterion. *Structural Optimization*, 9(1), 52–56. <https://doi.org/10.1007/bf01742645>
- Roehl, P., Mavris, D., & Schrage, D. (1995). Combined aerodynamic and structural optimization of a high-speed civil transport wing. In *36th structures, structural dynamics and materials conference*. <https://doi.org/10.2514/6.1995-1222>
- Schlueter, M. (2018). *Midaco Solver User Guide* (6.0).
- Schlüter, M., Egea, J. A., & Banga, J. R. (2009). Extended ant colony optimization for non-convex mixed integer nonlinear programming. *Computers & Operations Research*, 36(7), 2217–2229. <https://doi.org/10.1016/j.cor.2008.08.015>
- Schlüter, M., & Gerds, M. (2009). The oracle penalty method. *Journal of Global Optimization*, 47(2), 293–325. <https://doi.org/10.1007/s10898-009-9477-0>
- Schlüter, M., Gerds, M., & Rückmann, J.-J. (2012). A numerical study of MIDACO on 100 MINLP benchmarks. *Optimization*, 61(7), 873–900. <https://doi.org/10.1080/02331934.2012.668545>
- Sebaey, T., Lopes, C., Blanco, N., & Costa, J. (2011). Ant colony optimization for dispersed laminated composite panels under biaxial loading. *Composite Structures*, 94(1), 31–36. <https://doi.org/10.1016/j.compstruct.2011.07.021>
- Seresta, O., Gürdal, Z., Adams, D. B., & Watson, L. T. (2007). Optimal design of composite wing structures with blended laminates. *Composites Part B: Engineering*, 38(4), 469–480. <https://doi.org/10.1016/j.compositesb.2006.08.005>

- Serra, M., & Venini, P. (2006). On some applications of ant colony optimization metaheuristic to plane truss optimization. *Structural and Multidisciplinary Optimization*, 32(6), 499–506. <https://doi.org/10.1007/s00158-006-0042-x>
- Setoodeh, S., Abdalla, M., & Gürdal, Z. (2006). Approximate feasible regions for lamination parameters. In *11th AIAA/ISSMO multidisciplinary analysis and optimization conference*. <https://doi.org/10.2514/6.2006-6973>
- Setoodeh, S., Abdalla, M. M., IJsselmuiden, S. T., & Gürdal, Z. (2009). Design of variable-stiffness composite panels for maximum buckling load. *Composite Structures*, 87(1), 109–117. <https://doi.org/10.1016/j.compstruct.2008.01.008>
- Soremekun, G., Gürdal, Z., Kassapoglou, C., & Toni, D. (2002). Stacking sequence blending of multiple composite laminates using genetic algorithms. *Composite Structures*, 56(1), 53–62. [https://doi.org/10.1016/s0263-8223\(01\)00185-4](https://doi.org/10.1016/s0263-8223(01)00185-4)
- Stanford, B. K., & Dunning, P. D. (2015). Optimal topology of aircraft rib and spar structures under aeroelastic loads. *Journal of Aircraft*, 52(4), 1298–1311. <https://doi.org/10.2514/1.C032913>
- Sun, C., & Mao, K. (1988). A global-local finite element method suitable for parallel computations. *Computers & Structures*, 29(2), 309–315. [https://doi.org/10.1016/0045-7949\(88\)90264-7](https://doi.org/10.1016/0045-7949(88)90264-7)
- Tang, J., Xi, P., Zhang, B., & Hu, B. (2013). A finite element parametric modeling technique of aircraft wing structures. *Chinese Journal of Aeronautics*, 26(5), 1202–1210. <https://doi.org/10.1016/j.cja.2013.07.019>
- The MathWork Inc. (2011). Optimization toolbox user's guide.
- Thomsen, C. R., Wang, F., & Sigmund, O. (2018). Buckling strength topology optimization of 2d periodic materials based on linearized bifurcation analysis. *Computer Methods in Applied Mechanics and Engineering*, 339, 115–136. <https://doi.org/10.1016/j.cma.2018.04.031>
- Tonelli, L. (1915). Sur une méthode directe du calcul des variations. *Rendiconti del Circolo Matematico di Palermo*, 39(1), 233–264. <https://doi.org/10.1007/bf03015981>
- Tonelli, L. (1920). La semicontinuità nel Calcolo delle Variazioni. *Rendiconti del Circolo Matematico di Palermo*, 44(1), 167–249. <https://doi.org/10.1007/bf03014600>
- Townsend, S., & Kim, H. A. (2019). A level set topology optimization method for the buckling of shell structures. *Structural and Multidisciplinary Optimization*. <https://doi.org/10.1007/s00158-019-02374-9>
- Truesdell, C., & Wang, C. C. (1973). *Introduction to Rational Elasticity*. Noordhoff International Publishing.
- Truesdell, C. A. (1977). *A First Course in Rational Continuum Mechanics : Volume 1 General Concepts*. Academic Press.
- Tsai, S., & Hahn, T. (1980). *Introduction to composite materials*. Technomic.
- Tsai, S., & Pagano, N. J. (1968). *Invariant properties of composite materials* (tech. rep.). Air force materials lab Wright-Patterson AFB Ohio.
- van Campen, J., Seresta, O., Abdalla, M., & Gürdal, Z. (2008). General blending definitions for stacking sequence design of composite laminate structures. In *49th AIAA/ASME/ASCE/AHS/ASC structures, structural dynamics, and materials conference*. <https://doi.org/10.2514/6.2008-1798>

- Vankan, W. J., Maas, R., & Grihon, S. (2014). Efficient optimisation of large aircraft fuselage structures. *The Aeronautical Journal*, 118(1199), 31–52. <https://doi.org/10.1017/S0001924000008915>
- Vannucci, P., Gong, X., & Verchery, G. (1998). Determination des stratifiés quasi-homogènes par l'approche polaire [(Arcachon, France)], In *Proc. of jnc11 - journées nationales sur les composites*.
- Vannucci, P., & Verchery, G. (2001a). A special class of uncoupled and quasi-homogeneous laminates. *Composites Science and Technology*, 61(10), 1465–1473. [https://doi.org/10.1016/S0266-3538\(01\)00039-2](https://doi.org/10.1016/S0266-3538(01)00039-2)
- Vannucci, P., & Verchery, G. (2001b). Stiffness design of laminates using the polar method. *International Journal of Solids and Structures*, 38(50-51), 9281–9294. [https://doi.org/10.1016/S0020-7683\(01\)00177-9](https://doi.org/10.1016/S0020-7683(01)00177-9)
- Vannucci, P., & Verchery, G. (2002). A new method for generating fully isotropic laminates. *Composite Structures*, 58(1), 75–82. [https://doi.org/10.1016/S0263-8223\(02\)00038-7](https://doi.org/10.1016/S0263-8223(02)00038-7)
- Vannucci, P., & Verchery, G. (2010). Anisotropy of plane complex elastic bodies. *International Journal of Solids and Structures*, 47(9), 1154–1166. <https://doi.org/10.1016/j.ijsolstr.2010.01.002>
- Vannucci, P. (2002). A special planar orthotropic material. *Journal of Elasticity*, 67(2), 81–96. <https://doi.org/10.1023/a:1023949729395>
- Vannucci, P. (2009). On special orthotropy of paper. *Journal of Elasticity*, 99(1), 75–83. <https://doi.org/10.1007/s10659-009-9232-2>
- Vannucci, P. (2012a). A Note on the Elastic and Geometric Bounds for Composite Laminates. *Journal of Elasticity*, 112(2), 199–215. <https://doi.org/10.1007/s10659-012-9406-1>
- Vannucci, P. (2012b). The design of laminates as a global optimization problem. *Journal of Optimization Theory and Applications*, 157(2), 299–323. <https://doi.org/10.1007/s10957-012-0175-6>
- Vannucci, P. (2017, July 10). *Anisotropic elasticity*. Springer-Verlag GmbH. <https://doi.org/10.1007/978-981-10-5439-6>
- Vannucci, P., Desmorat, B., & Vincenti, A. (2012). Design problems of anisotropic structures: Some recent results. In *Springer optimization and its applications* (pp. 395–426). Springer US. https://doi.org/10.1007/978-1-4614-2435-2_17
- Venkataraman, S., & Haftka, R. T. (2004). Structural optimization complexity: what has Moore's law done for us? *Structural and Multidisciplinary Optimization*, 28(6), 375–387. <https://doi.org/10.1007/s00158-004-0415-y>
- Verchery, G. (1979). Les invariants des tenseurs d'ordre 4 du type de l'élasticité' [Published in 1982 by Editions du CNRS, Paris, pp. 93–104 (in French)]. *Colloque Euromech 115, Villard-de-Lans*.
- Verchery, G. (1982). Les invariants des tenseurs d'ordre 4 du type de l'élasticité. In *Mechanical behavior of anisotropic solids / comportement mécanique des solides anisotropes* (pp. 93–104). Springer Netherlands. https://doi.org/10.1007/978-94-009-6827-1_7
- Verchery, G., & Vong, T. S. (1986). Une méthode d'aide graphique à la conception des séquences d'empilement dans les stratifiés. In *Comptes rendus de jnc5 (5èmes journées nationales sur les composites)*.

- Viglietti, A., Zappino, E., & Carrera, E. (2019). Free vibration analysis of variable angle-tow composite wing structures. *Aerospace Science and Technology*, 92, 114–125. <https://doi.org/10.1016/j.ast.2019.05.068>
- Wang, W., Guo, S., Chang, N., & Yang, W. (2010). Optimum buckling design of composite stiffened panels using ant colony algorithm. *Composite Structures*, 92(3), 712–719. <https://doi.org/10.1016/j.compstruct.2009.09.018>
- Warren, F., & Norris, C. B. (1953). *Mechanical properties of laminate design to be isotropic* (tech. rep. No. 1841). Forest Product Laboratory.
- Watson, J. D., & Crick, F. H. C. (1953). Molecular structure of nucleic acids: A structure for deoxyribose nucleic acid. *Nature*, 171(4356), 737–738. <https://doi.org/10.1038/171737a0>
- Whitcomb, J. (1991). Iterative global/local finite element analysis. *Computers & Structures*, 40(4), 1027–1031. [https://doi.org/10.1016/0045-7949\(91\)90334-i](https://doi.org/10.1016/0045-7949(91)90334-i)
- Wu, B., Xu, Z., & Li, Z. (2007). A note on imposing displacement boundary conditions in finite element analysis. *Communications in Numerical Methods in Engineering*, 24(9), 777–784. <https://doi.org/10.1002/cnm.989>
- Wu, K. M., & Avery, B. L. (1992). Fully Isotropic Laminates and Quasi-Homogeneous Anisotropic Laminates. *Journal of Composite Materials*, 26(14), 2107–2117. <https://doi.org/10.1177/002199839202601406>
- Ye, H.-L., Wang, W.-W., Chen, N., & Sui, Y.-K. (2015). Plate/shell topological optimization subjected to linear buckling constraints by adopting composite exponential filtering function. *Acta Mechanica Sinica*, 32(4), 649–658. <https://doi.org/10.1007/s10409-015-0531-5>
- Zein, S., Colson, B., & Grihon, S. (2011). A primal-dual backtracking optimization method for blended composite structures. *Structural and Multidisciplinary Optimization*, 45(5), 669–680. <https://doi.org/10.1007/s00158-011-0716-x>
- Zhang, B., Dai, R., Ma, W., Wu, H., Jiang, L., Yan, C., & Zhang, Y. (2019). Analysis and design of carbon fibre clamping apparatus for replacement of insulator strings in ultra-high voltage transmission line. *The Journal of Engineering*, 2019(16), 2212–2215. <https://doi.org/10.1049/joe.2018.8907>
- Zhao, A., Zou, H., Jin, H., & Wen, D. (2019). Structural design and verification of an innovative whole adaptive variable camber wing. *Aerospace Science and Technology*, 89, 11–18.
- Zhu, W., Yu, X., & Wang, Y. (2019). Layout optimization for blended wing body aircraft structure. *International Journal of Aeronautical and Space Sciences*, 20(4), 879–890. <https://doi.org/10.1007/s42405-019-00172-7>

A Note on the Square of the Sum of n Terms

Consider the square of the sum of terms a_1, a_2, \dots, a_n , $n \in \mathbb{N}$. Hence, it is easy to see that

$$\left(\sum_{k=1}^n a_k \right)^2 = \sum_{k=1}^n a_k^2 + 2 \sum_{k=1}^{n-1} a_k \sum_{j=k+1}^n a_j = \sum_{k=1}^n a_k^2 + 2 \sum_{k=1}^{n-1} \sum_{j=k+1}^n a_k a_j, \quad (\text{A.1})$$

where the distributivity property of sum and product operators has been used (see, for instance, (Graham et al., 1994, Chapter 2)).

The number of the double-product terms is equal to

$$\sum_{k=1}^{n-1} \sum_{j=k+1}^n 1 = \sum_{k=1}^{n-1} (n - k) = n \sum_{k=1}^{n-1} 1 - \sum_{k=1}^{n-1} k = n(n-1) - \frac{n(n-1)}{2} = \frac{n(n-1)}{2}. \quad (\text{A.2})$$

If an n -term sequence $\{a_k\}$ has indices k progressively taking values in an arbitrary, but ordered, set of n natural numbers, say \mathcal{A} , the square of the sum of the sequence's elements can be written as

$$\left(\sum_{k \in \mathcal{A}} a_k \right)^2 = \sum_{k \in \mathcal{A}} a_k^2 + 2 \sum_{\substack{k, j \in \mathcal{A} \\ j > k}} a_k a_j. \quad (\text{A.3})$$

Of course, the result of Eq. (A.2) still holds.

Therefore, for a laminate having N plies and m distinct orientations, Eq. (9.3) reads

$$\begin{aligned}\rho_0 &= \frac{1}{N} \sqrt{\left(\sum_{j=1}^N \cos 4\theta_j\right)^2 + \left(\sum_{j=1}^N \sin 4\theta_j\right)^2} \\ &= \frac{1}{N} \sqrt{\left(\sum_{j=1}^m n_j \cos 4\theta_j\right)^2 + \left(\sum_{j=1}^m n_j \sin 4\theta_j\right)^2}.\end{aligned}\tag{A.4}$$

Applying Eq. (A.1) to Eq. (A.4), one has

$$\begin{aligned}\rho_0 &= \frac{1}{N} \sqrt{\left(\sum_{j=1}^m n_j \cos 4\theta_j\right)^2 + \left(\sum_{j=1}^m n_j \sin 4\theta_j\right)^2} \\ &= \frac{1}{N} \left[\sum_{j=1}^m n_j^2 \cos^2 4\theta_j + \sum_{j=1}^m n_j^2 \sin^2 4\theta_j \right. \\ &\quad \left. + 2 \sum_{k=1}^{m-1} \sum_{j=k+1}^m n_k n_j \cos 4\theta_k \cos 4\theta_j + 2 \sum_{k=1}^{m-1} \sum_{j=k+1}^m n_k n_j \sin 4\theta_k \sin 4\theta_j \right]^{1/2} \\ &= \frac{1}{N} \sqrt{\sum_{j=1}^m n_j^2 + 2 \sum_{k=1}^{m-1} \sum_{j=k+1}^m n_k n_j \cos 4(\theta_k - \theta_j)} \\ &= \frac{1}{N} \sqrt{\sum_{j=1}^m n_j^2 + 2 \sum_{k=1}^{m-1} \sum_{j=k+1}^m n_k n_j (2 \cos^2 2(\theta_k - \theta_j) - 1)} \\ &= \text{Eq. (9.24)} \quad (m = 3),\end{aligned}\tag{A.5}$$

where the identity $\cos(2\alpha) = 2 \cos^2 \alpha - 1$ has been used. In a similar manner, the expression of ρ_1 of Eq. (9.4) can be rearranged as Eq. (9.25).

Study of $\mathbf{B}^* = 0$ for Blending Constraints

Uncoupling condition on laminates is $\mathbf{B}^* = 0$, which can be stated as follows:

$$\sum_{k=1}^N b_k e^{i\beta\theta_k} = 0, \quad \beta = 2, 4. \quad (\text{B.1})$$

Considering Eqs. (4.23) and (4.30), Eq. (B.1) may be expressed as:

$$\frac{N(N+1)}{2} \rho_{0K} e^{i4\Phi_1^{A*}} = \sum_{k=1}^N k e^{i4\theta_k}, \quad (\text{B.2})$$

$$\frac{N(N+1)}{2} \rho_1 e^{i2\Phi_1^{A*}} = \sum_{k=1}^N k e^{i2\theta_k}. \quad (\text{B.3})$$

As already done in Section 6.2, consider two laminates denoted with labels p and q , such that, without loss of generality, $N_p > N_q$. Writing Eqs. (B.2) and (B.3) for the two laminates, subtracting member-by-member, taking the square of both members, one obtains:

$$\begin{aligned} & \left[\Delta_{pq} \left(\frac{N(N+1)}{2} \rho_{0K} c_4 \right) \right]^2 + \left[\Delta_{pq} \left(\frac{N(N+1)}{2} \rho_{0K} s_4 \right) \right]^2 = \\ & \left(\sum_{k \in \mathcal{NB}} k \cos 4\theta_k + \sum_{k=1}^{N_q} [\mathcal{B}(k) - k] \cos 4\theta_k \right)^2 \\ & + \left(\sum_{k \in \mathcal{NB}} k \sin 4\theta_k + \sum_{k=1}^{N_q} [\mathcal{B}(k) - k] \sin 4\theta_k \right)^2, \end{aligned} \quad (\text{B.4})$$

and

$$\begin{aligned} \left[\Delta_{pq} \left(\frac{N(N+1)}{2} \rho_1 c_2 \right) \right]^2 + \left[\Delta_{pq} \left(\frac{N(N+1)}{2} \rho_1 s_2 \right) \right]^2 = \\ \left(\sum_{k \in \mathcal{NB}} k \cos 2\theta_k + \sum_{k=1}^{N_q} [\mathcal{B}(k) - k] \cos 2\theta_k \right)^2 \\ + \left(\sum_{k \in \mathcal{NB}} k \sin 2\theta_k + \sum_{k=1}^{N_q} [\mathcal{B}(k) - k] \sin 2\theta_k \right)^2. \end{aligned} \quad (\text{B.5})$$

Consider, for the sake of simplicity, the right-hand side of Eq. (B.4) (akin considerations hold for Eq. (B.5)). It can be expressed as:

$$\begin{aligned} & \left(\sum_{k \in \mathcal{NB}} k \cos 4\theta_k \right)^2 + \left(\sum_{k=1}^{N_q} [\mathcal{B}(k) - k] \cos 4\theta_k \right)^2 \\ & + 2 \left(\sum_{k \in \mathcal{NB}} k \cos 4\theta_k \right) \left(\sum_{k=1}^{N_q} [\mathcal{B}(k) - k] \cos 4\theta_k \right) \\ & + \left(\sum_{k \in \mathcal{NB}} k \sin 4\theta_k \right)^2 + \left(\sum_{k=1}^{N_q} [\mathcal{B}(k) - k] \sin 4\theta_k \right)^2 \\ & + 2 \left(\sum_{k \in \mathcal{NB}} k \sin 4\theta_k \right) \left(\sum_{k=1}^{N_q} [\mathcal{B}(k) - k] \sin 4\theta_k \right) \\ & =: c_1 + c_2 + c_3 + c_4 + c_5 + c_6. \end{aligned} \quad (\text{B.6})$$

Considering Appendix A and the elementary trigonometric identity $\cos \alpha \cos \beta + \sin \alpha \sin \beta = \cos(\alpha - \beta)$, the sum $c_1 + c_4$ gives:

$$\sum_{k \in \mathcal{NB}} k^2 + 2 \sum_{\substack{k, j \in \mathcal{NB} \\ j > k}} k j \cos 4(\theta_j - \theta_k). \quad (\text{B.7})$$

In a complete similar manner, the sum $c_2 + c_5$ simplifies to

$$\sum_{k=1}^{N_q} [\mathcal{B}(k) - k]^2 + 2 \sum_{k=1}^{N_q-1} \sum_{j=k+1}^{N_q} [\mathcal{B}(k) - k] [\mathcal{B}(j) - j] \cos 4(\theta_k - \theta_j). \quad (\text{B.8})$$

The sum $c_3 + c_6$ can be rewritten as (using the distributivity property of sum and product operators and the aforementioned trigonometric identity)

$$\begin{aligned}
& 2 \sum_{k=1}^{N_q} \sum_{j \in \mathcal{NB}} [\mathcal{B}(k) - k] j \cos 4\theta_j \cos 4\theta_k + 2 \sum_{k=1}^{N_q} \sum_{j \in \mathcal{NB}} [\mathcal{B}(k) - k] j \sin 4\theta_j \sin 4\theta_k \\
&= 2 \sum_{k=1}^{N_q} \sum_{j \in \mathcal{NB}} [\mathcal{B}(k) - k] j (\cos 4\theta_j \cos 4\theta_k + \sin 4\theta_j \sin 4\theta_k) \\
&= 2 \sum_{k=1}^{N_q} \sum_{j \in \mathcal{NB}} [\mathcal{B}(k) - k] j \cos 4(\theta_j - \theta_k).
\end{aligned} \tag{B.9}$$

Assembling Eqs. (B.7), (B.8) and (B.9), Eq. (B.6) simplifies to:

$$\begin{aligned}
& \sum_{k \in \mathcal{NB}} k^2 + 2 \sum_{\substack{k, j \in \mathcal{NB} \\ j > k}} k j \cos(4(\theta_j - \theta_k)) + \sum_{k=1}^{N_q} [\mathcal{B}(k) - k]^2 \\
&+ 2 \sum_{k=1}^{N_q-1} \sum_{j=k+1}^{N_q} [\mathcal{B}(k) - k] [\mathcal{B}(j) - j] \cos 4(\theta_k - \theta_j) \\
&+ 2 \sum_{k=1}^{N_q} \sum_{j \in \mathcal{NB}} j [\mathcal{B}(k) - k] \cos 4(\theta_k - \theta_j).
\end{aligned} \tag{B.10}$$

It is simple to see that

$$\begin{aligned}
\text{Eq. (B.10)} &\leq \sum_{k \in \mathcal{NB}} k^2 + 2 \sum_{\substack{k, j \in \mathcal{NB} \\ j > k}} k j + \sum_{k=1}^{N_q} [\mathcal{B}(k) - k]^2 \\
&+ 2 \sum_{k=1}^{N_q-1} \sum_{j=k+1}^{N_q} [\mathcal{B}(k) - k] [\mathcal{B}(j) - j] + 2 \sum_{k=1}^{N_q} \sum_{j \in \mathcal{NB}} j [\mathcal{B}(k) - k],
\end{aligned} \tag{B.11}$$

since terms of the form $(\mathcal{B}(\cdot) - \cdot)$ are always non-negative, because of property **b** of Definition 6.3.

Consider the particular case for which $\mathcal{B}(k) = k$; it follows that $\mathcal{NB} = \{i \mid N_q + 1 \leq i \leq N_p\}$. Equation (B.11) simplifies to:

$$\begin{aligned}
\sum_{k=N_q+1}^{N_p} k^2 + 2 \sum_{i=N_q+1}^{N_p-1} \sum_{j=i+1}^{N_p} i j &= \frac{1}{4} [N_p^4 + N_q^4 + 2(N_p^3 + N_q^3) + N_p^2 + N_q^2 \\
&- 2N_p N_q (N_p N_q + N_p + N_q + 1)] =: C_B.
\end{aligned} \tag{B.12}$$

The final blending constraints, for the considered particular case, read:

$$\begin{aligned}
 g_{\text{blend}-0}^{\text{C}_B} &:= \left[\Delta_{pq} \left(\frac{N(N+1)}{2} \rho_{0K} c_4 \right) \right]^2 + \left[\Delta_{pq} \left(\frac{N(N+1)}{2} \rho_{0K} s_4 \right) \right]^2 - C_B, \\
 g_{\text{blend}-1}^{\text{C}_B} &:= \left[\Delta_{pq} \left(\frac{N(N+1)}{2} \rho_1 c_2 \right) \right]^2 + \left[\Delta_{pq} \left(\frac{N(N+1)}{2} \rho_1 s_2 \right) \right]^2 - C_B, \\
 g_{\text{blend}-i}^{\text{C}_B} &\leq 0, \quad i = 0, 1.
 \end{aligned} \tag{B.13}$$

Figure B.1 shows, for the reference laminate of Section 6.2, that conditions of Eq. (6.43) is stricter than the one expressed by Eq. (B.13). Even though C_B is not the sharpest upper-bound of Eq. (B.11), the fact that the condition $\mathbf{B}^* = \mathbf{0}$ does not introduce further constraints on PPs can be inferred. In fact, if there exists another estimate $C > C_B$ (for which Eq. (B.13) would read $g_{\text{blend}-i}^C \leq 0, i = 0, 1$, with a clear meaning of notation), the feasible domain can only be larger than the (green) one in Figure B.1. The result may

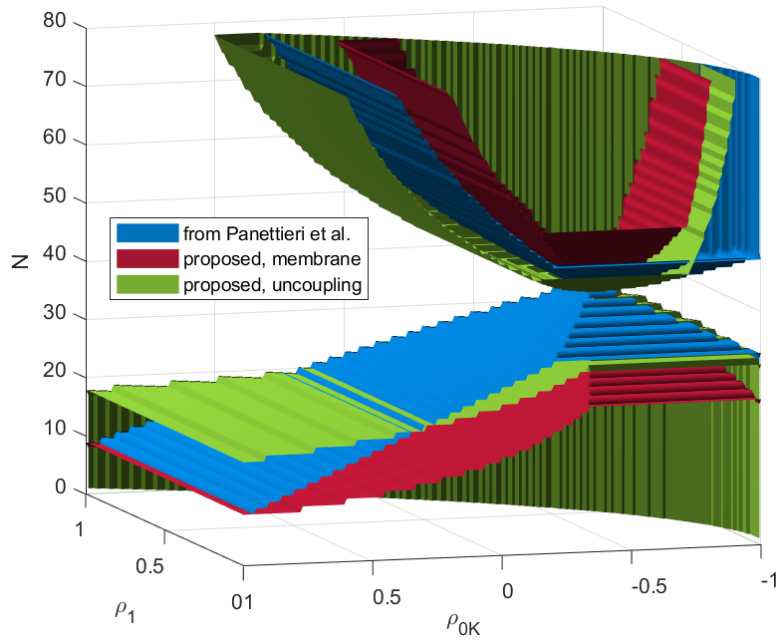


Figure B.1: Comparison between blending constraints

be due to the fact that increasing separately the “angle terms”, as done in Eq. (B.11), and the “arrangement terms”, as done in Eq. (B.12), is too rude. Indeed, a coupling between the aforementioned terms exists, which makes finding a good estimate of Eq. (B.10) a cumbersome, probably impossible, task.

Analytic Expression of Stiffness Matrix Gradient

The unconstrained equilibrium system of the GFEM is of the form

$$\hat{\mathbf{K}}\hat{\mathbf{u}} = \hat{\mathbf{f}}, \quad (\text{C.1})$$

where $\hat{\mathbf{K}} \in \mathbb{M}_s^{n_{\text{DOF}} \times n_{\text{DOF}}}$ is the unconstrained (singular) stiffness matrix, while n_{DOF} is the number of DOFs of the GFEM before the application of the BCs.

If BCs are of the type $u_j = 0$ for $j \in I_{\text{BC}} \subset \{i \mid i = 1, \dots, n_{\text{DOF}}\}$, $\#I_{\text{BC}} = n_{\text{BC}}$, Eq. (C.1) can be transformed in a reduced problem of the form and size considered in Eq. (6.1) by posing $\mathbf{K} := \mathfrak{R}(\hat{\mathbf{K}}, I_{\text{BC}}, I_{\text{BC}})$, $\mathbf{u} := \mathfrak{R}(\hat{\mathbf{u}}, I_{\text{BC}})$ and $\mathbf{f} := \mathfrak{R}(\hat{\mathbf{f}}, I_{\text{BC}})$.

The analytical form of $\partial\mathbf{K}/\partial\xi_j$ can be easily determined. In fact, the expression of $\hat{\mathbf{K}}$ is:

$$\hat{\mathbf{K}} = \sum_{e=1}^{N_e} \hat{\mathbf{L}}_e^{\text{T}} \int_{\Omega_e} \mathbf{B}_e^{\text{T}} \mathbf{K}_e^{\text{lam}} \mathbf{B}_e \, \text{d}\Omega_e \hat{\mathbf{L}}_e, \quad (\text{C.2})$$

where N_e is the number of elements of the GFEM, Ω_e is the integration domain for the e -th element, \mathbf{B}_e is the operator defined in Eq. (6.26), $\mathbf{K}_e^{\text{lam}}$ is the element stiffness matrix defined in Eq. (4.15), expressed in the global frame of the GFEM, whilst $\hat{\mathbf{L}}_e \in \mathbb{M}^{24 \times n_{\text{DOF}}}$ is a linear map $\hat{\mathbf{L}}_e : \hat{\mathbf{u}} \mapsto \mathbf{u}_e$. By differentiating Eq. (C.2) with respect to the generic ξ_j , one obtains:

$$\frac{\partial \hat{\mathbf{K}}}{\partial \xi_j} = \sum_{e=1}^{N_e} \hat{\mathbf{L}}_e^{\text{T}} \int_{\Omega_e} \mathbf{B}_e^{\text{T}} \frac{\partial \mathbf{K}_e^{\text{lam}}}{\partial \xi_j} \mathbf{B}_e \, \text{d}\Omega_e \hat{\mathbf{L}}_e. \quad (\text{C.3})$$

It follows that

$$\frac{\partial \mathbf{K}}{\partial \xi_j} := \mathfrak{R} \left(\frac{\partial \hat{\mathbf{K}}}{\partial \xi_j}, I_{\text{BC}}, I_{\text{BC}} \right). \quad (\text{C.4})$$

Analytic Expression of Laminate Strength Matrices Gradient

Matrix \mathbf{G}_A^* can be decomposed as:

$$\begin{aligned}
 \mathbf{G}_A^* &= \underbrace{\begin{bmatrix} \Gamma_0 + 2\Gamma_1 & -\Gamma_0 + 2\Gamma_1 & 0 \\ & \Gamma_0 + 2\Gamma_1 & \\ & & \Gamma_0 \end{bmatrix}}_{\mathbf{G}_{A0}^*} + \Lambda_0^{G_A^*} \underbrace{\begin{bmatrix} c_4 & -c_4 & s_4 \\ & c_4 & - \\ & & 4 \end{bmatrix}}_{\mathbf{G}_{A1}^*} + \Lambda_1^{G_A^*} \underbrace{\begin{bmatrix} 4c_2 & 0 & 2s_2 \\ & -4c_2 & 2 \\ 0 & & \end{bmatrix}}_{\mathbf{G}_{A2}^*} \\
 &:= \mathbf{G}_{A0}^* + \rho_{0K} \Lambda_0 \mathbf{G}_{A1}^* + \Lambda_1 \rho_1 \mathbf{G}_{A2}^*,
 \end{aligned} \tag{D.1}$$

with

$$\begin{aligned}
 c_2 &= \cos 2 \left(\frac{\pi}{2} \phi_1 + \Omega_1 - \Phi_1 \right), & c_4 &= \cos 4 \left(\frac{\pi}{2} \phi_1 + \Omega_0 - \Phi_0 \right), \\
 s_2 &= \sin 2 \left(\frac{\pi}{2} \phi_1 + \Omega_1 - \Phi_1 \right), & s_4 &= \sin 4 \left(\frac{\pi}{2} \phi_1 + \Omega_0 - \Phi_0 \right).
 \end{aligned}$$

Similarly, matrix \mathbf{G}_H^* can be decomposed as:

$$\mathbf{G}_H^* = \underbrace{\begin{bmatrix} \Gamma & 0 \\ \text{sym} & \Gamma \end{bmatrix}}_{\mathbf{G}_{H0}^*} + \Lambda \rho_1 \underbrace{\begin{bmatrix} c_2^{G_H^*} & s_2^{G_H^*} \\ \text{sym} & -c_2^{G_H^*} \end{bmatrix}}_{\mathbf{G}_{H1}^*} := \mathbf{G}_{H0}^* + \Lambda \rho_1 \mathbf{G}_{H1}^*, \tag{D.2}$$

with

$$c_2^{G_H^*} = \cos 2 \left(\Omega - \frac{\pi}{2} \phi_1 + \Phi_1 \right), \quad s_2^{G_H^*} = \sin 2 \left(\Omega - \frac{\pi}{2} \phi_1 + \Phi_1 \right).$$

Since quasi-homogeneity holds, $\mathbf{G}_B^* = \mathbf{0}$ and $\mathbf{G}_D^* = \mathbf{G}_A^*$.

Let $h = t_{\text{ply}} n_0 n_{\text{ref}}$, with reference to Eq. (4.32) be the thickness of the laminate. There-

fore, the following derivatives read:

$$\begin{aligned} \frac{\partial \mathbf{G}_A}{\partial n_0} &= \frac{h}{n_0} \mathbf{G}_A^*, & \frac{\partial \mathbf{G}_A}{\partial \rho_{0K}} &= h\Lambda_0 \mathbf{G}_{A1}^*, & \frac{\partial \mathbf{G}_A}{\partial \rho_1} &= h\Lambda_1 \mathbf{G}_{A2}^*, \\ \frac{\partial \mathbf{G}_A}{\partial \phi_1} &= 2\pi h\Lambda_0 \rho_{0K} \begin{bmatrix} -s_4 & +s_4 & c_4 \\ & -s_4 & - \\ & & 4 \end{bmatrix} + \pi h\Lambda_1 \rho_1 \begin{bmatrix} -4s_2 & 0 & 2c_2 \\ & +4s_2 & 2 \\ 0 & & \end{bmatrix}. \end{aligned} \quad (\text{D.3})$$

Similarly, for matrix \mathbf{G}_D and matrix \mathbf{G}_H :

$$\begin{aligned} \frac{\partial \mathbf{G}_D}{\partial n_0} &= \frac{h^2}{4} \frac{\partial \mathbf{G}_A}{\partial n_0}, & \frac{\partial \mathbf{G}_D}{\partial \rho_{0K}} &= \frac{h^2}{12} \frac{\partial \mathbf{G}_A}{\partial \rho_{0K}}, & \frac{\partial \mathbf{G}_D}{\partial \rho_1} &= \frac{h^2}{12} \frac{\partial \mathbf{G}_A}{\partial \rho_1}, & \frac{\partial \mathbf{G}_D}{\partial \phi_1} &= \frac{h^2}{12} \frac{\partial \mathbf{G}_A}{\partial \phi_1}, \quad (\text{D.4}) \\ \frac{\partial \mathbf{G}_H}{\partial n_0} &= \frac{h}{n_0} \mathbf{G}_H^*, & \frac{\partial \mathbf{G}_H}{\partial \rho_{0K}} &= \mathbf{0}, & \frac{\partial \mathbf{G}_H}{\partial \rho_1} &= h\Lambda \mathbf{G}_{H1}^*, & \frac{\partial \mathbf{H}}{\partial \phi_1} &= -\pi h\Lambda \rho_1 \begin{bmatrix} -s_2^{G_H^*} & c_2^{G_H^*} \\ \text{sym} & s_2^{G_H^*} \end{bmatrix}. \end{aligned} \quad (\text{D.5})$$

Finally, for the generic variable ξ_j , for an orthotropic quasi-homogeneous laminate,

$$\frac{\partial \mathbf{G}}{\partial \xi_j} = \text{diag} \left(\frac{\partial \mathbf{G}_A}{\partial \xi_j}, \frac{\partial \mathbf{G}_D}{\partial \xi_j}, \frac{\partial \mathbf{G}_H}{\partial \xi_j} \right). \quad (\text{D.6})$$

Analytic Expression of Laminate Stiffness Matrices Gradient

Under the hypothesis of orthotropic laminate, the expression of the homogenised membrane stiffness matrix in terms of the dimensionless PPs reads:

$$\begin{aligned}
 \mathbf{A}^* &= \underbrace{\begin{bmatrix} T_0 + 2T_1 & -T_0 + 2T_1 & 0 \\ & T_0 + 2T_1 & \\ & & 0 \end{bmatrix}}_{\mathbf{A}_0^*} + R_{0K}^{A^*} \underbrace{\begin{bmatrix} c_4 & -c_4 & s_4 \\ & c_4 & - \\ & & 4 \end{bmatrix}}_{\mathbf{A}_1^*} \\
 &\quad + R_1^{A^*} \underbrace{\begin{bmatrix} 4c_2 & 0 & 2s_2 \\ & -4c_2 & 2 \\ 0 & & \end{bmatrix}}_{\mathbf{A}_2^*} \tag{E.1} \\
 &:= \mathbf{A}_0^* + R_{0\rho_{0K}} \mathbf{A}_1^* + R_{1\rho_1} \mathbf{A}_2^*,
 \end{aligned}$$

with

$$c_2 = \cos \pi\phi_1, \quad c_4 = \cos 2\pi\phi_1, \quad s_2 = \sin \pi\phi_1, \quad s_4 = \sin 2\pi\phi_1.$$

Similarly, matrix \mathbf{H}^* can be decomposed as:

$$\mathbf{H}^* = \underbrace{\begin{bmatrix} T & 0 \\ \text{sym} & T \end{bmatrix}}_{\mathbf{H}_0^*} + R_{\rho_1} \underbrace{\begin{bmatrix} c_2^{H^*} & s_2^{H^*} \\ \text{sym} & -c_2^{H^*} \end{bmatrix}}_{\mathbf{H}_1^*} := \mathbf{H}_0^* + R_{\rho_1} \mathbf{H}_1^*, \tag{E.2}$$

where

$$c_2^{H^*} = \cos 2\Phi^{H^*}, \quad s_2^{H^*} = \sin 2\Phi^{H^*}, \quad \Phi^{H^*} = \Phi + \Phi_1 - \frac{\pi}{2}\phi_1.$$

Since quasi-homogeneity holds, $\mathbf{B}^* = \mathbf{0}$ and $\mathbf{D}^* = \mathbf{A}^*$.

Let $h = t_{\text{ply}}n_0N_{\text{ref}}$, with reference to Eq. (4.32), be the thickness of the laminate. Therefore, the following derivatives read:

$$\begin{aligned} \frac{\partial \mathbf{A}}{\partial n_0} &= \frac{h}{n_0} \mathbf{A}^*, \quad \frac{\partial \mathbf{A}}{\partial \rho_{0K}} = hR_0 \mathbf{A}_1^*, \quad \frac{\partial \mathbf{A}}{\partial \rho_1} = hR_1 \mathbf{A}_2^*, \\ \frac{\partial \mathbf{A}}{\partial \phi_1} &= 2\pi hR_0 \rho_{0K} \begin{bmatrix} -s_4 & +s_4 & c_4 \\ & -s_4 & - \\ & & 4 \end{bmatrix} + \pi hR_1 \rho_1 \begin{bmatrix} -4s_2 & 0 & 2c_2 \\ & +4s_2 & 2 \\ 0 & & \end{bmatrix}. \end{aligned} \quad (\text{E.3})$$

Similarly, for matrix \mathbf{D} and matrix \mathbf{H} :

$$\frac{\partial \mathbf{D}}{\partial n_0} = \frac{h^2}{4} \frac{\partial \mathbf{A}}{\partial n_0}, \quad \frac{\partial \mathbf{D}}{\partial \rho_{0K}} = \frac{h^2}{12} \frac{\partial \mathbf{A}}{\partial \rho_{0K}}, \quad \frac{\partial \mathbf{D}}{\partial \rho_1} = \frac{h^2}{12} \frac{\partial \mathbf{A}}{\partial \rho_1}, \quad \frac{\partial \mathbf{D}}{\partial \phi_1} = \frac{h^2}{12} \frac{\partial \mathbf{A}}{\partial \phi_1}, \quad (\text{E.4})$$

$$\frac{\partial \mathbf{H}}{\partial n_0} = \frac{h}{n_0} \mathbf{H}^*, \quad \frac{\partial \mathbf{H}}{\partial \rho_{0K}} = \mathbf{0}, \quad \frac{\partial \mathbf{H}}{\partial \rho_1} = hR \mathbf{H}_1^*, \quad \frac{\partial \mathbf{H}}{\partial \phi_1} = -\pi hR \rho_1 \begin{bmatrix} -s_2^{H^*} & c_2^{H^*} \\ \text{sym} & +s_2^{H^*} \end{bmatrix}. \quad (\text{E.5})$$

Finally, for orthotropic quasi-homogeneous laminates, for the generic ξ_j :

$$\frac{\partial \mathbf{K}_e^{\text{lam}}}{\partial \xi_j} = \text{diag} \left(\frac{\partial \mathbf{A}_e}{\partial \xi_j}, \frac{\partial \mathbf{D}_e}{\partial \xi_j}, \frac{\partial \mathbf{H}_e}{\partial \xi_j} \right). \quad (\text{E.6})$$

List of Publications

Most of the content of this Thesis may also be found in the following journal papers:

1. Picchi Scardaoni, M., & Montemurro, M. (2020). A General Global-Local Modelling Framework for the Deterministic Optimisation of Composite Structures. *Structural and Multidisciplinary Optimization*. <https://doi.org/10.1007/s00158-020-02586-4>.
2. Picchi Scardaoni, M., Montemurro, M., Panettieri, E., & Catapano, A. (2020). New Blending Constraints and a Stack-Recovery Strategy for the Multi-Scale Design of Composite Laminates. *Structural and Multidisciplinary Optimization*. <http://dx.doi.org/10.1007/s00158-020-02725-x>.
3. Picchi Scardaoni, M., & Montemurro, M. (2020). Convex or non-convex? On the nature of the feasible domain of laminates. *European Journal of Mechanics - A/Solids*. <https://doi.org/10.1016/j.euromechsol.2020.104112>.
4. Picchi Scardaoni, M., Montemurro, M., Panettieri, E., Cipolla, V., & Binante, V. (2020). Multi-scale Deterministic Optimization of Blended Composite Structures: Case Study of a Box-Wing. In preparation.
5. Picchi Scardaoni, M., & Paroni, R. (2020). Linear Models of a Stiffened Plate via Γ -convergence. In preparation.

and in the following conference works:

1. Picchi Scardaoni, M., Montemurro, M., Panettieri, E., & Catapano, A. (2020, September). Blending in Multi scale Design of Composite Structures. *ICCS23 MECHCOMP6*. Porto.

2. Picchi Scardaoni, M., Cipolla, V., & Binante, V. (2019, July). Overall Preliminary Sizing and Optimization of the Metallic Structures of a PrandtlPlane Civil Transport Aircraft., *8th Eucass Conference*. Madrid. [10.13009/eucass2019-802](https://doi.org/10.13009/eucass2019-802).

The content of other works, correlated to my Ph.D. project but not included in this Thesis, may be found in the following journal papers:

1. Picchi Scardaoni, M. (2020). A Simple Model for Minimum Induced Drag of Multiplanes: Could Prandtl Do the Same?, *Aerotecnica Missili & Spazio*. [10.1007/s42496-020-00058-y](https://doi.org/10.1007/s42496-020-00058-y).
2. Picchi Scardaoni, M., Panettieri, E., & Montemurro M. (2020) PrandtlPlane wing box least-weight design: a multi scale approach. *Aerospace Science and Technology*. <https://doi.org/10.1016/j.ast.2020.106156>
3. Picchi Scardaoni, M., Magnacca, F., Massai, A., & Cipolla, V. (2020). A methodology for aircraft turnaround time estimation in early design phases: an application to box-wing architecture. *Journal of Air Traffic Management*. Submitted.
4. Frediani, A., Cipolla, V., Abu Salem, K., Binante, V., & Picchi Scardaoni, M. (2019). Conceptual design of PrandtlPlane civil transport aircraft. *Proceedings of the Institution of Mechanical Engineers, Part G: Journal of Aerospace Engineering*. <https://doi.org/10.1177/0954410019826435>.
5. Picchi Scardaoni, M., & Frediani, A. (2019). Analytical and Finite Element Approach for the In-plane Study of Frames of Non-conventional Civil Aircraft. *Aerotecnica Missili & Spazio*. [10.1007/s42496-018-00004-z](https://doi.org/10.1007/s42496-018-00004-z).
6. Picchi Scardaoni, M., & Frediani, A. (2019). General closed-form solution of piecewise circular frames of aircraft. *AIAA journal*. [10.2514/1.J057712](https://doi.org/10.2514/1.J057712).
7. Picchi Scardaoni, M., Binante, V., & Cipolla, V. (2017). WAGNER: a new code for parametrical structural study of fuselages of civil transport aircraft. *Aerotecnica Missili & Spazio*. [10.19249/ams.v96i3.311](https://doi.org/10.19249/ams.v96i3.311).

and in the following conference works:

1. Cipolla, V., Abu Salem, K., Picchi Scardaoni, M., & Binante, V. (2020, January). Preliminary design and performance analysis of a box-wing transport aircraft. *AIAA Scitech 2020 Forum*, Orlando. [10.2514/6.2020-0267](https://doi.org/10.2514/6.2020-0267)
2. Picchi Scardaoni, M., Izzi, M. I., Panettieri, E., & Montemurro, M. (2019, September) PrandtlPlane aircraft Least Weight Design: a multi scale Optimisation Strategy. *XXV AIDAA International Congress*. Rome.
3. Izzi, M. I., Panettieri, E., Picchi Scardaoni, M., & Montemurro, M. (2019, July). Design of an aircraft composite posite wing-box: integrating a global/local modelling approach into the multi-scale optimisation method. *21ème Journées Nationales sur les Composites*. Bordeaux.

-
4. Cipolla, V., Frediani, A., Abu Salem, K., Picchi Scardaoni, M., & Binante, V. (2019, January). The Project Parsifal: Prandtlplane Architecture For The Sustainable Improvement Of Future Airplanes, *MATEC Web of Conferences*. [10.1051/mateconf/201930401024](https://doi.org/10.1051/mateconf/201930401024)
 5. Cipolla, V., Frediani, A., Abu Salem, K., Picchi Scardaoni, M., Nuti, A., & Binante, V. (2018, June). Conceptual design of a box-wing aircraft for the air transport of the future, *AIAA AVIATION Forum*. Atlanta. [10.2514/6.2018-3660](https://doi.org/10.2514/6.2018-3660)
 6. Frediani, A., Cipolla, V., Abu Salem, K., Binante, V., & Picchi Scardaoni, M. (2017, July). On the Preliminary Design of PrandtlPlane Civil Transport Aircraft. *7th EU-CASS conference*, Milan. [0.13009/EUCASS2017-546](https://doi.org/0.13009/EUCASS2017-546)